



Structures de déformation induites par surpressions de fluide dans les environnements sous-glaciaires et marin profonds : implications paléoenvironnementales et réservoirs

Edouard Ravier

► To cite this version:

Edouard Ravier. Structures de déformation induites par surpressions de fluide dans les environnements sous-glaciaires et marin profonds : implications paléoenvironnementales et réservoirs. Sciences de la Terre. Université de Bourgogne, 2014. Français. NNT : 2014DIJOS053 . tel-01134153

HAL Id: tel-01134153

<https://theses.hal.science/tel-01134153>

Submitted on 23 Mar 2015

HAL is a multi-disciplinary open access archive for the deposit and dissemination of scientific research documents, whether they are published or not. The documents may come from teaching and research institutions in France or abroad, or from public or private research centers.

L'archive ouverte pluridisciplinaire **HAL**, est destinée au dépôt et à la diffusion de documents scientifiques de niveau recherche, publiés ou non, émanant des établissements d'enseignement et de recherche français ou étrangers, des laboratoires publics ou privés.

UNIVERSITE DE BOURGOGNE

UFR Sciences Vie Terre Environnement

Ecole Doctorale Environnement Santé

THÈSE

Pour l'obtention du grade de

Docteur en Sciences de la Terre

Par

Edouard RAVIER

**Structures de déformation induites par surpressions de fluide dans les environnements sous-glaciaires et marins profonds:
Implications paléoenvironnementales et réservoirs.**

Soutenue le 11 décembre 2014 à Dijon, devant le jury composé de:

O. Bourgeois , <i>Maître de Conférence</i>	Université de Nantes	Rapporteur
J.-F. Buoncristiani , <i>Maître de Conférence</i>	Université de Bourgogne	Examineur
M. Guiraud , <i>Professeur</i>	Université de Bourgogne	Directeur de thèse
D.P. Le Heron , <i>Professeur</i>	Université de Londres (<i>Royal Holloway</i>)	Examineur
A. Moscariello , <i>Professeur</i>	Université de Genève	Rapporteur
J. Menzies , <i>Professeur</i>	Université de Brock	Examineur
E. Portier , <i>Ingénieur Réservoir</i>	GDF SUEZ EPI	Examineur
E. Vennin , <i>Professeur</i>	Université de Bourgogne	Présidente du jury

Avant-propos

• En premier lieu, je souhaite remercier MM. **Olivier Bourgeois** et **Andrea Moscariello** d'avoir accepté de rapporter mon travail de thèse, ainsi que MM. **John Menzies** et **Daniel Paul Le Heron** d'avoir accepté d'en être les examinateurs. Merci également à **Emmanuelle Vennin** de faire partie du jury en tant qu'examinatrice. En licence, en master, ou en thèse, j'ai toujours apprécié et profité de ses connaissances, de sa passion pour la sédimentologie, et de sa gentillesse au quotidien.

• Un grand merci à **Eric Portier** pour toutes les discussions (scientifiques ou non) que l'on a pu avoir sur le terrain. Au Maroc, en Irlande, aux Etats-Unis ou en Ecosse, j'ai beaucoup appris à ses côtés, et ce toujours dans la bonne humeur. Sa passion pour la géologie dépasse largement le cadre de la géologie réservoir ce qui ne pouvait que me ravir. Merci également à **Guy Desaubliaux** pour les quelques discussions scientifiques enrichissantes que l'on a pu avoir au cours de cette thèse. Par l'intermédiaire de ces deux personnes c'est également l'entreprise **GDF Suez** que je tiens à remercier pour le financement des recherches entreprises pendant ces trois années de thèse.

• I will just switch in English for few words to thank **John Menzies**. When I contacted John a bit more than two years ago to build a collaboration between him and our team in Dijon, I never thought that he will be so enthusiastic. Few months later I was spending three enriching weeks working with him in Ontario. Since that, our collaboration continued during all my thesis and I am glad he accepted to cross the ocean to attend the defense.

John, I enjoyed very much working and discussing with you. Thank you for sharing your knowledge of glacial sediments. I hope we will stay in contact and we will keep collaborating in the future as I have still much to learn from you.

• Je remercie vivement **Michel Guiraud** de m'avoir fait confiance et d'avoir accepté d'être mon directeur de thèse. Sa passion communicative pour la géologie structurale a finalement réussi à me contaminée, même si ce n'était pas gagné d'avance. Nos discussions scientifiques, parfois animées, m'auront en tout cas permis de progresser dans ce domaine, mais aussi d'en comprendre l'utilité dans l'analyse des déformations glaciaires.

• Enfin je tiens à remercier **Jean-François Buoncrisiani** qui fut une personne majeure et déterminante tout au long de mon parcours universitaire. Merci d'avoir grandement contribué à devenir l'apprenti chercheur que je suis aujourd'hui. Depuis plus de 5 ans, j'ai toujours pu bénéficier de ses conseils sur le terrain ou à la fac. Ma passion pour les glaciers a pu se concrétiser professionnellement grâce à lui, de même que ma passion pour la géologie de terrain. Merci également pour ces soirées passées à discuter autour de quelques verres sur le terrain ou au Quentin. Je lui serais toujours reconnaissant et j'espère que l'opportunité de travailler de nouveau ensemble sur les glaciers actuels et/ou anciens se présentera dans un futur proche...

• Mes remerciements s'adressent également à tous les membres du laboratoire Biogéosciences, enseignants chercheurs et personnels de l'UMR que j'ai pu côtoyer tout au long de ces années. Merci pour les diverses discussions mais aussi pour les aides administratives.

- La suite sera consacrée à mes amis et à ma famille, car la recherche c'est réjouissant mais la vie serait bien triste et monotone si il n'y avait pas tous ces gens là à mes côtés.

- Mes amis d'abord, qui m'ont permis de me détendre pendant ces années de dur labeur que ce soit le week-end, le soir, la nuit, au petit matin, etc...

- Tout d'abord, mes pensées se tournent vers mes amis thésards ou anciens amis de Master. Je les citerais par ordre chronologique, en espérant n'oublier personne: Bastien (dit: «sharkaille», «bastos», «goupos», ou encore «rideau de», bien plus qu'un ancien collègue de promo!), Tom (anarchiste disparu), JB (langue de vipère capée d'une bonne choucroute capillaire) et Morgane (caractère bien trempé, pour pas dire de m...), Jean-David Roselmack (filet de moustache), Sylain Montebourg (et son remake de l'oreille cassé en Irlande), Ben Pierrafeu (daddy cool), Aurélie, Christophe Goumi Roston Roulpaf (parfois mal luné mais on s'y attache malgré tout), Julien Rastafary yeah man (peace), Luca drum'n bass Forza Italia coupe de cheveux de vendeur de Kebab (ps: on a bien compris que l'Italie c'est mieux, mais tu resteras quand même le bienvenu ici!), Anthony aka «bout'» (je t'assure que ton chat n'est pas en dépression), Etienne «gros tinou de Saône et Loire», Triple Axelle Merckx, Jessicapeach, Juju boulish, et tous les autres...Merci également aux étudiants de master qui m'ont donné un sérieux coup de main pendant ces trois années de thèse: Arthur (le vrai, l'unique, l'authentique bourguignon), Agathe, Lucie et Anaïs.

- Enfin mes amis d'enfance, d'adolescence ou de jeune adulte qui n'auront rien retenu de mes années de thèse à part qu'un géologue c'est juste un «casse-caillou», mais qui auront eu pour qualité première d'égayer mes week-ends. Je les citerai par ordre de préférence bien sur: Bastos (encore lui) et sa femme Gwendo, les marnailles (Polo et Lolo), VV (la brique qui fait craquée les «meufs»), Sim (Mr Bean de Felipe de Borbon), Coline (intermittente du spectacle en résidence à l'industrie), Flash (recherché activement...), Valou aka le marocain au teint blanc (merci d'avoir fait le déplacement, j'espère bien prendre le thalys dans un an pour la tienne...), Gregory (conducteur aux verrins solides), Jacques Mayol, ^{su}Fabou (supertramp fun, merci pour ton caillou d'Alaska!), Quentin (le «cainri»), Siavoshe (l'aladin belge sur son tapis volant), Lucie (Franc-comtoise néo-thaïlandaise), Eliott et Emira (un mélange unique et fusionnel couscous/vin rouge/poutine), Jo the french teach' (un grand merci pour la relecture), camille (la flûte enchantée), ma petite pilloute (déversoir...), tibo p'tit nouvo, Laure, et enfin **Léa**. Désolé pour ceux que j'ai, sans le faire ou en faisant exprès, oublié.

Les amis, vous connaissez tous mon humour de m...je sais donc que vous ne m'en voudrez pas pour ce concentré de petits pics vous concernant, mais qu'au contraire vous pourrez tous y trouver une attention personnalisée.

- Enfin un dernier petit mot pour ma famille. Merci à tous, et surtout merci à mes parents de m'avoir toujours soutenu dans mes choix et de m'avoir grandement contribué à vivre mon rêve islandais. Merci à ma soeur Ana (et Vincent cornetto soft) et à mon frère JB de me supporter, de m'avoir souvent fourni un toit, à manger ou à boire, et de me faire passer de si bons moments depuis tant d'années.

Résumé

Les structures de déformation pré-lithification s'observent dans le registre sédimentaire, depuis l'Archéen jusqu'à nos jours et se retrouvent dans presque tous les environnements sédimentaires. Elles sont particulièrement abondantes dans les domaines sous-glaciaires et marins profonds, notamment en raison du développement de fortes pressions de fluide (i.e., surpressions) dans les sédiments. A partir de cas d'études choisis dans ces deux environnements, ces structures de déformation pré-lithification sont étudiées dans cette thèse, dont la problématique a permis de définir leurs implications sur les **(1) reconstructions paléoenvironnementales**, mais également leurs impacts sur les **(2) morphologies glaciaires**, et sur les **(3) propriétés pétrophysiques** des réservoirs sableux.

(1) L'analyse combinée des régimes de contrainte (cisaillement pur, simple, général), des mécanismes de déformation (fragile, hydroplastique, liquéfaction, fluidisation), et de la chronologie associés à la mise en place des structures de déformation ont permis de mieux contraindre les paléoenvironnements sédimentaires, au Quaternaire (Irlande et Islande), et à l'Ordovicien (Maroc et Algérie). Ainsi, plusieurs critères, basés sur l'analyse détaillée de ces structures, ont été identifiés afin de différencier les environnements de dépôt sous-glaciaire, submarginal, et proglaciaire. Puis, l'analyse structurale des déformations pré-lithifications a été utilisée comme un «proxy» afin d'estimer les variations de la vitesse d'écoulement, de l'épaisseur de glace, et de la production d'eaux de fonte. Cette nouvelle approche permet également d'affiner la dynamique des oscillations d'une marge glaciaire au cours du temps.

(2) Les séries sédimentaires des vallées tunnels ordoviciennes (Maroc) enregistrent la mise en place de nombreuses structures de déformation d'origine sous-glaciaire. La description détaillée des déformations liées aux surpressions de fluide a permis de proposer un nouveau modèle de creusement des vallées. Sous la glace, l'augmentation de la pression de fluide dans les aquifères confinés préglaciaires déclenche des processus de remobilisation sédimentaire. Ces processus se caractérisent par une fracturation hydraulique des dépôts préglaciaires, et par l'évacuation du matériel bréchifié et fluidisé au sein de chenaux sous-glaciaires. Ce nouveau modèle de creusement, lié aux surpressions de fluide (Alnif, Maroc), semble être favorisé dans les zones d'inter *ice-stream*, car l'infiltration des eaux de fonte dans le substrat sous-glaciaire est prédominante. A l'inverse, dans les couloirs d'*ice-stream*, l'écoulement des eaux de fonte se produit préférentiellement à l'interface glace-substrat et est à l'origine de la formation de vallées tunnels aux morphologies ondulantes (Foum Larjamme, Maroc).

(3) Les processus d'hydrofracturation et d'injection de sédiments fluidisés, liés aux augmentations de la pression de fluide, ont un impact sur les propriétés pétrophysiques des sédiments, et sur la géométrie des réservoirs sableux. Les études pétrophysiques menées sur des grès déposés en environnements marins profonds (bassin Vocontien, France) et sur des grès glaciaires (bassin de Sbaa, Algérie) ont permis de mettre en évidence l'impact des surpressions de fluide sur les propriétés réservoirs (porosité, perméabilité) des sables. Si les processus de remobilisation et de fluidisation sont capable de créer des réservoirs très poreux et perméables, les processus d'élutriations qui leurs sont associés peuvent avoir un effet inverse, et réduire la porosité et la perméabilité. Dans ces deux environnements, la distribution des propriétés pétrophysiques des réservoirs est contrôlée par les surpressions de fluide, mais elle semble très hétérogène, notamment en raison des processus de fluidisation. Cependant, certains paramètres contrôlant la distribution des propriétés réservoirs ont pu être mis en évidence tels que: l'épaisseur des injectites, la distance à la source, et les environnements de dépôts.

Mots-clés: Structures de déformation pré-lithification; pression de fluide; environnement sous-glaciaire, environnement marin profond; reconstructions paléoenvironnementales; propriétés réservoirs; vallées tunnels.

Abstract

Soft-sediment deformations occur in unconsolidated and sometimes water-saturated sediments, during or shortly after their deposition. Soft-sediment deformation structures (SSDs) are observed in the sedimentary record from the Archean until today, and occur in most sedimentary environments. SSDs are particularly abundant in subglacial and deep-marine environments because of the frequent development of high porewater pressure (i.e., fluid overpressure) in the sediment. Case studies of these two sedimentary environments were used **(1) to reconstruct palaeoenvironments from SSDs (2) to define the impact of SSDs on glacial morphologies, and (3) to determine the petrophysical properties of sand reservoirs affected by SSDs.**

(1) Combined analyses of strain regimes (pure, simple, or general shear), deformation mechanisms (brittle, hydroplastic, liquefaction, fluidisation), and chronologies (cross-cutting relationships) in SSDs served to improve palaeoenvironmental reconstructions. Using detailed SSDs and sedimentological analyses, palaeoenvironments were determined in the Pleistocene (Ireland and Iceland) and the Ordovician (Morocco and Algeria) glacial sedimentary record. Using this method, criteria facilitating the discrimination between subglacial, submarginal and proglacial environments were identified. In addition, the description and interpretation of these structures were used as “proxies” to estimate variations in palaeo-ice flow velocities, ice thickness, and meltwater production. This new approach, based on the analyses of chronologies and deformational sequences in the sedimentary record also contributed to refine the dynamics of ice-front oscillations through time.

(2) The sedimentary series of Ordovician tunnel valleys (Morocco) record numerous subglacial SSDs induced by fluid overpressure. The detailed description of these deformation structures was used to characterize a new model of tunnel valley formation controlled by the increase of porewater pressure in the preglacial substratum. Beneath the ice, the increase of porewater pressure within confined aquifers controls the initiation of sedimentary remobilisation processes. These remobilisations occur through hydraulic fracturing of the preglacial deposits, and evacuation of the brecciated and fluidised «mélange» within subglacial pipes. This porewater pressure-driven model (Alnif, Morocco) is more likely to occur in inter-ice stream zones, where meltwater is preferentially transferred to the preglacial substratum. In ice-stream corridors, meltwater circulates at the ice-substratum interface and promotes the formation of tunnel valleys driven by meltwater processes (Foum Larjamme, Morocco). The distribution of ice streams influences the mechanisms involved in the formation of tunnel valleys and controls their morphologies.

(3) Remobilisation processes (hydrofractures and fluidisation) triggered by the increase of fluid pressure have an impact on the granular framework of the sediments and on the geometry of sand reservoirs. Petrophysical studies of subglacial (Sbaa Basin, Algeria) and deep-marine (Vocontian Basin, France) sandstones demonstrated the impact of fluid overpressure on reservoir properties. Processes of remobilisation and fluidisation are responsible for the increase in porosity and permeability, while the elutriation processes associated with fluid overpressure lead to a decrease in these petrophysical properties. In both cases, the distribution of petrophysical properties at outcrop- or core-scale is highly heterogeneous, notably because of fluidisation processes. However, it was possible to identify the following parameters controlling the distribution of reservoir properties: injectite thickness, distance from the source bed and depositional environment.

Keywords: Soft-sediment deformation structures; fluid pressure; subglacial environment; deep-water environment; palaeoenvironmental reconstructions; reservoir properties; tunnel valleys.

Sommaire

INTRODUCTION GENERALE.....	1
1. Contexte de l'étude.....	1
2. Problématiques.....	3
3. Méthodes et choix des sites d'études.....	6
4. Construction du manuscrit.....	9
 CHAPITRE I - ETAT-DE-L'ART.....	13
▶ INTRODUCTION.....	15
▶ <i>PARTIE 1: SSDs definition, physical aspects, triggers and methods</i>.....	17
1. Definition.....	19
2. Elementary notions on SSDs mechanics.....	20
3. Prerequisites.....	30
4. Triggers.....	31
5. Methods.....	32
▶ <i>PARTIE 2: SSDS in subglacial environments</i>.....	37
1. Introduction.....	39
2. Parameters controlling deformation.....	39
3. Theoretical distribution of stresses and porewater pressure.....	46
4. Terminology and methods to classify SSDs.....	51
5. Classification of subglacial SSDS.....	58
6. Micromorphology of tills.....	75
7. Subglacial distribution of SSDS.....	79
8. Glaciodynamic and palaeoenvironmental reconstructions.....	79
9. Limits and particular cases.....	85
▶ <i>PARTIE 3: SSDS in deep-marine environments</i>.....	93
1. Introduction.....	95
2. Deep-marine depositional environments.....	95
3. Turbidite systems.....	97
4. Types of SSDS in deep-marine environments.....	102
5. In-situ deformation structures.....	103
6. Injected deformation structures.....	106
7. Morphology of clastic injections.....	110
8. Internal sedimentary structures.....	117
9. Parameters controlling the geometry & orientation of clastic injections.....	120
10. Impacts on reservoir geology.....	124
▶ CONCLUSIONS.....	129

CHAPITRE II - STRUCTURES DE DEFORMATION PRE-LITHIFICATION: MARQUEURS PALEOENVIRONNEMENTAUX..... 131

► INTRODUCTION	133
► PARTIE 1: Discrimination des dépôts fluviaux sous-glaciaires et des dépôts de cônes de déjections juxtaglaciaires	135
1. Objectifs.....	135
2. Précédents travaux.....	136
3. Contexte de l'étude.....	138
4. Méthodes.....	139
5. Article publié dans <i>Sedimentology</i>	140
6. Annexes.....	170
► PARTIE 2: Modèle de développement d'un réseau d'injections clastiques: processus et implications pour les reconstructions de la dynamique glaciaire	175
1. Objectifs.....	175
1. Précédents travaux.....	176
2. Contexte de l'étude.....	177
3. Méthodes.....	178
4. Article en préparation.....	178
► PRINCIPAUX RESULTATS	251

CHAPITRE III - DEFORMATION PAR SURPRESSIONS DE FLUIDE: IMPACTS SUR LES MORPHOLOGIES GLACIAIRES..... 255

► INTRODUCTION	257
► PARTIE 1: Contrôle de la pression d'eau interstitielle sur les remobilisations sédimentaires sous-glaciaires et la formation de vallées tunnels	259
1. Objectifs.....	259
2. Précédents travaux.....	260
3. Contexte de l'étude.....	261
4. Méthodes.....	262
5. Article publié dans <i>Sedimentary Geology</i>	263
► PARTIE 2: Comparaison des modèles de formation des vallées tunnels à l'Ordovicien et relations avec la dynamique des ice-streams	291
1. Objectifs.....	291
1. Précédents travaux.....	292
2. Contexte de l'étude.....	293
3. Méthodes.....	295
4. Article soumis à <i>Paleontology Paleoecology Paleoclimatology</i>	295
► PRINCIPAUX RESULTATS	337

CHAPITRE IV - DEFORMATION PAR SURPRESSIONS DE FLUIDE: IMPACTS SUR LES PROPRIETES RESERVOIRS.....	341
► INTRODUCTION.....	343
► PARTIE 1: Structures micro- et macroscopique, séquence diagénétique et caractéristiques pétrophysique de deux réseaux d'injectites.....	345
1. Objectifs.....	345
2. Précédents travaux.....	346
3. Contexte de l'étude.....	347
4. Méthodes.....	348
5. Article soumis à <i>Marine and Petroleum Geology</i>	349
► PARTIE 2: Les coatings argileux dans les grès glaciaires: processus de mise place et implications pétrophysiques.....	411
1. Objectifs.....	411
1. Précédents travaux.....	412
2. Contexte de l'étude.....	413
3. Méthodes.....	415
4. Rapport.....	417
5. Annexe.....	453
► PRINCIPAUX RESULTATS.....	457
CONCLUSIONS ET PERSPECTIVES.....	459
1. Synthèse des principaux résultats.....	461
2. Perspectives.....	473
BIBLIOGRAPHIE.....	477

Liste des figures et tableaux

Chapitre I

Partie 1

Figure 1: Illustration du concept des vecteurs contraintes.....	20
Figure 2: Illustration des concepts d'états de contrainte et d'ellipsoïdes des contraintes.....	21
Figure 3: Ellipsoïde des déformation résultant des différentes régimes de contraintes.....	22
Figure 4: Illustration des concepts de rhéologie dans l'espace en fonction de la contrainte différentielle (σ) et de la vitesse de déformation (ϵ).....	23
Figure 5 : Illustration des principes de déformation fragile et ductile.....	24
Figure 6: Diagramme de Knipe.....	26
Figure 7: Synthèse des processus et mécanismes de déformation, leurs caractéristiques physiques, leurs comportement rhéologiques, et leurs impacts sur la structure du sédiment.....	27
Figure 8: Représentation graphique du cercle de Mohr-Coulomb.....	28
Figure 9: Illustration de l'impact de l'augmentation de la pression de fluide sur le critère de rupture de Mohr-Coulomb.....	29
Figure 10: Illustration des critères permettant de reconnaître les structures de déformation pré-lithification.....	33
Figure 11: Description de la méthode facilitant la reconnaissance, la description et l'interprétation des structures de déformation pré-lithification.....	34

Partie 2

Figure 12: Illustration des différents paramètres contrôlant la déformation des sédiments dans les environnements sous-glaciaires.....	40
Tableau 1: Valeurs de cohésion et d'angles de friction de différents matériels géologiques.....	40
Figure 13: Planche photographique illustrant le découplage de la glace et du substrat.....	41
Figure 14: Diagramme illustrant des différents paramètres contrôlant la contrainte cisailante à la base du glacier.....	42
Figure 15: Illustration des différents paramètres contrôlant la pression d'eau interstitielle dans le substrat sous-glaciaire.....	43
Figure 16: Caractéristiques lithologiques et distribution des sédiments meubles potentiellement sujet à des déformations induites par le glacier.....	45
Figure 17: Distribution théorique des contraintes et de la pression d'eau interstitielle sous une calotte glaciaire.....	48
Figure 18: Illustration de la variation latérale des vitesses d'écoulement de la glace et de la contrainte cisailante basale sous une calotte glaciaire.....	50
Figure 19: Planche photographique illustrant la similarité des structures de déformation formées dans les environnements sous-glaciaires et métamorphiques à l'échelle macroscopique.....	52
Figure 20: Planche photographique illustrant la similarité des structures de déformation formées dans les environnements sous-glaciaires et métamorphiques à l'échelle microscopique.....	53
Tableau 2: Tableau synthétisant les différents paramètres contrôlant la déformation des sédiments sous la glace.....	54
Figure 21: Distribution des états de contraintes sous une calotte de glace en faisant varier la contrainte normale (σ_{ice}), la containte cisailante (τ_{flow}) et la pression de fluide (F_p).....	55

Figure 22: Evolution des état de contraintes dans l'espace et dans le temps en fonction des changements de pressions de fluide et des vitesses d'écoulement de la glace.....	57
Figure 23: Planche photographique illustrant les structures de déformation fragile sous-glaciaire induites par un cisaillement pur.....	59
Figure 24: Photographie illustrant une cataclase de grain d'origine sous-glaciaire.....	60
Figure 25: Planche photographique illustrant les structures de déformation fragile sous-glaciaire induites par un cisaillement général.....	61
Figure 26: Planche photographique illustrant les structures de déformation hydroplastique induites par cisaillement pure et général (boudins).....	63
Figure 27: Planche photographique illustrant les structures de déformation hydroplastique induites par cisaillement général (plis).....	64
Figure 28: Planche photographique illustrant les structures de déformation hydroplastique induites par cisaillement général (plans de schistosité).....	65
Figure 29: Planche photographique illustrant des structures de déformation rotationnels («turbate structures») induites par cisaillement général.....	66
Figure 30: Planche photographique illustrant des dykes clastiques <i>per descensum</i>	68
Figure 31: Planches photos illustrant des sills, des sills en marche d'escalier, et des dykes clastiques <i>per ascensum</i>	70
Figure 32: Planche photographique illustrant des structures de bréchification hydraulique.....	71
Figure 33: Planche photographique illustrant des structures induites par liquéfaction/fluidisation des sédiments.....	72
Figure 34: Planche photographique illustrant des structures liées à l'élutriation des particules argileuses (conduits d'élutriation et coatings argileux).....	73
Figure 35: Planche photographique illustrant des surfaces striées et flutées.....	74
Figure 36: Représentation schématique des différentes microstructures affectant les sédiments glaciaires.....	76
Figure 37: Illustration des relations entre les fabrique plasmiques et la dynamique glaciaire.....	78
Figure 38: Distribution théorique des structures de déformation syn-sédimentaires selon les différents environnements sous-glaciaires précédemment définis.....	81
Figure 39: Diagramme illustrant l'évolution de l'orientation et du sens de propagation des hydrofractures et des injections en fonction des variations d'épaisseur de la glace et du changement de vitesse d'écoulement de la glace.....	80
Tableau 3: Les différents styles de déformation en fonction des différents environnements glaciaires d'après McCarroll et Risdijk (2003).....	84
Figure 40: Planche photographique illustrant des structures formées dans les complexes glaciectoniques proglaciaires.....	85
Figure 41: Diagramme illustrant le concept d'espace disponible pour la propagation de la déformation dans les environnements sous-glaciaires et proglaciaires.....	86
Figure 42: Modèle dynamique illustrant différents exemples de chemins de déformations.....	88
Figure 43: Planche photographique illustrant des recoupement entre différents structures de déformation afin de mettre en évidence les «chemins» de déformation.....	89
Figure 44: Diagramme illustrant les différents chemins de déformations possible en faisant varier le champs de contraintes et la pression d'eau interstitielle.....	90
Figure 45: Représentation schématique du modèle mosaïque entre la glace et son substrat où zones en cours de déformation coexistent avec des zones non déformées.....	91
Figure 46: Illustrations du principe de substrat sous-glaciaire mosaïque à l'aide d'évidence terrains et de modélisation numérique.....	92

Partie 3

Figure 47: Diagramme illustrant les différents processus sédimentaires et les dépôts associés dans les environnements marins profonds.....	96
---	----

Figure 48: Classification des différentes séquences sédimentaires associés aux différents types d'écoulements gravitaire en domaine marin profond.....	98
Figure 49: Diagramme illustrant la distribution des différents faciès sédimentaires dans un système turbiditique.....	99
Figure 50: Diagramme illustrant la mise en place des chenaux turbiditiques sableux et leur obturation par des sédiments fins imperméables.....	100
Figure 51: Planche photographique illustrant les caractéristiques faciologiques et géométriques des dépôts turbiditiques.....	101
Figure 52: Diagramme représentant les trois grands types de déformation pré-lithification dans les environnements marins profonds.....	102
Figure 53: Photographie illustrant les déformations syn-sédimentaires (convolutes) associées au dépôt d'une turbidite.....	103
Figure 54: Planche photographique illustrant les différentes structures de déformation syn-sédimentaires in-situ associées aux dépôts des turbidites.....	106
Figure 55: Diagramme illustrant les différents mécanismes responsable du développement de surpressions de fluide dans les chenaux turbiditiques.....	107
Figure 56: Illustration du principe d'hydrofracturation à l'aide du cercle de Mohr.....	108
Figure 57: Diagramme illustrant l'impact de l'augmentation de la pression d'eau interstitielle sur l'évolution de la structure granulaire et sur la mise en place d'un réseau d'injection clastique en domaine marin profond.....	109
Figure 58: Les différents types et morphologies d'injections clastiques observées dans le registre sédimentaire marin profond.....	110
Figure 59: Diagramme représentant le partitionnement caractéristique d'un système d'injection clastique.....	111
Figure 60: Planche photographique illustrant les différentes morphologies de dyke clastiques observées en domaine marin profond.....	112
Figure 61: Planche photographique illustrant les différentes morphologies de sill clastique observées en domaine marin profond.....	113
Figure 62: Planche photographique illustrant la morphologies des injectites résultant de connexions multiples entre dykes et sills.....	114
Figure 63: Planche photographique illustrant les morphologies des extrudites.....	115
Figure 64: Planche photographique illustrant les autres morphologies d'intrusions clastiques observées à l'affleurement et en subsurface.....	117
Figure 65: Planche photographique illustrant quelques structures sédimentaires observées dans les remplissages sédimentaires d'intrusions clastiques.....	118
Figure 66: Planche photographique montrant quelques exemples de brèches observés dans le remplissage de certaines intrusions clastiques.....	119
Figure 67: Photographies comparant la texture des grains dans les injections et dans l'unité parente à l'échelle microscopique.....	120
Figure 68: Modèle schématique illustrant l'évolution du type et de la morphologie des injections en fonction de la profondeur d'enfouissement.....	121
Figure 69: Diagramme illustrant le type et la morphologie des injections en fonction de l'absence ou présence de fractures préexistantes.....	123
Figure 70: Diagramme illustrant l'influence des remobilisations sédimentaire sur les réservoirs clastiques des domaines marins profonds.....	125
Figure 71: Graphiques montrant l'influence des remobilisations sédimentaires sur les valeurs de porosité des sédiments en environnement marin profond.....	126
Figure 72: Diagramme illustrant les différentes phases d'écoulement de fluides associé a l'injection puis a la diagenèse des injectites.....	128

Chapitre II

Partie 1

Tableau 1: Synthèse des critères sédimentologiques, déformationnels, morphologiques et topographiques facilitant la reconnaissance des faciès sédimentaires sous-glaciaires..... 136

Figure 1: Localisation géographique du site d'étude et paléogéographie de la calotte glaciaire Britannique-Irlandaise au Quaternaire..... 139

Article publiée dans *Sedimentology*

Figure 1: Localisation géographique de la carrière de Ballyhorsey et paléogéographie de la calotte glaciaire Britannique-Irlandaise au Quaternaire..... 143

Figure 2: Panorama interprété illustrant l'arrangement stratigraphique des associations de faciès sédimentaire et présentation des logs sédimentologiques réalisés sur le site d'étude..... 144

Tableau 1: Synthèse des principales caractéristiques de chaque faciès et associations de faciès sédimentaires..... 145

Figure 3: Planche photographique illustrant les différents faciès sédimentaires sous-glaciaires.... 147

Figure 4: Panorama interprété comparant le «stacking pattern» et la géométrie des dépôts sous-glaciaires et proglaciaires..... 149

Figure 5: Direction de pendage des dykes et direction de vergence des plis au sein des faciès sous-glaciaires reportés au sein de diagrammes circulaires..... 150

Figure 6: Illustration des différentes structures de déformation syn-sédimentaires observés dans les faciès sédimentaires sous-glaciaires..... 151

Figure 7: Diagramme schématisant les différents mécanismes responsables de la mise en place des structures de déformations dans les dépôts sous-glaciaires..... 152

Figure 8: Planche photographique illustrant les différents faciès sédimentaires proglaciaires..... 154

Figure 9: Direction de pendage des dykes, de vergence des plis et de pendages des failles normales reportés dans des diagrammes circulaires + illustration des différentes structures de déformations pré-lithification observées dans les sédiments proglaciaires..... 155

Figure 10: Schéma de corrélation stratigraphique et cartographie des structures de déformation pré-lithification..... 157

Figure 11: Diagramme comparant les caractéristiques des séquences sédimentaires sous-glaciaires et proglaciaires..... 128

Figure 12: Diagramme illustrant l'impact de la production et du drainage des eaux de fonte sur le dépôt et la déformation de sédiments sous la glace..... 163

Figure 13: Diagramme synthétisant les principaux résultats de cette étude et plus particulièrement les critères sédimentologiques, stratigraphiques, géométriques et déformationnel permettant de discriminer des faciès sédimentaires triés sous-glaciaires et proglaciaires..... 165

Partie 2

Figure 1: Localisation géographique du site d'étude..... 177

Article en cours de préparation

Figure 1: Localisation géographique de l'affleurement analysé dans cette étude et cartographie des principales moraines glaciaires à la marge Sólheimajökull..... 184

Tableau 1: Tableau synthétisant les caractéristiques des différents faciès sédimentaires..... 187

Figure 2: Log sédimentologique du site d'étude et planche photographique illustrant les différents faciès sédimentaires..... 188

Figure 3: Distribution granulométrique, moyenne, et médiane de la fraction inférieure à 2 mm des différents faciès sédimentaires définis dans cette étude.....	190
Figure 4: Panorama interprété illustrant l'empilage des différents faciès sédimentaires et la géométrie du réseau d'injection clastiques.....	194
Figure 5: Photographies interprétées illustrant la cinématique associée aux différentes structures de déformation pré-lithification affectant les sédiments encaissants.....	195
Figure 6: Panorama interprété illustrant la morphologie des injections dans la zone où elles présentent la plus forte densité.....	197
Figure 7: Projection stéréographique obtenue avec le pendage et la direction de pendage des dykes composant le réseau d'injection.....	198
Figure 8: Plaque photographique illustrant les différents types de remplissage observés dans le réseau d'injection clastique.....	199
Figure 9: Diagramme synthétisant les différents types de remplissage observés dans le réseau d'injection.....	200
Figure 10: Graphiques illustrant les variations de la distribution granulométrique (fraction < 2 mm) à l'intérieur d'un dyke, et en s'éloignant de la source.....	202
Figure 11: Graphique illustrant les variations granulométriques au sein d'un sill.....	203
Figure 12: Indices granulométriques calculés pour les différents faciès et pour le remplissage des injections reportés dans un diagramme de Passega.....	204
Figure 13: Plaque photographique illustrant les séquences sédimentaires observées dans le remplissage de certaines injections.....	204
Figure 14: Photographie interprétée illustrant les recoupements entre les différentes générations d'injections clastiques.....	205
Figure 15: Photographie interprétée mettant en évidence les différentes générations d'injections clastiques observables à l'échelle macroscopique.....	206
Figure 16: Photographie interprétée illustrant deux phases d'injections observées à l'échelle mésoscopique.....	207
Figure 17: Photographie illustrant la cinquième et ultime phase d'injection.....	208
Figure 18: Position des différents échantillons prélevés pour la réalisation de lames minces (1).....	209
Figure 19: Position des différents échantillons prélevés pour la réalisation de lames minces (2).....	210
Figure 20: Scan et interprétation lame mince 1.....	211
Figure 21: Scan et interprétation lame mince 2.....	212
Figure 22: Scan et interprétation lame mince 3.....	213
Figure 23: Scan et interprétation lame mince 4.....	214
Figure 24: Scan et interprétation lame mince 5.....	215
Figure 25: Scan et interprétation lame mince 6.....	216
Figure 26: Scan et interprétation lame mince 7.....	217
Figure 27: Scan et interprétation lame mince 8.....	218
Figure 28: Scan et interprétation lame mince 9.....	219
Figure 29: Scan et interprétation lame mince 10.....	220
Figure 30: Scan et interprétation lame mince 11.....	221
Figure 31: Scan et interprétation lame mince D1.....	222
Figure 32: Scan et interprétation lame mince D2.....	223
Figure 33: Diagramme synthétisant les interprétations des lames minces 1 à 8 et D1, D2.....	224
Figure 34: Diagramme synthétisant les interprétations des lames minces 9 à 11.....	225
Figure 35: Plaque photographique illustrant la morphologie des coatings argileux tapissant les grains dans le remplissage des injections clastiques.....	226
Figure 36: Photographie interprétée mettant en évidence la possible présence de laminations entrecroisées dans le remplissage d'un sill.....	227
Figure 37: Diagramme synthétisant les caractéristiques morphologiques des 5 générations d'injections clastiques.....	230

Figure 38: Diagramme illustrant le modèle de «crack and seal» responsable de la formation des lamines dans les injections clastiques.....	234
Figure 39: Diagramme schématisant la distribution et la morphologie théorique des injections clastiques sous et a la marge d'un glacier.....	236
Figure 40: Diagramme représentant les différentes étapes de la déformation affectant les sédiments fins laminés.....	240
Figure 41: Diagramme illustrant les différentes phases de sédimentation et d'injection au cours du temps.....	243
Figure 42: Reconstruction et datation des différentes phases d'avancée glaciaire à l'aide des moraines terminales et de datation au carbone 14.....	245

Chapitre III

Partie 1

Figure 1: Localisation géographique de la vallée tunnel d’Alnif et reconstitution de la paléogéographie du continent Gondwana et de sa calotte glaciaire à l’Hirnantien.....	262
---	-----

Article publié dans la revue *Sedimentary Geology*.

Figure 1: Localisation de la vallée tunnel d’Alnif sous la calotte glaciaire Gondwanienne durant la glaciation Hirnantienne et sur une carte structural et géologique actuelle.....	266
Figure 2: Chronostratigraphie des dépôts Ordoviciens Supérieur et log sédimentologique présentant les dépôts préglaciaires, la profondeur de l’incision et le remplissage de la vallée tunnel.....	268
Figure 3: Carte géologie des dépôts de l’Ordovicien supérieur sur le secteur d’Alnif, et cartographie des deux unités glaciaires dans la vallée tunnel d’Alnif. La distribution géographique du conglomérat basal est également représentée sur cette carte.....	269
Figure 4: Photographie panoramique de la vallée tunnel d’Alnif interprétée et modèle synthétique du remplissage de la vallée tunnel d’Alnif.....	270
Figure 5: Log sédimentologique détaillée de la basse du remplissage de la vallée tunnel d’Alnif et distribution stratigraphique des différentes structures de déformation pré-lithification observées dans les dépôts préglaciaire et dans le remplissage glaciaire.....	271
Tableau 1: Tableau synthétisant les principales caractéristiques des différents faciès sédimentaires observés à la base de la vallée tunnel.....	272
Figure 6: Photographie interprétée illustrant la géométrie des dépôts mise en place à la base de la vallée tunnel.....	272
Figure 7: Planche photographique illustrant les différents faciès sédimentaires de la base du remplissage de la vallée tunnel.....	273
Figure 8: Photographies interprétées décrivant les différentes structures de déformation pré-lithification observées sous la vallée tunnel.....	275
Figure 9: Photographies interprétées illustrant les différentes structures de déformations pré-lithification observées à l’intérieur des clasts composant le conglomérat basal.....	276
Figure 10: Photographies interprétées illustrant la relation entre la morphologie des clasts préglaciaires et la fracturation du matériel préglaciaire.....	277
Figure 11: Photographies interprétées décrivant les différentes structures de déformations pré-lithification observées dans le conglomérat basal.....	278
Figure 12: Photographies interprétées illustrant les différents types de déformation affectant la matrice du conglomérat.....	279
Figure 13: Photographies interprétées illustrant les différents types de structure de déformation observés dans les grès, à la base de la vallée tunnel.....	280
Figure 14: Diagramme synthétisant la chronologie de mise en place des différentes structures de déformation. La cinématique et la pression d’eau interstitielle associées à chaque structure est représentée sur cette figure.....	282
Figure 15: Modèle de formation et de remplissage de la vallée tunnel d’Alnif.....	285

Partie 2

Figure 1: Localisation géographique de la vallée tunnel d’Alnif et de Fourn Larjamme, et reconstitution de la paléogéographie du continent Gondwana et de sa calotte glaciaire à l’Hirnantien (Ordovicien terminal).....	294
---	-----

Figure 1: Localisation de la vallée tunnel d’Alnif sous la calotte glaciaire Gondwanienne durant la glaciation Hirnantienne.....	300
Figure 2: Corrélations chronostratigraphiques entre les régions de Foug Larjamme et d’Alnif....	301
Figure 3: Diagramme et photographies panoramiques interprétés illustrant la morphologie et le remplissage sédimentaire des vallées tunnels d’Alnif et de Foug Larjamme.....	302
Figure 4: Log sédimentologique, distribution stratigraphique des structures de déformation pré-lithification et planche photographique illustrant les différentes faciès sédimentaires de la vallée tunnel d’Alnif.....	304
Figure 5: Log sédimentologique, distribution stratigraphique des structures de déformation syn-sédimentaires et planche photographique illustrant les différentes faciès sédimentaires de la vallée tunnel de Foug Larjamme.....	306
Figure 6: Photographies interprétées illustrant les différentes structures de déformation pré-lithification observées sous la deuxième incision glaciaire.....	308
Figure 7: Photographies illustrant l’absence de déformation sous la vallée tunnel de Foug Larjamme à échelle macroscopique et microscopique.....	310
Figure 8: Planche photographique illustrant les différents structures de déformations pré-lithification observées dans le remplissage sédimentaire basal de la vallée tunnel d’Alnif et de Foug Larjamme.....	314
Figure 9: Modèle de formation et de remplissage de la vallée tunnel d’Alnif.....	318
Figure 10: Modèle de formation et de remplissage de la vallée tunnel de Foug Larjamme.....	321
Figure 11: Localisation de la vallée d’Alnif et de Foug Larjamme sur une carte de reconstitution des paléo <i>ice-streams</i> de la calotte Gondwanienne.....	325
Figure 12: Diagramme synthétisant les principales caractéristiques des vallées de Foug Larjamme et d’Alnif et leur relations avec la distribution des <i>ice-streams</i>	327

Chapitre IV

Partie 1

Figure 1: Localisation géographique des deux site d'études et délimitation de la paléo marge passive du bassin Vocontien..... 348

Article soumis à la revue *Marine and Petroleum Geology*

Figure 1: Localisation géographique des deux site d'études, délimitation de la paléo marge passive du bassin Vocontien et distribution des sédiments Aptien-Albien.....	355
Figure 2: Log sédimentologique/corrélation stratigraphique entre les sites de Rosans et Bevons.	357
Figure 3: Planche photographique illustrant les principaux faciès sédimentaires des deux sites d'études.....	358
Figure 4: Panorama photographique interprété du réseau d'injectites observé sur le site de Bevons et positionnement des différents échantillons récoltés pour l'étude pétrophysique.....	360
Figure 5: Panorama photographique interprété du réseau d'injectites observé sur le site de Rosans et positionnement des différents échantillons récoltés pour l'étude pétrophysique.....	361
Figure 6: Granulométrie et composition des sables composant respectivement les turbidites, les dykes et les sills sur les sites de Bevons et Rosans.....	362
Figure 7: Diagramme illustrant la méthode pour estimer la porosité primaire à partir d'une lame mince.....	363
Figure 8: Planche photographique illustrant les différentes morphologies de dykes et de sills observées sur les sites de Bevons et Rosans.....	365
Figure 9: Planche photographique illustrant les différentes structures de déformation observées dans les marnes encaissantes, le long des injectites.....	368
Figure 10: Planche photographique illustrant les différentes structures internes formées pendant l'injection du sable.....	370
Figure 11: Photographie interprétées illustrant les différentes structures observées dans les injectites et mise en place par des mouvements d'eau interstitielle.....	372
Figure 12: Photographies interprétées illustrant les différentes structures observées dans les injectites et induites par la compaction mécanique précoce.....	374
Figure 13: Photographie interprétée et modèle de mise en place des injections secondaires.....	376
Figure 14: Diagramme synthétisant la chronologie, les processus, et la cinématique associés à la mise en place précoce des différentes structures observées dans les injectites.....	377
Figure 15: Diagramme présentant la séquence diagénétique généralisée aux deux sites d'études.	380
Figure 16: Planche photographique illustrant les différentes phases diagénétiques observées au sein des deux réseaux d'injectites.....	381
Figure 17: Diagramme illustrant la large gamme de porosité actuelle et de porosité primaire observée au sein des réseaux d'injectites.....	383
Figure 18: Graphiques présentant les valeurs de porosité primaire des dykes, sills et turbidites sur les sites de Rosans et Bevons.....	385
Figure 19: Graphiques comparant les valeurs de porosité primaire en fonction de l'épaisseur des injectites sur le site de Bevons.....	387
Figure 20: Graphiques comparant les valeurs de porosité primaire en fonction de l'épaisseur des injectites puis en fonction de la distance à la source sur le site de Rosans.....	388
Figure 21: Carte d'interpolation des valeurs de porosité primaire calculées sur le site de Bevons.	389
Figure 22: Carte d'interpolation des valeurs de porosité primaire calculées sur le site de Rosans.	391
Figure 23: Diagramme illustrant la profondeur d'enfouissement à laquelle s'est développé les systèmes d'injectites en se basant sur leurs morphologies, et sur le report des valeurs de porosité primaire maximum sur une courbe de compaction des sables.....	393

Figure 24: Diagramme illustrant les trois phases majeurs d'évolution de la porosité au sein des systèmes d'injectites de Bevens et de Rosans.....	395
Figure 25: Diagramme synthétisant l'impact des différentes structures et phases diagénétiques sur l'évolution de la porosité et sur les écoulements de fluide au sein des réseaux d'injectites, de l'injection à aujourd'hui.	401

Partie 2

Figure 1: Localisation géographique du bassin de Sbaa et position du site d'étude sous la calotte glaciaire Gondwanienne.....	414
--	-----

Rapport sur la mise en places des coatings argileux sur les grès glaciaires du bassin de Sbaa.

Figure 1: Planche photographique illustrant différentes morphologies de coatings argileux.....	420
Figure 2: Diagramme illustrant les différents modèles de mise en place des coatings argileux dans les environnements glaciaires.....	423
Figure 3: Localisation géographique du bassin de Sbaa et carte géologique et structural simplifiée de la région d'étude.....	426
Figure 4: Stratigraphie et lithologie des sédiments paléozoïque du bassin de Sbaa.....	428
Figure 5: Carte d'extension maximum de la calotte glaciaire gondwanienne et localisation du bassin de Sbaa.....	429
Figure 6: Diagramme illustrant les différentes méthodes utilisées au cours de cette étude.....	430
Figure 7: Log sédimentologique ODZ-6 présentant les différents faciès, la distribution des différentes structures de déformation pré-lithification, les valeurs d'abondance en coatings argileux ainsi que les données pétrophysiques (porosité, perméabilité).....	432
Figure 8: Légende du log sédimentologique ODZ-6.....	436
Figure 9: Planche photographique présentant les structures de déformation liées au cisaillement de la glace sur le substrat.....	434
Figure 10: Planche photographique illustrant les différentes structures de déformation liées à l'augmentation de la pression d'eau interstitielle.....	435
Figure 11: Photographies de lames minces où les coatings argileux sont absents ou présents.....	437
Figure 12: Photographies des coatings argileux des grès du bassin de Sbaa réalisées au microscope électronique à balayage.....	438
Figure 13: Graphiques présentant les données d'abondance des coatings argileux vs. porosité/perméabilité.....	439
Figure 14: Graphique présentant la distribution de l'abondance des coatings argileux sous le plancher glaciaire.....	440
Figure 15: Diagramme illustrant les variations localisées d'abondance en coatings argileux.....	441
Tableau 1: Tableau présentant les moyennes d'abondance en coatings argileux entre les grès sous-glaciaires et proglaciaires.....	442
Figure 16: Modèles de mise en place des coatings argileux dans les grès glaciaires ordoviciens d'Algérie.....	445

INTRODUCTION GENERALE

Introduction générale

1. Contexte de l'étude

Les structures de déformation syn-sédimentaire à syn-lithification affectent les sédiments de manière précoce, avant leur complète lithification (Lowe, 1975; Allen, 1982; Mills, 1983; Maltman, 1984, 1994; van Loon, 2009; Owen et al., 2011). Ces structures peuvent donc être considérées comme des structures de déformation pré-lithification. Leur taille varie de l'échelle millimétrique (Lowe et LoPiccolo, 1974; Hurst et Buller, 1984; van der Meer, 1993; van der Wateren et al., 1995) à l'échelle plurimétrique (Boehm et More, 2002; Vigorito et al., 2008; Moreau et al., 2011), on les retrouve dans l'enregistrement sédimentaire depuis l'Archéen jusqu'à aujourd'hui (van Loon, 2009). Ces structures de déformation ont été décrites pour la première fois il y a plus de 150 ans (Lyell, 1841; Vanuxem, 1842; Dana, 1849; Darwin, 1851), mais n'étaient pas alors considérées comme des structures intéressantes dans la reconstruction de l'histoire des sédiments. Dans les années 1960, lorsque la sédimentologie devint une discipline à part entière, les travaux visant à établir les premières classifications des structures de déformation pré-lithification se sont multipliés (Potter et Pettijohn, 1963; Pettijohn et Potter, 1964; Dzulynski et Walton, 1965; Nagtegaal, 1965). A la fin des années 70, et au début des années 80, la compréhension des déformations pré-lithifications a nettement évolué, en effet de nombreux travaux ont mis en évidence l'importance de ces structures dans la reconstitution des environnements de dépôts (Sims, 1978; Allen, 1982; Mills, 1983). C'est également durant cette même période que les géologues structuraux se sont de plus en plus intéressés à l'étude des déformations pré-lithifications (Maltman, 1984).

A l'heure actuelle, ces structures de déformation pré-lithification sont très étudiées puisqu'elles ont des implications: (1) **académiques**, (2) **sociétales**, et (3) **environnementales**.

(1) **Implications académiques**. Les structures de déformation pré-lithification sont actuellement un outil facilitant les reconstitutions paléoenvironnementales ou paléogéographiques. En effet, ces structures ont notamment permis de mieux contraindre les caractéristiques d'un environnement de dépôt (hydrodynamisme, taux de sédimentation, etc...) (Owen, 1987; Molina et al., 1998; Marshall,

2000; Oliveira; 2009, 2011) mais elles ont aussi facilité les reconstitutions paléogéographiques et l'analyse de la dynamique des anciennes calottes glaciaires (Brodzikowski et Van Loon, 1980, 1983, 1985; Williams, 1996; McCarroll et Rijdsdijk, 2003; Le Heron et al., 2005; Denis et al., 2010).

(2) **Implications sociétales.** L'analyse des déformations pré-lithifications est utilisée dans le cadre de la prévention contre les risques naturels. Il est notamment possible de déterminer le risque sismique d'une région en étudiant la récurrence, l'ampleur, et le type de structures de déformation pré-lithification liés aux tremblements de terre (i.e., séismes) (Guiraud et Plaziat, 1993; Obermeier, 1996; Rosseti, 1999; Gruska et van Loon, 2007; Mugnier et al., 2011). De la même manière, des structures de déformation pré-lithification typiques associées au passage de tsunamis ont été décrites, permettant ainsi de définir le risque potentiel sur une région (Minoura et Nakata, 1994; Le Roux et al., 2008; Meshram et al., 2011; Aslop et Marco, 2012).

(3) **Implications économiques.** Plus récemment, le nombre d'études visant à caractériser l'impact des structures de déformations sur les propriétés pétrophysiques des sédiments est en nette hausse, en raison de l'intérêt économique associé aux réservoirs géologiques. En effet, la découverte de nombreux réseaux d'injections sableuses dans les réservoirs clastiques (Dixon et al., 1995; Lonergan et al., 2000; Braccini et al., 2008), et la modification de la structuration des grains provoquée par les processus de fluidisation influencent la géométrie et les propriétés pétrophysiques des réservoirs clastiques (Duranti et al., 2002; Briedis et al., 2007; Scott et al., 2013). Ces structures jouent donc un rôle essentiel dans le stockage ou la migration d'hydrocarbures.

Les structures de déformations peuvent se former dans une multitude d'environnements sédimentaires, continentaux ou marins, au sein desquels les environnements glaciaires et marins profonds sont les mieux documentés (Mc Carroll et Risdijk, 2003; Hurst et al., 2011). Ces deux environnements sédimentaires présentent une grande variété de structures et sont notamment caractérisés par la présence de déformations liées aux fortes pressions de fluides, autrement connu sous le terme de surpression de fluide. L'analyse et l'interprétation de ces structures de déformation dans ces deux environnements sédimentaires constituent l'élément principal de ce manuscrit, avec un intérêt particulier porté aux déformations pré-lithifications induites par des surpressions de fluide.

2. Problématiques

Les problématiques développées dans ce travail de recherche aborderont les structures de déformation pré-lithification à travers leurs implications dans (1) les **reconstitutions paléoenvironnementales**, ainsi que leurs impacts sur les (2) **morphologies glaciaires**, et sur les (3) **propriétés réservoirs** des sédiments clastiques.

• Problématique 1: Paléoenvironnement

Ce premier axe de recherche permettra de définir précisément le cadre environnemental dans lequel se mettent en place les structures de déformation précoces.

Cet axe de recherche se focalise sur les déformations en domaines glaciaires et plus particulièrement celles se mettant en place sous et à la marge d'un glacier. Une grande variété de structures peut s'y former, et leurs analyses permettent d'obtenir des informations sur la dynamique glaciaire passée (Boulton et Caban, 1995; Boulton, 2001; McCarroll et Risdjik, 2003; Denis et al., 2010). En effet, chaque structure enregistre les variations de la vitesse d'écoulement de la glace et de la pression d'eau interstitielle (i.e., pression de fluide), ces deux paramètres étant caractéristiques de l'environnement où se met en place la déformation (i.e., sous-glaciaire, marginal ou proglaciaire).

Questions

- ☐ Quels sont les critères sédimentologiques et déformationnels qui permettent d'identifier les faciès sédimentaires triés déposés sous la glace.
- ☐ L'identification de dépôts fluviatiles sous-glaciaires permet-elle de caractériser la dynamique sédimentaire sous-glaciaire?
- ☐ Peut-on reconstruire la dynamique glaciaire et estimer les variations de la pression de fluide en se basant sur une analyse détaillée des structures de déformation ?
- ☐ Peut-on mettre en évidence des séquences de déformation liées à des oscillations de la marge glaciaire ? Quels impacts pour les reconstitutions paléogéographiques ?

• Problématique 2: Morphologies glaciaires

Ce deuxième axe de recherche a pour objectif de mieux contraindre l'impact des remobilisations

sédimentaires liées aux surpressions de fluide sur les morphologies glaciaires. Afin de pouvoir estimer cet impact, les vallées tunnels d'origine glaciaire seront étudiées.

Le terme de mobilisation ou remobilisation sédimentaire s'applique aux processus de remise en mouvement d'un sédiment après son dépôt due à l'augmentation rapide de sa pression d'eau interstitielle (Lowe et al., 1975; Maltman, 1994; Maltman et Bolton, 2003).

Il existe de nombreux modèles de formation de vallées tunnels dans la littérature (Piotrowski, 1994; Johnson, 1999; Hooke et Jennings, 2006; Shaw, 2002, 2010), certains proposent que l'augmentation de la pression de fluide dans les sédiments est responsable de remobilisations sédimentaires et de la formation des vallées tunnels (Boulton et Hindmarsh, 1987; Janszen et al., 2012). Cependant, ces modèles guidés par des pressions de fluide élevées reposent sur des approches numériques (Boulton et Hindmarsh, 1987) ou alors sur des approches conceptuelles à partir de données sismiques (Janszen et al., 2012). Il n'existe à l'heure actuelle aucun argument terrain validant ces modèles de creusement des vallées tunnels.

Questions

- ☐ Quels sont les processus intervenant dans l'évacuation du matériel préglaciaire et donc dans la formation des vallées tunnels contrôlées par l'augmentation de la pression d'eau interstitielle ?
- ☐ Quels sont les paramètres contrôlant l'augmentation de la pression d'eau interstitielle dans les sédiments meubles préglaciaires ?
- ☐ Quels sont les critères terrains permettant de démontrer l'impact des surpressions de fluides et des processus de remobilisation dans le creusement des vallées tunnels ?
- ☐ Les vallées tunnels mises en place sur substrats meubles sont-elles toutes initiées par l'augmentation de la pression d'eau interstitielle ?
- ☐ Existe-t-il un lien entre les processus de creusement des vallées tunnels et la dynamique d'écoulement glaciaire (*ice-stream* vs. *inter ice-stream*) ?

• Problématique 3: Propriétés réservoirs

Ce troisième axe de recherche permettra de déterminer l'impact des structures de déformation pré-lithification liées aux fortes pressions de fluide sur les propriétés réservoirs des sédiments clastiques en environnements glaciaires et marins profonds.

Les sédiments déposés en domaines marins profonds et glaciaires constituent des réservoirs géologiques potentiels. De nombreux réservoirs contenant des hydrocarbures ont notamment été découverts dans des sédiments glaciaires Ordoviciens en Afrique du Nord ou encore au Moyen-Orient (Davidson et al., 2000; Hirst et al., 2002; Le Heron et al., 2009); mais aussi dans les sédiments marins profonds de la Mer du Nord, ou des marges ouest-africaine et brésilienne (Pettingil et Weimer, 2002). Les remobilisations sédimentaires liées aux fortes pressions de fluide sont communes dans ces deux environnements et ont un impact direct sur les réservoirs clastiques. A grande échelle, ces déformations pré-lithifications induisent une modification de la géométrie des réservoirs et de la connectivité entre les réservoirs (Dixon, 1995; Lonergan et al., 2000). A l'échelle microscopique, l'augmentation de la pression de fluide provoque des changements dans la structure granulaire des sédiments, mais également la remobilisation des particules les plus fines (élutriations). Ces processus se traduisent par une modification des propriétés pétrophysiques (Duranti and Hurst, 2004; Jonk et al., 2005; Scott et al., 2009, 2013). Cependant, dans ces environnements, l'impact des pressions de fluide sur les qualités réservoirs est encore relativement méconnu, notamment en raison du manque d'étude terrain visant à quantifier les variations latérales des propriétés pétrophysiques du sédiment à l'échelle de l'affleurement.

Questions

- ☐ Quelles sont les valeurs de porosité primaire (i.e., porosité pré-lithification) associées aux injections sableuses ?
- ☐ Quels sont les paramètres contrôlant la distribution de la porosité primaire au sein d'un réseau d'injectites à l'échelle de l'affleurement ?
- ☐ Quel est l'impact des déformations syn-sédimentaires sur la porosité primaire au sein d'un système d'injectites ?
- ☐ Quelle est l'origine des «coatings» argileux (i.e., tapissages argileux) dans les grès glaciaires Ordoviciens et quels impacts ont-ils sur les propriétés réservoirs?
- ☐ La mise en place des «coatings» argileux en environnement glaciaire est-elle liée à des processus d'élutriation induits par l'augmentation de la pression de fluide ?

3. Méthodes et choix des sites d'études

Afin de répondre à ces différentes problématiques, les travaux de recherche présentés dans ce manuscrit sont basés sur des études de terrain (Irlande, Islande, France, Maroc, Algérie) à différentes échelles (micro- et macro-échelles) et différentes périodes géologiques (Ordovicien, Crétacé et Pléistocène) (**Fig 1**). Les sites d'études ont été sélectionnés en fonction de la qualité des affleurements, des conditions de préservation (i.e., dépôts peu affectés par les déformations tectoniques post-lithifications) et de la connaissance du cadre paléogéographique, stratigraphique et sédimentologique. La méthode utilisée au cours de ces différentes études est identique et consiste en une analyse sédimentologique fine, couplée à une étude des structures de déformation pré-lithification à échelle macroscopique et microscopique.

► Problématique 1: Paléoenvironnements

Dans ce premier axe de recherche visant à utiliser les structures de déformation pré-lithification comme outil pour reconstruire les environnements et la dynamique glaciaire, deux chantiers Pleistocene ont été sélectionnés.

- Chantier Irlande (Ballyhorsey): Les affleurements se situent dans une carrière offrant d'excellentes conditions d'affleurements sur une épaisseur de 30 mètres. Ce site présente à la fois des dépôts sous-glaciaires et proglaciaires permettant ainsi d'observer, de caractériser, et de comparer les différents types de structures de déformation formés dans ces deux environnements.
- Chantier Islande (Sólheimajökull): Un affleurement de près de 300 mètres de long pour 20 mètres d'épaisseur recoupé par un réseau d'injection clastique est observé dans la plaine proglaciaire du Sólheimajökull. Le choix de ce site s'explique par le haut degré de préservation du réseau d'injections clastiques permettant ainsi une analyse fine des structures de déformations à échelles microscopique et macroscopique. Les indices géomorphologiques mais aussi la synthèse de précédents travaux (Thorarinsson, 1943; Norðdhal et al., 2008; Ingofólsson et al., 2010, Sigurdsson, 2010) permettent de bien contraindre la paléogéographie glaciaire locale et donc de comprendre l'impact de la dynamique

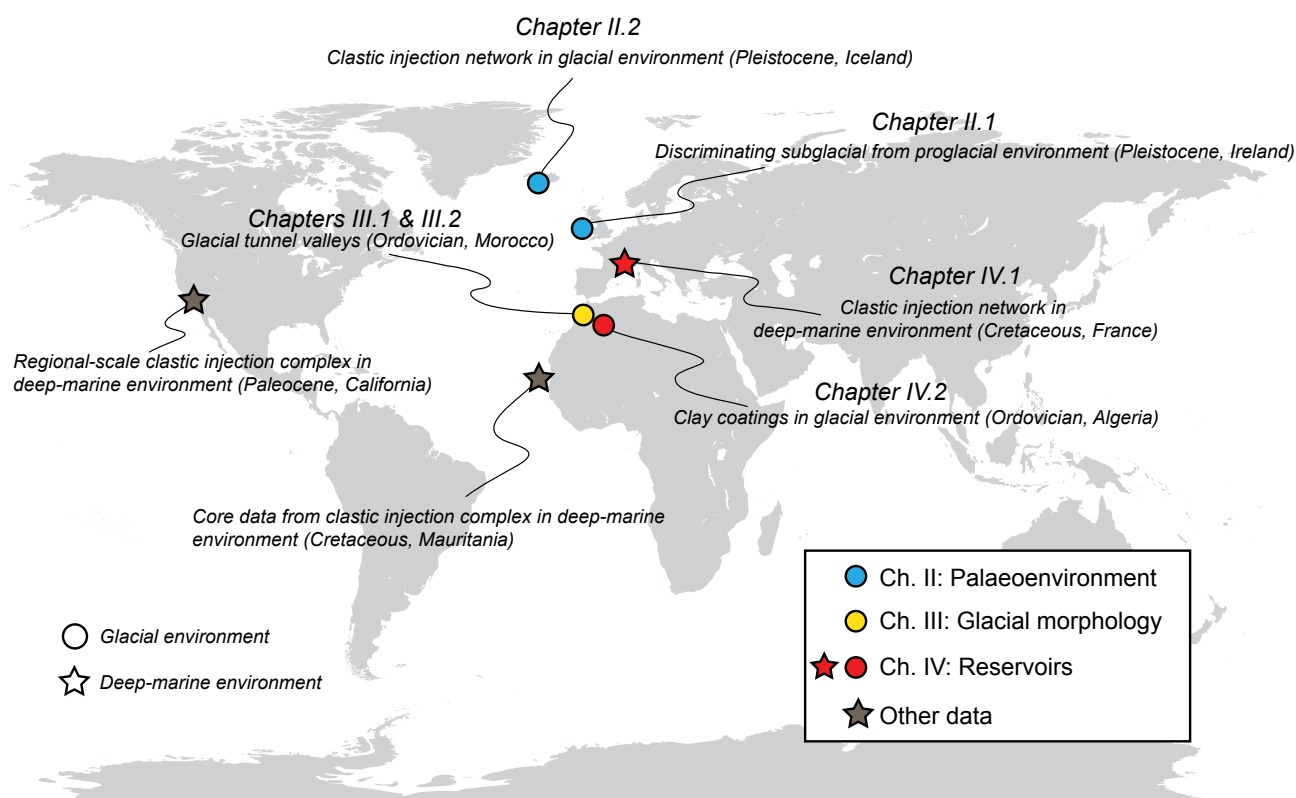


Figure 1. Presentation of the different sites studied during this thesis.

glaciaire sur la mise en place et la morphologie de ce réseau d'injections clastiques.

► Problématique 2: Morphologies glaciaires

Afin de tester l'impact des surpressions de fluide et des remobilisations sédimentaires sur la géomorphologie et plus particulièrement sur la formation de vallées tunnels, deux vallées tunnels glaciaires ordoviciennes situées au Maroc ont été choisies pour leurs qualités d'affleurements et pour la connaissance de leurs cadres stratigraphique, faciologique et morphologique (Le Heron, 2007; Clerc, 2012; Clerc et al., 2013).

- Chantier Maroc (Alnif): La très bonne connaissance des dépôts préglaciaires (Villas et al., 2006; Alvaro et al., 2007) et du remplissage glaciaire (Clerc et al., 2013), couplée à la qualité des affleurements plurikilométriques, ont fait de la vallée tunnel d'Alnif un choix évident pour tester l'impact des pressions de fluide sur le creusement d'une vallée tunnel.

- Chantier Maroc (Foum Larjamme): Cette vallée tunnel présente une morphologie et un remplissage sédimentaire très différents de ceux d'Alnif permettant ainsi de comparer et de proposer plusieurs

processus de formation pour les vallées tunnels ordoviciennes d'Afrique du Nord.

► Problématique 3: Propriétés réservoirs

Afin de tester l'impact des fortes pressions de fluide sur les propriétés réservoirs des sédiments dans les environnements glaciaires et marins profonds, deux chantiers ont été choisis. Le chantier marin profond se base sur l'étude des variations latérales de porosité à l'échelle de l'affleurement au sein d'un réseau d'injectites dans le sud-est de la France (Bassin Vocontien, Crétacé). Le chantier glaciaire s'appuie sur des données pétrophysiques ainsi que sur l'analyse microscopique d'échantillons issus de carottes sédimentaires prélevées dans une vallée tunnel ordovicienne algérienne.

- Chantier France (bassin Vocontien): Ce site présente de très bonnes qualités d'affleurements d'échelles kilométriques où les connexions entre chenaux turbiditiques et réseaux d'injectites sont visibles. Le cadre stratigraphique ainsi que l'architecture du réseau d'injectites sont bien documentés (Parize, 1988; Friès et Parize, 2003; Parize et al., 2007). La séquence diagénétique, composée d'une phase de cimentation carbonatée bloquant la porosité de manière précoce, permet d'estimer la porosité pré-lithification (i.e., porosité primaire) et ses variations au sein des réseaux d'injectites à l'échelle de l'affleurement.

Chantier Algérie (bassin de Sbaa): Les carottes sédimentaires du bassin de Sbaa issues du remplissage de vallées tunnels glaciaires ont été décrites dans de précédents travaux (Tournier, 2010; Tournier et al., 2010). L'influence majeure des "coatings" argileux sur la diagenèse des grès et à terme sur leurs propriétés pétrophysiques a alors été mise en évidence. De plus, elles présentent de nombreuses structures de déformation pré-lithification, induites pour certaines d'entre elles par des fortes pressions de fluide. Un échantillonnage continu le long de carottes sédimentaires a permis d'étudier l'origine de ces "coatings", leur distribution, et leur abondance, afin de tester si leur mise en place est liée à l'augmentation de la pression d'eau interstitielle.

4. Construction du manuscrit de thèse

Le travail de recherche entrepris pendant cette thèse a permis la rédaction de cinq articles scientifiques publiés ou soumis dans des revues scientifiques internationales, et d'un manuscrit qui sera rapidement soumis à publication:

Article 1. Ravier, E., Buoncristiani, J.F., Clerc, S., Guiraud, M., Menzies, J. and Portier, E., 2014. Sedimentological and deformational criteria for discriminating subglaciofluvial deposits from subaqueous ice-contact fan deposits: A Pleistocene example (Ireland). *Sedimentology* 61, 1382-1410.

Article 2. Ravier, E., Buoncristiani, J.F., Guiraud, M., Menzies, J. and Portier, E. A new model for the development of the Sólheimajökull clastic injection network: trigger mechanisms, processes of injection and implications for ice dynamics. (En préparation)

Article 3. Ravier, E., Buoncristiani, J.-F., Guiraud, M., Menzies, J., Clerc, S., Goupy, B., Portier, E., 2014b. Porewater pressure control on subglacial soft sediment remobilization and tunnel valley formation: A case study from the Alnif tunnel valley (Morocco). *Sedimentary Geology* 304, 71-95.

Article 4. Ravier, E., Buoncristiani J.F., Menzies, J., Guiraud, M., Clerc, S. and Portier, E. Porewater pressure-driven (Alnif) vs. Meltwater-driven (Foum Larjamme): two models of tunnel valley formation existing during the Ordovician glaciation, and their relations with Ice-Stream dynamics (Morocco). (Soumis à *Palaeogeography, Palaeoclimatology, Palaeoecology*)

Article 5. Ravier, E., Guiraud, M., Guillien, A., Vennin E., Portier, E., Buoncristiani, J.F. Micro- to Macroscale internal Structures, Diagenesis and Petrophysical evolution of Injectite networks in the Vocontian basin (France): implications for Fluid Flows. (Soumis à *Marine and Petroleum Geology*).

Le manuscrit de thèse se décompose en quatre chapitres qui s'appuient sur des articles scientifiques mais également sur des données originales. Ils s'organisent ainsi:

• **Chapitre I:** «Structures de déformation pré-lithification dans les environnements sous-glaciaires et marins profonds: Etat-de-l'Art».

Ce chapitre présente une synthèse complète des structures de déformation pré-lithification dans les environnements sous-glaciaires et marins profonds et se décline en trois parties.

- 1) Une première partie présentera des généralités sur les notions de déformation pré-lithification, les principales notions physiques utiles dans l'analyse de ces structures, leurs mécanismes déclencheurs ainsi qu'une méthode facilitant leurs descriptions et leurs interprétations.
- 2) Une deuxième partie se focalisera sur les déformations dans les environnements sous-glaciaires.
- 3) La dernière partie évoquera les déformations pré-lithifications liées aux fortes pressions de fluides dans les environnements marins profonds.

Cette synthèse se base sur une compilation de précédents travaux scientifiques et les illustrations des différentes structures de déformation sont issues des différentes campagnes de terrain réalisées pendant cette thèse (cf. **Fig. 1**), mais également d'articles scientifiques.

• **Chapitre II:** «Structures de déformation pré-lithification: marqueurs paléoenvironnementaux».

Ce second chapitre vise à mettre en évidence la signification paléoenvironnementale des différentes structures de déformation pré-lithification en se focalisant sur les reconstitutions de la dynamique glaciaire.

Ce chapitre se divise en deux parties correspondant successivement à deux chantiers différents:

- 1) Chantier Irlande (**Fig. 1**): Cette première partie propose de différencier les environnements de dépôts sous-glaciaire et proglaciaire en se basant sur une étude sédimentologique et sur l'analyse de structures de déformation pré-lithification. Cette première partie contient un article publié dans la revue *Sedimentology* (Article 1).
- 2) Chantier Islande (**Fig. 1**): Cette seconde partie propose d'étudier un réseau d'injections clastiques mis en place en contexte glaciaire, et d'en utiliser les caractéristiques pour

reconstruire l'évolution de la pression d'eau interstitielle dans le substrat et les oscillations de la marge glaciaire au cours du temps. Cette seconde partie fait l'objet d'un article scientifique en cours de préparation (Article 2).

• **Chapitre III:** « Déformations par surpressions de fluide: impacts sur les morphologies glaciaires ».

Ce troisième chapitre aborde l'impact des pressions de fluide sur les processus de remobilisation sédimentaire et sur le creusement des vallées tunnels. Ce chapitre se construit sur l'interprétation de données terrain issues de deux vallées glaciaires ordoviciennes de l'Anti-Atlas marocain se développant sur substrat meuble. L'analyse de ces deux vallées fait l'objet de deux parties:

1) "Vallée tunnel" d'Alnif (**Fig. 1**): Cette première partie synthétise les différents arguments terrain en faveur d'un modèle de creusement contrôlé par les fortes pressions de fluide. Cette partie se focalise sur la description des processus de remobilisation sédimentaire responsables de la formation de cette vallée tunnel, et fait l'objet d'un article publié dans *Sedimentary Geology* (Article 3).

2) "Vallée tunnel" de Foug Larjamme (**Fig. 1**): Cette seconde partie compare les processus intervenant dans le creusement de la vallée tunnel d'Alnif et de Foug Larjamme afin de comparer différents modèles de formation des vallées tunnels. Dans un second temps, l'impact de la distribution des paléo-fleuves de glace sur la nature des processus intervenant dans le creusement de ces différentes vallées tunnels est discuté. Cette partie intègre un article soumis dans la revue *Palaeogeography, Palaeoclimatology, Palaeoecology* (Article 4).

• **Chapitre IV:** « Déformations par surpressions de fluide: impacts sur les propriétés réservoirs ».

Ce quatrième chapitre permettra d'étudier l'impact des déformations pré-lithifications induites par des surpressions de fluide sur les propriétés réservoirs des sédiments clastiques en domaines marins profonds et glaciaires. Ce chapitre s'étaye sur des données acquises au sein d'un réseau d'injectites situé dans le bassin vocontien (France), et au sein de carottes sédimentaires prélevées dans le remplissage sédimentaire d'une vallée tunnel ordovicienne (Algérie). Ce chapitre est subdivisé en deux parties présentant respectivement l'impact des pressions de fluide sur les réservoirs clastiques marins profonds, puis glaciaires.

1) Chantier France (marin profond) (**Fig. 1**): Cette première partie présente des données

de porosité primaire acquises au sein d'un réseau d'injectites mis en place dans le système turbiditique crétacé du bassin vocontien. L'analyse de la distribution des valeurs de porosité primaire au sein du réseau d'injection permet d'estimer l'impact des remobilisations sédimentaires sur les propriétés pétrophysiques, et les paramètres contrôlant leur distribution. L'évolution progressive de la porosité après les différentes phases de déformation pré-lithification et de diagenèse est également discutée, tout comme leurs impacts sur les écoulements de fluide dans le réseau d'injection au cours du temps. Les résultats sont discutés dans le cadre d'un article soumis à *Marine and Petroleum Geology* (Article 5).

2) Chantier Algérie (glaciaire) (**Fig. 1**): Cette seconde partie propose d'étudier l'impact des pressions de fluide sur la mise en place de "coatings" argileux au sein de grès glaciaires remaniés par des déformations pré-lithifications. L'influence majeure de l'abondance des "coatings" argileux sur les propriétés pétrophysiques des grès glaciaires ordoviciens représente la motivation principale de cette étude qui a pour but de comprendre les processus de mise en place de ces "coatings". L'hypothèse des pressions de fluide et des processus d'élutriation (i.e., remobilisation des particules les plus fines) qui leur sont associés est testée dans cette deuxième partie.

Enfin, les principaux résultats de ces différentes études seront synthétisés et les réponses aux différentes questions formulées précédemment seront apportées dans la conclusion. Les implications de ces résultats dans les domaines académiques et industriels seront présentées, et permettront de dresser les perspectives ouvertes par ce travail de recherche.

CHAPITRE I

**Déformations pré-lithifications dans les environnements
sous-glaciaires et marins profonds: Etat-de-l'Art**

Introduction

Cette thèse présente des travaux de recherche sur les structures de déformation pré-lithification formées dans les environnements sous-glaciaires et marins profonds. Les objectifs principaux de ce manuscrit sont de mieux comprendre la contribution de ces structures dans la reconstruction des paléoenvironnements et de la dynamique glaciaire, ainsi que de comprendre quels sont leurs impacts sur les propriétés pétrophysiques des réservoirs clastiques.

Ce premier chapitre a pour objectif de dresser l'état-de-l'art des structures de déformations pré-lithification dans ces deux environnements, et se divise en trois parties. Il sera rédigé en anglais afin de créer une base de donnée pour l'entreprise GDF Suez.

• **Partie 1:** «Soft-sediment deformation structures: Definition, physical aspects, triggers and methods of analyses».

Dans cette première partie, la notion de structure de déformation pré-lithification sera définie. Les principaux aspects mécaniques et physiques liés à la mise en place et au fonctionnement de ces structures seront présentés (i.e., états de contrainte, pression d'eau interstitielle, rhéologie, mécanismes de déformation, ...). Les principes de déformation exogénique et endogénique seront également présentés dans cette partie. Enfin, une méthode facilitant l'identification, la description, et l'interprétation des structures de déformation pré-lithification sera proposée.

• **Partie 2:** «Soft-sediment deformation structures in subglacial environments».

Cette seconde partie se focalise sur les déformations pré-lithification en environnements sous-glaciaires. Les paramètres contrôlant la déformation seront d'abord introduits (poids de la glace, vitesse d'écoulement de la glace, pression d'eau interstitielle, lithologie, ...). La distribution des états de contrainte sous-glaciaire sur un profile longitudinal théorique de calotte sera ensuite établie. Les différentes structures de déformation liés aux différents états de contraintes prédéfinis seront ensuite présentées.

Les précédents travaux démontrant l'intérêt de ces structures de déformation dans la reconstruction

des paléoenvironnements, et de la paléodynamique glaciaire, seront également synthétisés dans cette deuxième partie.

Partie 3: «Soft-sediment deformation structures induced by fluid overpressure in deep-marine environments»

Cette troisième partie se focalise sur la description et l'interprétation des différentes structures de déformation pré-lithification induites par des surpressions de fluide (i.e., des pressions d'eau interstitielle élevées) dans les environnements marins profonds.

Tout d'abord les caractéristiques de l'environnement marin profond et plus particulièrement des systèmes turbiditiques seront introduites. Les paramètres contrôlant la déformation dans ce type d'environnement seront ensuite définis. Les morphologies et les processus de mise en place des différentes structures de déformations observés dans cet environnement seront présentés. Les facteurs responsables de l'augmentation de la pression de fluide, et les impacts de cette augmentation sur les propriétés pétrophysiques des réservoirs clastiques marins profonds seront déterminés.

**Soft-sediment deformation structures:
Definition, Physical aspects, Triggers, and Methods of analyses**



Seismogenic slump folds formed by gravity-driven tectonics (Dead Sea Basin) (Aslop and Marco, 2013)

1. Definition of soft-sediment deformation structures

Soft-sediment deformation is deformation that affects **unconsolidated sediments**, thus occurring during or shortly after deposition (Lowe, 1975; Allen, 1982; Mills, 1983; Maltman, 1984; Owen, 1987; Collinson, 2003; Van Loon, 2009; Owen et al., 2011). A definition has been proposed by van Loon (2009): “*Soft-sediment deformation structures in sediments are deformations that occur in still unlithified sediments or in sedimentary rocks that had not yet undergone lithification before the deformation structures started to form*”. Such deformations are also referred to early-diagenetic features as they are formed, in principle, prior to any significant lithification (van loon, 2009; Moretti et al., 2011). Other alternative names are occasionally found, such as soft-rock deformations, sedimentary deformational structures, penecontemporaneous deformations, synsedimentary deformations or pre-lithification deformations.

Such deformation usually occurs close to the surface as the increase of sediment shear strength, during burial and compaction, tend to prevent the deformation of sediments (Maltman, 1994). Unlithified sediments affected by deformations can be cohesive or cohesionless, but their physical properties are distinct from those of rock. The variety of soft-sediment deformation structures (SSDs) is considerable and the complexity of their structures illustrates the variety of processes and agents involved in their formations.

Numerous environments are concerned by SSDs: marine environments (e.g., shallow, deep-water, and tidal) (Molina et al., 1998; Greb and Archer, 2007; Chen et al., 2009; Oliveira et al., 2009, 2011), continental environments, including fluvial (Marshall, 2000; Went, 2005), volcanic (Smellie et al., 2006; Brown et al., 2007) lacustrine (Gruszka and Van Loon, 2007), and glacial environments (Benn and Evans, 1996; McCarroll and Rijdsdijk, 2003; Le Heron et al., 2005; Denis et al., 2010; Arnaud, 2012). Transitional environments may also be affected by soft-sediment deformations, especially in deltaic environments (Dugan and Flemings, 2002; Hickson and Lowe, 2002, Wignall and Best, 2004). Triggers for soft-sediment deformations can either be **endogenic** or **exogenic**, meaning that they can be directly related to the conditions existing in the depositional environments (i.e., endogenic: ice flow, mass movement, wave actions,...) or that triggers for deformations are completely independent of the depositional environments (i.e., exogenic: earthquakes, meteoric impacts,...).

In this first part, elementary **mechanical notions** and **triggers** of deformation will be presented as well as **methods** facilitating the recognition and interpretation of soft-sediment deformation structures.

2. Elementary notions on soft-sediment deformation mechanics

2.1. Stress and strain definitions

Structures formed by soft-sediment deformations are controlled by the **stress** exerted on sediments during deformation, **porewater pressure**, and **lithological characteristics** (e.g., grain-size, granular framework, and clay content). The change of shape or volumes of sediments related to sediment deformation under an applied stress is known as **strain**.

2.1.1 Stress

Stress (σ) is a measure of the intensity of a force acting upon a body as a function of its area. A stress acting on a plane can be seen as a vector which can be resolved into two major components, the **normal component** known as the normal stress (σ_n) and acting perpendicular to the plane and a **shear component**, referred to the shear stress (τ) and acting parallel to the plane (**Fig. 1**).

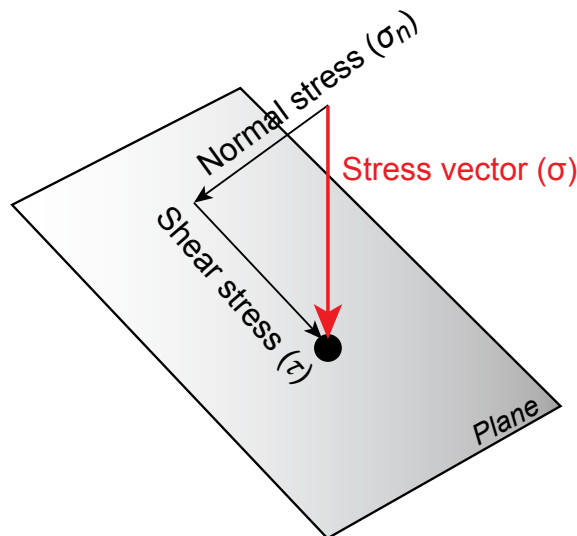


Figure 1. Illustration of the stress vectors concept (σ). Each stress vector can be decomposed into a normal stress (σ_n) acting perpendicular to a plane and a shear stress (τ) acting parallel to a plane.

To define the state of stress at a point inside sediments, three principal stress values are defined and expressed as σ_1 (the maximum compressive stress), σ_2 (the intermediate compressive stress) and σ_3 (the minimum compressive stress) and stress axes are normal to the three surfaces on which they act (**Fig. 2A**). Stress is also commonly illustrated by a stress ellipsoid with principal stress axes as symmetry axes and represents a useful mental tool for geometrically representing the state of three-

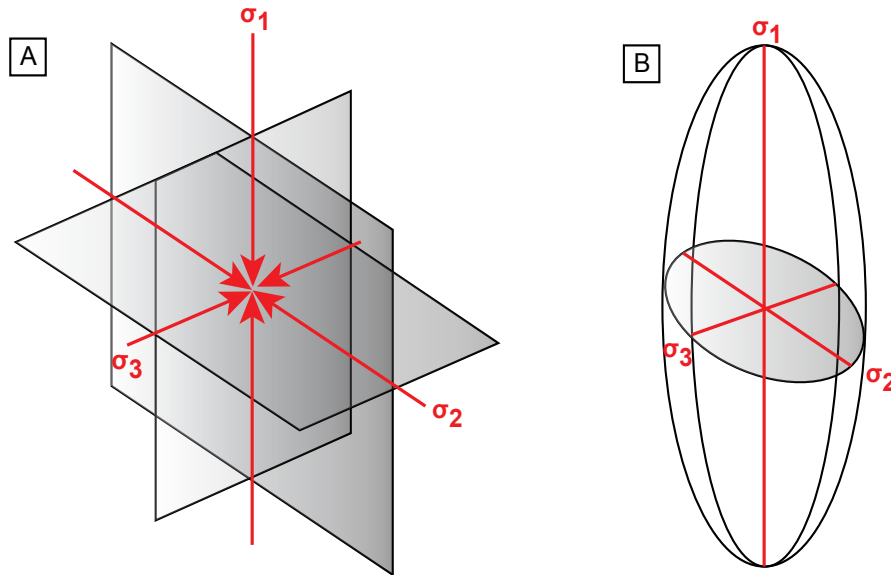


Figure 2. (A) The complete stress state at the point can be represented by three orthogonal vectors, operating on three orthogonal surfaces. (B) The principal stress vectors are symmetry axes of a stress ellipsoid.

dimensional stresses at a point (**Fig. 2B**).

When describing stresses exerted on soft-sediments, the porewater pressure must be taken into account as porewater naturally exerts a stress on the surrounding grains. This pressure known as **porewater pressure** is an **isotropic stress** (i.e., same in every directions) and acts on the grains in the opposite direction of all stresses exerted (e.g., total stress) on sediments. The **effective stress** (σ') derives from these characteristics, and is most simply expressed as the difference between the **total stress** (σ), corresponding to the combination of the lithostatic stress and the trigger stress, and the **porewater pressure** (P_{H_2O}):

$$(1) \sigma' = \sigma - P_{H_2O} \text{ (Terzaghi equation (1925))}$$

2.1.2. Strain

Strain (ϵ) corresponds to the dimensional change in the shape or volume of a body as a result of deformation under an applied stress. Strain is the ratio of the altered length, area, or volume to its original value. Strain may be homogeneous or inhomogeneous. Considering homogeneous deformation, and given an initial circle, it is possible to obtain strain ellipsoids with various shapes. The shape of the strain ellipsoid will depend on the **strain regimes** during deformation, known as **pure shear**, **simple shear** and **general shear**.

- *Pure Shear (homogeneous non-rotational strain)*

Pure shear is a three-dimensional constant-volume “homogeneous flattening” (Twiss and Moores, 1992). During homogeneous flattening a sphere is transformed into a pancake-like shape and a box is changed into a tablet or book-like form (**Fig. 3A**). Pure shear is a **non-rotational** or **irrotational** deformation.

- *Simple shear (homogeneous rotational strain)*

Simple shear is a three-dimensional constant-volume strain (Ferguson, 1994; Davis and Reynolds, 1996). A cube subjected to a simple shear event is converted into a parallelogram resulting in a rotation of the finite strain axes (**Fig. 3B**). Simple shear corresponds to a **rotational** deformation. The **angular shear strain (ψ)** is a measure of the angular rotation from two mutually perpendicular reference axes following simple shear and allow to estimate the shear strain rate. The **shear strain (γ)** is given as the tangent of angular shear (ψ). Rotational deformation leads to the development of **schistosity planes** (referred to as “**S**” planes) and **shear planes** (referred to as “**C**” planes) (**Fig. 3B**). The **θ angle** displayed between the “**S**” and “**C**” planes can be used as an indicator to easily estimate shear strain rates on the field (Choukroune et al., 1987; Passchier and Trouw, 2005) (**Fig. 3B**).

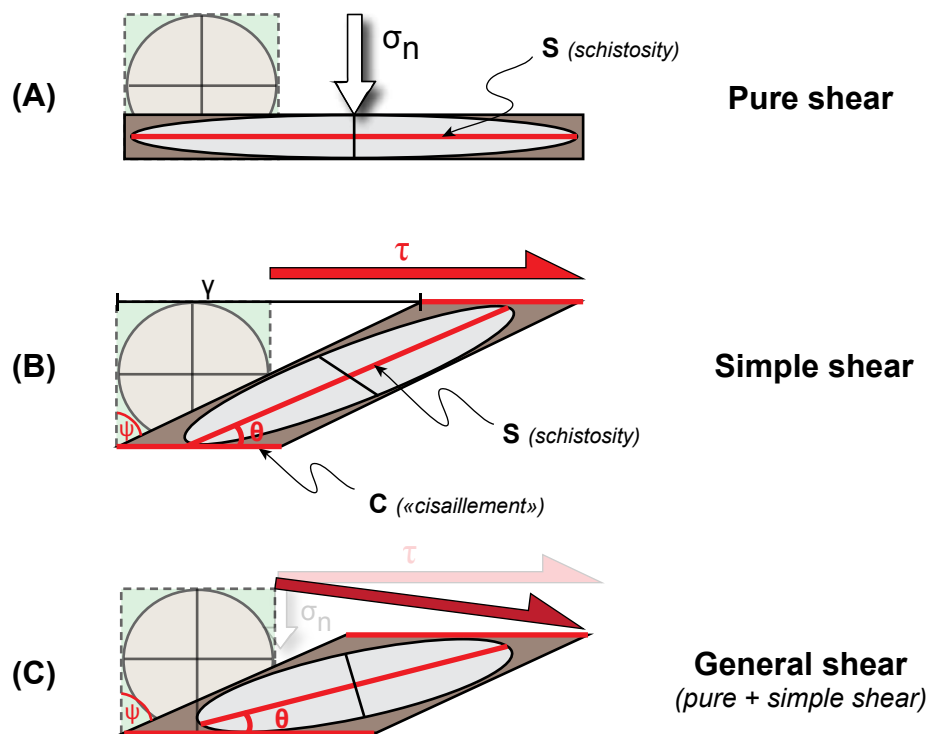


Figure 3. The above diagram represents the resulting strain ellipsoids corresponding to the different strain regimes. σ_n and τ respectively represents the contribution of the normal stress and shear stress during deformation of the ellipses. (A) Pure shear implies no rotation, only shortening and lengthening. (B) Simple shear involves rotation about a point. (C) General shear is a combination of pure shear and simple shear. The angular shear (ψ) helps to determine to what extent the plane was displaced during shear.

- *General shear (pure shear + simple shear)*

Pure and simple shear are often found together. The combination of pure shear and simple shear is called **general shear**. The resulting shape of the ellipsoid will depend if pure shear occurs followed by simple or inversely, or their relative contribution to strain if pure shear and simple shear occurs simultaneously (Fossen and Tikoff, 1993) (**Fig. 3C**).

2.2. Relations between stress and strain

The relation between **stress** and **strain** can be illustrated by a diagram which shows the change in strain under an applied stress through time (**Fig. 4**). This diagram shows that the increase of differential stress may exceed a limit the sediments can support, known as **yield strength**, which induces permanent deformation. Indeed, any rocks or sediments will show an **elastic behavior** under mean stress by a small decrease in volume, and under differential stress by a small change in shape (less than 1%) (Passchier and Trouw, 2005). Such elastic strain is recoverable if the stress is released (**Fig. 4**). However, if elastic strain in response to differential stress exceeds a limit that the rock can

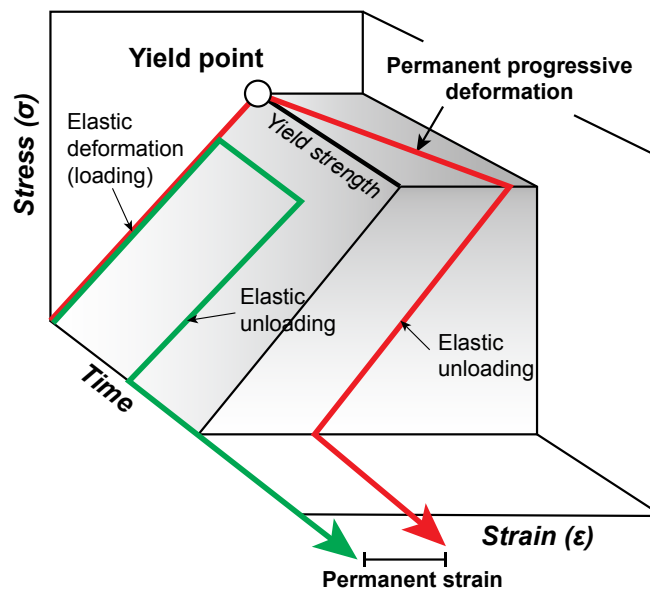


Figure 4. Illustration of some concepts of rheology in space, plotting differential stress (σ) and strain (ϵ) against time. The red and green curves illustrate loading and unloading of a sample in an experiment when differential stress is applied. Behavior is first elastic until the yield point is reached, beyond which permanent deformation begins. When stress is released, the elastic strain is relaxed and permanent strain remains. (After Passchier and Trouw, 2005).

support (i.e., the yield strength), the material will deform permanently. If the differential stress is released, only the elastic strain will be recovered (**Fig. 4**).

The **strain rate**, corresponding to the speed at which the rock changes permanently, is primordial

as the stress duration is very important in determining the strain behavior. Similarly to the yield strength, when sediments are subject to shear stress, the maximum shear stress value on an original cross section area that can be sustained is named **shear strength**. Sediment shear and yield strength variations depend on **temperature**, **confining pressure**, **shape**, **size**, **loading rate** and **porewater pressure**.

2.3. Rheology of sediment during deformation

Two types of strain behaviors are depicted during soft-sediment deformation: **brittle** and **ductile** behaviors. **Ductile** deformation is also referred to as **distributed** or **continuous** deformation in the literature while **brittle** deformation is usually referred to as **localized** and **discontinuous** deformation (Schmid and handy, 1991). Classically, when subject to a physical stress, sediments failing or breaking along particular planes exhibit a brittle behavior while sediments bending or flowing are inferred to behave on a ductile manner.

• Brittle deformation

Brittle deformations are driven by stresses whose magnitude exceeds the sediment yield strength and leads to **intergranular shear in cohesive sediments**, or **small-scale faults in cohesionless sediments** (Owen, 1987). It corresponds to the **abrupt failure of an elastic material** at a well-defined peak strength and is associated with a loss of cohesion and strong softening. The deformation is then achieved by sediments movements along clearly-defined surfaces (Twiss and Moores, 1992; Dehandschutter et al., 2005) (**Fig. 5A**). Brittle deformations are commonly associated with volume

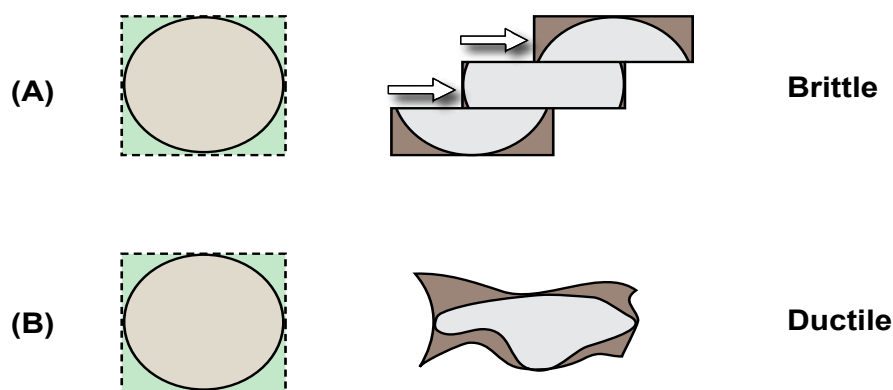


Figure 5. Representation of the two different sediment behaviors when sediments deform. (A) Brittle behavior corresponds to discontinuous deformations along clear surfaces. (B) Ductile behavior occurs when sediments undergo continuous and permanent deformation, without fracturing.

changes. Brittle deformations imply that sediments are characterized by relatively low porewater pressure and/or low clay content, or that deformations affect frozen sediments (Maltman, 1994).

- *Ductile*

Ductile deformations, also known as viscous flows, are deformations that derive from a strain distributed throughout the entire mass of sediments (**Fig. 5B**). It is possible when the sediments are temporarily in a weakened state, i.e., when the yield strength is reduced, so that sediments can behave as a viscous fluid or a plastic. Reduced yield strength sensibly enables ductile deformation (Owen, 1987). This type of deformation involves water-saturated sediment or/and sediments with a high clay content.

2.4. Mechanisms of soft-sediment deformations controlled by porewater pressure

Knipe (1986) illustrated the different types of syn- to post-lithification deformations in a diagram as a function of three principal parameters: the deformation ratio, the degree of lithification, and the fluid pressure (i.e., porewater pressure) (**Fig. 6**). In this diagram, the **Independent Particulate Flow (IPF)** corresponds to the area where the ductile deformation of soft-sediments occurs and defines the behavior of non-cohesive sediments. The variations of fluid pressure within these unlithified sediments can trigger momentary yield strength diminution. In this configuration, under an applied stress, sediments can become mobilized because it is in a condition of insufficient strength to resist the stresses driving it to move (Maltman and Bolton, 2003). The deformation and remobilization of water-saturated sediments are controlled by ductile processes occurring through **IPF**, causing sediments to behave as either a **plastic material (hydroplastic deformation)** or as a **viscous fluid (liquefaction/fluidization)** stressed beyond its yield strength (Lowe, 1975; Owen, 1987; Maltman, 1994) (**Figs. 6 and 7**).

- *Hydroplastic*

Hydroplastic deformations occur when sediments are characterized by a significant content of clay particles or/and a moderate porewater pressure. In this configuration, the sediment water-mixture will have a cohesive component to its strength, thus behaving as a **rheological plastic** which can sustain a certain value of shear stress before deformation begins (i.e., a significant yield strength). The

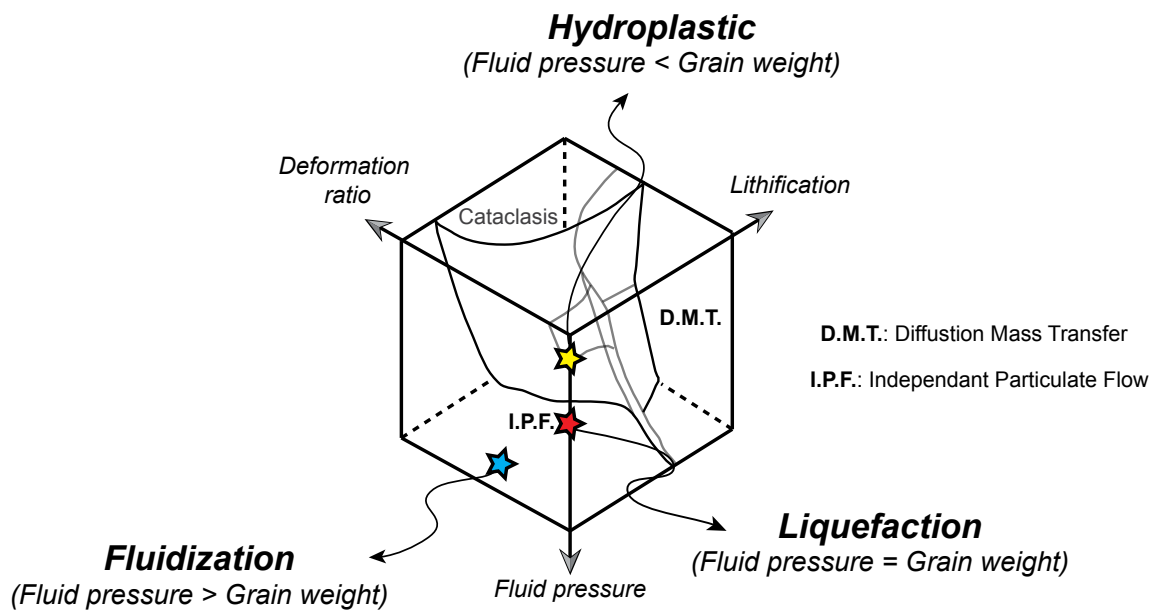


Figure 6. Diagram illustrating the characteristics of deformation mechanisms while the fluid pressure, the degree of lithification and the deformation ratio vary (modified after Knipe (1986) and Huguen et al., 2001). Hydroplastic, liquefaction and fluidisation correspond to the different types of independent particulate flow (IPF), depending on the fluid pressure.

required sediment cohesion for hydroplastic deformation can be achieved when sediment is damp but not water-saturated, sand which has dried out after being wet, partially cemented sand, frozen sand or muddy sand. Although sediments bend during hydroplastic deformation, **primary structures** are **preserved** and are **concordant** with the layering (So); elutriation of finer grains is negligible. Hydroplastic deformations are characterized by relatively **low to moderate porewater pressure**, **low water escape rate** and **preserved primary structures** (Fig. 7).

• Liquefaction

Liquefaction is a loss of strength related to an increase in pore fluid pressure (i.e., porewater pressure) to a level which equals the overburden pressure. Particles become temporarily dispersed in the pore fluid, the strength is reduced to zero and sediments behave as a **viscous fluid** (Lowe, 1975; Owen, 1987; Maltman and Bolton, 2003). During deformation, liquefaction occurs when the sediment is wholly sustained by the pore-fluid and cohesion is negligible. The sediment remains in a liquefied state until pore pressure is reduced and some inter-particulate frictional strength is restored. Liquefaction is characterized by a negligible yield strength, a **fluid pressure approximately equivalent to the lithostatic pressure**, and a moderate water escape rate. After deformation, primary structures can be **partly preserved but more generally destroyed, concordant, with an elutriation of finer grains ranging from minor to important** (Fig. 7).

• Fluidization

Fluidization occurs when the sediment strength was lost through moving interstitial fluids buoying the particles. The fluidization mechanism implies a continuous flow of fluid through the sediments. In this configuration, **the fluid-drag forces exceeds the particles weight**. In a fluidized state, sediments also behave as a **viscous fluid**. The fluidization mechanism implies that sediments have a negligible yield strength with a fluid pressure clearly superior to the lithostatic pressure. **Water escape rate is high and primary structures are completely destroyed and are generally discordant (Fig. 7)**. If the superficial fluid exceeds the particle settling velocity, fine particles are mobilized and **elutriation is significant** (Lowe, 1975; Allen, 1982).

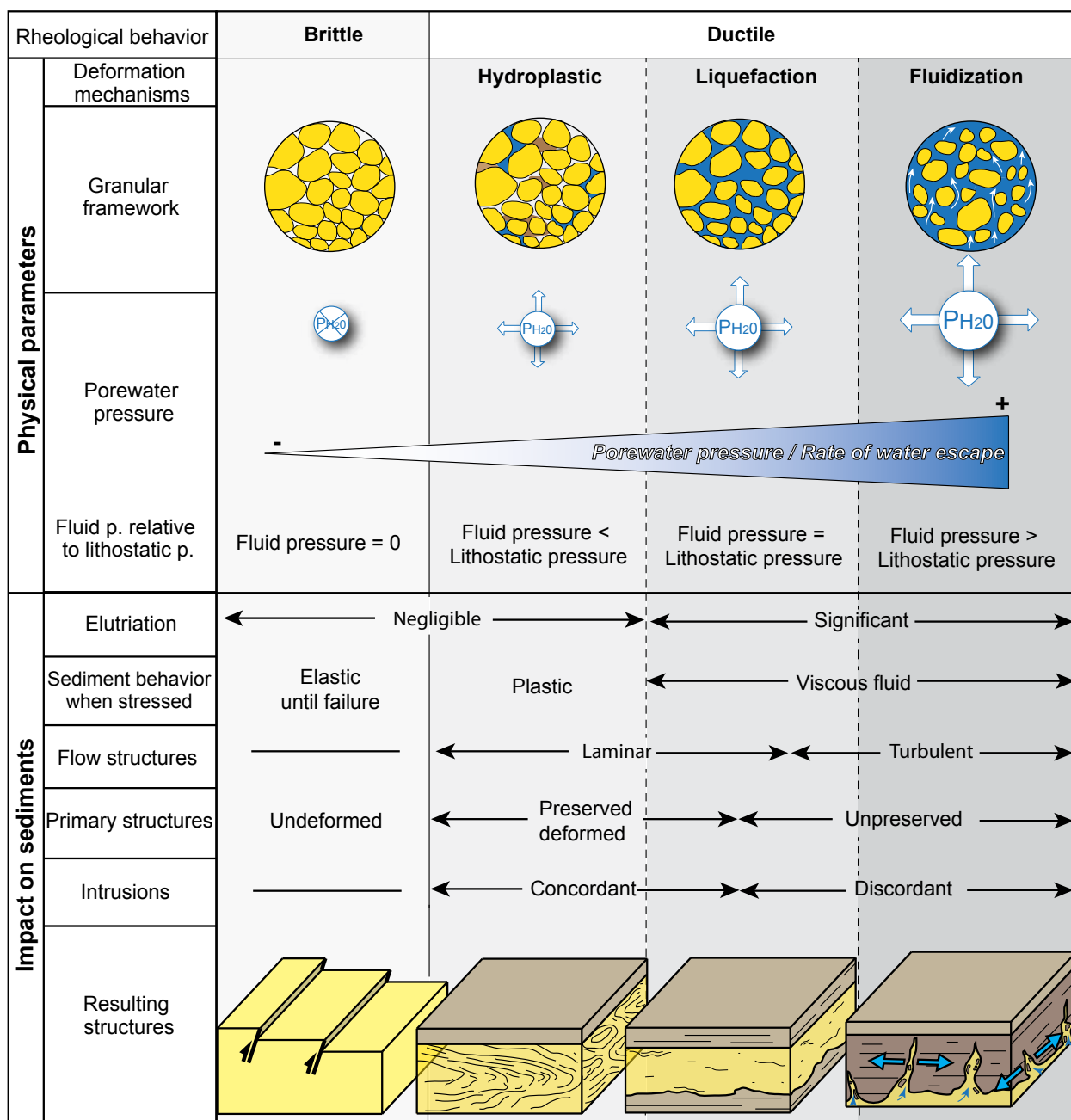


Figure 7. Processes of sediment deformation and their associated physical characteristics, behaviors, and products (modified after Lowe, 1975).

2.5. Sediment Failure and Hydrofracturing

2.5.1. Sediment failure

The Mohr-coulomb theory (1776) is a mathematical model used to describe the response of material to shear stress and normal stress. The time-honoured view of the relation between these parameters uses the **Mohr-Coulomb equation**. In the configuration of deformations affecting water-saturated sediments, the equation is as it follows:

$$(2) \tau_{\text{yield}} : C + \sigma' \tan \phi$$

τ_{yield} : yield strength; C: sediment cohesion; σ' : effective stress; ϕ : friction angle

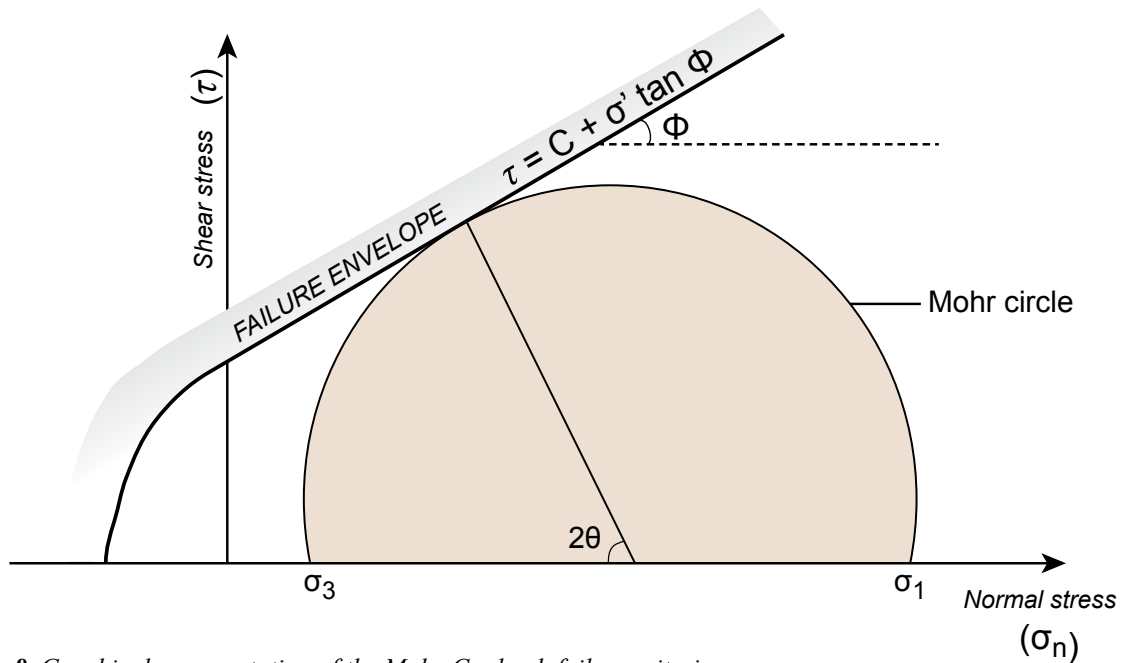


Figure 8. Graphical representation of the Mohr-Coulomb failure criterion.

This equation permits to draw the Mohr envelope, also called **failure envelope** and defines a linear relationship between normal and shear stresses (or maximum and minimum principal stresses) at failure. Mohr circles, representing two dimensional graphical representation of stress tensors can then be plotted on the diagram to determine if stresses exerted on material whether lead to failure or not.

Failure occurs when Mohr circles intercept the failure envelope (Fig. 8).

2.5.2. Hydrofracturing

The fluid pressure (i.e., porewater pressure) increase within sealed water-saturated sediments

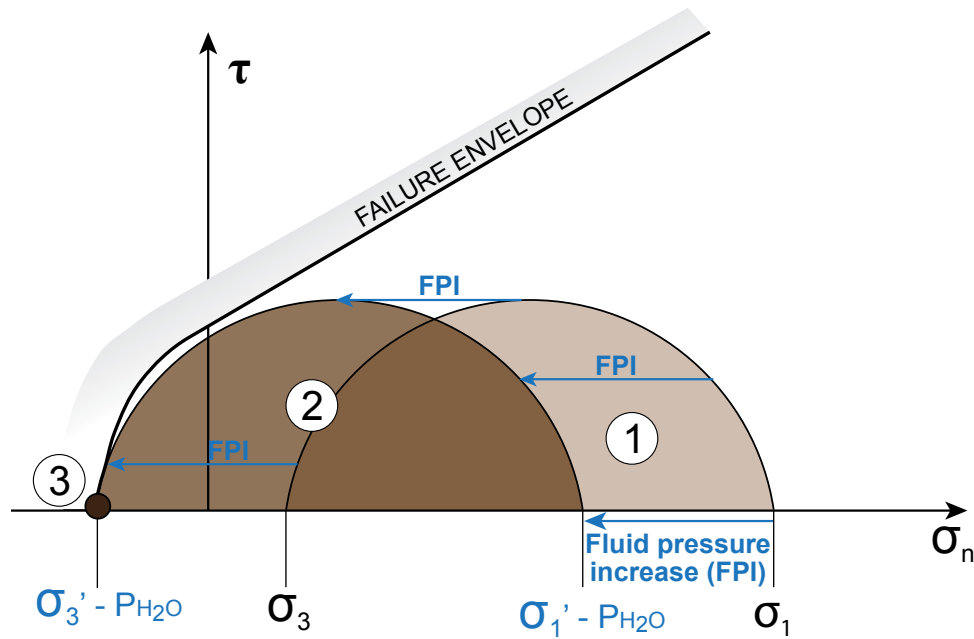


Figure 9. Mohr circle representation of three different stress states. (1) Solid line circle 1 will not cause failure. (2) The effect of fluid pressure increase is to move the stress state (1) to the left by an amount of P_{H_2O} (FPI), the resulting solid line circle 2 touches the failure envelope, hydraulic fracturing occurs. (3) Mohr circle 3. The increase of fluid pressure leads to the reduction of the differential stress until it becomes zero. This configuration describes a hydrostatic stress field.

triggers **fluid overpressure** development. Overpressure is associated with potential failure of sediments when the porewater pressure exceeds the tensile strength of the encasing sediments, plus the minimum compressive stress (σ_3). The hydrofracturing principle can be illustrated using a Mohr circle representation. In order to trigger failure, the Mohr circle must touch the brittle failure envelope. In Mohr circle 1, corresponding to a stable stress state configuration, failure will not occur (**Fig. 9**). The increase of fluid pressure (FPI) acts so as to oppose the compressive stress (σ_1 , σ_3) and cause them to be reduced to the effective stresses ($\sigma_1 - P_{H_2O}$, $\sigma_3 - P_{H_2O}$). The **increase of fluid pressure (FPI) induces lateral migration of the Mohr circle** to the left (Mohr circle 2) (**Fig. 9**). Mohr circle 2 touches the failure envelope indicating failure driven by increasing fluid pressure, known as **hydraulic fracturing**. Point number 3 represents a Mohr circle when the differential stress is 0, thus corresponding to a hydrostatic stress field. In that case, the normal stress across all planes is the same and there is no direction of relatively easy opening for fractures (e.g., **hydraulic brecciation**) (Cosgrove, 1995).

The direction of hydrofracture propagations will depend on the orientation of σ_3 implying that dykes will form when σ_3 is horizontal, while sills will form when σ_3 is vertical. In other terms, **hydrofractures propagates parallel to the maximum compressive stress (σ_1) and perpendicular to the minimum compressive stress (σ_3)** (Delanay et al., 1986; Cosgrove, 1995; Jolly and Lonergan, 2002).

3. Prerequisites on soft-sediment deformation structures.

Although pre-lithification deformation structures are widely observed and easily identifiable, it exists some settings where deformation or sediment mobility occurs that should not be considered as soft-sediment deformation structures (Moretti et al., 2011). Debated types of soft-sediment deformation structures are discussed thereafter.

- *Tectonic deformation*

Stresses delivered by tectonic activities may deform both near-surface unconsolidated sediments and more deeply buried rock (Storti and Vannucchi, 2007). The deformation of sediments represents soft-sediment deformation, although there may be a continuum of processes with deformation of lithified rock (Moretti et al., 2011).

- *Mass movements*

Slumps trigger deformation of unconsolidated sediments, leading to folding, faulting, thrusting, and fracturing of unlithified sediments, and therefore constitute SSDs. Nevertheless, there is a continuum of gravity-driven mass-movements and sedimentary gravity flow processes, many of which cannot be considered as SSDs, such as debris flows or turbidity currents.

- *Sediment remobilization in deeply buried deposits*

The development of fluid overpressures in buried and unlithified clastic sediments leads to the formation of clastic injections and diapiric structures. Although they are not related to deformation occurring within subsurface sediments, mobility of the sediments are driven by similar processes to near-surface sediments, implying that they can also be considered as soft-sediment deformation structures (Owen et al., 2011).

- *Igneous and Metamorphic rocks*

Although deformation occurring in these particular settings cannot constitute soft-sediment deformation structures, the structures formed in igneous and metamorphic rocks can be morphologically very similar to those observed in sedimentary environments (ex: subglacial shear zone vs. mylonite discussed in part 2, section. 4.1) (Wiebe and Collins, 1998; Passchier and Trouw, 2005; Phillips et

al., 2011).

4. Triggers for soft-sediment deformation structures

Triggers responsible for the deformation of soft sediments can either be **endogenic** or **exogenic**, meaning that triggers involved in sediment deformation can be dependent or independent of the depositional environments. The endogenic/exogenic distinction might be difficult to make. For example, tsunamis triggering sediment deformation in a wave-influenced environment (i.e., shoreface environment) represent an **endogenic trigger**, however waves developed during tsunamis can enter into the continent and affect terrestrial backshore deposits, thus corresponding to an **exogenic trigger** (Owen et al., 2011).

4.1. Endogenic triggers

- *Continental setting*

Soft-sediment deformation structures related to endogenic triggers are common in continental settings, most particularly in glacial, alluvial, and lacustrine environments. In glacial environments, **basal shear stresses imposed by overriding ice** represent the dominant trigger for soft-sediment deformations. Lacustrine and alluvial environments commonly contain SSDs triggered by **high sedimentation rates** and **gravity processes** along sedimentary slopes.

- *Transitional setting*

Deltaic and estuarine environments contain most of the soft-sediment deformation structures recorded in transitional environments, including deformations triggered by **high sedimentation rates** and **gravity processes**. In addition, transitional setting may contain structures induced by the shear stress exerted on sediments by **water waves** and **tides**.

- *Marine environments.*

In shoreface environments, deformations are triggered by **water waves** and **tides**, while the slope and offshore domains are mainly affected by deformations triggered by **gravity instabilities** and **high sedimentation rates**.

4.2. Exogenic triggers

Triggers are occasionally independent of the depositional environments implying that they can potentially be found in all the depositional environments previously described. The most widespread exogenic trigger is the **tectonic trigger**, frequently leading to **seismic activities** (Guiraud and Plaziat, 1993). Indeed, earthquakes trigger deformations due to sediments shaking by compressional and shear seismic waves. Similarly, **meteorite impacts** induce sediment deformation by resulting shock and seismic waves released during the impact (Roussell et al., 2003).

The **burial** of unlithified clastic sediments is associated with an **increase of overburden pressure**, **water released** by clay dehydrations or clay minerals transformations, or **oil/gas migrations** (Lonergan et al., 2000). The burial of sediments associated with the migrations of fluids may lead to the development of **fluid overpressures** within sealed water-saturated sediments and trigger soft-sediment deformations (i.e., clastic injections).

5. Methods for identifying, describing, and interpreting soft –sediment deformation structures

5.1. Identifying soft-sediment deformation structures in ancient system

Recognizing soft-sediment deformation structures in ancient sedimentary system can be difficult as they can be incorporated into orogens, where superimposed tectonic structures are present (Waldron and Gagnon, 2011).

Welded contacts have been proposed by other workers as a criterion to recognize SSDs (Pickering, 1987). Welded contacts are contact surfaces between deformed and undeformed rocks that show no indication of grain breakage, fabric development, veining, or other post-lithification deformation. Such contacts are commonly interpreted as depositional. Another criterion providing a reliable identification of soft-sediment is the overprinting of deformation structures by **sedimentary or organic structures that show grain-by-grain mobilizations**. For examples, trace fossils, sediment-filled dykes or dewatering pipes that cross-cut folded or faulted structures (**Fig. 10A, C**).

Studies of the mechanical properties of clastic sediments and sedimentary rocks show that under most circumstances, sands are stronger than penecontemporaneously deposited shales. However,

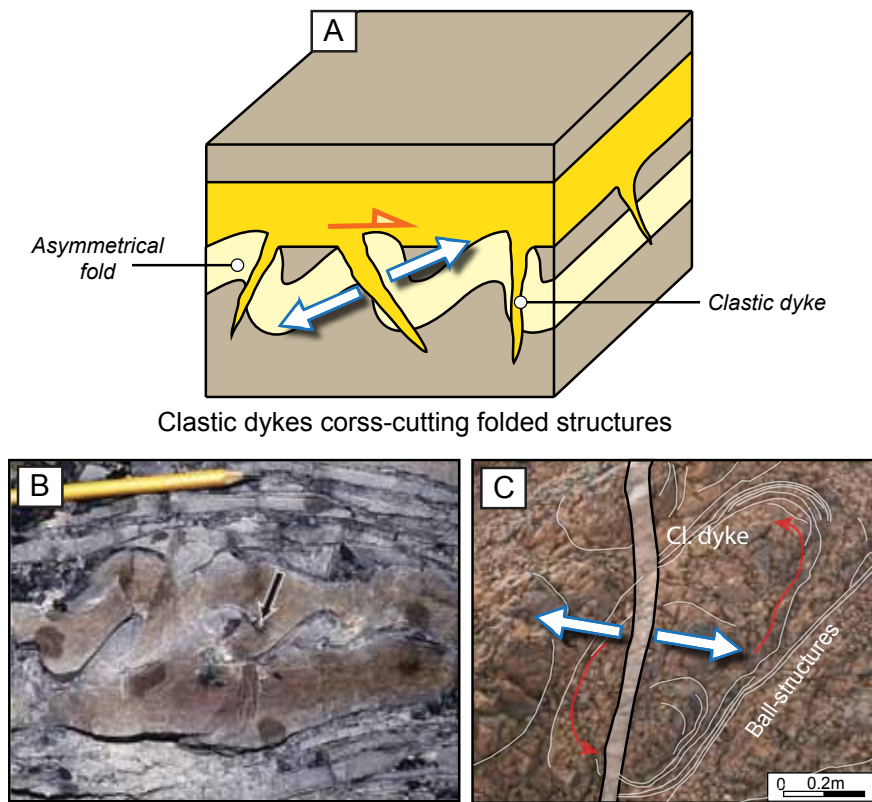


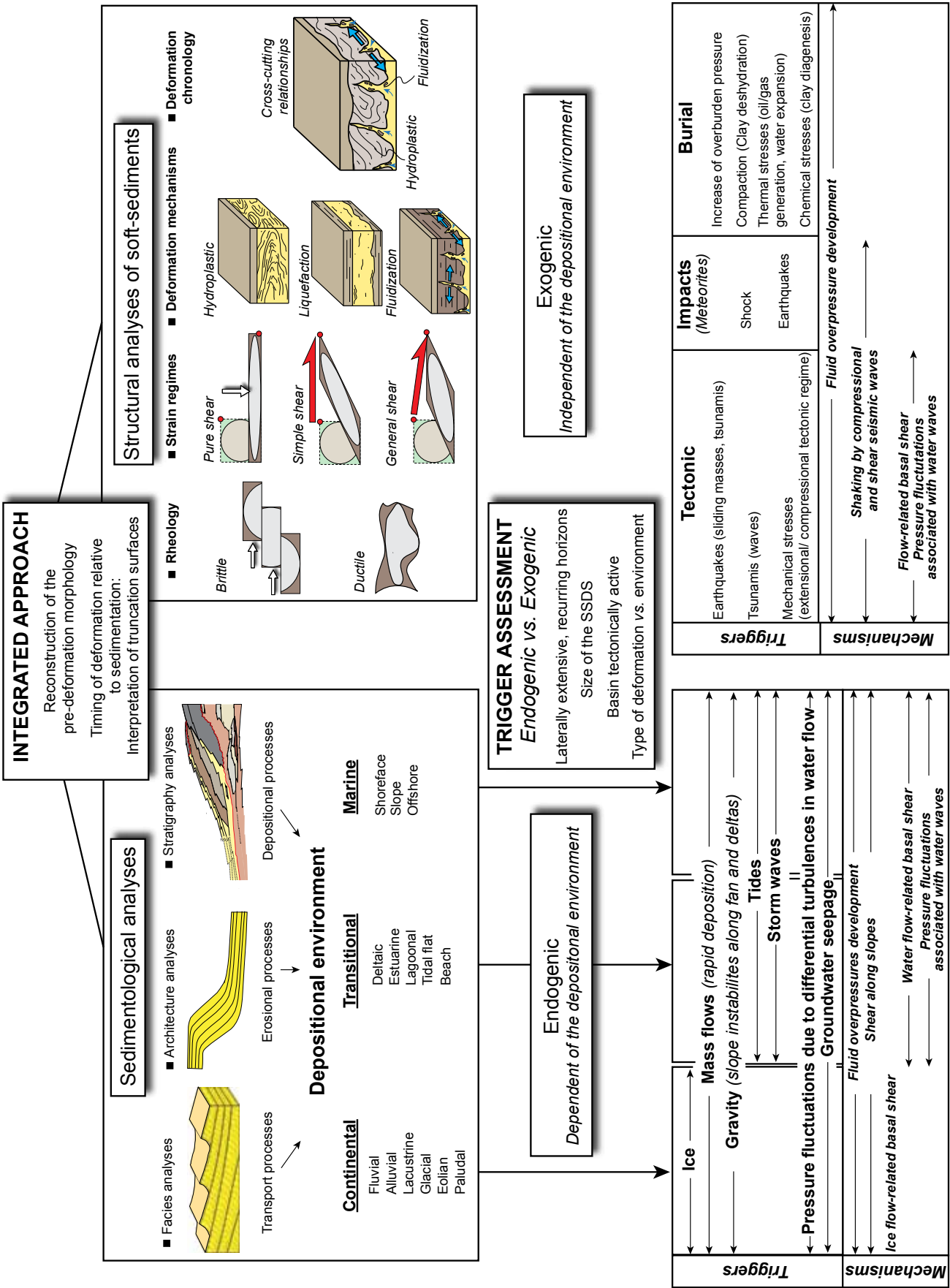
Figure 10. Representation of several criteria facilitating the recognition of soft-sediment deformation structures (A) A clastic dyke cross-cutting a folded structure suggests that folding affected unlithified sediments. (B) Folds in very thin mudstone beds between two thicker sandstone beds. Sandstone layers above and below the mudstone layer show thickening into the hinges of the folds, indicating that the sandstone was much less competent than the mudstone due to liquefaction during deformation (Nova Scotia, Late Palaeozoic)(Waldron, 2004). (C) A clastic dyke cross-cutting ball-structures indicates that ball-structures represent SSDs due to sediment liquefaction (Morocco, Ordovician).

liquefaction/fluidization can reverse this pattern by reducing effective strength of a granular sediment to near zero. This **strength reversal**, when it occurs, provides a relevant criterion for the recognition of soft-sediment structures (Waldron and Gagnon, 2011). The resulting structures notably include angular convex mudstone domains surrounded by concave sandstone domains within folds (**Fig. 10B**).

5.2. Methods to describe and interpret soft-sediment deformation structures

A method is proposed to describe/interpret soft-sediment deformation structures and to assess their triggers (**Fig. 11**). The first step of the method is to realize combined and detailed **sedimentological** and **structural** analyses.

A sedimentological analyze is required to reconstruct the pre-deformation morphology, to assess the timing of deformation relative to sedimentation by interpreting the truncation surfaces, and finally to determine the depositional environment. In parallel, soft-sediment deformation structures



must be analyzed to determine the **rheological behavior** of the sediments during deformation (brittle vs. ductile), the **strain regime** during deformation (pure shear, simple shear and general shear), and **mechanisms** involved during the deformation of ductile materials (hydroplastic, liquefaction, fluidization). **Cross-cutting relationships** must be established between the different structures to determine the relative deformation chronology. Once the depositional environment is constrained and the deformation structures described, the challenge is to determine the triggers responsible for the deformation of sediments. To assess if the trigger is either **endogenic** or **exogenic**, some other parameters must be studied. Indeed, the **lateral extension**, the **size** and the **recurrence** of deformation structures must be determined (**Fig. 11**). In addition, the **tectonic activity** of the sedimentary basin must be investigated. The analyses of deformation structures give information on the stress configuration and porewater pressure at time of deformation that must be compared to “classic” conditions occurring in the concerned depositional environment. These different parameters permit to differentiate exogenic triggers from endogenic triggers. For example, in a tectonically active basin, earthquakes (exogenic trigger) might be frequent resulting in laterally extensive deformations (e.g., seismites) that may be recurring within the sedimentary sequence.

Soft-sediment deformation structures in subglacial environments



Ice-bed coupling and bed deformation, Greenland. © JF Buoncristiani

1. Introduction

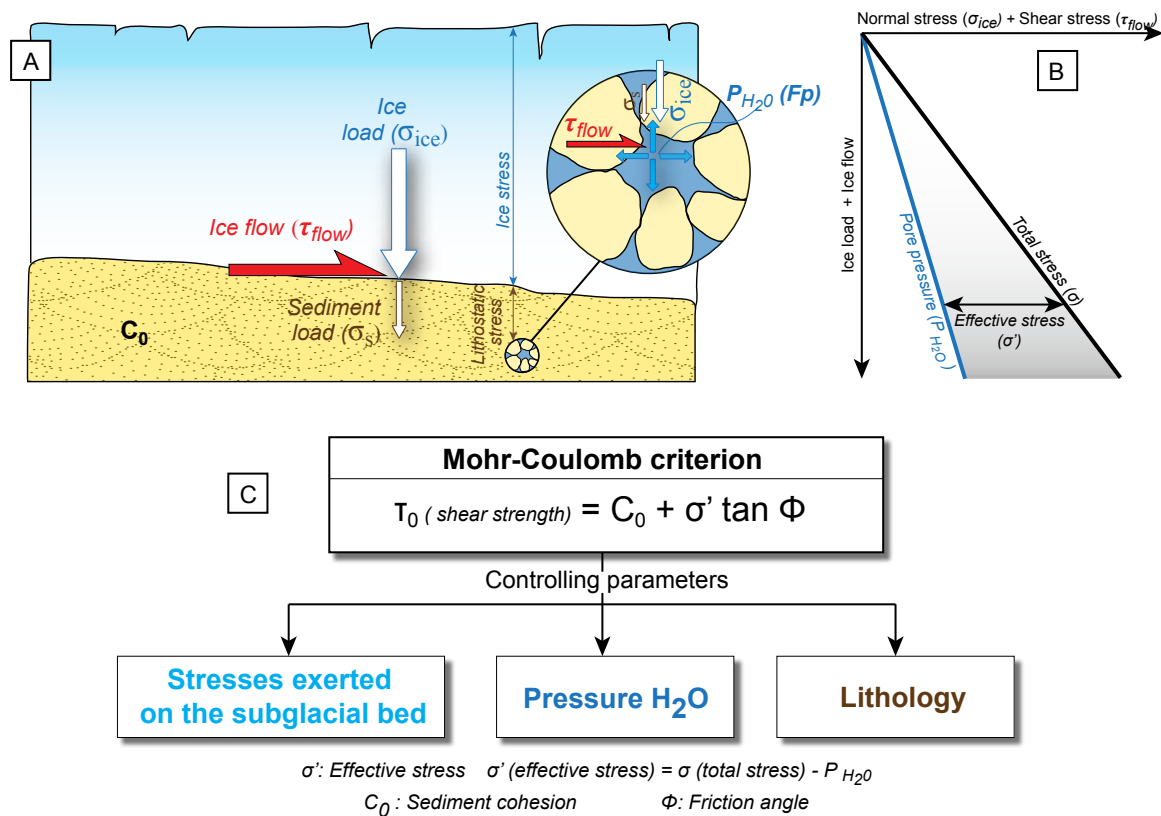
Some 10 % of the earth's land surface is currently covered by ice. During past glacier maxima (Neoproterozoic, Upper Ordovician, Permo-Carboniferous, Pleistocene), the glacier coverage has been considerably greater. Although glaciers frequently overly rigid bedrock, many glaciers lie or were lying on unlithified (i.e., soft) sediments, leading to the development of soft-sediment deformation structures. Soft-sediment deformation structures have been described at macro-scale for almost 90 years (Slater, 1926; Rotnicki, 1976; Boulton and Jones, 1979; Hart and Boulton, 1991; Benn and Evans, 1996; Lesemann et al., 2010), while the use of micromorphology in the description of soft-sediment deformations is much more recent (van der Meer, 1993; Menzies, 2000; 2012; Phillips et al., 2011). A glacial environment offers many opportunities of deformation, including deformation of the glacier bed, bulldozing of sediments at the ice sheet margins, ploughing of the sea floor by calving icebergs, or debris flow creeping down the glacier front for examples (Banham, 1977; van der Wateren et al., 1995; Boulton et al., 2001; Bennett, 2001; Winsemann, 2003; and many other authors). The different glacial environments are characterized by their own processes and mechanisms of soft-sediment deformations as well as their own types of deformation structures.

This review aims to present the **different type of structures formed in subglacial environments**. **Parameters controlling the deformation** in subglacial environments will be first presented. According to these parameters, a **theoretical subglacial distribution of stress/strain regimes** and **porewater pressure** conditions will be proposed. **Each subglacial deformation structures will be associated to a particular stress state and strain regime with a defined porewater pressure**. The different stress, strain, and porewater configurations will permit to use SSDs as a tool for precise **palaeoenvironmental reconstructions**.

2. Parameters controlling deformation in subglacial environments

Parameters controlling deformations of unlithified sediments in subglacial environments can be approached using the **Mohr Coulomb equation (Fig. 12)**. In the subglacial soft bed, the **basal**

Figure 12. (A) Diagram representing the different factors controlling the deformation of sediments in a subglacial environment, including the normal (σ_{ice}) and shear stress (τ_{flow}) (ice load and ice flow respectively), the porewater pressure (P_{H_2O}) and the sediment cohesion. (B) Schematic illustration of the Terzaghi equation in subglacial environments. (C) Mohr-coulomb criterion equation and first order parameters controlling the deformation of the subglacial bed.



shear strength (τ_0), also known as yield strength corresponds to the stress value at the onset of permanent deformation. The basal shear strength is controlled by the **sediment cohesion** (C_0), the **friction angle** (ϕ), and the **effective stress** (σ'). The sediment cohesion and frictional angle values required to calculate the shear strength indicate that lithologies influence soft-sediment deformations (**Table 1**). In addition, the effective stress (σ') plays a primordial role in establishing the basal shear strength of sediments. This necessity to include effective stress as a parameter controlling deformation indicates that **glacier dynamics** and **porewater pressure** (P_{H_2O}) (i.e., **fluid pressure** (F_p)) within the subglacial bed must be taken into account.

Material	Cohesion (C_0) (kPa)	Friction angle (Φ) (°)
Well-sorted sand	0	32-40
Poorly sorted sand	0	38-46
Well-sorted gravel	0	34-37
Poorly sorted gravel	0	45-48
Soft glacial clay	30-70	27-32
Stiff glacial clay	70-150	30-32
Till	150-250	32-35
Igneous rock	35000 - 55000	35-45

Table 1. Typical cohesion values and friction angles from some geologic materials (Selby, 1993)

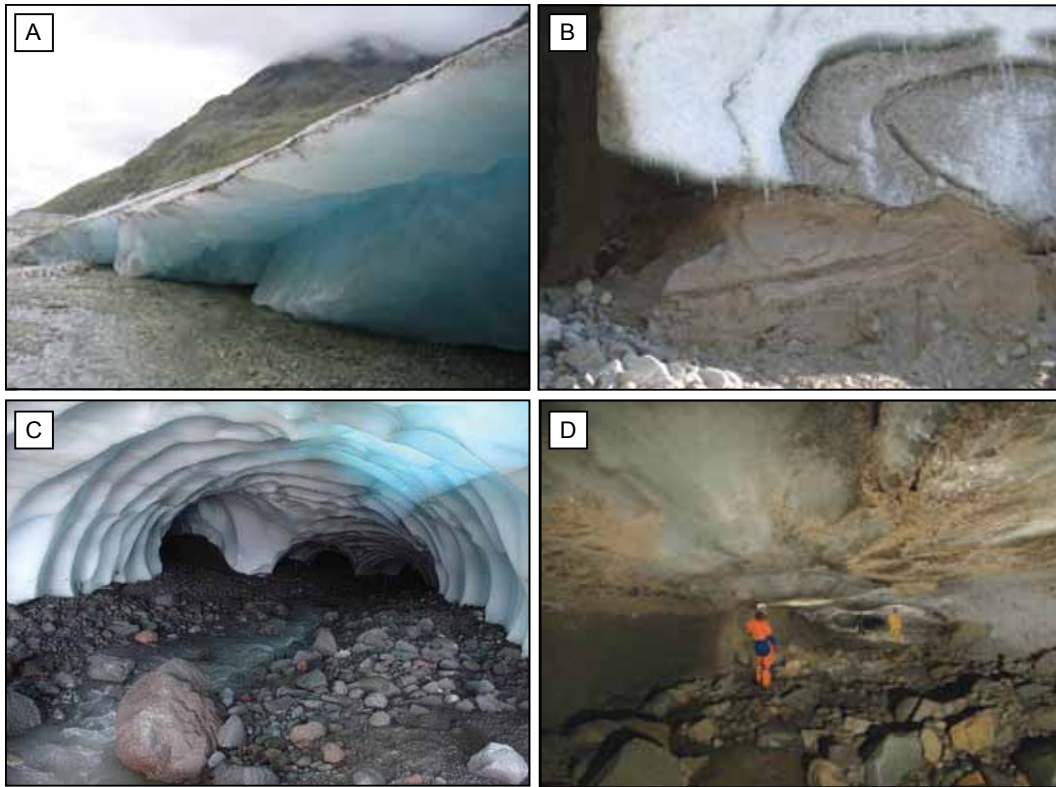


Figure 13. (A) Ice coupled to the bed (proglacial fluvial plain) (Switzerland) © JF Buoncristiani. (B) Ice coupled to the bed, deformation occurs at the base of the ice and within the subglacial bed (Greenland) © JF Buoncristiani. (C) Ice decoupled to the bed, development of a subglacial meltwater channel (Iceland)(geology.um.maine.edu). (D) Air-filled cavity beneath the Greenland ice sheet (nature.com).

2.1. Stresses in subglacial environments

In subglacial environments, the ice can either be **coupled** or **decoupled to the bed** (Fig. 13). During ice-bed coupling episodes, the **total stress** (σ_{total}) transmitted to the bed results from the combination of a **normal stress** acting perpendicular to the bed induced by the **ice load** (σ_{ice}), and a **shear stress** acting parallel to the bed surface exerted by the **ice flowing over the sediments** (τ_{flow}) (Fig. 12A). In subglacial environments, zones where ice is decoupled to its bed frequently occur (e.g., water films, water channels, subglacial lakes, air-filled cavities), implying that no stresses are transmitted to the bed, except the potential lithostatic load corresponding to the sediment pile (Fig. 13C, D).

Driving stresses at the base of the ice sheet can be approached by calculating the basal shear stress:

$$(3) \tau_b = \rho_i \cdot g \cdot H \cdot \tan \alpha$$

α : surface slope of the ice; g : gravitational constant; H : ice thickness; ρ_i : density of the ice.

The ice load, corresponding to the ice weight, is the vertical stress that is applied normal to the bed (σ_{ice}). The normal stress is function of **ice thickness** and has a direct influence on the basal shear stress (τ_b) exerted on sediments (Fig. 14A). Ice thickness is directly influenced by the **glacier mass**

Parameters controlling stresses exerted by the ice on subglacial sediments

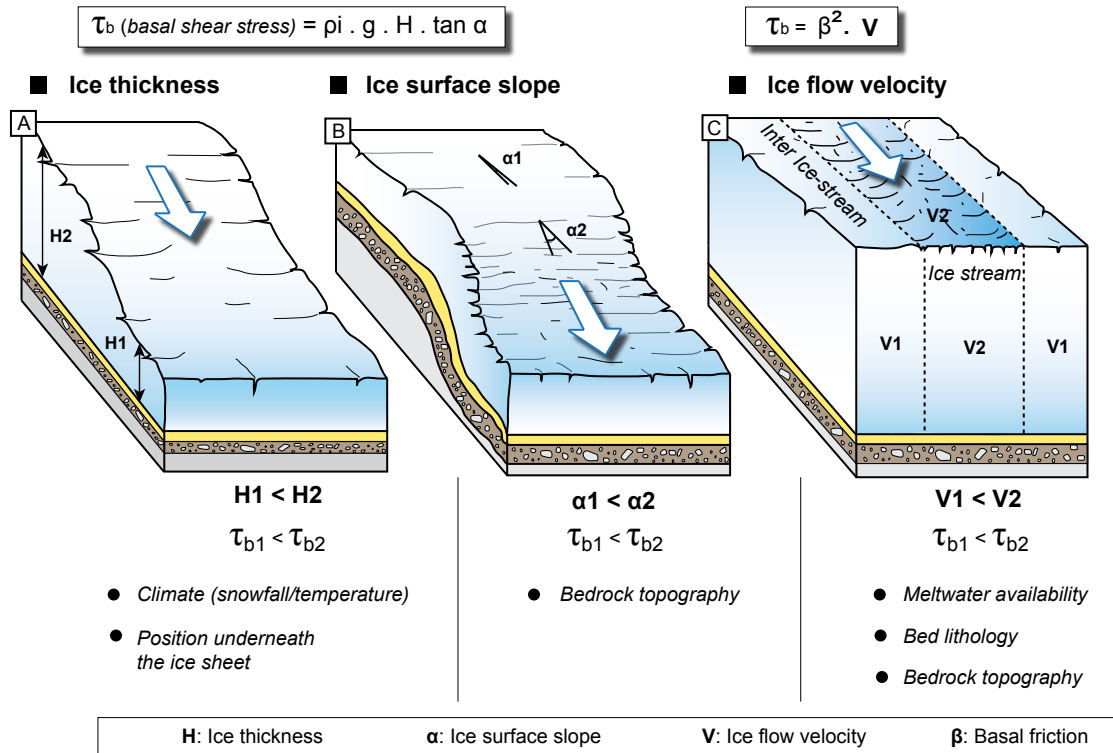


Figure 14. Schematic diagram illustrating the different parameters controlling the basal shear stress exerted by the ice on sediments during episodes of ice-bed coupling: (A) ice thickness, (B) ice surface slope, and (C) ice flow velocity.

balance that will lead to an increase or decrease of the ice thickness. This also implies that the basal shear stress will be higher in the inner part of an ice sheet than at the margin where ice thickness considerably decreases. When looking at equation (3), it also appears that the **ice surface slope** has an impact on the basal shear stress exerted on the bed, implying that bed topography will have an impact on the basal shear stress (**Fig. 14B**). In addition, **ice flow velocity** also influences considerably subglacial **shear stress values**. The contribution of the ice flow to the stress field is represented as an horizontal stress (τ_{flow}), acting parallel to the ice-bed interface. **The increase of ice flow speed is correlated with an increase of basal shear stress (τ_b)** (MacAyeal, 1992; Joughin, 2004) (**Fig. 14C**). Ice flow velocities are influenced by **bed topography**, and **meltwater availability** at the ice/bed interface or within the bed (porewater pressure).

2.2. Porewater pressure in subglacial environments

Porewater pressure (P_{H_2O}) (also referred to the fluid pressure (F_p)) has a considerable impact on processes of sediment deformation. The stress exerted by the porewater pressure is **isotropic** and reduce the total stress ($\sigma_{total} = \sigma_{ice} + \tau_{flow}$) exerted by the ice on sediments in every directions (**Fig.**

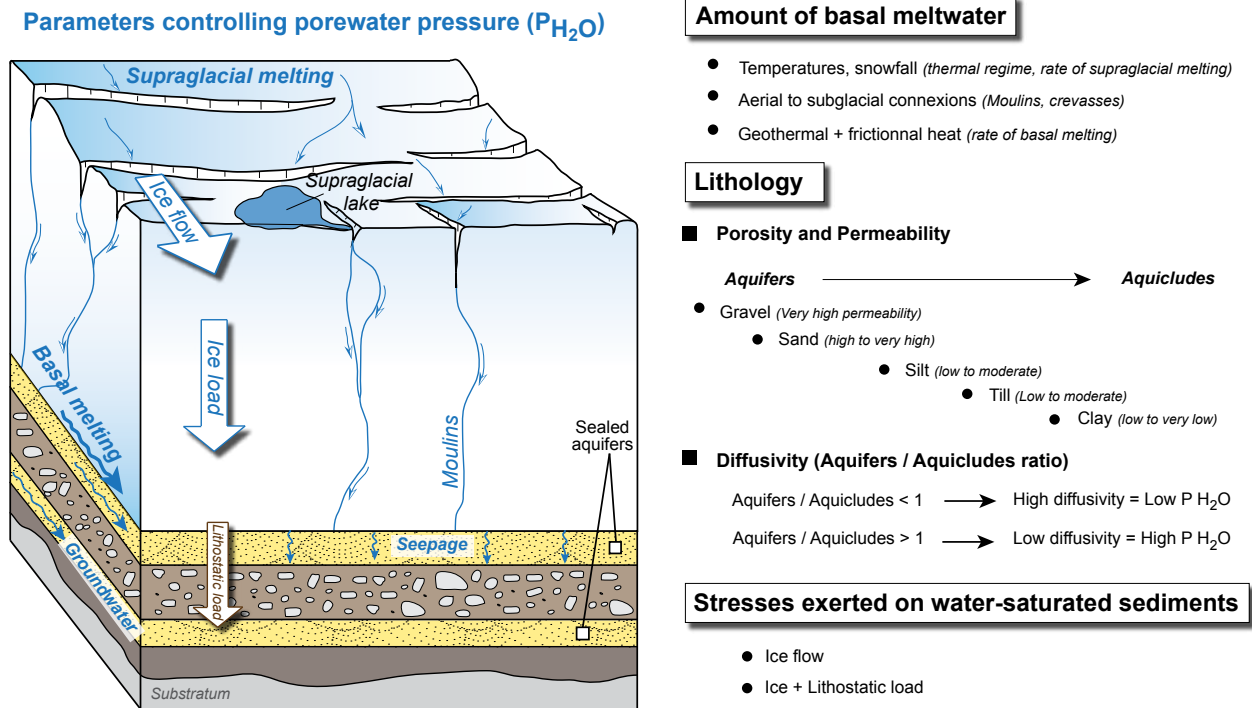


Figure 15. Schematic diagram illustrating the different parameters controlling the porewater pressure in sediments, beneath an ice sheet.

12). The increase of porewater pressure induces changes in the mechanisms controlling deformation, from brittle to ductile and from hydroplastic to fluidization. Porewater pressure in the subglacial bed is controlled by the amount of **basal meltwater**, the **lithology**, and the **stresses** exerted on the bed (**Fig. 15**). The amount of basal meltwater available depends on the **thermal regime of the ice sheet (wet-based vs. dry-based systems)** and is a function of variations of atmospheric temperatures. Temperatures control the rate of supraglacial meltwater production which in turns can be transmitted to the bed through moulins and crevasses (Zwally et al., 2002; Boon and Sharpe, 2003). At the base of the ice sheet, melting can also occur due to frictional heat, geothermal heat, or pressure melting. The produced meltwater can circulate at the ice-bed interface, can be transferred to the bed through infiltrations, or can be stored in subglacial lakes (**Fig. 15**).

Lithological characteristics of the subglacial bed considerably influence the porewater pressures. Porewater pressures will depend on the permeability of sediments as well as the stacking pattern of the subglacial sediments (Janszen et al., 2012; Clerc et al., submitted). The increase of porewater pressure within sediments implies that **high permeability sediments (aquifers)** must be sealed by **low-permeability sediments (aquicludes)** or alternatively by the ice (**Fig. 15**). Consequently, the evolution of the porewater pressure within the subglacial bed will highly depend on the **aquifers/ aquiclude ratio**. A ratio <1 will tend to promote meltwater diffusion, thus decreasing the porewater

pressure within the bed. In the other way, a ratio >1 implies an optimum configuration for the development of high porewater pressures as meltwater is entrapped between impermeable barriers and thus cannot escape (Clerc et al., submitted). This particular stratigraphical configuration promoting the development of overpressures has been referred to as the “layer-cake” configuration (Ravier et al., 2014b).

2.3. Lithology in glacial environments

The Mohr coulomb equation demonstrates that sediments, especially their **grain-size** characteristics and **sorting**, have a great influence on the style of deformation (**Fig. 12, Table 1**). Grain-size and sorting have a considerable impact on meltwater dynamics (i.e., porosity and permeability) within the soft bed and as a consequence an impact on the porewater pressure and deformation styles. A wide range of sediments characterized by different **grain-size**, **sorting**, **clay content** and **stacking pattern** can potentially be affected by glacial deformations, resulting in a various range of deformation structures (**Fig. 16**).

The clay content plays a major role in the deformation of sediments. Indeed, the increase of clay content will tend to change the rheology of the material during deformation (e.g., from brittle to ductile) but will also tend to decrease the permeability of sediments (Maltman, 1994). In addition, the influence of the sedimentary stacking pattern in the potential development of high porewater pressures have been demonstrated, especially the ratio of impermeable/permeable layers (**Fig. 15**) (Janszen et al., 2012; Clerc et al., submitted). **Subglacial**, **proglacial** or even **preglacial** soft sediments can experience deformation by overriding ice.

- **Unlithified preglacial bedrock** can be affected by subglacial deformations when, for example, an ice sheet advance over **unlithified or semi-lithified marine sediments** (Le Heron et al., 2005a). This notably occurred during the Ordovician glaciation in North Africa where a preglacial “layer-cake” composed of alternating sand and shale beds deposited in marine environments have been intensely deformed during ice sheet growth (Ravier et al., 2014b).
- Deformation can affect **sediments deposited subglacially (till or sorted sediments)** when the subglacial deposition of sediments is followed by episodes of ice recoupling with the bed (Lesemann et al., 2010; Menzies and Ellwanger, 2011; Reinardy et al., 2011).
- At last, subglacial deformation can also be recorded within **sediments deposited in a proglacial**

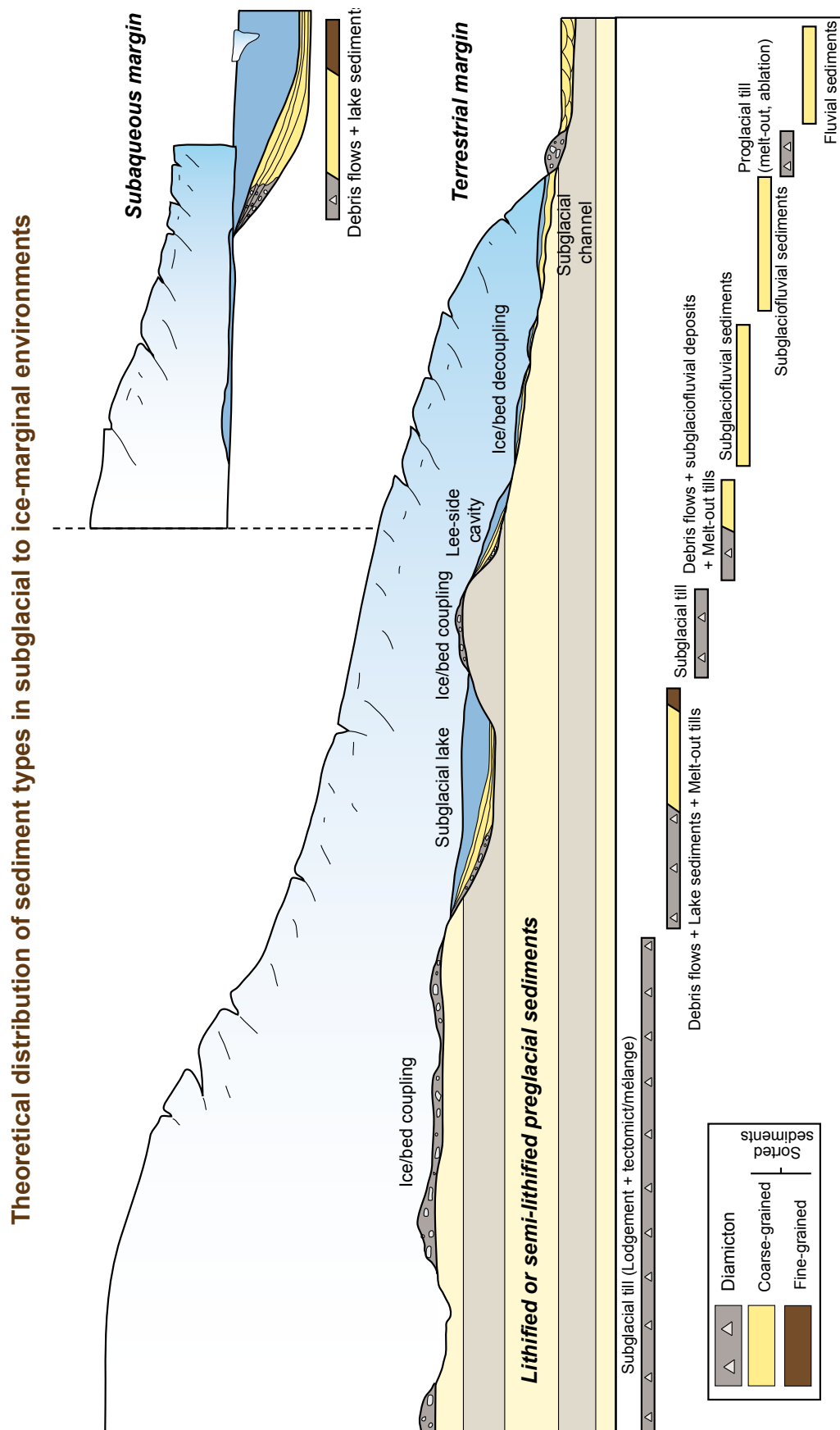


Figure 16. Characteristics of sedimentation in subglacial and proglacial environments, and theoretical distribution of sediment types (diamicton vs. sorted sediments) along an ice sheet profile.

environment when sedimentation is followed by episodes of ice advance (Roberts et al., 2009; Waller et al., 2011).

In subglacial environments, **diamicton** and **sorted sediments** with various grain-size can be deposited (from clay to gravel). Diamicton containing clays to boulder-size clasts can deposit during episodes of ice-bed coupling (lodgement till) but also during episodes of ice bed decoupling, within subglacial lakes or cavities (debris flows, hyperconcentrated flows, melt-out tills) (Evans et al., 2006; Livingstone et al., 2012). Although the deposition of sorted sediments are often ascribed to proglacial environments, sorted sediments can also be deposited subglacially (Munro-Stasiuk, 2000; Lesemann et al., 2010; Clerc et al., 2012). Deposition of sorted sediments can occur within subglacial lakes and cavities (Livingstone et al., 2012) (**Fig. 16**). When the meltwater pressure is higher than the ice weight, ice-bed decoupling occurs, thus permitting a subglaciofluvial system to develop and sorted sediments to deposit (Lesemann et al., 2010). In marginal settings, large subglacial channels (N- or R-channels) develop allowing a considerable amount of sorted sediments to be deposited (eskers) (Brennand, 2000) (**Fig. 16**).

During episodes of ice readvances, deformation of sediments triggered by overriding ice are common and can affect proglacial sediments (Thomas and Chiverrell, 2007). Diamiction deposits are common in proglacial settings, particularly at the proximity of ice sheet margin (**Fig. 16**). Diamicton resulting from ice melting at the margin in either subaqueous settings or terrestrial settings (ablation till and melt-out tills) are frequently concerned by deformations induced by ice-bed interactions (Evans et al., 2006). In subaqueous environments, debris flow or hyperconcentrated flows deposited in the vicinity of the grounding line produce diamicton that can also be latter deformed during ice readvance. In both terrestrial and subaqueous settings, sorted sediments are deposited within subaqueous fans and within proglacial alluvial plains (**Fig. 16**).

The exceptional **variation in deformation structures** found in glacial environments is notably due to the **wide range of sediment types and stratigraphical pattern** affected by deformation.

3. Theoretical subglacial distribution of stresses and porewater pressures

3.1. Theoretical longitudinal distribution

Within an ice sheet, **ice thickness**, **ice flow** and **meltwater availability** vary laterally and

longitudinally. However, an ice sheet can be theoretically divided into three principal domains where subglacial conditions are different: the **ice dome area**, the **intermediate area** and the **marginal area** (Kleman and Borgström, 1996).

- *Ice dome area:*

A first domain corresponds to the ice dome area in the inner part of the ice sheet. This area situated below the accumulation zone is generally characterized by **cold-based conditions** and a **dry-based system**, implying an absence of meltwater at the base of the ice sheet (Dyke, 1993) (**Fig. 17**). Within the ice dome area, **ice flow is null or very slow** and the **ice pile is at its thickest**. Subglacial conditions in this zone are characterized by a **high normal stress component** (σ_{ice}) induced by the significant ice load. The stagnant to slow-moving ice and the absence of basal sliding induces a weak or even **null shear stress component** (τ_{flow}) acting parallel to the subglacial bed. The very low meltwater content available beneath the ice implies **low porewater pressure**. The plausible stress and porewater pressure configuration indicates that deformation structures within sediments principally form in response to **brittle deformation** controlled by **pure shear strain**.

- *Intermediate area*

The intermediate area is located beyond the equilibrium line and implies a switch in the subglacial hydrological system from a dry-bed system to a **wet-bed system** (Kleman and Borgström, 1996) (**Fig. 17**). This also implies **basal sliding** at the ice-bed interface. Within the intermediate area, the complexity of glacier dynamics induces that the stress fields and the meltwater availability can highly vary. Two main configurations can be envisaged when ice is coupled to the bed. The first one is related to moderate ice flow associated with elevated ice thickness and could be envisaged in the inner part of the intermediate zone. In this configuration, **the normal stress** (σ_{ice}) **is high** while the **shear stress** (τ_{flow}) **is moderate** implying that deformation is controlled by **general shear** with a higher contribution of pure shear stress (PS) (i.e., **PS > SS**). Alternatively, closer to the margin (or within ice stream pathways), ice thickness decreases while ice flow velocity increases resulting in deformations structures influenced by **general shear** with a simple shear stress being predominant (i.e., **SS > PS**). In the intermediate area, meltwater availability and porewater pressures within the bed can be highly variable, illustrating that all deformation mechanisms including **brittle** and **ductile** (including hydroplastic, liquefaction and fluidization) deformation must be considered.

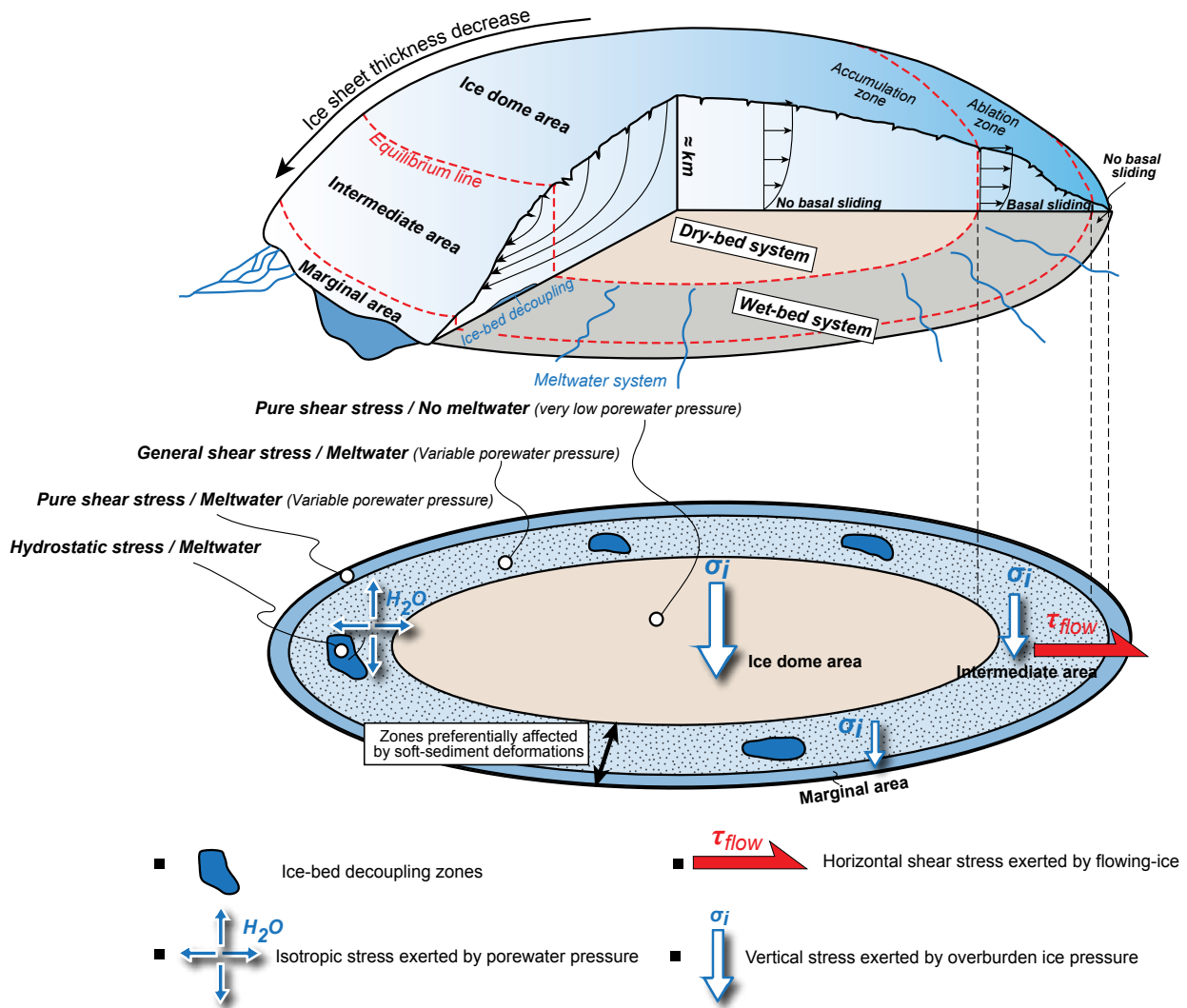


Figure 17. Schematic illustration of the three distinct zones (ice dome, intermediate, marginal) along an ice sheet profile, defined according to variations in ice flow, ice load and meltwater characteristics. (Significantly modified after Kleman and Borgström, 1996)

Locally, when porewater pressures within the bed become superior to the total stress exerted by the overlying ice mass, **ice-bed decoupling** can occur. In this configuration, sediments are subject to an **isotropic stress field related to the hydrostatic stress** (Fig. 17). The porewater pressure required to overcome the ice overburden pressure induces that sediments are in a **fluidized state** during deformation.

• Marginal area

In the marginal zone, considering a terrestrial ice front, **ice flow velocity** decreases until becoming **null** and **ice thickness** is considerably **reduced**. In this configuration, sediment deformation is controlled by stresses exerted by the **ice load** exerted on sediments (σ_{ice}) implying that deformation structures are governed by **pure shear strain regimes**. When ice sheet terminates in water, the ice

keeps flowing implying that general shear stresses governs sediment deformation in marginal zones. Porewater pressure are variables and every deformation mechanisms must be expected (e.g., **brittle and ductile**).

3.2. Theoretical transverse distribution

Although the ice dome and the marginal areas are rather stables across the ice sheet in terms of stresses (i.e., Stagnant ice), the intermediate area is subject to high lateral variations of subglacial stresses over short time scales (10^1 - 10^3 ka) (Kleman and Glasser, 2007).

These variations result in a very **heterogenous distribution of ice flow velocities** that can laterally shift through time, thus influencing the basal shear stress transmitted to the bed.

In an ice sheet, four major ice-dynamical components can be laterally distinguished: **ice streams, ice stream tributaries, sheet flows and frozen bed patches (Fig. 18A, B)**. These different components are characterized by different ice flow velocities. Ice stream networks represent narrow zones fast flowing-ice in ice sheets that are otherwise dominated by slow sheet flows (Bennett, 2003). Typically ice stream velocities are up to two orders of magnitude faster than the surrounding sheet flows (**Fig. 17B**). Tributaries to ice streams flow display intermediate ice flow velocities between ice streams and sheet flows (Hulbe et al., 2000) (**Fig. 17B**). Frozen-bed patches correspond to localized areas where the ice flow is close to be null and have been identified under inter-stream ridges of the Antarctic ice sheet (Rose, 1979; Vogel et al., 2003; Engelhardt, 2004) (**Fig. 17B**). These different elements and associated flow velocities characteristics induce a **high transversal variations in the shear stress (τ_{flow})** transmitted parallel to the bed. (**Fig. 17C**). Due to very dynamic changes beneath ice sheets, basal conditions including basal shear stress can highly evolve through time and space (Habermann et al., 2013).

The spatial and temporal variations of thermal bed regime below the ice sheet, **oscillating between cold-based and wet-based**, greatly influence the availability of **meltwater**, the **distribution of sediments**, and the **development of SSDs** (Eyles and Miall, 1984; Menzies, 1989; Hicock, 1990). As a consequence, the thermal bed regime accounts for the high lateral variations in flow velocities and porewater pressures which may also create high lateral variations in subglacial shear stress values (Piotrowski and Kraus, 1997; Piotrowski et al., 2004). At shorter time scales, variations in ice flow velocities can occur due to **daily** or **seasonal** variations in meltwater production and passage beneath

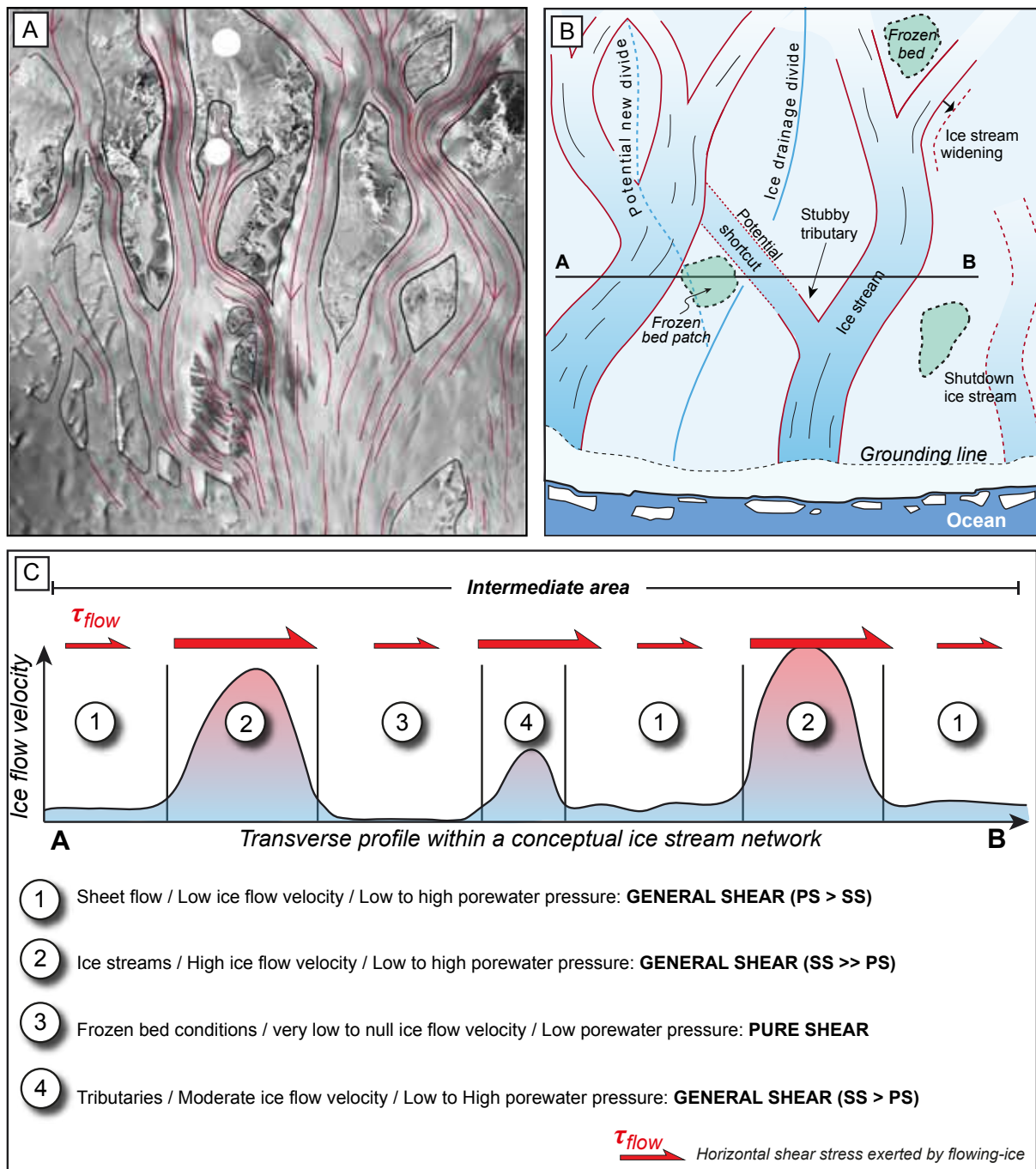


Figure 18. Illustration of the transverse variations of ice flow velocities and subglacial shear stresses within an ice sheet. (A) Ice surface radar imagery in East Antarctica showing the pattern of ice stream distribution and the resulting lateral variations in ice flow velocities. (from Kleman and Glasser, 2007). (B) Conceptual model of an ice stream web, and the different ice-dynamical components: ice stream, tributaries, sheet flow, and frozen bed patches. (Modified after Kleman and Glasser, 2007). (C) Theoretical transverse profile showing the lateral evolution of ice flow velocities and shear stresses within an ice sheet. See position of the A-B profile in Figure 17B.

the ice (Tulaczyk, 1999; Zwally et al., 2002; Mair et al., 2003; Joughin et al., 2008; Bartholomew et al., 2011; Bartholomew et al., 2012), implying **cyclic** and **short-term variations in basal shear stress** transmitted to soft sediments. Such seasonal variations have been evidenced in repetitive sequences of soft-sediment deformations recorded within sediments below the Irish Sea Ice Sheet (Ravier et al., 2014a).

4. Terminology and methods used to classify subglacial soft-sediment deformation structures

4.1. Comparisons between subglacially deformed sediments and mylonites

Soft-sediment deformation structures in subglacial environments have been subject to many studies, however terms used to describe structures are numerous and variable between the different works. At the micro-scale, micromorphologists preferentially used the **soil science terminology** to describe deformation structures in subglacial sediments (van der Meer, 1993; Carr, 2004; Menzies, 2006). Other studies tried to characterize deformation structures using the **structural geology terminology** (van der Wateren, 1999; van der Wateren et al., 1995, 2000; Denis et al., 2010; Phillips et al., 2011).

The morphology of deformation structures found at both micro and macro-scale in subglacially deformed sediments are similar to structures developed within **polydeformed metamorphic and mylonitic rocks (Figs. 19 and 20)**. Slater (1926) and Banham (1975, 1977), were among the first to recognize the similarities between the deformation structures present in glacial sediments and those in deformed metamorphic rocks. In both cases, deformation are similar and principally controlled by **shear within ductile shear zones**, implying that structures represent good **kinematic and strain indicators** for assessing shear orientations and shear strain values. Structures are comparable although strains involved in the deformation of metamorphic rocks and mylonitic rocks are significantly higher than those in subglacially deformed sediments (Iverson et al., 1996; van der Wateren et al., 2000; Thomson and Iverson, 2006). These typical deformations occur in glacial environments under much lower values of cumulative strain due to high porewater pressure in water-saturated sediments. In metamorphic rocks, new minerals or grain growths are common due to prolonged periods of elevated temperature and pressure while absent in glacial sediments due to different strain values and temperatures. In **subglacial and metamorphic shear zones, porewater pressure and temperature** variations are respectively parameters controlling the mechanisms involved in ductile deformations. Although differences between subglacial environments and cataclastic faults rocks or mylonites subsist, their kinematic and geometric similarities could justify the use of a common descriptive terminology with structural geology (van der Wateren et al., 2000). Indeed, a single terminology will considerably simplify the description and the classification of glacially deformed sediments at both micro- and macroscale. In the classification of subglacial deformation structures (section 5), the

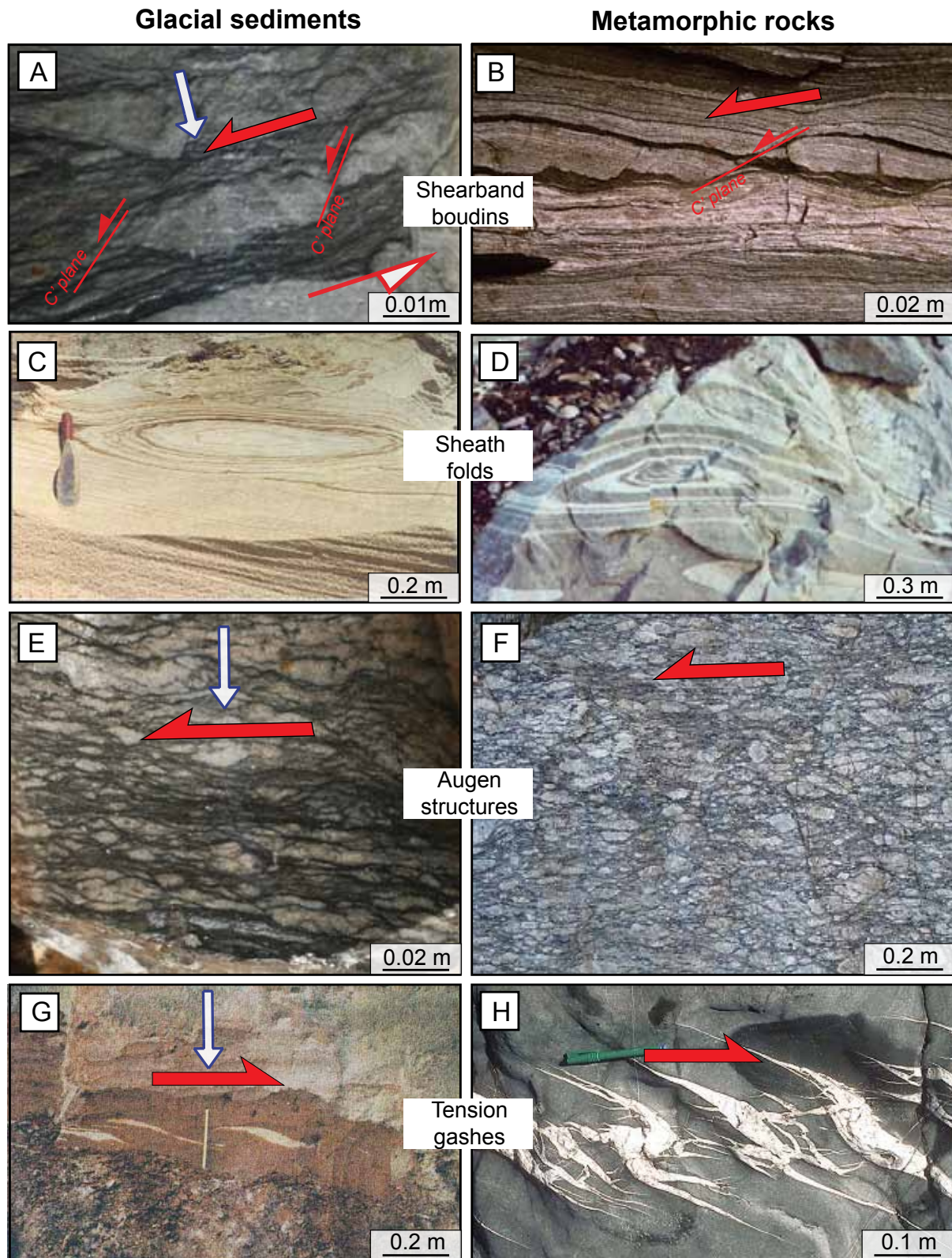


Figure 19. Illustration of the similarities between deformation occurring in subglacial sediments and in metamorphic zones at the macro-scale. (A) General shear (Simple Shear > Pure shear). Asymmetrical boudins in subglacial sediments (Algeria, Ordovician) referred to as shearband boudins in structural geology and the equivalent structures found in mylonites (B) (www.geol.ucsb.edu). (C) General shear (Simple shear > Pure shear). Sheath folds found in pleistocene soft-sediments (Denmark, Lesemann et al., 2010) and a comparable structure formed in metamorphic rock (D) (bio-geo-terms.blogspot.com). (E) General shear (Pure shear > Simple shear). Slightly asymmetrical and flattened boudinage observed in glacial sediments (Algeria, Ordovician) and the analogous structures observed in metamorphic zones (F) (geocaching.com). (G) Tension gashes formed as a response of basal shear in Pleistocene subglacial sediments (Netherlands, van der Meer et al., 2006) and the equivalent structures formed in metamorphic rocks (H) (see.leeds.ac.uk). Note that the size of the red arrows is function of the shear stress component.

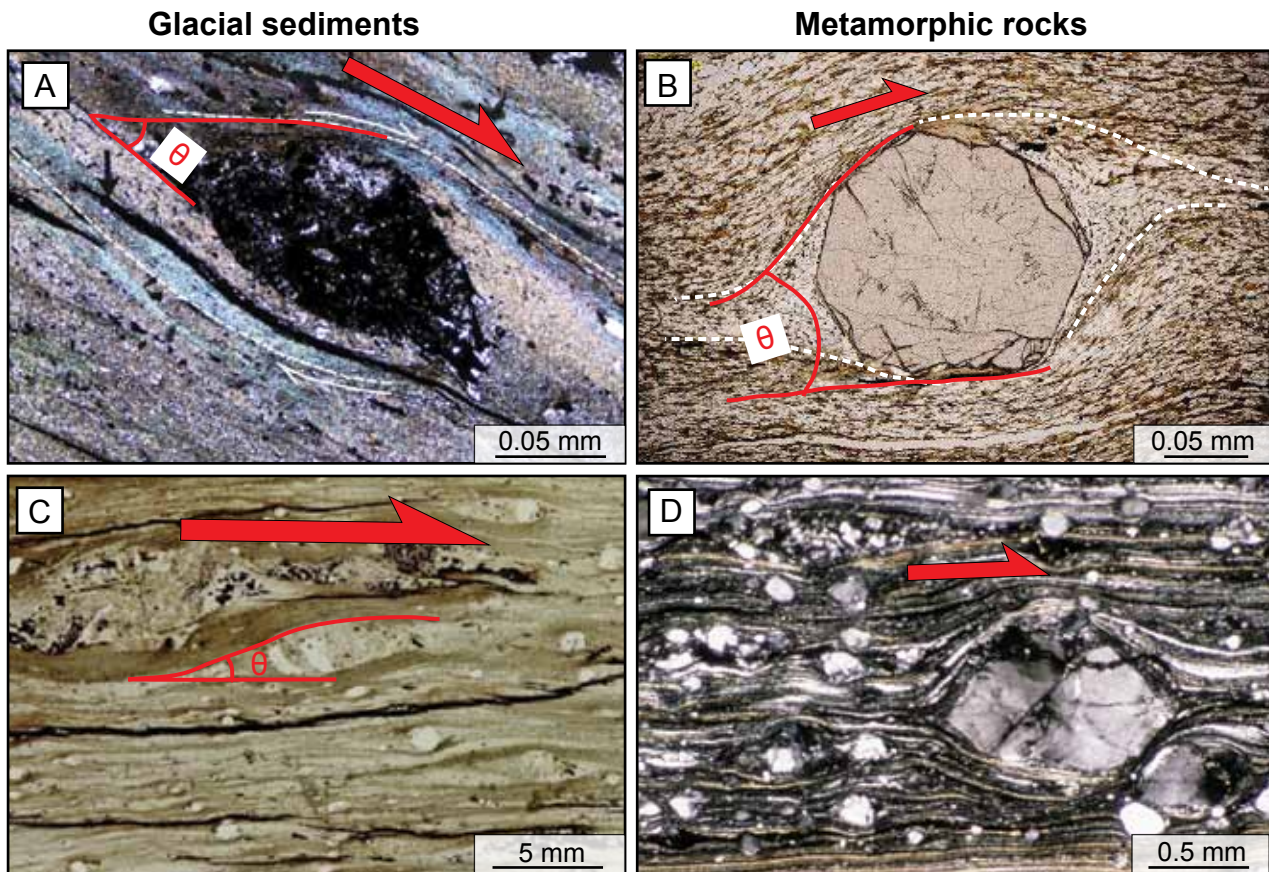


Figure 20. Illustration of the similarities between deformation occurring in subglacial sediments and metamorphic zones at the micro-scale. (A) General shear (Simple shear > Pure shear). Strain shadows (or pressure shadows) observed around grains in subglacial sediments (Namibia, Neoproterozoic, Busfield and Le Heron, 2013) and metamorphic zones (www2.geo.ua.edu) (B). (C) (Simple shear > Pure shear). Boudins structures at the micro-scale within subglacial sediments (Namibia, Neoproterozoic, Busfield and Le Heron, 2013) and metamorphic rocks (ged.rwth-aachen.de) (D). Note that the size of the red arrows is function of the shear stress component.

description and interpretation of the different structures will be realized using the structural geology terminology (cf. Maltman 1994; Passchier and Trouw, 2005; or Fossen, 2010 for further details on the terminology and basic concepts).

4.2. A new method to classify and interpret subglacial SSDs based on structural geology

The classification of soft-sediment deformation structures will be based on the theoretical distribution of **porewater pressure** and **strain regimes** beneath the ice (**Fig. 17**).

The strain regimes vary longitudinally and transversely along an ice sheet profile according to fluctuations in the **ice load induced-normal stress** (σ_{ice}) and the **ice flow velocity induced-shear stress** (τ_{flow}). The relative contribution of ice load and ice flow stresses during deformation of the sediments will lead to different strain regimes:

- **Pure shear** occurs when the deformation is solely driven by the vertical stress exerted by the ice

load.

- **Simple shear** strain does not occur in subglacial environments as the ice load exerts a vertical stress on sediments during deformation.

- **General shear strain** is certainly the most dominant style of deformation in subglacial environments. General shear represents a **combination of pure shear simple strain**, called general shear . The variable contribution of the ice load and the ice flow during deformation induced by general shear implies that two strain regime must be considered:

- **General shear (pure shear > simple shear)**: the vertical stress exerted by the ice load is dominant.

- **General shear (simple shear > pure shear)**: the horizontal basal shear stress exerted by the ice flow is dominant.

In total, three stress configurations occur in subglacial environment (**Table 2**).

Variables controlling the type of deformation structure in subglacial environments	
Stresses	Porewater pressure
<ul style="list-style-type: none"> ■ Pure shear ■ General shear (<i>Pure shear > Simple shear</i>) ■ General shear (<i>Simple shear > Pure shear</i>) 	<ul style="list-style-type: none"> ■ Very low porewater pressure (<i>brittle</i>) ■ Moderate to high porewater pressure (<i>hydroplastic/liquefaction</i>) ■ Very high porewater pressure (<i>liquefaction/fluidisation</i>)

Table 2. List of the main variables controlling subglacial deformation structures.

Along the ice-sheet profile, the meltwater content at the base of the ice is highly variable. These variations influence the porewater pressure within the subglacial soft bed, and therefore control the type of deformation mechanisms.

In this classification, three ranges of porewater pressure values are proposed (**Table 2**). These different ranges of porewater pressure are function of the changes of rheological behaviors and the deformation mechanisms they will induce when sediments are stressed beyond their shear strength.

- **Very low porewater pressure**: When stressed under very low porewater pressures, **brittle deformation structures** will preferentially form in sediments.

- **Moderate to high porewater pressure**: The increase of porewater pressure will tend to promote the formation of **hydroplastic to liquefaction-type deformation structures**.

- **Very high porewater pressure**: The considerable increase of porewater pressure will trigger **liquefaction to fluidization** of the subglacial sediments.

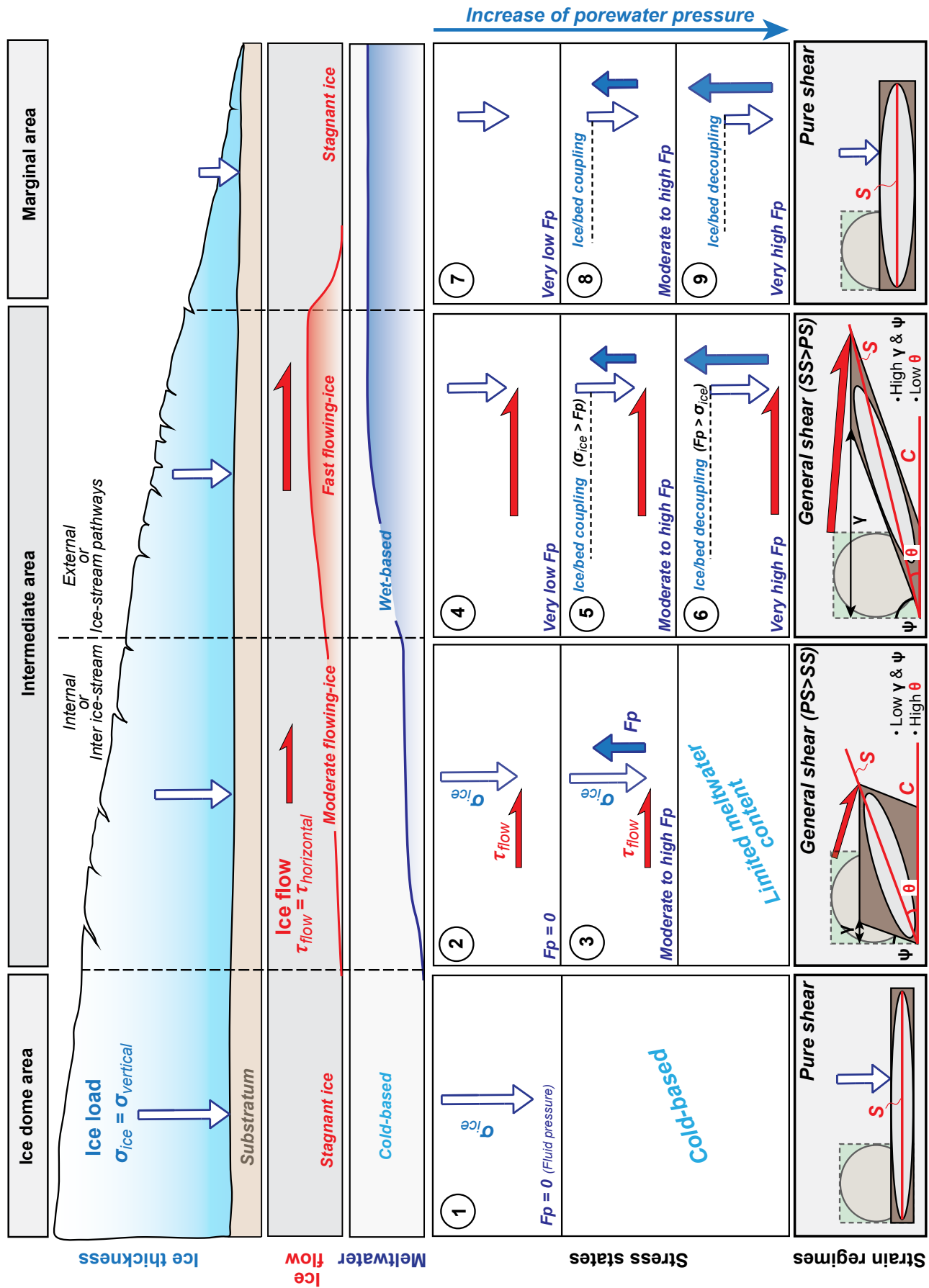


Figure 21. Schematic diagram illustrating the variations of ice thickness, ice flow, and meltwater along a theoretical ice sheet profile. Stress states and corresponding strain regimes are replaced beneath the profile.

The variations of the three controlling parameters beneath the ice can be represented using **three stress vectors**: the **ice load** (σ_{ice}), the **ice flow** (τ_{flow}), and the **fluid pressure** (F_p). Lengths of the stress are functions of the estimated values of these different parameters.

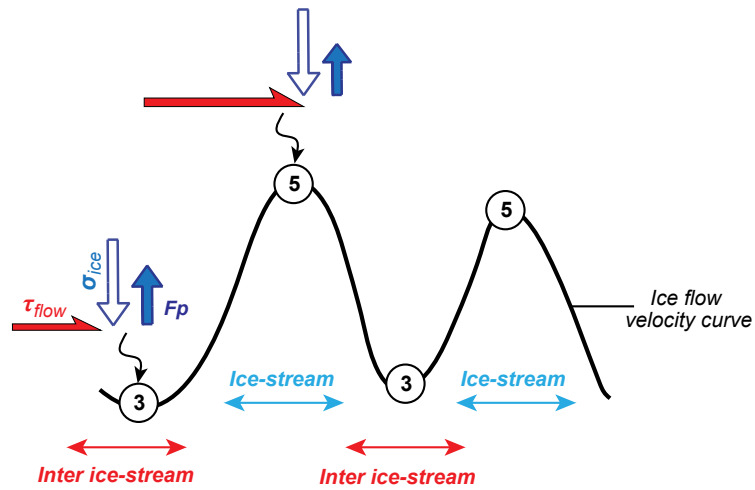
The different subglacial zones, characterized by different ice-dynamical and meltwater characteristics, determined in section 3 (cf. Figs. 17, 18), allow to define **nine stress configurations** (Fig. 21). The nine stress configurations lead to **three different strain regimes**: **pure shear**, **general shear (pure shear > simple shear)** and **general shear (simple shear > pure shear)** (Fig. 21). When ice load-induced normal stress is higher than the fluid pressure, deformation related to **ice-bed coupling** occurs (Stress states 1, 2, 3, 4, 5, 7 and 8). However when the contribution of fluid pressure becomes higher than the normal stress, **ice-bed decoupling** occurs (Stress states 6 and 8).

Although the stress states and their associated strain regimes are described along a longitudinal ice sheet profile, they can also vary transversely and through time. These variations result from geographical and temporal fluctuations in ice flow velocities and porewater pressures (Fig. 22). In **Figure 17**, the different values of basal shear stress transmitted to the bed, in an between ice streams, have been illustrated (Joughin, 2004; Kleman and Glasser, 2004). These lead to lateral changes of stress states during deformation of the sediments (Fig. 22A).

Cyclic changes of porewater pressure in the substratum have also been evidenced in the sedimentary record (Denis et al., 2010; Lesemann et al., 2010; Ravier et al., 2014a). These cycles are highly related to meltwater production and can be annual or longer-lived when related to a phase of deglaciation. They also control the evolution of the stress configuration through time (Fig. 22B).

A

An example of transverse stress states sequence
(Ice flow velocities variations)



B

An example of temporal stress states sequence
(porewater pressure variations)

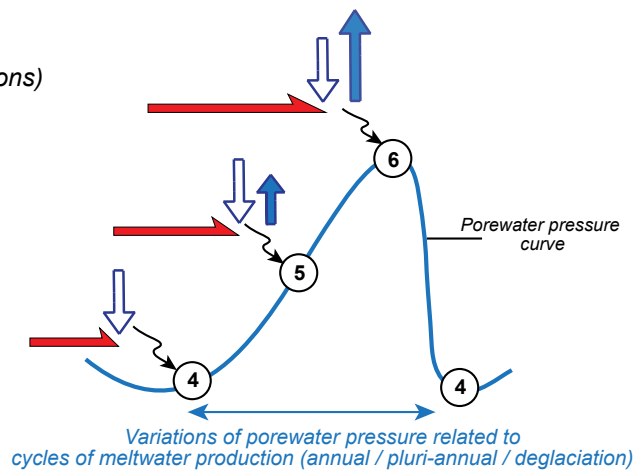


Figure 22. Schematic diagram illustrating the geographical and temporal evolution of stress states according to changes in ice flow velocities (A), and porewater pressures (B).

5. Classification of soft-sediment deformation structures

Soft-sediment deformation structures observed in subglacial environments can be classified using the theoretical distribution of stress states beneath the ice defined earlier (**Fig. 21**). The different processes of sediment deformation controlled by variations of **fluid pressure (F_p)**, including **brittle**, **hydroplastic** and **liquefaction/ fluidization**, will be successively presented. For each stress state corresponds a strain regime, including **pure shear** and **general shear strain (Pure Shear > Simple Shear; Simple Shear > Pure Shear)**. Deformation structures observed at both **macro-and micro-scale** are described thereafter.

5.1. Brittle deformation structures

Cohesionless sediments that are not entirely water-saturated, or alternatively sediments that contain frozen porewater (Kleman and Hättestrand, 1999) preferentially form brittle deformation when stresses exceeds the yield strength of sediments (Maltman, 1994).

5.1.1. Ice-bed coupling structures

First, structures that are directly the result of ice-bed interactions will be presented. Ice-bed coupling episodes imply that **the fluid pressure (F_p)** is lower than the **ice load (σ_{ice})** (**Fig. 21**). The structures will vary according to changes in stress states induced by changes in glaciodynamics (ice flow + ice load).

□ Pure-shear induced deformation structures (**Stress states 1 and 7**)

In case of stagnant to slow flowing-ice that is coupled to cohesionless sediments with low porewater pressure and clay content or alternatively to frozen sediments, the predominant vertical stress (σ_{ice}) leads to a pure shear strain regime, and a brittle rheological behavior.

- **Radial step normal faults** also referred as radial extensional normal microfaults are typical deformation structures illustrating ice-bed coupling conditions (Biju-Duval et al., 1974; Denis et al., 2010; Clerc et al., 2013) (**Fig. 23A, B**). These structures illustrate extensional radial deformation triggered by the ice load (σ_{ice}). These faults generally display mm to cm-scale offset along fault

planes that are generally high angle (50° - 80°). Surfaces displaying radial step normal faults can occur over quite extensive areas (100's m^2) (Biju-Duval et al., 1974). Radial step normal faults have been ascribed to subglacial deformation underneath ancient ice sheet, in Niger, Morocco, Algeria and Lybia (Ordovician) (Biju-Duval et al., 1974; Denis et al., 2010; Clerc et al., 2013) and Ireland (Pleistocene) (Ravier et al., 2014a). Radial step normal faults with undulating fault planes can also occur, indicating a slight increase in porewater pressure responsible for the development of “hydroplastic” step normal faults (Clerc et al., 2013).

• **Dihedral conjugate normal faults** or fractures occur in subglacial sediments as a response of pure-shear induced deformation, and are recognized as sets of normal faults characterized by moderate to steeply dipping conjugate pairs (**Fig. 23C, D, E**). Such structures are similar to compactional shear bands which frequently occur within sediments when the increase of the confining pressure induced by the vertical lithostatic stress triggers sediment failure (Fossen et al., 2007). In a glacial context, these faults can be interpreted as structures induced by lateral extension associated with a predominant vertical stress exerted on sediments by the ice weight (σ_{ice}) (McCarroll and Rijdsdijk, 2003; Flemming et al., 2012).

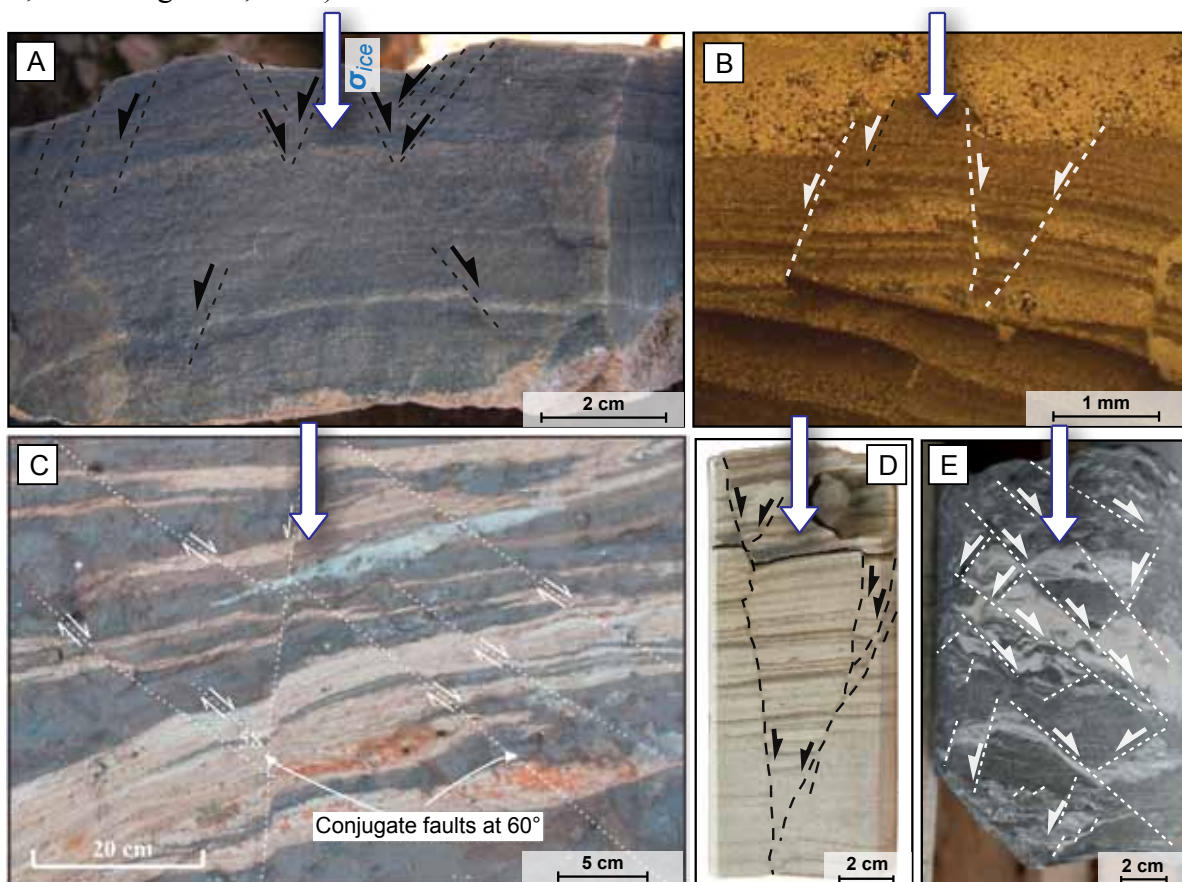


Figure 23. Brittle deformation structures induced by pure shear. (A) Radial step normal faults (Morocco, Ordovician). (B) Radial step normal faults observed in thin sections (Scotland, Pleistocene). (C) Dihedral conjugate normal faults (England, Pleistocene) (Flemming et al., 2012). (D), (E) Dihedral conjugate sets of normal faults observed at core-scale (Algeria, Ordovician).

□ *General shear-induced deformation structures (Pure shear > Simple shear) (Stress state 2)*

In case of moderate flowing-ice, the combined action of horizontal (τ_{flow}) and vertical stress (σ_{ice}), respectively related to ice flow and ice weight leads to a configuration where general shear strain regimes occur in the sediments. In moderate flow configuration, the normal stress induced by ice weight (σ_{ice}) is supposedly superior to the shear component inferred from ice flow (τ_{flow}) ($PS > SS$). Cataclased quartz grains under striae observed in Niger represents brittle deformation that must have been formed under flowing-ice with significant ice load (σ_{ice}) (Denis et al., 2010) (**Fig. 24**).

This stress configuration associated with brittle failure during deformation leads to the development of high angle reverse faults characterized by a high θ angle (i.e., the angle displayed between S_0 (bedding) and the fault plane) (Lesemann et al., 2010; Flemming et al., 2012) (**Fig. 25A, B**). In subglacial configuration, fault offsets are generally mm to cm-sized.

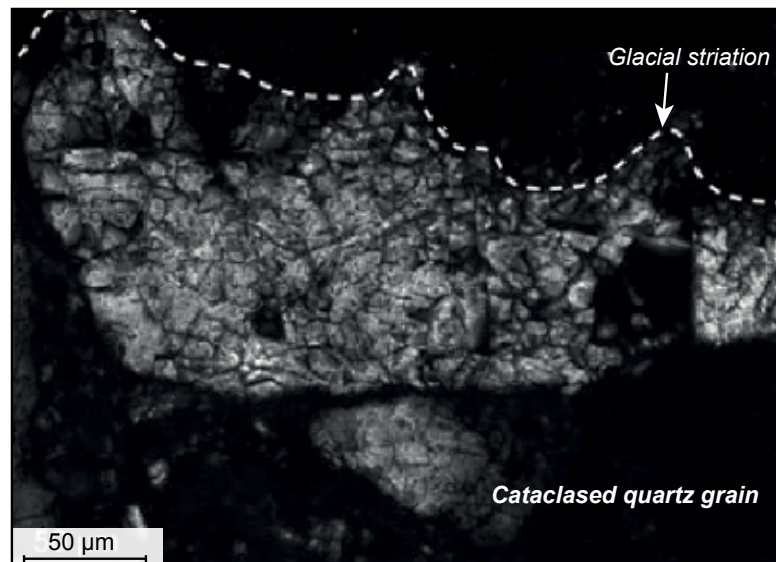


Figure 24. Brittle deformation induced by general shear ($PS > SS$). Truncated and cataclased quartz grain at the former ice/bed contact. (Denis et al., 2010).

□ *General shear-induced deformation structures (Simple shear > Pure shear) (Stress state 4)*

When increasing the basal shear stress (τ_{flow}) component due to increasing ice flow velocities, simple shear strain exceeds pure shear strain resulting in the **decrease of the dip angles of reverse fault planes (Fig. 25.C, D, E)**.

• **Low-angle reverse faults** (also referred to as thrust faults) characterized by **low θ angle values** illustrate this increase in horizontal shear strain. Fault offsets are generally smaller than those observed in large thrust faults in a proglacial morainal complexes (< 1 m) (Bennett, 2001) (**Fig. 25.C, D**). Thrusts faults are frequently associated with sets of normal faults, known as **riedel shears** and **conjugate riedel shears (Fig. 25E, F)**. Thrust and riedel shears are typical of **brittle shear zones** that

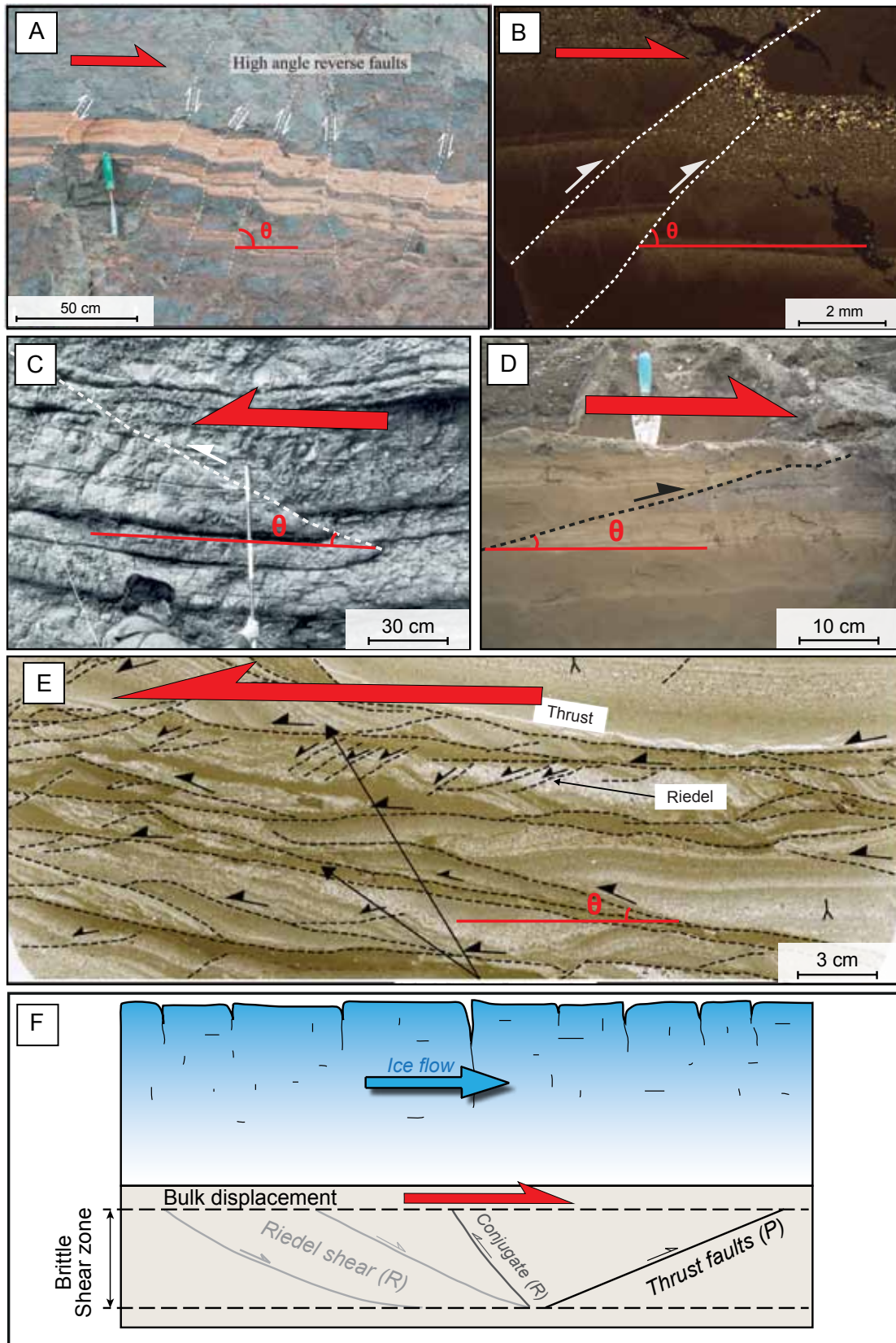


Figure 25. Brittle deformation structures induced by general shear. (A) ($PS > SS$) High angle reverse faults (England, Pleistocene) (Flemming et al., 2012). (B) ($PS > SS$) High angle reverse faults in thin section (Scotland, Pleistocene). (C) ($SS > PS$) A thrust fault at outcrop scale (Denmark, Pleistocene) (Pedersen, 1996). (D) ($SS > PS$) A thrust fault at outcrop scale (Iceland, Pleistocene) (© Ingofolssen) (E) ($SS > PS$) Thrust faults and associated riedel faults in thin section (Scotland, Pleistocene) (Phillips et al., 2007). (F) Illustration of a brittle shear zone composed of thrust faults, riedel and conjugate riedel shears. Note the variation of the θ angle illustrating fluctuations of the basal shear stress during deformation. Note that the size of the red arrows is function of the shear stress component.

can notably be found in subglacial environments (Phillips et al., 2007).

- Very high basal shear strain can lead to a high density of faults implying considerable fracturing of sediments. This high fracture concentration results in the formation of breccia-like structures referred to as in-situ **brittle shear breccias**, also termed **shear-induced breccias** (Passchier, 1998; Phillips et al., 2013a).

5.1.2. Background deformations

"Background" deformation structures are soft-sediment deformation structures that can be potentially formed in **all glacial environments**, including subglacial and marginal environments, because deformations are not necessarily related to interactions between the ice sheet and the bed.

Radial step normal faulting can be observed within both subglacial and proglacial environments.

- Although radial step normal faults can be formed in response to ice-bed coupling, this faulting pattern may alternatively result from sediment compaction triggered by the vertical pressure exerted by the overlying sediments (e.g., lithostatic stress).
- The progressive melting of buried ice triggers collapse of the overlying sediments and subsequent formation of step normal faulting (i.e., kettle hole) (Winsemann et al., 2003). Step normal faults do not display a radial pattern and can be discriminated from the radial step normal faults previously described.
- Faulting triggered by seismic waves could also occur in subglacial environments. Although tectonic activity is thought to be the first mechanism for the production of earthquakes, basal “icequakes” also transmit seismic waves to the bed and can be triggered by crevasse openings, or changes in subglacial water pressures (Deichmann et al., 2000; Walter et al., 2008).

5.2. Hydroplastic deformation structures

When the cohesion of sediments increases due to an increase of porewater pressure and/or clay content, sediments can deform on a plastic manner, known as hydroplastic deformation.

5.2.1. Ice-bed coupling structures

□ *Pure shear-induced deformation structures (Stress state 8)*

When stagnant to slow-moving ice is coupled to a sedimentary pile constituted by bed of different competences (i.e. different degree of resistance to deformation in terms of relative mechanical strength), the normal stress (σ_{ice}) exerted by the ice load on cohesive sediments leads to preferential stretching of the more competent beds implying formation of **symmetrical boudins**. These boudins formed as a response of pure shear stress and are also referred to as **drawn boudins** in structural geology (Goscombe et al., 2004) (**Fig. 26.A**). Symmetrical boudins are characterized by the absence of slip motion on the inter-boudins surfaces. Individual boudins are generally up to few centimeters although boudins up to 1 m wide have been described by Benn and Prave (2005) (**Fig. 26A**). Boudins structures regularly affect sand layers or lenses contained within till deposits because of the differences of competence between these two different materials.

□ *General shear induced deformation structures (Pure shear > Simple shear) (Stress state 3)*

Deformations controlled by general shear (PS>SS) affecting cohesive sediments with moderate porewater pressure lead to hydroplastic deformation structures, including slightly asymmetrical

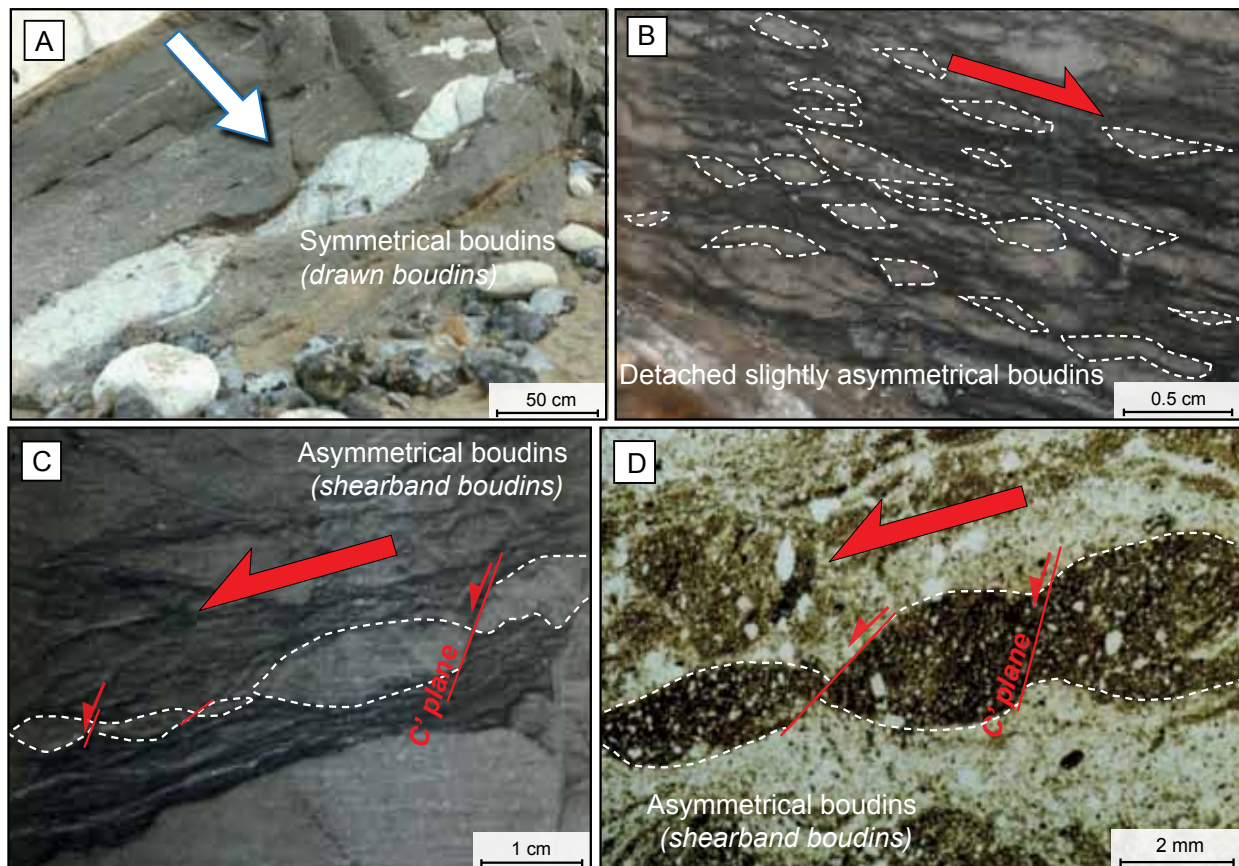


Figure 26. (A) Pure shear. Symmetrical boudins (England, Pleistocene) (Benn and Prave, 2005). Hydroplastic deformation induced by general shear: (B) (PS>SS) Detached and slightly asymmetrical boudins structures at core-scale (Algeria, Ordovician). (C) (PS>SS) Shearband boudins and associated C' plane at core-scale (Algeria, Ordovician). (D) (PS>SS) Shearband boudins and associated C' plane in thin section (Algeria, Ordovician). Note that the size of the red arrows is function of the shear stress component.

boudins, asymmetrical folds and high-angle S-C structures (**Figs. 26, 27, 28**).

- The increase of horizontal shear stress related to increasing flow velocities (τ_{flow}) within the cohesive bed characterized by layers of different competence leads to the formation of **slightly asymmetrical boudins (Fig. 26B)**.
- **Asymmetrical folds** characterized by high-angle axial planes have their fold hinges dipping towards the sense of shear (i.e., the ice flow direction) and correspond to moderate strain rates (**Fig. 27A, B**). The (θ) angle value between the axial plane and the bedding surface (S_0) corresponds to the plunge of the fold, and is an indicator of strain rates applied during folding but also an indicator of the contribution of the simple shear stress component during deformation (Choukroune et al., 1987). The

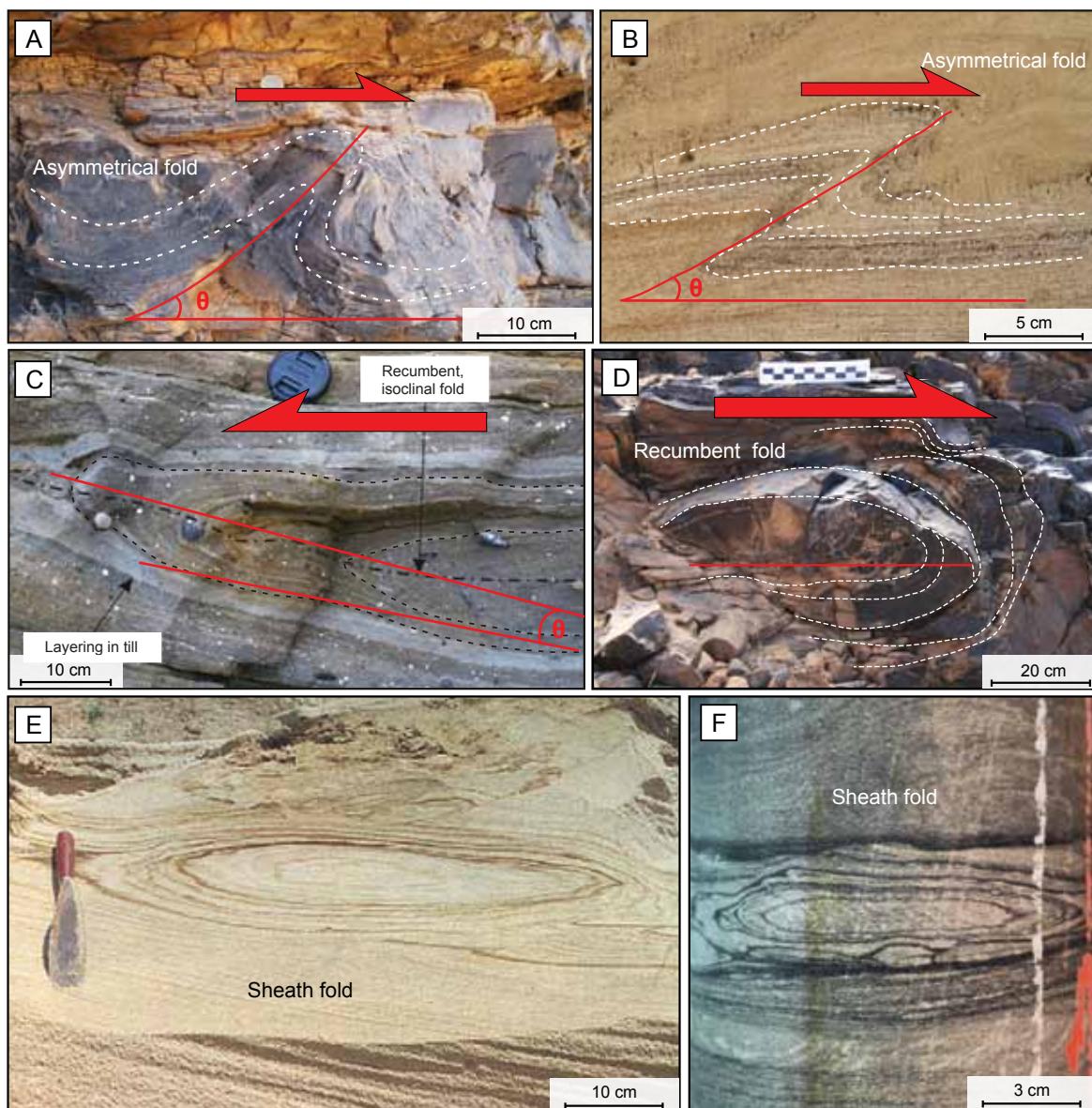


Figure 27. Hydroplastic deformation induced by general shear. (A) (PS>SS) Asymmetrical fold at outcrop scale (Morocco, Ordovician). (B) (PS>SS) Asymmetrical fold at outcrop scale (Pleistocene, Ireland). (C) (SS>PS) Recumbent fold at outcrop scale (England, Pleistocene)(Phillips et al., 2008). (D) (SS>PS) Recumbent fold at outcrop scale (Morocco, Ordovician). (E) (SS>PS) Sheath fold at outcrop scale (Denmark, Pleistocene) (Lesemann et al., 2010) (F) (SS>PS) Sheath fold at core scale (Algeria, Ordovician).

high (θ) angle values characterizing asymmetrical folds indicate prevailing pure shear strain.

- In subglacial shear zones, the development of **S-C fabric** (“S” for schistosity; “C” for cisaillement) occurs and can be observed at different scales (from mm to tens of cm). The (θ) angle displayed between the S- and C- planes indicates the strain intensity, and the contribution of the simple shear strain during deformation of sediments. In a stress configuration where pure shear prevails, the **angle between the S- and C-planes (θ)** is expected to be **high (Fig. 28A)**.

□ *General shear induced deformation structures (Simple shear > Pure shear) (Stress state 5)*

When increasing the horizontal shear stress component, simple shear stress becomes predominant over pure shear stress. In this configuration, asymmetrical boudins, recumbent to sheath folds, and low-angle S-C structures occur.

- The increase of basal shear strain related to the horizontal stress (τ_{flow}) increase induced by ice flow speed-up leads to the formation of **asymmetrical boudins** displaying sigmoid shape and are referred to as **shearband boudins** (Goscombe et al., 2004). The formation of shearband boudins is

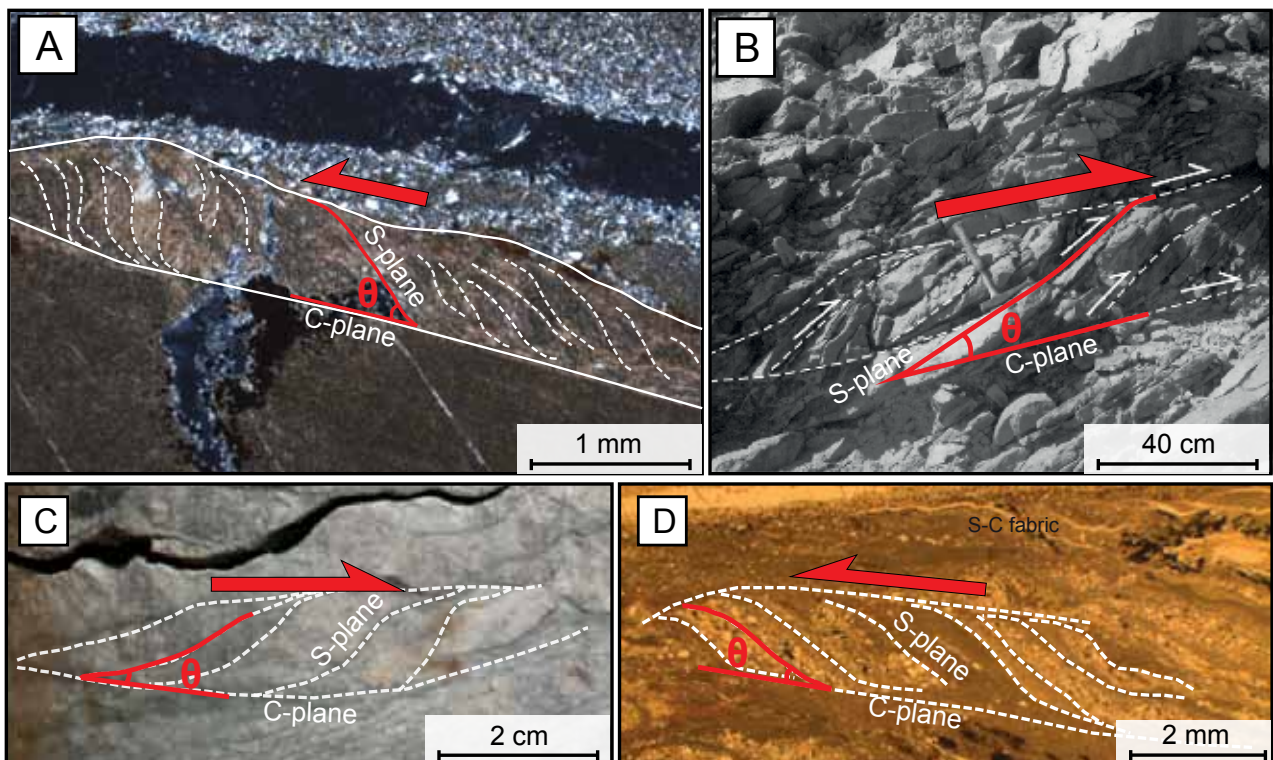


Figure 28. Hydroplastic deformation induced by general shear: (A) (PS>SS) High-angle S-C fabric in thin section (Scotland, Pleistocene) (B) (SS>PS) Low-angle S-C fabric at outcrop scale (Morocco, Ordovician). (C) (SS>PS) Low-angle S-C fabric at core scale (Algeria, Ordovician). (D) (SS>PS) Low-angle S-C fabric in thin section (Scotland, Pleistocene).

occasionally associated with the development of normal faults (C' plane), separating cm-wide sigma-shaped boudins (Fig. 26C, D).

- The increase of the simple shear strain component also leads to the decrease of the plunge (θ) in folds, illustrated by the formation of **recumbent to sheath folds** where **the θ is close to be null (Fig. 27C, D, E, F)**. Similarly, the **low-angle S-C structures** demonstrate a predominant simple shear stress, and a high finite shear strain (**Fig. 28B, C, E**).
- When the simple shear stress component is very elevated, **turbate structures** (also referred to as rotational structures) characterized by circular grains or clast re-arrangements can develop in conglomerate and diamictons (van der Meer, 1993; Menzies et al., 2006). Turbate structures are mainly recognized at micro-scale (few mm in diameters) although few macroscale examples (up to 1 m) have been described (Le Heron et al., 2013; Ravier et al., 2014b) (**Fig. 29A, B**). Turbate structures can either contain a stone or matrix core. The absence of clast-to-clast or grain-to-grain contacts within turbate structures may indicate that deformation occurred in conjunction with high porewater pressures.

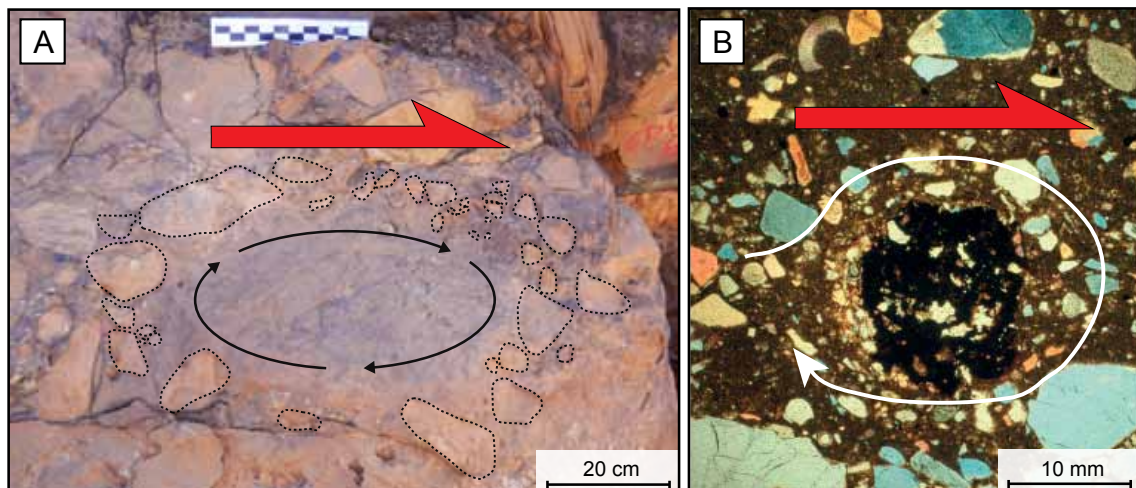


Figure 29. General shear ($SS > PS$). (A) Macro-scale turbate structure at outcrop scale (Morocco, Ordovician). (B) Micro-scale turbate structure with stone core in thin section (England, Pleistocene) (Hart, 2007).

5.2.2. Background deformations

Hydroplastic deformation structures are also commonly observed in marginal environments and are therefore not diagnostic of a subglacial environment. **Folding** is very common in morainal complex at the ice margin although fold scales and thickness affected by deformation are higher in proglacial environments (Bennett, 2001; Benediktsson et al., 2008). In proglacial environments, the space available to accommodate deformation is much higher, and folds formed by sediment compression at the ice margin tends to affect the greater part of the overridden sediments (cf. section 8.2.2 for further details). Structures related to hydroplastic shear are also common in proglacial subaqueous environments, within slumped deposits. Indeed, **folds**, **boudins**, and **S-C fabrics** have been described

in such deposits (Pisarska-Jamroz and Weckwerth, 2013). **Load structures** represent hydroplastic deformations resulting from the foundering of a denser layer into a less dense layer (Maltman, 1994). A set of structures are generally attributed to sediment loading, including load casts, flame structures or load balls. Such structures can occur in every environments containing a sequence of sediments characterized by different densities, and therefore subject to **density inversions** (Maltman, 1994).

5.3. Liquefaction/Fluidization

Over large areas, subglacial drainage system is likely to produce high porewater pressures in the subglacial soft bed, reducing the effective stresses to level low enough to induce deformation by liquefaction or fluidization processes. When the porewater pressure significantly increases, porewater pressure exceeds the pressure exerted by grain weights. In this configuration, sediments start to behave as a viscous fluid. In this section, we describe structures induced by liquefaction and fluidization together as it is often difficult to distinguish between fluidization and liquefaction structures. Nichols (1995) proposed the term liquifaction that include both liquefaction and fluidization deformation mechanisms and is used to describe any processes that transforms sediment into a liquid-like state (Allen, 1982). During the deformation of the substratum, ice remains coupled to the bed when the fluid pressure is lower than the pressure exerted by the ice load (**Fig. 21**). Inversely, when the porewater pressure is higher than the ice load, ice-bed decoupling occurs.

5.3.1. Ice-bed coupling structures

□ Pure shear-induced deformation structures (**Stress state 8**)

In subglacial environments, when the porewater pressure is elevated and exceeds the tensile strength of the host strata, **hydrofractures develop parallel to the direction of the principal stress (σ_1)**. In a configuration where pure shear stress operates, the dominant stress exerted by the ice on sediments is vertical and related to the pressure exerted by the ice weight on sediments ($\sigma_1 = \sigma_{ice}$). Resulting hydrofractures are **vertical to subvertical and propagate downwards (Fig. 30A)**. Once hydrofractures open, **liquefied to fluidized sediments are injected** into the fracture. When the system comes to a rest, injected sediments are generally **structureless** because of processes of sediment homogenization occurring during injection of fluidized material. However, multi-phased infills of

clastic dykes frequently occur, and lead to internal laminations, deposited parallel to the intrusion margins (Le Heron and Etienne, 2005; Phillips et al., 2013).

Downwards propagating dykes are also known as *per descensum* clastic dykes and represent deformation structures that typically form in subglacial sediments during ice-bed coupling (Le Heron and Etienne, 2005; van der Meer et al., 2009; Clerc et al., 2012; Phillips et al., 2013b; Ravier et al., 2014a). The width of clastic dykes formed subglacially ranges from mm to m (up to 1-2 m) and their

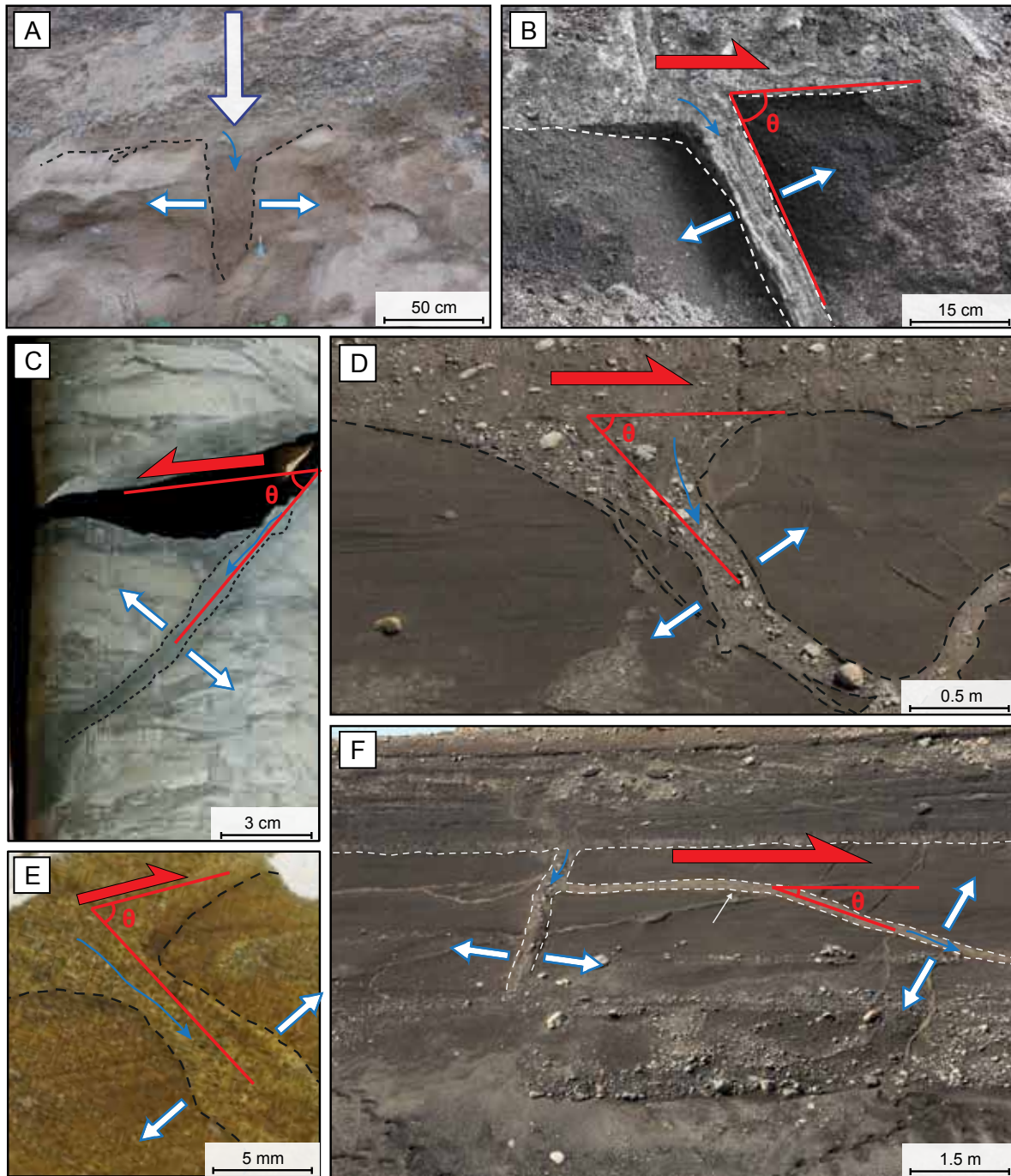


Figure 30. *Per descensum* clastic dykes with various angles, related to hydrofracturing and injection of fluidized/liquefied material. (A) (PS) Vertical clastic dyke at outcrop scale (Ireland, Pleistocene) (Clerc et al. 2012) (B) (PS>SS) High-angle clastic dyke (Iceland, pleistocene). (C) (PS>SS) High-angle clastic dyke at core-scale (Algeria, Ordovician) (D) (PS>SS) High-angle clastic dyke at outcrop scale. (E) Clastic dyke in thin section (Iceland, Pleistocene). (F) (SS>PS) Low-angle clastic dyke at outcrop scale (Iceland, Pleistocene).

vertical extension can reach tens of meters (van der Meer et al., 2009; Clerc et al., 2012; Phillips et al., 2013b).

□ *General shear (Pure shear > Simple shear) (Stress state 3)*

The relative increase of the basal shear component during hydrofracturing leads to progressive **decrease of the angle (θ)** between the bedding (S_0) and the dip angle. When pure shear strain prevails, **downwards propagating high-angle dykes** are preferentially formed (**Fig. 30B, C, D, E**).

□ *General shear (Simple shear > Pure shear) (Stress states 5 and 6)*

The increase of the basal shear (τ_{flow}) induced by the augmentation of the ice flow velocity leads to the formation of **low-angle per descensum clastic dykes** (**Fig. 30F**).

In submarginal to marginal settings, hydrofractures and associated sediment **injections can propagate upward (e.g., per ascensum)** as the result of drastic ice sheet thickness decrease at the ice margin (Boulton and Caban, 1995; Phillips et al., 2013b) (**Fig. 31B**). The decrease of ice sheet thickness triggers a distinct reduction in the ice overburden pressure (e.g., decrease of σ_{ice}) allowing **dykes to climb upwards and sills to form** (**Fig. 31A**). Geometries of climbing upwards clastic dykes are random although the dip angle of *per ascensum* clastic dykes seem to be controlled by the **surface gradient of the ice front** (Phillips et al., 2013b). Gently inclined margins will tend to form gently inclined *per ascensum* hydrofractures, while steeply inclined hydrofractures will tend to promote the formation of *per ascensum* clastic dykes, with high dip angles.

5.3.2. Ice-bed decoupling structures (Stress states 6, 9)

When porewater pressure exceeds the sum of pressures exerted by the ice on grain weights, ice becomes **decoupled** to its bed. In this configuration, injections parallel to bedding (S_0) (i.e., sills) develop and are comprised between few mm and few tens of centimeters thick at most (**Fig. 31C, D**). During these episodes of ice-bed decoupling, the required high porewater pressure conditions imply that sediments are in a fluidized state. In the sedimentary record, lenses that are homogenized without preservation of original sedimentary structures may indicate fluidization related to ice-bed

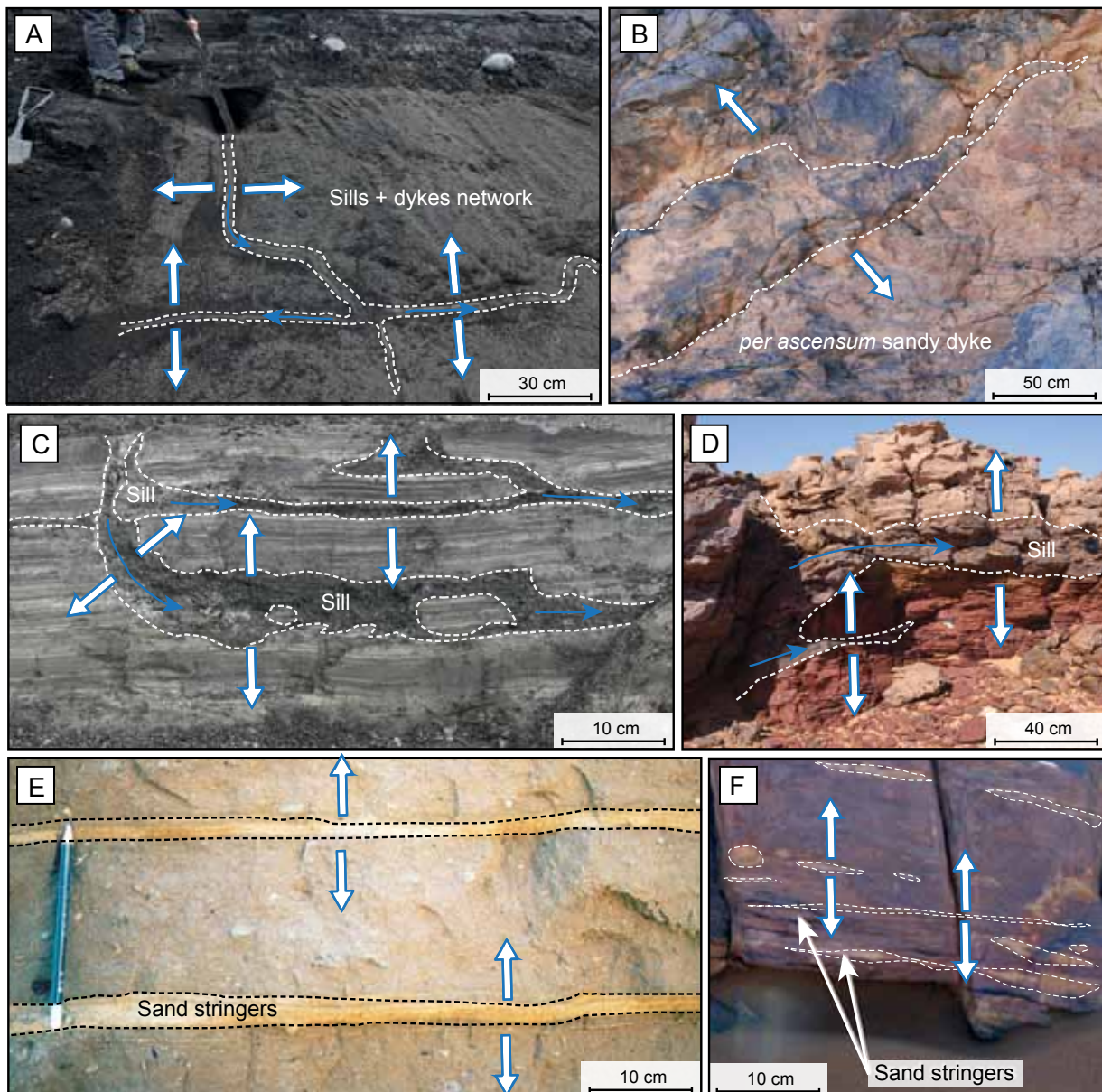


Figure 31. (A) Sills and dykes networks deposited in submarginal settings (Iceland, Pleistocene). (B) *per ascensum* clastic dykes deposited in a marginal setting (Morocco, Ordovician). (C) A sill network deposited in submarginal setting promoted by the decrease of ice overburden pressure (Iceland, Pleistocene). (D) Sills formed subglacially (Niger, Ordovician) (Denis et al., 2010). (E) Sand stringers deposited subglacially when porewater pressure locally exceeds the ice flotation point (Germany, Pleistocene) (Piotrowski et al., 2006). (F) Sand stringers (e.g., sills) deposited during localized ice-bed decoupling (Niger, Ordovician) (Denis et al., 2010).

decoupling. These structures have been referred to as **fluidized bed** or **sand stringers** in the literature (Piotrowski et al., 2006; Denis et al., 2010) (**Fig. 31E, F**).

Similarly, when porewater pressure is very high and ice decoupled to its bed, sediments are in a **hydrostatic stress**, implying that no stress exerted by the ice is transmitted to the bed. In this stress configuration, hydrofractures and injections of sediments develop in every directions, leading to **in-situ hydraulic brecciation**. “Jigsaw-like” fabrics surrounded by fluidized sediments are characteristics of hydraulic brecciation (**Fig. 32B, C**). Such fabric is rarely preserved since such breccias are generally transported away from the site of brecciation (Ravier et al., 2014b). Although sills and breccias can

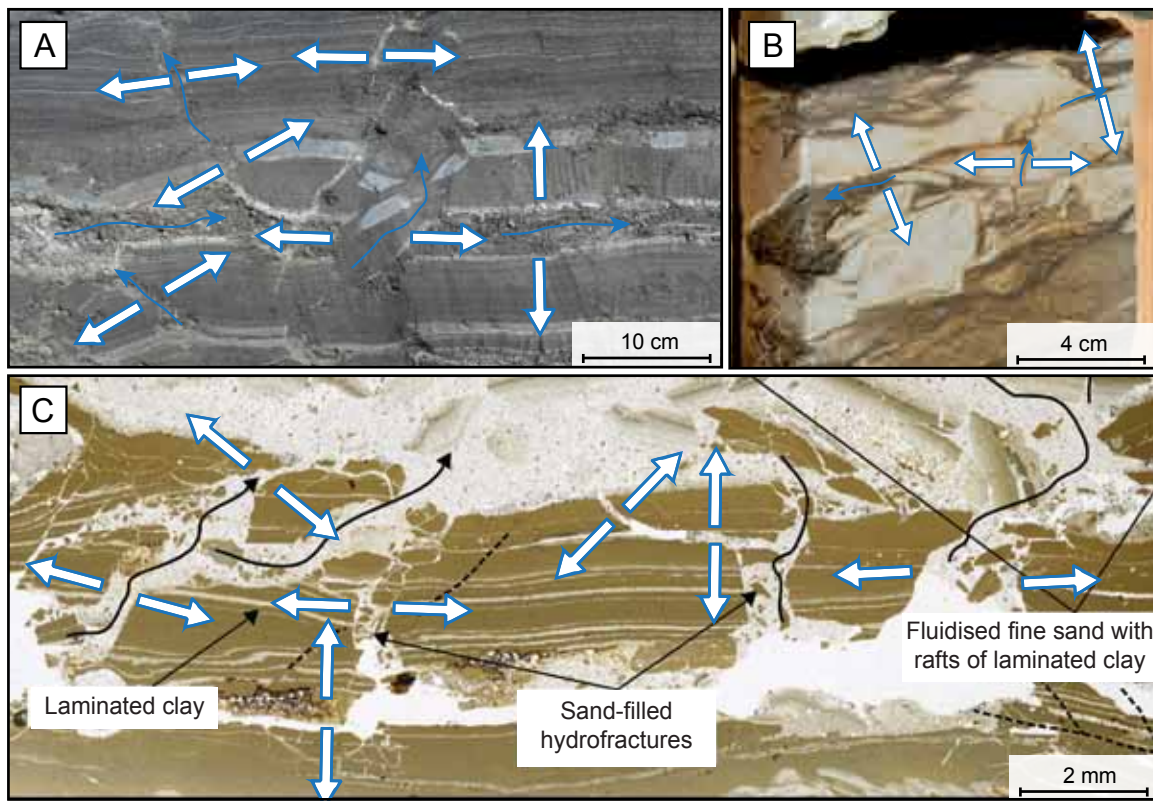


Figure 32. (A) Hydraulic breccia resulting in angular clasts formation (Iceland, Pleistocene). (B) Hydraulic breccia at core-scale forming a jigsaw-like fabric (Algeria, Ordovician). (C) Hydraulic breccia in thin sections formed by closely spaced hydrofractures (Scotland, Pleistocene) (Phillips et al. 2007).

form in subglacial settings, similar structures can be formed in submarginal settings when ice is still coupled to the bed. In such setting, sills and dykes complex can form because the significant decrease of ice thickness reduces the ice weight pressure (σ_{ice}) and allow hydrofractures to develop upwards and parallel to bedding, forming "**stepped sills**" (Phillips et al., 2013b) (Fig. 31A). Occasionally, where the concentration of dykes and sills is high, **breccia-like fabrics** occasionally form (**Fig. 32A**).

5.3.3. Background deformations

Background deformations related to liquefaction or fluidization are numerous, and include convoluted bedding, dish structures, sheet dewatering structures, elutriation bands, ball and pillow structures. These structures induced by high porewater pressures can develop in proglacial and subglacial environments and generally never exceeds few tens of centimeters.

Ball and pillow structures represent isolated “nodules” that may form as a response of water escape and ascending liquefied to fluidized sediments (Cheel and Rust, 1986; Maltman, 1994) (**Fig. 33A**).

Convolutes indicate partial liquefaction of the sediments and record the internal foundering of liquefied sediment layers upon themselves, commonly in conjunction with active upward water escape

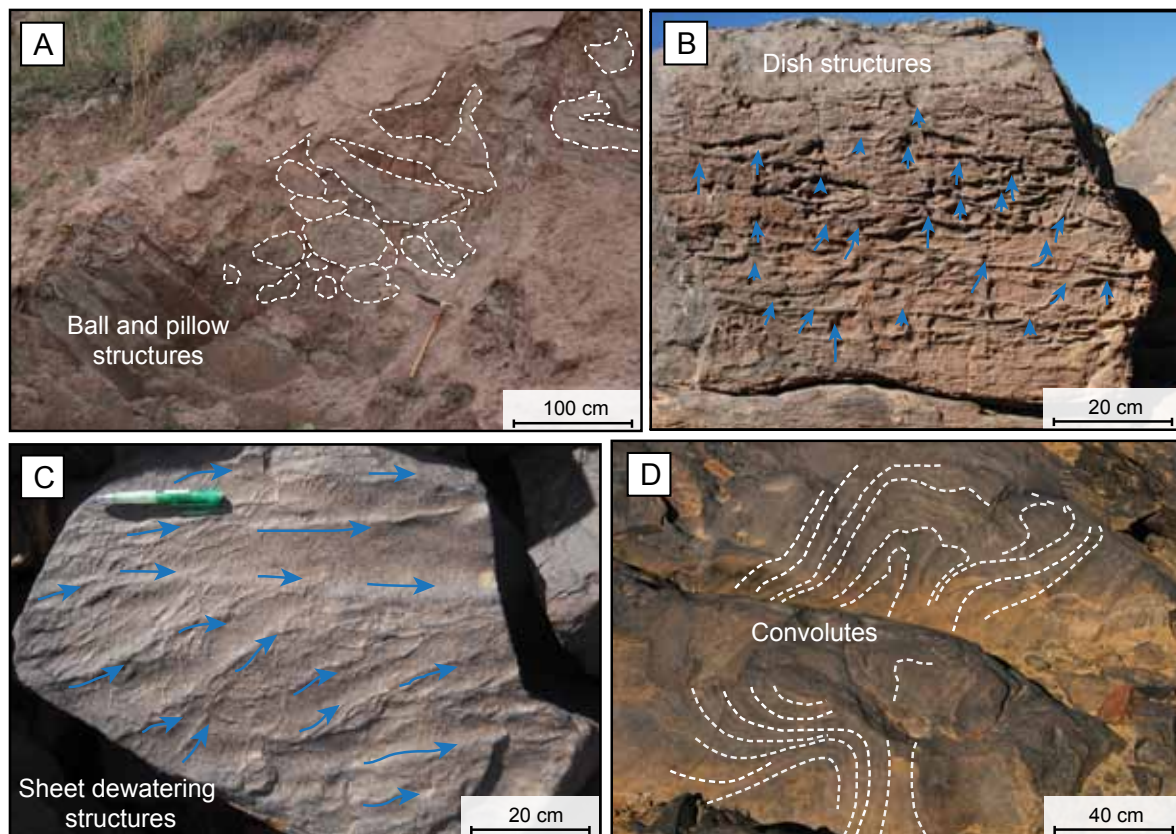


Figure 33. (A) Ball and pillow structures formed as a result of density inversion (Canada, Pleistocene). (B) Dish structures illustrating local-clay enrichment formed by upward dewatering (Morocco, Ordovician). (C) Sheet dewatering structures formed by the horizontal dewatering of sand and triggers by clay-enrichment along elutriation conduits (Morocco, Ordovician). (D) Convolute beds formed by sediment liquefaction (Morocco, Ordovician).

(Maltman, 1994) (**Fig. 33D**). When convolutes are overturned in a preferred directions, it implies that their formations occurred in conjunction with a simple shear stress component, either induced by sediment flow or ice flow. Convolute beds are generally irregularly distributed in a sediment unit and often localized within an intact bed. However, they are expected to occur over quite extensive areas in case of an exogenic trigger (e.g., seismic shock).

Dish and pillar structures, sheet dewatering structures, and elutriation bands, are features observed within sand that were affected by elutriation processes occurring during the increase of porewater pressure (Lowe, 1975; Maltman, 1994). Elutriation processes correspond to the transport of fine particles (e.g., clays) together with the escaping porewater excess. These deformation structures locally modify the texture of the sediments by preferentially enriching or depleting the sand in clay particles (Maltman, 1994).

Dish and pillar structures reflect the local clay enrichment of small zones within sand (Lowe, 1975) (**Fig. 33B**). Dish are centimetric-scale concave-upwards structures. Pillar structures have more or less vertically elongated zones which cross the dishes and often stem from their upturned edges. The local enrichment in clay particles defines the dishes. **Sheet dewatering structures** are similar

to pillar structures but are more linear in plan view. Sheet dewatering structures are composed of a anastomosed system of mm-sized conduits where elutriation processes occur (**Fig. 33C**).

Elutriation bands are similar to sheet dewatering structures, although the conduits where elutriation processes are ongoing are vertical or subvertical. The conduits are generally anastomosed but can also

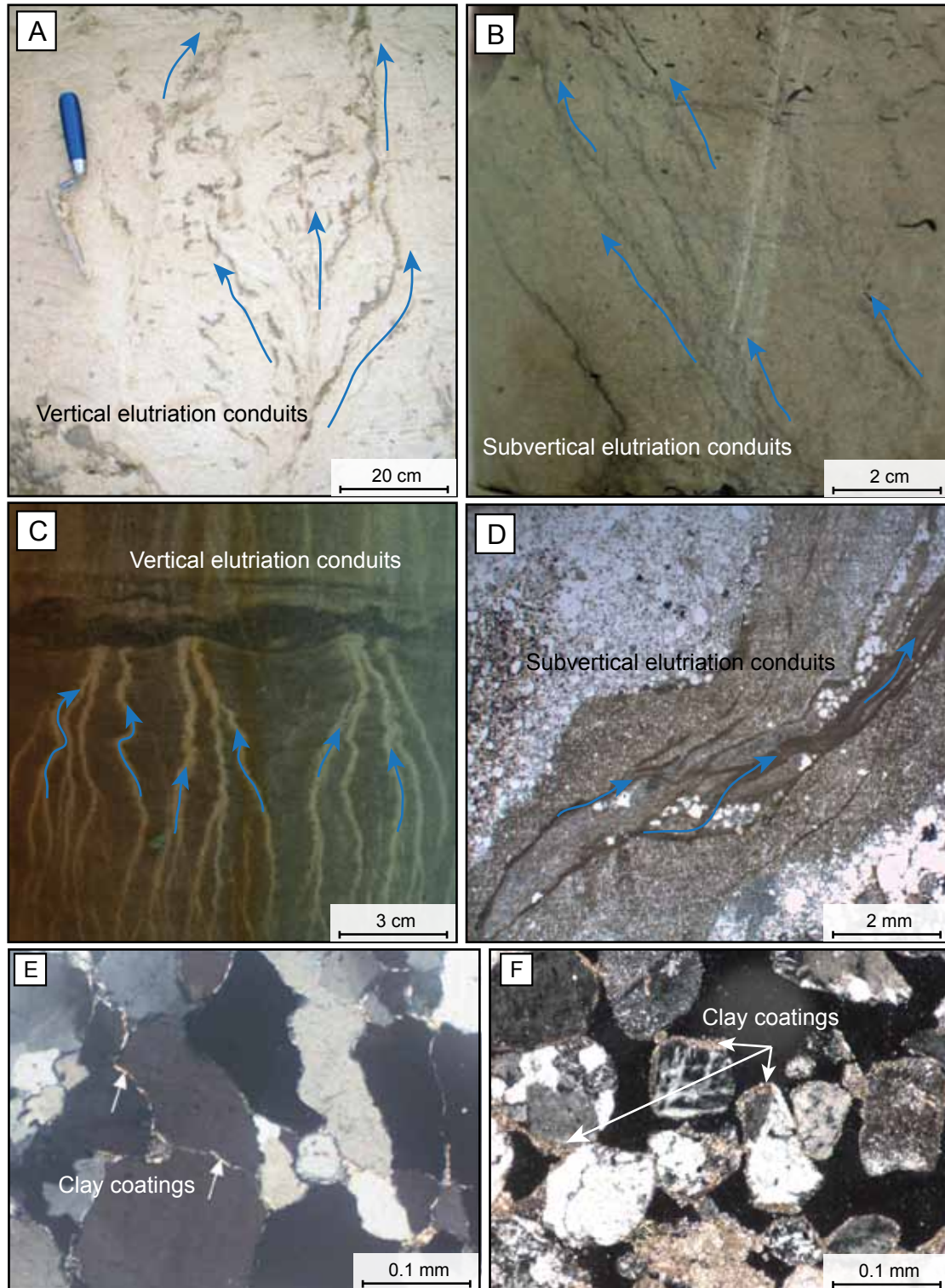


Figure 34. (A) Anastomosing vertical bands enriched in clays, corresponding to elutriation bands (Germany, Pleistocene) (Brandes and Winsemann, 2013). (B) Subvertical dark lineations corresponding to thin elutriation conduits enriched in clay particles (Algeria, Ordovician). (C) Anastomosing conduits depleted in clay particles (Algeria, Ordovician). (D) Anastomosed clay-rich conduits related to elutriation (Antarctica, Miocene). (E) Clay (illite) coatings around quartz grains (Algeria, Ordovician). (F) Detrital clay coating around grains (Switzerland, Pleistocene).

be parallel (**Fig. 34A, B, C, D**). The elutriation processes are notably responsible for the emplacement of **clay coatings** (also known as clay cutans). Clay coatings are thin clay films surrounding grains in sediments (**Fig. 34E, F**). The development of clay coatings in glacial environments are often interpreted to be the result of **porewater movement** within overpressurized sediments (Tournier, 2010; Menzies and Ellwanger, 2011). They are thought to directly influence diagenesis and petrophysical properties in ordovician sandstones (Tournier et al., 2010).

5.3. Other deformation structures

In subglacial environments, some other deformation structures affecting unlithified sediments are not associated with the deformation mechanisms presented before (e.g., brittle, hydroplastic, liquefaction/fluidization). Striae and fluted surfaces are frequently observed within the glacial sedimentary record. These two structures are formed by flowing-ice during episodes of ice-bed coupling.

Striae are scratches incised into bedrock oriented parallel to the palaeo ice flow directions and have long been recognized as evidence for scoring by particles embedded in basal glacier ice (**Fig. 34A**). Striae can be directly formed at the ice-bed interface, but also at the interface between two beds being sheared at different strain rates (e.g., intraformational striae) (Girard et al., 2012) (**Fig. 34A**).

Fluted surfaces are elongated morphologies oriented parallel to the ice flow. They are generally a few tens of centimetres to a few metres high and wide, and up to several hundreds of meters long (**Fig. 35B**). Flutes generally occur in groups of sub-parallel ridges and are the result of soft-bed deformations

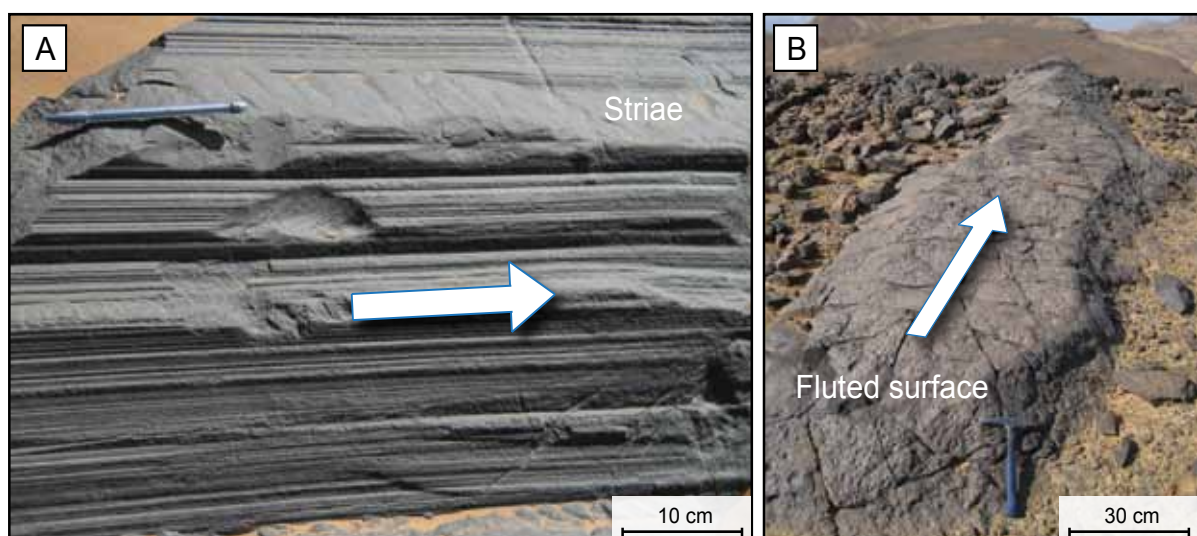


Figure 35. (A) Intraformational striae in soft sediments (Lybia, Ordovician) © JF Buoncristiani. (B) Fluted surface characterized by an elongated morphology parallel to the palaeoflow direction (Clerc et al., 2013).

underneath flowing-ice (Boulton, 1976; Rose, 1987; Gordon et al., 1992). The **elongation ratio of flutes (length/width) is indicative of basal shear strain** (Hart and Smith, 1997). The higher the ratio is, the higher the simple shear stress component is, implying that very elongated flutes will tend to form under fast-ice flow conditions.

6. Micromorphology of tills

Tills are **heterometric deposits** and contain a wide variety of grain-size, from clay to boulders. During deformation, this type of deposits leads to a wide range of structures and fabrics, only observed at microscale, indicative of subglacial deformation. The micromorphology of tills and unconsolidated sediments permits the arrangement of particles and matrix to be fully analyzed (van der Meer and Menzies, 2011). Numerous works have been led on the deformation of till at the micro-scale, and the list of deformation structures is considerable (van der Meer, 1993; Carr, 2004; Menzies et al., 2006, 2012). Although most of the deformation structures are similar to those previously described, the terms used to characterize these different deformation structures differ, because till micromorphology is a subject using the soil science terminology. Using the soil science terms, tills are subdivided into two major components: (1) particles $<25-30\ \mu\text{m}$ defined as the **plasma** and corresponding to the matrix of the till and (2) particles $>35\ \mu\text{m}$ in size, termed **skeleton grains (S-matrix)**. Deformation structures affecting the plasma and S-matrix are divided and listed in **Figure 36**.

The formation of each microstructures are controlled by variations in the rheological behaviour during deformation, which is function of the **porewater pressure**, and/or **clay contents**, and the applied **stress**. Many structures are similar at micro and macro-scale, including **folds** (e.g., fold structure, crenulation foliation), **reverse and normal faults** (e.g., faulted domains and reverse faults), **boudinage**, **sill and dyke structures** and **dewatering structures** (*sensu largo*). Some structures are predominantly observed at the micro-scale, including **crushed grains**, **silts and clay coatings**, **strain caps and shadows**, **rotational structures**, **turbate structures** and **matrix deformation** (e.g., **plasmic fabric**).

Crushed grains are in-situ fractured grains, indicating brittle deformation induced by the overriding ice. Prerequisites for the fracturing processes to occur are: ice-bed coupling conditions, high confining ice pressures preventing dilatant strain behaviour, and grain-to-grain contacts within the bed. In this configuration, loading and shear induced by overriding ice flow induce tensile stresses at grain

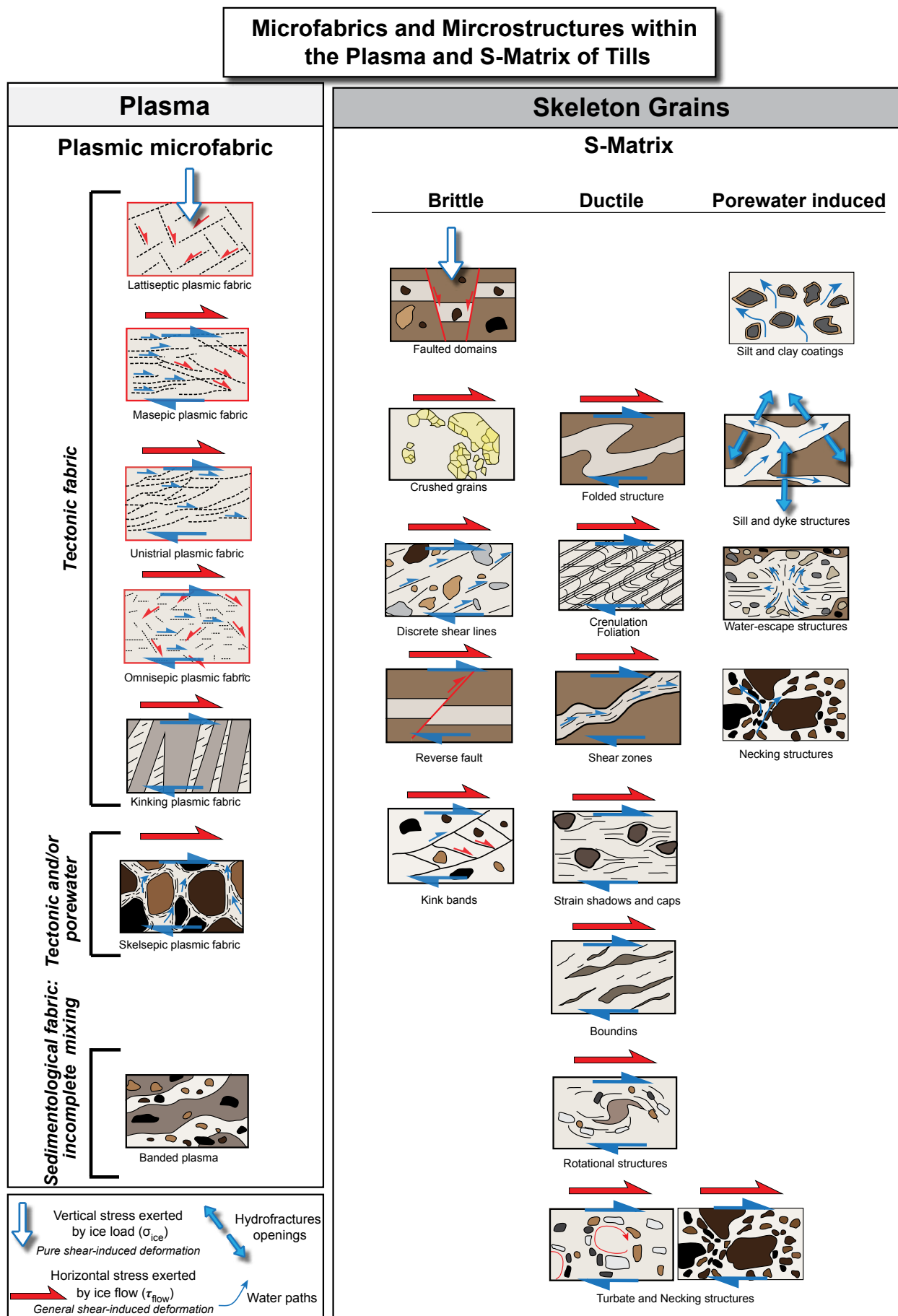


Figure 36. Microstructures related to subglacial deformation of tills. Structures affecting the plasma and the skeleton grains are separated (modified after van der Meer, 1993 and Menzies, 2000)

contacts and potentially trigger grain crushing (Boulton, 1974; Hiemstra and van der Meer, 1997).

Strain caps and shadows, rotational structures and turbate structures are formed by clasts rotation within diamictons and represent high strain deformation induced by prevailing simple shear stress (van der Meer, 1993). The morphology of rotational structures and strain shadows (also referred as pressure shadows) can indicate the strain intensity, because the lengths of these structures are proportional to shear strain (van den Driessche and Brun, 1987).

In subglacial environments, **silt and clay coatings** are mainly thought to be the result of transmission of fine particles through pores by overpressurized meltwater (e.g., elutriation processes) (Menzies, 2000; van der Meer et al., 2003; Tournier, 2010; Menzies and Ellwanger, 2011).

The **plasmic fabric**, recording the deformation of the till matrix, can only be recognized at the micro-scale and record the stress configuration at time of deformation. There are five plasmic fabric that may give information on the stress orientations and values exerted on sediments: the **lattiseptic**, **unistrial**, **masepic**, **omnisepic** and **skeleptic** plasmic fabrics.

- The **lattiseptic plasmic fabric** is defined by oriented domains in two perpendicular directions and therefore mimics **conjugate bands** (van der Meer, 1993) (**Figs. 36, 37B**). In a subglacial context where the overburden exerts a vertical pressure on sediments, these perpendicular and conjugate bands could be considered as compactional shear bands (McCarroll and Risdijk, 2003; Fossen, 2007; Ballas et al., 2013). Such fabric is related to pure-shear enhanced deformation related to a vertical stress exerted by the ice overburden pressure (σ_{ice}).
- When the horizontal stress (e.g., basal shear stress induced by ice flow (τ_{flow})) increases, the shear strain increases and the plasmic fabric becomes **unistrial**. This plasmic fabric is defined by relatively continuous domains, defining **discrete shears** (van der Meer, 1993) (**Fig. 36, 37D**). Discrete shear planes triggered by flowing-ice represent S-plane (i.e., schistosity plane) that are commonly found in ductile shear zones (van der Wateren et al., 2000).
- The **masepic plasmic fabric** is characterized by the presence of two directions of oriented domains (van der Meer, 1993) that are not set at right angles and consist in a wide variety of potential plasmic fabrics. However, masepic fabric formed within ductile shear zone are characterized by two directions of oriented domains corresponding to **S-planes** and **C'-planes** (**Fig 37E**).
- The **omnisepic fabric** consists in plasma re-oriented in one or more distinct directions (van der Meer, 1993), and the actual motions of the particles are difficult to deduce. However, when the plasma is re-oriented in several different directions, and is found associated with rotational

structures, such fabric may develop in response to high basal shear stress (van der Meer, 1993).

- The **skelsepic plasmic fabric**, characterized by oriented domains parallel to the surface of large grains, may either form in response to rotational movements or to clay translocations due to circulation of overpressurized meltwater (i.e., clay coating) (van der Meer, 1993, Menzies et al., 2006).

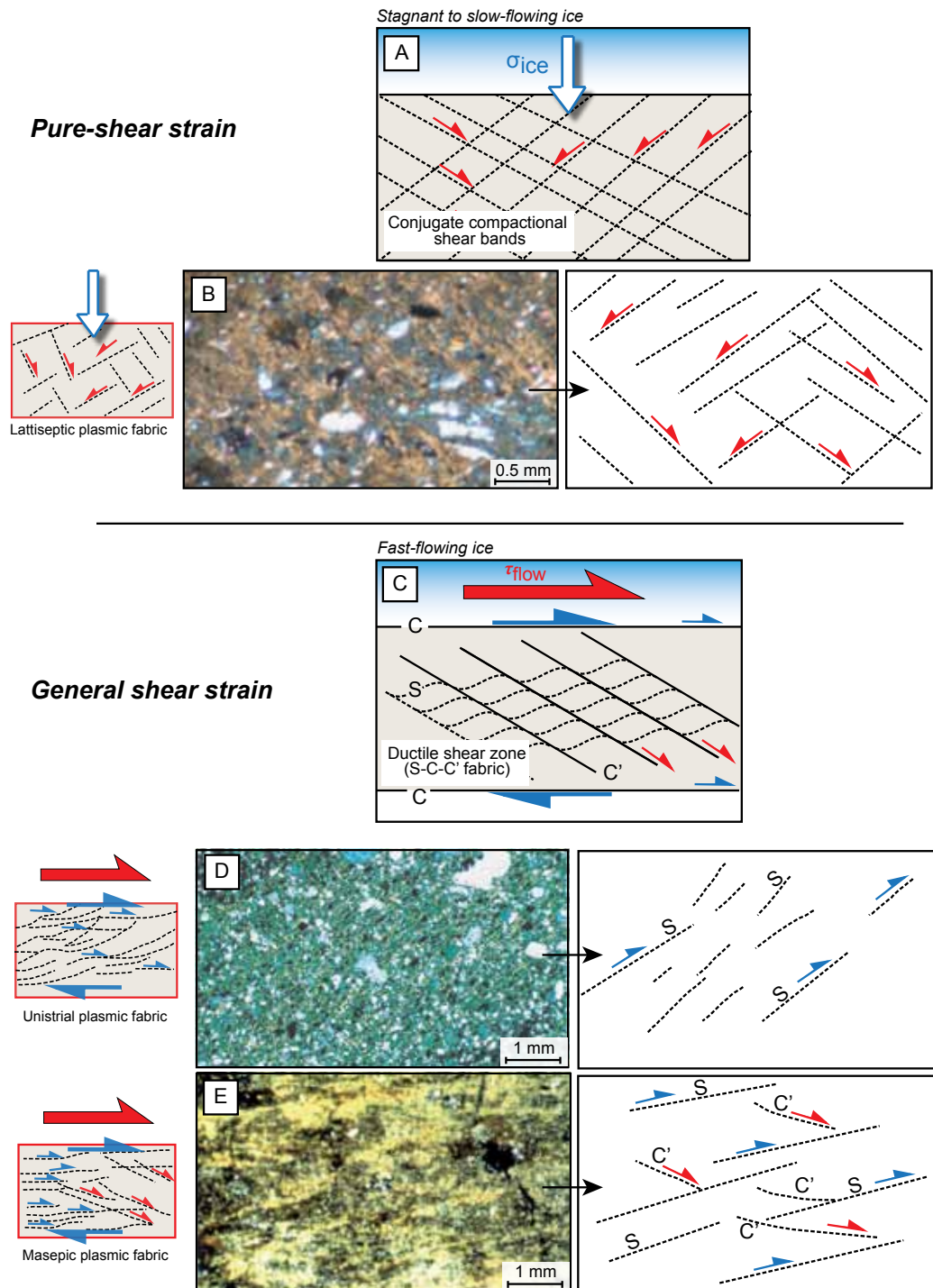


Figure 37. (A) Illustration of brittle pure shear deformation induced by stagnant to slow-flowing ice, resulting in the formation of conjugate compactional shear bands. (B) Lattiseptic plasmic fabric in subglacial till induced by pure shear deformation (from Reinardy et al., 2011). (C) Illustration of a ductile shear zone where fast-flowing ice leads to the formation of S-C fabric. (D) Unistrial plasmic fabric evidenced by faint shear planes (e.g., schistosity planes) related to general shear (from van der Meer et al., 2003). (E) Masepic plasmic fabric formed during general shear-induced deformation. The masepic plasmic fabric results from the combination of S and C' planes generated during shear deformation (from van der Meer, 1993).

7. Distribution of micro- and macro-scale soft-sediment deformation structures along an ice sheet

All deformation structures previously described are compiled in **Figure 38** and classified according to the stress states, the strain regimes, and the porewater pressure involved during deformation (cf. **Fig. 21; Stress states 1 to 9**). These subglacial deformation structures are replaced along a theoretical ice sheet profile where **ice flow velocity**, **ice thickness**, and **porewater pressure** are longitudinally/laterally variable (**Fig. 38**).

8. Deformation structures as a tool for glaciodynamic and palaeoenvironmental reconstructions

8.1. Glaciodynamics reconstructions

• The θ angle

The dynamics of glaciers describe the ice motion and is a function of ice flow velocities. The variations in glacier dynamics have a direct influence on the distribution of the forces exerted on the subglacial sediments during ice-bed coupling, which in turns indicate that distribution of subglacial stress states will highly vary. Three configurations of ice flow velocities are considered: stagnant to slow-flowing ice, moderate flowing-ice and rapid flowing-ice. The progressive increase of ice flow velocity tends to increase the basal shear component, i.e., the stress acting parallel to the subglacial bed (τ_{flow}). In the case of **stagnant** or **slow flowing-ice**, the **basal shear stress is close to be null** and the sediments are subject to a normal stress acting vertically related to the pressure exerted by **the ice weight** (σ_{ice}). The variety of deformation structures induced by general shear are significant and directly derives from the **ratio pure shear strain / simple shear strain**, i.e., the relative contribution of basal shear stress (τ_{flow}) to normal stress (σ_{ice}) (**Figs. 21, 38**). For most of the general shear-induced deformation structures, the **θ angle allows to estimate the contribution of simple shear stress relative to pure shear** stress during the subglacial deformation of sediments (**Figs. 21, 38**). The **angular relationship (θ)** between fabric elements **decreases together with the increase of the shear strain** (Choukroune et al. 1987; van der Wateren. et al., 2000). In subglacial environments, the basal shear stress and strain increase with the ice flow velocity. Rapid flowing-ice will modify the stress states due to the increase of the horizontal basal shear (τ_{flow}) induced by increasing basal sliding. The

possibility to calculate the θ angle on several structures serves to investigate the basal shear strain during deformation and to characterize the ice sheet dynamic characteristics at the deformation spot. Changes in reverse fault dips (reverse faults vs. thrust faults) (**Fig. 25**), in fold plunges (asymmetrical vs. recumbent or sheath folds) (**Fig. 27**), in angles between S- and C- planes within shear zones (high-angle vs. low-angle) (**Fig. 28**) or in the dip angles of *per descensum* clastic dykes (high-angle vs. low-angle) (**Fig. 30**) are indicative of changes in the basal shear strain and ice flow velocities.

• Dyke morphologies

In subglacial environments, **dyke morphologies** can give reliable information on the palaeo stress fields and the inferred ice flow velocity and ice thickness (**Fig. 39**). **Sand stringers and sills** suggest localized ice-bed decoupling conditions that favors fast flowing-ice (Kjaer et al., 2006; Piotrowski et al., 2006; Denis et al., 2010, Hughes et al., 2011) (**Fig. 39A**). In subglacial settings, and under stagnant to moderate flowing-ice, clastic dykes will tend to be **vertical**. The increase of the basal shear stress (τ_{flow}) induced by ice flow speed-up will form ***per descensum* oblique dykes**, with the θ angle being function of the contribution of simple shear stress relative to pure shear stress (**Fig. 39B,C**). In marginal settings, the decrease of the ice thickness and flow significantly reduces the **total stress** ($\sigma_{\text{ice}} + \tau_{\text{flow}}$) exerted on sediments during hydrofracturing. In this configuration, formation of "**stepped**" sills and ***per ascensum* dykes** are promoted (Boulton and Caban, 1995; Phillips et al., 2013b) (**Fig. 39D, E**). The **angle of climb** of clastic dykes formed in marginal settings may give reasonable information on the **morphology of the ice sheet margin** (Phillips et al., 2013b). A gently

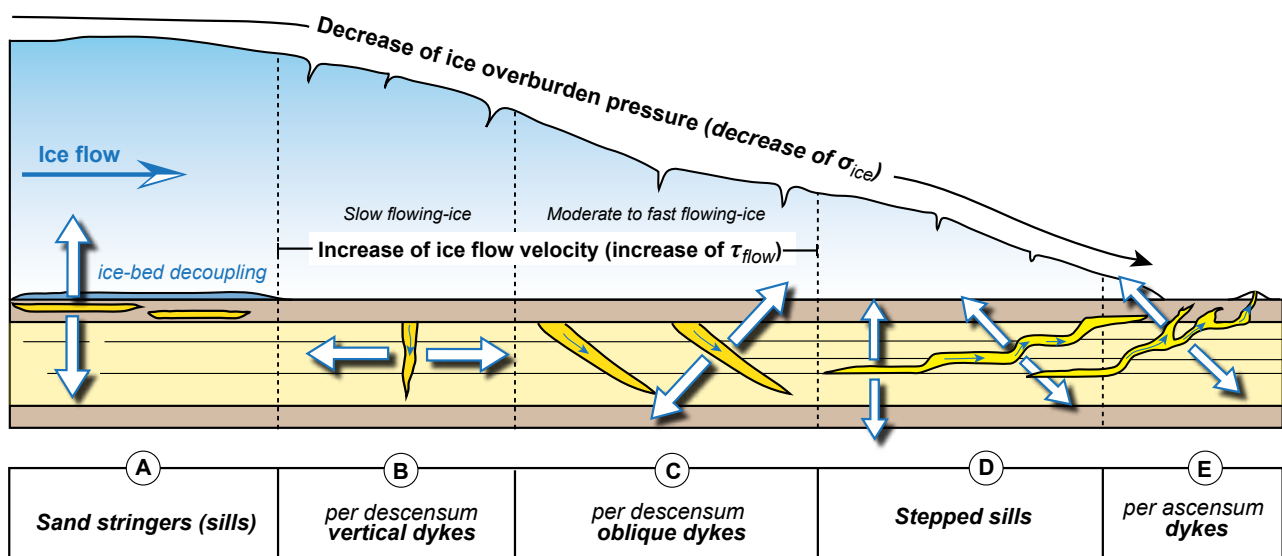


Figure 39. Illustration of the evolution of hydrofractures and subsequent clastic injection morphologies with changes in ice sheet thickness and ice flow velocities

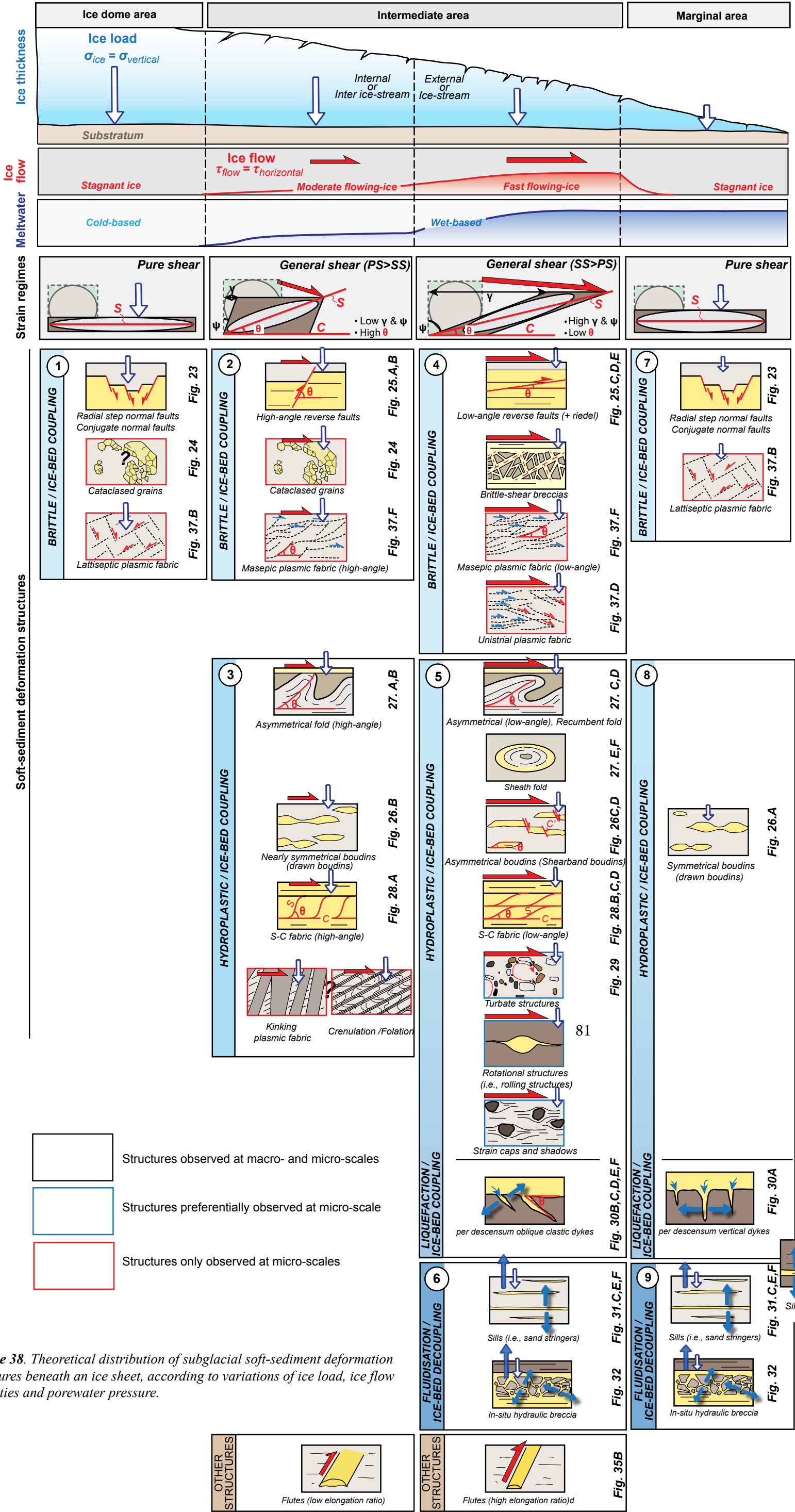


Figure 38. Theoretical distribution of subglacial soft-sediment deformation structures beneath an ice sheet, according to variations of ice load, ice flow velocities and porewater pressure.

inclined margin will result in gently inclined *per ascensum* clastic dykes, which in turns indicate periods of ice sheet decay. Inversely, steep margins are associated with steeply inclined clastic dykes, and therefore indicate periods of ice sheet growth.

- *Deformation mechanisms*

Ice motion is also considerably influenced by the subglacial meltwater content and drainage, which lubricate the ice-bed interface, and promote high ice flow velocities (Winsborrow et al., 2010). Porewater pressure conditions give reasonable information on the subglacial hydrological system since circulation of meltwater is likely to produce high porewater pressures within the subglacial soft bed. Soft-sediment deformation structures record the mechanism (e.g., brittle, hydroplastic, liquefaction/fluidization) responsible for the deformation of the subglacial bed, indicating the porewater pressure conditions at time of deformation. The occurrence of soft sediment deformation structures related to **liquefaction/fluidization** formed in the subglacial bed has often been used as a "proxy" for fast flowing-ice (**i.e., ice streaming**) (Piotrowski et al., 2006; Denis et al., 2010).

- *Elongation ratio of flutes.*

Flutes are streamlined subglacial bedforms indicating ice velocity (Rose, 1987; Boyce and Eyles, 1991; Clark, 1994). The **elongation ratio** (Length / Width) can be used as a "**proxy**" for **reconstructing the basal shear strain and the ice flow velocities** (Hart and Smith, 1997). The highest the elongation ratio is, the highest the basal shear strain and the ice flow velocities are.

8.2. Palaeoenvironmental reconstructions

8.2.1. Previous works and new contributions

- *Previous works*

The analyzes of soft-sediment deformation structures have always been used as a fundamental key to reconstruct **glacial palaeoenvironments**, although the study of deformation should always be part of an integrated investigation, combining sedimentological, stratigraphical and structural approaches.

McCarroll and Risdijk (2003) used deformation styles as a key for interpreting glacial depositional

environments and to discriminate subglacial, ice marginal, proglacial (terrestrial) glaciolacustrine and glaciomarine depositional environments. They defined four main deformation styles including: **pure shear deformation**, **simple shear deformation**, **compressional deformation**, **vertical deformation** (i.e., induced by gravity) and **deformations related to icebergs** that will be very common, common, rare or absent in these different environments (**Table 3**).

At the micro-scale, other studies have proposed to discriminate subglacial from proglacial depositional

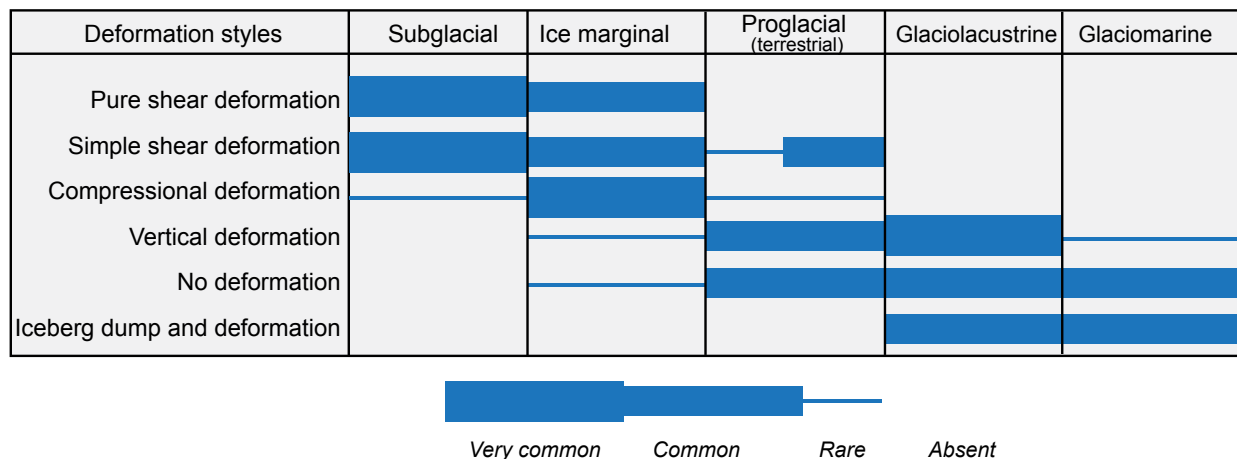


Table 3. Relative degree of dominance of deformation styles in the different glacial environments (modified after McCarroll and Rijdsdijk, 2003).

environments (van der Meer, 1993; Roberts, 1995; Carr, 2001). Carr (2001) used thin section micromorphology to discriminate between fine-grained diacmities that have been deposited within subglacial and glaciomarine environments. The occurrence of crushed quartz grains, augen-shaped intraclasts (i.e., boudins), pressure shadows, rotational structure and unistrial/masepic plasmic fabrics have been proposed to recognize sediments deposited in subglacial environment.

• New contributions

Using the **distribution of subglacial stress states (Fig. 21)**, it is possible to refine the classification proposed by Mc Carroll and Risdijk (2003). The different stress states and porewater pressure configurations are associated with typical soft-sediment deformation structures and divided into **three different domains (Figs. 21 & 38)**. An inner zone, corresponding to the ice dome area and characterized by the absence of meltwater and basal sliding, an intermediate area where basal sliding and basal meltwater occur, and a marginal area where the ice sheet thickness and ice flow decrease drastically. Detailed analyses of deformation structures allow to propose a more precise palaeoenvironmental reconstruction underneath the ice (**Fig. 38**). However, discriminating subglacial to ice-marginal deformation structures still remains challenging as processes involved during

deformation of sediments and resulting structures are often very similar.

8.2.2. Discriminating subglacial from marginal deformation

Although subglacial and marginal deformation styles are very similar, some criteria facilitate the identification of deformation structures formed subglacially. Subglacial deformation structures are generally **restricted to single sediment layers**, while in an ice-marginal environment, deformations **affect the greater part of the overridden sediments** during successive phases of glaciers retreat and advance (Bennett, 2001; Lesemann et al., 2010; Clerc et al., 2012). In subglacial environments, due to repeated phases of ice-bed decoupling and coupling, **coeval and cyclical deposition and deformation** occurs, indicating that sediments deform shortly after deposition.

Proglacial deformations, generally referred to as **proglacial glacitectonics**, are related to compression and are therefore very similar to deformation structures and deformational processes occurring during continental collision and mountain building. Proglacial glacitectonics refer to the **compression** and the subsequent large-scale displacement of proglacial and sub-marginal materials due to stresses imposed by glacier ice, and involve **ductile** and **brittle** deformations (van der Wateren, 1995; Bennett, 2001; Williams et al., 2001; Benn and Evans, 2010) (**Fig. 40**). The brittle deformations mainly involve **thrusting** along planes of failure marked by planes of “décollement” while ductile deformations

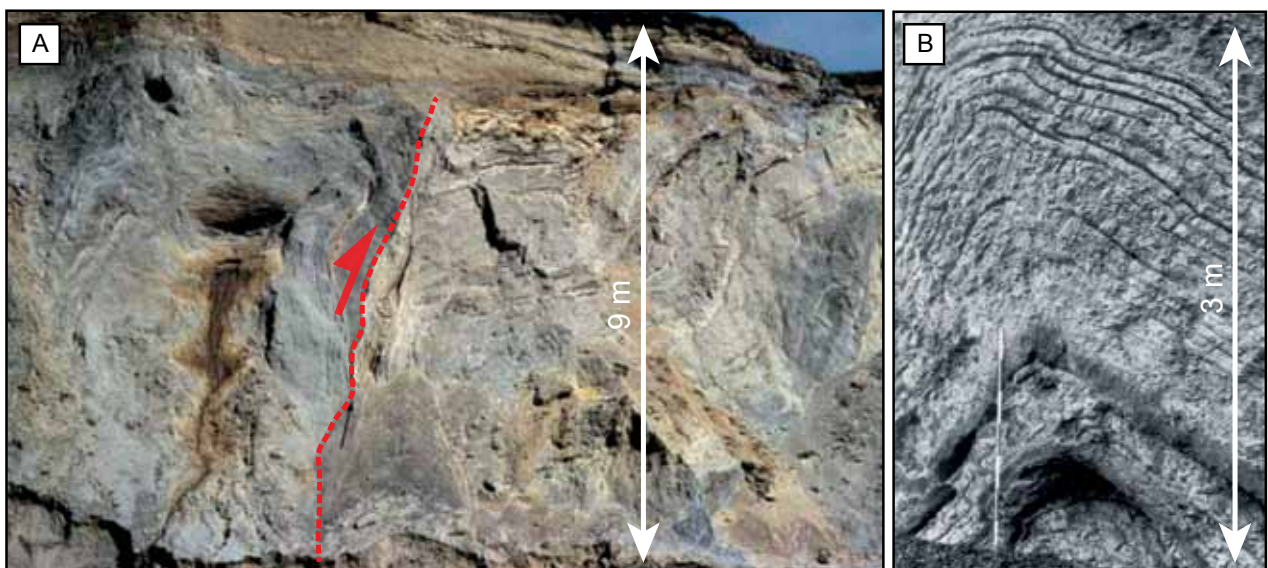


Figure 40. (A) Upright thrust sheets developed within a proglacial glacitectonic complex (Denmark, Pleistocene) (Pedersen, 2005). (B) High-amplitude fold exposed in a proglacial glacitectonic complex (Denmark, Pleistocene) (Asbjørn and Pedersen, 1996).

involve **folding** of sediments (Pedersen, 1993). Folds in proglacial environments can display long wavelengths (open folds) or small wavelengths (isoclinal or recumbent folds), other fold types notably

include chevron folds, box folds or polyclinal folds (van der Wateren, 1995; Bennett, 2001).

In the vicinity of the ice margin, the expulsion of overpressurized meltwater frequently occurs, resulting in **ascending water escape structures** (*per ascensum* clastic dykes, blow-out structures) (Boulton and Caban, 1995; Benediktsson et al., 2008) while subglacial hydrofracturing mainly consists in *per descensum* **dyke morphologies** (Le Heron and Etienne, 2005; Clerc et al., 2012).

Another criterion that may contribute to identify subglacial deformation structures is the space available for sediment deformation. When deformation occurs during episodes of **ice-bed coupling**, the **space available for propagation of the deformation is limited**, because it is constrained by the presence of the overlying ice roof (**Fig. 41A**).

The shear stress exerted by flowing ice leads to a dominant horizontal tectonic transport during

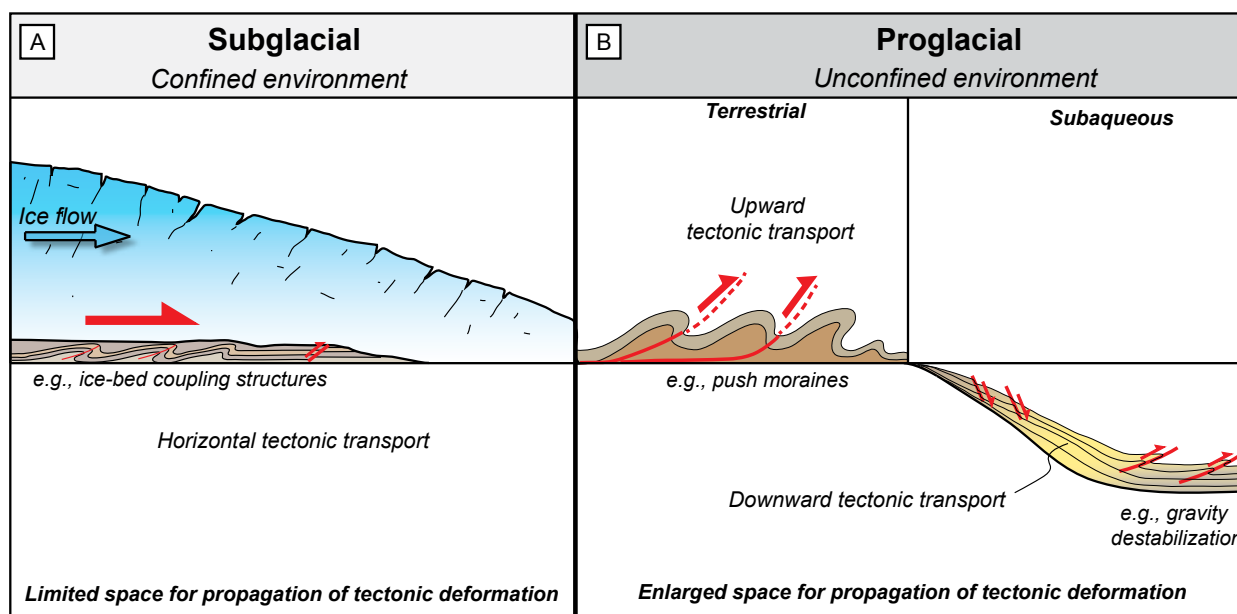


Figure 41. Illustration of the "propagation space for sediment deformation concept" in a confined subglacial environment (A) vs. in an unconfined proglacial environment (B).

deformation. In **proglacial settings**, the unconfined space results in an **enlarged space for propagation of deformation**. This includes large-scale upward tectonic transport along thrust planes in proglacial glacitectonics (e.g., push moraines) or downward tectonic transport induced by gravity destabilisation along fan slopes in subaqueous settings (**Fig. 41B**). Metric-scale thrust faults with meter-size fault offsets are commonly observed in proglacial environments (Pedersen, 2005) while thrust or reverse faults formed in subglacial environments generally range from millimetric to centimetric scale (**Figs. 25A, 40A**). Similarly, high-amplitude folds (e.g., m-scale) will preferentially form within glacitectonic complex in proglacial environments, whereas subglacial folds are generally restricted to single beds and display low-amplitudes (**Figs. 27, 40B**).

9. Interpretation of subglacial deformation structures: limits and particular cases

The array of deformation of deformation structures formed subglacially has been described and their theoretical distribution proposed in this review (**cf. section 5 and Fig. 38**), however **complex glaciodynamics, variations in the stress field orientation and values through time and space, and multiple cycles of deformations** may complicate the analyses and interpretations of these deformation structures.

9.1. Deformation pathways

In subglacial environments, stress field orientations and values vary through time due to changes in environmental parameters (**ice-bed decoupling /recoupling, increase/decrease of basal sliding, groundwater recharge/discharge, etc...**). This implies that sediments composing the subglacial bed may undergo several episodes of deformation of various strains, known as **strain pathways (Fig. 42)**. Deformation structures and associated strains are controlled by variations in stresses and porewater pressure through time, although it may be difficult to assign a time sequence to the different deformation pathways (Menzies, 2012). However, the deformation pathway route can sometimes be investigated when clear overprinting between different deformation structures are observed (**Fig. 43**). The **complex multi-strain history is time-progressive** and remnant deformation structures may survive various previous deformation phases (Bolton et al., 1998; Phillips et al., 2011; Menzies, 2012).

The two main parameters controlling sediment strains through time is the **evolution of stress** and the **porewater pressure**. Strain pathways can be very complex and the deformation structures observed in sediments generally record the **higher strain events**, obliterating previously formed structures (**Fig. 42**).

The progressive increase of basal shear stress produced by ice flow speed-up implies progressive transition from low strain to very high strain, illustrated for example by boudinage structures evolving from **symmetrical to asymmetrical (Fig. 44A)**. In conjunction with variations of the stress orientations and values inferred from ice dynamics, **porewater pressure** may also vary, further

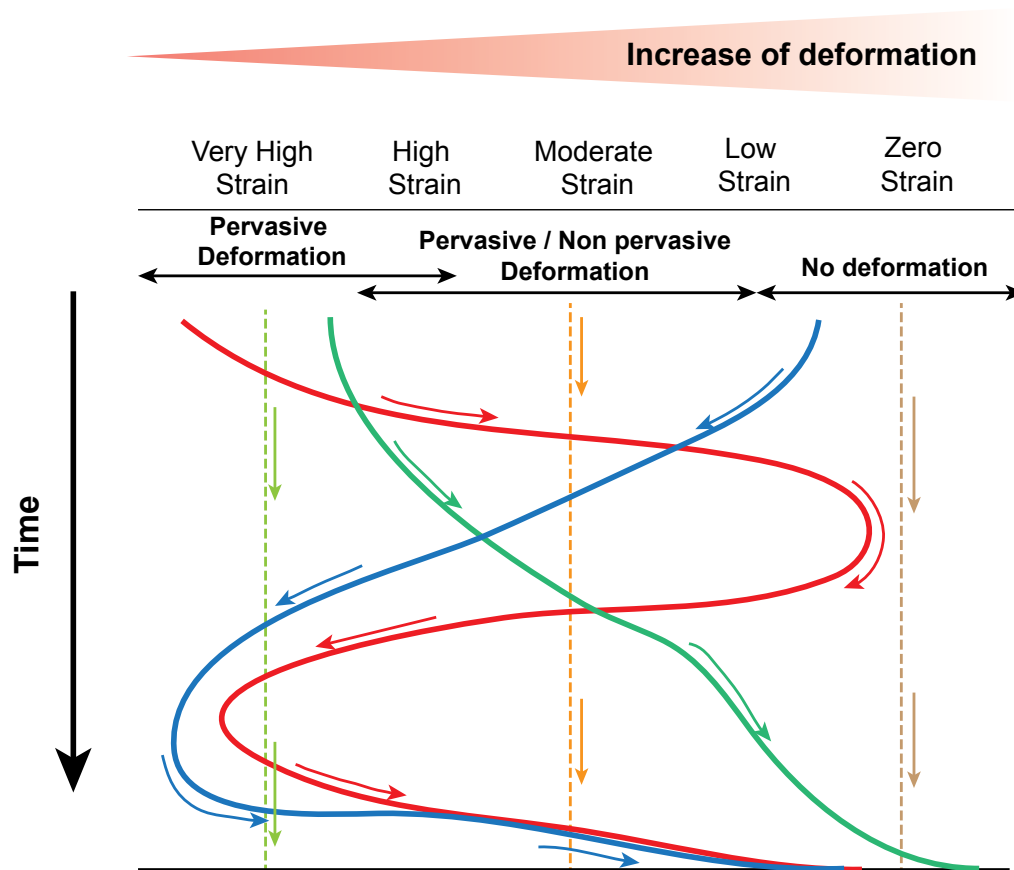


Figure 42. Kinematic model showing different examples of strain pathways (Menzies, 2012).

complicating strain pathways. During a whole cycle of shear strain, sediments may undergo both **brittle** and **ductile** deformations through time, with one often overprinting the other (Muir Wood, 1998) (**Figs. 43A, C, D, 44B**). Sediments usually dewater with compaction, leading to a typical sequence where deformation mechanisms evolve from ductile to brittle. Alternatively, an inverse sequence from brittle to ductile deformation has been observed when sediments experience water recharges during deformation (Tarplee et al., 2011). An example of the influence of water recharge during a deformation cycle is illustrated in **Figure 44B**, where the increase of porewater pressure leads to changes of deformation styles, from **brittle** to **hydroplastic** to **liquefaction/fluidization**. Cross-cutting relationships between deformation structures allow to better constrained the possible strain pathways and their relative chronologies.

The sheet dewatering structures, indicating sediment liquefaction/fluidization, are cross-cut by radial step normal faults, which demonstrate that sediments have dewatered between two episodes of deformation (**Fig. 43A**). Similarly, clayey clastic dykes being cross-cut by a set of conjugate normal faults indicate a decrease of the porewater pressure, probably induced by sediment dewatering (**Fig. 43D**). Alternatively, dewatering structures using a palaeo-conjugate set of fractures to propagate,

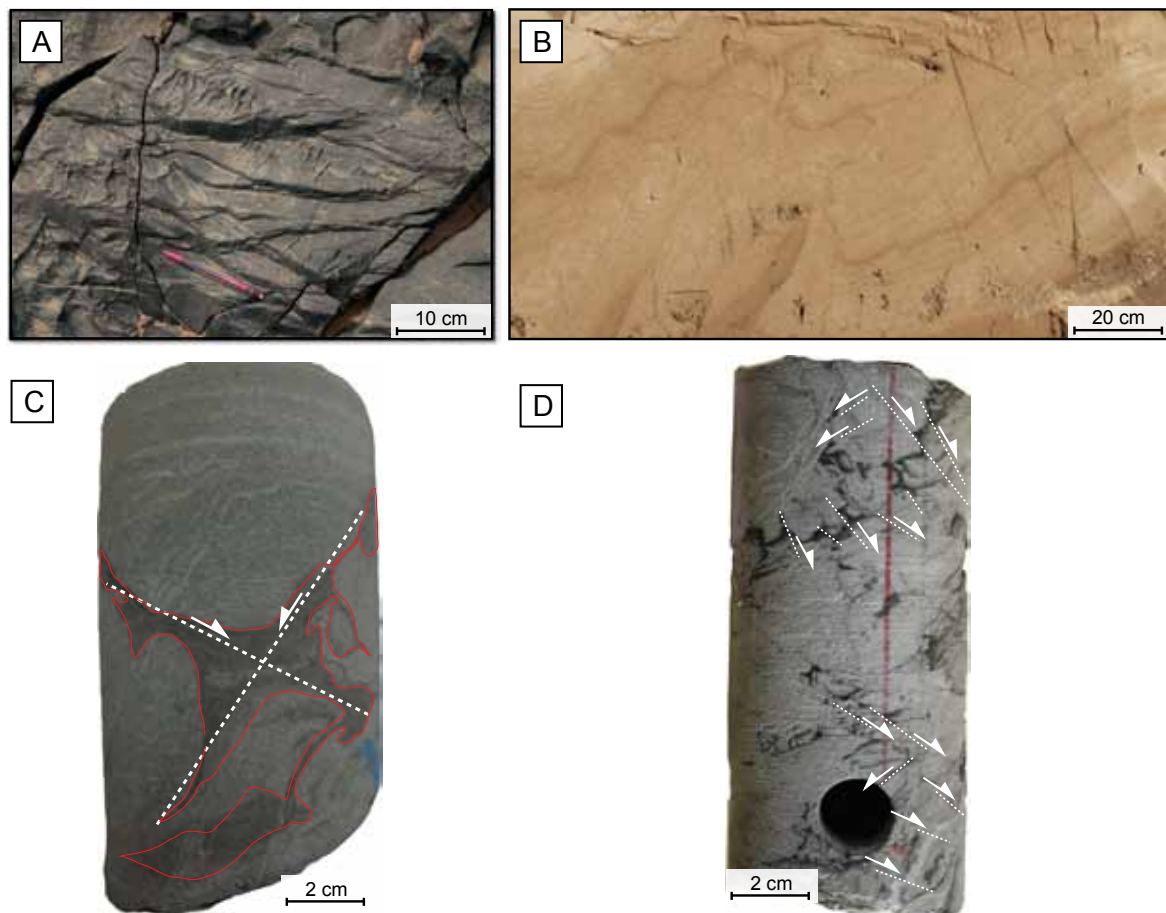


Figure 43. (A) Sheet dewatering structures cross-cut by radial step normal faults (Lybia, Ordovician). (B) Asymmetrical fold affecting convoluted beds (Ireland, Pleistocene). (C) Dewatering structures propagating along a set of conjugate fractures (Algeria, Ordovician). (D) Clayey clastic dykes affected by a set of conjugate normal faults (Algeria, Ordovician).

illustrate a reverse deformation path (e.g., from brittle to liquefaction/fluidization), plausibly demonstrating a water recharge (**Fig. 43C**).

9.2. Heterogeneous deformation: the mosaic bed model

In order to simplify analyses and interpretation of deformation structures in subglacial environments, a theoretical distribution of stress states and porewater pressure was proposed (**Fig. 21**), although subglacial stresses and porewater pressures can vary at a very local scale as illustrated by the **deforming spot model** (Piotrowski, 2001; van der meer et al., 2003) (**Fig. 45**). This model (also known as the "**mosaic bed model**") illustrates that the subglacial bed is a mosaic where **deforming zones occur in the proximity of undeformed zones**. Deforming zones are zones where active deformation occurs and correspond to a state where the **subglacial basal shear (τ_b)** stress exceeds the **shear strength of the subglacial bed (τ_f)** (**Fig. 45**). The mosaic is not stable though time implying that deforming zones change positions through time. This model of heterogeneous

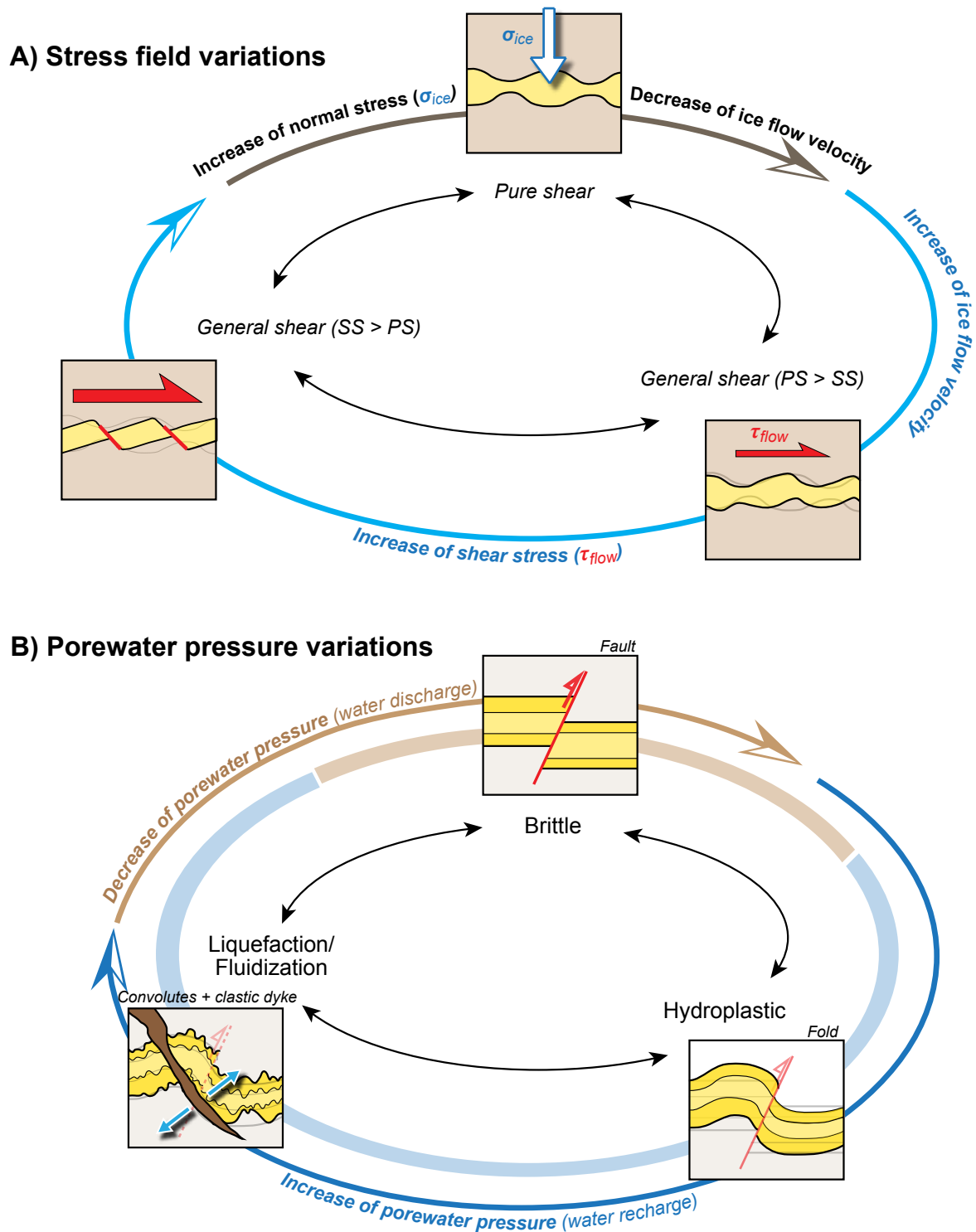


Figure 44. Potential deformation or strain pathways occurring in the subglacial bed. (A) Variations in the orientation and value of the stress field induce evolution of the structures formed during deformation. (B) Variations in porewater pressures through time imply temporal changes in the deformation mechanisms (e.g., from brittle to ductile).

subglacial shear stress and subsequent heterogeneous bed deformations have been suggested using the sedimentary record, where stable zones laterally coexist with deformed zones (**Fig. 46A, B**). In addition, computed basal shear stress distributions beneath Pine Island and Thwaites Glaciers (Antarctica) show similar results. Indeed, the presence of riblike patterns of very high basal shear

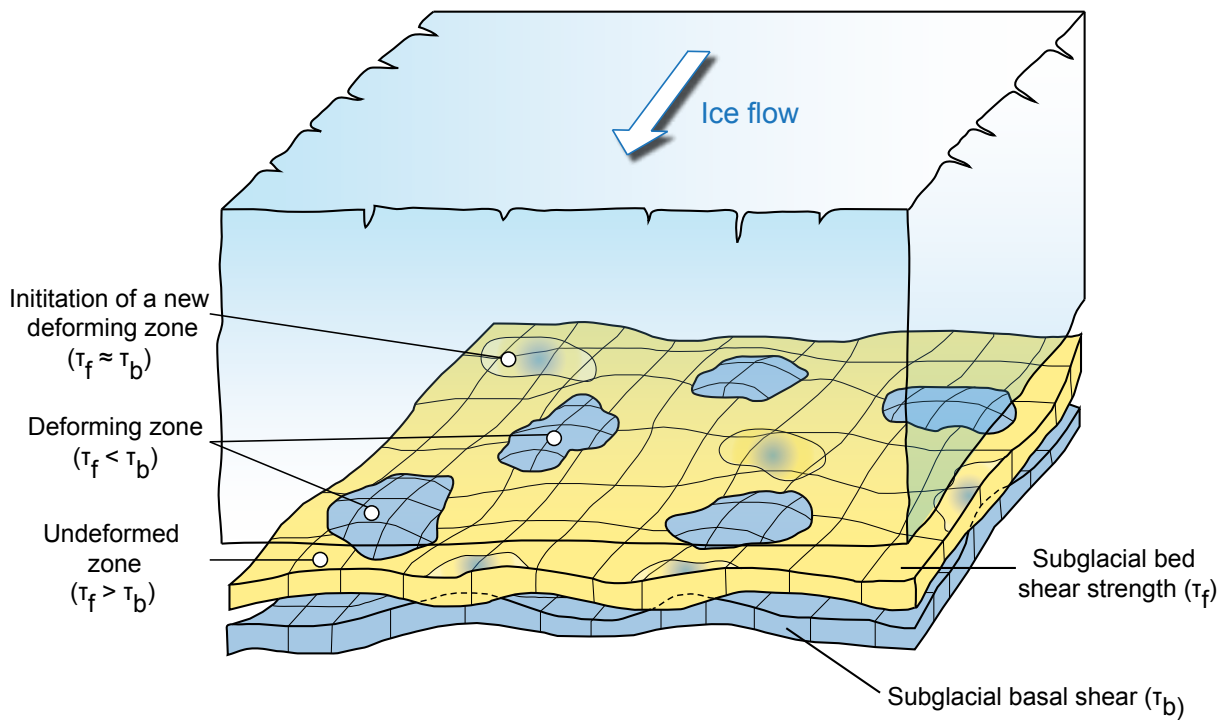


Figure 45. Schematic representation of the relationship between the subglacial shear stress (τ) and the shear strength of subglacial sediments (τ_f) in a ice-bed mosaic model (modified after Piotrowski and Kraus, 1997). In this model, deforming zones coexist with zones where sediments remains undeformed. The ice-bed mosaic model is highly unstable and deformed and undeformed zones laterally shift through time.

stress embedded within much larger areas with zero basal shear stress demonstrates heterogeneous subglacial deformation (Sergienko and Hindmarsh, 2013) (**Fig. 46C**).

van der Meer et al. (2003) illustrated that the deforming bed continuously changes its configuration over space and time and that these lateral changes are function of the combination of **spatial changes in bed water** and **clay contents**. Alternatively, Piotrowski and Kraus (1997) suggested that the stable/deforming mosaic is the result of complex **coexistence of zones of ice-bed coupling and zones of ice-bed decoupling** that will laterally shift through time. The reduced basal coupling limits the transmission of the glacier basal shear stress to the bed, and is illustrated by the lack of sedimentological evidence for widespread pervasive bed deformation (**Fig. 46A**). Nevertheless, the existence of deformed zones suggests that ice-bed coupling locally led to deformation of the subglacial bed (**Fig. 46B**). A mosaic bed model characterized by zones of ice-bed coupling and uncoupling implies that the distribution of **porewater pressure** within the bed controls deformation. Ice-bed uncoupling (also known as decoupling) occurs where porewater pressure was close to the **ice-flotation point**. Uncoupling seems to occur especially within zones of **low hydraulic conductivity**, thus emphasizing the importance of the **subglacial lithology** during bed deformation (Piotrowski and Kraus, 1997; Piotrowski et al., 2004).

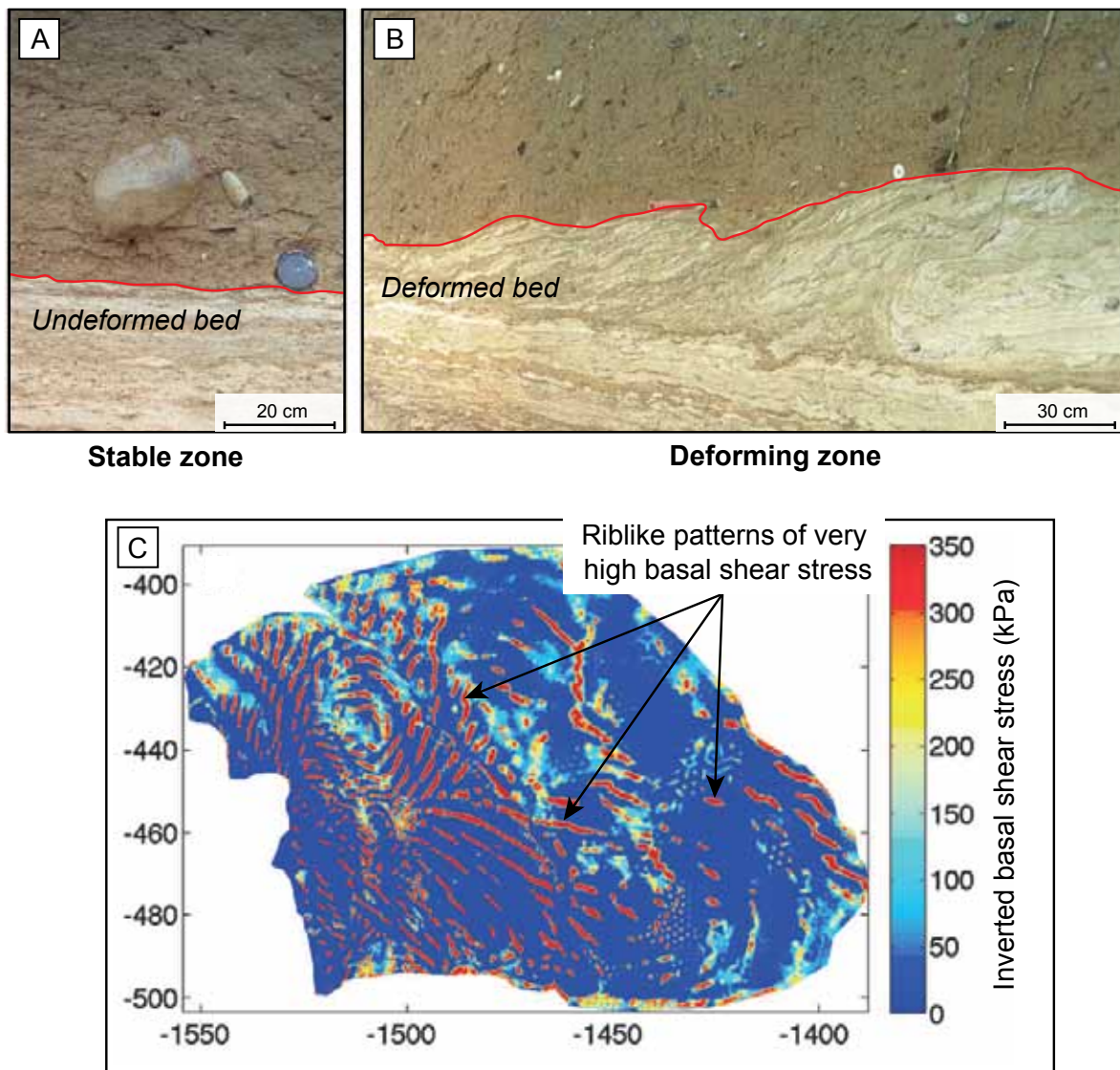


Figure 46. Photographs of a single outcrop (Germany, Pleistocene) illustrating the concept of mosaic subglacial bed. Along the outcrop, stable zones (i.e., undeformed) coexist with deforming zones (Piotrowski et al., 2004). (A) Largely intact glaciolacustrine sediments overlain by a till deposit: the stable zone. (B) Sheared and deformed glaciolacustrine deposits overlain by a till deposit: the deforming zone. (C) Inverted basal shear stress (in kilopascals) beneath the Thwaites Glacier, illustrating the riblike pattern of high stress enclosed within zones of zero stress (from Sergienko and Hindmarsh, 2013).

Soft-sediment deformation structures in deep-marine environments
(induced by fluid overpressure)



Giant injectites complex formed in deep-marine sediments (Panoche Hills, California)

1. Introduction

In the past 40 years, **reservoirs** related to sediments deposited by gravity flows in **deep-marine environments** have received an increasing interest (Pettingill and Weimer, 2002). Hydrocarbon accumulations associated with such reservoirs, generically called **turbidites**, have been discovered in many sedimentary basins around the world, including the North Sea, gulf of Mexico, deep offshore Basins in West Africa (Congo, Angola, Gabon, Nigeria) and Brazil (Pettingill and Weimer, 2002). Architecture, geometries, and sedimentary processes involved in deep-water environments are well-documented (Mutti, 1985; Shanmugan and Moiola, 1988; Mutti et al., 1999; Shanmugan, 2000; Mulder, 2011). This depositional environment is certainly the most affected by **soft-sediment deformation structures induced by fluid overpressures** (Jolly and Lonergan, 2002). These numerous soft-sediment deformation structures significantly modify **reservoir geometries, reservoir connectivities, and petrophysical properties** (Lonergan et al., 2000). Active research on these soft-sediment deformation structures controlled by fluid overpressure started 20 years ago, when their impacts on **hydrocarbon systems** have undeniably been recognized (Dixon et al., 1995).

The aim of this literature review is to present all the **deformation structures related to high fluid pressures in turbiditic environments**, and the mechanisms and processes involved in their formations. The **impacts of such structures on reservoir geology**, including their control on reservoir geometries, petrophysical properties, diagenesis, and fluid flows will also be presented. As a preamble, the **deep-water depositional environment** will be briefly presented, with a special focus on **gravity flow processes** that are responsible for the development of **turbiditic systems** and deposition of clastic sediments into the deep-sea.

2. Deep-marine depositional environments

The sediments in deep-marine environments consist of clastic particles derived from eroded rocks and sediments, particles formed during volcanic eruptions, particles formed by living organisms and particles formed by chemical precipitations (Mulder et al., 2011). **Deep-marine environments** correspond to the area situated **beyond the shelf break**, and include the **continental slope**, the **continental rise**, and the **abyssal plain (Fig. 47)**. Sedimentary processes and resulting sedimentary deposits are numerous in deep-marine environments.

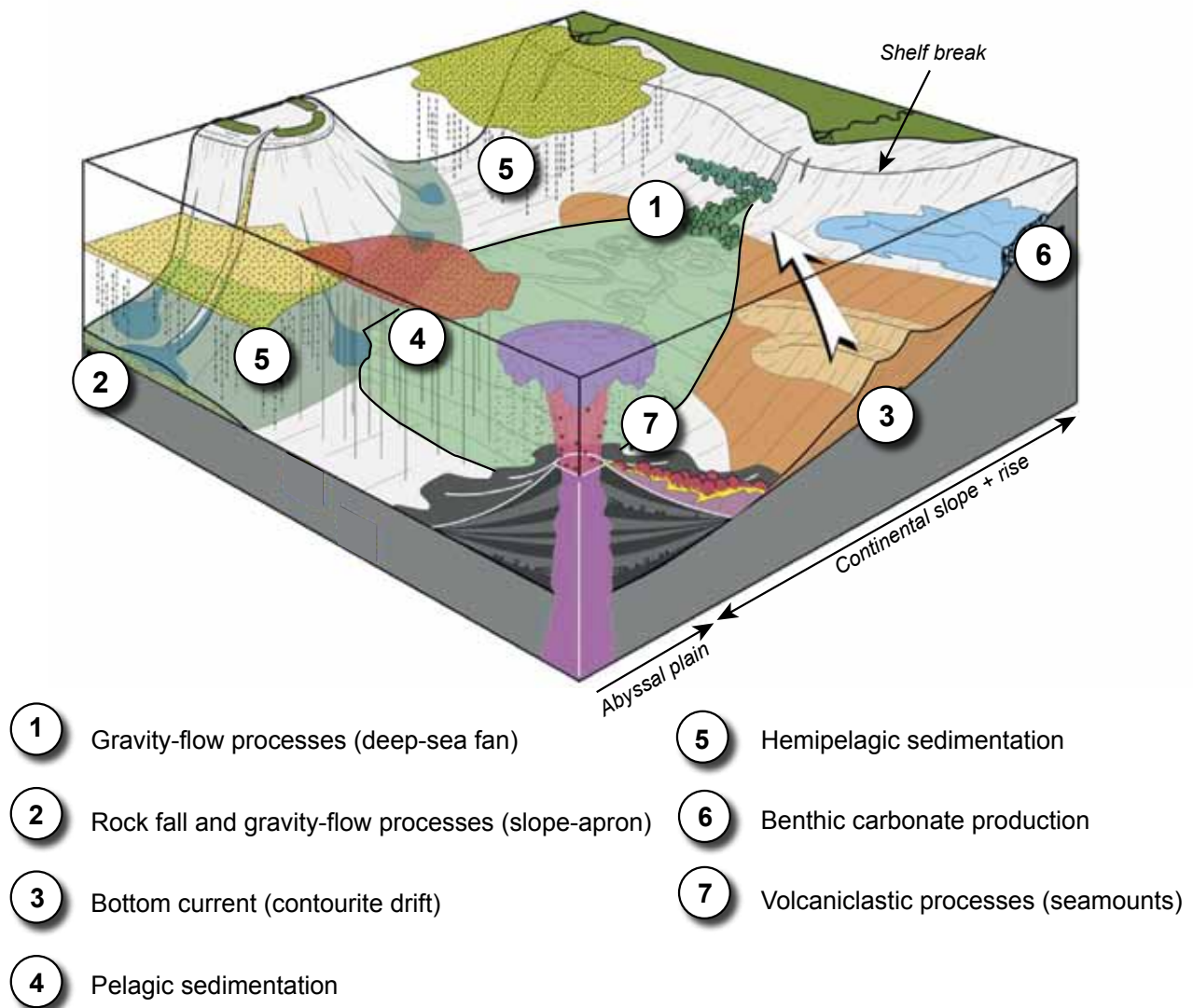


Figure 47. Sedimentary processes and products in deep-marine environments (modified after Mulder et al., 2011).

(1) (2) **Gravity flow processes** are related to gravity-driven sediment transport occurring in more or less close contact to the sea floor. These gravity-driven processes are responsible for the development of large submarine fans or aprons composed of siliciclastic deposits. The main type of flow processes are rock or consolidated material **avalanching**, **creeping** and **failures**, **slides**, **slumps**, **flows** (cohesive and non-cohesive), and **turbulent flows** (Fig. 47).

(3) **Bottom current processes** are related to geostrophic currents flowing principally along the continental slope, following the thermohaline circulation. Resulting deposits are known as «**contourites**», and develop perpendicular to gravity-driven deposits. Contourites correspond to sediment deposited by bottom currents or to sediments that are significantly affected by these currents (Fig. 47).

(4) **Pelagic processes** refer to particles settling in the oceanic water column. Phytoplankton, and zooplankton greatly contribute to the pelagic sediment factory. The amount of pelagic sediments

deposited at the bottom of the ocean is controlled by the production, fluxes and preservations of tests of living organisms (**Fig. 47**).

(5) **Hemipelagic processes** correspond to the settling in water column of muddy sediments formed close to the continental margins. Within hemipelagic sediments, biogenic materials comprise 5-75 % of the total volume, while terrigenous materials can reach 40% of total volume (**Fig. 47**) (Mulder et al., 2011).

(6) **Benthic deep-marine carbonates** correspond to biogenic and authigenic carbonate production within the darkness of the deep sea. They depend on biogenic productivity, variations in supply of siliciclastic detritus, and dissolution parameters (**Fig. 47**).

(7) The last sedimentary process involved in the deposition of sediments in the deep sea is related to **submarine volcanic activity**. Volcaniclastic processes lead to sediment deposition near mid-ocean ridges, seamounts, large volcanic islands, and subduction zones (**Fig. 47**).

Most of the soft-sediment deformation structures induced by high porewater pressures are closely associated with the emplacement of sandy material in deep-sea fans (Jolly and Lonergan, 2002; Hurst et al., 2011). The development of sand bodies in such environments are mainly related to sediment deposition by **turbidity currents**.

3. Turbiditic systems

Although sedimentological characteristics of turbidites are beyond the scope of this review, a brief introduction to their **depositional processes**, **sedimentary facies** and **geometries** is necessary. Deep-sea turbidites systems are well-documented and many models are proposed in the literature to explain the emplacement of these siliciclastic deposits (Mutti, 1985; Shanmugan and Moiola, 1988; Mutti et al., 1999; Shanmugan, 2000; Mulder and Alexander, 2001; Talling et al., 2012; and many other authors). Clastic sediments deposited in deep-sea fans can originate from turbidity currents triggered by **slope failures**, or by the **input of considerable amount of clastic material carried by fluvial systems** into the sea. Deposition of sediments within deep-sea fans occurs through **subaqueous cohesive to non-cohesive density flows** (Mutti et al., 1999; Mulder and Alexander, 2001; Talling et al., 2012). Cohesive flows characterized by **laminar flows** progressively evolve into **non-cohesive flows**, characterized by **turbulent flows**, passing through **transitional hybrid**


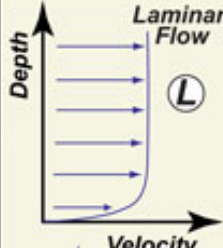
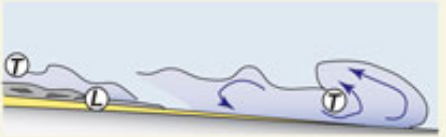
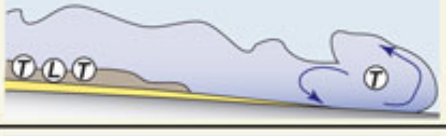
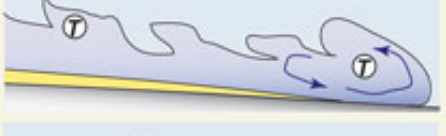
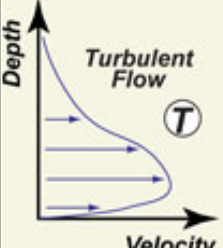
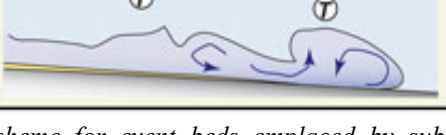
EVENT TYPES		DEPOSITS	BEHAVIOUR
DEBRIS FLOW	COHESIVE	 Debrite D	 Laminar Flow (L)
CO-GENETIC FLOWS	HYBRID	 'Linked' debris LD	
SLURRY FLOW	TRANSITIONAL	 'Banded' sandstone SF	
HIGH-DENSITY TURBIDITY CURRENT	NON-COHESIVE	 HDT	 Turbulent Flow (T)
LOW-DENSITY TURBIDITY CURRENT		 LDT	

Figure 48. Classification scheme for event beds emplaced by subaqueous sediment gravity flows in deep-water environments (from Houghton, 2006).

flows (Fig. 48). Sedimentary sequences deposited by the different flow types vary according to the flow behaviour during the transport of sediments (i.e., laminar vs. turbulent). Turbidity currents are non-cohesive flows sustained by fluid turbulence, and represent the most important transporters of coarse-grained sediments into deep water. Turbidity currents are thought to move rapidly down the continental slope or submarine canyons along the sea bed, and to deposit originally shallow-water sediments at the foot of the slope or on the abyssal plain.

From the shelf break to the basin plain, the evolution of transport and depositional processes lead to **lateral changes in grain-size and sedimentary structures** recorded in the clastic deposits. The characteristics of the **facies tract**, illustrated in **Figure 49**, mainly depend on the textural composition of **parental flows** (i.e., from dense cohesive to non-cohesive turbulent flows), the **amount of bed erosion**, the **flow efficiency**, and the **basin configuration** (Mutti et al., 1999). The facies tract evolves from **conglomerate** in the vicinity of the submarine erosional conduit exit to **planar parallel coarse sand** deposits in the lobe region, and to **finer deposits** with **fining-upward sequences** characteristics of turbidity currents in the distal lobe and the basin plain regions (**Fig. 49**).

Turbiditic systems are composed of several architectural elements that can be depicted at different scales. At the smaller scale, sediments deposited by turbulent flows form different beds, recording

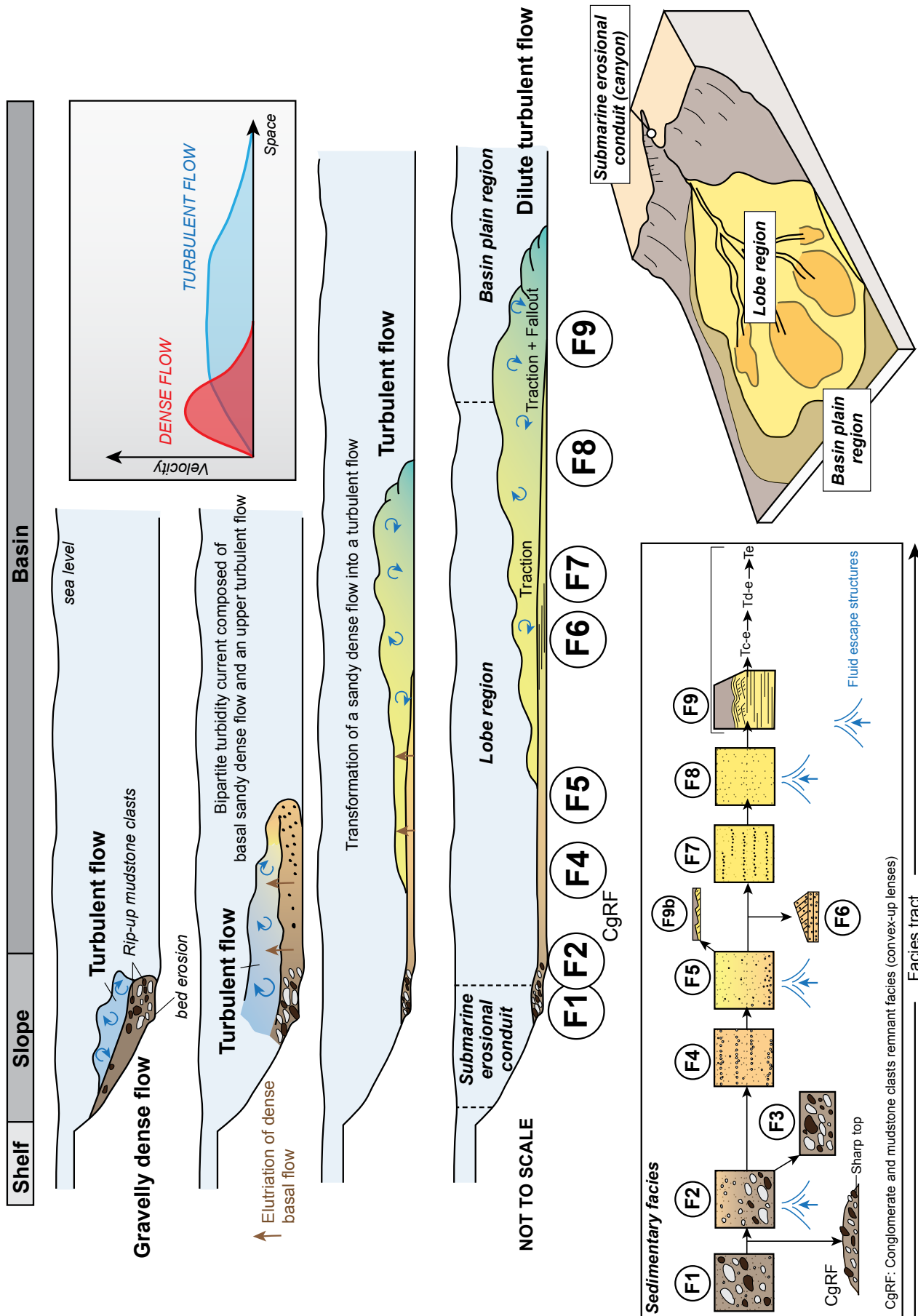


Figure 49. Schematic diagram illustrating the facies tract in turbiditic system. Dense flows evolve into turbulent flows with distance to the shelf break, and grain-size progressively decreases (after Mutti et al., 1999).

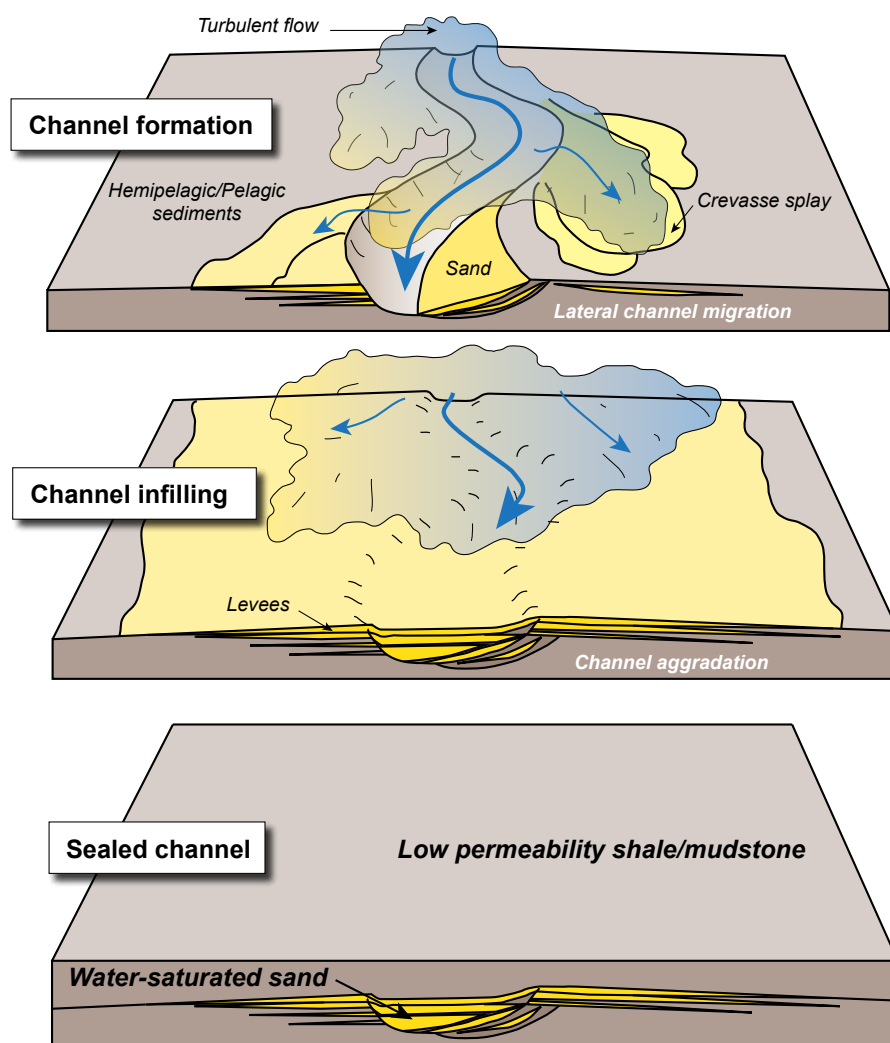


Figure 50. Schematic diagram illustrating processes of channel erosion and sedimentary infill by turbidity flows in deep-marine environments. When the input of clastic sediments ceased, the channels become progressively sealed by hemipelagic/pelagic sediments (modified after Lien et al., 2003).

single events, and are composed of particular **sedimentary sequences** and sedimentary facies (Cf. facies tract in **Fig. 49**). These single sand beds vertically stack within lenticular elements corresponding to **turbidite channels** (**Fig. 50**). The migration of these channels through time leads to **stacked channel systems** embedded within host mud. The different channels inside which clastic sediments are deposited form the **lobate system** (e.g., **deep-sea fans**), which also migrates or stacks through time (**Figs. 49, 50**) .

The lateral migration of the channelized deposits through time combined with the deposition of **fine-grained hemipelagic/pelagic sediments** lead to progressive **sealing of the turbidite channels** (**Fig. 50**). The importance of sealed sand bodies in the generation of fluid overpressures will be later discussed (Cf. section 6.1).

At outcrop scale, deep-sea fans and turbidites can be recognized due to their typical sedimentary sequences characterized by **grading** (i.e., **Bouma sequence**, **Lowe sequence**, **Stow sequence**) and

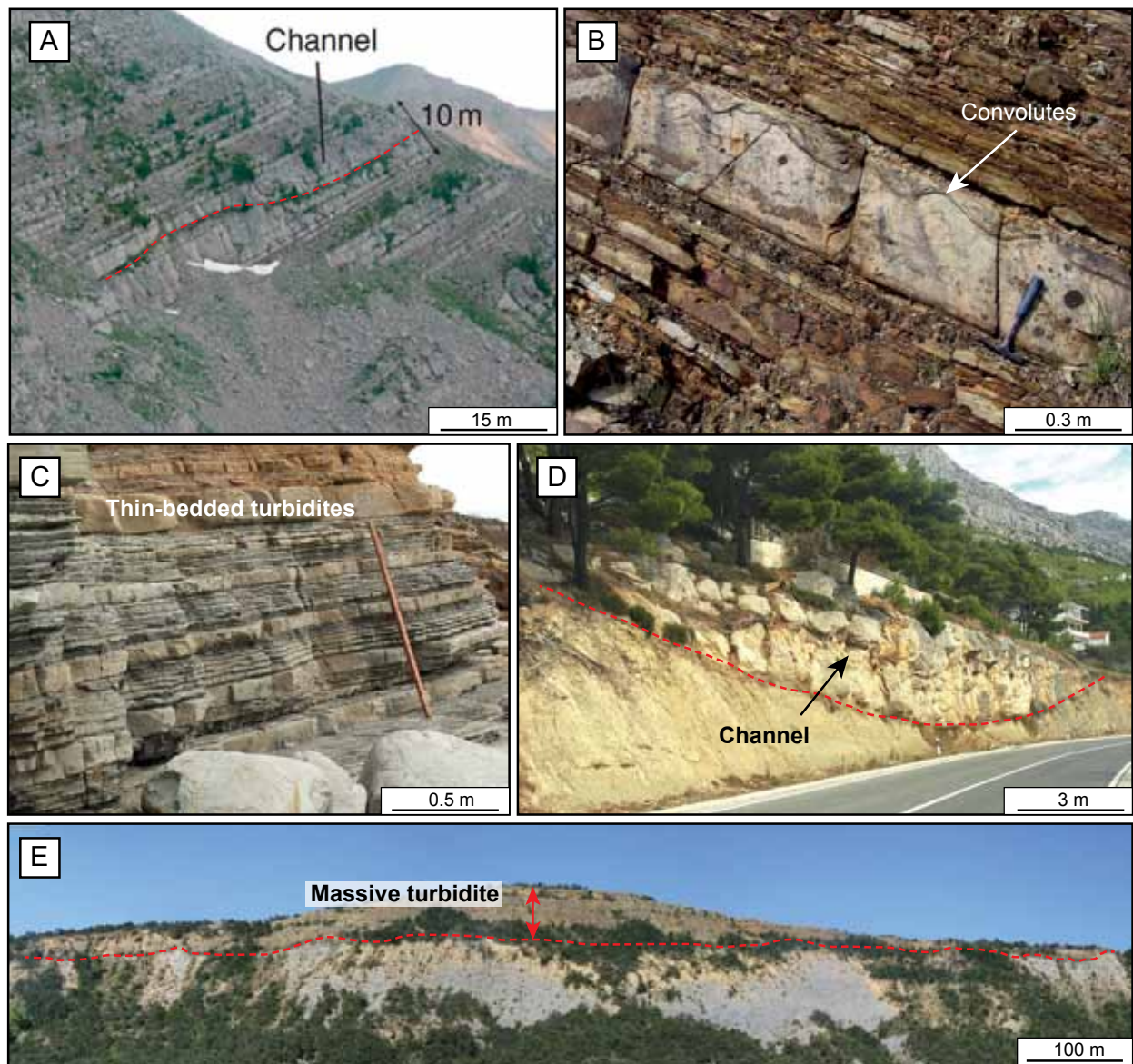


Figure 51. (A) Turbiditic channels at Trois Evêchés, Annot sandstone (SE France) (Mulder, 2011). (B) Sand bed with convolute laminations corresponding to sediment deposition by turbidity flow in the Norton Gully Sandstone (Australia) (vic.gsa.org.au). Convolute laminations correspond to sediment liquefaction triggered by rapid sedimentation. (C) Repetitive alternation of sandstone/mudstone beds corresponding to thin-bedded turbidites (California) ([clastic detritus.com](http://clasticdetritus.com)). (D) Turbiditic channel with erosive base in the Makarska Flysch (Croatia) (picture: W Nemec). (E) Giant and massive turbiditic channels in the Vocontian Basin (SE France).

syndepositional water-escape structures, but also due to their particular **stacking patterns** and **architectures/geometries**. Turbidites commonly show predictable changes in bedding from coarse layers at the bottom to finer laminations at the top, known as **Bouma sequences**. These sequences result from different settling velocities of the particle sizes during waning flows (Bouma, 1962). Alternation of sand beds with shales or mudstones are also good indicators for sediment deposition in deep-marine environments (**Fig. 51A, B, C**). Sedimentary sequences and architecture of the clastic deposits highly depend on their position along the turbiditic system (i.e., conduit exit, slope, lobate system or basin plain). **Channelized morphologies** with **erosive bases**, **scours** and **levees** are frequent in the **lobate region**, while **sheet-like geometries** with thin sand beds are more common in

the **basinal region** (Figs. 49, 51A, D, E). Turbidites can also be **massive** and structureless without preservation of their typical sedimentary sequences and deposited by **high-density turbidity flows** (Lowe, 1982; Mulder and Alexander, 2001) (Fig. 51E).

4. Soft-sediment deformation structures in deep-marine environments

In deep-marine environments, the products of soft-sediment deformation can be classified as:

(1) **in situ**, (2) **detached**, and (3) **injected** (Oliveira et al., 2009) (Fig. 52).

(1) **In-situ deformations** occur without significant downslope movement and generate small-scale structures (less than a meter) that generally form during **rapid deposition** of density flows. They comprise structures related to sediment **liquefaction**, such as convolute laminations, dish structures, ball and pillow structures, pillar structures, etc.,... (Fig. 52).

(2) **Detached soft-sediment deformation structures** are related to laminar sediment transport via **downslope mass flows**. Commonly detached deformation products include large-scale contorted laminations, folding, and faulting (e.g., **slides and slumps**) (Fig. 52).

(3) **Injected deformation structures** involve pressure-driven sediment **remobilization** and forceful **injection** of fluidized sediment into **hydrofractures**. Injection morphologies include dykes, sills, sand volcanoes, etc, ... (Fig. 52).

In this review, we focus on deformations structures that are triggered by increasing porewater pressures (i.e., in-situ and injected deformation structures).

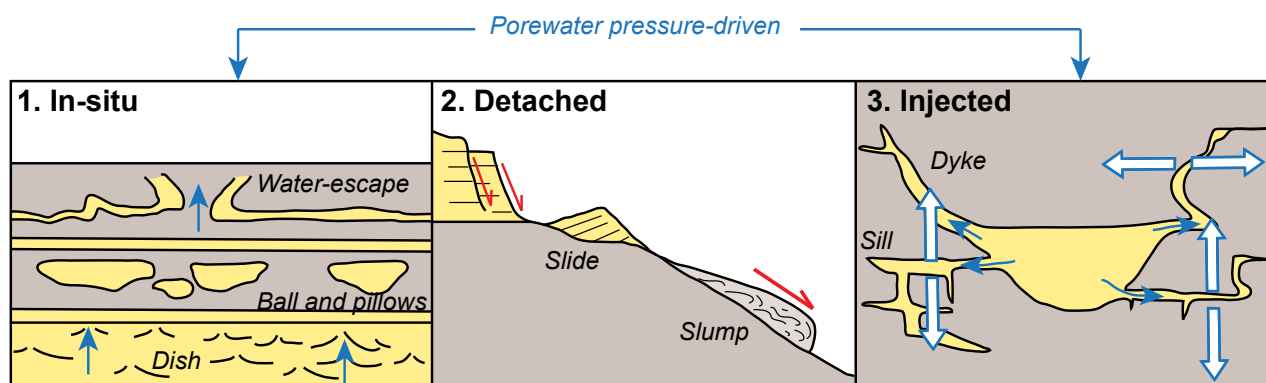


Figure 52. Three groups of soft-sediment deformation structures are identified in deep-water environments. (1) In-situ, (2) Detached, and (3) Injected. In-situ and injected deformation structures are driven by porewater pressure fluctuations within turbidites. (modified after Oliveira et al., 2009).

5. In-situ deformation structures

5.1. Types, morphologies, and processes of formation

In-situ soft-sediment deformation structures mainly correspond to **syndepositional structures**. These deformation structures are common in density flows, especially within turbidite beds, and are generally triggered by **rapid sedimentation** (Lowe, 1975; Allen, 1982). Within turbidite systems, the very rapid deposition of the sediments implies that large amount of water become entrapped in pore throats. This syndepositional excess of porewater pressure is responsible for the early deformation of sediments (Sanders, 1965; Stromberg and Bluck, 1997; Moretti et al., 2001).

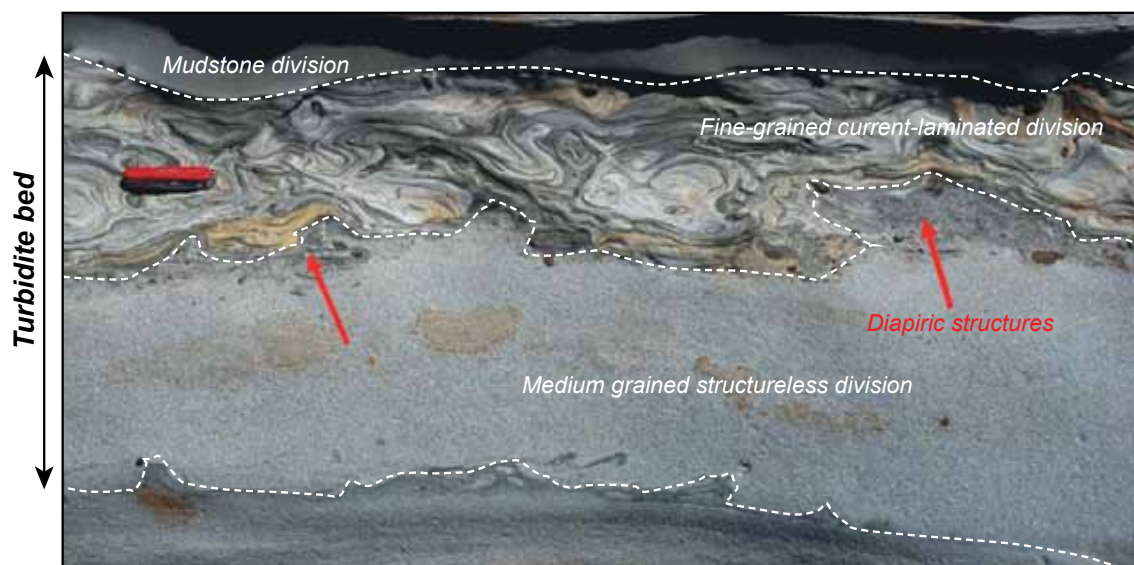


Figure 53. Fining-upward turbiditic bed displaying convolute laminations within the C-unit of a Bouma sequence.

These syndepositional deformations include structures formed by **liquefaction/fluidization** such as: **dish structures, convolute laminations, sheet dewatering structures, pillar structures, balls and pillows, and load casts**.

- **Convolute laminations** are deformation structures that occur most commonly within a single bed. They involve original sedimentary laminations being highly contorted as a result of fluid pressure increase and subsequent sediment liquefaction (Maltman, 1994). They are very common in turbidites and are generally observed within the laminated and cross-laminated parts (C-unit) of a turbiditic sedimentary sequence, sensu Bouma (1962) (**Figs. 53, 54C, D**).
- **Dish structures** are concave disruptions of the layering formed by the upward movement of fluids that are few cm to tens of cm across (**Fig. 54A, B**). They are generally easily recognized because dish morphologies are enriched in clay particles, as evidenced by abundant clay coatings (Hurst

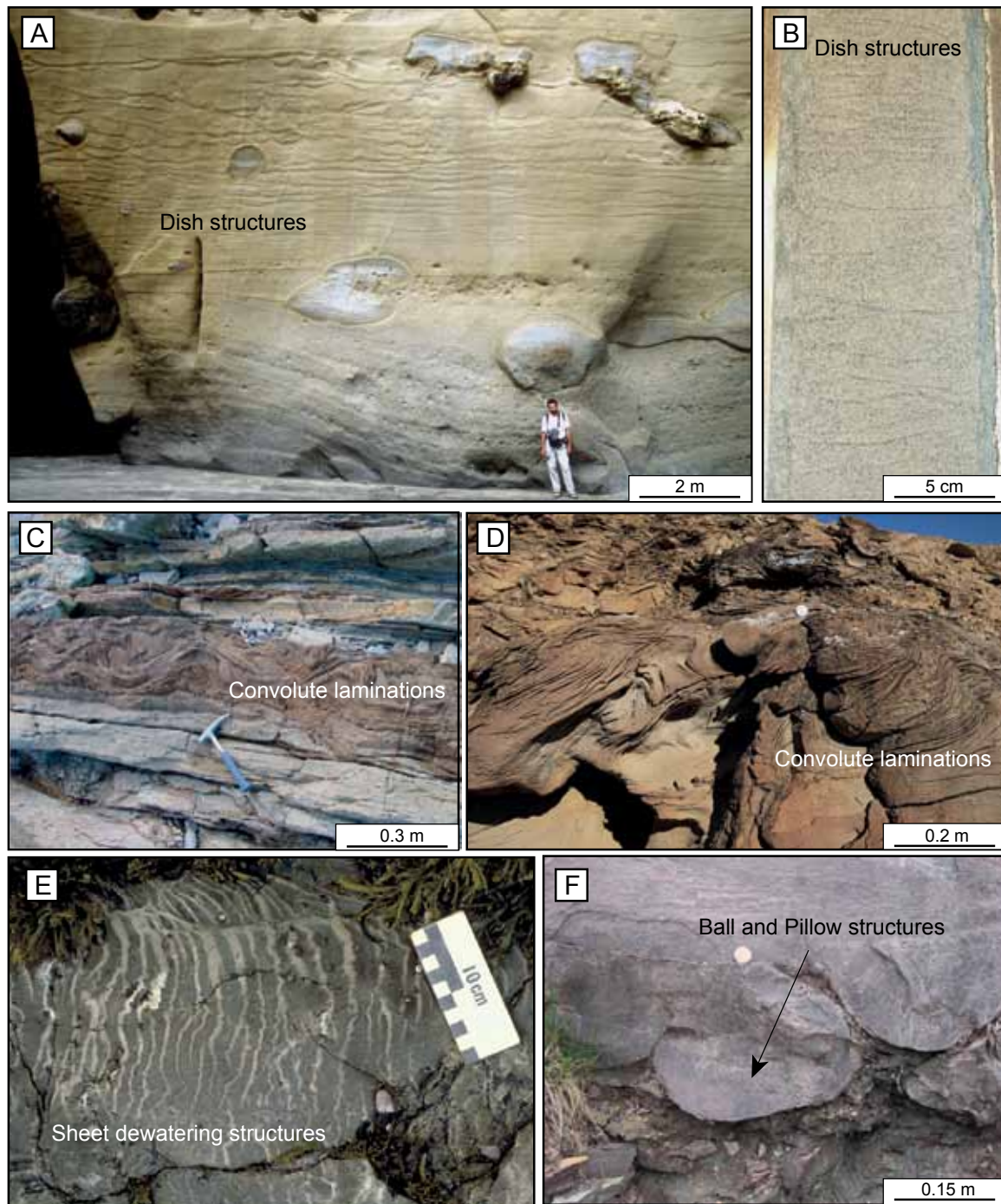


Figure 54. (A) Giant dish structures in turbidites (Peru). (B) Centimetric dish structures in a fine-to-medium grained sandstone turbidite (North sea Basin, Norway) (Jackson et al., 2007). (C) Convolute laminations in turbidites (Basque Flysch, SW France) (Mulder, 2011). (D) Convolute laminations in turbidite bed (Panoche Hills, California). (E) Sheet dewatering structures in a turbidite bed (Irishtown Formation, Canada) (www.ualberta.ca). (F) Ball and pillow structures in turbidite (Swift Run Formation, Virginia) (blogs.agu.org).

and Buller, 1984; Hurst and Cronin, 2001). They form when the porewater excess encounters small horizontal barriers of lower permeability, forcing water to flow until it finds a place to release upward this water excess.

- **Pillar structures** are vertical water-escape pipes that can be simple tubes or have a vertical sheet-like morphology (Maltman, 1994). Dish and pillar structures generally occur together within sediments containing a high water content (e.g, liquefied flows). During the deposition of liquefied

flows, successive freezing from the base to the top of the flow is responsible for ascending fluid-escape structures, such as dish structures or pillar structures (Middleton and Hampton, 1973). It is also thought that pillar structures form during early compaction by the explosive escape of water along vertical, or subvertical columnar, or planar flow paths (Lowe and LoPiccolo, 1974).

- **Sheet dewatering structures** (or dewatering sheets) are similar to pillar structures but are more linear in plan view, and may be closely spaced within the bed (**Fig. 54E**) (Maltman, 1994). Sheet dewatering structures are evidenced by a network of conduits that are generally enriched in clay particles, emplaced during elutriation processes.
- **Ball and pillow structures** are ellipsoidal structures varying from few centimetres to several metres in diameter. These structures are generated by the foundering of sand into mud, especially when a good supply of sand covers rapidly unconsolidated mud (**Fig. 54F**). Their formations are promoted by the liquefaction of sediments (Maltman, 1994).

Soft-sediment deformation structures affecting turbidite beds rarely exceeds few cm thick. However, m-sized deformed beds occasionally occur as illustrated by the giant dish structures observed in Neogene turbidites from Peru (**Fig. 54A**).

5.2. Impacts on reservoir quality

Although no recent studies have been realized on the impact of syn-depositional deformation structures on petrophysical properties, older works demonstrated that **porosity** and **permeability** values within beds affected by soft-sediment deformations structures are highly controlled by the **clay content** (Hurst and Buller, 1984). In such beds, the clay content is often influenced by the elutriation dynamics.

Horizontal and vertical permeabilities are best in units affected by pillar structures because of the very low clay content. Horizontal permeability within dished units remain relatively good even though clay content is high because of the presence of clay-free “washed” zones occurring between individual dishes (Lowe and LoPiccolo, 1974; Hurst and Buller, 1984). However, the vertical permeability in dished units is low because the concentration of the clay into horizontal dishes reduces the permeability values (Hurst and Buller, 1984).

6. Post-burial deformation structures (Injected structures)

Once deposited, **sand bodies** in deep-water environments most commonly become **sealed by low permeability muds** implying that water contained in pore throats is entrapped (**Fig. 50**). The increase of **porewater pressure** within the sealed sand is responsible for the formation of **clastic injections** which represent very common structures in deep-water environments (Dixon et al., 1995; Lonergan et al., 2000; Jolly and Lonergan, 2002; Hurst et al., 2011).

6.1. Conditions for the development of fluid overpressure

Sand represent the dominant grain-size found within **injectites** and derive from the **remobilization** of water-saturated sand deposited within turbiditic channels. To generate high porewater pressures and subsequent **fluid overpressures** within these channels, the water-saturated sand bed must be enclosed in low-permeability material such as mud. Mud prevents the expulsion of porewater from the water-saturated bed. Overpressure is then generated when the **pore fluid pressure is greater than the hydrostatic pressure** (Maltman, 1994), and is function of the permeability of the host material, and the rate at which the pore fluid pressure increases (Glennie and Hurst, 2007).

6.2. Triggers for overpressure development

Three principal external triggers for porewater pressure increase have been identified in deep-water environments: (1) **seismicity and tectonic activity** (Obermeier, 1996; Boehm and Moore, 2002), (2) **rapid loading** (Truswell, 1972; Rowe et al., 2002), and (3) the **migration of additional fluids** (Brooke et al., 1995; Davies et al., 2006; Monnier, 2013) (**Fig. 55**). Seismicity and rapid loading are the most commonly cited triggers for the development of high porewater pressures within sand bodies (Jolly and Lonergan, 2002).

(1) **High magnitude earthquakes (> 6)** can trigger an increase of porewater pressures and soft-sediment deformation 15 to 20 km away from seismic epicentres (Rosetti, 1999). The generation of high porewater pressure is the result of cyclical shear stresses affecting the water-saturated sediments during earthquakes shaking (Obermeier, 1996) (**Fig. 55A**).

(2) **Rapid loading** caused by the transport and **deposition of mass-flows** is responsible for the

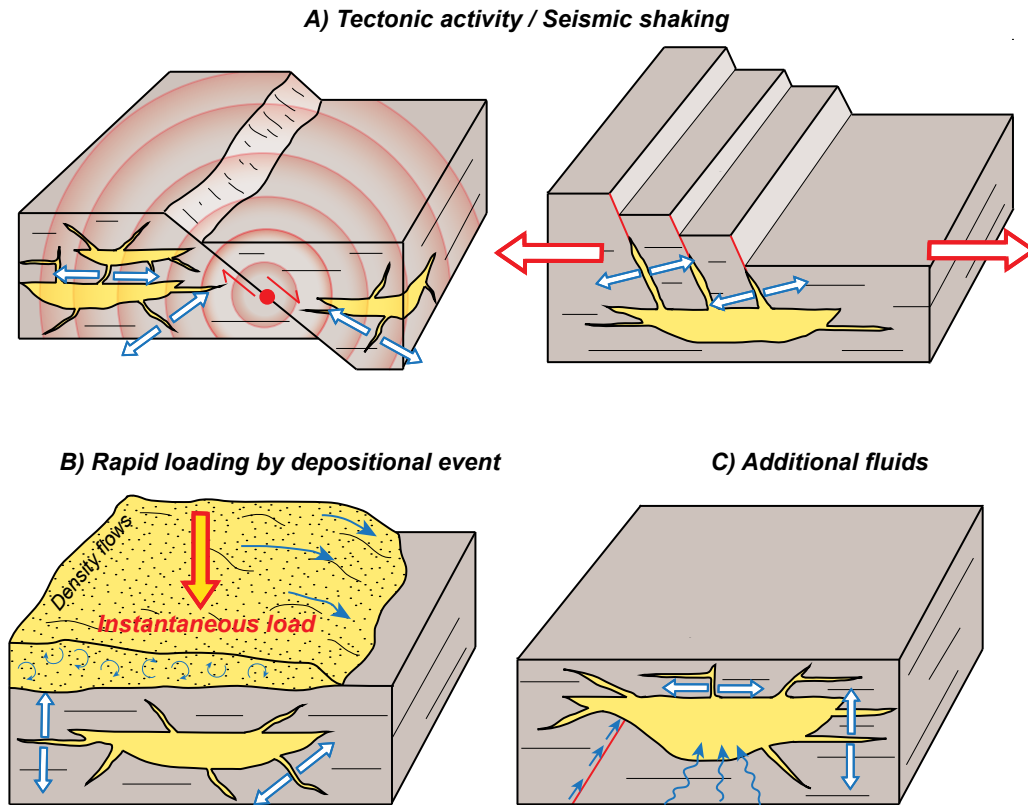


Figure 55. External triggers proposed for the development of high porewater pressures and the generation of clastic injections.

development of high porewater pressures within sealed sand bodies located near sea floor (Rowe et al., 2002; Strachan, 2002; Jonk et al., 2007). Mass-transports are generally triggered by gravitational instabilities along submarine slopes. Storm waves can also induce sudden loading of the sea floor and potentially high fluid pressure within sealed sand bodies (Hildebrandt and Egenhoff, 2007) (**Fig. 55B**).

(3) **Rapid migration of fluids** into depositional and sealed sand bodies may also generate high fluid pressures. Fluids may originate from mineralogical phase changes (Davies et al., 2006), or rapid migration of hydrocarbon gas (Brooke et al., 1995). The migration of fluids into sand bodies can also be facilitated by faults (Monnier, 2013) (**Fig. 55C**).

6.3. Processes of clastic injections formation

The increase of porewater pressure within sealed sand bodies frequently triggers the formation of hydrofractures filled by injected sediments.

6.3.1. Hydrofracturing

When the **porewater pressure** within the sand bodies exceeds the **tensile strength** of the seal lithology, seal failure occurs by **hydraulic fracturing (i.e., hydrofracturing)**. The increase of fluid pressure acts so as to oppose the compressive stress (σ_1, σ_3), and cause them to be reduced to the effective stresses ($\sigma_1 - P_{H_2O}$; $\sigma_3 - P_{H_2O}$). The increase of fluid pressure induces lateral migration of the **Mohr circle** to the left (**Fig. 56**). The Mohr circle touches the failure envelope indicating failure driven by increasing fluid pressure, known as hydraulic fracturing. The sudden increase of fluid pressure responsible for the development of hydrofractures is promoted by the conjunction of **overburden pressure increase (σ_1)** during burial and an **external trigger (Figs. 55, 57C)**.

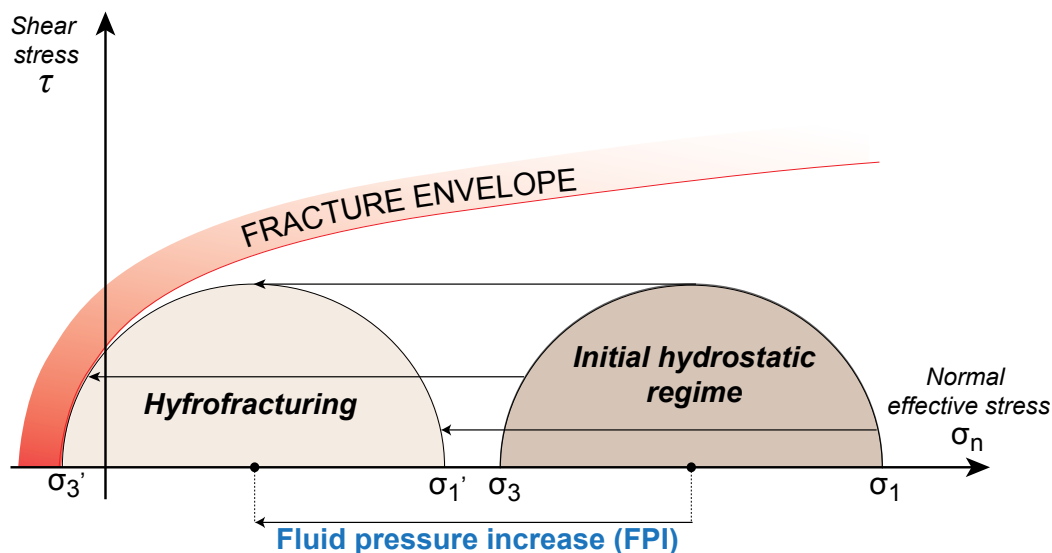


Figure 56. Mohr circle representation of the hydrofracturing principle. The effect of fluid pressure increase is to move the Mohr circle to an amount equal to the increase of fluid pressure (FPI) until it touches the failure envelope. Failure induced by this increase of porewater pressure is referred to as hydraulic fracturing (i.e., hydrofracturing).

6.3.2. Injection of fluidized sediments

The excess of porewater into the sealed sand units is responsible for sediment **liquefaction/ fluidization**. Liquefaction/fluidization occurs when grains are no longer supported by intergranular friction but are momentarily suspended by the ambient pore fluid (Lowe, 1975). The fluidization of sediments implies a continuous flow of fluids through the sediments, indicating that the **fluid-drag forces balance or exceed the particles weight (Fig. 57D)**. Although processes of liquefaction have been associated to the injection of clastic sediments in seismically-induced overpressurized sand units (Obermeier, 1996; Takahama et al., 2000), fluidization remains the main mechanism involved during the injection of clastic material into hydrofractures (Duranti and Hurst, 2004). Clastic injections are

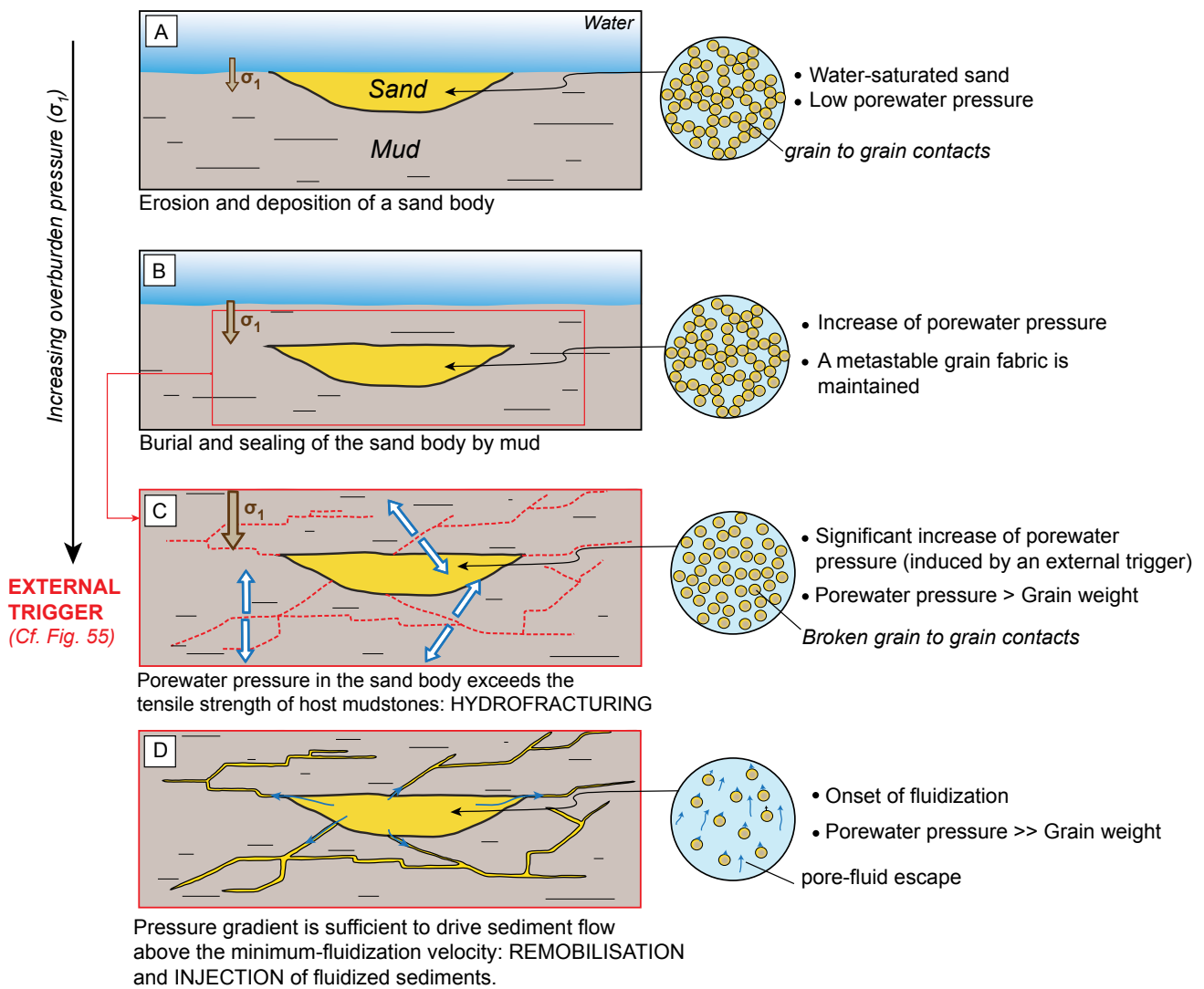


Figure 57. Schematic diagram illustrating the evolution of the grain fabric with progressive development of hydrofractures and clastic injections in deep-marine environments. (A) Deposition of a water-saturated sand lens that become progressively sealed by low-permeability mud (B). (C) The increase of overburden pressure during burial combined with the stress exerted by an external trigger promote the development of fluid overpressures within the sand. Overpressure is released through processes of hydrofracturing. (D) Once hydrofractures form, pressure gradient in sand is sufficient to trigger fluidization, remobilization and injection of sediments into the hydrofractures (Modified after Hurst et al., 2011).

considered to form by the complete fluidization of sediments into a fracture when the pressure gradient is sufficient to drive upward-flow above the minimum fluidization velocity (Gallo and Woods, 2004). During the injection of sediments, erosion of the hydrofracture margins are common and result from the interaction between high-velocity fluidized sand and the host strata (Werther and Reppenhagen, 2003; Diggs, 2007; Scott et al., 2009).

The fluidized flow regime during sand injection is still debated and is thought to be **laminar** (Sturkell and Ormö, 1997) or alternatively to be **turbulent** (Duranti, 2007; Hubbard et al., 2007; Levi et al., 2011). The lack of consensus on the type of flow regime during injection is explained by contrasting interpretations of the grain-size variations recorded in certain clastic injections. In sandstones dykes, normal grading has been interpreted as a record of turbulent flows during the injection (Hubbard et

al., 2007) but have alternatively been used as evidence for viscous laminar flow regime (Peterson, 1968). The occasional occurrence of laminae and imbricated clasts within injected sandstones suggests that bedload layers moved during sustained periods of traction (Kawakami and Kawamura, 2002; Scott et al., 2009).

7. Morphology of clastic injections

Clastic injections networks can be subdivided into four main geometrical elements: **dykes**, **sills** (i.e., **clastic intrusions**), **clastic extrusions** and **parent units** (Figs. 58, 59). **Clastic dykes** are discordant structures cross-cutting host bedding at high and low angles. **Clastic sills** are tabular bodies that are concordant to the host bedding (Fig. 58). **Clastic extrusions** are formed by the venting of sand on palaeo-sea floor (Fig. 58). Some other injection morphologies have described in the literature, especially when using subsurface data (e.g., conical injections, wings, “saucer-shaped” injections) (Jackson, 2007; Monnier et al., 2014) (Fig. 58). Parent units correspond to the depositional

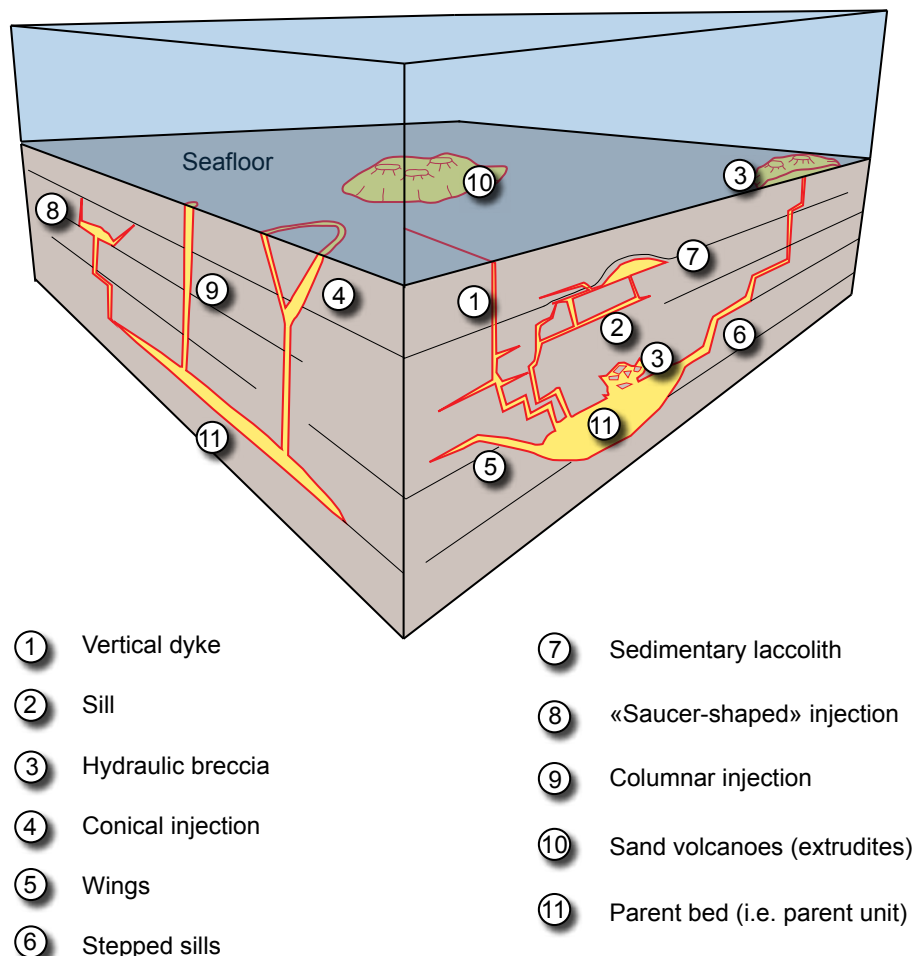


Figure 58. Terminology and morphology of the different elements potentially found in clastic injection networks. (modified after Hurst and Cartwright, 2007; Braccini et al., 2008; Monnier, 2013).

sandstones remobilized during sand injection and represent the source for the formation of clastic intrusions and extrusions (**Fig. 59**).

A **tri-partite organization** has been ascribed to clastic injection networks (Vigorito et al., 2008; 2010; Scott et al., 2013) involving **parent sandstone units** feeding an **intrusive complex** (composed of dykes and sills) and an **extrusive complex** with sand volcanoes sourced from the underlying intrusive complex (**Fig. 59**).

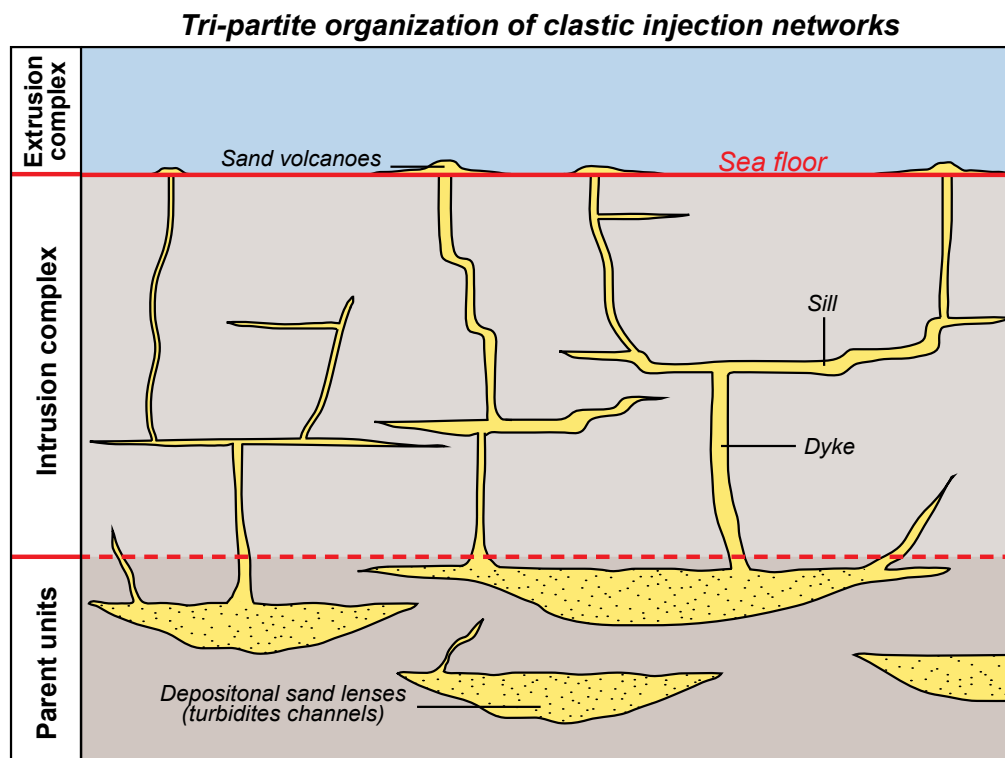


Figure 59. Schematic diagram illustrating the tri-partite organization of clastic injection networks, with parent units at the base, the intrusion complex in an intermediate zone, and the extrusion complex reaching the sea floor at the top.

- Clastic dykes

Clastic dykes display a wide range of geometries from straight and planar to highly irregular, bulbous, and curved (Taylor, 1982; Parize et al., 2007). Planar dykes are generally indicative of sand injections along planar fractures (**Fig. 60B, C**). The formation of irregular and bulbous dykes are thought to reflect the anisotropy of the host strata and post-injection folding and boudinage induced by compaction (Truswell, 1972). Tapering, bifurcating, or braided dyke morphologies are also common (Strachan, 2002; Hubbard et al, 2007; Vetel and Cartwright, 2010) (**Fig. 60D**). Depending on the fracturation of the host rock, some other geometries can be observed including “en echelon”, or “zig-zag” geometries (Huang, 1988; Hoek, 1991; Vétel and Cartwright, 2010). Ptygmatic features caused by post-injection compaction are frequent and evidenced by the frequent occurrence of folded

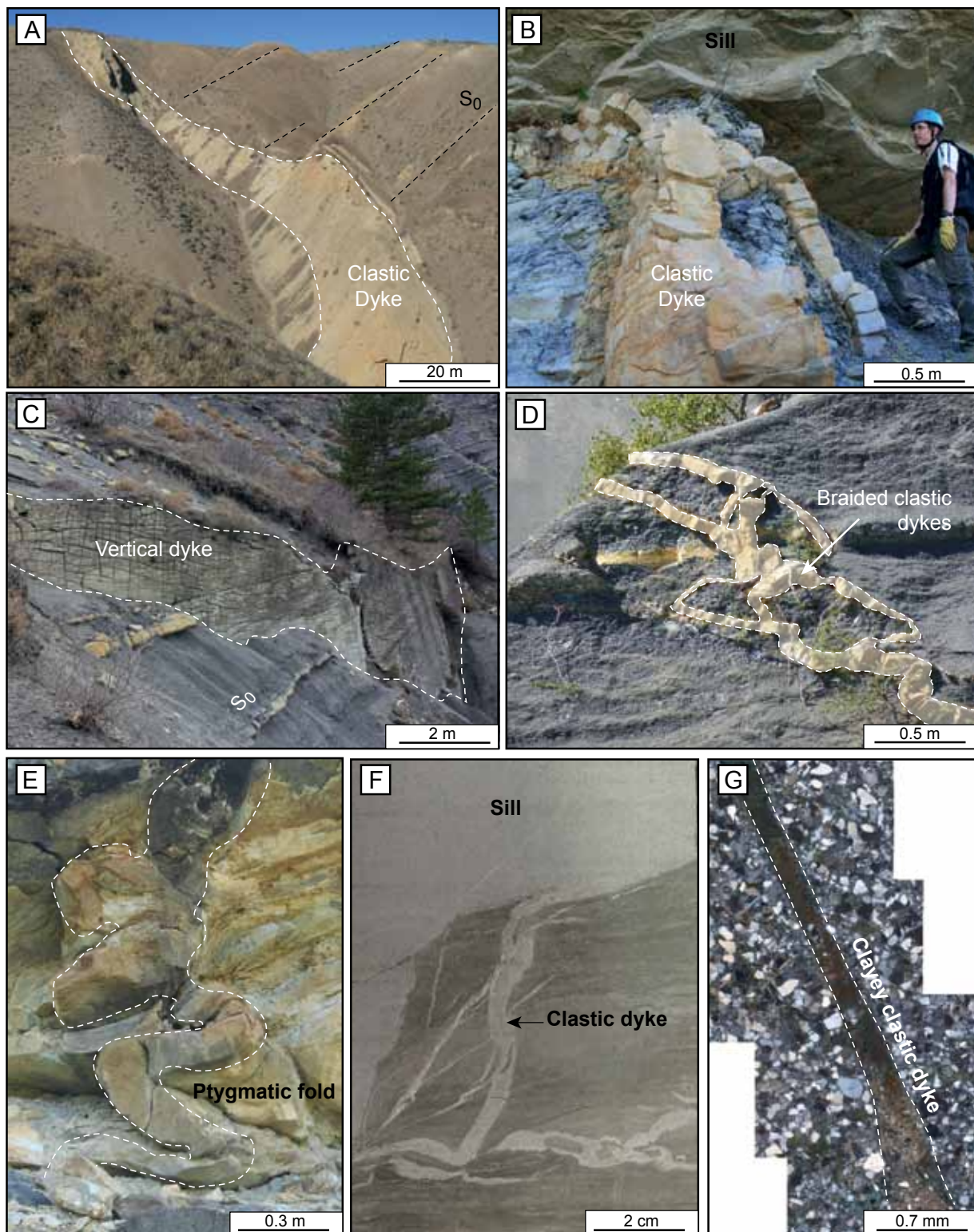


Figure 60. Multi-scale dyke morphologies. (A) Giant clastic dyke in the Panoche Hills (California). (B) Straight clastic dykes connected to a sill (Vocontian Basin, SE France). (C) Sandstone wall formed by the development of a straight and vertical dyke (Vocontian Basin, SE France). (D) Braided dyke morphology (Vocontian Basin, SE France). (E) Ptygmatic folds in a clastic dyke caused by post sand injection compaction (Vocontian Basin, SE France). (F) Small-scale clastic dyke connected to a sill observed at core-scale (Offshore Mauritania). (G) Micro-scale clastic dyke composed of clayey material (Vocontian Basin, SE France).

dykes (Hillier and Cosgrove, 2002) (**Fig. 60E**). The dyke thickness varies from mm to m and can be few cm to hundreds of m long (**Fig. 60A, F, G**). Clastic dykes tend to become thinner away from the source (Jonk et al., 2003; Kane, 2010). They are generally more abundant close to the parent units,

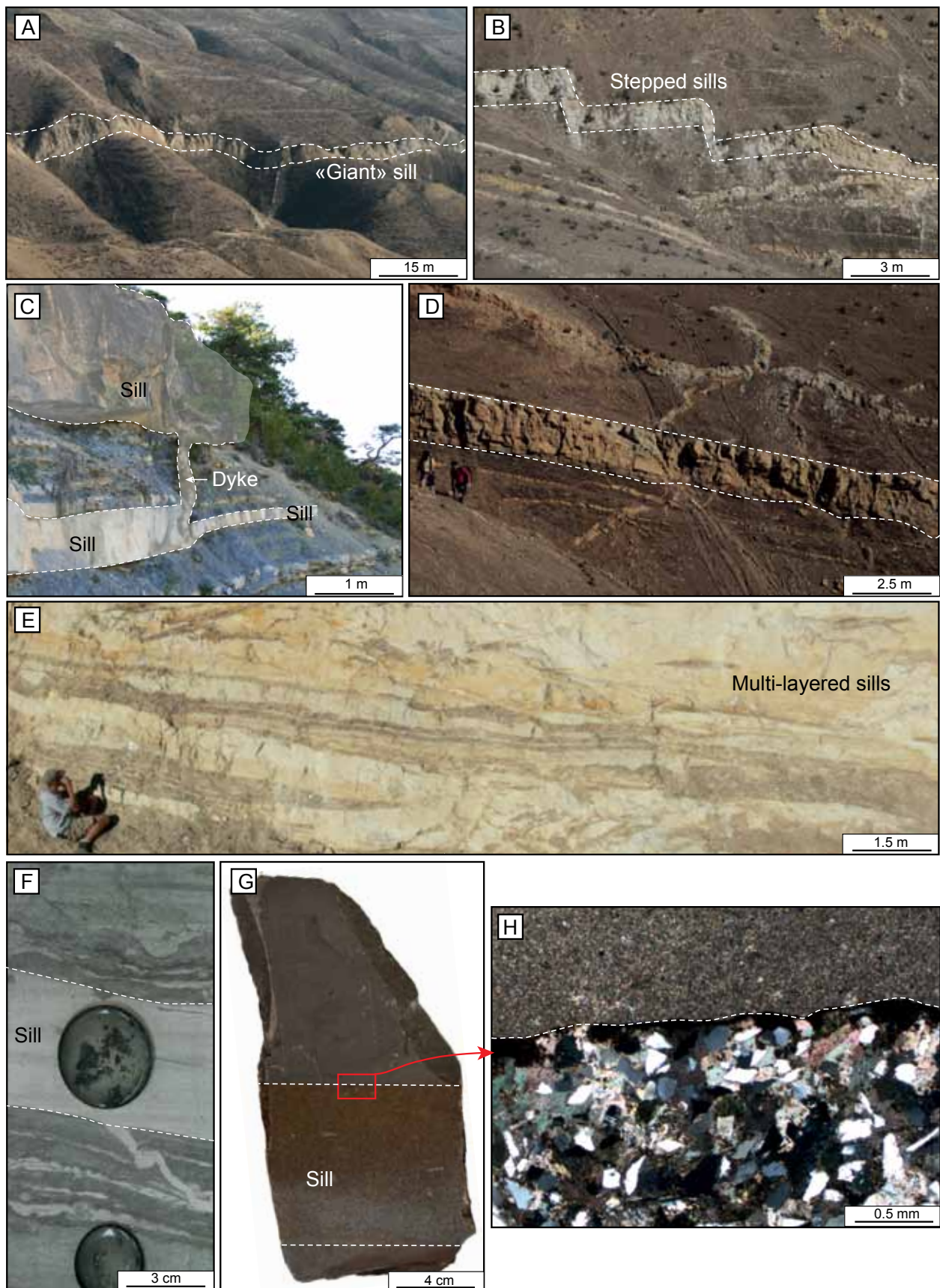


Figure 61. Multi-scale sill morphologies. (A) Giant sill in the Panoche Hills (California). (B) Staircase sill morphology referred to as stepped sills (Panoche Hills, California). (C) A rapid lateral change of sill thickness induced by a dyke connection (Vocontian Basin, SE France). (D) Thick sill developing parallel to the bedding (Panoche Hills, California). (E) Multi-layered sills (Panoche Hills, California) (Hurst et al., 2011). (F) Clastic sill composed of homogenized fine-grained sand (offshore Mauritania). (G) A clastic sill with straight margins. (H) Close-up on the straight contact between injected sand and host limestone (Vocontian Basin, SE France).

and where host sediments are cross-cut by faults (Huang et al., 1988). On the margins of sandstones dykes, mm to cm-sized marks frequently occur, including flute marks (Peterson, 1968; Hubbard et al., 2007), grooves (Surlyk and Noe-Nygaard, 2001), rills (Diggs, 2007), scours (Martill and Hudson, 1989), and frondescant/gutter marks (Surlyk and Noe-Nygaard, 2001; Keighley and Pickerill, 1994). These different marks observed along the margins record the interaction between the pressurized fluidized sand and the host strata during injection.

- Clastic sills

Although **sills** are clastic intrusions that are concordant with host strata, they often bifurcate, taper and step (Hillier and Cosgrove, 2002; Huuse et al., 2004; Lonergan et al., 2007; Parize et al., 2007; Scott et al., 2013). Three main geometries are recognized in sills: staggered, multi-layered and stepped sills (**Fig. 61B, E**) (Vigorito et al., 2008; Vigorito and Hurst, 2010; Scott et al., 2013). The sill thickness varies from mm to m and can locally reach tens of m thick. Their thickness tend to decrease away from the parent bed (Surlyk and Noe-Nygaard, 2001; Parize et al., 2007) (**Fig. 61A, F, G**). The thickness of sills can laterally change; pinch and swell structures are common (**Fig. 61C**) (Diggs,

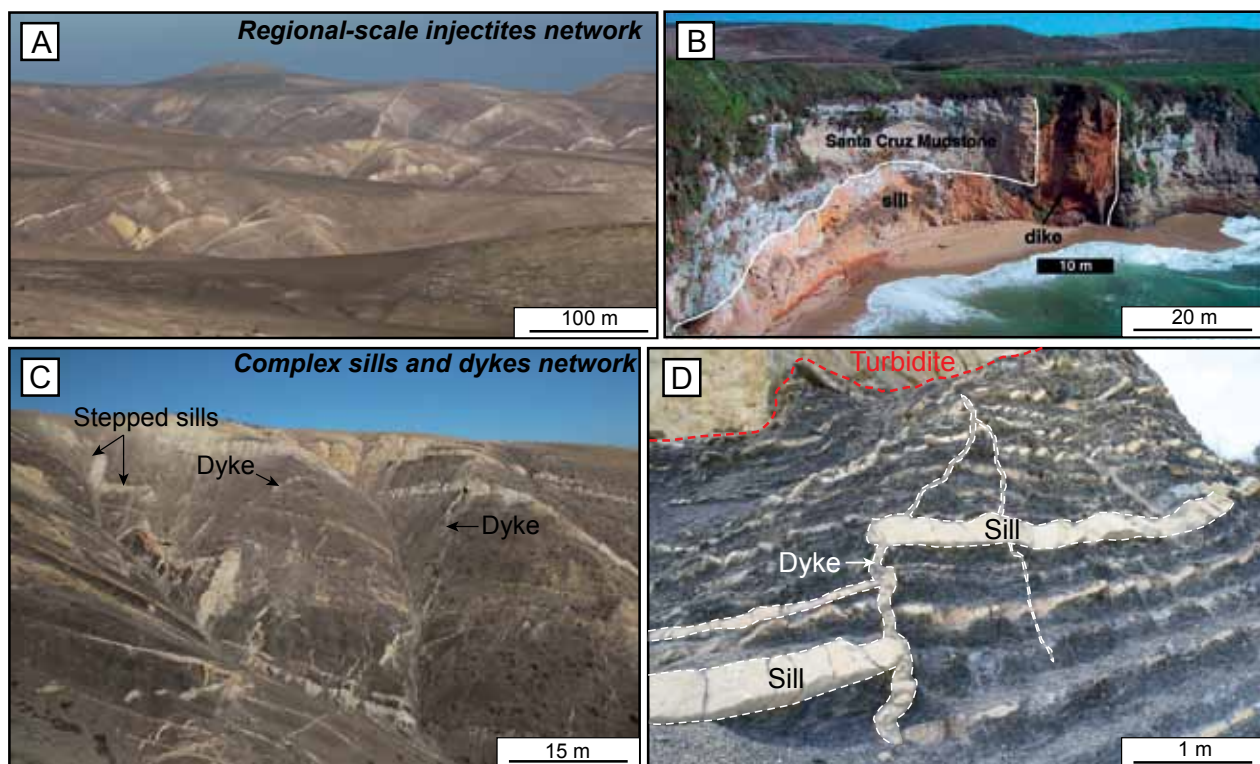


Figure 62. Sills and dykes networks. (A) Regional-scale injectites network composed of sills and dykes (Panoche Hills, California). (B) Giant sill and dyke network (Yellow Bank Creek, California) (Boehm and Moore, 2002). (C) Outcrop-scale network composed of stepped sills, sills, and high-angle dykes (Panoche Hills, California). (D) High-angle dykes and sills network (Vocontian Basin, SE France).

2007). The lateral extent of sill can reach several km, although mean extents generally reach few tens of m (Obermeier, 1996; Parize et al., 2007). Sills preferentially propagate along stratigraphical (bottom or top of sedimentary beds) or sedimentological heterogeneities (abrupt changes in lithology). Sill margins can be straight (**Fig. 61G, H**) or irregular due to erosion of the host strata during injection of fluidized sediments (**Fig. 61E**) (Kawakami and Kawamura, 2002; Scott et al., 2009; Kane, 2010). Erosional features occur at both upper and lower margins which help to discriminate sills from parent beds. Along sills, up to 4 m of erosion into overlying mudstones has been observed (Scott et al., 2009). Similarly to dykes, marks recording the injection of fluidized sand along the margins occur, and notably include flutes, scours and grooves (Kawakami and Kawamura, 2002). Dykes and sills frequently occur together forming complex networks with multiple connections at microscale to regional scale (**Fig. 62**).

- Clastic extrusions

Clastic extrusions, also referred to as **extrudites** (Hurst et al., 2006), consist in **sand volcanoes** or **composite sheet-sand units**. Sand volcanoes are the most common elements formed during sand extrusions, they display typical conical to elliptical geometries that are sourced by individual dykes (**Fig. 63A, B**). Sand volcanoes can reach 0.75 m thick and their diameters generally range between 0.3 and 3 m (Hurst et al., 2011). Some sand volcanoes could reach much higher dimensions as illustrated by a giant volcano ($5.3 \cdot 10^7 \text{ km}^3$) recognized in the North sea subsurface data (Andresen et al., 2009). Instead of building sand volcanoes, the extrusion of fluidized sediments can form sand sheets that can reach 3 m thick and extend laterally for several hundred of m (Boehm and moore, 2002; Hurst et al.,

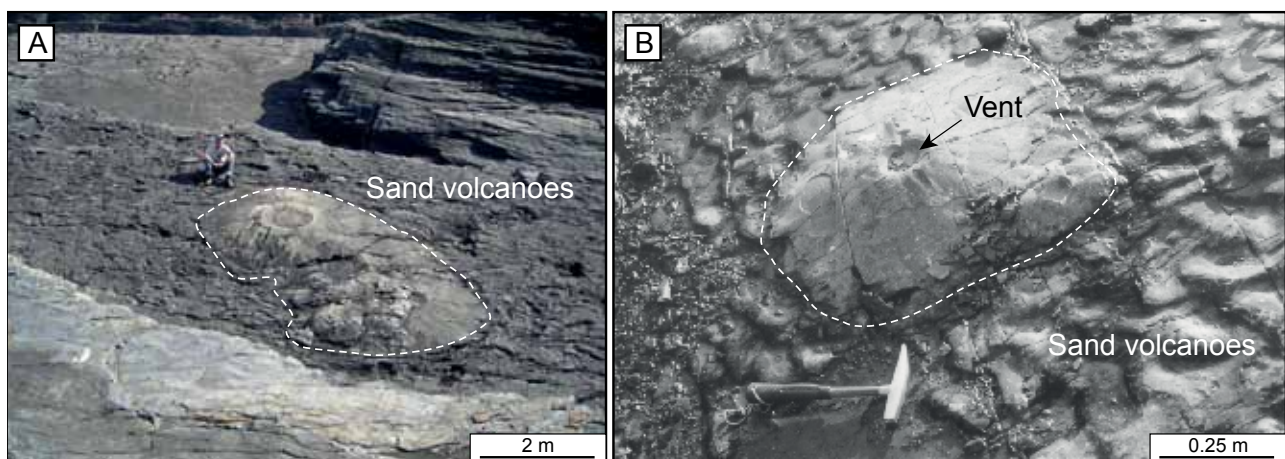


Figure 63. Clastic extrusions. (A) Sand volcanoes in deep-marine sediments (Ross Formation, County Clare, Ireland) (www.sepmstrata.org). (B) Sand volcanoes (Ross Formation, County Clare, Ireland) (Jonk et al., 2007).

2006; Vigorito et al., 2008).

- Other injection morphologies

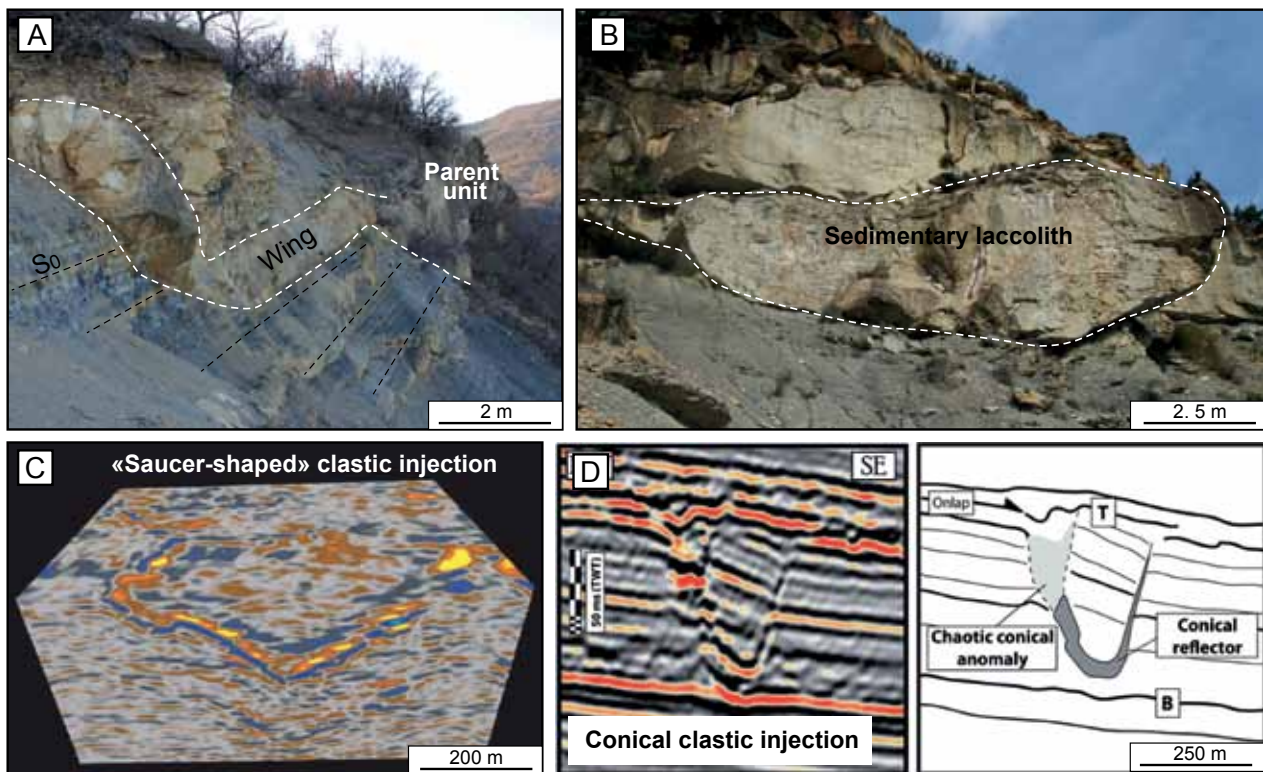
Other injection morphologies include **wings**, **conical injections**, «**saucer-shaped**» injections and **sedimentary laccoliths**. These morphologies are commonly found within tertiary deep-water sediments of the North sea and determined on the basis of subsurface data (Huuse et al., 2007; Cartwright et al., 2008). However, such morphologies have rarely been identified along outcrops (Vigorito and Hurst, 2010).

Wings correspond to sills and dykes emanating from the parent bed and are generally evidenced by two low-angle (10-40°) high-amplitude seismic reflectors connected to depositional sand bodies (Huuse et al., 2004; Jackson et al., 2007; Monnier et al., 2014) (**Fig. 58**). Such geometries have also been recognized on the field (Monnier, 2013) (**Fig. 64A**). Winglike morphologies can reach hundreds of m long and few m thick (Jackson, 2007; Jackson et al., 2011). Wings generally propagate upwards (Waterson, 1950) but occasionally downwards (Parize et al., 2007). Wings can laterally propagate over few kilometers (Huuse and Mickelson, 2004).

Conical injections or **saucer-shaped injection** morphologies are intrusions emanating upwards from deep sand bodies (Molyneux et al., 2002; Huuse et al., 2007; Cartwright et al., 2008; Monnier et al., 2014) (**Fig. 58**). The base of conical intrusions is planar, while saucer-shaped intrusions display v-shaped bases (Cartwright et al., 2008) (**Fig. 64C, D**). Conical anomalies detected on seismic data indicate that these clastic intrusions can reach few hundreds of m in diameter and tens of m high (Monnier et al., 2014).

Sedimentary laccoliths represent concordant sheet-like intrusions that have been injected between two layers of the host sediments (Cartwright et al., 2008). The pressure exerted by the upward flow of overpressurized sediments is high enough that the overlying strata are forced upwards giving the sedimentary laccoliths a dome or mushroom-like form, with a planar base (**Fig. 64B**). Sedimentary laccoliths are connected to dykes. The lateral extent of sedimentary laccoliths can reach hundreds of m and tens of m thick (Monnier, 2013).

Figure 64. Other clastic intrusions morphologies. (A) Wing morphology observed at outcrop scale (Vocontian Basin, SE France). (B) Outcrop-scale sedimentary laccolith (Vocontian Basin, SE France). (C) Three-dimensional visualization of a conical injection using subsurface data (Viking Graben, North Sea) (Huuse et al., 2007). (D) Saucer-shaped anomalies related to clastic intrusions and interpretative geological line drawing (Lower Congo Basin, Congo) (Monnier et al., 2014).



- Parent units

Modifications of the **parent unit** external geometries after remobilization and multiple injections have been observed using subsurface data (Hillier and Cosgrove, 2002), however the absence of outcrop examples does not allow to assess detailed post-remobilization changes in external morphologies. The increase of porewater pressure combined with fluidization processes and sediment remobilization triggered modifications of pre-existing depositional structures. **Remobilization and injection** due to porewater pressure increase is recorded in parent units through progressive **grading of preserved depositional structures into upward deformed laminae, giant pillars and structureless sandstones** (Hurst et al., 2003; Duranti and Hurst, 2004). In a typical sequence of increasing porewater pressure and fluidization intensity, structureless sandstones occur at the top of the sequence (Duranti and Hurst, 2004).

8. Internal sedimentary structures

The deposition of **fluidized sediments** tends to generate **homogenized clastic injections**, thus forming **structureless fractures-fills** (Hillier and Cosgrove, 2002; Parize et al., 2007). Most of the clastic injections are composed of fine to medium sand because such grain-sizes are characterized

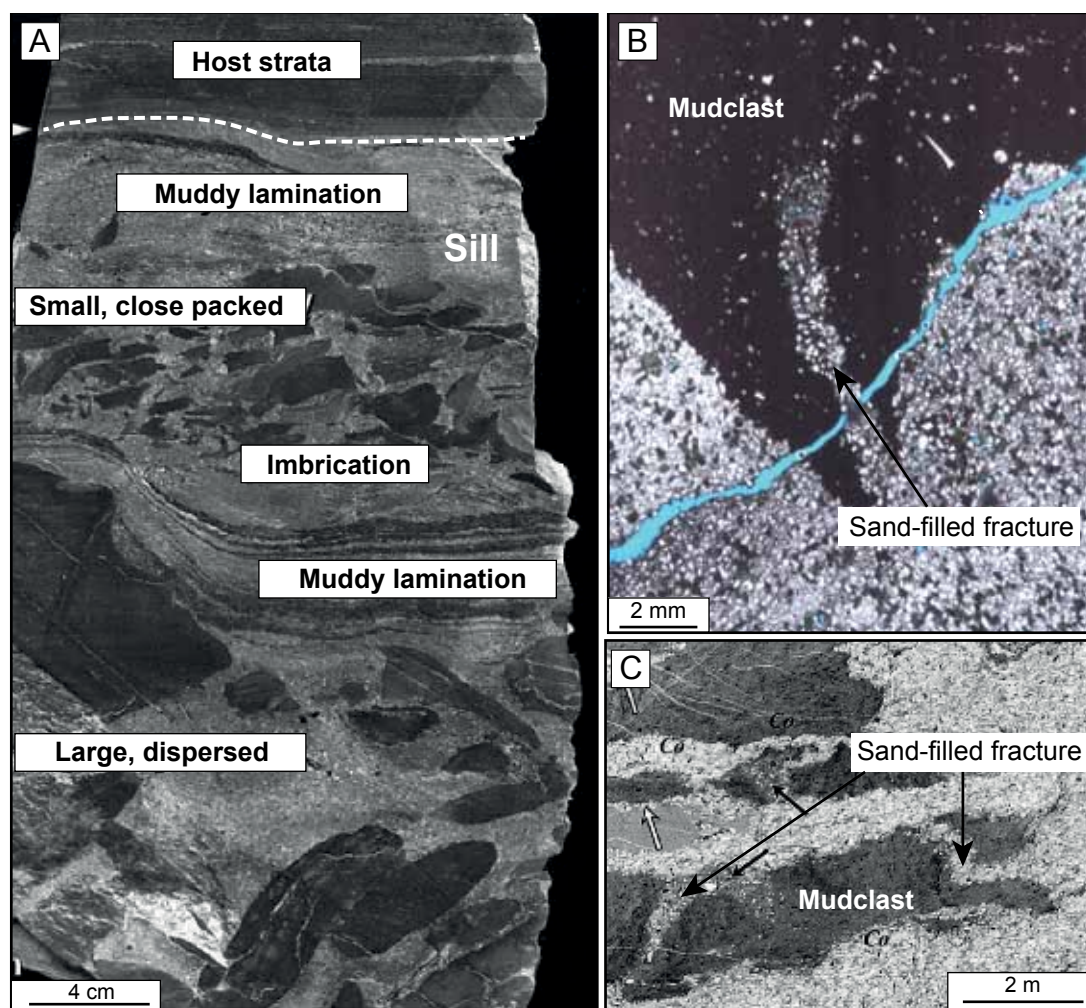


Figure 65. Internal sedimentary structures. (A) Well-developed muddy laminations in a sandy sill. Laminations are bounded by the different layers of size-differentiated mud clasts (Osawa Formation, Japan) (Kawakami and Kawamura, 2002). Microscale intraclasts displaying a microfracture infilled by fine-grained sand (sample taken in a clastic dyke) (Vocontian Basin, SE France). (C) Microscale intraclasts displaying wedge-shaped fractures filled by sand, sample is taken in a clastic sill (Osawa Formation, Japan) (Kawakami and Kawamura, 2002).

by low minimum fluidization velocities, thus being more easily remobilized (Lowe, 1975). However, structures and grain-size variations frequently occur within injectites. Variations in grain-size depend on the composition of the parent unit, but also on the internal concentration of mudstone intraclasts (Kawakami and Kawamura, 2002).

Banding and laminae oriented parallel to the margins of the injection have frequently been reported in dykes (Hillier and Cosgrove, 2002; Diggs, 2007), and more occasionally within sills (Kawakami and Kawamura, 2002) (**Fig. 65A**). Bands or laminae are bounded by sharp contacts and can be easily distinguished due to the difference in grain-size between single elements (Taylor, 1982; Hubbard et al., 2007). Bands are generally comprised between 0.01 m and 0.1 m thick while laminae never exceeds 1 mm thick. The formation of bands and laminae is attributed to multiple episodes of injection (Taylor, 1982; Le Heron and Etienne, 2005; Diggs, 2007), irregularities in the rate of fracture opening (Peterson, 1968), or variations in both velocity and viscosity of the injected fluidized material

(Peterson, 1968; Taylor, 1982; Diggs, 2007).

Grading frequently occurs within dykes and sills, perpendicular to the margins of the injection but also along the injection length. Both normal and reverse grading have been depicted within clastic injections (Hubbard et al., 2007). The grading in sandstone injection is poorly constrained. Hubbard et al. (2007) suggested that turbulent flows during injection are responsible for normal grading, while Taylor (1982) interpreted these grain-size variations as laminar flow deposits. Within sandstone extrusions, low-angle beds and laminae dipping away from the central venting point are frequently observed (Pringle et al., 2007; Jonk et al., 2007). Cross-bedding like structures can also be distinguished in extrudites, reflecting the interfingering and stacking of different volcanic cones (Hurst, 2004).

Host-mudstone or limestones clasts are frequently observed within clastic injections. Clasts can vary from mm to m for their longest axis and are generally angular, elongated and slab-shaped (**Figs. 65, 66**). Although clasts can be isolated, they are frequently clustered forming a **breccia-like fabric** (**Fig. 65**). Host strata clasts are sometimes cross-cut by sand-filled mm wide micro-fractures and also

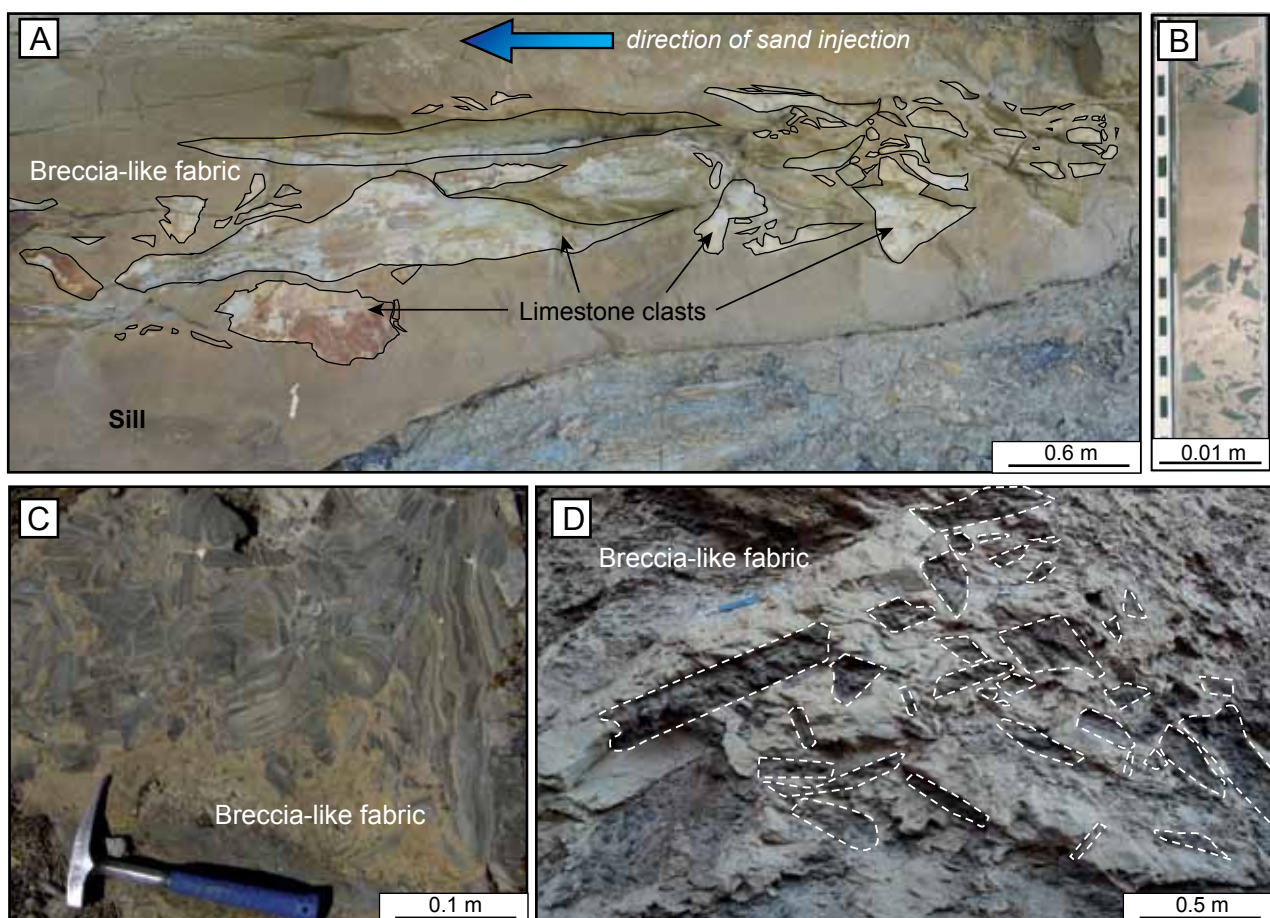


Figure 66. Breccia-like fabrics in clastic injections. (A) Clustered angular limestone clasts within a sill (Vocontian Basin, SE France). (B) Core-scale breccia-like fabric distinguished within a dyke, also referred to as intrusion breccia (Gryphon Field, North Sea) (Lonergan et al., 2007). (C) Intrusion breccia composed of angular slab-shaped clasts (Odonne et al., 2011). (D) Clustered angular clasts within a clastic sill (Panoche Hills, California).

contain embedded quartz grains (**Fig. 65B, C**). The occurrence of such clasts has been interpreted as the result of **corrasion**, **scouring** and **fracturing** of the hydrofracture margins during injection of fluidized sand (Kawakami and Kawamura, 2002; Scott et al., 2009). Embedded quartz grains illustrate processes of grains impingements upon the margins of the fractures during sand injection, at high velocity and at non-zero angles (Scott et al., 2009). Clusters of mudclasts forming a “jigsaw-like” breccia fabric is interpreted as **in-situ hydraulic brecciation** without subsequent transport (Duranti and Hurst, 2004) (**Fig. 66C**). Alignments of grains and mudclasts imbricated parallel to the margins of the clastic injections are common in dykes and sills (Kawakami and Kawamura, 2002; Scott et al., 2009) (**Fig. 66A**). These alignments suggest sustained periods of **traction** during injection of sediments (Kawakami and Kawamura, 2002). Evidence of grading perpendicular to dyke margins are attributed to sorting of clasts during sand injection (Obermeier, 1996; Diggs, 2007; Macdonald and Flecker, 2007). At the micro-scale, pore-filling clay size particles (forming **clay coatings**) partly or completely obstruct pore throats (Duranti and Hurst, 2004) (**Fig. 67A**). Clastic intrusions are generally enriched in clay coatings compared to the parent units because of the elutriation of clay-size particles during fluidization and remobilization of parent units (Duranti et al., 2002; Duranti and Hurst, 2004) (**Fig. 67B**).

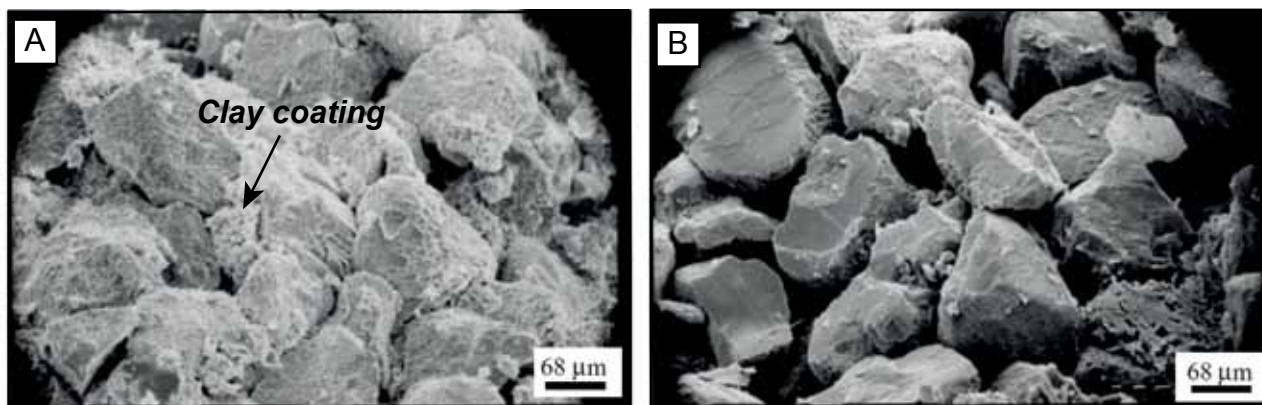


Figure 67. Scanning electron images of injected sand (A) and depositional sand (B). (A) Tightly packed grains and occurrence of fine clay mineral coatings on sand grains. (B) Stratified depositional sandstone with rather clean grains (Alba Formation, North Sea) (Duranti and Hurst, 2004).

9. Parameters controlling the geometry, the orientation, and the direction of propagation of clastic injections

The geometry, orientation, and direction of propagation of the clastic injections are controlled by the **state of stress** and the **distribution of preexisting weakness planes** (Jolly and Lonergan, 2002). The **stress state** is highly controlled by the **burial depth** and the nature of the **external**

trigger responsible for overpressure development. Weakness planes are represented by **pre-existing fractures** and **bedding anisotropy**.

9.1. Burial depth

The evolution of the **horizontal** and **vertical stresses** (σ_h , σ_v) during progressive **burial** of the parent unit leads to different geometries of clastic injections. At shallow depth (cm to 10 m), the **differential stresses** ($\sigma_v - \sigma_h$) are **small**, and the **bedding anisotropy** favours the formation of **sills** (**Fig. 68A**). If the parent unit is buried a little bit deeper (up to 10's of m), the lithostatic stress increase triggers the formation of short **dykes propagating upwards** (**Fig. 68B**). Dykes propagate upwards until **fluid pressure exceeds the vertical stress** exerted by the overburden pressure, implying that the dyke will evolve into a sill propagating at bed interfaces. The evolution of the stress with burial can notably explain the connexions between *per ascensum* dykes and sills. If hydrofracturing occurs at high burial depths (> 100 m), **longer clastic dykes** form because of increasing distance between the parent unit and the formation depth of sills (**Fig. 68C**).

This theoretical distribution of clastic injections styles and geometries, depending on the burial depth,

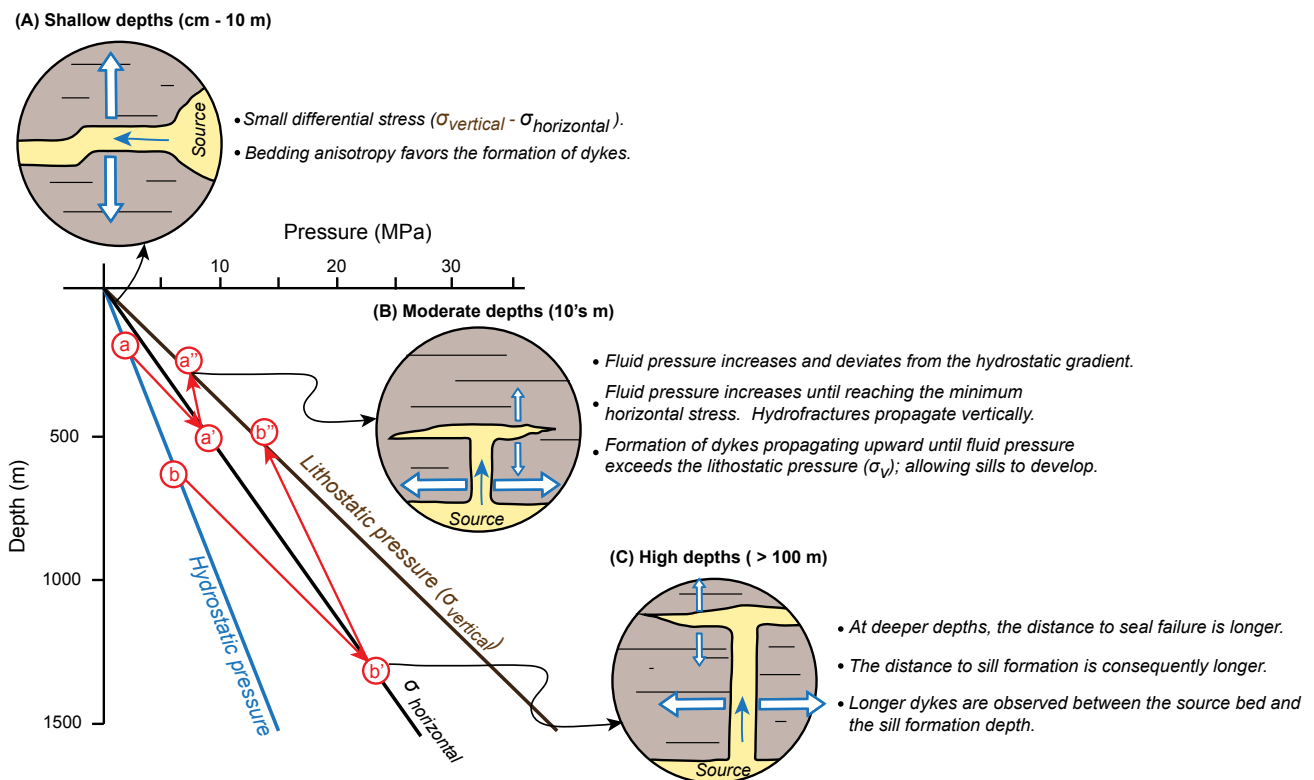


Figure 68. Simplified and theoretical model illustrating the evolution of clastic injection types according to the burial depth at which hydrofractures form. (A) At shallow depths, sills preferentially form. (B) At moderate depths, small vertical dykes pass upward into sill, while (C) at significant depths, longer dykes propagate before sills can develop. (Modified after Jolly and Lonergan, 2002).

has been observed along few outcrops, notably in the Panoche Hills (California) (Smyers and Peterson, 1971; Vigorito and Hurst, 2010) and in the Rosroe Peninsula (Ireland) (Jolly and Lonergan, 2002).

9.2. External trigger

Hydrofractures can propagate upwards or downwards, thus forming either *per ascensum* or *per descensum* clastic dykes. The sense of hydrofracture propagation is highly dependant on the **stress state** at time of hydrofracturing (Jolly and Lonergan, 2002).

During the forceful injection of sediments, **hydraulic fractures** propagate in the direction of the **water pressure gradient**, i.e., generally towards the sea floor (Jolly and lonergan, 2002). In this configuration, clastic injections propagate upwards, forming *per ascensum* injectite networks. In most sedimentary basins, clastic injections in deep-water environments usually propagate **upward or laterally** (Truswell, 1972; Hiscott, 1979; Hillier and Cosgrove, 2002; Cartwright et al., 2008; Vigorito et al., 2010; and many other authors). Few examples of *per descensum* injectite networks are described in the literature although they sometimes remain controversial (Parize, 1988; Scholz, 2010; Monnier, 2013). The overpressure development in near surface sand bodies caused by the **rapid deposition of mass flows** may be responsible for the formation of *per descensum* clastic dykes. Indeed, the **vertical stress** exerted by rapid deposition of the mass flows may force the **hydrofractures to propagate downward** (Parize, 1988; Parize et al., 2007; Rowe et al., 2002).

9.3. Preexisting fractures

During **burial** of the depositional sand bodies, the maximum **principal stress** (σ_1) is **vertical** due to increasing lithostatic stress and the minimum principal stress (σ_3) is horizontal. In a configuration where the sedimentary basin is filled by homogeneous sediments without preexisting fractures, if the **fluid pressure** (F_p) within the parent unit exceeds the **minimum principal stress** (σ_3) plus the **tensile strength** (T) of the host sediments, **vertical hydrofractures** will form (Jolly and Lonergan, 2002) (**Fig. 69A**).

When **preexisting fractures** characterized by little or no tensile strength occur in the host sediments, the **fluid pressure** (F_p) only needs to exceed the stress normal to the fracture for hydrofractures to form (Jolly and Lonergan, 2002). In this configuration, the **orientation and dip of the dykes will**

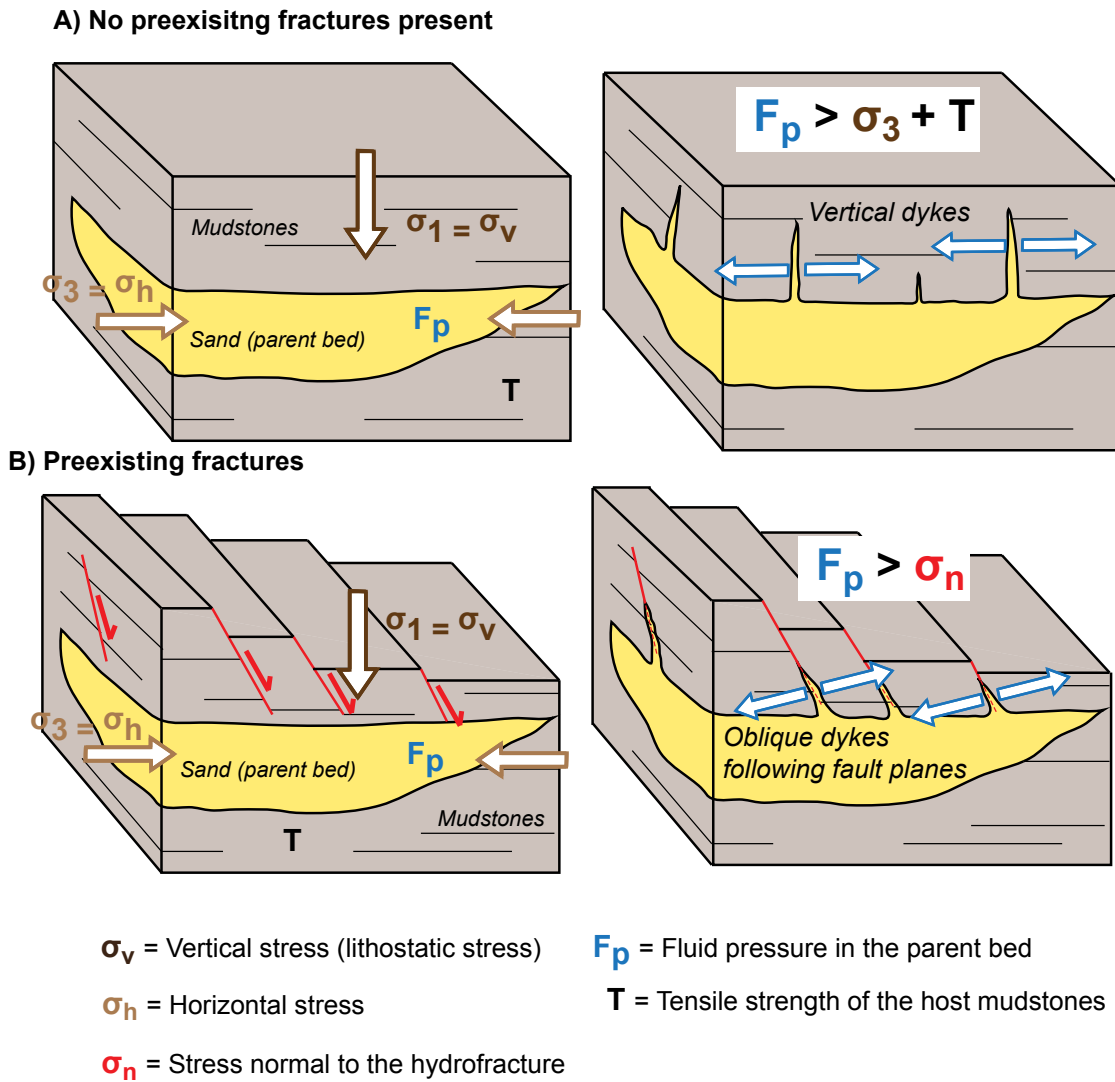


Figure 69. Schematic diagram illustrating the mechanisms by which seal fails during hydrofracturing in two particular cases. (A) No preexisting fractures and (B) preexisting fractures. (Modified after Jolly and Lonergan, 2002).

depend on the preexisting fractures network (Fig. 69B). With increasing fluid pressure, a larger range in fracture orientations is able to reopen and to be injected by fluidized sand (Delaney et al., 1986; Jolly and Sanderson, 1997; Cosgrove, 1995).

9.4. Bedding anisotropy

The **anisotropy** induced by **sediment layering** and **bedding** is responsible for two tensile strength, a first one perpendicular (T_v) to the sediments, and a second one parallel to the sediments (T_h). When the **fluid pressure** (F_p) exceeds the maximum **principal vertical stress** (σ_1) and the **tensile strength perpendicular to the bedding** (T_v), bedding anisotropy will favor the formation of **sills** (Price and Cosgrove, 1990).

10. Impacts of clastic injections on reservoir geology

10.1. Reservoir geometries

Processes of **sand remobilization** and **injection** are responsible for the modifications of reservoir geometries. The development of clastic intrusions networks tend to create more complex geometries than would have been if only primary turbiditic depositional processes were responsible for the formation of these sandy reservoirs. There are four main changes of reservoir geology induced by processes of sand remobilization (Lonergan et al., 2000) (**Fig. 70**).

(1) **Reservoir geometry**: Steepening of original depositional sand lenses geometries commonly occurs after remobilization of sand (Rye-Larsen, 1994). The development of pod-like sand bodies and sand intrusions directly emanating from the original reservoir is also observed (Dixon et al., 1995) (**Fig. 70A**).

(2) **Reservoir properties**: The increase of porewater pressure within depositional sand bodies tend to homogenize sand texture, and reservoir properties. **Fluidization** promotes the **homogenization** of sediments and the elutriation of clay-size particles during injection (**Fig. 70B**). The obliteration of original sedimentary structures during fluid pressure increase makes difficult the interpretation of such deposits as they could equally correspond to grainflows, debris flows, or high-density turbidity flows (Lowe, 1982; Shanmugan, 2000; Mulder and Alexander, 2001).

(3) **Reservoir connectivity**: Clastic intrusions can alter the transmissivity by forming connections between isolated sand reservoirs (Lonergan, et al., 2000) (**Fig. 70C**).

(4) **Top reservoir structure/depth surface**: Processes of sand remobilization tend to modify the top reservoir depth as the original planar surface may be transformed into a surface of small-to medium scale undulations (MacLeod et al., 1999) (**Fig. 70D**).

10.2. Petrophysical properties

Most of the petrophysical data measured in injectite networks were obtained from boheroles (Duranti et al., 2002; Duranti and Hurst, 2004; Lonergan et al., 2007), even though a recent study estimated outcrop-scale variations of permeabilities in the injectites network of the Panoche hills (California) (Scott et al., 2013).

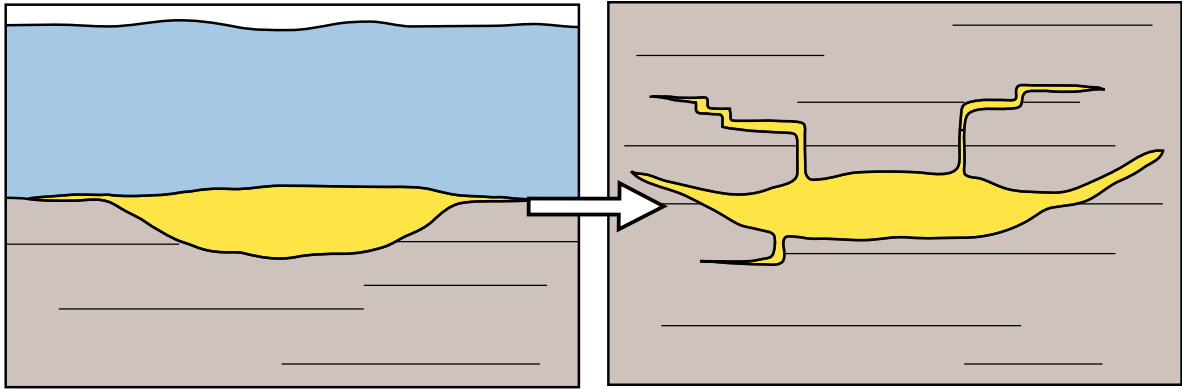
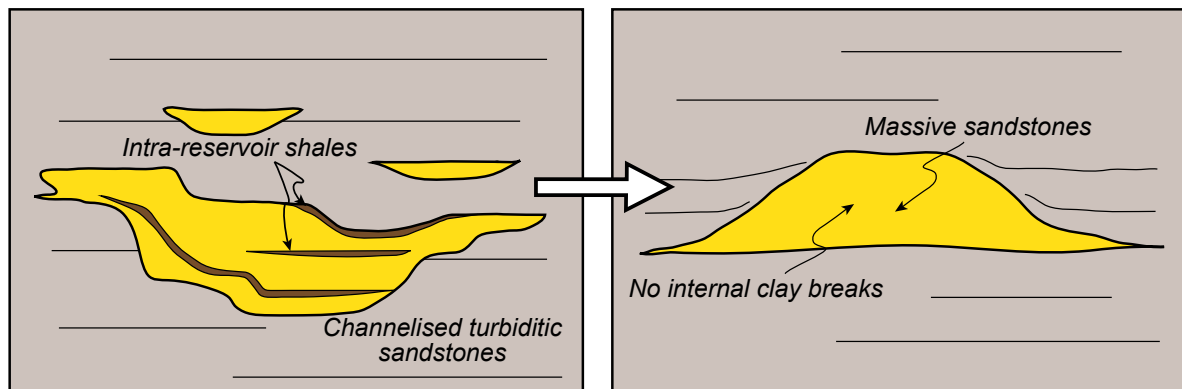
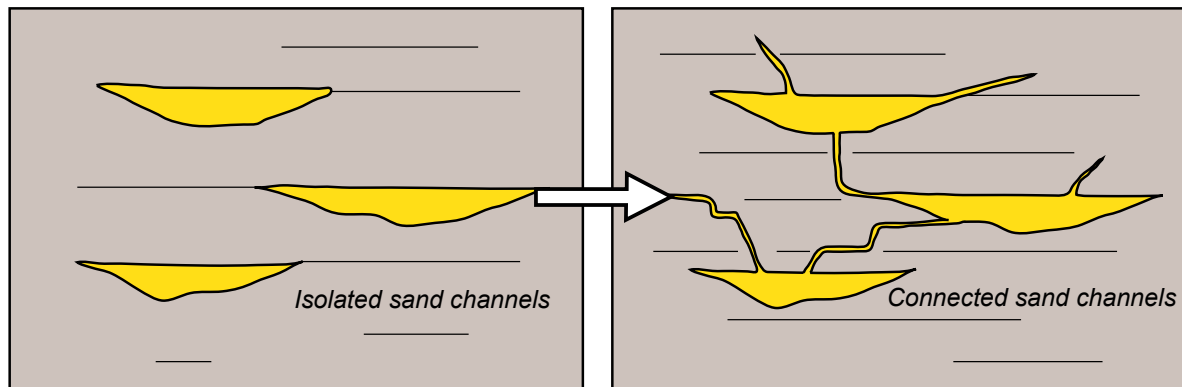
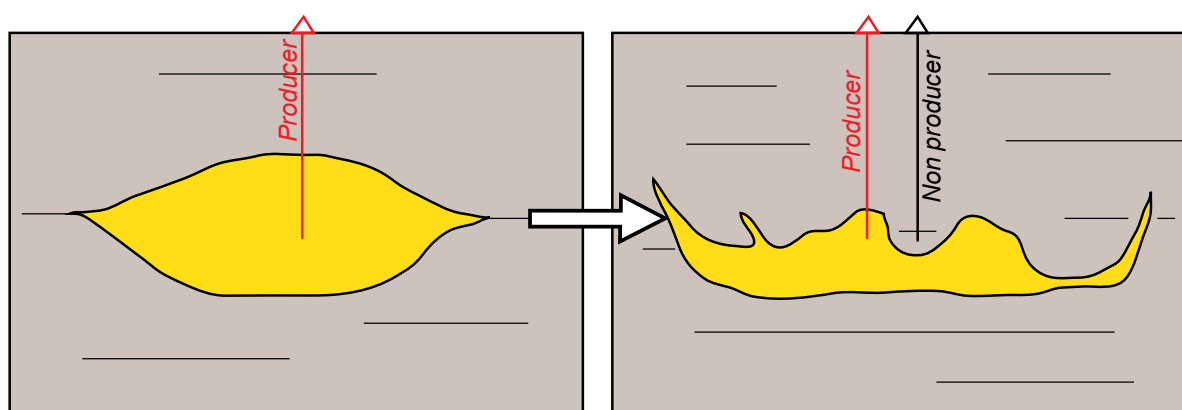
A) Change in reservoir geometry**B) Change in reservoir properties****C) Change in reservoir connectivity****D) Change in top reservoir surface and in reservoir volumetries**

Figure 70. Schematic diagram illustrating the influence of sand remobilization and clastic injection on reservoir geology in deep-marine environments (modified after Lonergan et al., 2000).

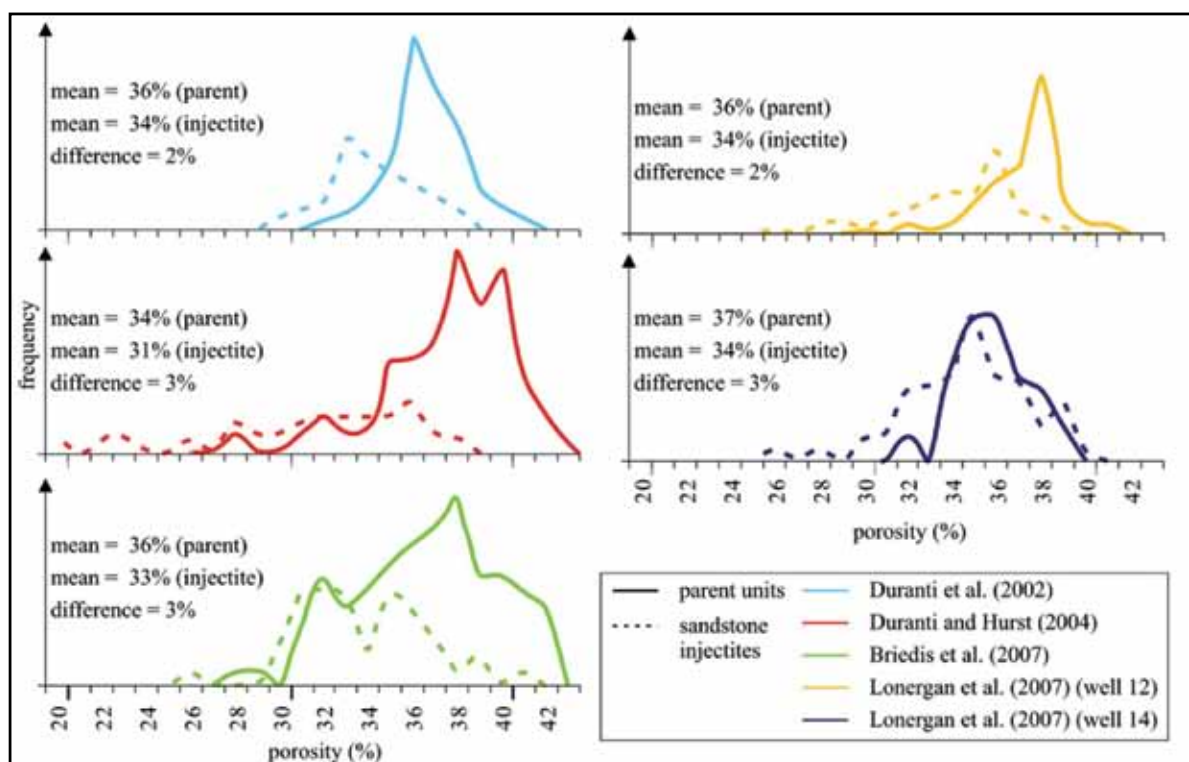


Figure 71. Frequency distribution of porosity (%) in parent units affected by sand remobilization and their associated clastic injections (injectites). In all cases, injectites display lower porosities compared to their respective parent units. Porosity data from North Sea samples (Hurst et al., 2011).

Porosity measurements conducted in boreholes show that **porosity is on average slightly lower in sandstones intrusions related to sandstone parent units** (Duranti et al., 2002) (**Fig. 71**). Similarly, permeability measurements show that **sandstones intrusions are slightly less permeable**. The lower porosity of sandstone intrusions has been attributed to a tighter grain packing (Hurst and Cronin, 2001) and a slightly higher clay content. High clay content is related to the elutriation of clay-size particles during fluidization and remobilization of parent units (Duranti et al., 2002; Duranti and Hurst, 2004) (**Fig. 71**).

Alternatively, Lonergan et al. (2007) proposed that high mudstone clast content and deformation bands are responsible for the lower porosities found in sandstones intrusions. Sandstone intrusions generally display broader porosity values compared to their source, possibly because of the wide range of textures and grain packing resulting from fluidization processes (**Fig. 71**) (Scott et al., 2009). Whether depositional or injected, higher porosities are observed within wider sand bodies. Since injectites are generally thinner than most depositional bodies, injectite tends to display lower porosities as they become quicker and pervasively compacted and cemented by carbonates (Jonk et al., 2005). This explains why the very thick injectites recognized in the North sea can maintain relatively high porosity at high burial depths (Lonergan et al., 2000; Duranti et al., 2002).

Permeability measurements conducted on the giant injectite complex of the Panoche Hills were used to characterize outcrop-scale variations of reservoir properties (Scott et al., 2013). Results showed that **high-angles dykes were approximately seven times less permeable than low-angle clastic dykes**. In addition, this study demonstrated that **staggered and stepped sills are seven times more permeable than multi-layered sills** (Scott et al., 2013).

10.3. Diagenesis and fluid flows

Diagenetic sequences affecting injectite networks are site-dependant. Although a single diagenetic sequence cannot be generalized to all injectite networks, Jonk et al. (2005a, b) proposed a simplified sequence based on six field examples.

Once injected, sand is unlithified and behaves as fluid flow conduits. The stress exerted on clastic injections by the overburden pressure leads to the development of **deformation bands** representing early diagenetic imprints (Jonk et al., 2003, 2005a). They generally form conjugate to subparallel sets of normal faults and are associated with the formation of **authigenic quartz cements** (Jonk et al., 2005). These quartz cements, resulting from pressure/solution processes, are promoted by fresh and highly reactive surfaces formed during abrasion and crushing of quartz grains along shear planes (Fossen et al., 2007). As the early quartz cements are very localized, clastic injections remain unlithified and the **circulation of carbonate-rich fluids can lead to pervasive cementation** (Jonk et al., 2005a, b).

Clastic injections tend to be more pervasively cemented by carbonate cements than parent units as thin bodies become more rapidly cemented compared to larger sand bodies. The carbonate source responsible for the emplacement of calcite cement may result from the release of Ca-rich fluids during compaction of the host strata, especially with host sediments that are composed of marl/limestone alternations (Monnier, 2013). The distribution of carbonate cements is notably controlled by injectite geometries, because high-angles of discordance between dykes and host strata may form particular contact that enhance fluid flows. In this configuration, enhance fluid flux from the surrounding mudstones will promote the carbonate cementation (Jonk et al., 2005a, b). **Late brittle fracturing** related to tectonic deformation can reopen cemented injectites inside which carbonate-rich fluids can circulate and precipitate to form **calcite veins** (Jonk et al., 2005a).

The typical diagenetic sequence implies that clastic injection networks can either behave as **fluid**

flow conduits or **fluid flow barriers**. After injection, sediments are unlithified and promote fluid flows (**Fig. 72A**). Basinal fluids continue to use these sand injection networks until they become completely and pervasively cemented by carbonates. According to Jonk et al., (2005a, b), clastic injections become cemented in the first kilometer of burial, thus causing the network to behave as flow barriers during further burial (**Fig. 72B**). Tectonic events and associated brittle deformations can affect the injection networks and more particularly the more competent well-cemented sandstones intrusions. Injectites are then reactivated as fluid flow conduits through the freshly open fractures (Jonk et al., 2005b) (**Fig. 72C**).

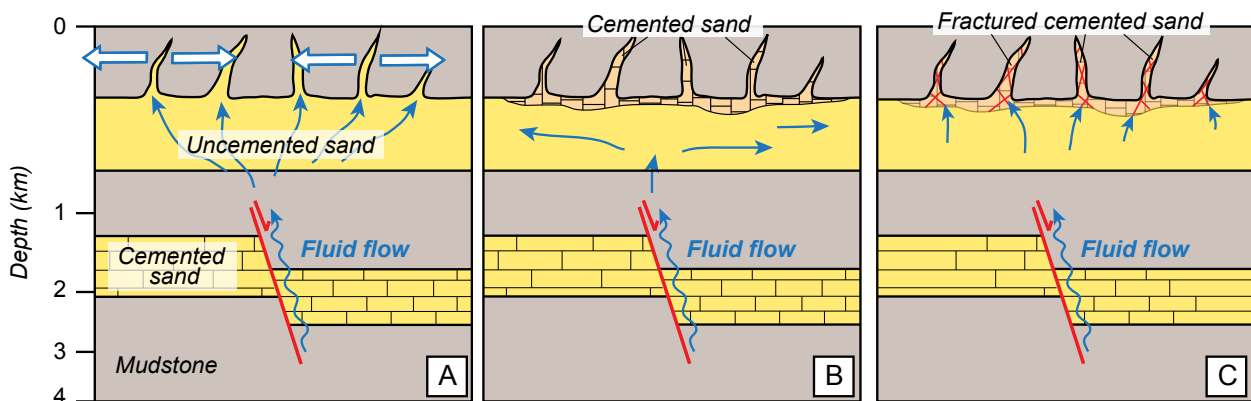


Figure 72. Schematic diagram illustrating the three main stages of fluid flows associated with sand injection emplacement and diagenesis. (A) Development of clastic injections. (B) Carbonate cementation in the first km of burial. Fluid flows continue until complete cementation of the clastic injections. (C) Late tectonic events and associated brittle deformation induce the reactivation of injectites as fluid conduits (Modified after Jonk et al., 2005b).

Conclusions

Les structures de déformation pré-lithification s'observent dans la plupart des environnements sédimentaires. Elles se distinguent à différentes échelles (millimétrique à kilométrique) et s'enregistrent dans les sédiments depuis le Néoprotérozoïque. La mise en place de ces structures est principalement contrôlée par l'orientation et la valeur des contraintes exercées sur les sédiments, la pression d'eau interstitielle, et le type de sédiments.

Les environnements sous-glaciaires et marins profonds présentent les plus fortes concentrations de structures de déformation pré-lithification, et sont caractérisés par l'abondance de structures induites par surpressions de fluide (i.e., pression d'eau interstitielle élevée).

► Les environnements sous-glaciaires présentent une large gamme de structures de déformations pré-lithification en raison de l'importante fluctuation des champs de contraintes et de la pression d'eau interstitielle. Chaque structure enregistre un état de contrainte particulier qui est associé au poids et à la vitesse d'écoulement de la glace, ainsi qu'à une pression de fluide particulière. Les variations de l'épaisseur de la glace, de la vitesse d'écoulement, ou encore de la pression d'eau interstitielle peut être représenter le long d'un profile théorique de calotte glaciaire. La calotte se divise en trois zones: une zone interne («ice dome area»), une zone intermédiaire («intermediate area»), et une zone externe («marginal zone»), qui sont chacune caractérisée par différents paramètres et différents états de contraintes. La distribution théorique de ces états de contraintes associée aux variations de la pression d'eau interstitielle permet de donner une signification paléoenvironnementale aux différentes structure de déformation observées dans le registre sédimentaire glaciaire. Cependant, les variations de la vitesse d'écoulement ou de la production d'eaux de fonte, dans l'espace et au cours du temps, peuvent notamment compliquer l'interprétation paléoenvironnementale de certaines structures.

► Dans les environnements marins profonds, la majorité des structures de déformation pré-lithification est provoquée par l'augmentation rapide de la pression d'eau interstitielle. Il existe deux grands types de déformation pré-lithification induits par surpressions de fluide dans ce type d'environnement: (1) les structures *in-situ* et (2) les structures injectées.

La mise en place des structures de déformation *in-situ* est contemporaine de la sédimentation. Ces structures résultent de l'augmentation de la pression de fluide liée au piégeage rapide d'eau interstitielle lors du dépôt rapide des écoulements de masse (ex: «dish», convolutes, ...).

La mise en place des structures injectées est liée à l'hydrofracturation et l'injection de sable fluidisé dans un encaissant imperméable, et sont postérieur à l'enfouissement de chenaux turbiditiques. L'augmentation rapide de la pression de fluide, nécessaire à la mise en place de réseaux d'injections clastiques, est généralement provoquée par des tremblements de terre, des migrations de fluides, ou une surcharge rapide. La morphologie de ces injections varie en fonction de la fracturation préexistante de l'encaissant, de l'anisotropie liée au litage de l'encaissant, ou encore de la profondeur d'enfouissement.

Les réseaux d'injection sont très étudiés puisqu'ils ont un impact majeur sur les propriétés réservoirs des sédiments clastiques marin profond. En effet, les processus d'hydrofracturation et de fluidisation liés à l'injection ont pour conséquence de modifier la structuration granulaire des sédiments et la géométrie des corps sableux.

Dans la littérature, des études sur l'analyse des structures de déformation ont été menés pour différentes raisons. Dans les environnements glaciaires, ces structures ont principalement été utilisées comme un outil facilitant les reconstructions de la dynamique glaciaire et des paléoenvironnements. En revanche, dans les environnements marins profonds, ces structures ont été étudiés afin de mieux contraindre leurs impacts sur les propriétés réservoirs des sédiments clastiques.

CHAPITRE II

**Structures de déformation pré-lithification:
Marqueurs Paléoenvironnementaux**

Introduction

Les modèles sédimentologiques réalisés à partir de la succession de différents faciès sédimentaires permettent de proposer des reconstitutions paléoenvironnementales. Cependant, la cinématique, les taux de déformation, ou encore les pressions d'eau interstitielle associés aux différentes structures de déformation pré-lithification permettent de valider ou de mieux contraindre les modèles paléoenvironnementaux et de caractériser la paléodynamique d'une calotte glaciaire (Williams, 1996; Le Heron et al., 2005; Piotrowski et al., 2006; Denis et al., 2010). Différents travaux ont permis de mettre en évidence ces relations entre paléoenvironnements et structures de déformations, à micro- et macro-échelles (Brodzikowski et van Loon, 1985; van der Meer, 1993; Carr, 2001; Mc Carroll et Risdijk, 2003; Le Heron et al., 2005; Phillips et al., 2013; ainsi que beaucoup d'autres auteurs).

L'objectif de ce chapitre est de présenter des cas d'études où les structures de déformation permettent de reconstituer de manière précise les environnements glaciaires, d'estimer les oscillations d'une marge glaciaire, de caractériser la paléodynamique glaciaire ou encore de déterminer s'il existe des séquences de sédimentation/déformation contrôlées par des cycles climatiques. Ce chapitre est composé de deux articles scientifiques présentant respectivement les données récoltées lors de deux campagnes de terrains:

• **Partie 1:** «Sedimentological and deformational criteria for discriminating subglaciofluvial deposits from subaqueous ice-contact fan deposits: A Pleistocene example (Ireland)». (Article 1)

Cette première partie se focalise sur la différenciation des environnements proglaciaires et sous-glaciaires via l'étude de dépôts sédimentaires pléistocènes situés en Irlande. L'étude sédimentologique combinée à l'analyse de la déformation pré-lithification permet de discriminer ces deux environnements et de proposer des critères de reconnaissance de l'environnement sous glaciaire (et plus précisément des environnements fluviaux sous-glaciaires). Cette méthode d'analyse permet aussi d'étudier le lien entre sédimentation/déformation, dynamique glaciaire, cycle de production des

eaux de fonte et déglaciation.

• **Partie 2:** «A new model for the development of the Sólheimajökull clastic injections network: trigger mechanisms, processes of injection and implications for the reconstruction of ice dynamics». (Article 2)

Cette seconde partie se propose d'étudier des déformations liées à des pressions de fluide élevées le long d'un affleurement situé au devant d'une langue glaciaire islandaise. Le réseau d'injections clastiques sera étudié dans le détail et à plusieurs échelles afin de déterminer la relation entre sa mise en place et les oscillations de la marge glaciaire. La très bonne préservation des structures de déformation permettra également de mieux comprendre les processus et mécanismes intervenant dans le processus d'injection et d'appréhender les variations de la pression d'eau interstitielle au cours du temps.

Partie 1

«Critères sédimentologiques et structures de déformation permettant de discriminer les dépôts fluviatiles sous-glaciaires des dépôts de cônes de déjections juxtaglaciaires: un exemple Pléistocène (Irlande)»

Cette première partie fait l'objet d'une publication dans la revue *Sedimentology*:

Article 1

Ravier, E., Buoncristiani, J.F., Clerc, S., Guiraud, M., Menzies, J. et Portier, E. 2014. Sedimentological and deformational criteria for discriminating subglaciofluvial deposits from subaqueous ice-contact fan deposits: A Pleistocene example (Ireland). *Sedimentology* 61, 1382-1410.

Objectifs:

- *L'objectif de cette première partie est de décrire, interpréter et comparer les sédiments déposés en environnements proglaciaires et sous-glaciaires ainsi que les structures de déformation pré-lithification qu'ils contiennent.*
- *Si l'origine sous-glaciaire de certains diamictons argileux (e.g., les tills) est bien établie dans la littérature, les faciès sédimentaires triés sont généralement interprétés comme des dépôts proglaciaires, malgré l'existence avérée de ce type de dépôt sous la glace. L'un des principaux objectifs de cette étude est donc d'apporter de nouveaux arguments permettant de discriminer les faciès triés proglaciaires des faciès triés sous-glaciaires en se basant notamment sur une analyse détaillée des structures de déformation.*
- *Enfin, le troisième objectif de cette première partie est de déterminer si les séquences sédimentaires et les séquences de déformation permettent de caractériser les variations de la dynamique glaciaire, les variations de la production d'eaux de fonte, et les mécanismes intervenant dans les processus d'écoulement d'un ice-stream.*

1. Précédents travaux

De précédentes études ont mis en évidence des critères d'ordre sédimentologique, stratigraphique, structural, morphologique et topographique facilitant la reconnaissance des faciès sédimentaires triés (sables et graviers) d'origine sous-glaciaire. Si chacun de ces critères diagnostiques, pris seul, ne permet pas de tirer une conclusion sur l'origine des dépôts sédimentaires, la combinaison de plusieurs de ces critères (**cf. Tableau 1**) pourrait permettre de reconnaître des faciès triés mis en place dans un environnement sous-glaciaire.

Criteria	Description/Interpretation	Ref.
■ Sedimentological & Stratigraphical		
□ Alternating and interfingering subglacial till with sorted sediments	This demonstrates alternation of ice/bed coupling and decoupling and indicates that deposition of sorted sediment may occur subglacially.	1, 2, 3, 4, 5, 6, 7, 8, 9.
□ Conformable subglacial tills/sorted sediments contacts	Conformable contacts between till and underlying sediments suggest subglacial deposition and a transition from ice/bed decoupling (cavity) to ice/bed coupling.	9, 10.
□ Sub and Intra- till lenses of sorted sediments	In such configuration, lenses of sorted sediments indicate localized ice/bed decoupling and deposition by meltwater current.	4, 9, 11, 12, 13
□ Amalgamated sorted sediments associated with rhythmic change in grain-size	Rhythmically alternating coarse and fine-grained sediments with sharp and erosive contacts indicate highly variable hydrodynamism and changes in sediment supply or flow competence. These features are typical of subglacial hydrology and reflect a limited accommodation space.	2, 14
□ Planar/tabular beds of sorted sediments	Subglacial flows within ice/bed decoupling cavities are inferred to have a sheet-like geometry, producing planar-tabular beds containing bedforms.	15
□ Evenly distributed dropstones (<i>debris rain-out</i>)	Ice-roof melting releases debris evenly within water-filled cavities, this can even lead to diamicton deposition when debris release is very high.	2, 16, 17, 18
□ Evidence for subglacial till reworking	Reworking of nearby subglacial till by meltwater should be imprinted in cavity deposits.	16, 17
■ Deformational		
□ Coeval and cyclical deposition and deformation	Subglacial deformation structures are separated by erosion surfaces. This means that ice episodically recouples with the bed between phases of sediment transport and deposition demonstrating subglacial deposition of sediments.	2, 17
□ Small-scale deformations affecting discrete beds	Since deformation generally occurs in between phases of sedimentation, deformation structures should affect discrete beds, rather than the entire sediment pile as it would be expected in proglacial setting.	2, 17
□ Typical subglacial deformation structures	To interpret subglacial coeval deposition and deformation, deformation structures have to be of a subglacial origin.	
● General shear-induced		
<i>General shear structures related to flowing-ice over sediments</i>		
○ Asymmetrical Folds	Recumbent, sheath, overturned, shear, elongate....Types of folds are various in subglacial settings, even though, they generally have their fold axis/hinges dipping up towards the ice flow direction.	15, 19, 20, 21
○ Augen/Boundins	They represent elongated lenses of sediments displaying slab-like shape, resulting from simple shearing of sediments by basal ice.	22, 23, 24, 25, 26
○ Tectonic laminae	Tectonic laminations are formed by intense attenuations of sediments during subglacial simple shearing of soft material.	24, 27, 28
○ Realigned clasts	Clasts can also overprint subglacial shearing by realignment of their long axes in the direction of the ice flow.	2, 22
○ Thrust/reverse faults	Thrust/Reverse faults are triggered by brittle failure of material as the result of simple shear strain exerted by the ice flow on sediments.	21, 29, 30
○ Shear planes/Shear zones	Discrete shear planes/zones affecting sediments are related to deformation by flowing ice during ice/bed coupling episodes.	19, 21, 31
○ Macro-scale rotational structures	Rotational clast rearrangements due to simple shear exerted by ice flow	32

Criteria	Description/Interpretation	Ref.
★ Overpressure-induced	The weight of hundreds meters of ice exerted on basal meltwater, including porewater, leads to overpressurized conditions in the sediments.	
○ <i>per descensum</i> oblique clastic dykes	Overpressurized water can flow through hydrofractures together with sediments leading to hydrofracture infill, forming clastic dykes. Oblique clastic dykes are formed when the maximum compressive strain (λ_3) is oblique, implying both ice-bed coupling and shear stress exerted by flowing-ice.	2, 33, 34, 35, 36, 37
● Pure shear-induced	<i>Pure shear structures are related to slow- or fast-moving ice</i>	
○ Steps faulting	Step normal faulting, indicating brittle failure of sediments, is typical of radial extensional regime related to ice-bed coupling and low water-content sediment.	2, 14, 18
★ Overpressure-induced		
○ <i>per descensum</i> vertical clastic dykes	<i>per descensum</i> vertical clastic dykes are formed when λ_1 is horizontal and λ_3 is vertical, such strain configuration suggests ice/bed coupling conditions associated with slow-flowing ice.	2, 36, 37,
○ Sills	Sills are produced when λ_3 is horizontal and λ_1 is vertical. In this strain configuration, ice is not weighing on the bed indicating ice/bed decoupling conditions.	2, 18, 38
○ In-situ Breccias	Fluidization-induced breccias displaying no evidence for displacement imply in-situ fragmentation of lithified or semi-lithified material. Fragmentation occurs during hydrofracturing induced by glacier overloading.	39
■ Morphological		
□ Channel pattern	Channel patterns under ice, i.e. under high pressure, may display different features compared to their free-surface counterparts: they show a higher braiding intensity, a higher variability of flow directions, and more sharply defined margins.	2, 14, 40
■ Topographical		
□ Sediment located behind topographic roughness	Occurrence of bed roughness transverse to ice flow may provide the topographical framework for development of subglacial cavities.	16, 41, 42, 43, 44, 45, 46
□ Topographic basin under the ice	Beneath ice sheet, bed depressions may in particular cases host large water bodies leading, to sorted sediment deposition within cavities.	47, 48, 49
□ Irregular sediment elevation	Topography derived from sediments deposited within cavities tends to vary considerably from site to site.	5, 10
□ Topographical impossibilities of proglacial water storage	Deposits elevation relative to drainage network may in particular cases require a subglacial origin, as a proglacial water mass would have drained.	5, 10

Table 1. Compilation of the main sedimentological, stratigraphical, deformational (macro-scale), morphological and topographical criteria for identifying subglacial sorted deposits. These criteria based on previous studies are either inferential or theoretical (1. Boyce & Eyles, 2000; 2. Clerc et al., 2012; 3. Fisher & Taylor, 2002; 4. Munro-Stasiuk, 2000; 5. Munro-Stasiuk, 2003; 6. Ng, 2000; 7. Piotrowski & Kraus, 1997; 8. Piotrowski & Tulaczyk, 1999; 9. Wysota, 2007; 10. McCabe & Ó Cofaigh, 1994; 11. Shaw, 1983; 12. Shaw, 1987; 13. Evans et al., 2006; 14. Clerc et al., 2013 ; 15. Lesemann et al., 2010; 16. Gibbard, 1980; 17. Brodzikowski & Van Loon, 1991; 18. Bennett et al., 2006; 19. Denis et al., 2010; 20. Ghienne et al., 2007; 21. van der Wateren, 1999; 22. Benn & Evans, 1996; 23. Benn & Prave, 2006; 24. Hart & Boulton, 1991; 25. Roberts and Hart, 2005; 26. Waller et al., 2011; 27. Hart & Roberts, 1994; 28. Hart, 1998; 29. Brandes & Le Heron, 2010; 30. Lee & Phillips., 2008; 31. Le Heron, 2007; 32. Le Heron et al., 2012; 33. Boulton & Caban, 1995; 34. Denis et al., 2009; 35. Le Heron & Etienne, 2005; 36. Risdjik et al., 1999; 37. Risdjik et al., 2010; 38. Phillips et al., 2013; 39. Passchier, 1998; 40. Catania & Paola, 2001; 41. Dardy & Hanvey, 1994; 42. Kamb, 1987; 43. Linden et al., 2008; 44. Lliboutry, 1979; 45. Sugden et al., 1992; 46. Walder, 1986; 47. Christoffersen et al., 2008; 48. Nye, 1976; 49. Shoemaker, 2003).

Des cycles de sédimentation et de déformation se produisant sous la glace ont été décrits par plusieurs auteurs (Munro-Stasiuk, 2000; Piotrowski et al., 2006; Wysota, 2007; Lesemann et al., 2010; Clerc et al., 2012) et semblent être liés aux changements de pression d'eau interstitielle au sein du substrat.

Ces cycles sont généralement induits par les variations cycliques de la production d'eaux de fonte (Lesemann et al., 2010). Les variations de la production de l'eau ont pour conséquence de faire varier la pression d'eau dans les sédiments sous-glaciaires et donc de provoquer des épisodes de découplage et de couplage entre la glace et son substrat. Lors du découplage, les faciès sédimentaires triés peuvent se déposer alors que pendant des épisodes de couplage glace/substrat, ces sédiments se déforment (Piotrowski et al., 2004; Denis et al., 2010; Lesemann et al., 2010; Clerc et al., 2012). Les cycles répétés de sédimentation/déformation ont un impact sur la dynamique glaciaire, notamment sur les mécanismes et les vitesses d'écoulement de la glace (Piotrowski et al., 2004; Denis et al., 2010; Lesemann et al., 2010).

2. Contexte de l'étude

Le site d'étude est une carrière localisée en Irlande, à 50 km au sud de Dublin et à proximité de la localité de Ballyhorsey (**Fig. 1A**). Cette carrière, constituée de sables et graviers déposés pendant le Dernier Maximum Glaciaire (DMG), présente une séquence sédimentaire de déglaciation déposée lors du retrait progressif de la calotte glaciaire irlandaise (**Fig. 1B**). Cette région fut notamment sélectionnée en raison de la description de faciès sédimentaires triés, d'origine sous-glaciaire, déposés au sein d'un paléo-système de drainage composé de chenaux, cavités, et lacs sous-glaciaires (**Fig. 1A**) (Eyles et McCabe, 1989; McCabe et O'Cofaigh, 1994; Clerc et al., 2012).

Au cours du Pleistocène moyen et supérieur, le continent européen est marqué par une succession de périodes glaciaires et interglaciaires, associée à des phases de croissance et de fonte de grandes calottes glaciaires (Ehlers et Gibbard, 2004; Gibbard et Cohen, 2008). Au niveau de l'Irlande, de nombreuses études ont caractérisé la chronologie des oscillations des calottes glaciaires centrées sur l'Irlande et les îles britanniques durant le dernier cycle glaciaire (e.g., glaciation Weichselienne ou Devensienne) (Eyles et McCabe, 1989; Bowen et al., 2002; Ballantyne et al., 2006; McCabe et al., 2005, 2007; Ó Cofaigh et Evans, 2007; Livingstone et al., 2012). Les différentes reconstitutions paléogéographiques de la calotte glaciaire durant cette période montrent que le site d'étude était localisé dans une zone caractérisée par la confluence de plusieurs flux de glace (Charlesworth, 1928; Farrington, 1934; Warren et Creighton, 1993; Ballantyne et al., 2006; Smith and Knight, 2011):

- Un flux principal correspondant à l'*ice-stream* de la Mer d'Irlande qui drainait alors les régions du Nord de l'Ecosse et de l'Irlande avec un écoulement dirigé vers le sud (**Fig. 1A**).

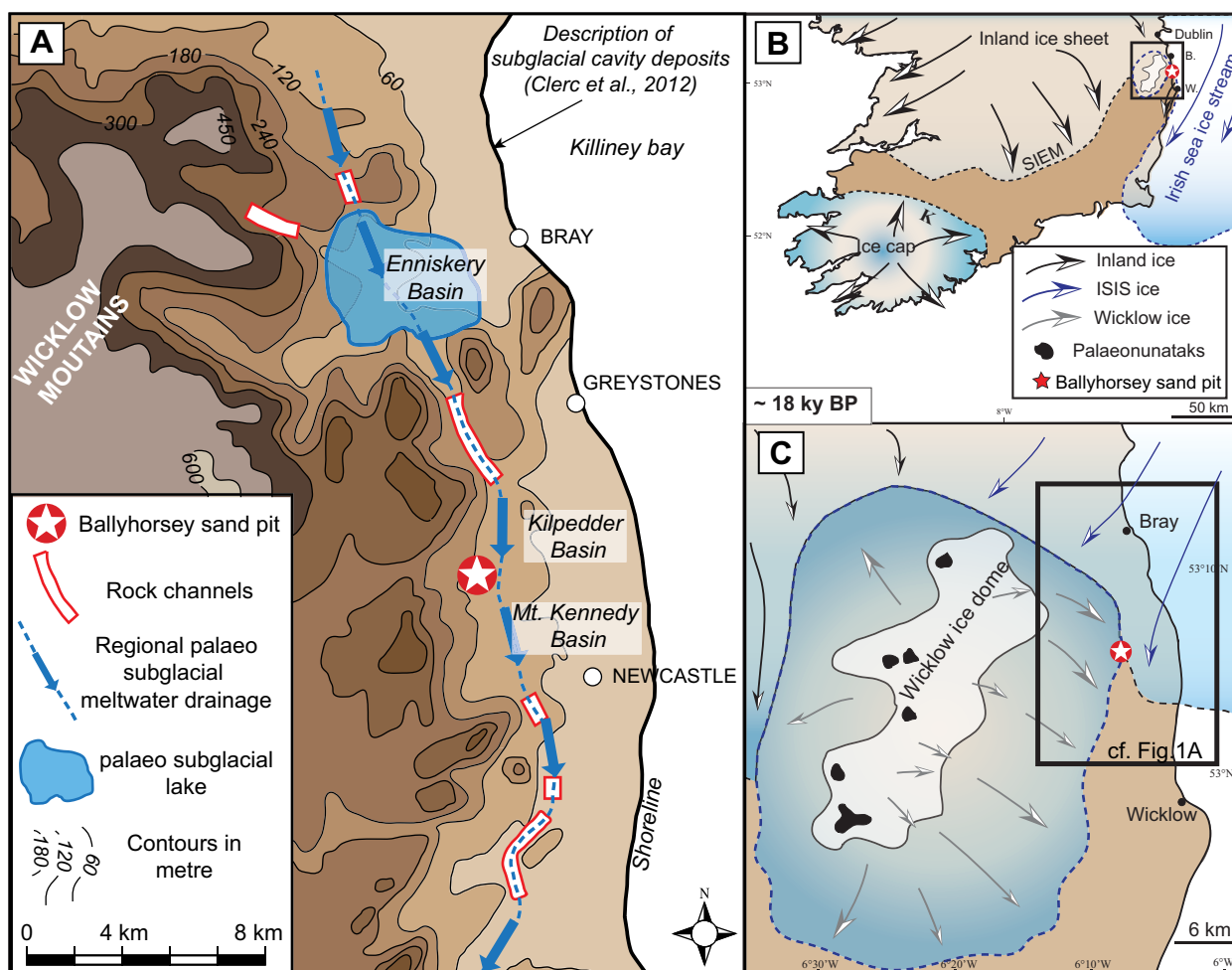


Figure 1. (A) Elevation map showing the position of the study area (red star). Basins and the palaeo-subglacial meltwater drainage system described by McCabe & O'Cofaigh (1994) are represented. (B) Late deglaciation palaeogeographic reconstructions of the British-Irish ice sheet over central and southern Ireland. (C) Close up of the study area, showing the Ballyhorsey sand pit in an ice-marginal position. Ice sheet and ice-flow reconstructions are based on Warren & Creighton (1993) and Ballantyne et al. (2006).

- Un écoulement venant des régions internes d'Irlande avec une direction sud-est (**Fig. 1A**).
- Un écoulement de glace local prenant sa source sur les «Wicklow Mountains» caractérisé par un écoulement dirigé vers le sud-est au niveau de la zone d'étude (**Fig. 1A**).

Si la zone d'étude fut probablement couverte de glace autour de 28 à 26 ka BP, son désenglacement est estimé autour de 17.4 ka BP (Warren et Creighton, 1993; Bowen et al., 2002; McCabe et Clark, 2003; Ballantyne et al., 2006; O'Cofaigh et al., 2012) ce qui implique une probable succession d'environnements sous-glaciaires et proglaciaires (**Fig. 1B,C**).

3. Méthodes

La méthode consiste en une étude intégrée combinant une analyse sédimentologiques (faciès, stratigraphie, géométrie) et une analyse fine des structures de déformations pré-lithification associés aux différents faciès sédimentaires préalablement définis.

L'étude se base sur l'acquisition de nouvelles données dans le but de déterminer de nouveaux critères diagnostiques permettant d'identifier des faciès sédimentaires triés déposés dans un environnement sous-glaciaire et les structures de déformations pré-lithification qui les caractérisent. L'analyse faciologique et structural des dépôts de la carrière de Ballhyorsey permet également de définir les mécanismes impliqués dans la déglaciation de l'*ice-stream* de la mer d'Irlande.

4. Article publié dans *Sedimentology*

«Sedimentological and deformational criteria for discriminating subglaciofluvial deposits from subaqueous ice-contact fan deposits: A Pleistocene example (Ireland)».

L'article est structuré de la façon suivante: (1) La première partie présente les différents faciès et associations de faciès sédimentaires, la stratigraphie et les structures de déformations pré-lithification. Dans cette première partie, les faciès sédimentaires sont interprétés en termes de processus de dépôt et les mécanismes associés aux différentes structures de déformations sont établis. (2) Dans une deuxième partie, une synthèse comprenant une corrélation stratigraphique à l'échelle du site d'étude ainsi qu'une cartographie complète de toutes les structures de déformations recensées sur le site est proposée. Dans cette même partie, les séquences sédimentaires types observées dans la carrière sont décrites. (3) Dans la troisième partie, l'environnement de dépôt des différentes associations de faciès est défini en se basant principalement sur la distribution et le type de structures de déformation observées au sein des sédiments. (4) Dans une dernière partie, l'enregistrement sédimentaire du site de Ballyhorsey et son implication sur les variations de la production d'eau de fonte, les mécanismes d'écoulement de la glace et sur la dynamique de déglaciation de l'*ice-stream* de la mer d'Irlande seront discutés.

Sedimentological and deformational criteria for discriminating subglaciofluvial deposits from subaqueous ice-contact fan deposits: A Pleistocene example (Ireland)

EDOUARD RAVIER*, JEAN-FRANÇOIS BUONCRISTIANI*, SYLVAIN CLERC*†, MICHEL GUIRAUD*, JOHN MENZIES‡ and ERIC PORTIER†

*Laboratoire Biogeosciences UMR/CNRS 6282 Université de Bourgogne, 6 Bd Gabriel, 21000 Dijon, France (E-mail: edouard.ravier@u-bourgogne.fr)

†GDF Suez, Exploration Production International, 1 place Samuel de Champlain, Faubourg de l'Arche, 92930 Paris La Défense Cedex, France

‡Department of Earth Sciences, Brock University, 500 Glendridge Avenue, St. Catharines, Ontario, Canada L2S 3A1

Associate Editor – Nick Eyles

ABSTRACT

A pit located near Ballyhorsey, 28 km south of Dublin (eastern Ireland), displays subglacially deposited glaciofluvial sediments passing upwards into proglacial subaqueous ice-contact fan deposits. The coexistence of these two different depositional environments at the same location will help with differentiation between two very similar and easily confused glacial lithofacies. The lowermost sediments show aggrading subglacial deposits indicating a constrained accommodation space, mainly controlled by the position of an overlying ice roof during ice-bed decoupling. These sediments are characterized by vertically stacked tills with large lenses of tabular to channelized sorted sediments. The sorted sediments consist of fine-grained laminated facies, cross-laminated sand and channelized gravels, and are interpreted as subglaciofluvial sediments deposited within a subglacial de-coupled space. The subglaciofluvial sequence is characterized by glaciotectionic deformation structures within discrete beds, triggered by fluid overpressure and shear stress during episodes of ice/bed recoupling (clastic dykes and folds). The upper deposits correspond to the deposition of successive hyperpycnal flows in a proximal proglacial lake, forming a thick sedimentary wedge erosively overlying the subglacial deposits. Gravel facies and large-scale trough bedding sand are observed within this proximal wedge, while normally graded sand beds with developed bedforms are observed further downflow. The building of the prograding ice-contact subaqueous fan implies an unrestricted accommodation space and is associated with deformation structures related to gravity destabilization during fan spreading (normal faults). This study facilitates the recognition of subglacial/submarginal depositional environments formed, in part, during localized ice/bed coupling episodes in the sedimentary record. The sedimentary sequence exposed in Ballyhorsey permits characterization of the temporal framework of meltwater production during deglaciation, the impact on the subglacial drainage system and the consequences on the Irish Sea Ice Stream flow mechanisms.

Keywords East central Ireland, proglacial subaqueous deposits, soft-sediment deformation structures, subglacial de-coupled space, subglaciofluvial deposits.

INTRODUCTION

Within glacial environments, subaqueous sedimentation can occur in proglacial and subglacial environments (Boulton, 1990; McCabe & O'Cofaigh, 1994; Lønne, 1995; Powell & Domack, 1995; Munro-Stasiuk, 2000, 2003; O'Cofaigh *et al.*, 2001; Bennett *et al.*, 2002, 2006; Knutz *et al.*, 2002; Powell, 2003; Hornung *et al.*, 2007; Winsemann *et al.*, 2007, 2009; Lindén *et al.*, 2008; Lesemann *et al.*, 2010; Clerc *et al.*, 2012). Sedimentary structures occurring in these different environments are comparable and often result in deposits that are very similar and sometimes difficult to discriminate. Although the origin of subglacial till is well-understood (Menziés & Shilts, 2002; Evans *et al.*, 2006; Benn & Evans, 2010), the subglacial origin of sorted sediments is subject to debate. Sorted sediments are often, and mistakenly, ascribed to proglacial environments, and the possibility of widespread subglacial emplacement of sorted sediments has not received the same level of enquiry (Eyles *et al.*, 1982; Lesemann *et al.*, 2010). Observations of processes occurring underneath the ice are generally difficult or impossible; consequently, information on processes relies on the interpretation of sediments deposited below or in front of former ice sheets. In a subglacial environment, meltwater is able to drain through channels, linked cavity systems, water films and via groundwater flow, leading to transport and deposition of sediments. Several studies have proposed sedimentological and stratigraphical criteria to identify sediments deposited subglacially by meltwater flow (Piotrowski & Tulaczyk, 1999; Munro-Stasiuk, 2000; Piotrowski *et al.*, 2001; Wysota, 2007; Livingstone *et al.*, 2012). The deformational characteristics including timing and type of deformation structures have also been used as indicators of subglacial deposits (Denis *et al.*, 2010; Lesemann *et al.*, 2010; Clerc *et al.*, 2012).

It is thought, based on a preliminary examination of the site at Ballyhorsey, that the exposed deformed sediments at the base of the pit may be indicative of a subglacial environment with localized deposition of sorted sediments within a subglacial space formed during episodes of ice-bed decoupling. Using sedimentary, stratigraphical or deformational criteria allows an interpretation of the basal sequence as subglaciofluvial deposition alternating with till deposition. In contrast, the upper part of the sediment package at the site displays prograding

sediments interpreted to have been deposited in a proglacial lake. Implications on the temporal framework of subglacial production of meltwater, ice-flow mechanisms and deglaciation of the Irish Sea Ice Stream (ISIS) will be also discussed.

GEOLOGICAL SETTING

This study is based on the examination of exposures of Upper Pleistocene glacial sediments in Ballyhorsey sand pit (53°06.317'N/06°07.319'W), an abandoned quarry located 1.6 km north-west of Newtownmountkennedy, County Wicklow, and ca 28 km SSE of Dublin (Fig. 1A to C). The site was covered by an ice sheet during the Last Glacial Maximum beginning ca 28 to 26 ka BP (Warren & Creighton, 1993; O'Cofaigh *et al.*, 2012; Bowen *et al.*, 2002; McCabe & Clark, 2003; Ballantyne *et al.*, 2006; Clark *et al.*, 2012). The study area lies in the area of a well-recognized confluence of ice emanating from the Irish Sea basin and ice of the local Wicklow Mountain ice cap (Charlesworth, 1928; Farrington, 1934; Warren & Creighton, 1993; Ballantyne *et al.*, 2006; Smith & Knight, 2011) (Fig. 1A and B). The deglaciation of the study area occurred ca 17.4 ka BP (Bowen *et al.*, 2002; McCabe & Clark, 2003).

A large basin enclosed between bedrock ridges occurs a few kilometres south-west of Killiney Bay (Enniskerry Basin), and has been interpreted as a palaeo-subglacial lake (McCabe & O'Cofaigh, 1994) (Fig. 1C). This large water-filled cavity is part of a more regional subglacial drainage network, ca 30 km in extension from north to south composed of aligned subglacial channels separated by topographic basins (McCabe & O'Cofaigh, 1994). The Ballyhorsey sand pit is located within the Kilpedder Basin that constitutes one of these basins (Fig. 1C). Sediments have not been described in the Kilpedder Basin and no studies indicate whether subglacial or proglacial sediments have accumulated within this topographic basin.

FACIES DESCRIPTIONS, STACKING PATTERN AND DEFORMATION STRUCTURES

The sedimentary succession at Ballyhorsey is composed of 11 distinct sedimentary facies (F), grouped into three major facies associations

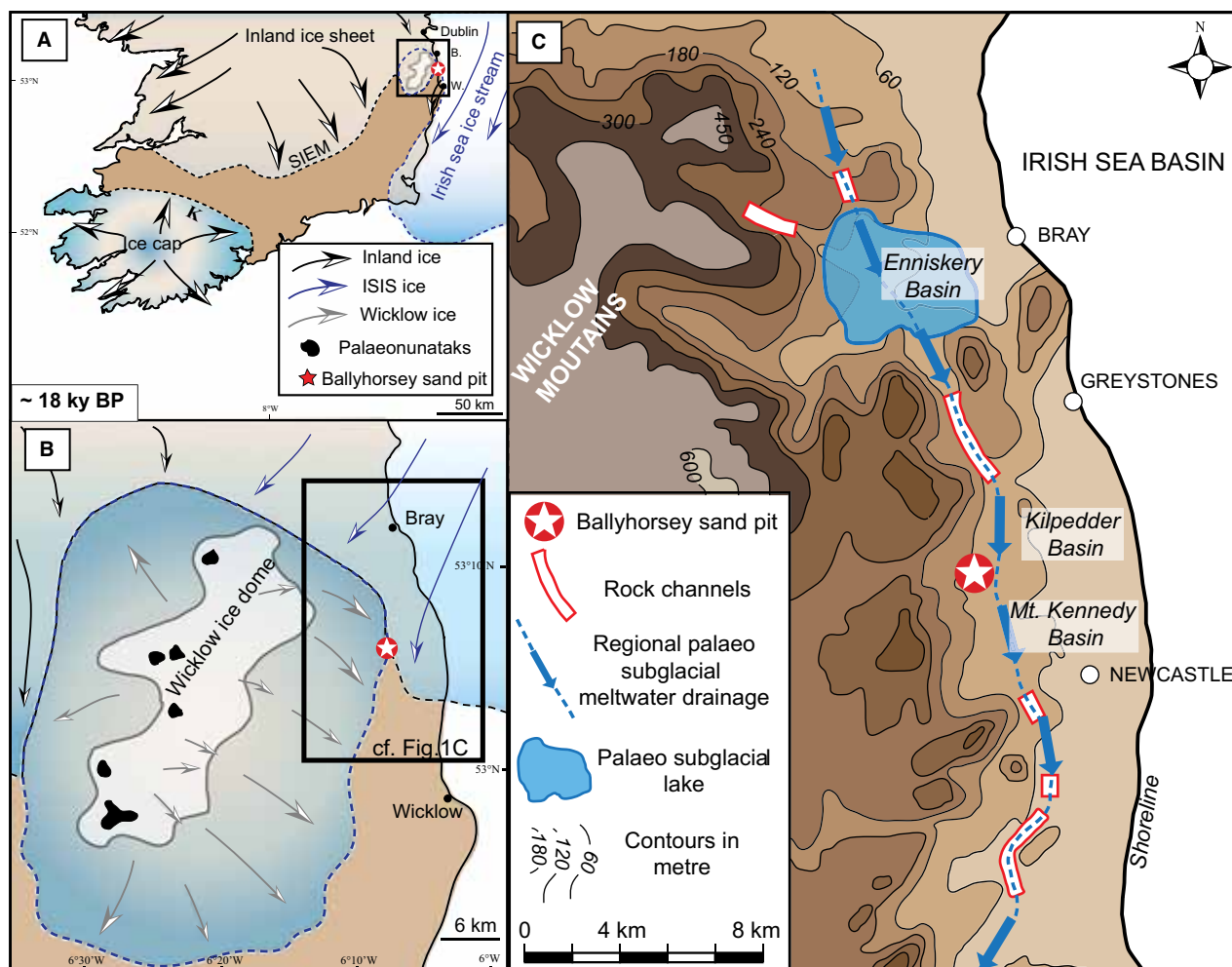


Fig. 1. (A) Late deglaciation palaeogeographic reconstructions of the British-Irish ice sheet over central and southern Ireland. (B) Close up of the study area, showing the Ballyhorsey sand pit in an ice-marginal position. Ice sheet and ice-flow reconstructions are based on Warren & Creighton (1993) and Ballantyne *et al.* (2006). (C) Elevation map showing the position of the study area (red star). Basins and the palaeo-subglacial meltwater drainage system described by McCabe & O'Cofaigh (1994) are represented.

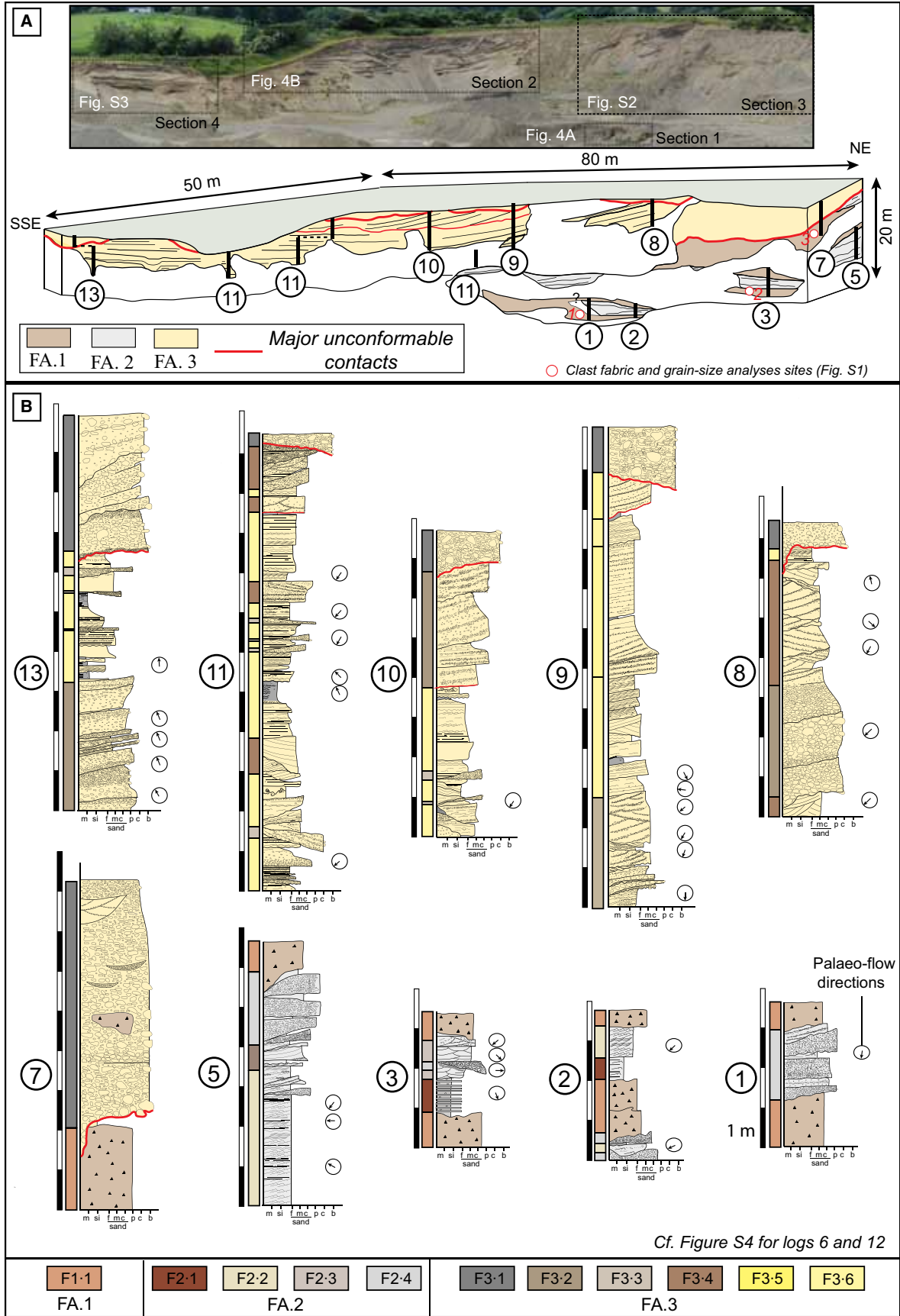
(FA), each defined on the basis of their grain-size, sedimentary structures and geometries. The main features of each sedimentary facies are classified and summarized in Table 1. The general stacking pattern of the facies associations and component facies are illustrated in a panoramic photograph representing an overview of the sand pit (Fig. 2A) and can notably be observed in 10 log sections (Fig. 2B).

Facies Association 1: Clay-rich diamicton deposits

Description

These deposits are characterized by massive, poorly sorted, matrix-supported granules to

boulders in a brownish clayey matrix (Fig. 3A). Facies Association 1 (FA.1) is observed at the bottom of the pit and consists of tabular/horizontal and interdigitated massive clay-rich diamicton layers (F1.1); F1.1 displays sharp and irregular basal contacts that are locally erosive. Diamicton layers are generally 1.5 to 2 m thick, but can occasionally reach 5 m thick and are traceable throughout the pit. Clast content varies significantly in the different layers of diamicton (25 to 50%). Grain-size distribution of the <2 mm fraction displays a bimodal grain-size distribution (Fig. S1A). Clasts are subangular to subrounded, often faceted and polished, displaying crescentic gouges and striations (Fig. 3A and C). Clast fabrics within the



Subglaciofluvial deposits versus ice-contact fan deposits 1385

Table 1. Classification of sedimentary facies (F) and facies associations (FA).

FA	Component facies	Description	Geometry/Bed contacts	Bed thickness	Interpretation
FA.1	F1.1 Massive clay-rich diamicton	Massive matrix-supported diamicton characterized by the presence of granule to boulder-sized clasts in a muddy matrix. Clasts are faceted, polished and show striations	Sheet-like/Sharp, irregular erosive	1.5 to 5.0 m	Deposition by glaciogenic processes (subglacial traction till)
	F2.1 Laminated clay and silt/sand	Alternations of massive clay and silt to sand beds displaying ripple cross-laminations. Clay beds contain numerous clasts from granule to cobble-size deforming underlying beds	Sharp/Sheet-like	0.01 to 0.05 m	Deposition by suspension settling with debris rain-out, alternating with traction deposition
	F2.2 Planar parallel-laminated and ripple cross-laminated sand	Individual beds consist of planar parallel-laminated sand with scattered gravels passing upward into climbing ripple cross-laminated sand	Sheet-like/Sharp	0.2 to 0.6 m	Deposition from traction processes associated with low-density laminar flow
	F2.3 Small-scale trough and planar cross-bedded sand	Trough and planar cross-stratified coarse sands are observed and contain numerous floating granules. Troughs are 0.1 m deep and 0.5 m wide	Sheet-like/Sharp or erosive	0.6 to 1.2 m	Traction deposition and downflow migration of 2D/3D dunes
FA.2	F2.4 Massive, and normally graded gravel	Clast-supported to matrix-supported gravel passing upwards into pebbly sand or ripple cross-laminated sand. Lenses of normally graded gravels are occasionally observed	Erosive/Lenticular	0.2 to 0.8 m	Deposition from waning hyperconcentrated or concentrated channelized density flows
	F3.1 Massive and poorly sorted gravel	Clast-supported to matrix-supported granules to boulders in a coarse sandy matrix. Clasts generally lack preferential orientation. Clusters of openwork clasts locally occur	Wedge-shaped/Erosive	1.5 to 6 m	Deposition by coarse-grained hyperconcentrated density flows
	F3.2 Normally or inversely graded sorted gravels	Upward-fining sequences of sorted clast-supported to matrix-supported gravel to pebble with a matrix consisting of medium-grained to coarse-grained sand	Wedge-shaped/Erosive	0.8 to 1.2 m	Deposition from waning high-density flows (hyperconcentrated to concentrated?)
	F3.3 Massive sorted gravels	Clast-supported and massive sorted gravel with few outsized clasts	Erosive/Lenticular	0.2 to 0.4 m	Deposition from channelized high-density flows
FA.3	F3.4 Trough cross-stratified gravel and sand	Large-scale and low-angle trough cross-bedded coarse sand to gravel. Downflow decrease in trough dimensions. Cross-strata vary from distinct to amalgamated	Wedge-shaped/Sharp or erosive	0.5 to 1.5 m	Traction deposition and downflow migration of 2D/3D dunes
	F3.5 Diffusely graded planar parallel sand and pebbly sand	Diffusely graded planar parallel sand and pebbly sand. Outsized clasts up to cobble size are observed within the diffusely graded sand	Wedge-shaped/Sharp or erosive	0.1 to 0.4 m	Traction deposition from high-density turbidity flows
	F3.6 Normally graded sand to mud beds	Individual beds are characterized by planar parallel-laminated sand followed by climbing ripples. This typical sequence fines upwards into massive or laminated clay. Outsized clasts up to cobble size are scattered throughout this facies and deform underlying sediments	Sheet-like/Flat or sharp	0.2 to 1.0 m	Deposition from waning low-density turbidity flows (T _{b-d} , cf. Bouma), with ice melting releasing dropstones

Subglaciofluvial deposits versus ice-contact fan deposits 1387

Fig. 2. (A) Arrangement of the three facies associations in the Ballyhorsey pit and localization of the sedimentological logs and interpreted sections. (B) Sedimentological logs measured in Ballyhorsey sand pit.

different till layers reveal unimodal to bimodal distributions with principal eigenvalues (S1) ranging from 0.73 to 0.77 (Fig. S1D). Results of Principal Component Analyses show that eigenvalues S1 and S2 account for between 90% and 93% of total data variance collected within the different till layers. These values, when plotted, show that clast fabrics at the study site are clustered in nature (Fig. S1B). Intra-diamicton lenses of stratified sorted sediments (1 m wide and 0.3 m thick) with upper conformable contacts and erosive concave-up bases are observed (Fig. 3B); they show fining-upwards trends with small-scale trough cross-stratified coarse sand to granules passing upwards into laminated clay containing abundant clasts with deformed bottom contacts. These lenses are not tilted and appear concordant with the host diamicton units.

Interpretation

This clay-rich diamicton was initially formed at the glacier bed, as illustrated by the bimodal grain-size distribution, the faceted clasts and the abundant striations observed on clasts. The different striation orientations denote clast re-orientations and re-alignments during wear and subglacial transport (Hicock, 1991; Benn, 1995). The clast fabrics ternary diagram indicates a cluster flat shape implying that the diamicton has undergone some degree of shearing and subsequent clast re-orientations during and/or after deposition. This clay-rich diamicton corresponds to material formed at the glacier sole (i.e. till) that could have been re-mobilized later (Evans *et al.*, 2006). If the diamicton was deposited subglacially, lenses of sorted sediments embedded within clay-rich diamicton may result from sediment deposition within ephemeral subglacial meltwater channels during episodes of localized ice/bed decoupling (Boyce & Eyles, 2000; Piotrowski *et al.*, 2004; Wysota, 2007; Lesemann *et al.*, 2010), or represent rafted intra-clasts (Menzies, 1990; Hoffmann & Piotrowski, 2001; Waller *et al.*, 2011). The preserved lenticular geometry and the absence of tilting suggest that this sorted material results from *in situ* sediment deposition rather than entrainment of sediment blocks into debris-rich basal ice. The transition from trough cross-bedded sand to dropstone-rich laminated clay suggests a

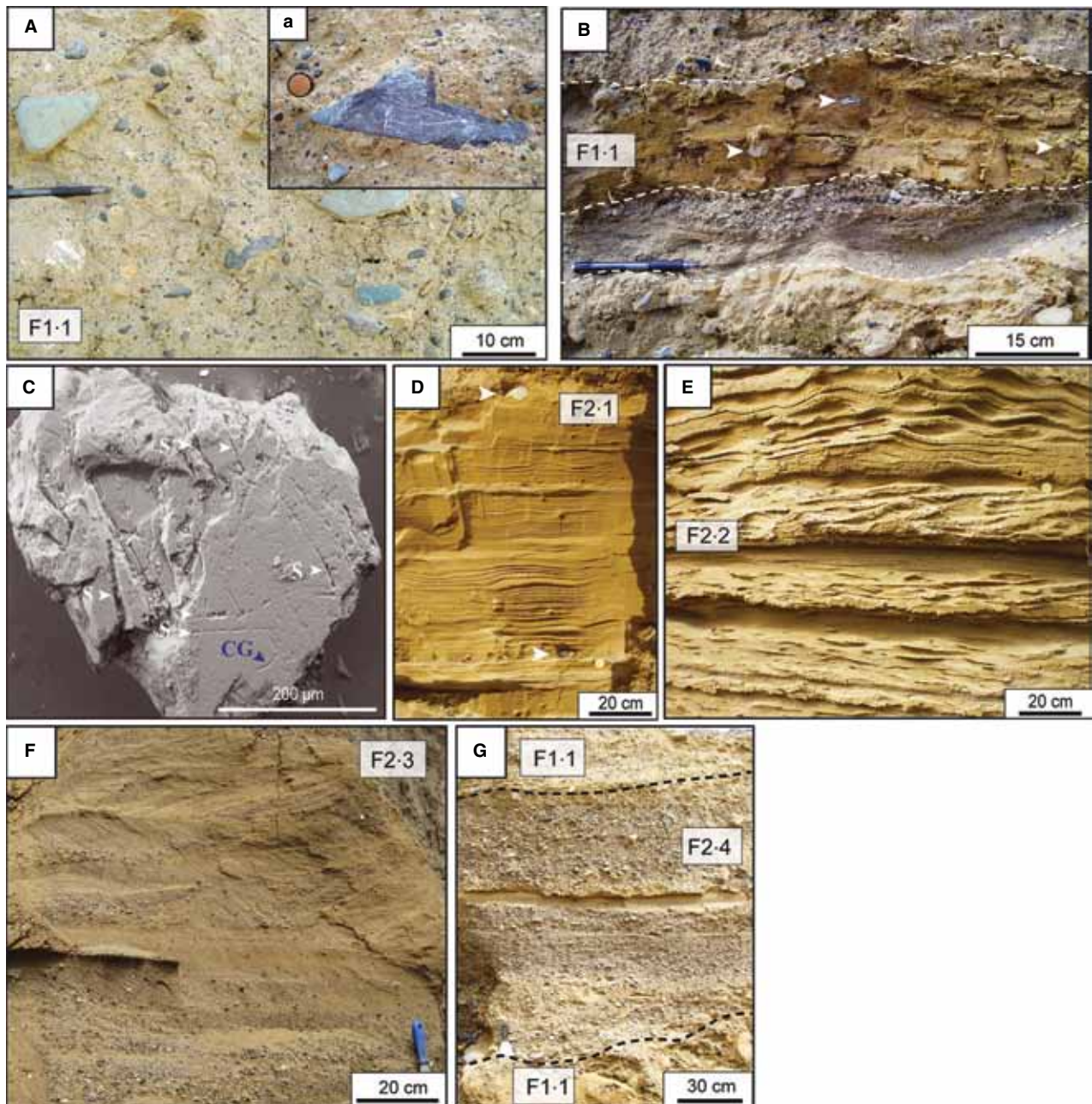
decrease in meltwater discharge and/or a decrease in sediment supply, which may indicate progressive isolation of a cavity (Lesemann *et al.*, 2010). Clasts with deformed bottom contacts suggest that they are dropstones that may indicate rain-out processes (Bennett *et al.*, 2006). *In situ* lenses of sorted sediments are uncommon within mass flow deposits, suggesting that deposition of FA.1 may occur at the glacier bed (Nemec, 1990; Lønne, 1995; Mulder & Alexander, 2001). In addition, the diamicton layers lie on flat and tabular beds without steep enough slopes to trigger gravity destabilization, and therefore do not support the mass flow deposit hypothesis.

Facies Association 2: Lenses of stratified and tabular sorted deposits

Description

This facies association is characterized by large lenses (up to 100 m long and 2 to 6 m thick) of vertically stacked, horizontal, tabular sorted sediments entrapped between layers of diamicton (F1.1) (Fig. 2A and B, logs 1, 2, 3 and 5; Fig. 4A). Facies Association 2 (FA.2) includes laminated alternating clay and silt beds (F2.1), planar parallel-laminated and ripple cross-laminated sands (F2.2), small-scale trough and planar cross-bedded sands (F2.3) and massive to normally graded gravel sequences (F2.4). These lenticular bodies are characterized by an overall upwards increase in sediment grain-size, from F2.1, passing upwards into F2.2 and/or F2.3, and erosively overlain by F2.4.

Laminated fine-grained sediments (F2.1), displaying a tabular geometry, overlie the diamicton deposits with sharp contacts and are characterized by a 0.5 to 1 m thick interbedding of silt to fine sand beds with clay beds (Fig. 3D). Single beds of clay are generally 0.01 m thick, with some layers exceeding 0.05 m. Silt to very fine sand beds are 0.02 to 0.05 m thick and show conformable contacts; some beds display current ripples. Clay layers contain numerous clasts from granule to cobble size with occasional deformed bottom contacts. This laminated fine-grained facies is either overlain by planar parallel-laminated and ripple cross-laminated sands (F2.2) or small-scale trough and planar cross-bedded sands (F2.3).



Facies F2.2 is composed of large sets of very fine to medium sand climbing ripple cross-laminations and planar parallel-laminations, frequently characterized by fining-upward sequences, each 0.2 to 0.6 m thick (Fig. 3E). These beds are characterized by cyclic alternations of planar parallel-laminated coarse sands, passing upwards into fine to medium sand, A-type climbing ripples and B-type climbing ripples, sometimes overlain by S-type climbing ripples. Thin clay layers sometimes drape over the climbing ripples.

Facies F2.3 is characterized by small-scale trough and planar cross-stratified coarse sand (0.1 m deep and 0.5 m wide) containing floating pebbles (Fig. 3F). Single beds of F2.3 are up to 1.2 m thick. Laminated fine-grained facies (F2.1) and cross-laminated sand (F2.2/F2.3) are overlain by lenticular bodies of massive to normally graded gravel (F2.4) with distinctive erosional contacts.

The size of the gravel lenses (F2.4) ranges from 0.3 to 2 m thick and metres to tens of metres in length. These lenses display a 0.2 to

Subglaciofluvial deposits versus ice-contact fan deposits 1389

Fig. 3. Facies associations FA.1 and FA.2 exposed in Ballyhorsey sand pit. (A) Clay-rich diamicton containing abundant striated and faceted clasts inset (a) (F1.1). Coin for scale in (A) is 2 cm in diameter. (B) An intra-diamicton lens of trough cross-stratified coarse sand to granules, overlain by dropstone-rich laminated clays. White arrows indicate dropstones. (C) SEM observations of a quartz grain belonging to F1.1; S: Striations; CG: crescentic gouges. (D) Laminated fine-grained sediments displaying alternations of clay beds with silt to fine sand beds (F2.1), white arrows correspond to dropstones. (E) Alternations of planar parallel-laminated sand with climbing ripple cross-laminations (F2.2). (F) Small-scale trough cross-stratified coarse sand (F2.3). (G) Massive clast-supported gravels with an interbed of coarse sand (F2.4).

0.8 m thick massive to normally graded sequence of matrix-supported or locally clast-supported imbricated gravels interbedded with 0.1 to 0.2 m thick planar parallel-stratified or ripple cross-laminated medium sand beds (Fig. 3G). Trough cross-bedding structures, gravel openwork structures and sandy soft clasts locally occur within F2.4. Flow directions, measured from ripple cross-laminations, trough cross-bedding structures and imbricated gravel, range from 90°N to 280°N within FA.2 (Fig. 2B).

Interpretation

The overall lenticular geometry of FA.2, associated with aggrading, tabular and horizontally stratified deposits, suggests a constrained accommodation space. The overall upward coarsening trend characterizing FA.2 indicates an increase in meltwater discharge and/or sediment supply through time. Laminated fine-grained deposits (F2.1) indicate deposition by settling of finer suspended particles during quiescent phases alternating with silt to very fine sand deposition by low-energy underflows (Plink-Björklund & Ronnert, 1999; Mulder & Alexander, 2001; Bennett *et al.*, 2006).

Granule to cobble-sized clasts deforming underlying sediments are dropstones, characterizing a proglacial setting in shallow ponds, or a glaciolacustrine setting with icebergs and floating ice, or a subglacial environment with rainout processes. Suspension settling processes are followed by traction processes, as indicated by the presence of cross-laminated sand (F2.2 and F2.3) right above F2.1. Fining-upward sequences with ripple cross-laminated sequences (F2.2) reflect traction deposition from successive waning flows.

Small-scale trough and planar cross-bedding structures (F2.3) are related to traction current deposition representing successive two-dimensional and three-dimensional megaripples migrating downflow. Lenticular bodies of massive to normally graded gravel (F2.4) with internal sandy rip-up clasts and erosive contacts are related to erosion and deposition from waning

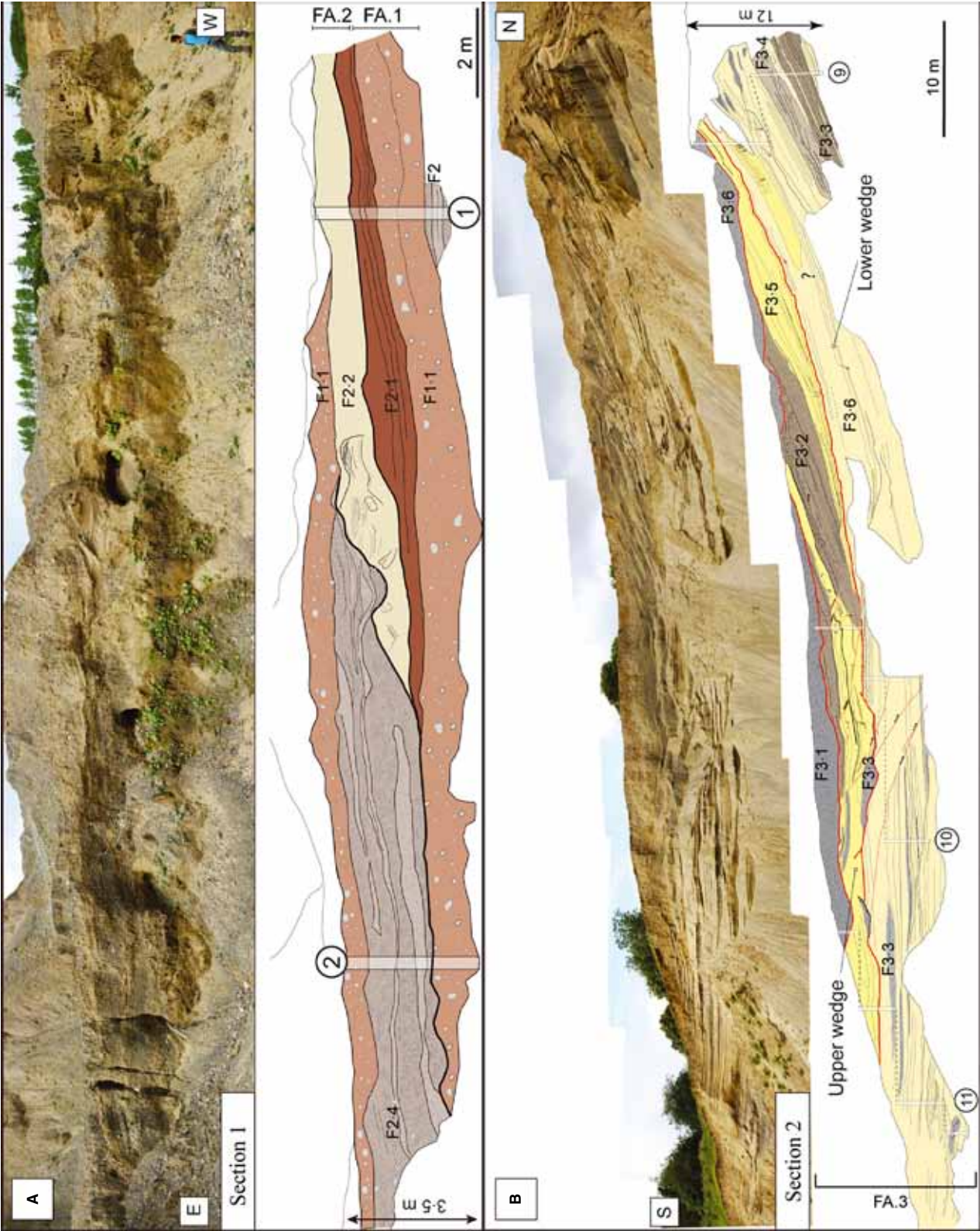
density flows within channels. Interbeds of planar or ripple cross-laminated sand indicate traction deposition during flow quiescence after deposition of gravel beds (Allen, 1982; Mulder & Alexander, 2001). The sharp or erosional contacts between the different facies (F2.1 to F2.4) and the upward changes in sediment grain-size record transport and deposition under highly variable flow conditions, ranging from quiescent slackwater conditions to high-energy conditions.

Deformation structures within Facies Association 2

Description

Deformation structures encompass clastic injections, folds and step normal faults. Within FA.2, 55 clastic dykes occur, including oblique and vertical dykes. Clastic dykes are dominantly oblique and dipping towards the south-east and are produced by the downward injection of sandy material (Figs 5 and 6A). Sills are also common ($n = 7$) within FA.2. Clastic dykes range from 0.03 to 0.5 m in width and are up to 1 m long; their sedimentary infills are composed of fine to medium sand and generally lack internal laminations. Dykes and sills occasionally occur together as part of complex branching patterns. A complex network characterized by the association of oblique/vertical dykes and sills with cross-cutting relations occurs within a 1 m thick sandy horizon (Fig. 6A). This network shows a predominance of oblique clastic dykes with a south to south-east dip direction (60%). Locally clastic dykes are overlain by folded structures (Fig. 6C).

Low-amplitude folds (up to 0.3 m), including recumbent and overturned types, are asymmetrical and limited to discrete beds ($n = 6$). Folds propagate horizontally and mostly display a south-east vergence (Fig. 5). Folds are sometimes eroded by the overlying clay-rich diamicton (Fig. 6B). Locally, a SSE-verging recumbent fold (Horizon 1) is observed directly above two overturned folds (Horizon 2) occurring in the hangingwalls of south-east dipping thrust faults (sense of displacement towards the NNW)



Subglaciofluvial deposits versus ice-contact fan deposits 1391

Fig. 4. Interpreted sections 1 and 2. (A) Photograph of section 1 and sketch of sedimentary facies arrangement. Channelized gravel (F2.4) erodes tabular sand (F2.2) and fine-grained laminated sediments (F2.1). This typical upward coarsening sequence of tabular sorted sediments (FA.2) is entrapped between two units of clay-rich diamicton (F1.1). (B) Photograph of section 2 and sketch of sedimentary facies arrangements. This section shows two stacked sequences of prograding sedimentary wedges of sorted sediments (FA.3), separated by an unconformable and erosive contact. Note that normal faults are abundant through both sedimentary wedges.

(Fig. 6B). Horizons H1 and H2 represent two superimposed horizons of deformation exhibiting two opposite senses of displacement (SSE versus NNW). These two horizons lay on an undeformed horizon (Horizon 3).

Normal step faulting is also observed within these deposits; they are high-angle and display low offsets from 0.05 to 0.1 m (Fig. 6D). These step faults are constrained to discrete beds and are intercalated between undeformed deposits.

Interpretation

The combination of clastic injections, folds and step normal faults within FA.2 indicates that porewater pressure was fluctuating during deformation of the water-saturated bed. Hydrofracturing and sand injection illustrate episodes of pressurized water release and injection of fluidized sediments while folding indicates hydroplastic deformation. Step normal faulting illustrates post-dewatering brittle deformation when porewater pressure was lower.

Facies Association 2 is principally characterized by the relative abundance of clastic injections that are either discordant (dykes) or concordant (sills) to the host strata. The main process leading to sand intrusions is hydrofracturing (Hurst *et al.*, 2011) and is triggered when pressure is greater than the weight of an equivalent column of water (Cosgrove, 1995; Jolly & Lonergan, 2002; Cobbold & Rodrigues, 2007). This state is defined as overpressure and can be reached subglacially where the weight of ice is exerted on basal meltwater or proglacially by aquifer compression at the margin (Broster, 1991; Rijdsdijk *et al.*, 1999; van der Meer *et al.*, 1999, 2009; Boulton & Caban, 1995; Phillips, 2006; Phillips *et al.*, 2012). The clay-rich diamicton layers (FA.1) intercalated between FA.2 represent low hydraulic conductivity sediments contributing to overpressure development within the water-saturated deposits. The dominant south to south-east dip directions of the oblique dykes are consistent with a shear stress direction inferred from a palaeo-ice flow sourced from the Wicklow ice dome inferred from Warren & Creighton (1993), suggesting a subglacial to submarginal origin (Fig. 5).

The sills observed within FA.2 may form in both subglacial and submarginal environments during episodes of fluid overpressure release and exploit the bedding as a preferential path for hydrofractures development (Denis *et al.*, 2010; Phillips *et al.*, 2012). The occurrence of several dyke generations with various dips (Fig. 6A) indicates changes in the stress field over time, possibly indicating local changes in glacier dynamics because hydrofractures always propagate along an axis parallel to the maximum compressive strain (λ_3).

Clastic dykes are locally overlain by folds, illustrating the decrease in porewater pressure following the processes of hydrofracturing and sand injections (Fig. 7A). Folds may either form during ice/bed coupling phases in a subglacial environment or via sediment compression in an ice-marginal setting (McCarroll & Rijdsdijk, 2003; Lesemann *et al.*, 2010). In proglacial environments, compression is the dominant driving stress at the glacial front resulting in large thrust faults and folds generally affecting the greater part of the overridden sediments (Bennett, 2001; Bennett *et al.*, 2004; Benediktsson *et al.*, 2008). The overturned and recumbent fold types are constrained to single beds and show a horizontal tectonic transport that may be explained by subglacial deformation (Piotrowski *et al.*, 2004; Lesemann *et al.*, 2010). The local truncation of

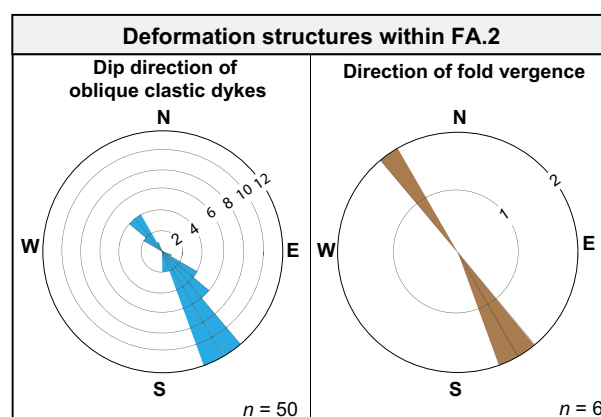


Fig. 5. Rose diagrams showing the dip direction of oblique clastic dykes ($n = 50$) and the direction of fold vergence ($n = 6$) within FA.2.

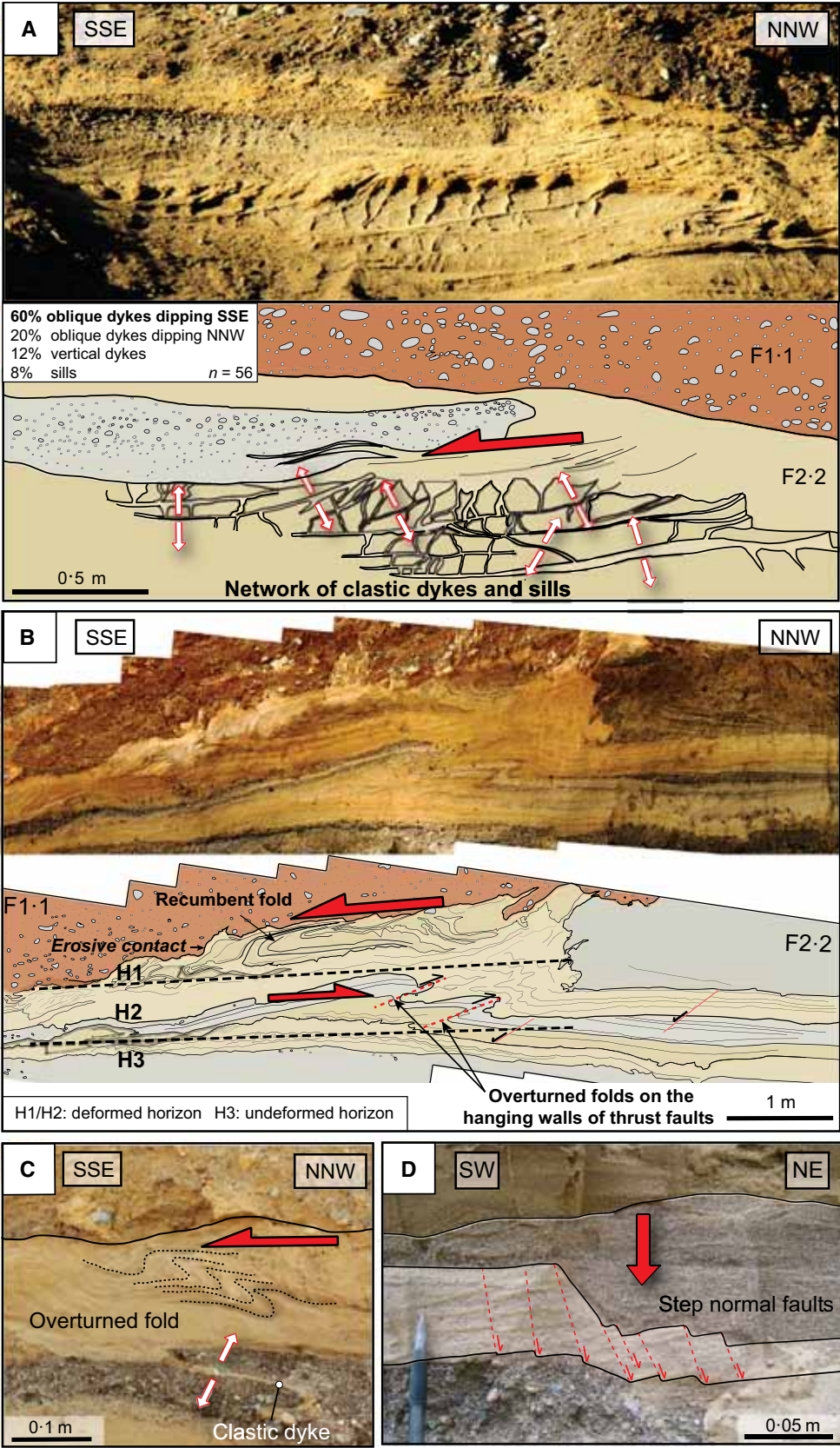


Fig. 6. Deformation structures observed within FA.2 (A) Clastic injections network within FA.2 occurring beneath diamicton deposits (FA.1), including oblique/vertical dykes and sills with a predominance of SSE dipping oblique dykes. (B) A SSE-verging recumbent fold overlying two NNW-verging overturned folds. Note that the recumbent fold is truncated by the overlying diamicton. The dotted lines correspond to the limit among three different horizons (H1/H2/H3) of deformation (refer to Fig. 7B for explanations). (C) An overturned fold overlying an oblique clastic dyke within FA.2. (D) Step normal faults entrapped between undeformed deposits.

fold structures indicates that deformation pre-dates the emplacement of the overlying till.

The deforming bed observed within Fig. 6B shows different horizons of deformation. During

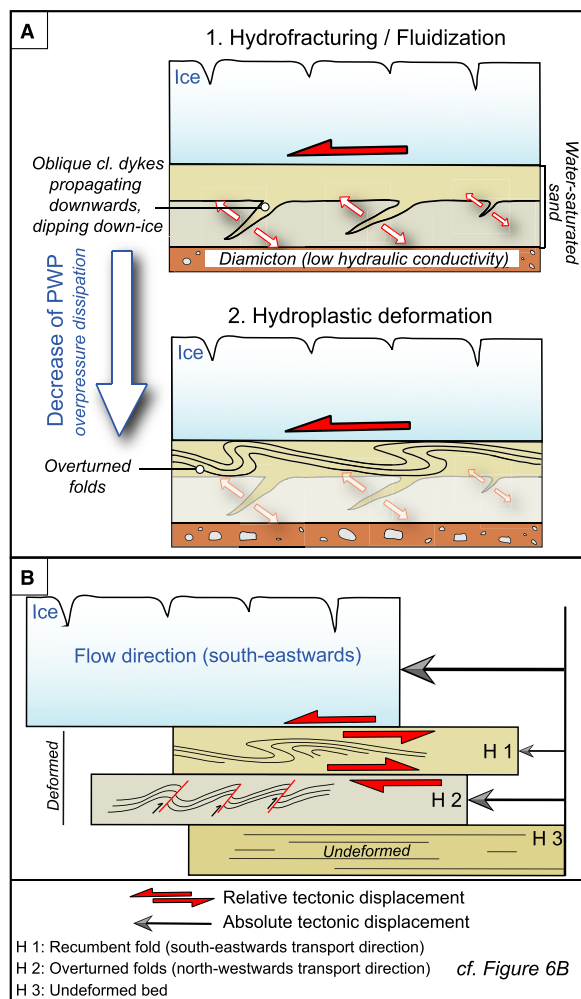


Fig. 7. (A) Diagram showing the change in deformation style due to decrease in porewater pressure. Hydrofracturing leads to dissipation of the overpressure and is followed by folding of the bed due to simple shear stress exerted by the overriding ice sheet (see Fig. 6C). (B) Deformable bed model when ice is coupled to the bed, explaining the reverse directions of tectonic transport between the Horizons 1 and 2. Shearing occurs at the ice/H1 interface and at the H1/H2 interface along a slip surface. H3 represents the stable horizon with no deformation (See Fig. 6B).

ice/bed coupling episodes, the shear stress exerted by flowing ice on the bed may trigger slip motion along the décollement surface induced by sediment layering. The occurrence of relative displacements within different layers of the subglacial bed allows determination of different horizons of deformation (Alley *et al.*, 1989; Kjær *et al.*, 2006). In the present study, the deforming bed is locally divided into three distinct horizons (H1 to H3) that deform at different strain rates. This configuration with different deformation rates leads to various absolute displacements, inducing shearing at horizon interfaces. Shear deformation occurs at the ice/H1 interface forming a fold with a southerly dipping axis, and also at the H1/H2 interface forming overturned folds with a northerly dipping axis (Fig. 7B). Horizon H3 represents the stable horizon with no deformations.

The presence of step normal faults within FA.2 suggests the occurrence of brittle deformation under low porewater pressure. These deformations affect discrete beds in between periods of sediment deposition because the step normal faults are entrapped in between two undeformed beds (Fig. 6D). The corresponding stress is related to radial extensional deformation (Guiraud & Seguret, 1987) and is generally associated with sediment compaction or glacier overloading. Single beds affected by step normal microfaults have been widely interpreted as subglacial deformation structures triggered by ice recoupling with the bed (Denis *et al.*, 2010).

Facies Association 3: Sedimentary wedge deposits

Description

This facies association is characterized by two major sedimentary wedges separated by an unconformable and erosional contact (Fig. 2A and B, logs 7, 8, 9, 10, 11 and 13; Fig. 4B). The sedimentary wedges display two different sets of prograding deposits dipping 20° to 22° towards the south, which form an unconformable and erosive contact with FA.1 and FA.2 (Fig. 2).

Facies Association 3 (FA.3) is characterized by a general decrease in mean grain size and

1394 E. Ravier *et al.*

wedge thickness towards the south. The lower wedge is up to 12 m thick, whereas the upper wedge is 4 to 5 m thick (Fig. 4B). The north to south decrease in grain size is illustrated by the progressive transition from cobbles to fine sand.

Within the lower wedge, massive and poorly sorted gravels (F3.1) laterally evolve into normally sorted gravels (F3.2), overlain by a wedge of trough cross-bedding coarse sands (F3.4). Upwards and laterally, diffusely graded planar parallel sands and pebbly sands occur (F3.5) and rapidly change into normally graded sand beds (F3.6), which represent the dominant facies observed in the lower wedge (Fig. 4B). Lenses of massive sorted gravels (F3.3) displaying erosive bases are scattered throughout F3.6. The upper wedge erosively overlies the lower wedge (Fig. 4B). This upper sequence displays diffusely graded sands and normally graded sorted gravels (Fig. 4B). In the uppermost part of the sedimentary sequence, both wedges are erosively in contact with massive and poorly sorted gravels (F3.1) that vary in thickness laterally (Figs 2 and 4B).

The massive and poorly sorted gravel facies (F3.1) displays an erosive base and varies in thickness from 1.5 to 6 m. This facies is composed of clast-supported to matrix-supported granules to boulders in a sandy matrix (Fig. 8A). These deposits show frequent clusters of open-work clasts and scours around larger clasts. Rip-up clasts of clay-rich diamicton (F1.1) locally occur within this facies.

Normal to inversely graded sorted gravels (F3.2) are characterized by moderately to well-sorted, clast-supported pebbles to cobbles (Fig. 8B and C). Thin interbeds of coarse sand to pebbly sand occur with some evidence of crude horizontal stratification.

Large-scale trough cross-stratified coarse sands (F3.4) are at a low angle and are generally 0.5 to 1.5 m thick and 1 to 6 m wide, with a downflow decrease in their dimensions (Fig. 8B). A few large clasts up to pebble size are observed. Flow directions measured from cross-bedding structures range between 170°N and 350°N.

Diffusely graded coarse sands (F2.5) with abundant pebble beds occur within both wedges; pebble content decreases downflow (Fig. 8D). Clasts up to cobble size are observed within this facies.

Normally graded sand beds (F3.6) represent the dominant facies in the southern part of the lower wedge (Fig. 4B). Individual beds consist

of planar parallel-laminated sands with scattered gravels fining upwards into A-type climbing ripples and passing upwards into B-type climbing ripples (Fig. 8E). Normally graded beds of sand are frequently topped by massive to laminated clays, especially in the downflow direction. Clayey rip-up clasts are locally scattered within F3.6, and flute casts are observed at the base of a few beds. Facetted and striated clasts up to cobble size, sometimes deforming underlying sediments, frequently occur throughout F3.6 (Fig. 8F). The abundance of these out-sized clasts varies within the different beds, even if a general upward decrease in clast content is observed. Some scour and fill structures are observed within this sandy facies (Fig. 8G).

Interpretation

Facies Association 3 is characterized by a thicker pile of sediments, different geometries, sedimentary facies and stacking patterns as compared with FA.2. These changes imply major changes in depositional processes, sedimentary dynamics and accommodation space.

Massive and poorly sorted gravel (F3.1) with clasts up to boulder-size and till intraclasts results from the deposition of coarse-grained hyperconcentrated density flows (Postma *et al.*, 1983; Nemec *et al.*, 1999; Mulder & Alexander, 2001; Winsemann *et al.*, 2009). Clusters of open-work clasts suggest a reworking of finer material by winnowing, which could be related to the vicinity of a subglacial conduit exit, coupled with high discharge. Occurrences of large rip-up clasts reflect basal erosion during sediment transport.

Beds of normally graded sorted gravels (F3.2) indicate deposition from waning high-density flows. Upwards, large-scale trough to planar cross-stratified coarse sand (F3.4) indicates deposition and downflow migration of 2D/3D dunes. Dunes need sustained flow conditions and continued sediment input to form, implying either quasi-steady concentrated density flows or quasi-steady turbulent flows (Gorell & Shaw, 1991; Winsemann *et al.*, 2007, 2009). The large change in direction of trough cross-bedding structures (180°) may reveal intense lateral shifting of flow directions, but it could also be related to flow expansion close to a subglacial conduit exit (Hornung *et al.*, 2007; Winsemann *et al.*, 2007, 2009). Large clasts correspond either to dropstones or isolated clasts acting as remnants when finer material has been removed by meltwater.

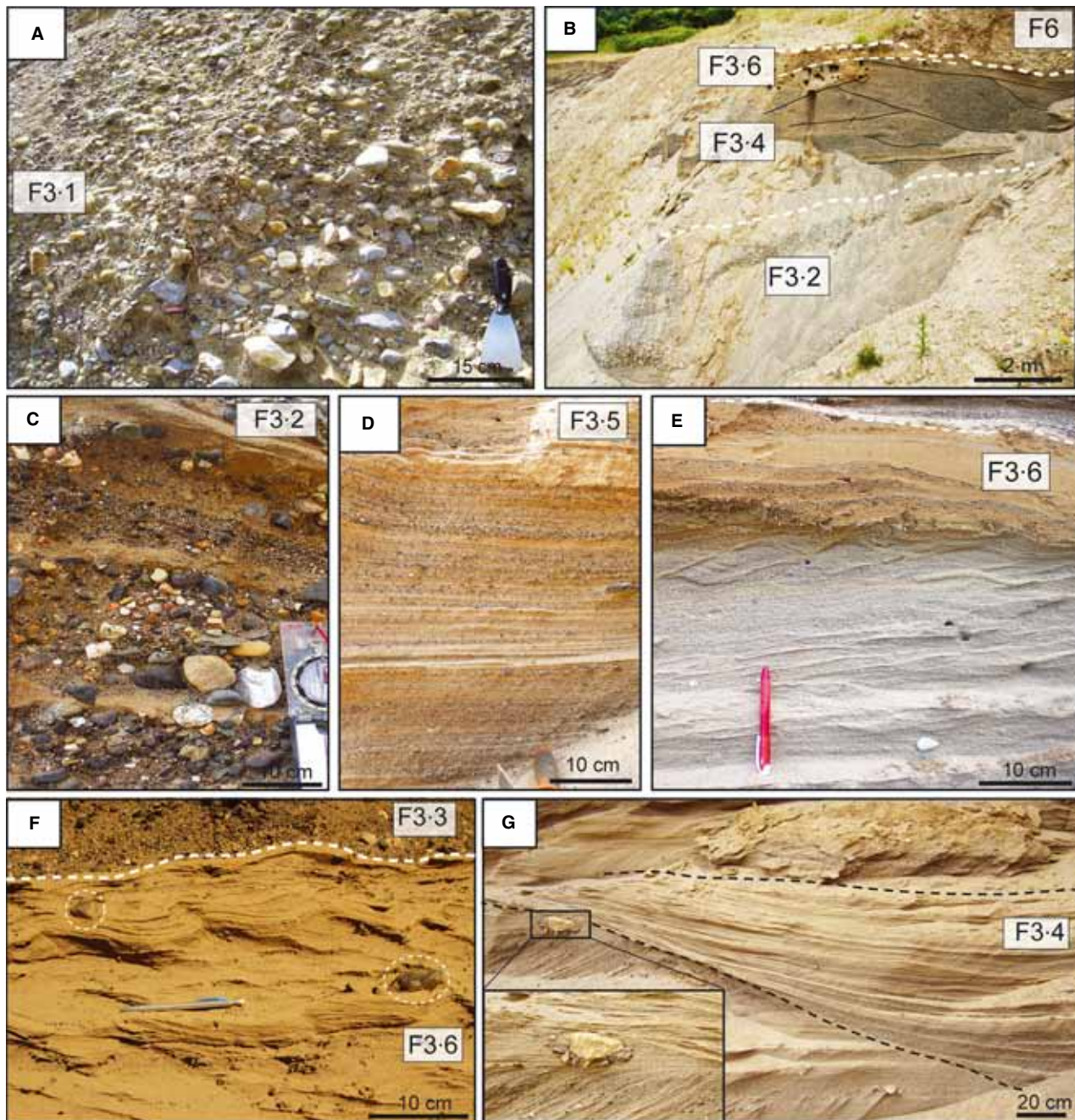


Fig. 8. Facies association 3 exposed at Ballyhorsey sand pit. (A) Massive and poorly sorted gravels (F3.1). (B) Normally graded sorted gravels (F3.2) overlain by large-scale trough cross-bedding coarse sands, passing upwards into cross-laminated sands (F3.6). (C) Normally graded sequence of gravels ending with massive sand beds (F3.2). (D) Diffusely graded coarse sands (F3.5). (E) Cross-laminated sand medium to coarse sand with a typical sequence showing alternations of type A and B climbing ripples, topped by silty beds (F3.6). (F) Sandy A-type climbing ripples (F3.6) containing dropstones, erosively overlain by channelized gravels (F3.3). (G) Scour and fill structures and clustered dropstones occasionally occurring within F3.6.

Diffusely graded sand and pebbly sands (F3.5) occurring in both wedges suggest traction deposition from high-density turbidity flows and imply rapid deposition under high-energy flows. Normally graded sand beds (F3.6) reflect

deposition from waning low-density turbidity currents; single beds are often characterized by base-absent Bouma sequences (T_{b-d}) (Bouma, 1962; Kneller, 1995). Flute casts represent erosion features formed by turbidity currents.

1396 E. Ravier et al.

Faceted and striated pebble-sized clasts deforming underlying sediments are interpreted as dropstones. Scattered lenses of massive and sorted gravels (F3.3), which sometimes display crude cross-stratifications, are related to deposition from pulsed and channelized high-density flows.

Deformation structures within Facies Association 3

Description

Deformation structures within FA.3 encompass clastic dykes, folds and normal faults (Figs 9 and S2). At the base of the lower sedimentary wedge, three large clastic dykes (3 to 10 m long

and 0.5 to 2 m wide) sourced in the underlying diamicton (F1.1) are observed within the massive and poorly sorted gravels (F3.1) (Fig. S2). The dykes are oblique and climb upwards with a SSW dip direction (Figs 9A and S2). The dykes locally display a branching pattern and are filled with a mix of clay, sand and clasts up to cobble size. One clastic dyke displays internal laminations parallel to the direction of dyke propagation, the base of the dyke is filled with massive clay to sand, passing into sand and gravel beds towards the edge. Within this dyke, clasts are re-aligned parallel to the margins of the injection structure.

A few overturned folds ($n = 3$), of centimetre to decimetre-scale occur in the upper part of the

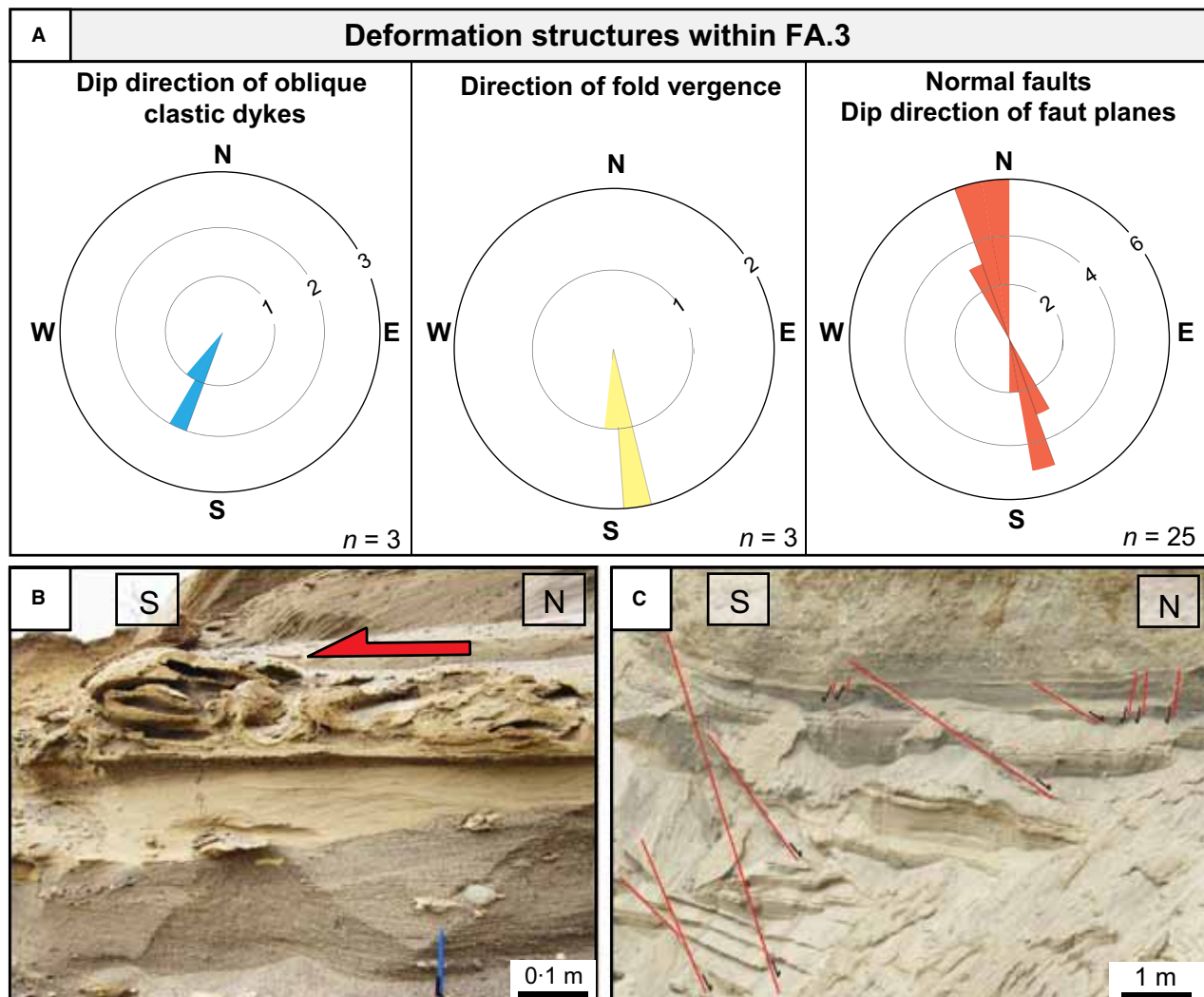


Fig. 9. (A) Dip direction of oblique clastic dykes, direction of fold vergence and dip direction of normal fault planes within FA.3, displayed on three different rose diagrams. (B) A south-verging overturned fold observed within FA.3. (C) Normal faults within the prograding fan (FA.3) dipping either towards the south or the north.

sedimentary wedge, principally within silt to very fine sand (F3.6). These deformation structures affect beds to a limited extent, along and down the slope of the sedimentary wedge. The folds display anticlines overturned towards the south (Fig. 9A and B).

Both wedges contain abundant normal faults that are either listric or straight-sided and low to high-angle (Figs 4B, 9A and 9C); they have a wide range of scales, varying from a few centimetres up to 7 m long, with an offset ranging from few centimetres up to a metre. Normal faults are antithetic; the dip direction of fault planes occurs either towards the NNW or SSE (Fig. 9A and C).

Interpretation

Oblique clastic injections are related to either subglacial or ice-marginal hydrofracturing (Broster, 1991; Boulton & Caban, 1995; Le Heron & Etienne, 2005). The emplacement of large clastic dykes propagating upwards is generally related to the release of overpressurized water from beneath the adjacent ice sheet in submarginal to marginal environments where a marked decrease in ice overburden pressure allows hydrofractures to climb upwards (Boulton & Caban, 1995; Phillips *et al.*, 2012). Internal laminations within one of the dykes indicate progressive infill by repeated fracture and extension of the sediments (Ramsay, 1980; Le Heron & Etienne, 2005; van der Meer *et al.*, 2009).

Fold anticlines are systematically directed towards the south, similar to the dip direction of the prograding foresets, indicating that deformations may have operated in conjunction with a down-slope mass movement (Maltman, 1994). In this case, folded beds are the product of slumping along the slope of the subaqueous fan. The dense network of normal faults downthrowing in opposite directions affect a large part of the sedimentary wedge, probably related to post-depositional gravity destabilization and subsequent spreading of the fan.

Iceberg keel-induced deformations

Description

In the distal part of the sedimentary wedge, a 3 m wide depression showing a scour structure, collapsed laminations and surrounded by intense deformations was observed (Fig. S3). The deformation structures are constrained to a 10 m wide and 2 m high area and occur within the distal part of the wedge (F3.6). The deformation struc-

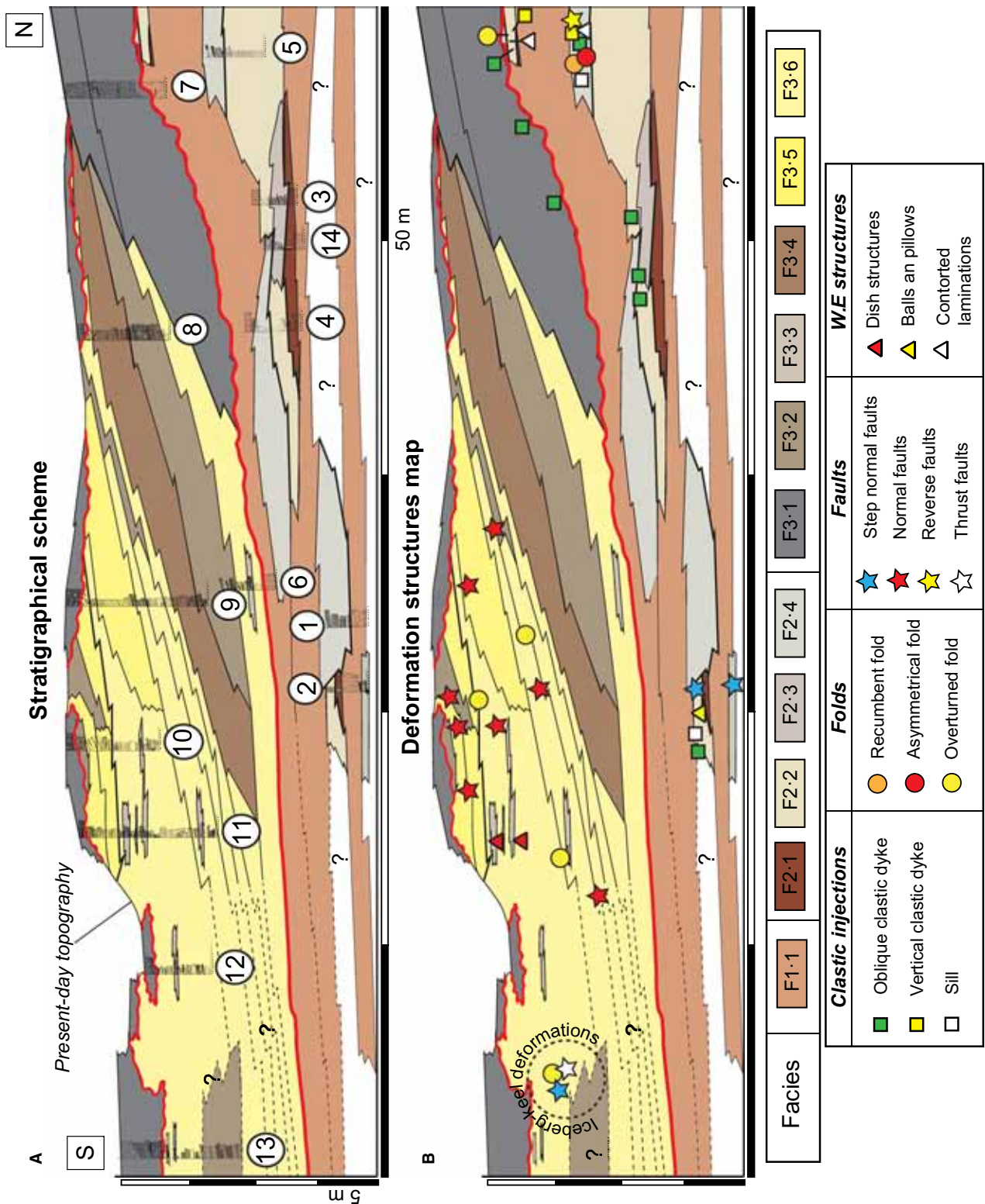
tures encompass highly convoluted bedding (centimetre to metre-scale), flame structures, load casts and small clastic dykes (2 cm wide and up to 15 cm long). On each side of the scour, SSE dipping low-angle thrust faults (<20°) and NNW asymmetrical verging folds are observed (Figure S3). Normal faults are numerous; they display steps on each side of the depression and often cross-cut the deformation structures previously mentioned. Fault offsets are low, ranging from centimetre to decimetre-scale.

Interpretation

Localized and intense deformation, including structures such as thrust faults, asymmetrical folds, clastic dykes and normal faults, associated with intense and deep scouring, are related to the association of ductile and brittle deformation. Melting of buried ice and subsequent downwarping may be responsible for the emplacement of collapsed structures, step normal faults and convolute bedding (Gruszka & van Loon, 2011). However, thrust faults and folds are not structures that are consistent with processes of deformation induced by melting of buried ice because they indicate sediment compression. These deformation structures affect sediments that were formed by subaqueous density flows (F3.6), while dead-ice melting ice is more likely to occur within proglacial glaciofluvial deposits. Winsemann *et al.* (2003) described an example of ice buried within subaqueous deposits where the entrapped ice was thought to be the result of the break-up of a ploughed iceberg. The buried keel fragment of the iceberg remained within the subaqueous sediments, causing normal faulting and downwarping of the surrounding strata during progressive melting. In this study, lateral thrusting and folding, also associated with hydrofractures, may have been triggered by an iceberg keel ploughing the lake floor. This array of deformation structures can be attributed to deformation triggered by an iceberg keel scouring of sediments (Longva & Bakkejord, 1990; Woodworth-Lynas, 1996; Eden & Eyles, 2001; Lynch *et al.*, 2012).

STRATIGRAPHICAL CORRELATION AND SEDIMENTARY SEQUENCES

A stratigraphical interpretative scheme based on correlation of outcrop logging data is shown in Fig. 10A. Lateral and upward variations of sedimentary facies, as well as their geometries and stacking patterns, are represented in this model.



Subglaciofluvial deposits versus ice-contact fan deposits 1399

Fig. 10. (A) Stratigraphical scheme of Ballyhorsey sand pit based on log correlations, showing the lateral distribution of sedimentary facies. See Fig. 2 for log section positions within the pit. (B) Localization of the deformation structures observed at the study site. FA.2 is dominated by deformation structures formed during ice/bed coupling, while FA.3 displays structures induced by gravity destabilization and mass-movements along the foreset beds. NB: A localized and intense deformed area is observed within FA.3 and corresponds to deformation structures related to an iceberg ploughing the lake floor.

Deformation structures mapped in the pit are shown in Fig. 10B.

These scenarios show aggrading basal sediments (FA.1 and FA.2) corresponding to lenses of vertically stacked sorted sediments (FA.2) entrapped within interdigitated diamicton units (FA.1). These sorted deposits are characterized by repetitive sedimentary sequences composed of coarsening upward trending sediments from F2.1 to F2.4, with rapid upward changes in sediment grain size and erosional surfaces (Fig. 11A).

These lenses of sorted sediments frequently display deformation structures constrained to single beds. Deformation structures are numerous and include clastic injections, folds and step normal faults, mostly related to a shear deformation directed towards the south-east (Figs 5 and 10B). The predominance of clastic dykes indicates that porewater pressure was high enough to trigger repeated episodes of hydrofracturing.

Aggrading bottom deposits are unconformably and erosively overlain by two prograding sedi-

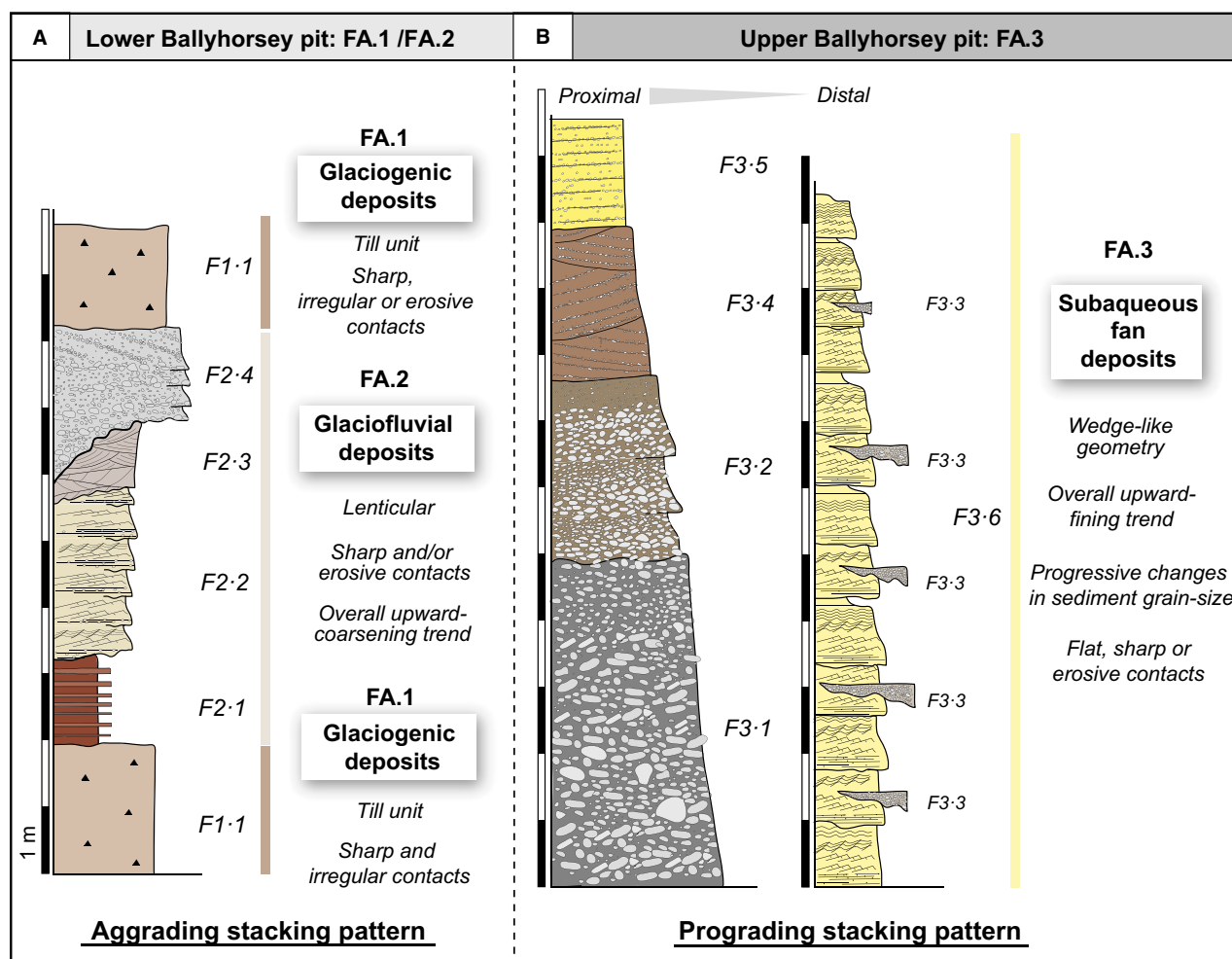


Fig. 11. (A) Typical sedimentary sequences observed at Ballyhorsey sand pit. (A) Lower Ballyhorsey pit showing an aggrading sedimentary sequence characterized by tabular and stratified sorted sediments (FA.2) intercalated between layers of clay-rich diamicton (FA.1). (B) Upper Ballyhorsey pit characterized by prograding sorted sediments (FA.3).

1400 E. Ravier *et al.*

mentary wedges (FA.3) characterized by a north to south decrease in sediment grain size from massive gravel (F3.1) to normally graded sand beds (F3.6). The wedges display a lateral and upward progressive grain-size fining trend with sharp or flat contacts between single beds compared to FA.2 (Fig. 11B). Deformation structures are mainly related to transport of sediments along the fan slope during episodes of gravity destabilization. Soft-sediment deformation structures include a dense network of normal faulting with fault dips oriented north/north-west and south/south-east and some overturned folding triggered by slumping (Fig. 10B). Apart from a few 'climbing' upwards clastic dykes at the base of the fan, folds and faults demonstrate conditions of low porewater pressure.

Different sedimentary sequences, stacking patterns and deformation structures allow FA.2 to be easily discriminated from FA.3 (Figs 10 and 11). Changes in accommodation space, meltwater discharge, sedimentary flux and porewater pressure are possibly responsible for the differences between FA.2 and FA.3, suggesting a possible shift in the type of glacial environment, i.e. from subglacial to proglacial.

DISCUSSION

The sedimentological, stratigraphical and deformational characteristics described in this study permit the discrimination of two different sedimentary units corresponding to two different glacial environments. The first, lowermost, unit corresponds to a subglacial/submarginal environment characterized by ice-bed coupling and decoupling episodes (FA.1/FA.2). The second unit corresponds to a proglacial environment characterized by sediment deposition in a proglacial lake (FA.3). Thereafter, the characteristics of these two environments and the criteria facilitating their recognition in the sedimentary record will be discussed.

This discussion will focus particularly on the subglacial depositional environment formed during ice-bed decoupling events because of the significant role played by subglacial processes and episodic meltwater drainage on the local ice stream dynamics. The lowermost unit is interpreted to be the result of repeated subglaciofluvial sediment deposition during ice-bed decoupling, followed by ice-bed recoupling, deformation of the bed and till deposition. The recurrence of ice-bed coupling and decoupling

episodes underneath the Irish Sea Ice Stream (ISIS) at this site will also introduce information on the temporal framework of the subglacial meltwater production and drainage, and its potential impact on ice-flow mechanisms. In addition, the transition from subglacial to proglacial sedimentary units can also be used to establish the dynamics of deglaciation of the ISIS at the regional scale.

Facies Association 1/Facies Association 2 – Subglacial/submarginal environment

Ice/bed decoupling and subglaciofluvial sediment deposition

The basal sedimentary sequence shows subglacial tills alternating with deposition and deformation of sorted sediments. This typical sedimentary sequence has already been ascribed to sedimentation within subglacial cavities or subglacial lakes characterized by periodic drainage leading to repeated glacier-bed decoupling and recoupling (Munro-Stasiuk, 2000; Wysota, 2007; Lesemann *et al.*, 2010; Livingstone *et al.*, 2012). Transport and deposition of sorted sediments can occur subglacially within a subglacial drainage system consisting of different types of individual elements: for example, channels, linked cavities, groundwater flow or pipe flow within tills (Hubbard & Nienow, 1997; Fountain & Walder, 1998; Eyles, 2006). Subglacial deposition may occur within less-side cavities where subaqueous fans are described (Walder, 1986; Kamb, 1987; Evans *et al.*, 2006; Lindén *et al.*, 2008; Clerc *et al.*, 2012). Deposition can also occur during episodes of decoupling when basal-water pressure exceeds ice-flotation pressure, within a subglacial de-coupled space. In this configuration, subglacial flows are inferred to have a sheet-like geometry producing planar-tabular beds (Piotrowski *et al.*, 2006; Lesemann *et al.*, 2010). The tabular and horizontal deposits characterizing FA.2 may indicate glaciofluvial deposition by laminar flow during episodes of ice-bed decoupling. Channelized gravels (F2.4) at the top of the lenses of sorted deposits erode planar-tabular beds implying destabilization of subglacial meltwater flows and their collapse into channelized flows (Walder, 1986; Creyts & Schoof, 2009; Lesemann *et al.*, 2010). Within FA.2, the increase in porewater pressure required to exceed the ice-flotation pressure can be triggered by reduced drainage into the subjacent bed, due to lower permeability within the clay-rich diamicton (FA.1) and/or an increase in

subglacial meltwater discharge. The aggrading pattern and the lenticular geometry characterizing FA.2 indicate that the subglacial accommodation space available for sediment deposition is restricted vertically and horizontally, as is expected underneath localized zones of ice/bed decoupling. The accommodation space for sediments in this specific subglacial de-coupled space is controlled and limited by the thickness of the basal-water layer and, consequently, by the melting and deformation of the overlying ice roof, the meltwater discharge, permeability of the bed, sediment flowing into the space and the sedimentation rate.

Facies Association 2 shows a recurrent sedimentary pattern, starting with tabular laminated fine-grained beds (F2.1) and sand beds (F2.2 and F2.3), overlain by channelized gravels (F2.4) with sharp and erosive bed contacts. This rhythmicity, inferred from repetitive changes in sediment supply or temporal changes in flow competence, is often associated with glacial environments, including subglaciofluvial environments (Knight, 2003; Clerc *et al.*, 2012; Lesemann *et al.*, 2010). The aggrading stacked pattern suggests progressive upwards motion and/or melting of the overlying ice roof, because aggradation occurs during periods of balance between rate of sediment deposition and rate of accommodation (Van Wagoner *et al.*, 1990). Because the sediment supply is expected to increase together with the meltwater discharge during the melt season, the available space for sediment deposition is also expected to increase to preserve the aggradational stacking pattern. The thermomechanical response of ice roof melting over a melt season is concordant with the increase in the subglacial de-coupled space. When the melt season ends, meltwater availability drastically decreases (FA.2) and ice can recouple with the bed. The excess of porewater pressure contained in the bed can be released through hydrofracturing (oblique clastic dykes within FA.2).

Ice-bed recoupling, deformation of subglaciofluvial sediments and till deposition

The discrete beds within the lenses of tabular subglaciofluvial deposits (FA.2) exhibit clastic injection, fold structures paralleling local palaeo-ice flow and step normal faults. These structures indicate glaciotectonic deformations under varying porewater pressure conditions (Figs 5 and 6).

In glacial environments, such deformation structures can be formed in either subglacial or

ice-marginal environments. In FA.2, the deformation structures are limited to single beds, sometimes separated by undeformed deposits (Fig. 6D), implying cyclical sediment deformation and coeval sediment deposition. Such patterns suggest subglacial deformation (with deformation occurring shortly after deposition) rather than successive phases of glacier retreats and re-advances (see Lesemann *et al.*, 2010). In an ice-marginal environment, deformation affects the greater part of the overridden sediments, whereas at the study site, evidence of deformation is generally restricted to single sediment layers (Bennett, 2001; Piotrowski *et al.*, 2004; Clerc *et al.*, 2012). The asymmetrical and low-amplitude folds observed within FA.2, including recumbent and overturned types, reveal a horizontal transport, related to shear deformation imposed by the overriding ice or mobile soft sediment. These folds may indicate that the space for propagation of sediment deformation is limited, i.e. deformation occurs in a confined environment. The abundance of clastic dykes indicates that sediments in FA.2 were impacted by high porewater pressure. In addition, dykes propagate downwards, towards the SSE, indicating that hydrofracturing occurred in conjunction with a shear stress induced by an overriding ice sheet. The predominance of oblique clastic dykes indicates that the ice flow exerted a primary control on the direction of hydrofracture propagation (van der Meer *et al.*, 2009; Clerc *et al.*, 2012; Phillips *et al.*, 2012). The dynamic changes in porewater pressure illustrated by the different styles of deformation (brittle, hydroplastic and fluidization) are probably a clear indication of the repetition of ice/bed decoupling and recoupling. Porewater pressure can increase due to meltwater input during decoupling stages, while release of overpressurized water by multiple hydrofracturing phases could occur during episodes of ice recoupling with the bed. After the release of porewater, pressure decreases progressively, implying an increase in the effective stress and a progressive change in sediment behaviour during deformation (from ductile to brittle). Deformations induced by the overriding ice sheet lead to the emplacement of asymmetrical folds (hydroplastic deformation) until porewater pressure is sufficiently low to form step normal faults (brittle deformation) (Fig. 6).

Deformation structures within FA.2 are located directly below clay-rich diamicton deposits (F1.1) (Fig. 10B). The deformation

structures are sometimes truncated by the overlying diamicton, indicating that deformation predates the emplacement of the diamicton (Fig. 6B). Deposition of the clay-rich diamicton may have occurred subglacially after ice-bed recoupling and deformation of the bed. Clast fabrics reveal that till layers have undergone some degree of shearing, possibly due to overriding ice or suprajacent mobile sediment (Fig. S1). These clay-rich diamictons can be considered as subglacial traction till deposits [sensu Benn & Evans (2010)]. The undeformed intra-till lenses of sorted sediments, concordant with layering, possibly indicate occasional localized decoupling or small-scale meltwater flow at the ice/bed interface or pipe flow within till. Such flow can settle and deposit sand when meltwater pressure exceeds the ice/sediment weight (Piotrowski & Tulaczyk, 1999; Munro-Stasiuk, 2000; Lesemann *et al.*, 2010).

Facies Association 3 – Proglacial environment

Ice sheet retreat, proglacial lake formation and ice-contact fan deposition

In the upper part of the pit, FA.3 corresponds to sediment deposition in a lake. Deformation structures related to iceberg keel scouring, associated with the occurrence of dropstones, indicate that sedimentation took place within an ice-contact proglacial lake associated with a calving ice margin. The occurrence of these proglacial deposits, unconformably (FA.3) overlying subglacial deposits, reveals an episode of glacier retreat (FA.1/FA.2) (cf. Fig. 10).

Facies Association 3 is composed of two sedimentary wedges displaying foreset bedding dipping down from the fan apex parallel to the fan surface at angles of 20 to 22°. The absence of topset deposits indicates that the wedges constitute grounding-line fans (Powell, 1990; Lønne, 1995; Nemec *et al.*, 1999; Thomas & Chiverrell, 2007). In the proximal zone of the fan, gravel facies (F3.1 and F3.2), often associated with scour structures and ripped-out clasts, indicate that deposition resulted from concentrated to hyperconcentrated meltwater flows within the zone of flow establishment (cf. Russell & Arnott, 2003, for terminology). Massive to poorly sorted gravels are proximal facies and indicate rapid deposition from turbulent hyperconcentrated flows, while normally graded gravels illustrate the downflow waning of more diluted high-density flows into a more distal part of the fan

(Russell & Arnott, 2003; Hornung *et al.*, 2007; Winsemann *et al.*, 2009). In the proximal fan zone, the frequent clusters of openwork clasts also indicate that the deposition of F3.1 and F3.2 occurs at, or near, the subglacial conduit exit (Russell & Arnott, 2003; Hornung *et al.*, 2007).

Laterally, the occurrence of diffusely graded sands indicates rapid deposition from sediment high-density flows under high energy within the zone of flow transition (Plink-Björklund & Ronnert, 1999; Russell & Arnott, 2003; Winsemann *et al.*, 2009). Development of large-scale cross-stratified coarse sands to granules is interpreted to represent the distal part of the zone of flow transition passing into the zone of established flow (Russell & Arnott, 2003; Hornung *et al.*, 2007; Winsemann *et al.*, 2009).

Within the distal zone of the fan, normally graded sands with ripple scale cross-laminations capped by massive or laminated clay to silt (F3.6) are related to low-density waning turbidity flows, with a net increase in suspension fallout away from the sediment influx point. These deposits are attributed to the zone of established flow (ZEF) and record the distal basinwards accretion of the fan (Russell & Arnott, 2003; Hornung *et al.*, 2007). Gravel lenses (F3.3) that are observed within distal deposits represent pulses of channelized and concentrated density flows during high discharge events.

The lateral and upward grain-size partitioning of the prograding sediments towards the south, from coarse-grained in the proximal zone to fine-grained in the distal zone, demonstrates the development of a subaqueous fan with a likely single sedimentary influx point. The prograding style of FA.3 and the thick sediment pile implies a larger accommodation space. The occurrence of two superimposed prograding wedges probably indicates a shifting of the subglacial conduit outlet position during deposition of FA.3.

Three climbing upwards clastic dykes are observed in proximal fan deposits and record the escape of porewater. The possibility of hydrofractures propagating upwards may be related to the marked decrease in ice overburden pressure at the margin (Boulton & Caban, 1995; Phillips *et al.*, 2012). The ice-contact fan is mainly characterized by deformation structures that are most likely to be induced by gravity due to spreading of the subaqueous fan. The emplacement of a dense network of normal faults illustrates the processes of fan spreading due to pressure equilibrium establishment within the fan. Faults and folds observed within

FA.3 illustrate that deformations occurred under low porewater pressure.

Implications for subglacial meltwater production and ice-flow mechanisms

Temporal control on subglacial meltwater production

The four sedimentary sequences deposited during periods of ice-bed decoupling display a similar coarsening upward pattern, demonstrating recurrent variations in subglacial meltwater discharge and/or sediment supply. The upward coarsening subglaciofluvial sedimentary sequences, entrapped between till layers suggest a temporal control of the meltwater production and sediment deposition, probably corresponding to seasonal or multi-episodic cycles of meltwater discharge increase. (1) A seasonal evolution of meltwater discharge has been underlined by several studies based on Alpine glaciers and ice sheets (Hubbard & Nienow, 1997; Nienow *et al.*, 1998; Bartholomew *et al.*, 2010; Chandler *et al.*, 2013). (2) Deglaciation is also often associated with pulses of temperature increase, leading to multi-episodic events of intense surface melting increase and developments of persistent subglacial drainage system (Le Brocq *et al.*, 2013).

1 The first hypothesis is the seasonal control on the subglacial sedimentary sequence, due to seasonal variations in meltwater discharge (Fig. 12). At the beginning of the melt season, meltwater production and basal meltwater pressure progressively increase, leading to localized ice/bed decoupling (Hubbard & Nienow, 1997). In this case, the early stages of decoupling and the development of a subglacial meltwater drainage system are characterized by the deposition of thin laminated clay and sand beds (0.01 to 0.05 m) (F2.1). Tabular sand beds indicate minor sheet flows during ice-bed decoupling, while clay beds imply suspension settling when the decoupled space is temporary disconnected from the main meltwater routing system. The increase in meltwater production during the melt season is highlighted by the occurrence of thicker tabular sand beds (0.2 to 0.6 m) (F2.2), implying sustained ice-bed decoupling. When the meltwater peak is reached during the melt season, the thickness of the subglacial meltwater layer tends to increase, triggering sheet flow instabilities and channelization, resulting in the deposition of channelized gravels (F2.4) (Walder, 1986; Creyts & Schoof, 2009; Lesemann *et al.*, 2010). When the melt

season ends, meltwater availability drastically decreases, water seeps through previously deposited permeable sorted sediments and ice can re-couple with the bed, leading to glaciotectionic deformations (i.e. oblique clastic dykes and folds) and till deposition (Fig. 12).

2 The subglacial sequence may alternatively reveal a multi-episodic control on the meltwater discharge and the development of perennial subglacial drainage networks underneath the ISIS (Fig. 12). During the last deglaciation, considerable fluctuations in temperature occurred (Andersen *et al.*, 2004). Episodes of rapid temperature increase impacted surface melting and meltwater discharge, resulting in the development of ice-bed decoupling zones with a subglacial meltwater drainage system remaining stable over several seasons. In this configuration, the timing of deposition is difficult to determine; subglaciofluvial sediments and till deposition could occur continuously depending on meltwater production and ice-bed coupling or decoupling dynamics.

Impact on ice-flow mechanisms

Ice-flow speed-up can be controlled by sediment deformation, but also by the passage of subglacial meltwater during decoupling events (Tulaczyk, 1999; Bartholomew *et al.*, 2011). The ice-bed decoupling episodes combined with a cyclical evolution of meltwater discharge are evidenced by the basal subglaciofluvial sedimentary sequence (FA.2) and probably have strong implications for ISIS dynamics. Similar to ice sheets today, the flow velocity of the ISIS may have increased seasonally in response to a meltwater production increase over the melt season and at other times in any one year (Mair *et al.*, 2003; Joughin *et al.*, 2008; Bartholomew *et al.*, 2012). At the end of a melt season, production of water would have decreased, ice re-coupled with the bed, subglaciofluvial sediments would have been deformed, tills deposited and ice-flow deceleration taken place (Knight, 2003; Clerc *et al.*, 2012) (Fig. 12). The multi-episodic meltwater discharge signal that could also be depicted from the subglaciofluvial sedimentary sequences would have also impacted the dynamics of the ISIS (Fig. 12).

These two hypotheses are concordant with studies below the Greenland Ice Sheet where it is demonstrated that seasonal to multi-episodic variations in ice accelerations are correlated with variations in the intensity of the surface melting (Zwally *et al.*, 2002).

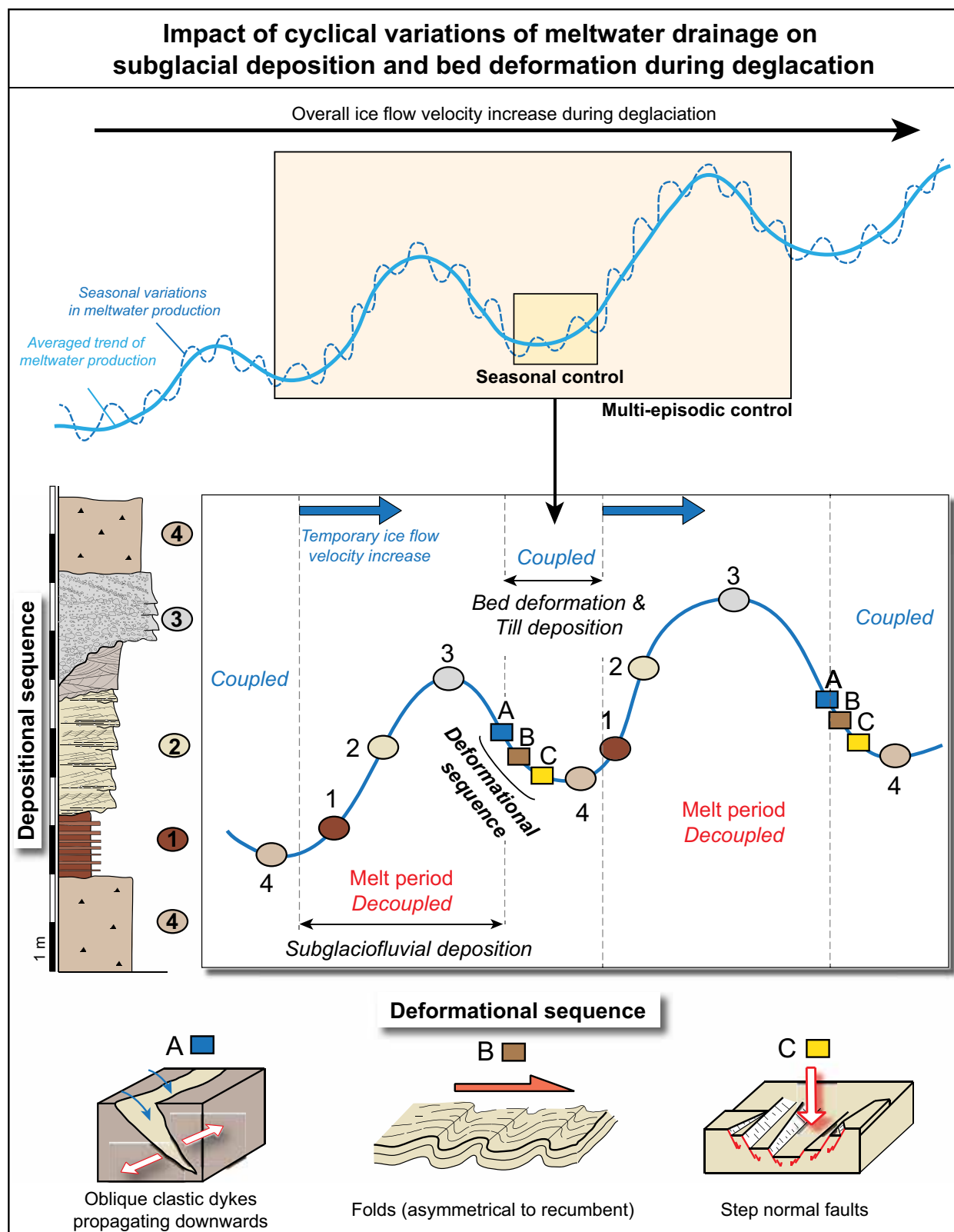


Fig. 12. Impact of cyclical variations of meltwater drainage on subglacial deposition and deformation. The subglaciofluvial sediments are deposited during ice-bed decoupling, implying episodes of ice-flow velocity increase, while deformation of the bed and till deposition occur during ice-bed coupling. This subglacial depositional and deformational sequence could be controlled by either seasonal or multi-episodic variations in meltwater discharge.

Implications for the deglaciation dynamics of the Irish Sea Ice Sheet

During ice sheet decay, ablation exceeds accumulation, leading to the formation of large volumes of meltwater, notably stored at or drained to the ice-bed interface. Previous studies in this area have described the occurrence of subglacial water bodies of various sizes, including kilometre-scale subglacial lakes (for example, at Enniskerry), metre-scale lee side cavities (for example, at Killiney Bay) and metre to centimetre-scale de-coupled space (for example, at Killiney Bay and Ballyhorsey) (McCabe & O'Cofaigh, 1994; Clerc *et al.*, 2012). The storage and drainage of a large amount of meltwater underneath the ISIS in subglacial to submarginal positions suggests an increase in meltwater production, probably triggered by an increase in surface melt during deglaciation. The upwards increase in hydrofracturing within the subglacial unit at Ballyhorsey and the dense networks of hydrofractures observed within subglacial deposits along Killiney Bay indicate high porewater pressure, also related to the increase in meltwater production within the subglacial bed during deglaciation (Rijsdijk *et al.*, 1999, 2010; Clerc *et al.*, 2012). The abundance of subglacial water bodies underneath this portion of the ISIS may have considerably increased basal ice-flow velocity (Bell, 2008). It has been demonstrated that subglacial lakes in Antarctica and development of subglacial meltwater drainage in Greenland control the increase in ice stream velocities (Shepherd *et al.*, 2009; Richter *et al.*, 2013). This relation implies that the retreat of the ISIS during deglaciation, illustrated by the deposition of proglacial sediments above subglacial sediments in Ballyhorsey and Killiney Bay, occurred in response to and along with high ice-flow velocity (Rijsdijk *et al.*, 2010; Clerc *et al.*, 2012). In addition, the development of ice-contact lakes could have further influenced ice-flow motion due to the thermomechanical feedback generated by the water in contact with the ice margin (Stokes & Clark, 2003).

The ice-contact fan in Ballyhorsey shows an apparent upwards decrease in dropstones, which could be related to changes in sedimentation rate, debris content of the ice and/or the ice margin calving rate. Fast flowing ice generally triggers an increase in calving rates (Sundal *et al.*, 2013), implying that the high dropstone concentration at the base of the fan may illustrate high calving rates during rapid ice

streaming. The relative upwards decrease in dropstone concentration associated with the upwards grain-size increase in the ice-contact fan may reveal an augmentation of meltwater discharge and sedimentation rates. The combined increase in meltwater discharge and sedimentation rates at the top of the sedimentary sequence exposed in Ballyhorsey (cf. upper wedge in the ice-contact fan; Fig. 10) may occur as a response to sustained surface melting increase due to a rise in post-LGM air-temperature in the last stages of deglaciation (Andersen *et al.*, 2004). Thinning of the glacier outlet due to calving and surface melting may have led to progressive retreat of the ISIS and decrease in the ice sheet volume. During deglaciation of the Jakobshavns Isbrae in Greenland, the initiation of a rapid ice stream was triggered by ice thinning and increased surface melting, implying that deglaciation of the ISIS may have been enhanced by rapid ice flow along ice streams (Long & Roberts, 2003). Within the overall pattern of ISIS, speed-up occurring during deglaciation, seasonal and/or multi-episodic accelerations of the ice sheet must have affected ice stream dynamics (Fig. 12).

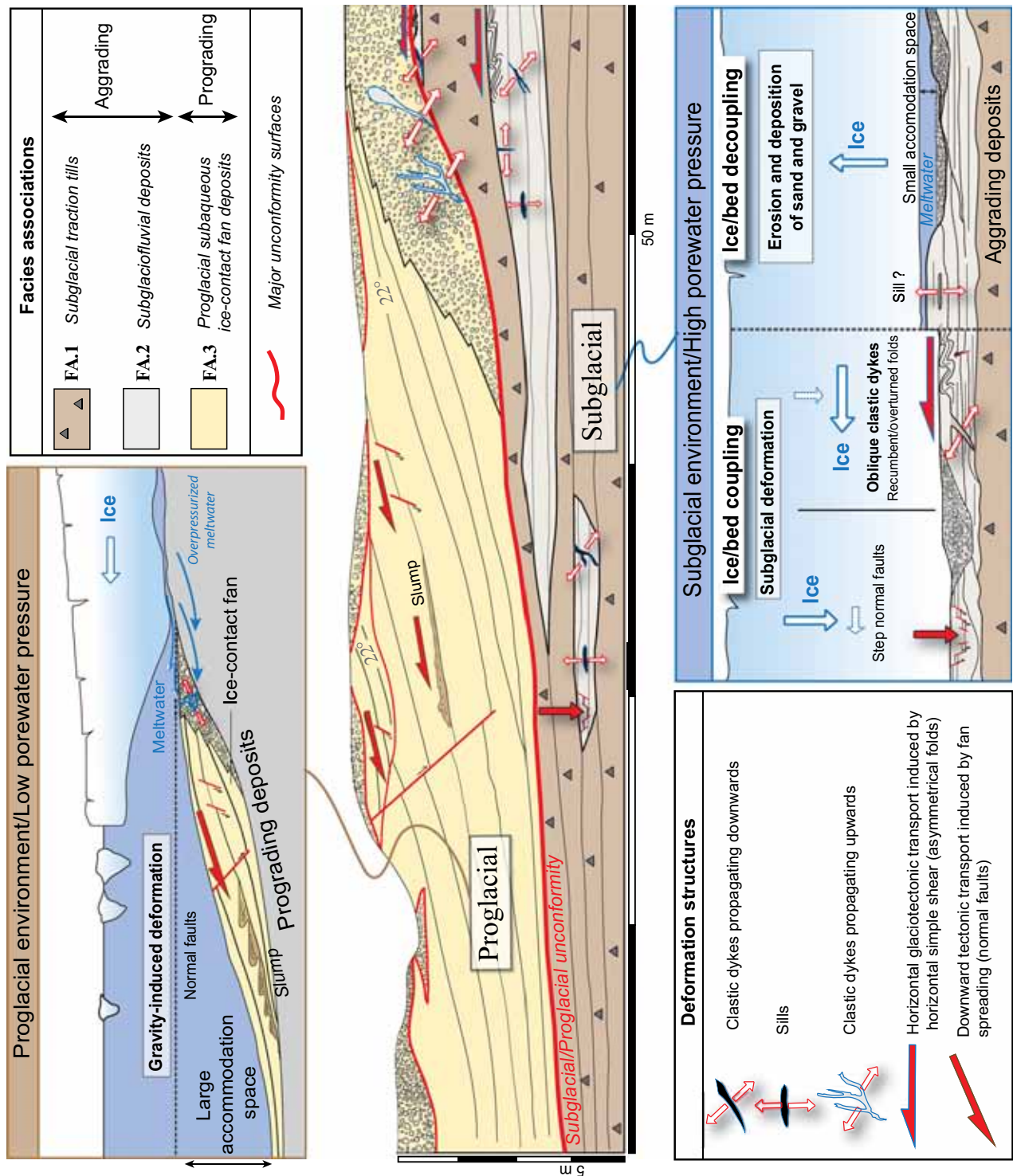
CONCLUSIONS

Field observations within the Ballyhorsey sand pit illustrate the transition from a subglacial to a proglacial depositional environment. Sediments located at the bottom of the sand pit were deposited within a closed subglacially confined environment, while the upper sediments were deposited in an open unconfined ice-contact proglacial lake. Different styles of sedimentation, geometries, stacking patterns and deformation structures permitted differentiation between subglacial and proglacial settings (Fig. 13).

1 Subglaciofluvial deposits, accumulating during ice/bed decoupling, are lenticular and entrapped between till units. These deposits display an overall coarsening upward trend, tabular deposit and an aggradational stacking pattern, affected by subglacial deformation structures constrained to discrete beds.

2 Ice-contact fan deposits are preserved and display a prograding stacking pattern with an upward and lateral grain-size decrease; deformation structures are related to fan spreading and gravity destabilization across the fan slopes.

Although no single element described in this study can be used as a key diagnostic criterion,



Subglaciofluvial deposits versus ice-contact fan deposits 1407

Fig. 13. This diagram summarizes the main sedimentological, geometrical, stratigraphical and deformational features of the Ballyhorsey pit. This figure shows the main differences between a subglacial environment characterized by vertically stacked and tabular subglaciofluvial sediment deposited during ice/bed decoupling and deformation structures formed during ice/bed coupling, and a proglacial environment characterized by a prograding ice-contact fan and deformations structures related to gravity destabilization.

taken together, the characteristics listed in this study permit the identification of a subglacial de-coupled space where sorted sediments can deposit. These criteria can be used for palaeoenvironmental reconstructions when studying both Pleistocene and Pre-Pleistocene sediments, and can be used to better constrain the impact of subglacial meltwater drainage on ice-flow dynamics. A temporal framework of meltwater production is illustrated by the sequence of subglaciofluvial deposition and deformation, impacting evolution of the Irish Sea Ice Stream (ISIS) flow velocity. The complete sedimentary sequence described in this study reveals an increase in meltwater production related to deglaciation, and fast retreat of the ISIS due to ice volume loss by calving and surface melting.

ACKNOWLEDGEMENTS

This study was made possible through research funds provided by the EAP department from the GDF SUEZ group. Liam O'Bharáin (Irish Geological Survey) is thankfully acknowledged for his comments on the paper. We are also very thankful to Sara McCune and Carmela Chateau for proof-reading the English. This study is a contribution of the UMR-CNRS 6282 Biogéosciences, Equipe SEDS. The authors thank Emrys Phillips, Niko Putkinen, Nick Eyles and an anonymous reviewer for their helpful comments that led to improvements to the original manuscript.

REFERENCES

- Allen, J.R.L. (1982) Sedimentary structures: their character and physical basis. *Dev. Sedimentol.*, **30**, 1–679.
- Alley, R.B., Blankenship, D.D., Rooney, S.T. and Bentley, C.R. (1989) Sedimentation beneath ice shelves: the view from Ice Stream B. *Mar. Geol.*, **85**, 101–120.
- Andersen, K.K., Azuma, N., Barnola, J.M., Bigler, M., Biscaye, P., Caillon, N., Chappellaz, J., Clausen, H.B., Dahl-Jensen, D., Fischer, H., Flückiger, J., Fritzsche, D., Fujii, Y., Goto-Azuma, K., Gronvold, K., Gundestrup, N.S., Hansson, M., Huber, C., Hvidberg, C.S., Johnsen, S.J., Jonsell, U., Jouzel, J., Kipfstuhl, S., Landais, A., Leuenberger, M., Lorrain, R., Masson-Delmotte, V., Miller, H., Motoyama, H., Narita, H., Popp, T., Rasmussen, S.O., Raynaud, D., Rothlisberger, R., Ruth, U., Samyn, D., Schwander, J., Shoji, H., Siggard-Andersen, M.L., Steffensen, J.P., Stocker, T., Sveinbjörnsdóttir, A.E., Svensson, A., Takata, M., Tison, J.L., Thorsteinsson, T., Watanabe, O., Wilhelms, F., White, J.W.C. and Project, N.G.I.C. (2004) High-resolution record of Northern Hemisphere climate extending into the last interglacial period. *Nature*, **431**, 147–151.
- Ballantyne, C.K., McCarroll, D. and Stone, J.O. (2006) Vertical dimensions and age of the Wicklow Mountains ice dome, Eastern Ireland, and implications for the extent of the last Irish Ice Sheet. *Quatern. Sci. Rev.*, **25**, 2048–2058.
- Bartholomew, I., Nienow, P., Mair, D., Hubbard, A., King, M.A. and Sole, A. (2010) Seasonal evolution of subglacial drainage and acceleration in a Greenland outlet glacier. *Nat. Geosci.*, **3**, 408–411.
- Bartholomew, I.D., Nienow, P., Sole, A., Mair, D., Cowton, T., King, M.A. and Palmer, S. (2011) Seasonal variations in Greenland Ice Sheet motion: Inland extent and behaviour at higher elevations. *Earth Planet. Sci. Lett.*, **307**, 271–278.
- Bartholomew, I., Nienow, P., Sole, A., Mair, D., Cowton, T. and King, M.A. (2012) Short-term variability in Greenland Ice Sheet motion forced by time-varying meltwater drainage: implications for the relationship between subglacial drainage system behavior and ice velocity. *J. Geophys. Res.-Earth Surf.*, **117**, F03002.
- Bell, R.E. (2008) The role of subglacial water in ice-sheet mass balance. *Nat. Geosci.*, **1**, 297–304.
- Benediktsson, Í.Ö., Möller, P., Ingólfsson, Ó., van der Meer, J.J.M., Kjær, K.H. and Krüger, J. (2008) Instantaneous end moraine and sediment wedge formation during the 1890 surge of Brúarjökull, Iceland. *Quatern. Sci. Rev.*, **27**, 209–234.
- Benn, D.I. (1994) Fabric shape and the interpretation of sedimentary fabric data. *J. Sed. Res.*, **A64**, 910–915.
- Benn, D.I. (1995) Fabric signature of subglacial till deformation, Breidamerkurjökull, Iceland. *Sedimentology*, **42**, 735–747.
- Benn, D.I. and Evans, D.J.A. (2010) *Glaciers and Glaciations*, 2nd edn. Edward Arnold, London.
- Bennett, M.R. (2001) The morphology, structural evolution and significance of push moraines. *Earth-Sci. Rev.*, **53**, 197–236.
- Bennett, M.R., Huddart, D. and Thomas, G.S.P. (2002) Facies architecture within a regional glaciolacustrine basin: Copper River, Alaska. *Quatern. Sci. Rev.*, **21**, 2237–2279.
- Bennett, M.R., Huddart, D., Waller, R.I., Cassidy, N., Tomio, A., Zukowskyj, P., Midgley, N.G., Cook, S.J., Gonzalez, S. and Glasser, N.F. (2004) Sedimentary and tectonic architecture of a large push moraine: a case study from Hagafellsjökull-Eystrí, Iceland. *Sed. Geol.*, **172**, 269–292.
- Bennett, M.R., Huddart, D. and Waller, R.I. (2006) Diamict fans in subglacial water-filled cavities – a new glacial environment. *Quatern. Sci. Rev.*, **25**, 3050–3069.

1408 E. Ravier et al.

- Boulton, G.S. (1990) Sedimentary and sea level changes during glacial cycles and their control on glacial marine facies architecture. *Geol. Soc. London Spec. Publ.*, **53**, 15–52.
- Boulton, G.S. and Caban, P.E. (1995) Groundwater flow beneath ice sheets: part II – its impact on glacier tectonic structures and moraine formation. *Quatern. Sci. Rev.*, **14**, 563–587.
- Bouma, A. (1962) *Sedimentology of some Flysch Deposits. A Graphic Approach to Facies Interpretation*. Elsevier Publications, Amsterdam, 168 pp.
- Bowen, D.Q., Phillips, F.M., McCabe, A.M., Knutz, P.C. and Sykes, G.A. (2002) New data for the last glacial maximum in Great Britain and Ireland. *Quatern. Sci. Rev.*, **21**, 89–101.
- Boyce, J.I. and Eyles, N. (2000) Subglacial deforming bed conditions recorded by late Quaternary sediments exposed in Vineland Quarry, Ontario, Canada. *J. Geol. Soc. London Bull.*, **112**, 98–118.
- Broster, B.E. (1991) Glaciotectonic deformation in sediment and bedrock, Hat Creek, British Columbia. *Géog. Phys. Quatern.*, **45**, 5–20.
- Chandler, D.M., Wadham, J.L., Lis, G.P., Cowton, T., Sole, A., Bartholomew, I., Telling, J., Nienow, P., Bagshaw, E.B., Mair, D., Vinen, S. and Hubbard, A. (2013) Evolution of the subglacial drainage system beneath the Greenland Ice Sheet revealed by tracers. *Nat. Geosci.*, **6**, 195–198.
- Charlesworth, J.K. (1928) The glacial retreat from Central and Southern Ireland. *Q. J. Geol. Soc.*, **84**, 393–3342.
- Clark, C.D., Hughes, A.L.C., Greenwood, S.L., Jordan, C. and Serjup, H.P. (2012) Pattern and timing of retreat of the last British-Irish ice sheet. *Quatern. Sci. Rev.*, **44**, 112–146.
- Clerc, S., Buoncristiani, J.F., Guiraud, M., Desaubliaux, G. and Portier, E. (2012) Depositional model in subglacial cavities, Killiney Bay, Ireland. Interactions between sedimentation, deformation and glacial dynamics. *Quatern. Sci. Rev.*, **33**, 142–164.
- Cobbold, P.R. and Rodrigues, N. (2007) Seepage forces, important factors in the formation of horizontal fractures and bedding-parallel fibrous veins ('beef' and 'cone-in-cone'). *Geofluids*, **7**, 313–322.
- Cosgrove, J.W. (1995) The expression of hydraulic fracturing in rocks and sediments. *Geol. Soc. Spec. Publ.*, **92**, 187–196.
- Creyts, T.T. and Schoof, C.G. (2009) Drainage through subglacial water sheets. *J. Geophys. Res.*, **114**, F04008.
- Denis, M., Guiraud, M., Konaté, M. and Buoncristiani, J.-F. (2010) Subglacial deformation and water-pressure cycles as a key for understanding ice stream dynamics: evidence from the Late Ordovician succession of the Djado Basin (Niger). *Int. J. Earth-Sci.*, **99**, 1399–1425.
- Eden, D.J. and Eyles, N. (2001) Description and numerical model of Pleistocene iceberg scours and ice-keel turbated facies at Toronto, Canada. *Sedimentology*, **48**, 1079–1102.
- Evans, D.J.A., Phillips, E.R., Hiemstra, J.F. and Auton, C.A. (2006) Subglacial till: formation, sedimentary characteristics and classification. *Earth-Sci. Rev.*, **78**, 115–176.
- Eyles, N. (2006) The role of meltwater in glacial processes. *Sed. Geol.*, **190**, 257–268.
- Eyles, N., Sladen, J.A. and Gilroy, S. (1982) A depositional model for stratigraphic complexes and facies superimposition in lodgement tills. *Boreas*, **11**, 317–333.
- Farrington, A. (1934) The Glaciation of the Wicklow Mountains. *Proc. Roy. Irish Acad.*, **42**, 173–209.
- Fountain, A.G. and Walder, J. (1998) Water flow through temperate glaciers. *Rev. Geophys.*, **36**, 299–328.
- Gorell, G. and Shaw, J. (1991) Deposition in an esker, bead and fan complex, Lanark, Ontario, Canada. *Sed. Geol.*, **72**, 285–314.
- Gruszka, B. and van Loon, A.J. (2011) Genesis of a giant gravity-induced depression (gravifossus) in the Enköping esker, S. Sweden. *Sed. Geol.*, **235**, 304–313.
- Guiraud, M. and Seguret, M. (1987) Soft-sediment microfaulting related to compaction within the fluvio-deltaic infill of the Soria strike-slip basin (northern Spain). In: *Deformation of Sediments and Sedimentary Rocks* (Eds M.E. Jones and R.M.F. Preston), *Geol. Soc. London Spec. Publ.*, **29**, 123–136.
- Hicock, S.R. (1991) On subglacial stone pavements in till. *J. Geol.*, **99**, 607–619.
- Hoffmann, K. and Piotrowski, J.A. (2001) Till mélange at Amsdorf, central Germany: sediment erosion, transport and deposition in a complex, soft bedded subglacial system. *Sed. Geol.*, **140**, 215–234.
- Hornung, J.J., Aspö, U. and Winsemann, J. (2007) Jet-efflux deposits of a subaqueous ice-contact fan, glacial Lake Rinteln, northwestern Germany. *Sed. Geol.*, **193**, 167–192.
- Hubbard, B. and Nienow, P. (1997) Alpine subglacial hydrology. *Quatern. Sci. Rev.*, **16**, 939–955.
- Hurst, A., Scott, A. and Vigorito, M. (2011) Physical characteristics of sand injectites. *Earth-Sci. Rev.*, **106**, 215–246.
- Jolly, R.J.H. and Lonergan, L. (2002) Mechanisms and controls on the formation of sand intrusions. *J. Geol. Soc. London*, **159**, 605–617.
- Joughin, I., Das, S.B., King, M.A., Smith, B.E., Howat, I.M. and Moon, T. (2008) Seasonal speedup along the western flank of the Greenland Ice Sheet. *Science*, **320**, 781–783.
- Kamb, B. (1987) Glacier surge mechanism based on linked cavity configuration of the basal water conduit system. *J. Geophys. Res.*, **92**, 9083–9100.
- Kjær, K.H., Larsen, E., van der Meer, J.J.M., Ingólfsson, Ó., Krüger, J., Benediktsson, Í.Ö., Knudsen, C.G. and Schomaker, A. (2006) Subglacial decoupling at the sediment interface: a new mechanism for rapid flowing ice. *Quatern. Sci. Rev.*, **25**, 2704–2712.
- Kneller, B.C. (1995) Beyond the turbidite paradigm: physical models for deposition of turbidites and their implications for reservoir prediction. In: *Characterization of Deep-marine Clastic Systems* (Eds A.J. Hartley and D.J. Prosser), *J. Geol. Soc. London Spec. Publ.*, **94**, 31–49.
- Knight, J. (2003) Temporal changes in subglacial meltwater activity: field evidence from the late Devensian in the north of Ireland. *Sed. Geol.*, **160**, 291–307.
- Knutz, P.C., Jones, E.J.W., Austin, W.E.N. and van Weering, T.C.E. (2002) Glacial marine slope sedimentation, contourite drifts and bottom current pathways on the Barra Fan, UK North Atlantic margin. *Mar. Geol.*, **188**, 129–146.
- Le Brocq, A.M., Ross, N., Griggs, J.A., Bingham, R.G., Corr, H.F., Ferraccioli, F., Jenkins, A., Jordan, T.A., Payne, A.J., Rippin, D.M. and Siegert, J.M. (2013) Evidence from ice shelves for channelized meltwater from beneath the Antarctic Ice Sheet. *Nat. Geosci.*, **6**, 945–948.
- Le Heron, D.P. and Etienne, J.L. (2005) A complex subglacial clastic dyke swarm, Sölheimajökull, southern Iceland. *Sed. Geol.*, **181**, 25–37.
- Lesemann, J.-E., Aslop, G.I. and Piotrowski, J.A. (2010) Incremental subglacial meltwater sediment deposition and deformation associated with repeated ice-bed decoupling:

Subglaciofluvial deposits versus ice-contact fan deposits 1409

- a case study from the Island of Funen, Denmark. *Quatern. Sci. Rev.*, **29**, 3212–3229.
- Linch, L.D., van der Meer, J.J.M. and Menzies, J. (2012) Micromorphology of iceberg scours in clays: glacial lake Agassiz, Manitoba, Canada. *Quatern. Sci. Rev.*, **55**, 125–144.
- Lindén, M., Møller, P. and Adrielsson, L. (2008) Ribbed moraine formed by subglacial folding, thrust stacking and lee-side cavity infill. *Boreas*, **37**, 102–131.
- Livingstone, S.J., Clark, S.D., Piotrowski, J.A., Tranter, M., Bentley, M.J., Hodson, A., Swift, D.A. and Woodward, J. (2012) Theoretical framework and diagnostic criteria for the identification of palaeo-subglacial lakes. *Quatern. Sci. Rev.*, **53**, 88–110.
- Long, A.J. and Roberts, D.H. (2003) Late Weichselian deglacial history of Disko Bugt, West Greenland, and the dynamics of the Jakobshavns Isbrae ice stream. *Boreas*, **32**, 208–226.
- Longva, O. and Bakkejord, K.J. (1990) Iceberg Deformation and Erosion in Soft Sediments, Southeast Norway. *Mar. Geol.*, **92**, 87–104.
- Lønne, I. (1995) Sedimentary facies and depositional architecture of ice-contact glaciomarine systems. *Sed. Geol.*, **98**, 13–43.
- Mair, D., Willis, I., Fischer, U.H., Hubbard, B., Nienow, P. and Hubbard, A. (2003) Hydrological controls on patterns of surface, internal and basal motion during three “spring events”: Haut Glacier d’Arolla, Switzerland. *J. Glaciol.*, **49**, 555–567.
- Maltman, A.J. (1994) *The Geological Deformation of Sediments*. Chapman and Hall, London.
- McCabe, A.M. and Clark, P.U. (2003) Deglacial chronology from County Donegal, Ireland: implications for the deglaciation of the British ice-sheet. *J. Geol. Soc. London*, **60**, 847–855.
- McCabe, A.M. and O’Cofaigh, C. (1994) Sedimentation in a subglacial lake, Enniskerry, eastern Ireland. *Sed. Geol.*, **91**, 57–95.
- McCarroll, D. and Rijdsdijk, K.F. (2003) Deformation styles as a key for interpreting glacial depositional environments. *J. Quatern. Sci.*, **18**, 473–489.
- van der Meer, J.J.M., Kjær, K.H. and Krüger, J. (1999) Subglacial water-escape structures and till structures, Sléttjökull, Iceland. *J. Quatern. Sci.*, **14**, 191–205.
- van der Meer, J.J.M., Kjær, K.H., Krüger, J., Rabassa, J. and Kilfeather, A.A. (2009) Under pressure: clastic dykes in glacial settings. *Quatern. Sci. Rev.*, **28**, 708–720.
- Menzies, J. (1990) Brecciated diamictites from Mohawk Bay, S. Ontario, Canada. *Sedimentology*, **37**, 481–493.
- Menzies, J. and Shilts, J. (2002) Subglacial environments. In: *Modern and Past Glacial Environments* (Ed. J. Menzies), pp. 183–278. Butterworth Heinemann, Oxford.
- Mulder, T. and Alexander, J. (2001) The physical character of sedimentary density currents and their deposits. *Sedimentology*, **48**, 269–299.
- Munro-Stasiuk, M.J. (2000) Rhythmic till sedimentation: evidence for repeated hydraulic lifting of a stagnant ice mass. *J. Sed. Res.*, **70**, 94–106.
- Munro-Stasiuk, M.J. (2003) Subglacial Lake McGregor, south-central Alberta, Canada. *Sed. Geol.*, **160**, 325–360.
- Nemec, W. (1990) Aspects of sediment movement on steep delta slopes. In: *Coarse-Grained Deltas* (Eds A. Colella and B.D. Prior), *Int. Assoc. Sedimentol. Spec. Publ.*, **10**, 29–73.
- Nemec, W., Lønne, I. and Blikra, L.H. (1999) The Kregnes moraine in Gauldalen, west-central Norway: anatomy of a Younger Dryas proglacial delta in a palaeofjord basin. *Boreas*, **28**, 545–576. Piotrowski
- Nienow, P.W., Sharp, M.J. and Willis, I.C. (1998) Seasonal changes in the morphology of the subglacial drainage system, Haut Glacier d’Arolla, Switzerland. *Earth Surf. Proc. Land.*, **23**, 825–843.
- O’Cofaigh, C., Dowdeswell, J.A. and Grobe, H. (2001) Holocene glaciomarine sedimentation, inner Scoresby Sund, East Greenland: the influence of fast-flowing ice sheet outlet glaciers. *Mar. Geol.*, **175**, 103–129.
- O’Cofaigh, C., Telfer, M.V., Bailey, R.M. and Evans, D.J.A. (2012) Late Pleistocene chronostratigraphy and ice sheet limits, southern Ireland. *Quatern. Sci. Rev.*, **44**, 160–179.
- Phillips, E.R. (2006) Micromorphology of a debris flow deposit: evidence of basal shearing, hydrofracturing, liquefaction and rotational deformation during emplacement. *Quatern. Sci. Rev.*, **25**, 720–738.
- Phillips, E.R., Everest, J. and Reeves, H. (2012) Micromorphological evidence for subglacial multiphase sedimentation and deformation during overpressurized fluid flow associated with hydrofracturing. *Boreas*, **42**, 395–427.
- Piotrowski, J.A. and Tulaczyk, S. (1999) Subglacial conditions under the last ice sheet in northwest Germany: ice-bed separation and enhanced basal sliding? *Quatern. Sci. Rev.*, **18**, 737–751.
- Piotrowski, J.A., Larsen, N.K. and Junge, F.W. (2004) Reflections on soft subglacial beds as a mosaic of deforming and stable spots. *Quatern. Sci. Rev.*, **23**, 993–1000.
- Piotrowski, J.A., Larsen, N.K., Menzies, J. and Wysota, W. (2006) Formation of subglacial till under transient bed conditions: deposition, deformation and basal decoupling under a Weichselian ice sheet lobe, central Poland. *Sedimentology*, **53**, 83–106.
- Piotrowski, J.A., Mickelson, D.M., Tulaczyk, S., Krzyszkowski, D. and Junge, F.W. (2001) Were deforming beds beneath past ice sheets really widespread? *Quatern. Int.*, **86**, 139–150.
- Plink-Björklund, P. and Ronnert, L. (1999) Depositional processes and internal architecture of Late Weichselian ice-marine submarine fan and delta settings, Swedish west coast. *Sedimentology*, **46**, 215–234.
- Postma, G., Roep, T.B. and Ruegg, G.H.J. (1983) Sandy-gravelly mass-flow deposits in an ice-marginal lake (Saalian, Leuvenumsche Beek valley, Veluwe, the Netherlands), with emphasis on plug-flow deposits. *Sed. Geol.*, **34**, 59–82.
- Powell, R.D. (1990) Glaciomarine processes at grounding-line fans and their growth to ice-contact deltas. In: *Glaciomarine Environments: Processes and Sediments* (Eds J.A. Dowdeswell and J.D. Scourse), *Geol. Soc. London Spec. Publ.*, **53**, 53–73.
- Powell, R.D. (2003) Subaquatic landsystems: fjords. In: *Glacial Landsystems* (Ed. D.J.A. Evans), pp. 313–347. Arnold, London.
- Powell, R.D. and Domack, E. (1995) Modern glaciomarine environments. In: *Glacial Environments, Vol. 1: Modern Glacial Environments: Processes, Dynamics and Sediments* (Ed. J. Menzies), pp. 445–486. Butterworth-Heinemann, Oxford.
- Ramsay, J.G. (1980) Shear zone geometry: a review. *J. Struct. Geol.*, **21**, 83–99.
- Richter, A., Fedorov, D.V., Fritsche, M., Popov, S.V., Lipenkov, V. Ya., Ekaykin, A.A., Lukin, V.V., Matveev, A. Yu., Grebnev, V.P., Roseneau, R. and Dietrich, R. (2013) Ice flow velocities over Vostok Subglacial Lake, East

1410 E. Ravier et al.

- Antartica, determined by 10 years of GNSS observations. *J. Glaciol.*, **59**, 315–326.
- Rijsdijk, K.F., Owen, G., Warren, W.P., McCarroll, D. and van der Meer, J.J.M. (1999) Clastic dykes in over-consolidated tills: evidence for subglacial hydrofracturing at Killiney Bay, eastern Ireland. *Sed. Geol.*, **129**, 111–126.
- Rijsdijk, K.F., Warren, W.P. and van der Meer, J.J.M. (2010) The glacial sequence at Killiney Bay, SE Ireland: terrestrial deglaciation and polyphase glaciotectionic deformation. *Quatern. Sci. Rev.*, **29**, 696–719.
- Russell, H.A.J. and Arnott, R.W.C. (2003) Hydraulic-jump and hyperconcentrated flow deposits of a glaciogenic subaqueous fan: Oak Ridge Moraine, southern Ontario, Canada. *J. Sed. Res.*, **73**, 887–905.
- Shepherd, A., Hubbard, A., Nienow, P., King, M., McMillan, M. and Joughin, I. (2009) Greenland ice sheet motion coupled with daily melting in late summer. *Geophys. Res. Lett.*, **36**, 4.
- Smith, M.J. and Knight, J. (2011) Palaeoglaciology of the last Irish ice sheet reconstructed from striae evidence. *Quatern. Sci. Rev.*, **30**, 147–160.
- Stokes, C.R. and Clark, C.D. (2003) The Dubawnt Lake palaeo-ice stream: evidence for dynamic ice sheet behaviour on the Canadian Shield and insights regarding the controls on ice-stream location and vigour. *Boreas*, **32**, 263–279.
- Sundal, A.V., Shepherd, A., van den Broeke, M., Van Angelen, J., Gourmelen, N. and Park, J. (2013) Controls on short-term variations in Greenland glacier dynamics. *J. Glaciol.*, **59**, 883–892.
- Thomas, G.S.P. and Chiverrell, R.C. (2007) Structural and depositional evidence for repeated ice-marginal oscillation along the eastern margin of the Late Devensian Irish Sea Ice Stream. *Quatern. Sci. Rev.*, **26**, 2375–2405.
- Tulaczyk, S. (1999) Ice sliding over weak, fine-grained tills: dependence of ice-till interactions on till granulometry. *Geol. Soc. Am. Spec. Pap.*, **337**, 159–177.
- Van Wagoner, J.C., Mitchum, R.M., Jr, Campion, K.M. and Rahmanian, V.D. (1990) Siliciclastic sequence stratigraphy in well logs, core, and outcrops: concepts for high-resolution correlation of time and facies. *AAPG Meth. Explor. Ser.*, **7**, 55.
- Walder, J.S. (1986) Hydraulics of subglacial cavities. *J. Glaciol.*, **32**, 439–445.
- Waller, R., Phillips, E.R., Murton, J., Lee, J. and Whiteman, C. (2011) Sand intraclasts as evidence of subglacial deformation of Pleistocene permafrost, North Norfolk, UK. *Quatern. Sci. Rev.*, **30**, 3481–3500.
- Warren, W.P. and Creighton, J.R. (1993) *Bray, Sheet 32/21 SW. Geological Survey of Ireland 1:25,000 Map Series: Quaternary Geology*. Geological Survey of Ireland, Dublin.
- Winsemann, J., Asprion, U., Meyer, T., Schultz, H. and Victor, P. (2003) Evidence of iceberg-ploughing in a subaqueous ice-contact fan, glacial Lake Rinteln, NW Germany. *Boreas*, **32**, 386–398.
- Winsemann, J., Asprion, U., Meyer, T. and Schramm, C. (2007) Facies characteristics of Middle Pleistocene (Saalian) ice-margin subaqueous fan and delta deposits, glacial Lake Leine, NW Germany. *Sed. Geol.*, **193**, 105–129.
- Winsemann, J., Hornung, J.J., Meinsen, J., Asprion, U., Polom, U., Brandes, C., Bubmann, M. and Weber, C. (2009) Anatomy of a subaqueous ice-contact fan and delta complex, Middle Pleistocene, North-west Germany. *Sedimentology*, **56**, 1041–1076.
- Woodworth-Lynas, C.M.T. (1996) Ice scour as an indicator of glaciolacustrine environments. In: *Past Glacial Environments 2* (Ed. J. Menzies), pp. 161–178. Butterworth-Heinemann, Oxford.
- Wysota, W. (2007) Successive subglacial depositional processes as interpreted from basal tills in the Lower Vistula valley (N Poland). *Sed. Geol.*, **193**, 21–31.
- Zwally, H.J., Abdalati, W., Herring, T., Larson, K., Saba, J. and Steffen, K. (2002) Surface melt-induced acceleration of Greenland ice-sheet flow. *Science*, **297**, 218–222.

Manuscript received 12 June 2013; revision accepted 23 December 2013

Supporting Information

Additional Supporting Information may be found in the online version of this article:

Figure S1. (A) Grain-size distributions of the matrix of different till layers (<2 mm). (B) Clast fabric plotted on a ternary diagram compared with data from other sites (in Benn, 1994). (C) Plot of S1/S3 eigenvalues for the Ballyhorsey clast fabric data, compared with data from other sites (Menzies & Shilts, 2002). (D) Schmidt equal-area projections of clast fabric data of the three different till layers observed at the base of the pit.

Figure S2. Interpreted section 3. Photograph showing the erosive contact between the clay-rich diamictite (F1.1) and the massive and poorly sorted gravel (F3.1). Note the occurrence of clastic dykes sourced in F1.1 that propagates upwards.

Figure S3. Interpreted section 4. Distal part of the wedge displaying mainly sandy deposits (F3.6) that are affected by intense deformation. The deformed zone is characterized by a 3 m wide depression bordered by step normal faults. This depression is surrounded by intense deformation structures including thrust faults (A), asymmetrical folds (B) and clastic dykes (C).

Figure S4. Sedimentary logs 6 and 12. See Fig. 2 for their localizations.

Annexes

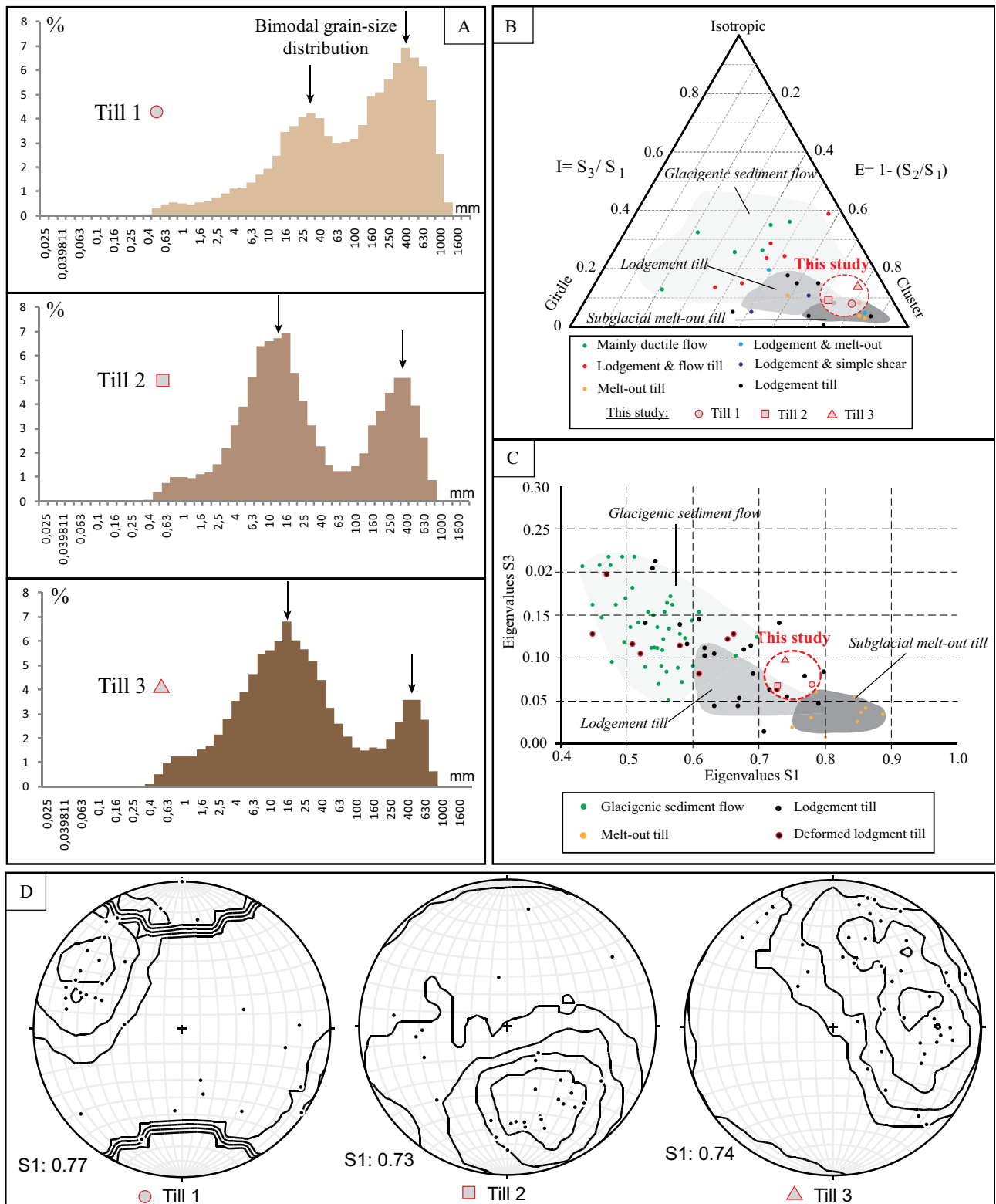


Figure S1. (A) Grain-size distributions of the matrix of different till layers (<2 mm). (B) Clast fabric plotted on a ternary diagram compared with data from other sites (in Benn, 1994). (C) Plot of S_1/S_3 eigenvalues for the Ballyhorsey clast fabric data, compared with data from other sites (Menziés & Shilts, 2002). (D) Schmidt equal-area projections of clast fabric data of the three different till layers observed at the base of the pit.



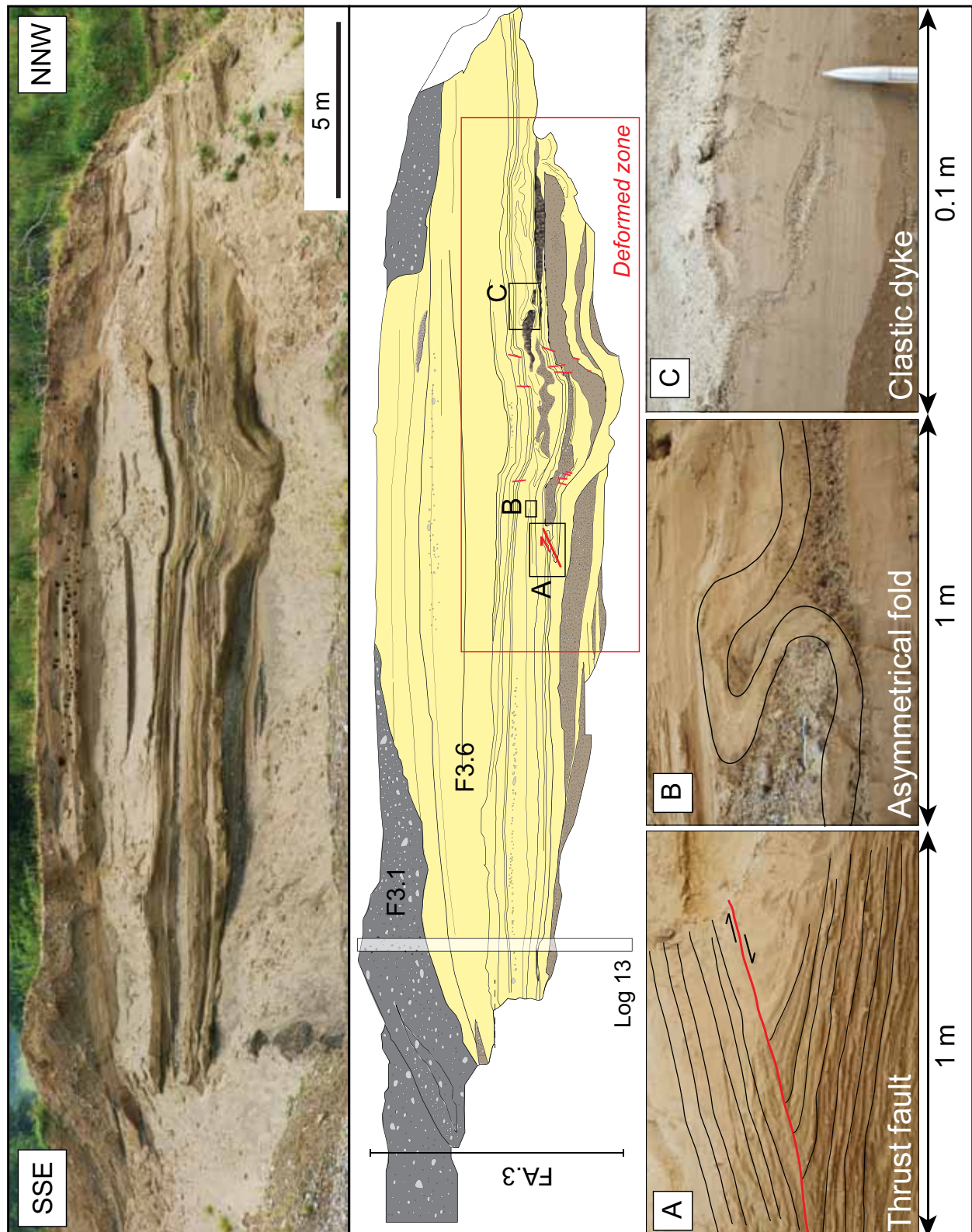


Figure S3. Interpreted section 4. Distal part of the wedge displaying mainly sandy deposits (F3.6) that are affected by intense deformation. The deformed zone is characterized by a 3 m wide depression bordered by step normal faults. This depression is surrounded by intense deformation structures including thrust faults (A), asymmetrical folds (B) and clastic dykes (C).

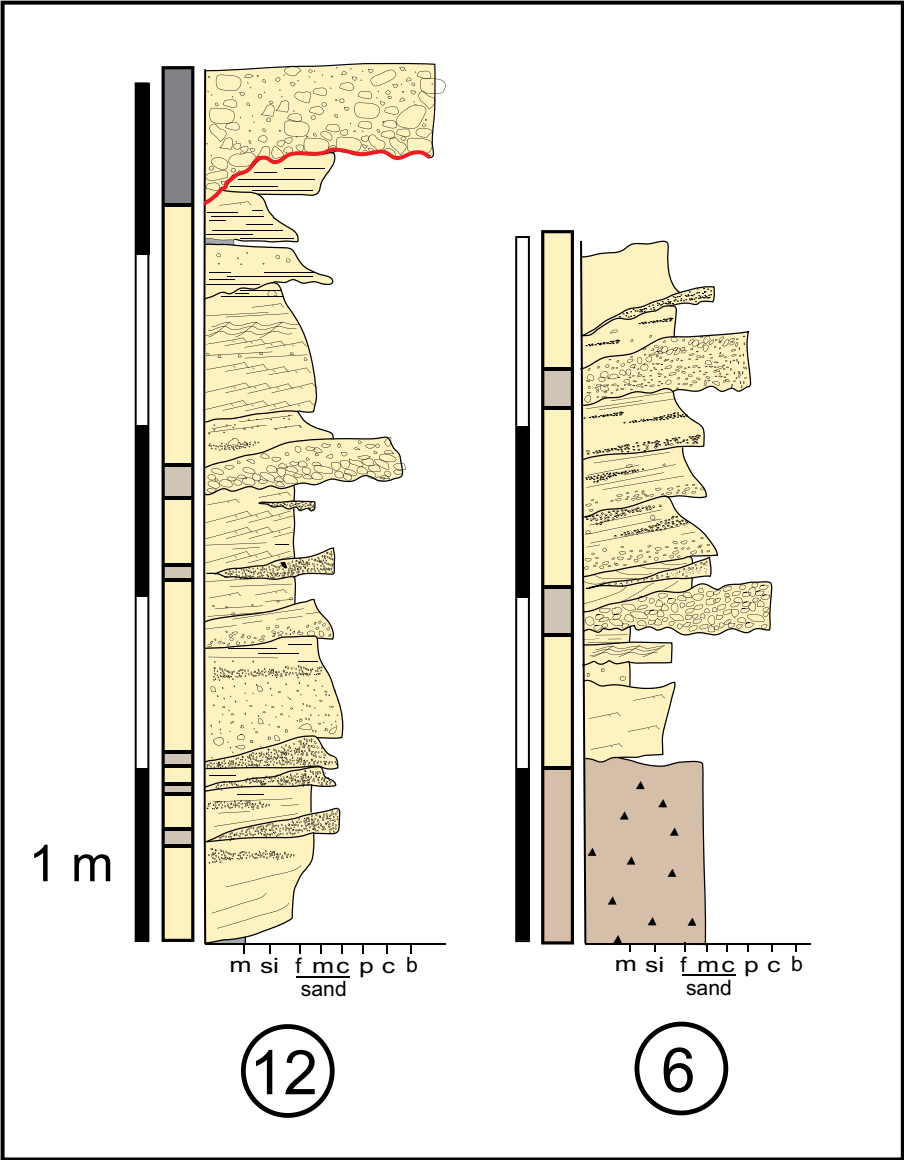


Figure S4. Sedimentary logs 6 and 12. See Fig. 2 for their localizations.

Partie 2

**«Un nouveau modèle pour le développement du réseau d'injections clastiques du Sólheimajökull:
mécanismes déclencheurs, processus d'injection, et
implications sur les reconstructions de la dynamique glaciaire».**

Cette seconde partie fait l'objet d'un article qui sera bientôt soumis à publication.

Article 2

Ravier, E., Buoncristiani, J.F., Guiraud, M., Menzies, J. et Portier, E. A new model for the development of the Sólheimajökull clastic injection network: trigger mechanisms, processes of injection and implications for the reconstruction of ice dynamics (in prep.).

Objectifs:

- *L'objectif principal de cette seconde partie est d'analyser un réseau d'injections clastiques à plusieurs échelles (micro- et macro-échelle).*
- *Dans un premier temps, le but sera de reconstituer les différentes phases de développement du réseau d'injections clastiques en s'appuyant sur les principes de recoupement entre les différents structures à micro- et macro-échelle.*
- *L'objectif sera ensuite de mieux comprendre les processus impliqués dans les phases successives d'hydrofracturation/injection en environnements glaciaires, grâce à l'analyse fine et multi-échelle du remplissage des injections.*
- *L'objectif de cette partie sera également d'analyser s'il existe une relation entre les mécanismes déclencheurs provoquant la mise en place de ces injections et la dynamique glaciaire.*
- *Enfin, le dernier objectif sera de déterminer quelles informations peuvent transmettre ces structures de déformation sur la dynamique glaciaire et plus particulièrement sur les oscillations de la marge glaciaire et les variations de la pression d'eau interstitielle.*

1. Précédents travaux

Les réseaux d'injections clastiques en environnements glaciaires ont connu un intérêt grandissant ces dernières années (Boulton et Caban, 1995; Risdijk et al., 1999; van der Meer et al., 1999, 2009; Le Heron et Etienne, 2005; Clerc et al., 2012; Phillips et al., 2013b, 2014). La majorité des études ont caractérisée ces injections à l'échelle macroscopique (Risidijk et al., 1999; Le Heron et Etienne, 2005; Clerc et al., 2012), cependant des travaux récents ont également décrit ces structures à l'échelle microscopique (van der Meer et al., 2009; Phillips et al., 2013b, 2014).

Les systèmes d'injections clastiques en domaine glaciaire sont principalement constitués de réseaux de dykes même si la présence de sills a déjà été observée (Denis et al., 2010; Phillips et al., 2013b). Ces réseaux sont généralement reliées à des processus d'injection de sédiments au sein d'hydrofractures. Si les processus d'hydrofracturation sont généralement responsables de la formation de ces injections clastiques, les processus intervenant dans leurs remplissages sont plus débattus. L'injection de sédiments dans un état fluidisé est généralement admise comme le processus principal de remplissage des hydrofractures (Jolly et Lonergan, 2002; Hurst et al., 2011). Cependant, les précédentes études portant sur les injections formées en domaines glaciaires suggèrent une liquéfaction des sédiments au moment de l'injection (Le Heron et Etienne, 2005; van der meer et al., 2009; Phillips et al., 2013). Dans les environnements glaciaires, les injections clastiques semblent dominées par des remplissages multiphasés (Le Heron et Etienne, 2005; van der meer et al., 2009; Phillips et al., 2013b) alors que les réseaux d'injections clastiques formés en domaine marin profond sont généralement constitués de remplissage homogène (Hillier et Cosgrove, 2002; Parize et al., 2007). Ces remplissages multiphasés sont le résultat de processus dit de «crack and seal» qui sont définis par des épisodes répétés d'hydrofracturation, d'expansion de la roche encaissante et du dépôt de sédiment le long de la fracture (Ramsay, 1980; Le Heron et Etienne, 2005; Phillips et al., 2013b).

L'orientation et le sens de propagation des injections sableuses en domaine glaciaire sont influencés par la dynamique glaciaire et plus principalement par la vitesse d'écoulement de la glace (Clerc et al., 2012). Les variations de la charge exercée sur le sédiments, induites par les changements d'épaisseur de la glace, entraînent également des modifications de la morphologie des injections (Phillips et al., 2013b).

Enfin, les différents épisodes d'injections, les variations de granulométrie au sein des remplissage, ainsi que les nombreux recoupements entre les différentes phases d'hydrofracturation impliquent d'intenses variations de la pression d'eau interstitielle au sein des dépôts glaciaires. Ces systèmes d'hydrofractures peuvent être réactivés de manière répétée et sur plusieurs dizaines d'années (Phillips et al., 2013b).

2. Contexte de l'étude

Afin de remplir les différents objectifs établis précédemment, un affleurement présentant un réseau d'injections clastiques d'échelle pluricentimétrique a été sélectionné dans la plaine proglaciaire du glacier Sólheimajökull en Islande. Ce site présente un affleurement de 250 m de long pour 20 m de puissance, formé par l'érosion de la berge de la rivière Jökulsa Fulilækur (**Fig. 1**). Il est situé à

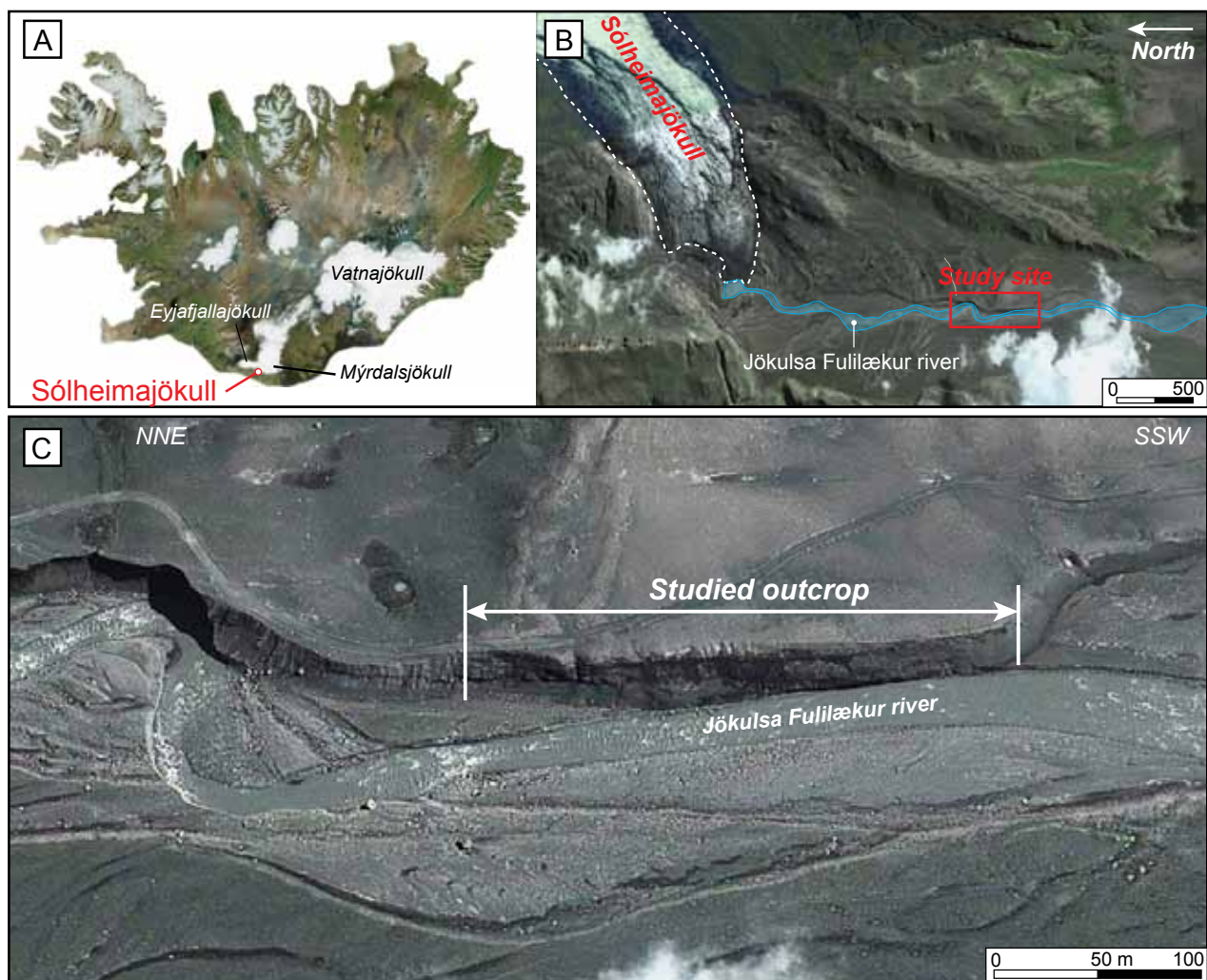


Figure 1. (A) Map of Iceland and location of the Mýrdalsjökull ice cap and the Sólheimajökull outlet glacier. (B) Aerial photograph of the Sólheimajökull outlet glacier and its proglacial outwash plain. The trajectory of the Jökulsa Fulilækur river is highlighted in blue and the position of the studied outcrop is marked. (C) Close-up on the aerial photograph showing the limits of the studied outcrop.

1.5 km de la marge actuelle du glacier (**Fig. 1**). Ce site fut l'objet d'une étude menée par Le Heron et Etienne (2005), qui s'était principalement focalisée sur les processus de mise en place de ces injections clastiques.

De nombreuses phases d'avancée et de recul de la marge glaciaire ont été mises en évidence sur le site d'étude, notamment par la présence de moraines terminales (Krüger et al., 2010) ou par la récurrence de moraines de fond («lodgement tills») (Le Heron et Etienne, 2005). Ces oscillations de la marge glaciaire permettent d'observer l'évolution de la morphologie des injections clastiques en fonction de la position du front du glacier.

3. Méthodes

Une étude stratigraphique et faciologique a tout d'abord été réalisée. Des échantillons ont été prélevés dans les différents faciès sédimentaires afin d'estimer la distribution granulométrique de la fraction inférieure à 2 mm (utilisation d'un granulomètre laser).

Dans un deuxième temps, le réseau d'injection clastique a été analysée. Tout d'abord le pendage et la direction de pendage ont été mesurés sur 46 dykes. Ensuite les différents types de remplissage observés au sein des injections ont été répertoriés. Des échantillons ont également été récoltés au sein du remplissage des injections sableuses afin d'en caractériser leurs granulométries. La distribution, la moyenne et la médiane ont été estimées pour la fraction < 2 mm de chaque échantillon. Les données granulométriques obtenues dans le remplissage des injections ont ensuite pu être comparées avec les données issues des différents faciès sédimentaires.

Enfin, treize blocs intacts ont été prélevés sur l'affleurement en utilisant des cylindres de 10 cm de diamètre afin de caractériser la morphologie des injections et leurs remplissages à l'échelle microscopique. A partir de ces blocs, des lames minces ont été réalisées après avoir remplacé l'eau contenue dans les échantillons par de l'acétone, puis par de la résine.

4. Article en cours de préparation

«A new model for the development of the Sólheimajökull clastic injection network: trigger mechanisms, processes of injection and implications for the reconstruction of ice dynamics».

L'article est structuré de la façon suivante: (1) Après avoir introduit le contexte géographique et glaciaire du site, (2) les différents faciès, leurs caractéristiques granulométriques, leurs relations stratigraphiques ainsi que les structures de déformation pré-lithification qu'ils contiennent sont présentés. Dans cette partie les différents faciès sédimentaires sont interprétés en termes de processus de dépôt.

(3) Dans une troisième partie, le réseau d'injections clastiques sera décrit de manière détaillée, tout d'abord à l'échelle macroscopique puis à l'échelle microscopique. Les caractéristiques morphologiques et géométriques seront présentées ainsi que la description des différents types de remplissage et leurs distributions granulométriques. Les différentes phases d'injections observées sur le site d'étude seront également établies.

(4) Enfin dans une dernière partie les différents résultats permettront de déterminer un modèle de dépôt, mais aussi les processus et mécanismes intervenant dans l'hydrofracturation et l'injection de sédiments. Les implications dans la reconstitution des variations de la pression d'eau interstitielle et des différentes oscillations de la masse glaciaire au cours du temps seront discutées.

(5) En conclusion sera présenté un modèle synthétique illustrant la mise en place progressive du réseau d'injection clastique du Sólheimajökull au cours du temps, et en fonction des phases de recul et d'avancée de la langue glaciaire.

**A new model for the development of the Sólheimajökull clastic injection network:
trigger mechanisms, processes of injection, and implications
for the reconstructions of ice dynamics. (*in prep.*)**

Edouard Ravier^a, Jean-François Buoncristiani^a, Michel Guiraud^a, John Menzies^b, Eric Portier^c.

^aLaboratoire Biogeosciences UMR/CNRS 6282 Université de Bourgogne, 6 Bd Gabriel, 21000 DIJON, France.

^bDepartment of Earth Sciences, Brock University, 500 Glenridge Avenue, St. Catharines, Ontario L2S 3A1, Canada

^cGDF Suez, Exploration Production International, 1 place Samuel de Champlain – Faubourg de l'Arche 92930 Paris La Défense Cedex – France.

1. Introduction

Clastic injections correspond to the intrusion of clastic sediments that are either discordant (dykes) or concordant (sills) to the bedding of their host strata. They form in response to the injection of remobilized liquefied to fluidized material within hydrofractures (Corsgrove, 2001; Jolly and Lonergan, 2002; Hurst et al., 2011). Hydrofracturing is triggered when the porewater pressure within sediments exceeds the tensile strength of the encasing unit, and injection is produced as a response of porewater excess release from an overpressurized parent bed (Jolly and Lonergan, 2002). Over the two past decades, the amount of works related to hydrofracturing and injection of clastic sediments have considerably increased because their major role in hydrocarbon systems have been demonstrated (intrusive traps, communications between reservoirs, ...) (Dixon et al., 1995). The occurrence of clastic injections has mainly been reported in deep-water and deltaic environments (Parize et al., 2007; Vigorito et al., 2010; Scott et al., 2013) although clastic injection networks in glacial environments have recently been subject to several studies (Le Heron and Etienne, 2005; van der Meer et al., 1999, 2009; Clerc et al., 2012; Phillips et al., 2013; Phillips and Hughes, 2014). Hydrofracturing and injection of sediments are predominant within subglacial and submarginal environments. The combination of high porewater pressures and basal shear stresses in such environments trigger the formation of *per descensum* clastic dykes dipping down-ice (van der Meer et al., 1999; Clerc et al., 2012). In marginal settings, the decrease in ice overburden pressure tends to promote the formation of sills controlled by bedding anisotropy and *per ascensum* dykes (Boulton and Caban, 1995; Rijdsdijk et al., 1999; Phillips et al., 2013). Massive and structureless hydrofracture-fills related to the injection of fluidized sediments are very common although banding or laminations have occasionally been observed and may correspond to different processes and mechanisms of sediment intrusion (Duranti and Hurst, 2004; Le Heron and Etienne, 2005). Clastic injection morphologies, dip directions and sediment-fills have often been used to determine variations of porewater pressures within the bed but are also thought to record ice front oscillations and the palaeo dynamics of glaciers (Clerc et al., 2012; Phillips et al., 2013; Ravier et al., 2014).

In this study, we propose to re-investigate the clastic injections network cropping in the Sólheimajökull forefield (South Iceland), first described by Le Heron and Etienne (2005). Grain-size and micromorphological analyses are added to the macro-scale description conducted by Le Heron and Etienne (2005). These multi-scale analyses permitted to define the different generations

of hydrofractures and the characteristics of the sediment-fills. These new data give the opportunity to better understand processes of hydrofracturing and injection, but also to discuss the relations between the different generation of clastic injections and the oscillations of the ice front through time. The integration of these new observations finally leads to a new model for the development of the Sólheimajökull clastic injection network.

2. Geological setting

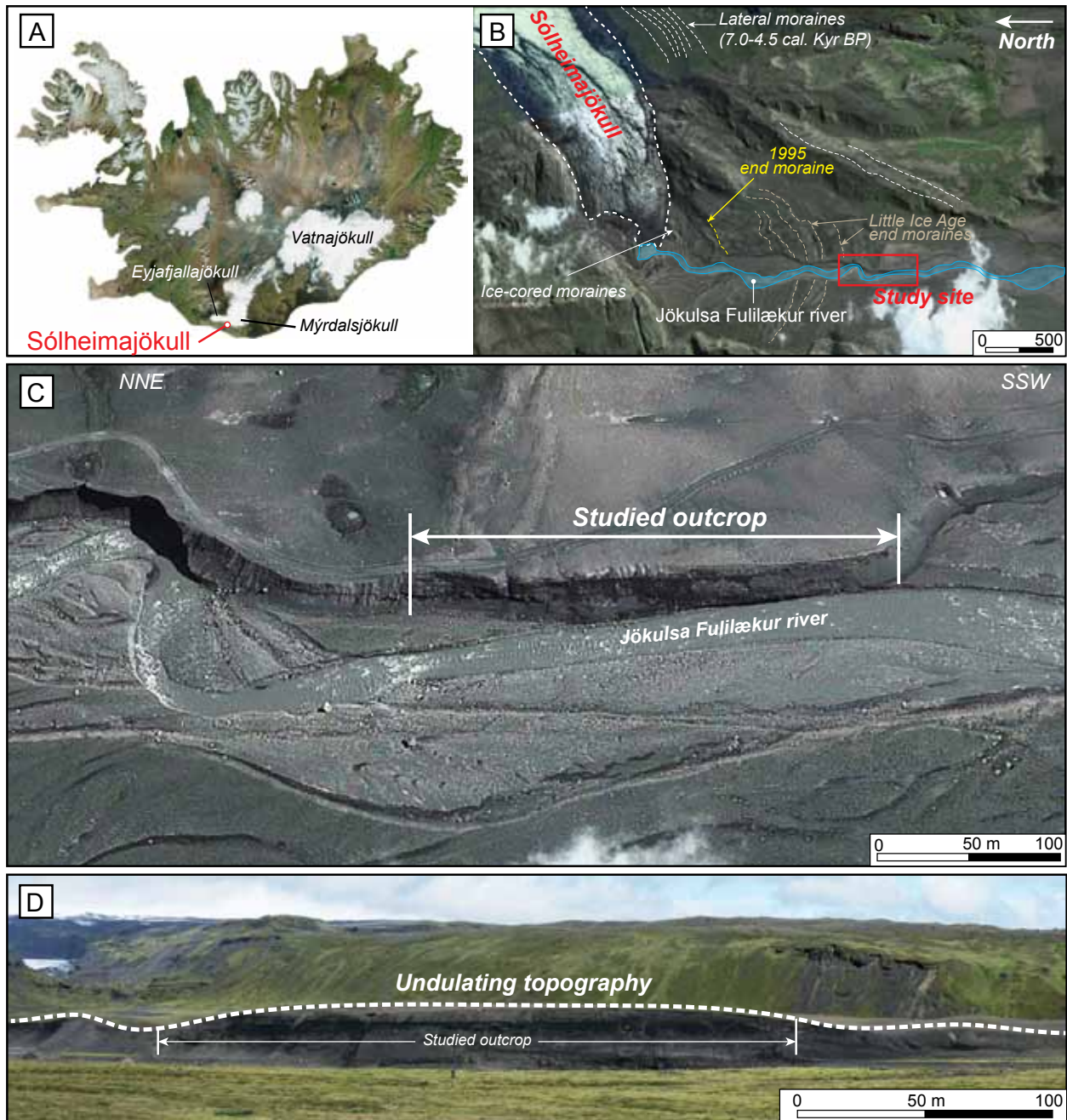


Figure 1. (A) Map of Iceland and location of the Mýrdalsjökull ice cap and the Sólheimajökull outlet glacier. (B) Aerial photograph of the Sólheimajökull outlet glacier and its proglacial outwash plain. The trajectory of the Jökulsa Fulilækur river is highlighted in blue and the position of the studied outcrop is replaced. Positions and age of the moraines are based on Dugmore (1989) and Ingólfsson et al., (2010). (C) Close-up on the aerial photograph showing the limits of the studied outcrop. (D) Undulating topography at the top of the outcrop.

The study site is located in south central Iceland, 1.5 km away from the southern margin of the Mýrdalsjökull ice cap (**Fig. 1A**). The ice cap develops atop one of the most active volcanic system of Iceland called Katla, situated along the eastern margin of the Eastern Volcanic zone of Iceland (Sturkell et al., 2010). The volcano produces Fe-Ti basalts and minor rhyolitic sub-alkalic rocks (Hildebrand and Thorssander, 1999). Eruptions within the Katla central volcano are phreato-magmatic and capable of producing glacial outbursts, referred to as jökulhlaups. The Mýrdalsjökull ice cap covers 600 km² and represents the fourth biggest ice cap in Iceland. The ice cap culminates at 1480 m a.s.l. and can be divided into two regions: the ice dome where ice forms and remain unbroken down to 1000-1300 m a.s.l., and below a peripheral zone where ice splits up into separate outlet glaciers (Krüger et al., 2010). The investigated site is situated at the margin of the Sólheimajökull which is a valley-type outlet glacier descending over rock steps and draining the Mýrdalsjökull ice cap down to 100 m a.s.l. towards the south (Krüger et al., 2010) (**Fig. 1B**). At the ice margin, ice-cored moraines are observed while further away a large proglacial outwash plain displaying a braided network develops (**Fig. 1B**). In this proglacial plain, bank erosion by the Jökulsa Fulilækur river gives the opportunity to observe fresh outcrops. Erosion by this river exposed a 250 m wide and 20 m thick outcrop on the eastern bank, oriented NNE-SSW (**Fig. 1B, C, D**). The undulating topography observed on top of the outcrop suggests that this site has been overridden by ice (**Fig. 1D**) (Evans, 2003).

During the Last glacial maximum, the entire island was covered by ice (Norðdhal et al., 2008). Due to extensive and extremely rapid environmental changes during the late Weichselian and early Holocene, the Icelandic ice sheet retreated and extensive areas became ice-free (Ingólfsson et al., 2010).

Numerous moraines are observed on the glacier forefield (**Fig. 1B**): (1) lateral moraines corresponding to a much wider outlet glacier dated from 7.0-4.5 cal. Kyr BP for the outermost ridges (Dugmore, 1989). (2) Little Ice Age (LIA) end moraines situated 1.5 to 2 km away from the actual ice margin and the 1995 end moraine corresponding to the 20th century glacier maxima (Dugmore and Sudgen, 1991; Ingólfsson et al., 2010). The Sólheimajökull experienced three glacier maxima during the LIA: around AD 1705, AD 1794 and AD 1820 (Thorarinsson, 1943; Ingólfsson et al., 2010). The study site was situated at the margin of the ice tongue during the Little Ice age maxima as evidenced by the LIA end moraine (Krüger et al., 2010) (**Fig. 1B**). The 20th century was time for a mass loss and subsequent glacier retreat (1 km between 1930 and 1969), except during the period 1970-1995 (Sigurdsson, 2010). During the period 1970-1995, the advance the Sólheimajökull was about 0.5 km while during the period 1995-2007, the ice tongue retreated by 0.5 km (Sigurdsson, 2010).

3. Methodology

Prior to sampling, the exposure was logged and the clastic injection geometries and sedimentary infills were described. The dips and strikes of clastic dykes were recorded and cross-cutting relationships between the different clastic injections analyzed. The different sedimentary facies defined during the description of the host sediments were sampled to assess grain-size analyses. The sedimentary infills of clastic injections were also collected for grain-size analyses, especially within injections showing internal laminations, where the sampling of single laminae was conducted. In addition, samples were collected near the source bed and at the tip of single dykes to estimate grain-size variations with increasing distance to the source. Once collected, the grain-size distribution of the < 2 mm fraction was obtained from a laser granulometer particle size analyzer. The mean, the mode, and the first percentile were calculated using grain-size distribution data. Results collected from grain-size analyses were plotted in the Passega diagram (1964) in order to estimate transport and depositional processes involved during the emplacement of host and injected sediments. The Passega diagram is a method for presenting the results obtained from grain-size analyses, wherein the values of the first percentile (C) are plotted against the median (M).

A total of 13 intact block samples of clastic injection sediment-fill and adjacent host sediments have been collected using 10 cm in diameter and length aluminium cylinders. Cylinders were pushed into the face to limit internal sediment disturbances. Positions, orientations, and way-up of each samples were recorded. To produce thin sections, porewater remaining in the sample was replaced by acetone, and then acetone progressively replaced by a resin.

4. Facies descriptions, stacking pattern and deformation structures in host sediments

4.1. *Sedimentary facies*

The host sediments are divided into 5 sedimentary facies, each defined on the basis of their grain-size, sedimentary structures, and geometries. The main features of each sedimentary facies are summarized in **Table 1**.

Facies code	Facies name	Bed contacts	Thickness	Description	Interpretation
F1	Fissile and overconsolidated diamicton	Sharp slightly erosive base	0.5 to 0.8 m	Overconsolidated and fissile massive matrix-supported diamicton containing clasts up to 1 m long. Diamicton layers are composed of a clayey to sandy matrix. Clasts are polygenic, faceted, polished, and striated. Diamicton colors vary from yellow grey, light brown to dark grey.	Subglacial sediment deposition, probably by lodgement processes (subglacial traction till).
F2	Underconsolidated diamicton	Sharp non erosive	0.6 m	Underconsolidated massive and matrix-supported diamicton containing clasts up to m-sized. Clasts are often faceted, polished and striated. Matrix is composed of silt to sand particles. This diamicton layer is composed of a dark grey matrix.	Sediment deposited during ice melting (melt-out till).
F3	Channelized sandy gravel	Erosive base	up to 7 m	Poorly sorted and matrix-supported sandy gravel, although clast-supported sandy gravel locally occurs (local clast openwork). Matrix is composed of coarse to very coarse sand. Clasts are up to 2 m-sized and are often imbricated towards the south. Gravely sand displays gently inclined foresets (< 5°) and lenticular channel morphologies underlined by boulder lags (5 to 10 wide, and 1 to 3 m deep).	Deposition by tractive currents. Cross-cutting channel-like morphologies record channel incision, abandonment and aggradation in a braided network.
F4	Planar-stratified to cross-stratified gravely sand	Slightly erosive base	up to 6 m	Gravely sand is moderately to well-sorted and composed of medium to coarse sand with frequent granules and gravels. Gravely sand consists in stacked fining-upward sequences (< 1m) showing planar stratifications and trough cross-stratifications.	Cross-bedding structures indicate traction deposition within channels under lower flow regime, while fining-upward sequences with planar-parallel laminations record sheetflood deposition under upper flow regime.
F5	Laminated clay to very fine sand	Sharp Non-erosive	1 m	Fine-grained laminated sediments composed of alternating clays and silts with occasional fine to medium sand layers. Single beds are generally inferior to 1 cm. Occasional ripple cross-laminations are observed within sand beds. Five cm-thick blue-green silty tephra layers are intercalated within the laminated sediments.	Deposition by suspension settling with occasional deposition by traction currents.

Table 1. Classification of sedimentary facies

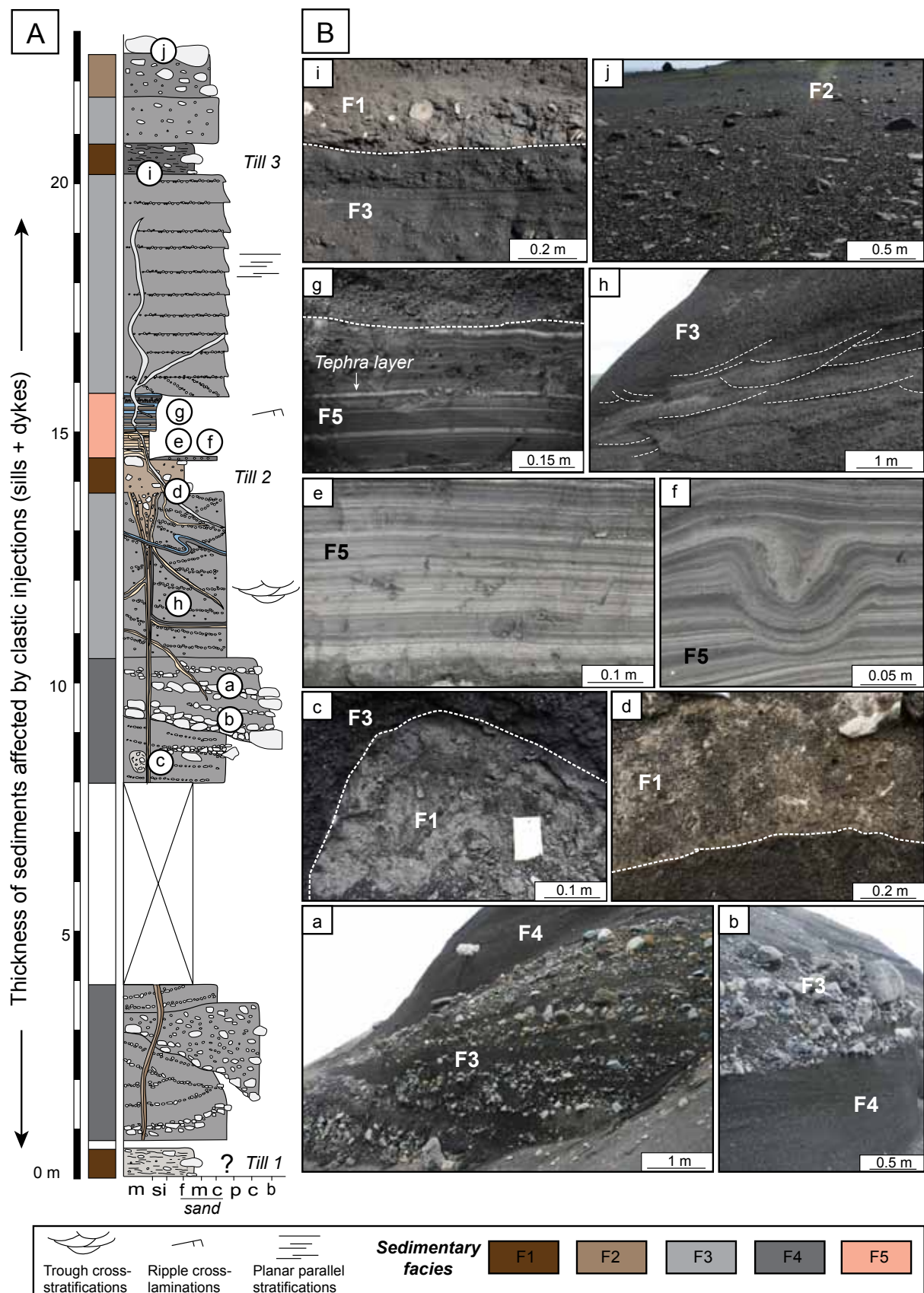


Figure 2. (A) Synthetic sedimentary log of the study site. (B) Photographs of the different sedimentary facies. (a) Sandy gravel (F3) with southward dipping foresets highlighted by boulder lags. **(b)** Gravely sand (F4) erosively overlain by sandy gravel (F4). **(c)** Rip-up till (F1) intraclast within F3. **(d)** Light brown lodgement till (F1) deposited over gravely sand (F4) with a sharp and slightly erosive basal contact. **(e)** Fine-grained laminated light brown clay to silt (F5). **(f)** Collapsed structures within fine-grained laminated sediments (F5). **(g)** Laminated dark grey silt to very fine sand with occasional dark brown clay layers (F5). Note the occurrence of blue green tephra layers. **(h)** Trough cross-stratifications within gravely sand (F4). **(i)** Dark grey fissile and overconsolidated till sharply deposited over gravely sand. **(j)** Underconsolidated till with boulders up to few meters across, deposited on top of the section.

- F1: Fissile and overconsolidated diamicton.

Description

F1 is composed of overconsolidated massive and matrix-supported diamicton presenting evidence of fissility (i.e., horizontal to subhorizontal pervasive joints) (**Fig. 2A, d, i**). Clasts are up to m-sized and the matrix is composed of clay to sand with a multimodal grain-size distribution for the < 2 mm fraction (**Fig. 3A**). Diamicton layers are subtabular/horizontal, their basal contacts are sharp and non to slightly erosive. Three overconsolidated diamicton layers occur along the exposure and their thickness varies between 0.5 m and 0.6 m (**Figs. 2A, 4**). Variations in diamicton colours are observed between the different diamicton layers from yellow grey, light brown to dark grey. Clasts contained within the diamicton are frequently faceted, polished and striated.

Interpretation

The multimodal grain-size distribution, the faceted and striated clasts indicate that the diamicton was initially formed at the glacier bed. The fissility observed in the diamicton deposits suggests shear-induced deformation or/and dewatering during or after deposition (Broster et al., 1979). Deformation induced by shear is typical of subglacial deposits, and triggered by the shear stress transmitted to the bed by overriding ice during ice-bed coupling periods. In addition, the diamicton is highly compacted resulting in an overconsolidated deposit due to the pressure exerted on sediments by the ice load. Fissile and overconsolidated diamicton containing faceted and striated clasts are generally interpreted as subglacial lodgement tills (Evans et al., 2006). Lodgement tills are deposited by plastering of glacial debris from a sliding glacier sole due to the combined effects of pressure melting and frictional drag (Evans et al., 2006). Variations in till colours are function of clay-contents and or sources.

- F2: Underconsolidated sandy diamicton

Description

F2 is composed of a massive and matrix-supported dark grey diamicton (**Fig. 2j**). Clasts, up to few meters wide, are embedded within an underconsolidated sandy matrix. Bed contacts are sharp and non erosive. F2 deposits occur at the top of the exposure and consist in a 0.6 m thick layer

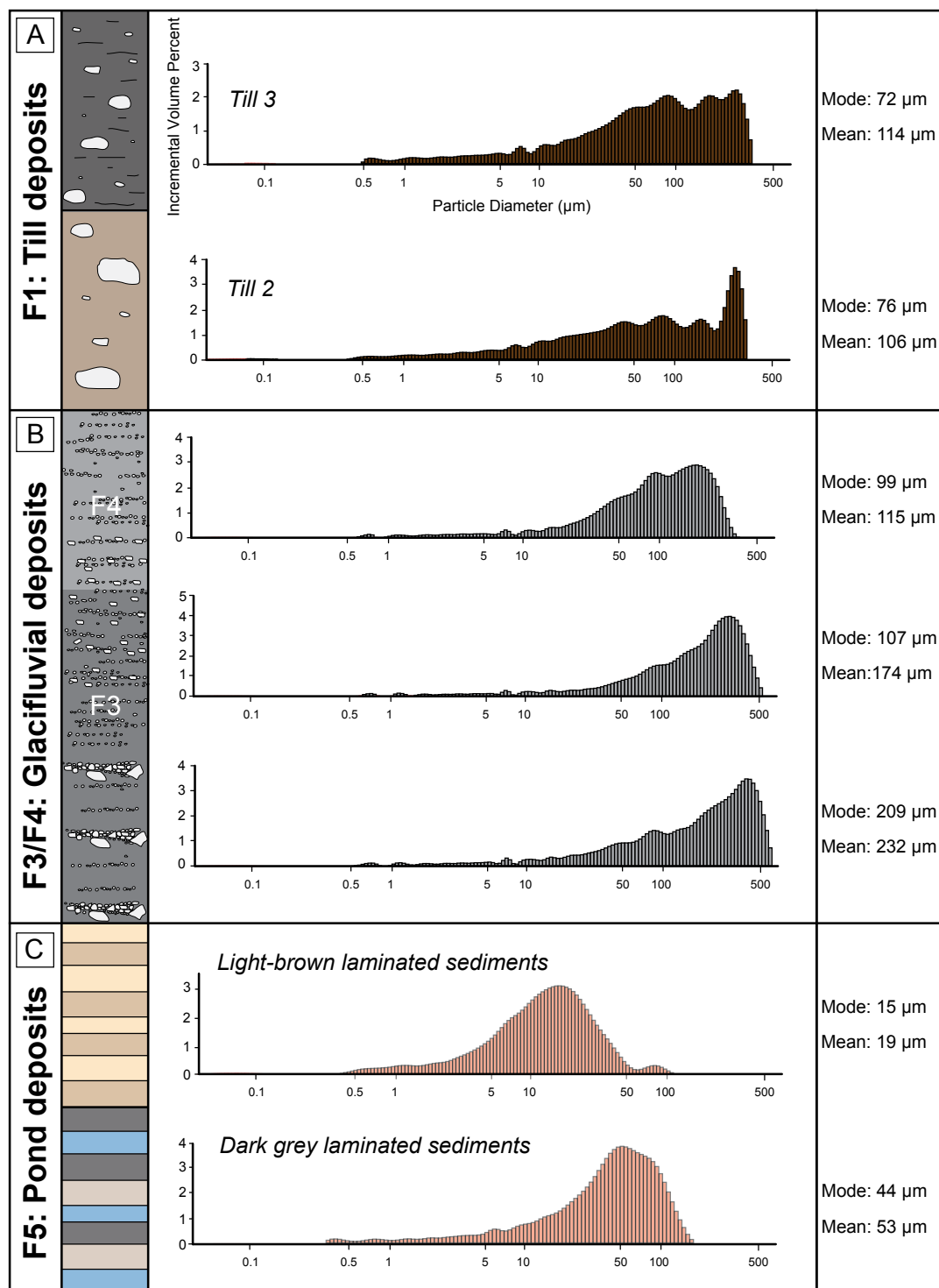


Figure 3. Grain-size distribution of the fraction < 2mm for the different sedimentary facies. The mean and mode are calculated for the different facies.

(Fig. 2A). Similar textures and characteristics occur within diamicton deposited at the present-day Sólheimajökull margin, in the ice-cored moraines.

Interpretation

The multimodal grain-size distribution, the faceted and striated clasts indicate that F2 deposits were initially formed at the glacier bed. However, this diamicton is underconsolidated, suggesting that

sediments were not deformed and compacted by glacier ice during deposition. The occurrence of similar deposits at the Sólheimajökull glacier outlet, 1.5 km away from the study site facilitates their interpretation. F2 can be considered as melt-out tills deposited by the passive release of subglacial, englacial, and supraglacial debris during ice melting (Evans et al., 2006; Benn and Evans, 2010).

- F3: Channelized sandy gravel

Description

F3 is composed of channelized morphologies filled by gravels to boulders (predominantly subangular) contained in a medium to very coarse sandy matrix. The distribution of the sandy matrix is unimodal (**Fig. 3B**). F3 is generally matrix-supported although clast-supported deposits locally occur, especially at the base of channels where m-sized boulders form basal lag deposits (**Figs. 2a, b and 4**). Lenticular channel-fills are 5 to 10 m wide and 1 to 3 m deep, and cross-cut each others. The base of F3 deposits is highly erosive, notably illustrated by the occurrence of m-sized till (F1) ripped-up intraclasts (**Fig. 2c**). F3 deposits are up to 7 m thick and display gently inclined foresets dipping towards the south ($< 5^\circ$) (**Fig. 4**).

Interpretation

Channelized lenses of matrix-supported gravel containing boulders and rip-up clasts reflect mass transport and rapid deposition by water. Such deposits could be interpreted as hyperconcentrated flows which are intermediate between stream flow and debris flow members (Mulder and Alexander, 2001). Intraclasts, ripped up from local tills, are particularly common in glacialfluvial flood deposits (Russell and marren, 1999; Russell and Knudsen, 2002). Subglacial eruptions underneath the Mýrdalsjökull ice cap frequently trigger outburst floods (jökulhlaup) in the proglacial outwash plain where hyperconcentrated flows occur (Russell et al., 2010). Cross-cutting channels indicate channel incision, abandonment and aggradation.

- F4: Planar to cross-stratified gravelly sand.

Description

F4 is composed of moderately to well-sorted gravelly sand, composed of medium to coarse sand

containing abundant granules and gravels. Distribution of the fraction < 2 mm is unimodal and slightly finer compared to F3 (**Fig. 3B**). Planar stratifications and trough cross-stratifications frequently occur in F4 (**Fig. 2A, h**) as well as fining-upward sequences < 1 m (**Fig. 2A**). Basal contacts are slightly erosive and F4 deposits can reach 6 m-thick.

Interpretation

Trough cross-bedding structures indicate traction deposition, and 2D to 3D dunes migration within channels, under lower flow regime (Allen, 1982). Fining upward sequences and planar parallel laminations record sediment deposition under upper flow-regime conditions, probably as sheet-flood deposition in interchannel positions (Collinson, 1996).

- F5: Laminated clay to very fine sand.

Description

F5 is composed of laminated fine-grained sediments composed of alternating clay to very fine sand beds (< 1 cm) with the occurrence of few well-sorted medium to coarse sand beds displaying ripple cross-laminations towards the top of this deposit (**Fig. 2A, e, g**). The laminated fine-grained deposits, up to 1 m thick, drape subglacial till deposits (F1) and laterally pinch-out (**Fig. 4**). Collapsed structures capped by overlying laminated sediments are observed within F5 (**Fig. 2f**). The base of the fine-grained deposits is composed of light brown beds that are enriched in clay-sized particles, while the upper part is composed of dark grey sediments characterized by a high silt to very fine sand content with occasional clay beds (**Figs. 2A, H and 3C**). Through F5 deposits, five blue-green silty and overconsolidated tephra layers occur, and are generally 1 to 2 cm thick (**Fig. 2g**).

Interpretation

The alternation of fine-grained sediments draping the till deposits and the preservation of silty tephra layers suggests deposition by suspension settling in quiescent water. Towards the top, the increase of grain-size with occasional medium to coarse sand beds displaying ripple cross-laminations indicates episodic deposition by tractive currents. Laminated sediments laterally pinch-out, indicating that sedimentation occurred in a relatively small-sized water body, corresponding to a proglacial water pound. Deposition of F5 occurred in a local subdued zone above a low-permeability till layer which

promoted the accumulation of water (**Fig. 4**). Localized collapsed structures suggest ice melting and that pieces of ice were entrapped within sediments during their deposition, therefore implying an episodic drainage of the pond.

4.2. *Stacking pattern*

The general stacking pattern of the different sedimentary facies is illustrated in two interpreted panoramic photographs (**Figs. 4** and **6**) and the sedimentary log (**Fig. 2A**).

The base of the exposure displays sandy gravel characterized by low-angle foreset beds dipping towards the south and channelized structures (F3). Although the base is not exposed, the occurrence of fissile and overconsolidated yellow grey till intraclasts within F3 may reveal the existence of a subjacent lodgement till layer, referred to as Till 1 (F1) (**Fig. 2A**). Lenticular channels infilled by hyperconcentrated flow deposits pass upwards into gravely sand displaying trough-cross stratifications (F4) resulting from channel filling under lower flow conditions. F3 and F4 corresponding to glacialfluvial deposits are overlain by a 0.6 m thick light brown subglacial lodgement till (F1) corresponding to Till 2 (**Figs. 2A, 4**). Localized deposition of fine-grained laminated sediments occur in topographic lows formed during deposition of Till 2 (F5) (**Fig. 4**). Above the pond deposits, gravely sand with fining-upward sequences and planar parallel-laminations (F4) record sheet-flood deposition, probably in interchannel positions. Gravely sand is overlain by 0.5 m thick overconsolidated fissile and dark grey till (F1) referred to as Till 3, which is overlain by a 1 m thick bed of gravely sand (F4). At the top of the exposure, a 1 m thick underconsolidated melt-out dark grey till (F2) is observed (**Figs. 2A, 4**).

4.3. *Soft-sediment deformation structures*

Soft-sediment deformation structures are sparse within the studied section or not observed because the predominant glacialfluvial facies, characterized by coarse-grained sediments and low clay content, makes difficult the observation of deformation at the macroscopic scale. The fissility characterizing lodgement till deposits have been previously described and results from the basal shear transmitted to the bed by the overriding ice, during or after deposition. Across the exposure, soft-sediment deformation structures are the most easily recognized within the fine-grained laminated sediments (F5). The deformation structures are not laterally extensive and occur within limited zones that are up

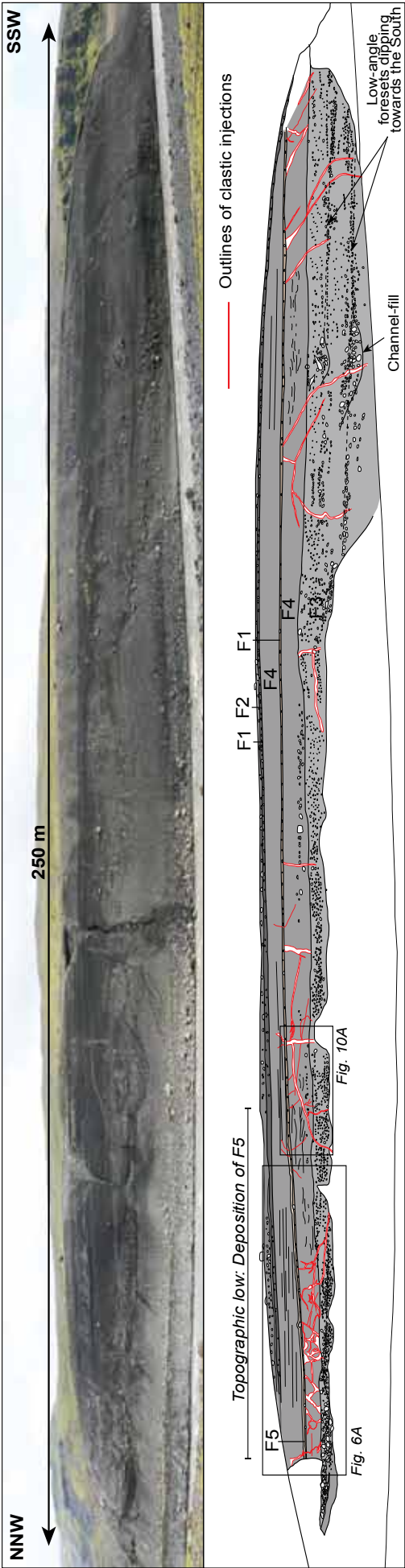


Fig. 4. Panoramic photograph and interpretation of sedimentary facies arrangements. The contours of clastic injections, cross-cutting host sediments, are highlighted in red.

to few meters wide (**Figs. 5, 6A**). Collapsed structures related to melting of buried ice affect locally the laminated sediments (few cm wide) (**Fig. 2f**).

Small-scale high-angle normal and reverse faults frequently disrupt the laminated sediments (**Figs. 5, 18, 19**). Sets of normal faults with centimetric fault offsets and undulating fault planes are observed within F5 and demonstrate sediment collapse (**Fig. 5A**). Sets of normal faults sometimes form steps and downthrow towards the NNE or the SSW. These normal faults are generally sealed by horizontally laminated sediments indicating that deformation is contemporaneous to the deposition of F5. Similarly, sealed reverse faults are locally observed within deformed zones with their fault planes either dipping towards the NNE or the SSW. Stacked asymmetrical folds with reverse directions of fold vergence (NNE and SSW) occur in the deposits (**Fig 5B, b**). They indicate sediment compression and changes in the direction of tectonic transport during deformation. These folds are sealed during deposition of F5 as illustrated by the laminated fine-grained sediments onlapping these folded structures (**Fig 5B**).

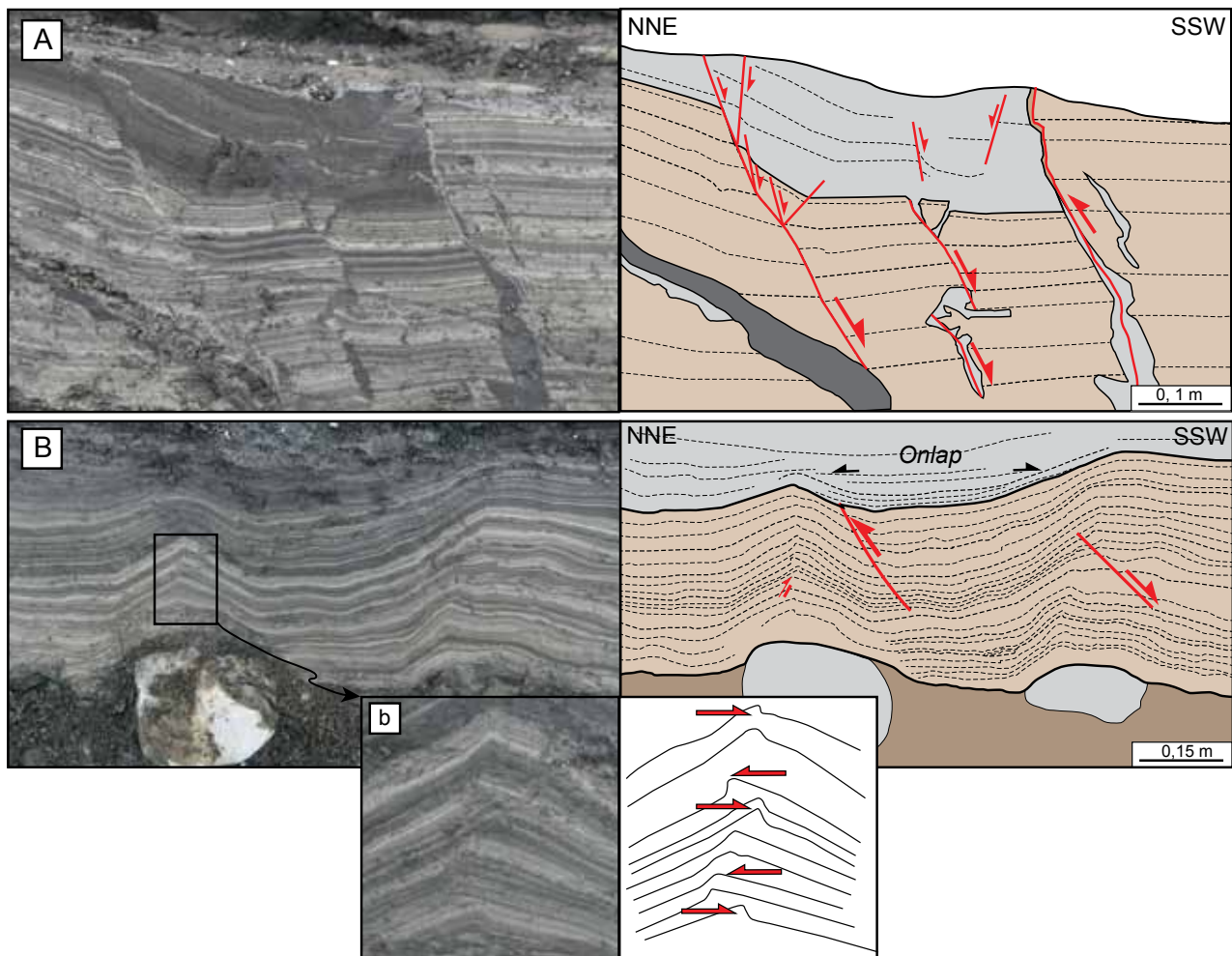


Figure 5. Soft-sediment deformation structures observed in facies 5. (A) Set of normal faults. (B) Reverse faults and asymmetrical folds sealed by laminated sediments. (b) Close-up on stacked asymmetrical folds displaying reverse directions of fold vergence.

5. Multi-scale descriptions of the clastic injection network

In this study, the clastic injection network has been described at different scales: the macroscale corresponding to large-scale observations (> 1 m), the mesoscale (between 0.05 and 1 m), and the microscale through the analyses of thin section (< 0.05 m). The morphology and geometry of the clastic injection network will be described as well as the nature and the origin of the sediments infilling the fractures. The timing of injection will be determined, using cross-cutting relationships.

5.1. Macroscale to mesoscale descriptions

5.1.1. Morphology and geometry

Sediments composing the Sólheimajökull outwash plain are cross-cut by a complex, anastomosed and multi-phased clastic injection system (**Figs. 4 and 6A**). Clastic injections occur along the whole outcrop (250 m) suggesting that network may have a much wider extent. The highest concentration of clastic injections is situated on the northern part of the outcrop, below the laminated fine-grained deposits (F5). Above till 2, clastic injections are seldom (**Figs. 4 and 6A**). The injection network displays sills coexisting with propagating upwards (i.e., *per ascensum*) or downwards (i.e., *per descensum*) clastic dykes of various dips. Clastic injections vary from few mm thick up to 1.5 m thick and their thickness generally decrease away from the source. If clastic dykes reach 1.5 m thick, sills never exceed 0.25 m thick. The longest clastic dykes exceeds 15 m (base not exposed) and the sills can reach 20 m in length. The clastic dykes dip in the range of 10-90° mainly towards the SSW, although few clastic dykes dipping in the opposite direction occur (**Fig. 7**). Clastic injection morphologies are wide and complex including: dykes, sills, «stepped» sills (i.e., interconnected dykes and sills describing steps), and anastomosed or bifurcating dyke morphologies (**Fig. 6B, C**). The intrusion of sediments sometimes follow preexisting normal or reverse faults, possibly evidenced by ‘Z-like’ injection morphologies (**Fig. 6D**). Sills follow bedding anisotropy and preferentially develop along low-permeability layers such as clay layers or well-indurated tephra layers (**Figs. 8C and 16**). Locally, dense networks of clastic intrusions lead to the in-situ brecciation of host sediments, thus forming angular slab-shaped rafts floating in the injected material (**Fig. 16**). Clastic injections display sharp margins with the host sediments although occasional abundant mm-sized apophyses branching

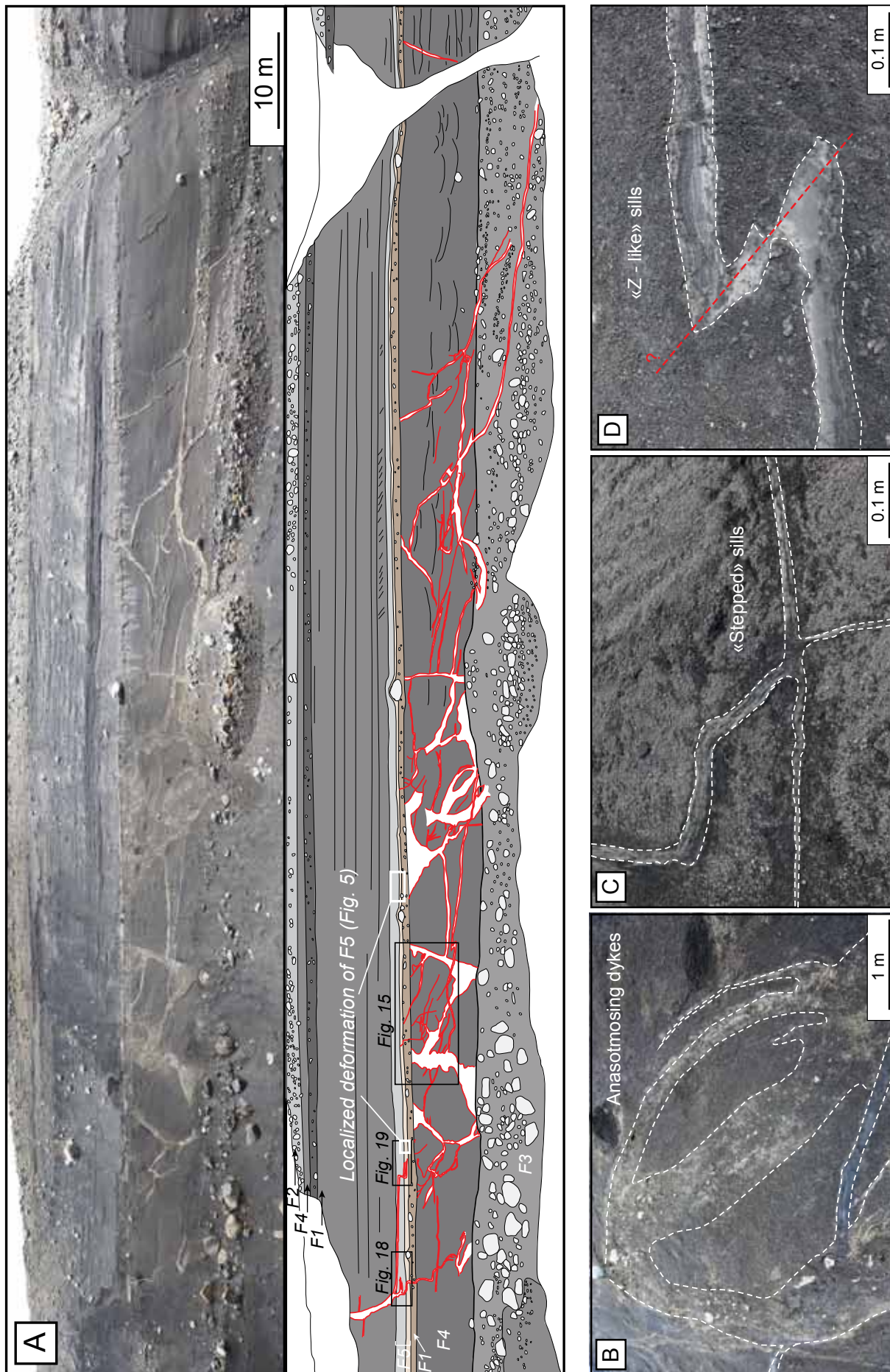


Figure 6. (A) Panoramic photograph and interpreted sketch of the northern part of the section where clastic injections are the most abundant. Note that the highest concentration of clastic injections occurs where fine-grained laminated deposits (F5) are thicker. (B) Anastomosing dyke network. (C) Stepped sill (D) «Z-like» sill morphology.

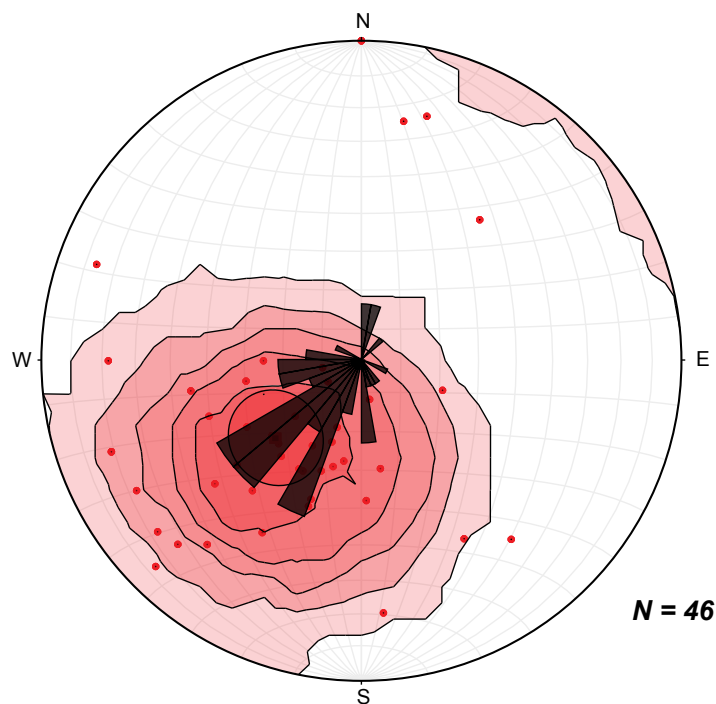


Figure 7. Lower-hemisphere stereographic projections showing the dip and dip direction data obtained from the clastic dyke network below Till 2.

out from the injections induce more diffused margins. The margins are either straight, bulbous or undulating.

5.1.2. Characteristics of sediment-filled hydrofractures

The clastic intrusions are characterized by a wide range of sedimentary infills controlled by changes of sediment sources and/or grain-size segregation during the successive injection events (**Figs. 8 and 9**). Most of the fractures display well-developed laminae that are parallel or subparallel to the orientation of the intrusions (**Fig. 8**). The laminae appear to be frequently lenticular and are therefore difficult to trace over long distance (< 1 m) (**Fig. 8F, G**). Lenticular shapes may result from erosion of the laminae by the fluid flows associated with the following episodes of injection. Occasionally, single or few laminae are deformed into a series of load casts where sand laminae founder into clay laminae, preferentially within sills (**Fig. 8D**). The number of lamina depicted within clastic intrusions vary between 3 and 16, and the thickness of single laminae ranges between 0.2 cm and 20 cm. Looking at the characteristics of sediments composing each laminae (grain-size, grain-size distribution, sorting, colours), it appears that their distribution is generally symmetric about the central axis of the clastic injection (**Figs. 8A, B, E, F, 9**). Another feature that is common to most of the fracture-fill is the increase of grain-size and clast content towards the injection centre, but a

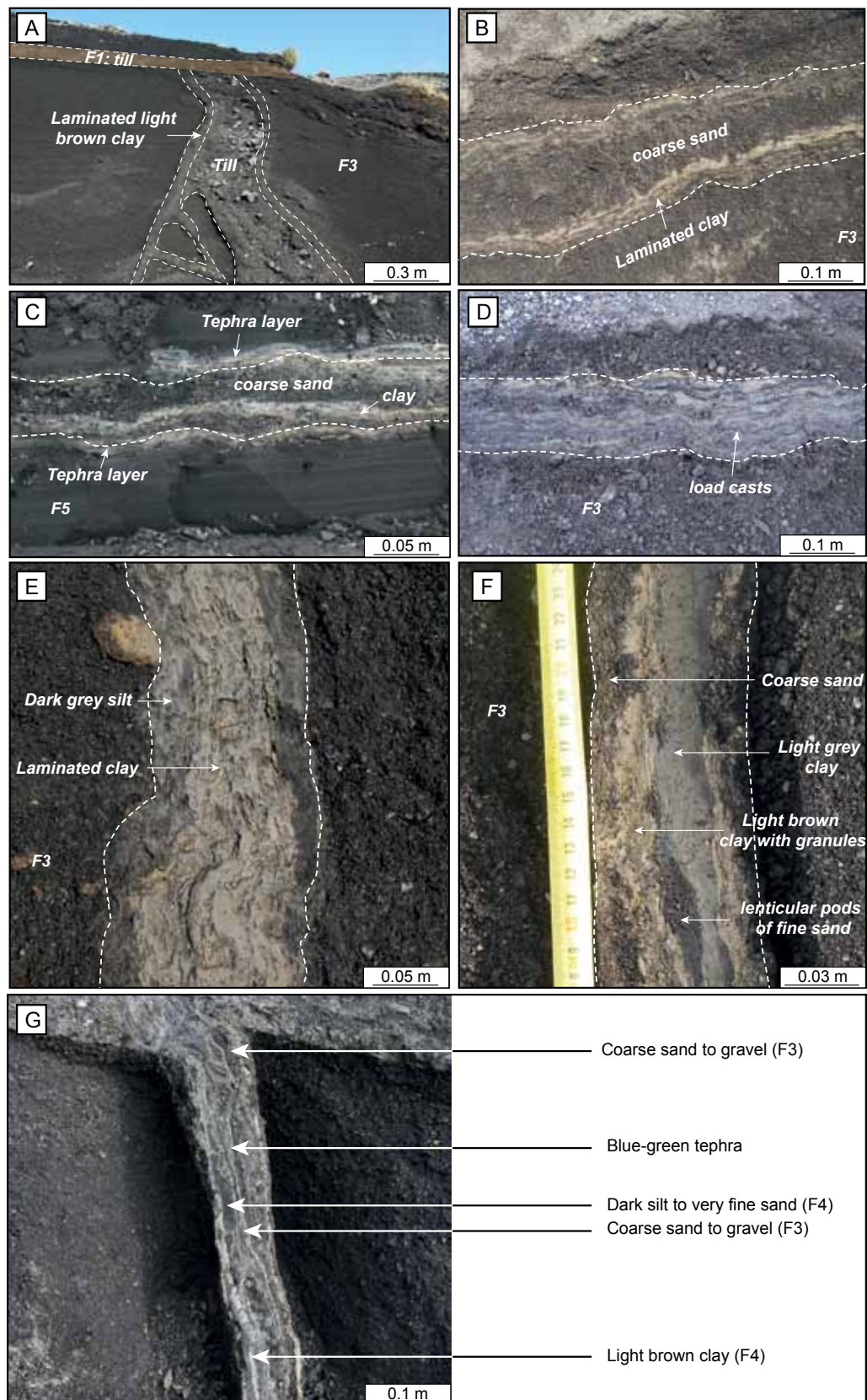


Figure 8. Different sediment-fills observed along the Sólheimajökull clastic injection network. (A) A clastic dyke directly in contact with Till 2 (source bed) filled by laminated clays along the sidewalls and diamicton in its core. (B) Laminated dyke-fill with laminated light brown clay along the margins and dark grey coarse sand in its core. (C) A sill intruding fine-grained laminated dark grey silt that contains light brown clay laminae and dark grey coarse sand. (D) Thinly laminated sill displaying alternating silt, clay, and sand with occasional load casts formed by foundering of denser sand into less dense clay laminae. (E) A dyke showing silty margins and clay laminations in its central part. (F) A dyke characterized by a composite fill composed of coarse sand, fine sand, light brown clay, and light grey clay. Note the lenticular shapes of the injected fine sand. (G) Complex sediment-fill with coarse sand, blue-green tephra, light brown clay and dark silt. Laminae often display lenticular shapes.

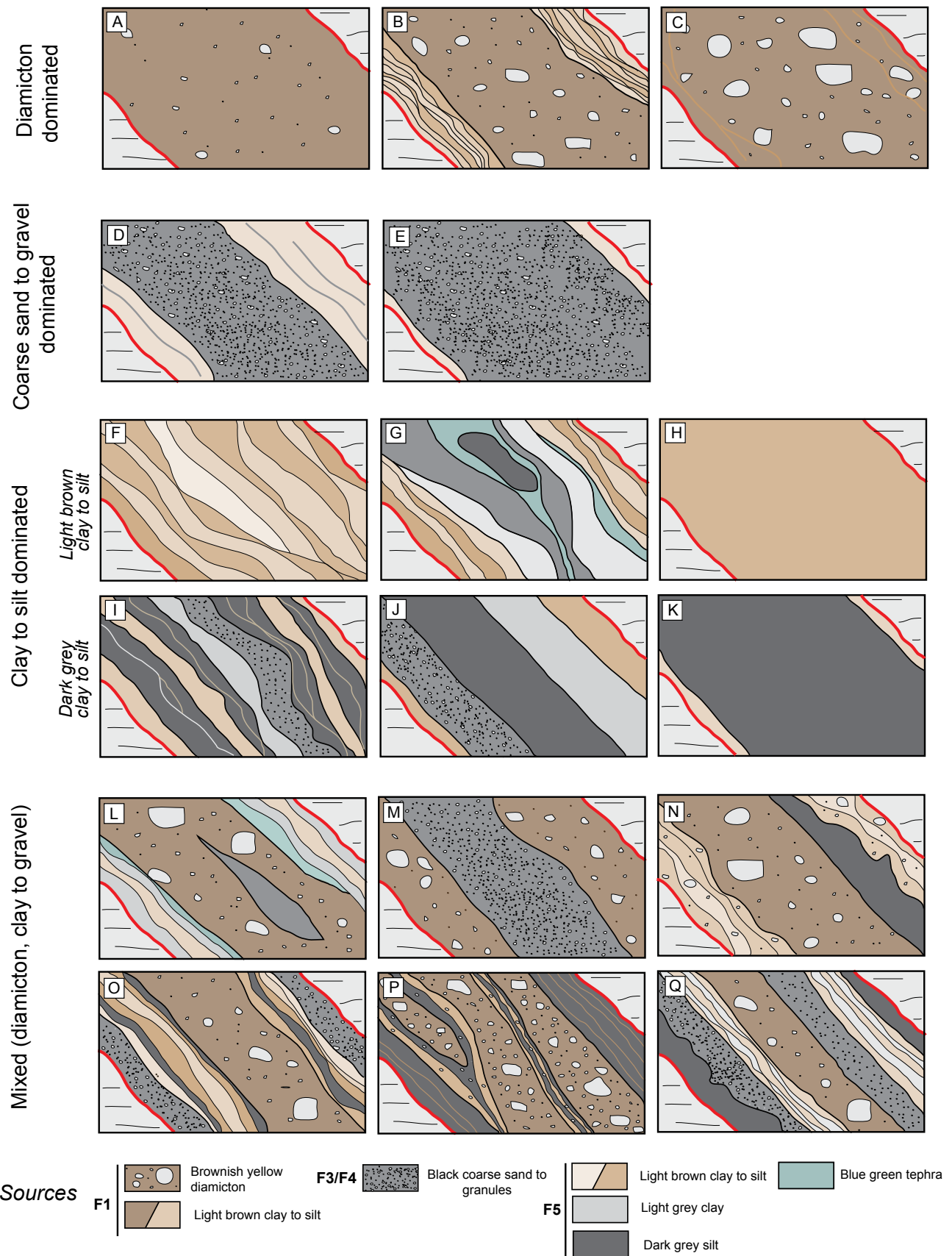


Figure 9. Schematic diagram illustrating the variety of sediment-fills encountered in the Sólheimajökull clastic injection system. (A) to (C) Sediment-fill dominated by diamicton (sourced in till: F1). (D) and (E) Sediment-fills dominated by dark grey coarse sand to gravel sourced in glaci-fluvial sediments (F3/F4). (F) to (K) Sediment-fills dominated by clay to silt either sourced in till (F1) or pond deposits (F5). (L) to (Q) Composite sediment-fills induced by variations in sediment source and/or grain-size segregation.

decrease in mean grain-size away from the source bed (**Figs. 8A, B, 9 and 10A**). Diamicton or gravely sand are generally observed at the core of the injection while the margins tend to display clay laminae (**Figs. 8A, B and 9B, D, E, I, N, L, O, Q**). Within a single clastic intrusion that can be traced over long distance, bulk sampling have been respectively realized 1 m and 6 m away from the source. The mode and mean of the < 2 mm fraction drastically decrease with distance to the source (**Fig. 10A**). Colour observations, textures, and grain-size distributions of the laminae composing the intrusions allow to define four main types of sediment-fill: (1) A first type where light brown diamicton is predominant within the sediment-fill (**Fig. 9A to C**), (2) a second one where coarse sand to gravel prevails (**Fig. 9D, E**), (3) a third one where fine-grained sediments (clay to silt) are dominant (**Fig. 9F to K**), and (4) a last one where sediment-fills are complex and characterized by clay, sand and/or diamicton laminae (**Fig. 9L to Q**). In case of sediment-fills predominantly composed of clay to silt, two subcategories can be defined: a first where light brown clays are dominant and a second one where dark grey clay to silt are prevalent. These variations in grain-size and colours indicate changes in the source bed or/and grain-size segregation during the different episodes of sediment injection.

A single dyke illustrates that each laminae is characterized by different grain-size distribution for the fraction < 2 mm (**Fig. 10B**). The mean and mode of the different laminae, compared to those calculated for host sediments, allow to determine a plausible source bed for each lamina (**Figs. 3A and 10B**). The different sources responsible for the laminated sediment-fills are the (1) light brown till, (2) the glacifluvial dark grey sand to gravel and (3) the pond deposits:

- (1) Light brown till (F1)

-Laminae 2 and 4, composed of a light brown matrix with clasts up to boulder size, display a multi-modal grain-size distribution, and similar grain-size mode/mean with Till 2. This indicates that Till 2 bed was injected within the fracture.

-Lamina 6 is composed of silt to clay with an unimodal grain-size distribution and seems to display similar grain-size characteristics with the light brown laminated pond deposits (**Figs. 3C and 10B**). However, the *per descensum* clastic dyke described in **Figure 10A** is not overlain by the laminated pond sediments due the limited lateral extension of such deposits (< 200 m; cf **Figs. 4 and 6**), suggesting that the light brown fine-grained material also derives from the remobilization of fine particles contained in Till 2 (**Fig. 10B**). This implies that during injection of the till within fractures, processes of grain-size segregation and partial sorting occur.

- (2) Glacifluvial dark grey sand

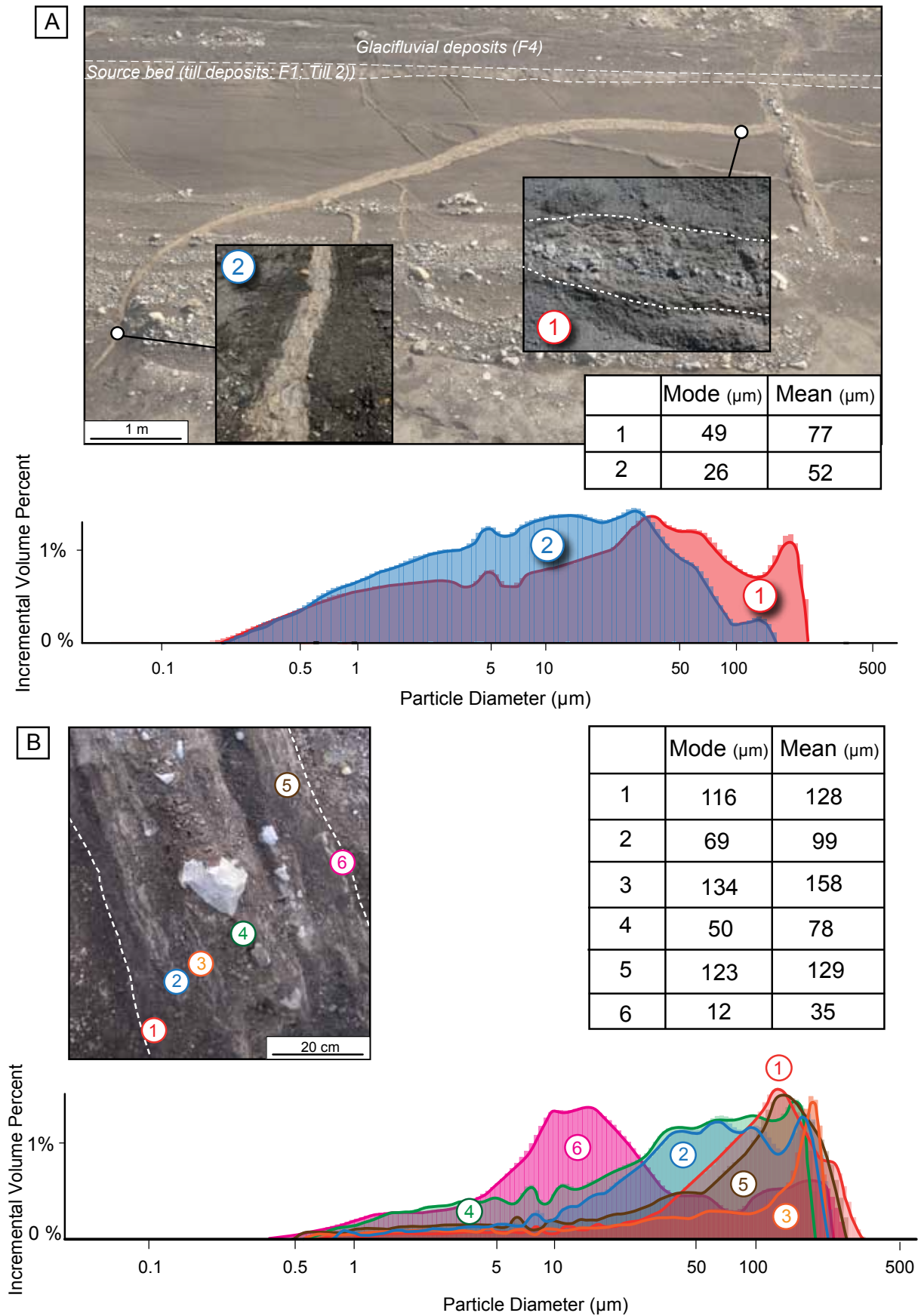


Figure 10. (A) Illustration of the decrease of grain-size with the distance from the source bed. (B) Variations of the grain-size characteristics between the different laminae composing a single dyke, suggesting variations of sediment source during sedimentary fill and/or grain-size segregation.

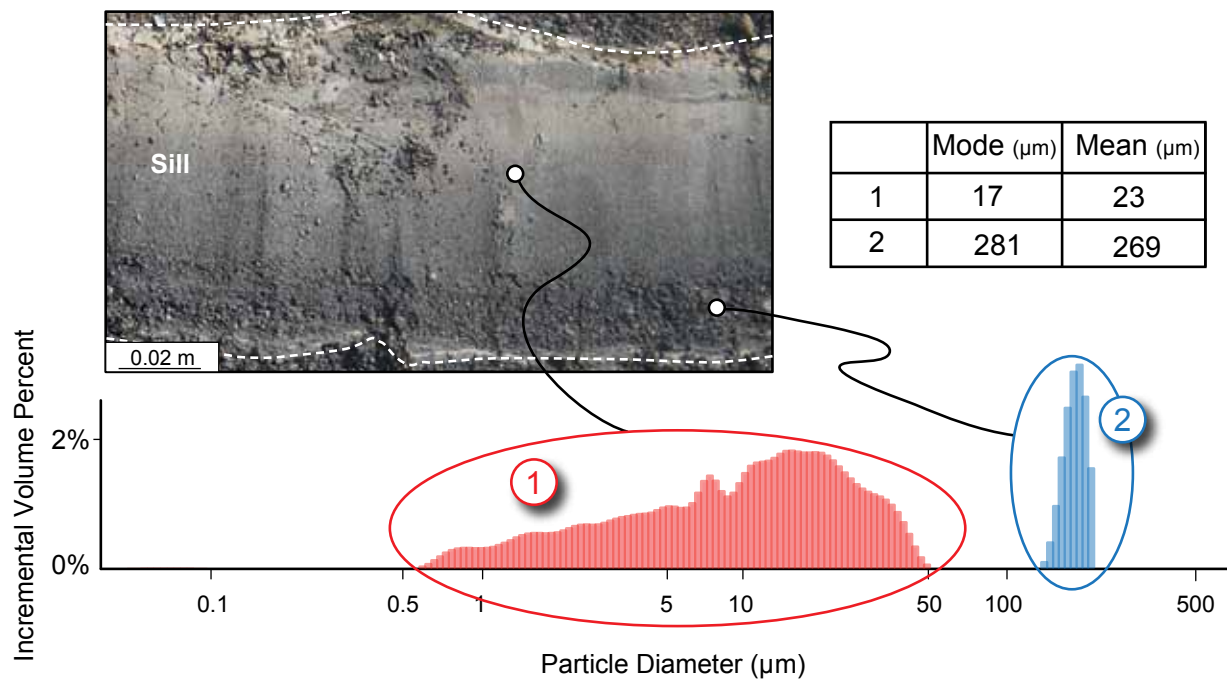


Figure 11. Grain-size distribution, mean, and mode of dark grey coarse sand and silt injected within a sill.

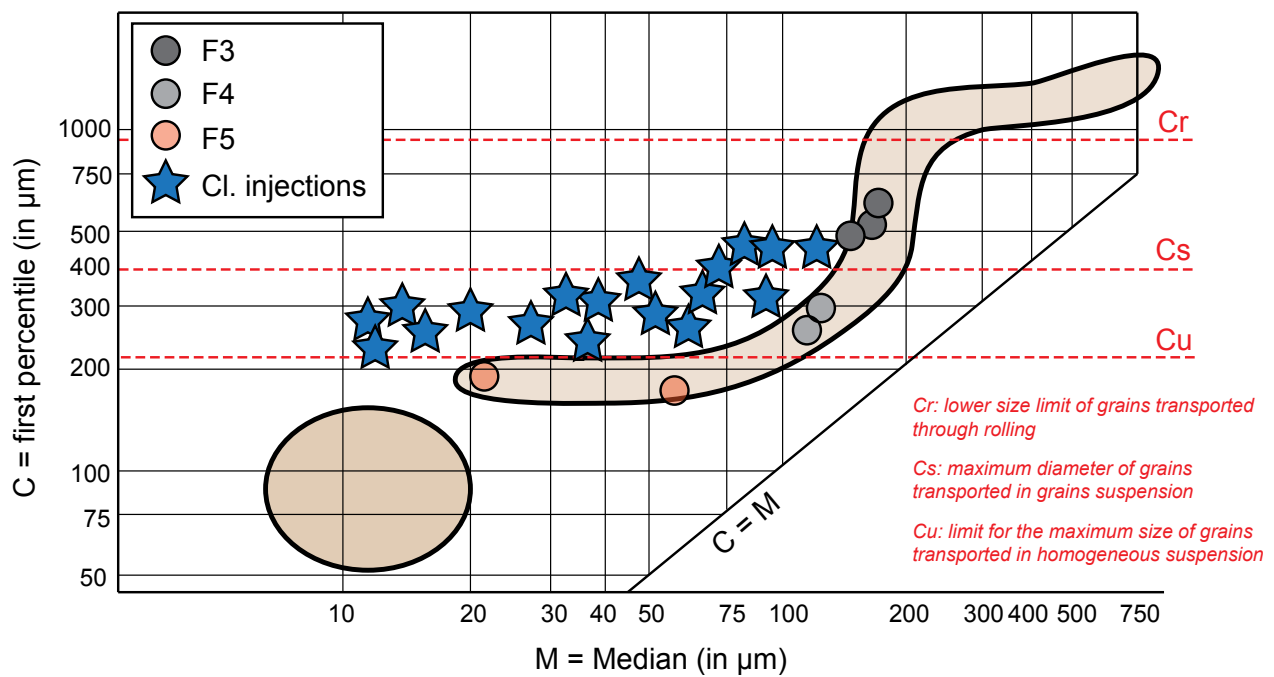
- A sill, composed of dark grey sand, displays an unimodal grain-size distribution and a mean grain-size exceeding 200 μm for the fraction <2 mm, illustrating that glaci-fluvial deposits have also been injected within the intrusion (**Figs. 3B and 11**).

• (3) Pond deposits (F5)

- The occurrence of typical and easily recognizable blue green tephra, dark silt or light grey clay in some clastic intrusions indicate that fine-grained laminated deposits (F5) have locally been remobilized and injected within fractures (**Fig. 8E, F, G and 9G, I, K, L**).

Results obtained from grain-size analyses in injected material and host sediments were plotted in a Passega diagram (1964) to characterize processes of transport and deposition during deposition and remobilization of sediments (**Fig 12**). As expected, grain-size characteristics of the laminated fine-grained sediments (e.g., median and first percentile) (F5) correspond to deposition by settling from suspension in stagnant meltwater, while glaci-fluvial deposits (F3/F4) correspond to transport and deposition in flowing water, mainly by rolling (**Fig. 12**). However, results obtained in sediment-fill of clastic injections show that grain-size distribution of sediments emplaced within clastic intrusions are not ruled by fluvial-like processes (i.e., saltation, rolling, or suspension), although few sedimentary

Figure 12. First-percentile and Median of glaci-fluvial and pond deposits plotted in C-M Passega diagram (1964). Values calculated within clastic injections are also replaced in the diagram.



structures have been observed (**Fig. 13**). Indeed, sills are sometimes filled by fining-upwards sedimentary sequences or pseudo cross-laminations, usually preserved within lenticular pods (**Fig. 13**). Fining upwards sequences consist of medium sand or silt progressively passing upwards into clays (**Fig. 13A**). The fining-upward sequences are structureless and composed of homogenized material.

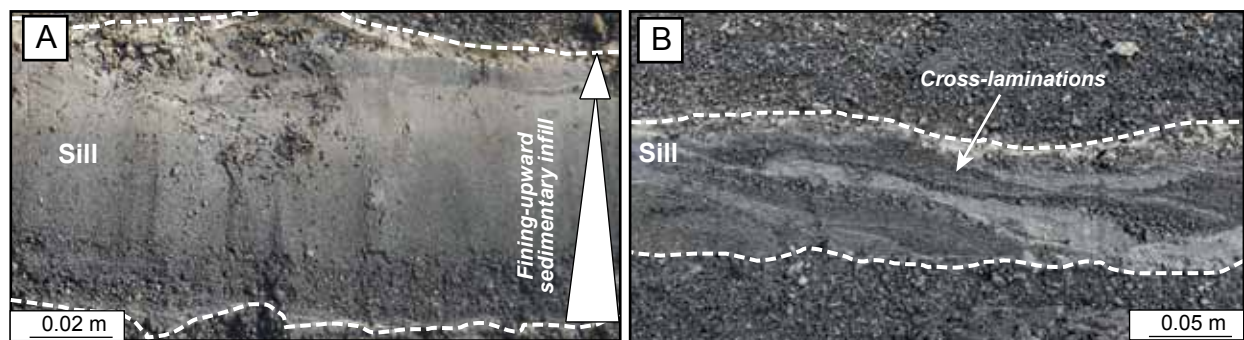


Figure 13. (A) Stacked fining-upward sequences within a sill composed of homogenized sediments. (B) Pseudo cross-laminations observed within a clastic sill.

5.1.3. Cross-cutting relationships

The numerous and complex cross-cutting relationships observed between the different intrusions demonstrate that the network developed in response to several and repeated phases of fracturing and injections (**Fig. 14**). At macro-scale, five generations of injections, composed of different sediment-fills can be determined (**Figs. 6, 14, 15 and 16**).

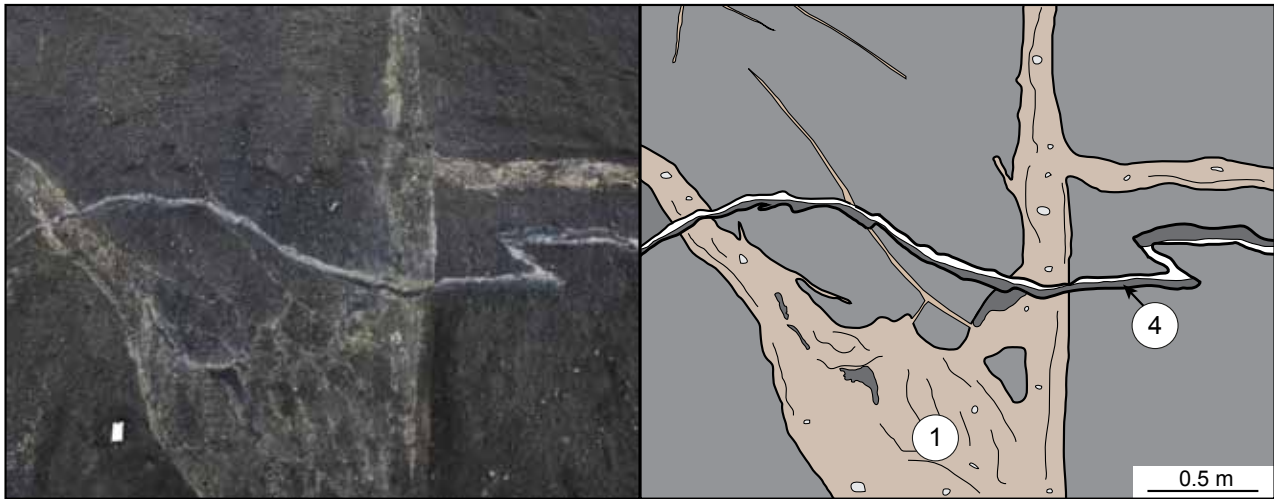


Figure 14. Cross-cutting relationships illustrated by a sill cross-cutting two merging clastic dykes. The first generation is predominantly composed of light Brown diamicton and is cross-cut by the fourth generation composed of silt to sand-rich sills.

- The first generation (1) of clastic injections propagates downwards (i.e., *per descensum*) within glaci-fluvial deposits (F3/F4) and takes its source in Till 2 (**Fig. 15**). This first generation is mainly constituted by high-angle dykes dipping towards the SSW that branch, split and rejoin (**Fig. 14** and **15**). Clastic dykes are composed of clay laminae with occasional sparse granules and gravels on the margins, and massive diamicton with clasts up to boulder size embedded in a clayey to sandy matrix in their centres (**Fig. 15; generation 1a**). This first generation contains the widest intrusions with clastic dykes up to 1.5 m wide (**Figs. 14** and **15**). Thin apophyses containing clay with sparse gravels branching out from this first generation propagate downwards and are probably penecontemporaneous to this first phase of injection (**Fig. 15; generation 1b**).
- The second generation (2) of clastic intrusions propagate upwards (i.e., *per ascensum*) and takes its source in the first generation of sediment injection (**Fig. 15**). The second generation is composed of several dykes that sometimes cross-cut each others, demonstrating different episodes of injection (generations 2a and 2b) (**Fig. 15**). Clastic dykes reach 0.1 to 0.15 m thick, and are characterized by thin light brown silty clay laminae with sparse granules (**Fig. 15**). The second generation of injection occasionally cross-cuts the fine-grained sediments (F5) and the base of the gravely sand (F4) (**Fig. 15**).
- The third generation (3) is evidenced by *per descensum* clastic dykes dipping towards the SSW, with a sediment-fill dominated by coarse sand originating from glaci-fluvial deposits (**Fig. 9D, E**). This generation locally cross-cuts the first generation and displays coarse sand on their margins (**Fig. 80**). Dark grey coarse sand being injected within the centre of preexisting clastic dykes also implies that

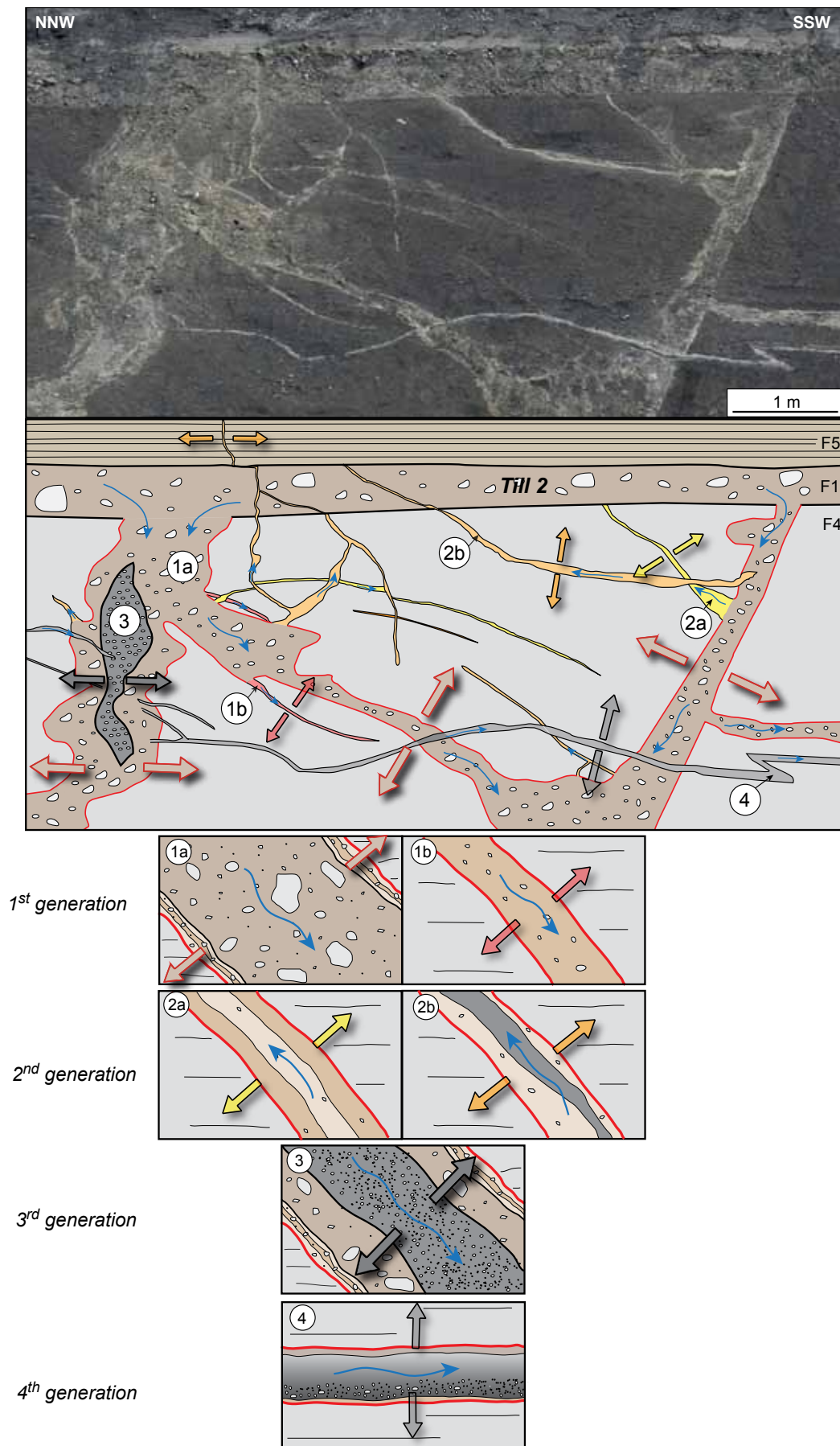


Figure 15. Close-up on the Sólheimajökull clastic injection system where several cross-cutting relationships can be observed. Four main generations of clastic injections are observed. (1a) Per descensum clastic dykes sourced in till. (1b) Small per descensum clastic dykes sourced in (1a). (2a) and (2b) Small per ascensum clastic dykes sourced in (1). The third generation (3) of injection locally reopen the first generation (1). (4) The fourth generation is composed of sills.

some older generations of clastic intrusions could have reopened during the development of this third generation (**Figs. 8D, E, I, M and 15**).

- The fourth generation (4) is characterized by sills developing along host sediment bedding and cross-cuts all previous generations (**Fig. 15**). Sills develop in glaci-fluvial sediments below Till 2 but also within the fine-grained laminated sediments where horizontal tephra or clay layers control the horizontal propagation of the intrusions (**Figs. 15 and 16**). Sills are sometimes connected to dykes propagating along preexisting fault planes, forming “stepped sills” morphologies (**Figs. 18 and 19**). Sills can reach 0.1 m thick and are composed of dark grey sandy gravel, dark grey silt and grey clay arranged in laminae or in fining-upward sequences (**Figs. 13A, 15 and 16**). Older dykes represent weakness planes which can locally deviate the horizontal propagation path of sills. Thin light brown clay laminae are sometimes observed along the margin of this fourth generation of clastic injection (**Fig. 16**). Light brown clay with sparse granules, dark grey silt/sand, and light grey clay suggest multiple sources during the sedimentary infill of the fourth generation (**Fig. 16**). Localized *per descensum* subvertical clastic dykes filled by homogenized sand cross-cutting this fourth generation have locally been observed (Cf. (4b) in **Fig. 16**).

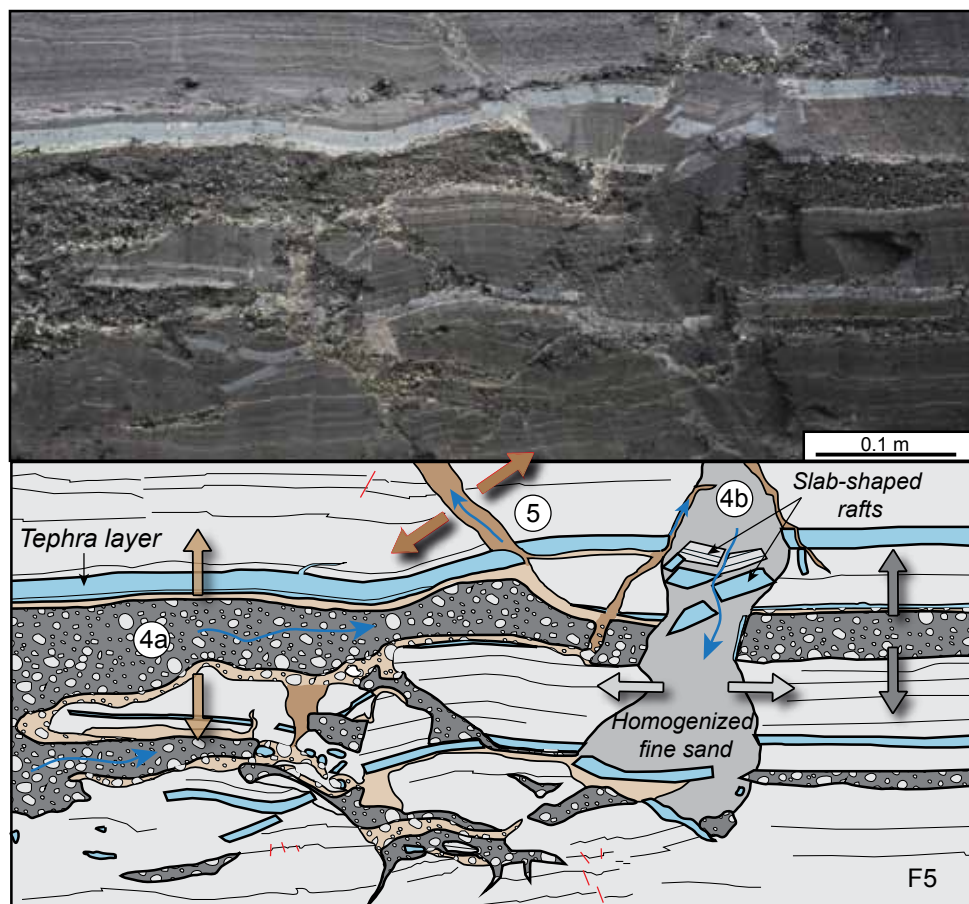


Figure 16. Cross-cutting relationships between the fourth and fifth generation of clastic injections at the meso-scale. Note that the propagation of the fourth generation follows the low-permeability blue green tephra layers.

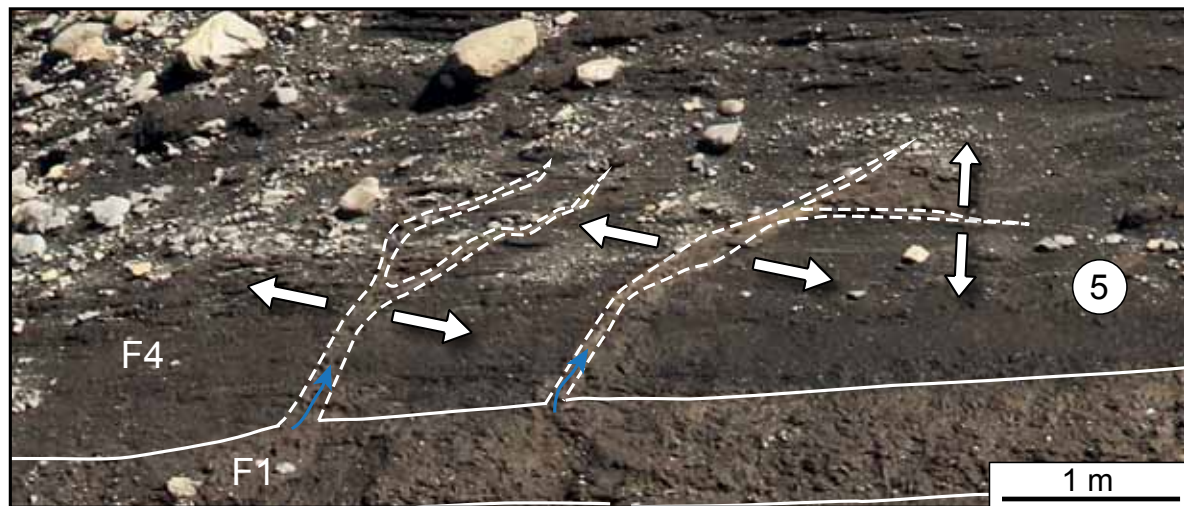


Figure 17. Close up on the fifth generation of clastic injections observed in the Sólheimajökull clastic injection network. The fifth generation is composed of *per ascensum* clastic dykes with minor sills branching out.

- The fifth generation (5) is composed of thin dykes, mainly propagating upwards and sourced within older clastic injections or within Till 2 (**Figs. 16 and 17**). This last generation is composed of thin dykes (< 0.1 m) and sometimes display connections with small sills (**Fig. 17**). This generation of intrusion is generally filled by a mix of clay and granules.

At the macro- and meso-scale, five principal generations of clastic injections were evidenced. Each of those are characterized by different grain-size and material injected (light brown diamicton, dark grey silt or sandy gravel, light brown clay and grey clay), different geometries (sills, stepped sills, low-angle dykes, high-angle dykes) and different senses of propagation (*per ascensum* vs. *per descensum*).

5.2. Microscale descriptions

Thin sections obtained from the sill-dominated network affecting the host fine-grained laminated sediments (F5) allow to refine the chronology of injection, but also to better understand the processes involved in their development (**Cf. Figs. 6, 18 and 19**). For reasons of clarity, characteristics and deformation affecting host sediments, the description of host/clastic injection contacts, characteristics of sediment-fill, and cross-cutting relationships will be described separately.

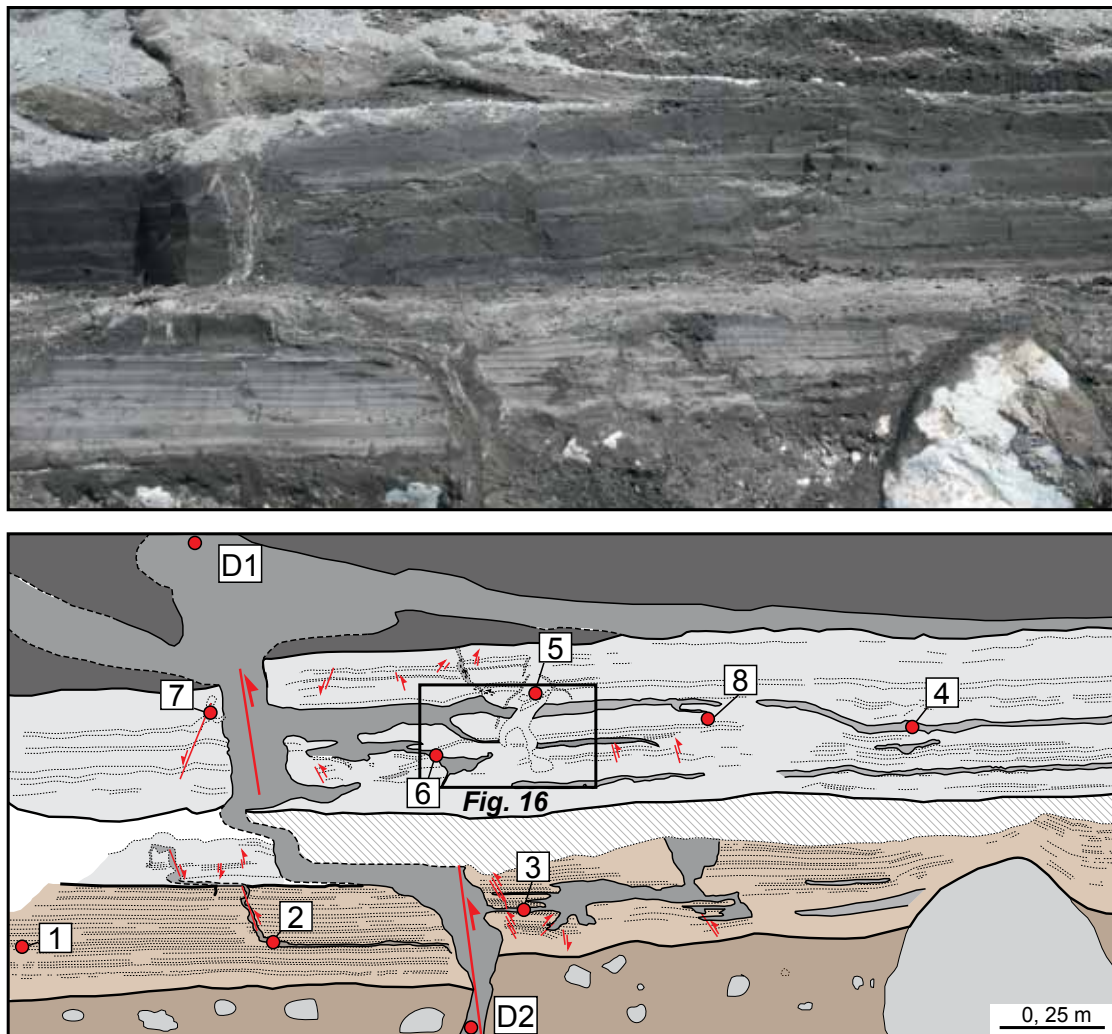


Figure 18. Close-up on the Sólheimajökull clastic injection network showing the location of samples 1 to 8, D1, and D2 collected for micromorphological analyses.

5.2.1. Deformation of host sediments

At the microscopic scale, host sediments are characterized by mm-thick laminated clay, silt and very fine sand beds. Faults cross-cutting few laminations with minor offsets (< 0.5 mm) frequently affect host sediments in the vicinity of clastic intrusions (**Figs. 25, 27 and 30**). In most cases, laminations appear to ‘drape over’ the small-scale faults affecting the host strata, indicating that deformation occurs during sedimentation. Normal faults are predominant although reverse and thrust faults are occasionally observed. In sample 2, a SSE directed thrust fault filled by silt occurs below a sill (**Fig. 21**). Smaller-scale reverse or thrust faults are frequently distinguished and are either directed towards the SSE or the NNW (**Figs. 23, 25 and 27**). In sample 6, conjugate reverse faults occur in the vicinity of clastic intrusions and may indicate radial compression that could be related to the development of the three dimensional intrusion network (**Fig. 25**). Step normal microfaults are sometimes observed in thin sections and represent compaction structures induced by the overburden pressure. In sample

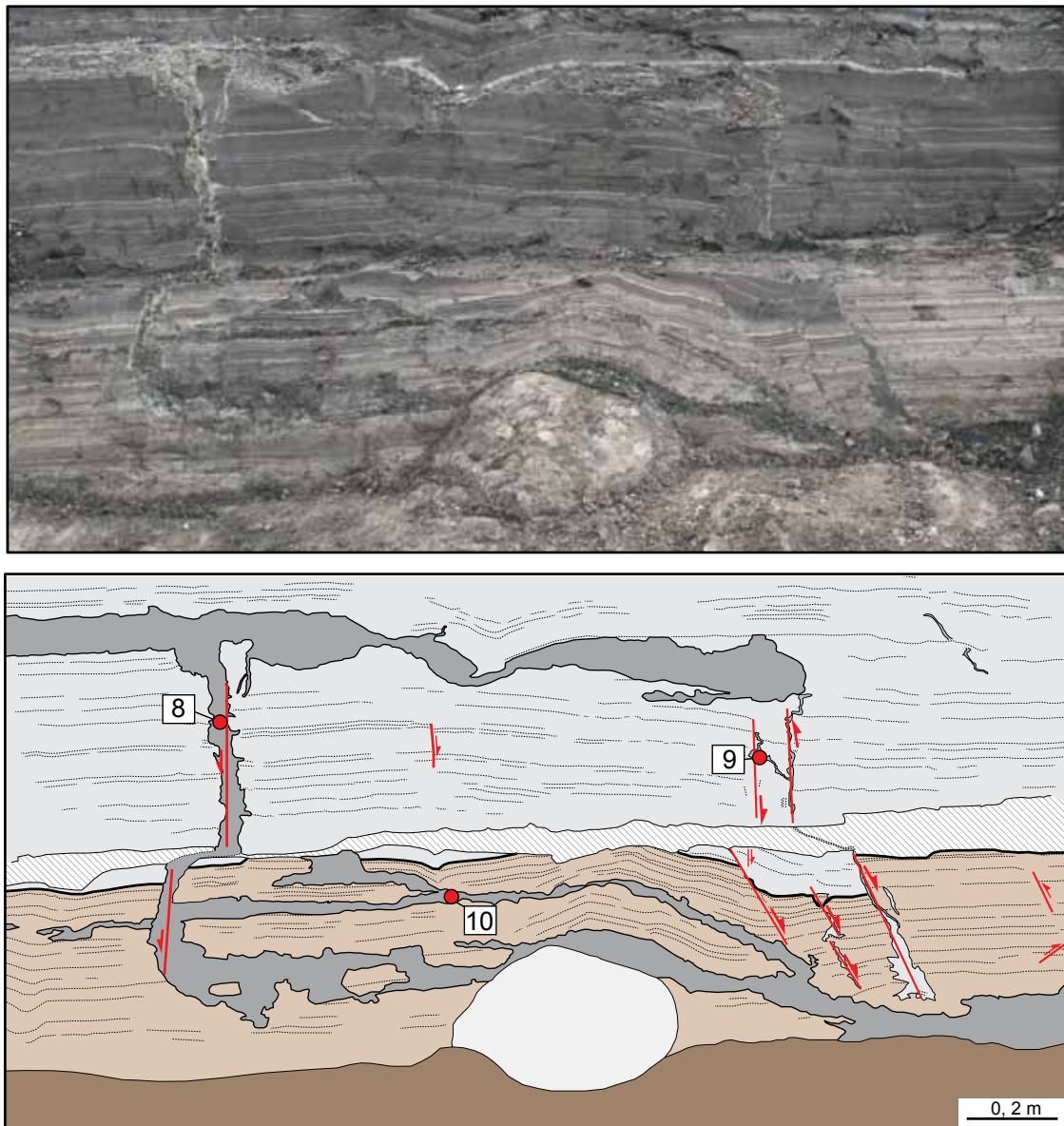


Figure 19. Close-up on the Sólheimajökull clastic injection network showing the location of samples 9 to 11 collected for micromorphological analyses.

4, these step normal faults cross-cut the last injection phase suggesting that compaction postdates the intrusion of sediments (**Fig. 23**). In sample 7, small-scale asymmetrical folds constrained to single beds and sealed by undeformed deposits verge towards the SSE (**Fig. 26**). Small-scale folds draped over by laminated sediments indicate that mechanisms responsible for deformation were short-lived. In sample 3, highly deformed host sediments are entrapped between two sills composed of gravely sand (**Fig. 22A, B**). The host sediments encompass load structures, contorted beds and numerous closely spaced hydrofractures filled by homogenized silt, forming an in-situ breccia-like fabric (**Figs. 22A, B and 29A, B**). The angular and slab-shaped intraclasts formed by hydraulic brecciation and erosion of host sediments are often remobilized during injection of sediments and float within homogenized sediments (**Figs. 23, 24, 27, 28 and 29**). Some of these intraclasts display internal sediment-filled

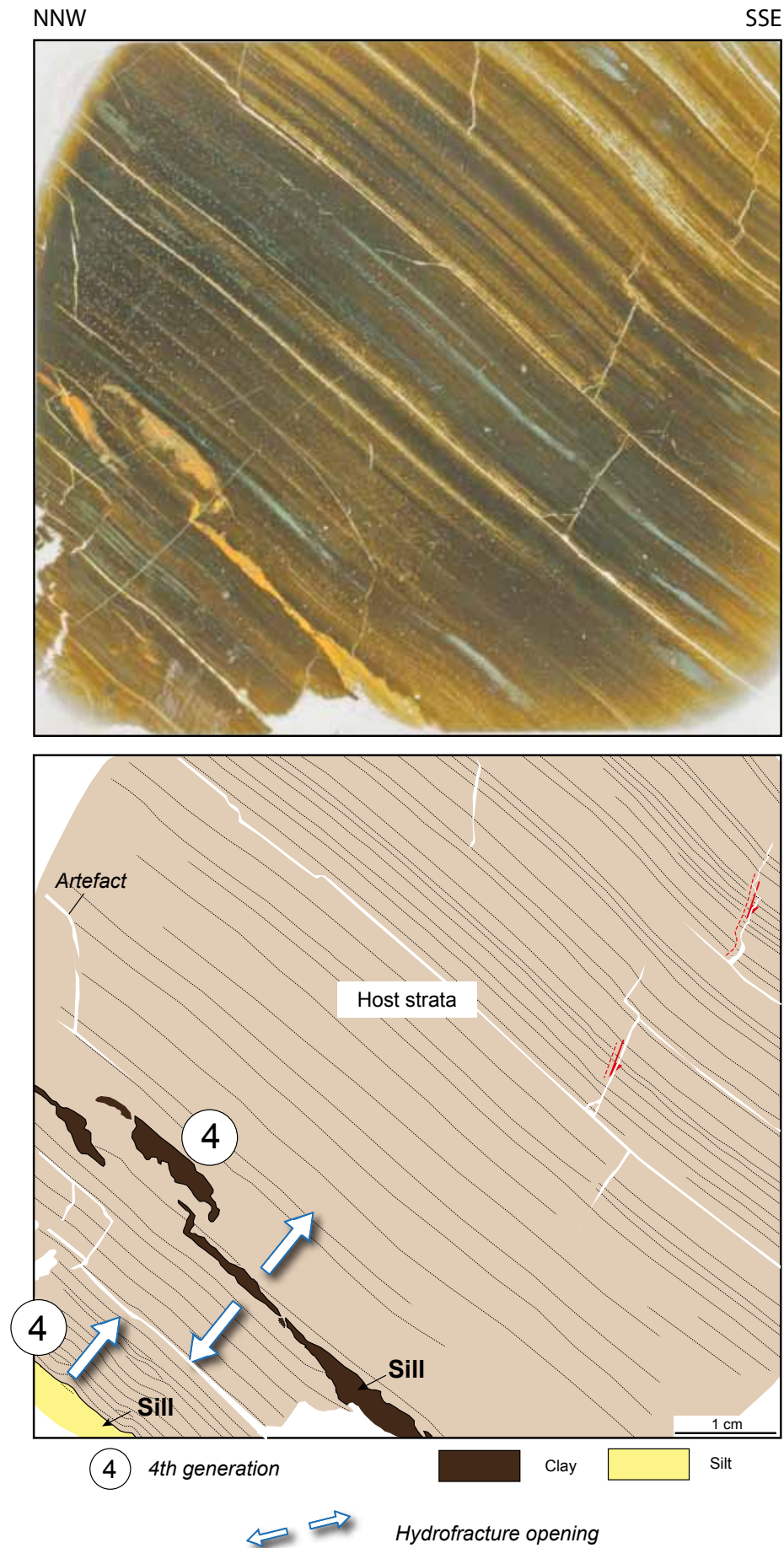


Figure 20. Scan and interpretation of sample 1. This thin-section is taken within the laminated fine-grained light brown clay and silt. Sills propagate along bedding and are either composed of clay or silt.

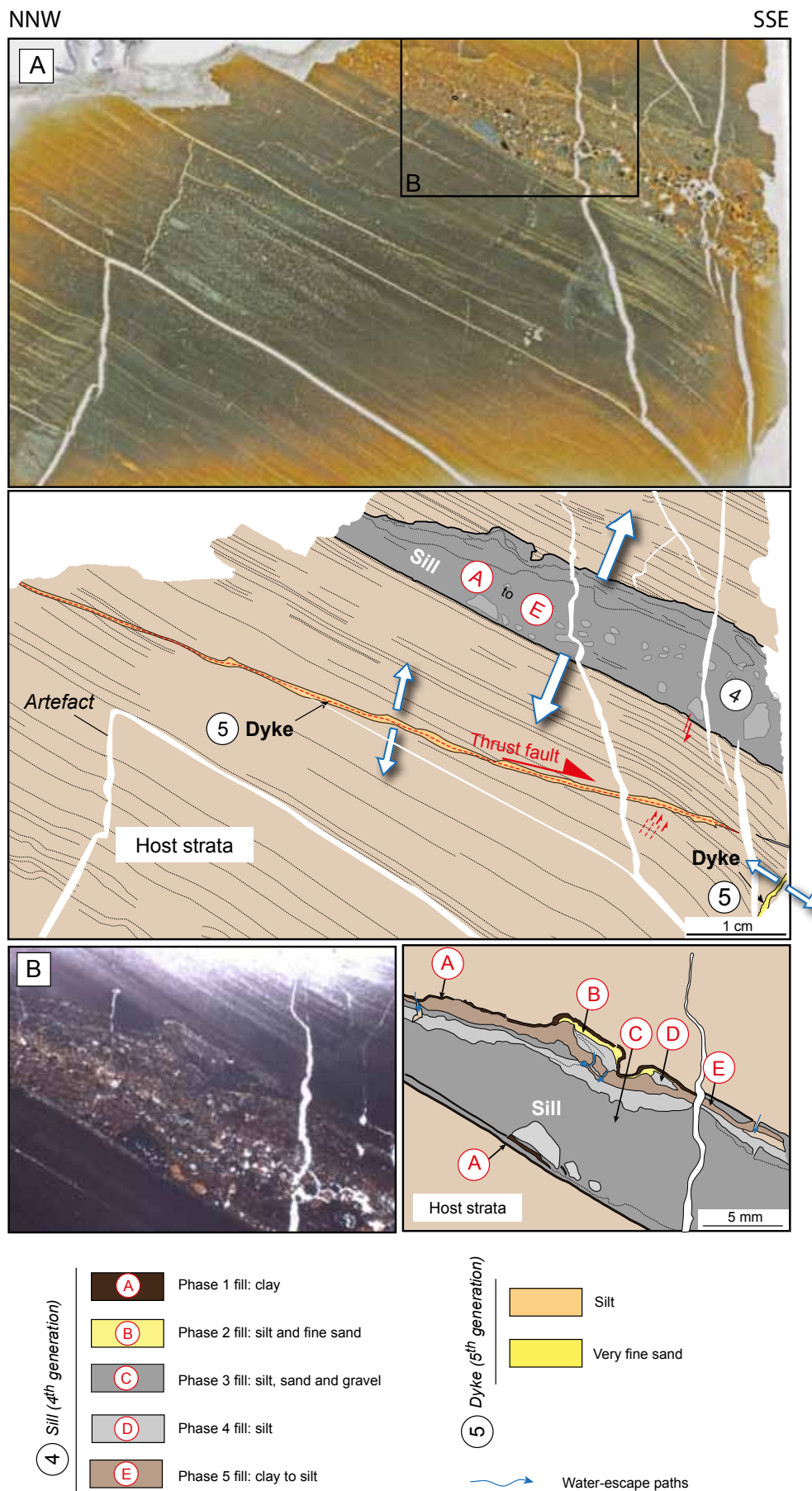


Figure 21. (A) Scan and interpretation of sample 2. A sand-rich sill develops parallel to bedding (4th generation) while two clastic dykes with different dip angles develop below the sill (5th generation). The low-angle dyke filled by silt propagates along a SSE-directed thrust fault. (B) Close-up on the sill. 5 phases of sediment-fill with an increase of grain-size towards the centre of the sill are observed

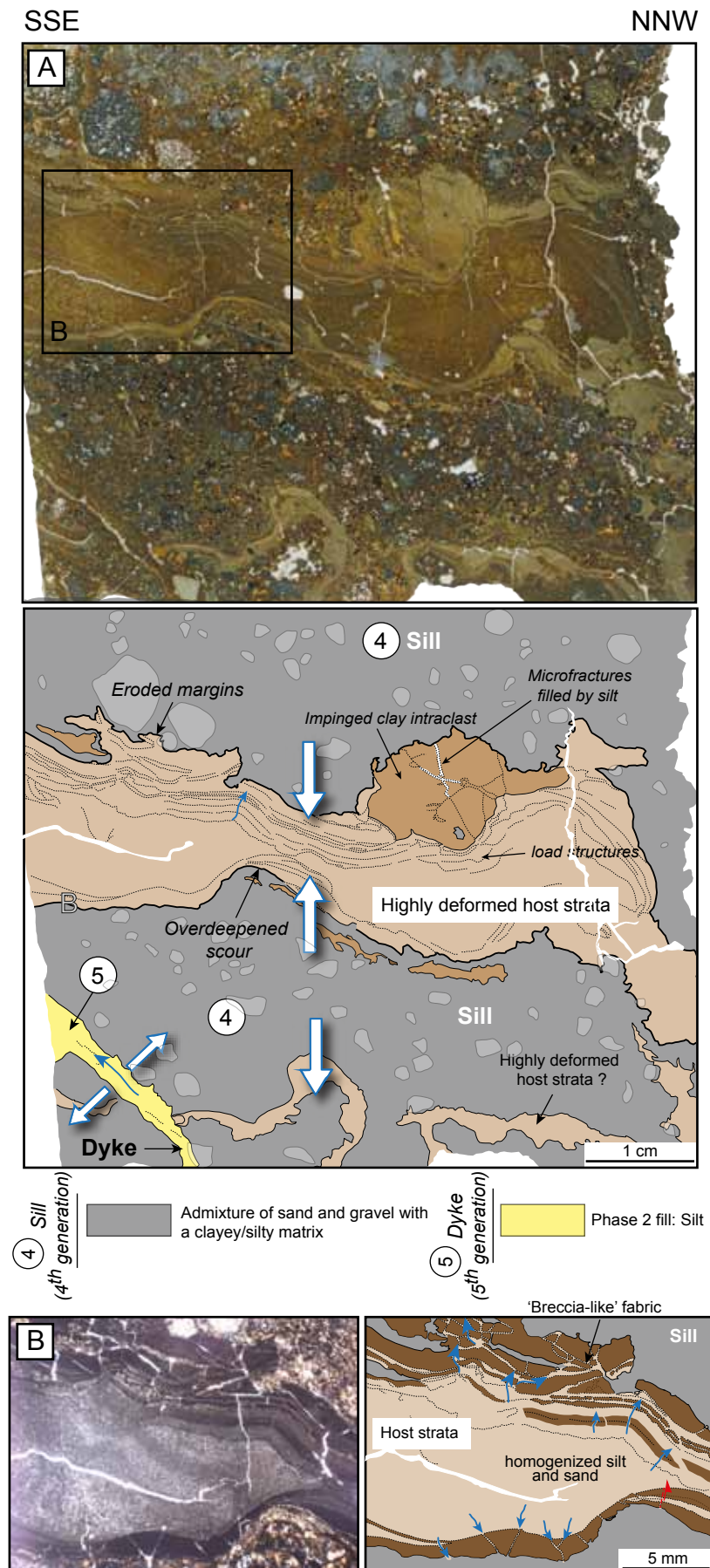


Figure 22. (A) Scan and interpretation of sample 3. The propagation of two closely spaced coarse sand-rich sills (4th generation) leads to the deformation of entrapped host sediments. Sills are cross-cut by a silt-rich clastic dyke propagating upward (5th generation). (B) Close-up on the deformed host strata where silt to fine sand become homogenized and structureless. In host sediments, the dense network of micro-fractures leads to in-situ brecciation.

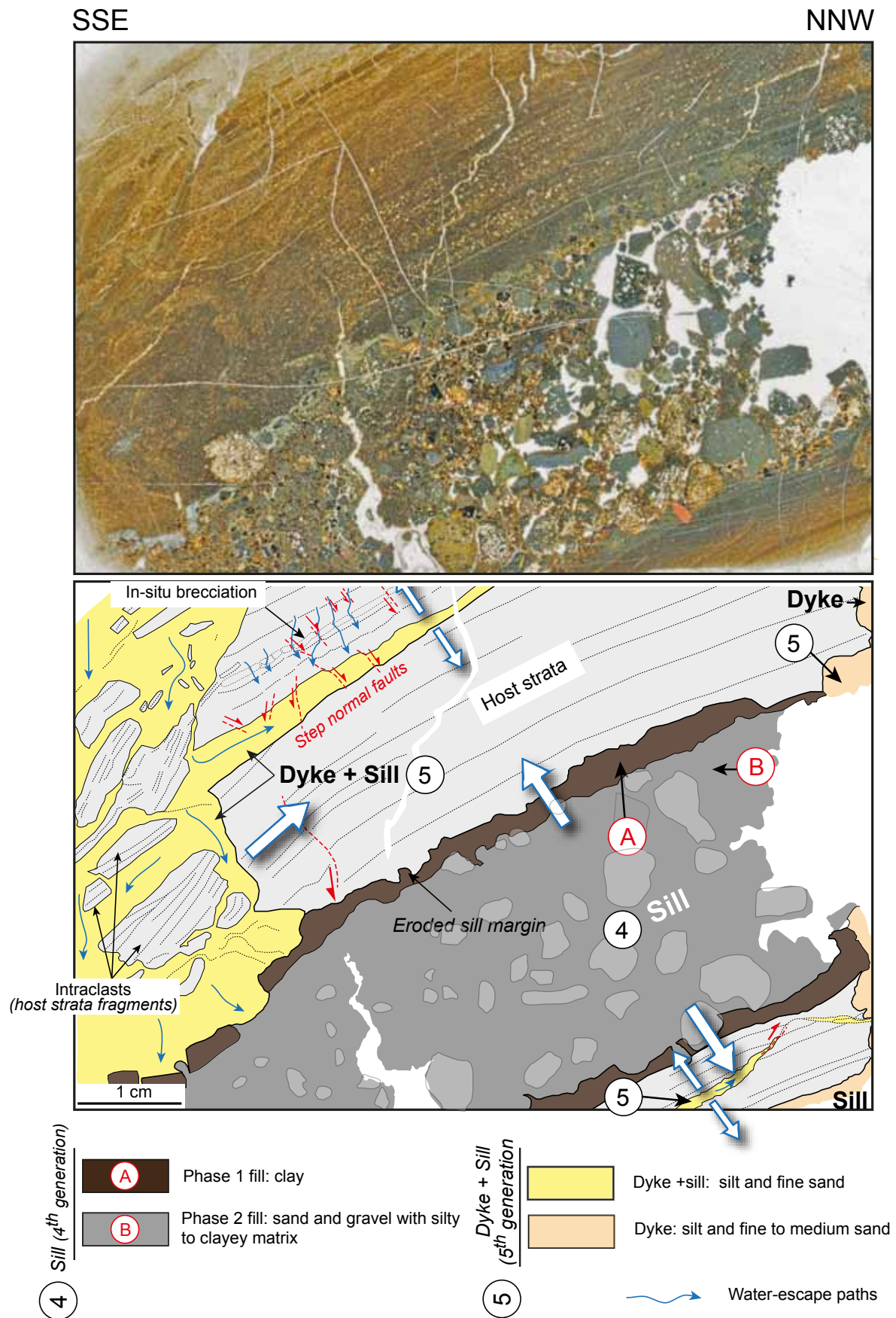


Figure 23. Scan and interpretation of sample 4. A generation of sill characterized by two phases of sediment-fill: clays, and sand to gravel, corresponding to the 4th generation. The sill is disrupted by another generation of clastic injection composed of a sill and dyke complex that triggers brecciation of the host strata (5th generation).

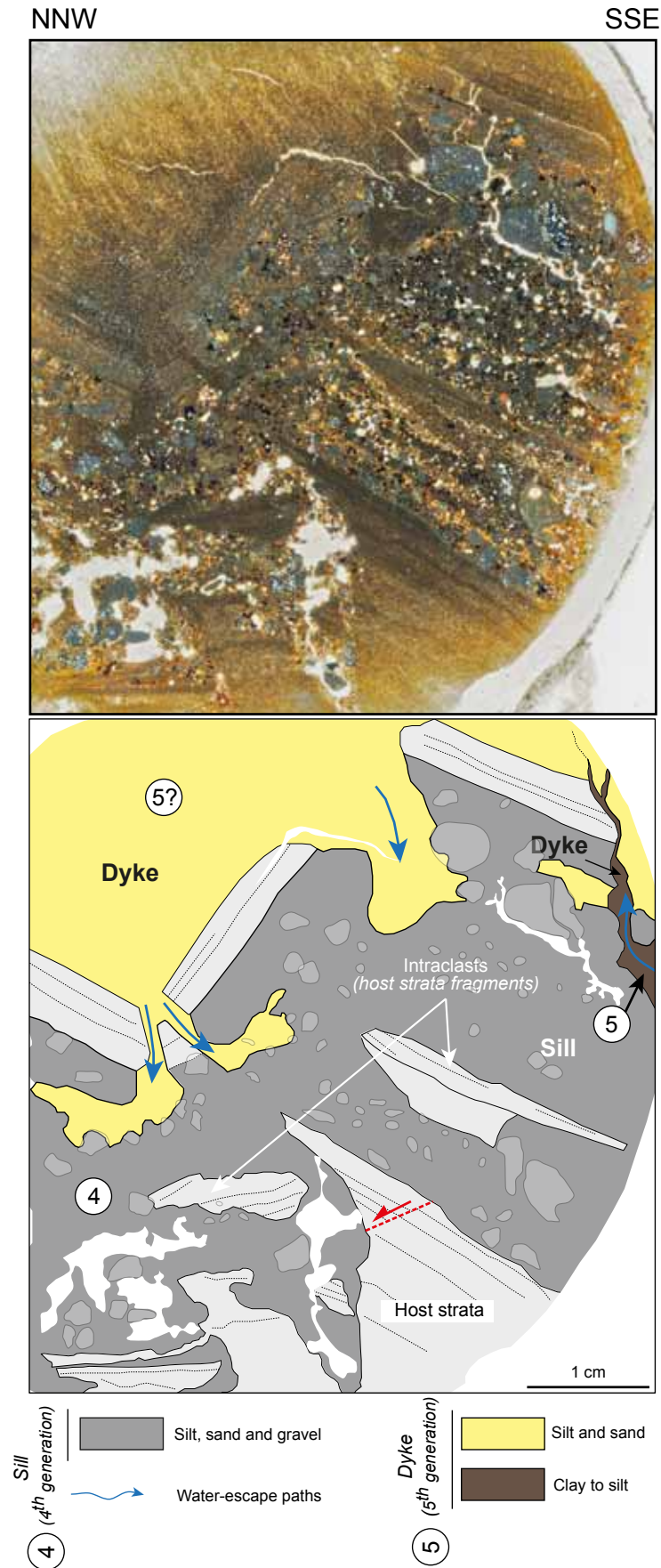


Figure 24. Scan and interpretation of sample 5. The 4th generation is composed of a coarse sand to gravel-rich sill containing angular intraclasts of host sediments. The following generation is composed of a dyke propagating downwards intruding the sill. The last episode is characterized by a per ascensum clayey injection, also corresponding to the 5th generation.

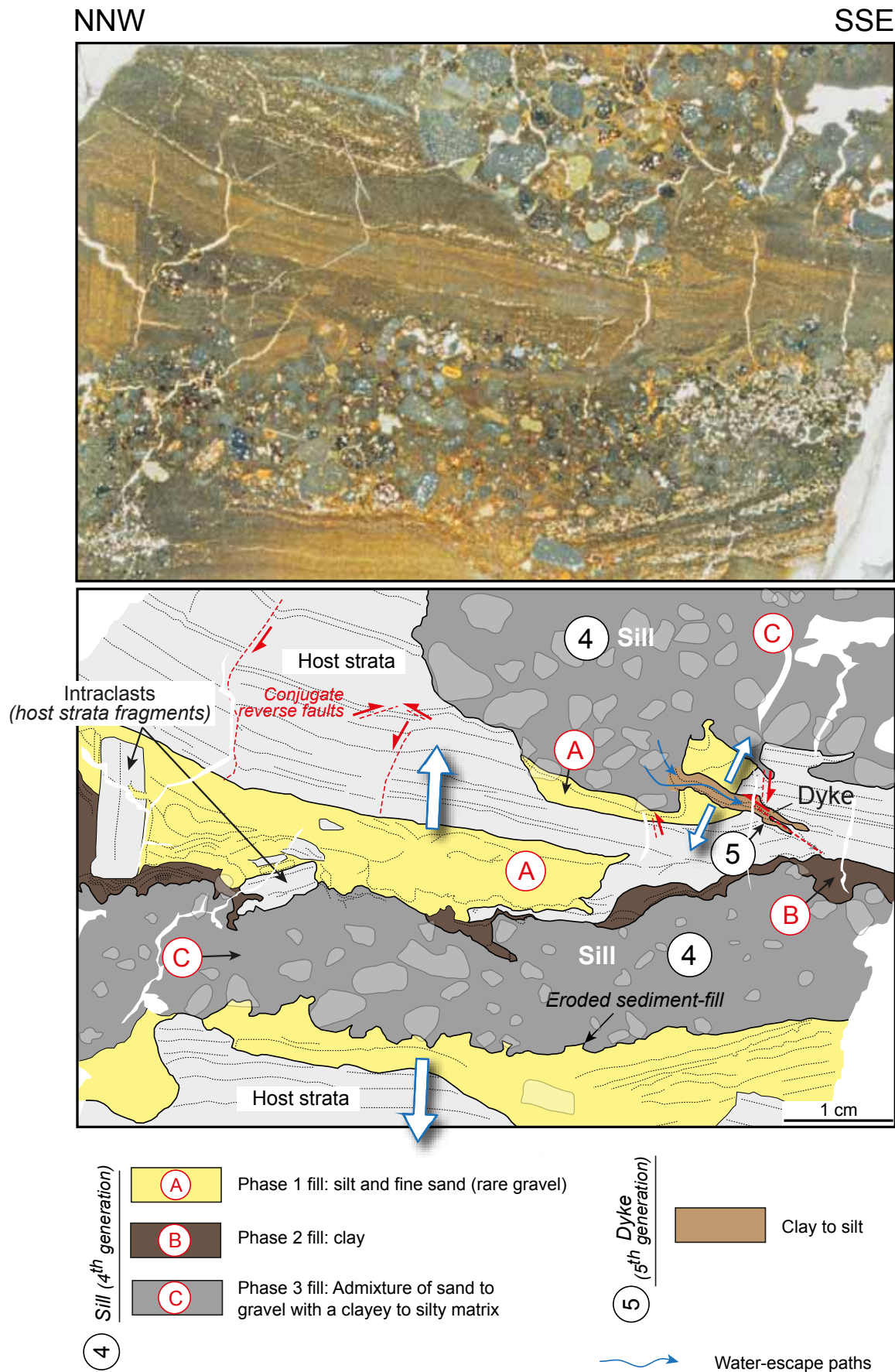


Figure 25. Scan and interpretation of sample 6. Development of two parallel sills that are characterized by three phases of sediment-fill, with an increase of grain-size towards the core of the sill (4th generation). Angular and slab-shaped intraclasts float within the sill. A late phase of injection following a preexisting fault plane leads to the formation of a clayey dyke (5th generation).

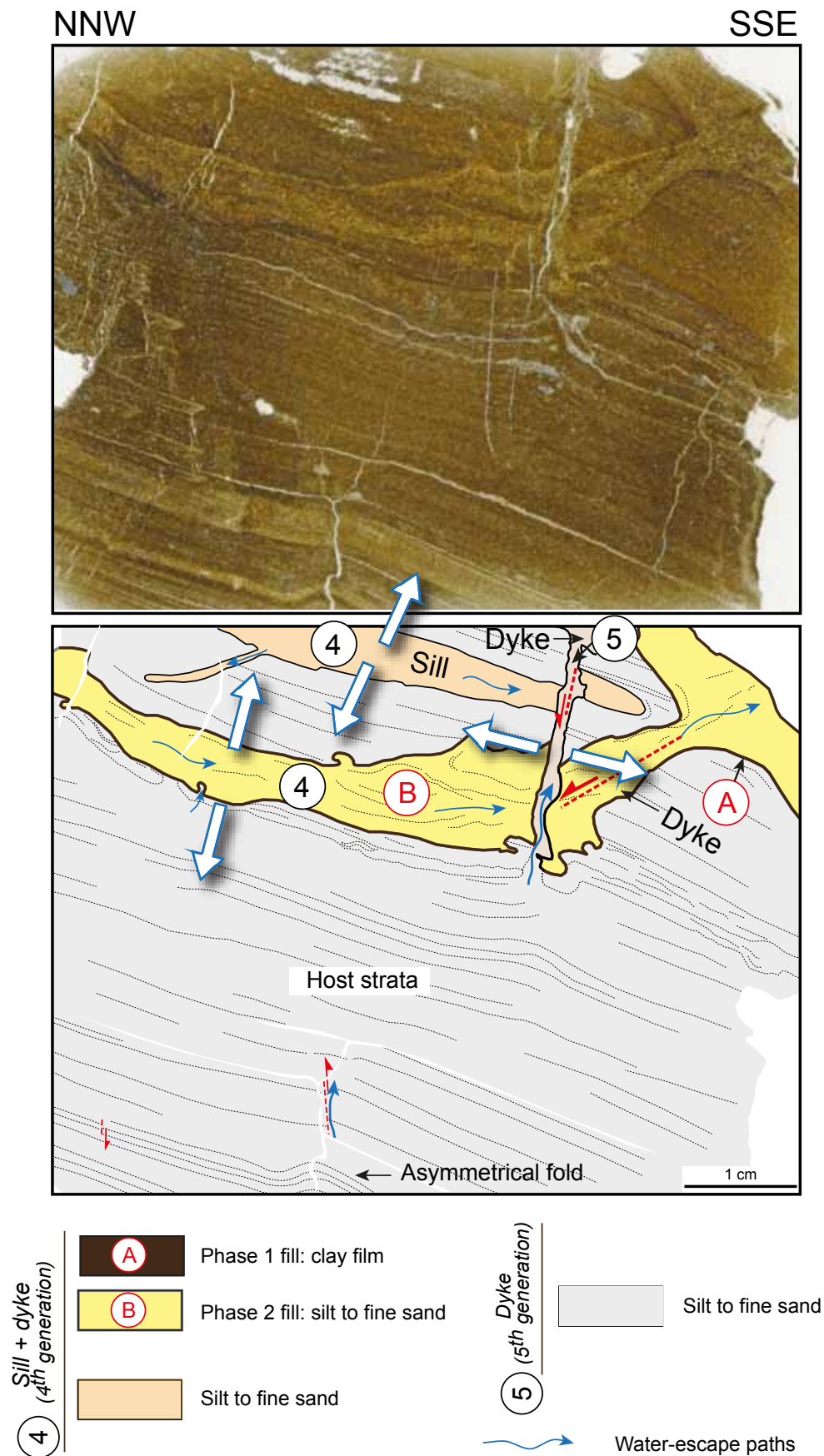


Figure 26. Scan and interpretation of sample 7. A dyke composed of homogenized silt to fine sand with a thin clay film on the sidewalls develop along a normal fault plane. This intrusion is followed by the development of an homogenized silt to fine sand-rich sill (4th generation). These two injections are cross-cut by the 5th generation of clastic injection, composed of a per ascensum clastic dyke propagating along a normal fault plane.

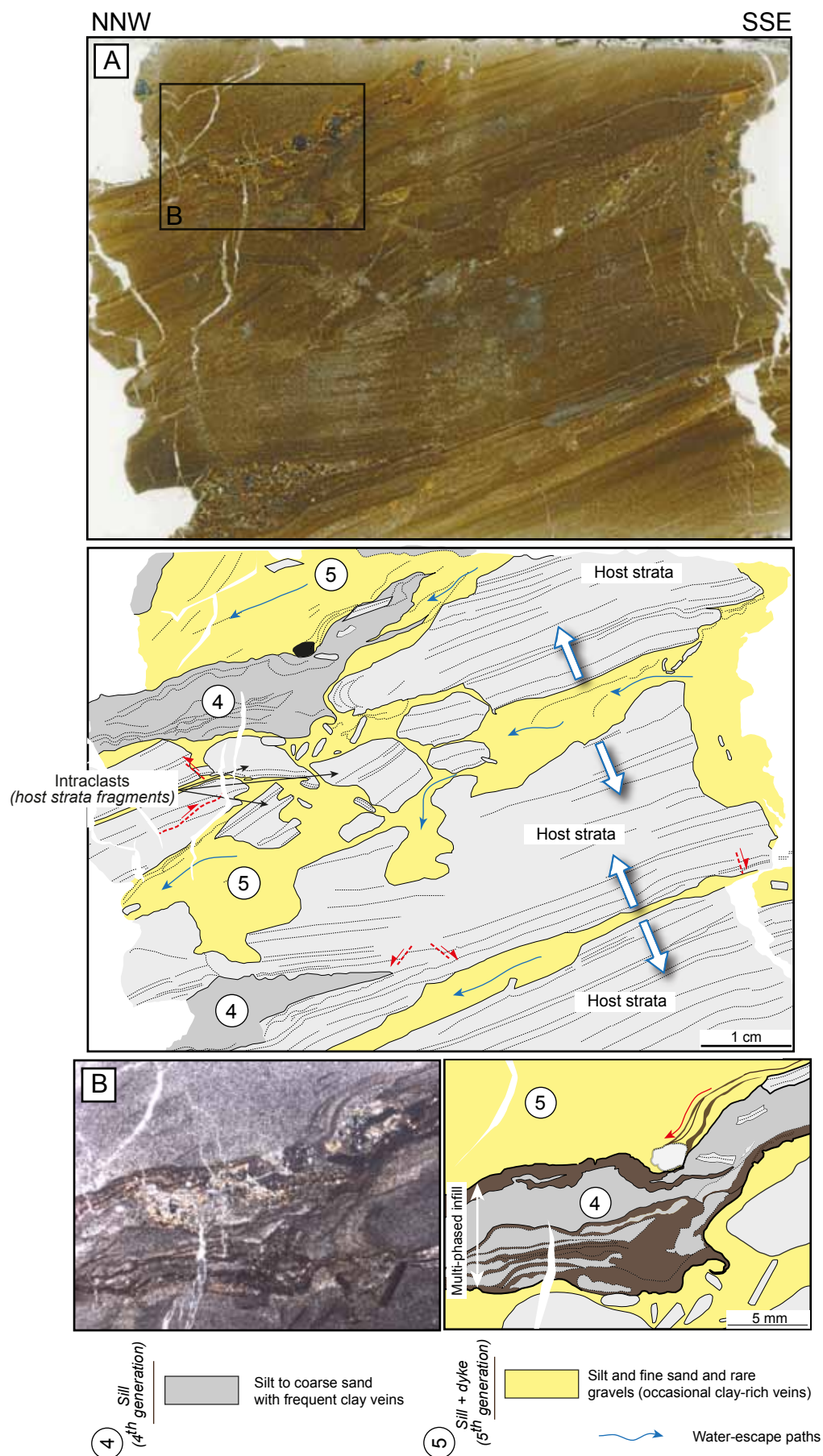


Figure 27. Scan and interpretation of sample 8. (A) A sill composed of silt to coarse sand (4th generation) is disrupted by the development of a network of dykes and sills filled by homogenized silt to fine sand (5th generation). The development of sills and dykes leads to intense brecciation of the host strata. (B) Close-up on the first generation of sill that is composed of silt to coarse sand with thin clay laminae suggesting multi-phased fill.

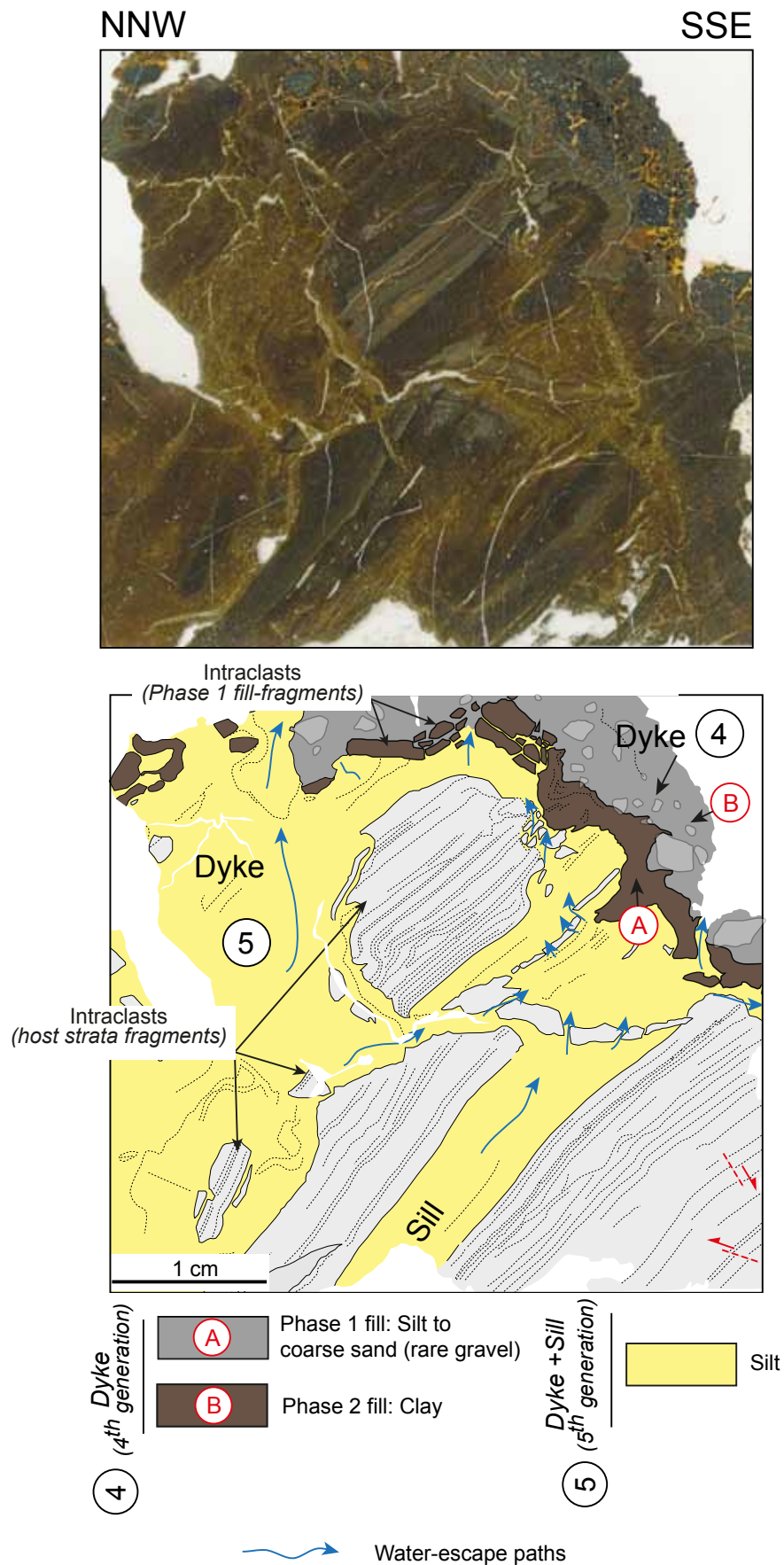


Figure 28. Scan and interpretation of sample 9. A dyke characterized by two phases of sediment fill (4th generation) is deformed and locally brecciated due to the development of a second generation composed of dykes and sills (5th generation). This second generation of dyke and sill is composed of homogenized silt with floating intraclasts.

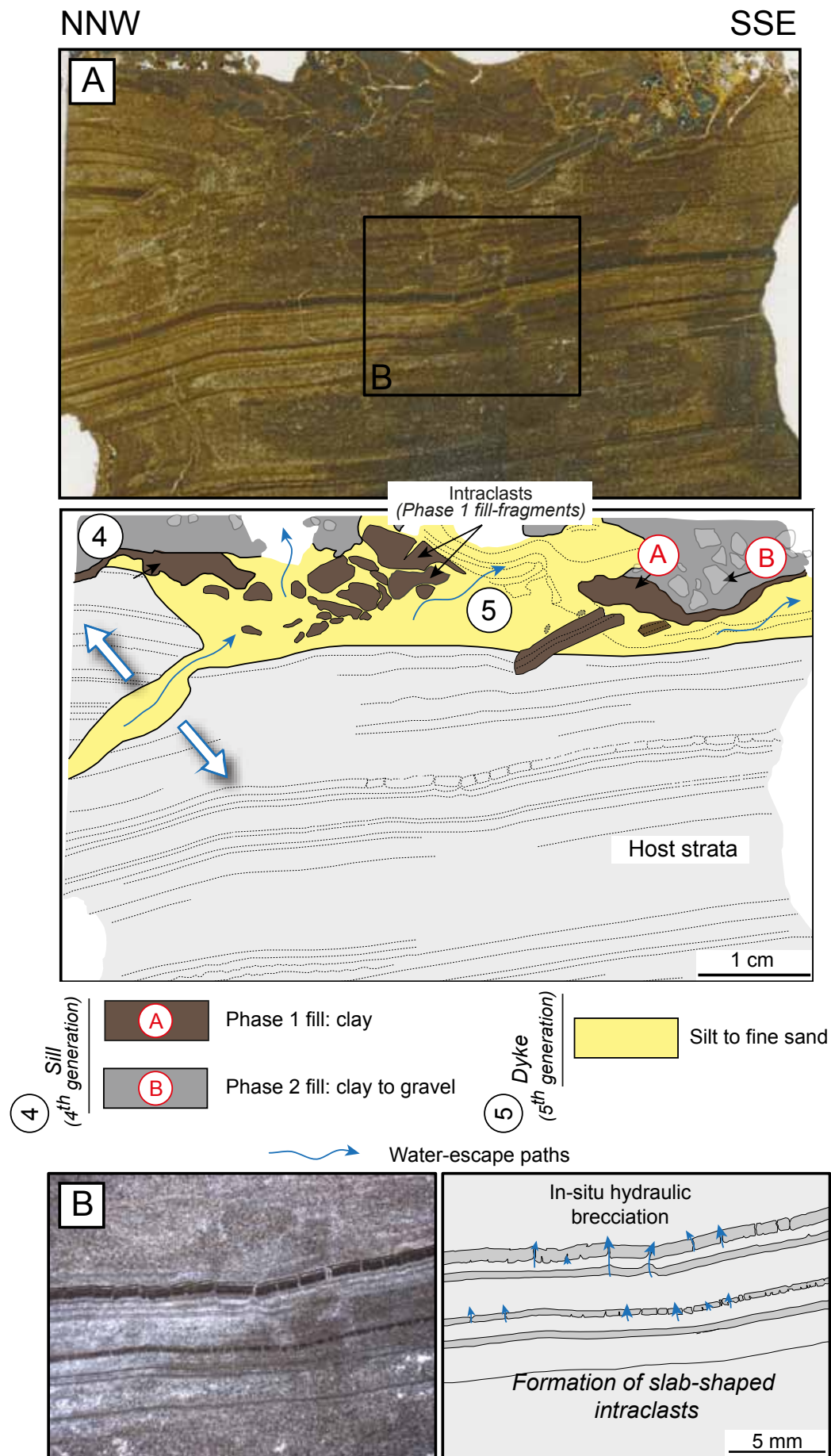


Figure 29. Scan and interpretation of sample 10. A sill characterized by two phases of sediment fill (clay + sand to gravel) is deformed and locally brecciated due to the development of a second generation composed of dykes propagating upwards (5th generation). The 5th generation of clastic injection is composed of homogenized silts with floating intraclasts.

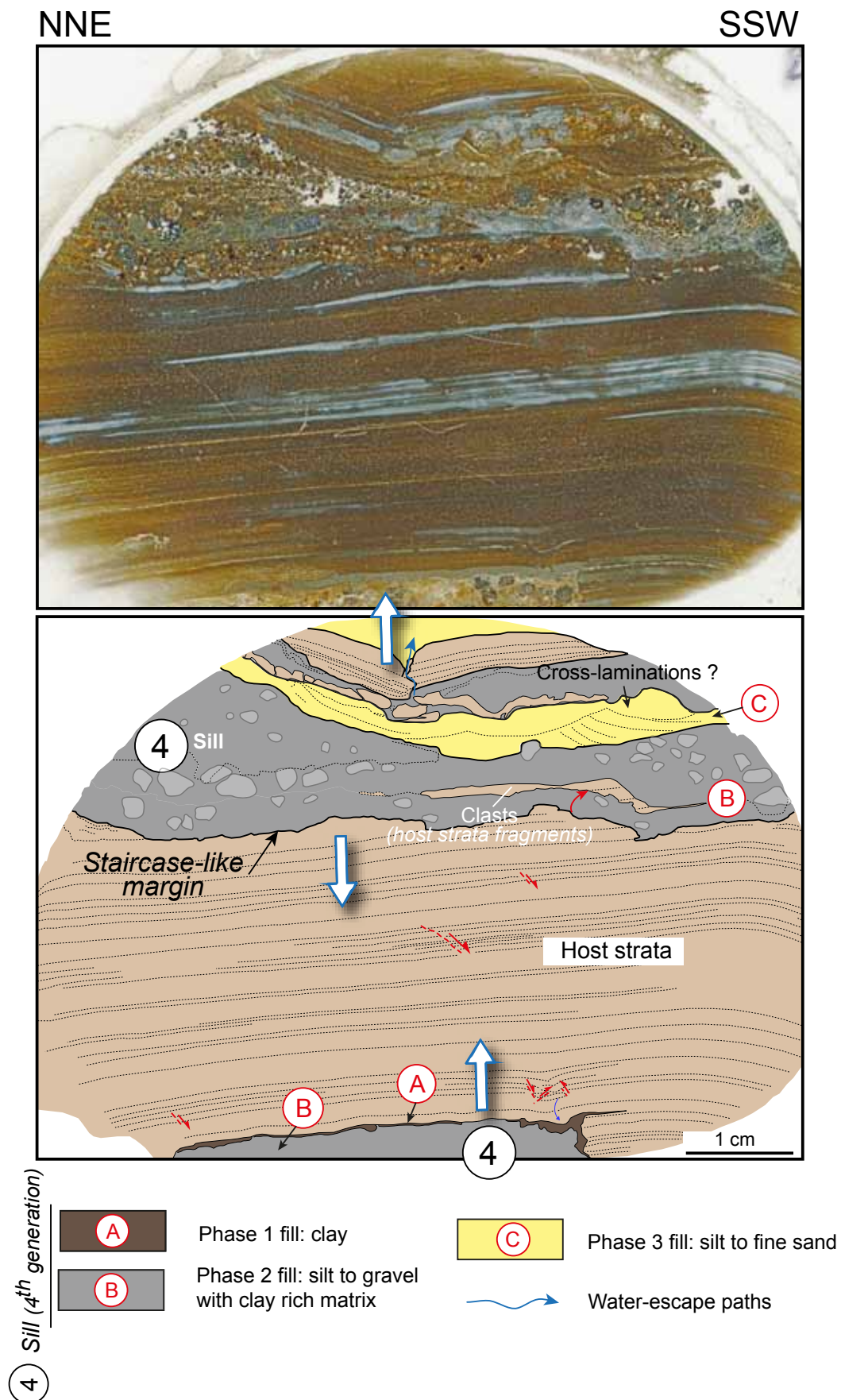


Figure 30. Scan and interpretation of sample 11. This sample displays sills that are characterized by three phases of sediment-fill (4th generation). Clay-rich fill is observed on the margins of the lower sill. The second phase is characterised by the injection of silt to gravel with a clay-rich matrix. The third phase of sediment fill is composed of silt to fine sand and seems to contain pseudo cross-laminations with SSW current directions. Note the staircase-like erosion of the sill margins.

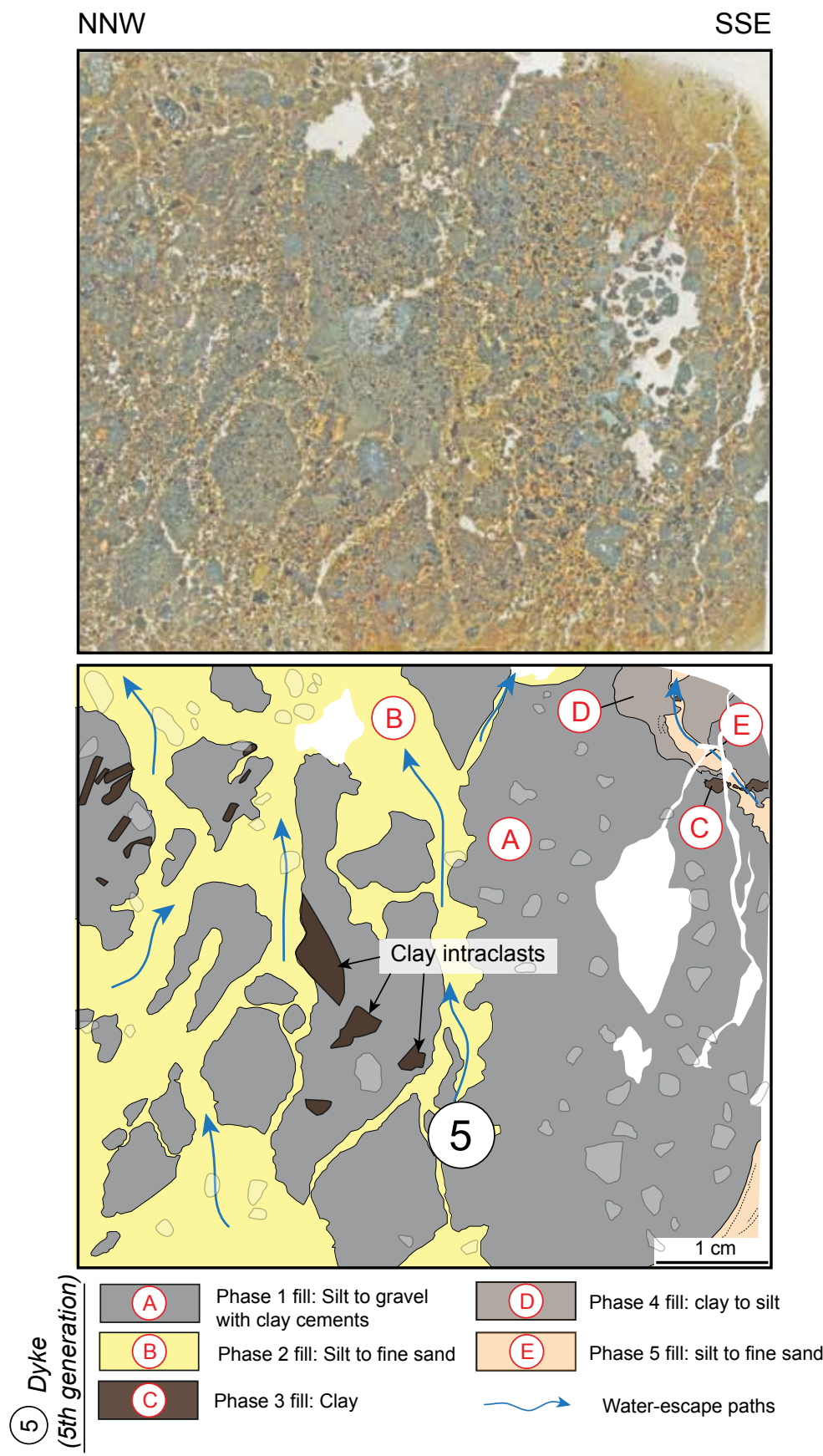


Figure 31. Scan and interpretation of sample D1. This sample is taken within a per ascensum clastic dyke corresponding to the 5th generation. At least 5 phases of sediment-fill can be depicted within this dyke. The first one corresponds to the emplacement of silt to gravel with a clay-rich matrix. The second generation leads to the brecciation of the first phase of sediment-fill. The third, fourth and fifth phases of sediment-fill are characterized by small clay to fine sand laminae in the right corner of the thin section.

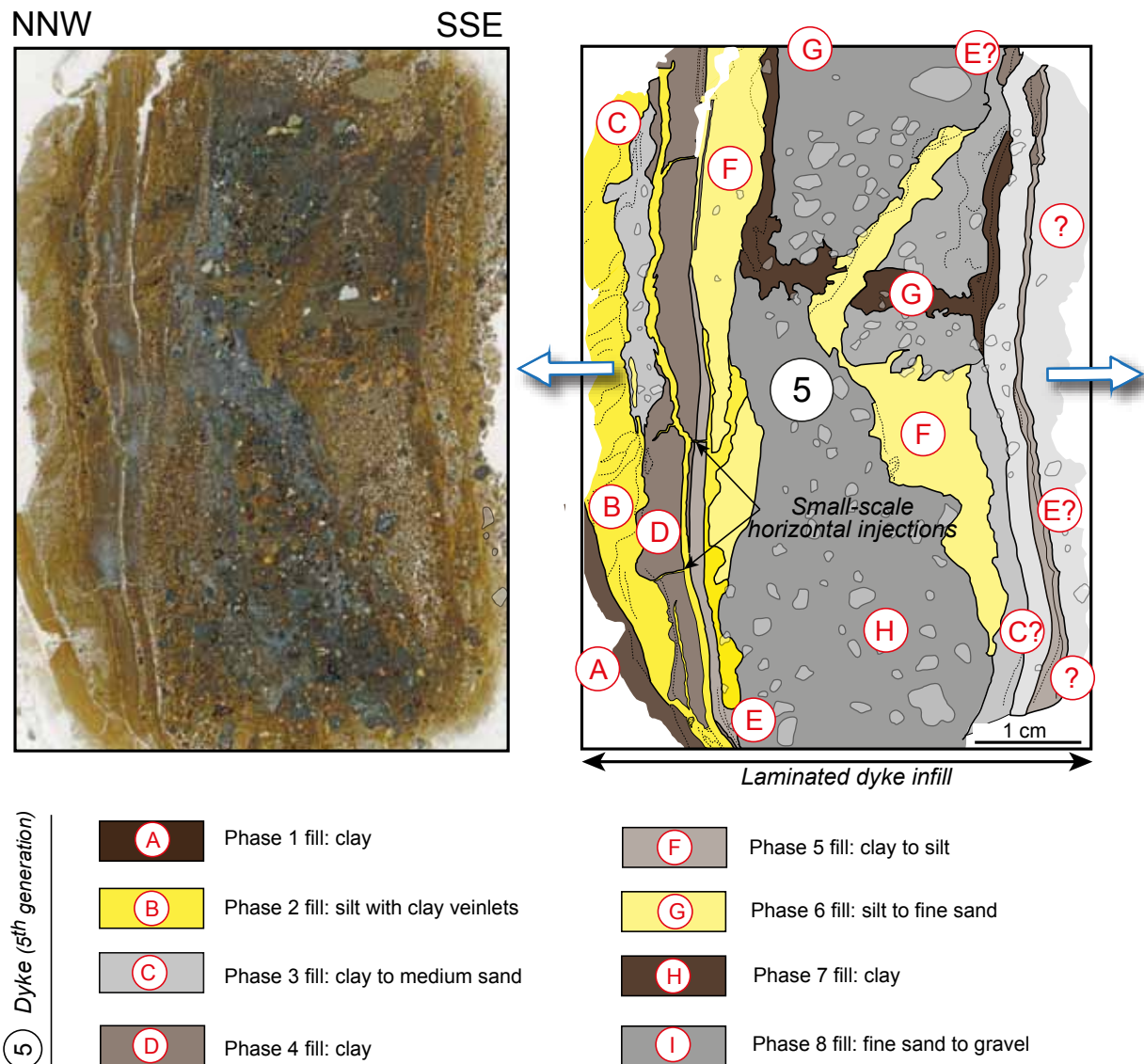


Figure 32. Scan and interpretation of sample D2. This dyke is composed of multi-phased fill (over 8 phases) with an increase of grain-size towards the centre of the dyke. Note that some laminae once injected can be later remobilized and form small-scale horizontal injection cross-cutting other laminae.

fractures illustrating that formation of intraclasts may have been triggered by hydrofracturing (Fig. 22).

5.2.2. Clastic injection morphologies (micro-scale)

Within fine-grained laminated sediments, sills are predominant and their thickness range between 0.5 cm and 5 cm. Dykes range between 0.5 cm and 3 cm thick. Sills develop along bedding, especially along low-permeability clay or tephra layers while dykes tend to propagate upwards and appear to

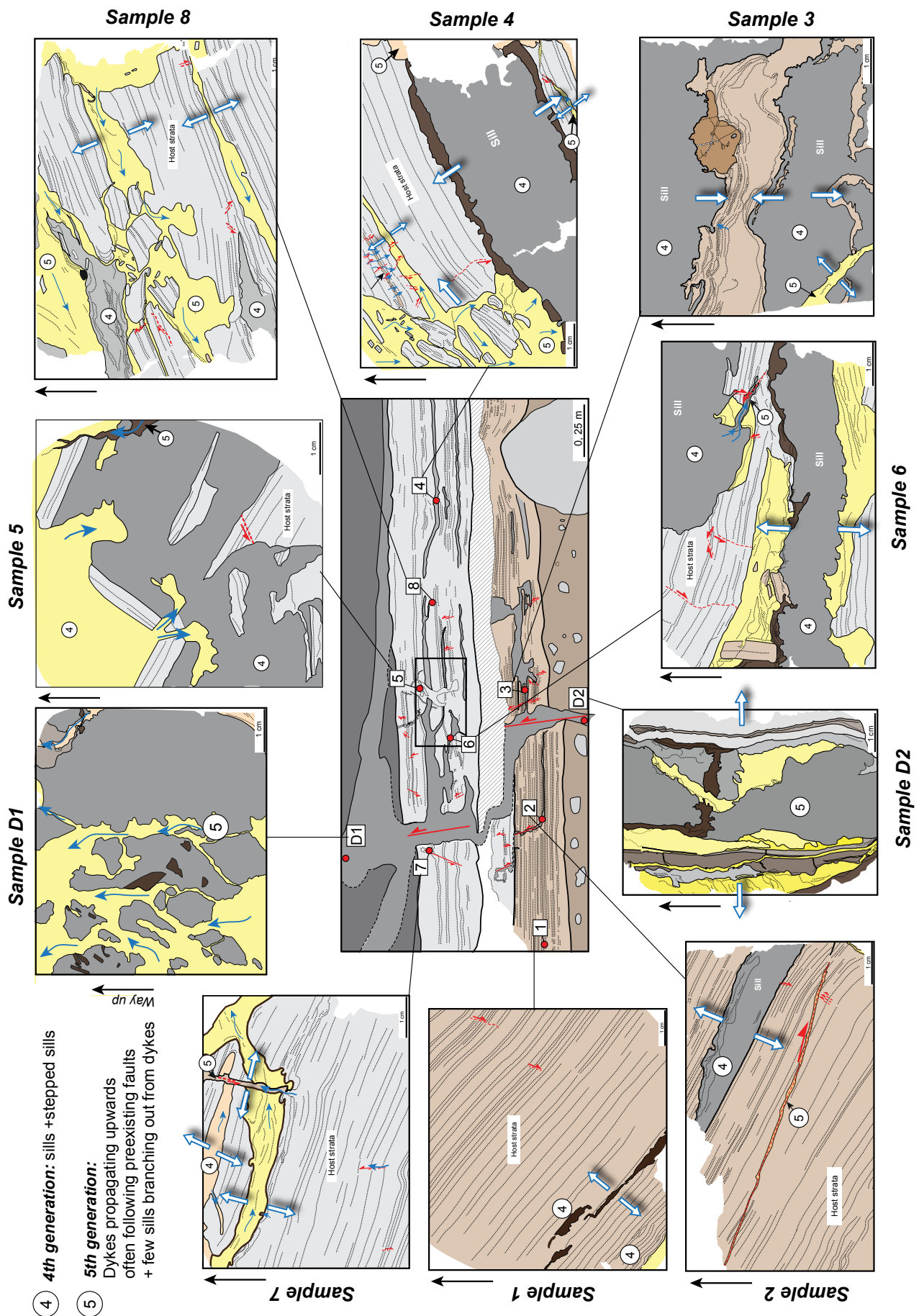


Figure 33. Diagram showing the positions and interpretations of the samples 1 to 8, D1 and D2 collected within the fine-grained laminated sediments (F5).

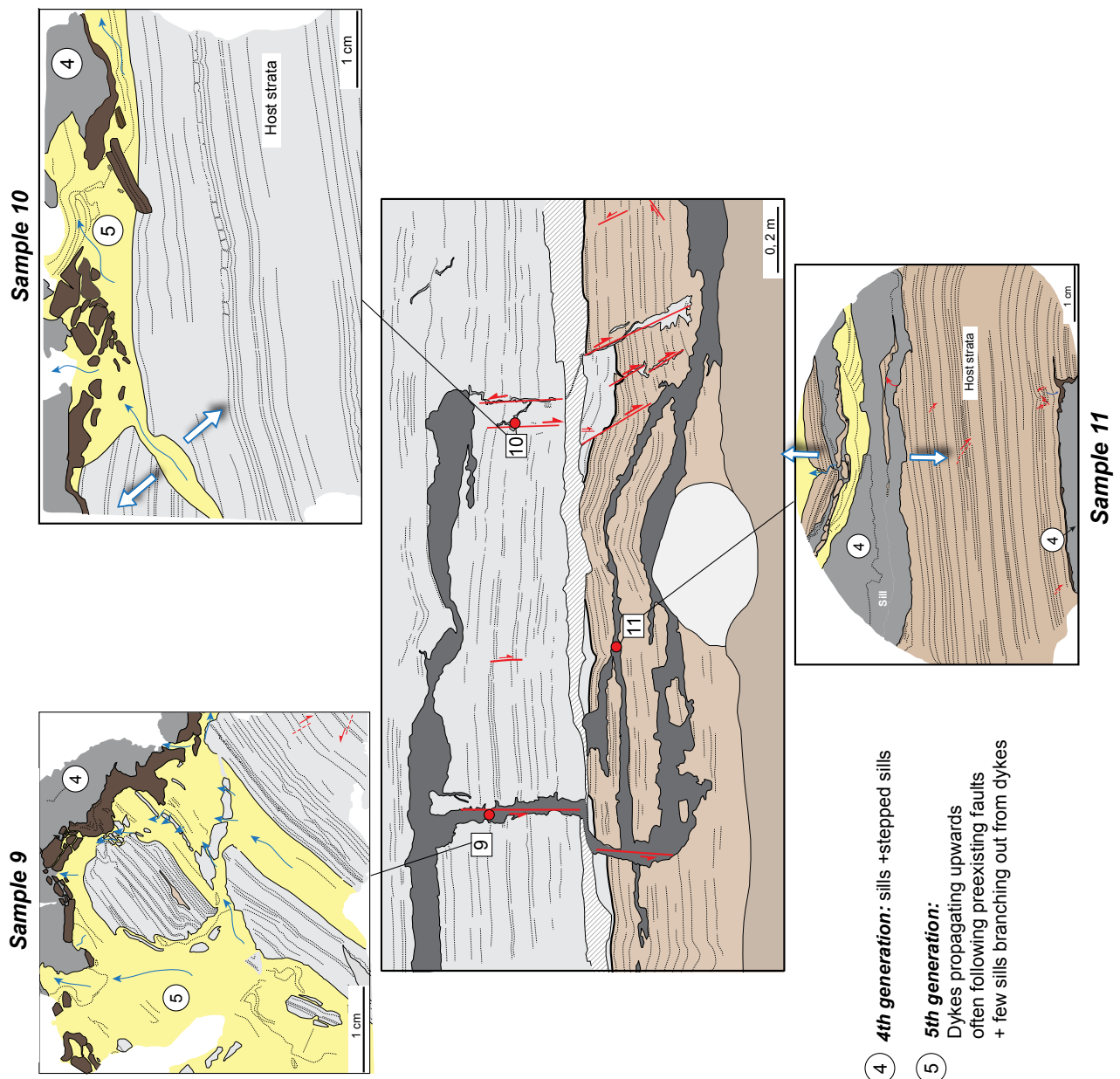


Figure 34. Diagram showing the positions and interpretations of the samples 9 to 11 collected within the fine-grained laminated sediments.

develop along preexisting fault planes (either reverse or normal faults) (**Figs. 20, 21, and 26**). The contacts between injected material and host sediments are generally erosive resulting in contorted and angular margins, especially when sand to gravel are injected (**Figs. 22, 23 and 25**). Erosional processes occurring at the margin of the injections are also emphasized by the recurrence of angular intraclasts. Intraclasts result from host strata fracturing, detachment and remobilization. Some intraclasts are sometimes impinged on the wall of the injection (**Fig. 22**). Occasionally, contacts between sills can be sharp with straight margins following horizontal bedding, especially along thicker clay beds (**Fig. 21**). “Staircase-like” margins and scours are locally observed along the margins of few sills (**Figs. 22, 25 and 30**).

5.2.3. Characteristics of sediment-fill (micro-scale)

Within most samples, sills and dykes coexist and cross-cut each other allowing to estimate the timing of injection. The fine-grained laminated deposits are cross-cut by the 2nd, 4th and 5th generation of clastic injections that have been determined at the macroscale (**Figs. 15 and 16**). Within single injections (sills or dykes), different phases of sediment-fill induced by several episodes of sediment injection can also be determined.

• Sills

All samples collected in laminated deposits display sills characterized by similar sediment-fills. Two main phases of sediments fills can be determined, referred to as the A- and B-phases in the interpretation of thin sections.

- Samples 2, 4, 6, 10, 11 display the A-phase characterized by clays deposited adjacent to the sill margins (**Figs. 21, 22, 23, 25, 29 and 30**). Injected clays are generally massive even though crude laminations are sometimes distinguished. The thickness of the clay-rich fill varies between 0.5 and 2 mm. In many samples, this first phase of sediment-fill is frequently eroded during the other phases of sediment injection. In response to erosion and fracturing, the clay-rich fill deposited parallel to the wall of the intrusion is discontinuous, or/and fractured, or even brecciated (**Figs. 23, 25 and 29**).

- In samples 4, 6, 8, 10 and 11, the phase B is composed of sand to gravel with local high silt to clay contents (**Figs. 23, 25, 29 and 30**). Clay coatings or clay matrix (i.e., clay cutans) are occasionally observed around grains within this second phase of sediment-fill and preferentially accumulate along the sill sidewalls. Clay coatings totally or partially surround grains while clay matrix completely fills

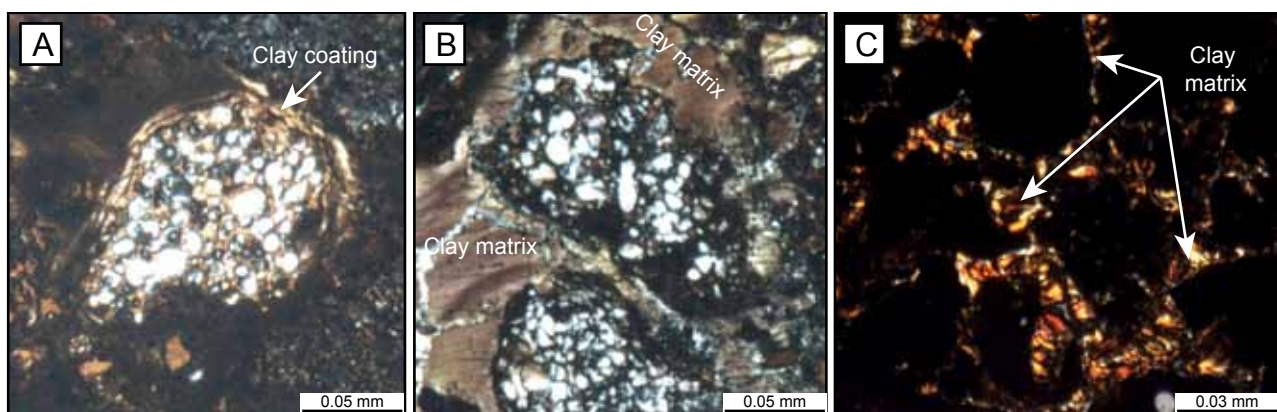


Figure 35. (A) Clay coatings characterized by a mm thin film of clay-sized particles totally surrounding a grain (sill, sample 11). (B) Clay matrix filling the free pore spaces (sill, sample 11). (C) Clay matrix filling free pore space in sand (dyke, sample D2).

the free pore spaces (Fig. 35A, B). Two main origins can be proposed for the emplacement of these clay coatings and matrix: the first model involves injection and deposition of an admixture of sand, gravel, and clays while the second model suggests late infiltration of clay-rich pressurized meltwater within gravely sand and deposition of clay into pore throats.

In sample 11, an additional phase of sediment-fill occurs (the C-phase) and is characterized by silt to fine sand inside which ‘pseudo’ cross-laminations are occasionally preserved (**Figs. 30 and 36**). Cross-laminations record an apparent southwesterly directed palaeoflow (**Fig. 36**).

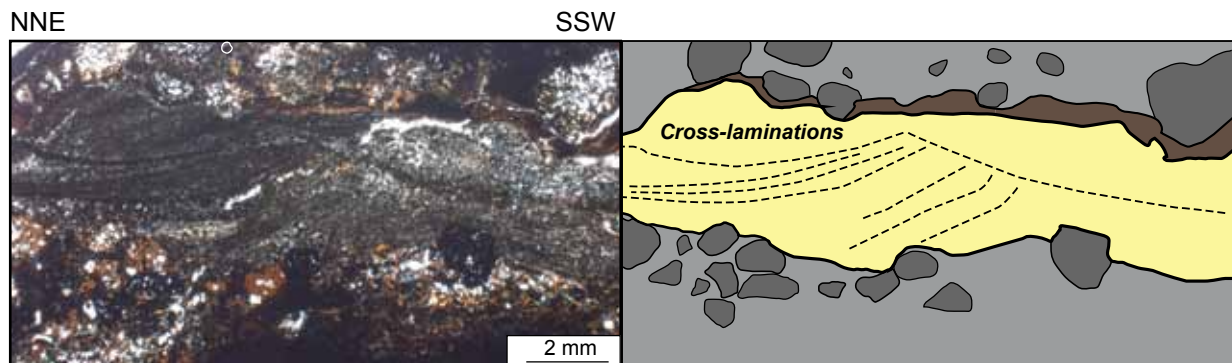


Figure 36. Close-up on cross-laminations observed within the third phase (C-phase) of sediment-fill observed in the sill (sample 11).

The emplacement of the different phases of sediment-fill is generally associated with the erosion and occasional fracturing of the host strata as illustrated by the abundant angular and slab-shaped clayey intraclasts embedded in the sills (**Figs. 24, 27, 29 and 30**). The last generation of sill formation occurs together with the formation of dykes (5th generation), and is generally composed of homogenized silt. The development of these networks of closely spaced sills and dykes trigger intense fracturing and brecciation of the host sediments (**Figs. 23, 27, 28 and 29**).

• Dykes

Most of the dykes are composed of homogenized silt to fine sand with occasional high clay content. Dykes are often associated with the late generation of sills previously described (5th generation) (**Figs. 23, 24, 27, 28 and 29**). These dykes are generally few mm thick with few examples reaching several cm thick.

Samples 7 and 9 display dykes that are composed of a first phase of clay-rich sediment-fill (A-phase) adjacent to the margins and a second phase of sediment-fill either characterized by silt to coarse sand with rare gravels or by homogenized silt to fine sand (B-phase) (**Figs. 26 and 28**). These dykes are characterized by the two same phases of sediment-fill distinguished in the sill generation (4th

generation), suggesting that they are closely associated and probably penecontemporaneous. Samples D1 and D2 collected within larger dykes show that dyke infill can be thinly laminated or more massive. Sample D1 was collected in the core of a 0.2 m thick dyke propagating upward (**Figs. 18 and 31**). The core of the dyke is chaotic and displays angular intraclasts of coarse sand to gravel cemented by clays. Intraclasts are slab-shaped and embedded within silt to medium sand (**Fig. 31**). The clay matrix contains within these angular clasts of coarse sand to gravel is totally filling the pore spaces (**Fig. 35C**). Inversely, the sample D2 collected in a vertical dyke displays a thinly laminated sediment-fill (**Figs. 18 and 32**). Over 14 laminations injected parallel to the dyke margins indicate that sediment-fill occurred through repeated phases of fluid flow. Margins of laminae are often very irregular or even truncated as a result of erosion by repeated fluid flows. The thickness of the different laminae varies between 0.2 and 3 cm. In sample D1, over 8 phases of sediment-fills are recognized with a general trend of grain-size increase towards the centre of the dyke. Once injected within the dyke, sediments can be later remobilized as illustrated by vertical laminae being laterally injected, thus transgressing horizontally other laminae (**Fig. 32**).

5.2.4. Cross-cutting relationships

Most of the thin sections contain the 4th generation of clastic injections affecting the host sediments. This fourth generation is generally characterized by sill morphologies that are filled by clays along the margins with a core composed of sand to gravel. During the emplacement of this gravel-rich sill system, a few dykes characterized by similar composition develop at the same time illustrating the development of vertical connections between sills (i.e., stepped sills) (**Fig. 28**). These connections between sills are often controlled by the presence of preexisting fault planes (**Figs. 18, 19 and 26**). The fifth generation has also been depicted at the microscopic scale, and generally cross-cuts sills of the 4th generation (**Figs. 26 and 29**). This latest generation displays dykes mainly propagating upwards (i.e., *per ascensum*) and sometimes associated with the propagation of sills (**Figs. 23, 27 and 28**). The predominant sediment-fill of the 5th generation is characterized by homogenized fine-grained deposits varying from clay to fine sand.

6. Multi-scale synthesis of clastic injection generations (micro- to macro-scales)

Different generations of clastic injections with different dips, geometries, and senses of propagation have been evidenced at the different scales. These observations allowed to define 5 main generations of injections characterized by different sediment-fills.

(1) The first generation of dyke is predominantly composed of *per descensum* and high-angle clastic dykes dipping towards the SSE (**Fig. 37A**). This generation is responsible for the formation of thick clastic dykes (up to 1.5 m thick) that are mainly composed of laminated light brown clays and light brown diamicton with an increase of the grain-size towards the centre of the injection. Grain-size size and colour analyses demonstrate that Till 2 is the source bed during sedimentary infill of the first generation of clastic injections.

(2) The following generation of clastic intrusions is constituted by *per ascensum* clastic dykes originating from the upward remobilization of sediments contained in the first dyke generation (**Fig. 37B**). This generation is composed of thin dykes (up to 0.1 m thick) that sometimes cross-cut each other. Sediment-fill is mainly characterized by light brown silt to clay containing sparse granules and gravels. These clastic dykes frequently cross-cut the overlying till, but also the pond and glacifluvial deposits.

(3) Few high-angle *per descensum* clastic dykes, dipping towards the SSE and filled by dark grey silt or sand along the sidewalls, represent a third phase of clastic intrusions. This phase of intrusion displays dykes that can reach 0.4 m thick. This generation of injection takes its source in the glacifluvial deposits (F3/F4) (**Fig. 37C**). The light brown diamicton observed in the core of these dykes indicates changes in sediment source through time. In addition, the occurrence of coarse sand in the core of 1st generation dykes implies local reopening of older injections (**Fig. 37C**).

(4) The fourth generation of clastic injection is characterized by the development of sills and stepped sills filled by dark grey silt and sand (**Fig. 37D**). Micro-scale observations show that clays were first injected in the sills as illustrated by the thin clay laminae along the sidewalls. The sediment-fill of this fourth generation derives from the remobilization of different source beds including glacifluvial, pond and till deposits. Lenticular pods containing cross-laminations or fining-upward sequences occasionally occur within this generation.

(5) The last phase is composed of high angle *per ascensum* clastic dykes with few branching out sills. This last phase is generally composed of thin dykes (< 0.1 m) displaying a wide range of sediment-

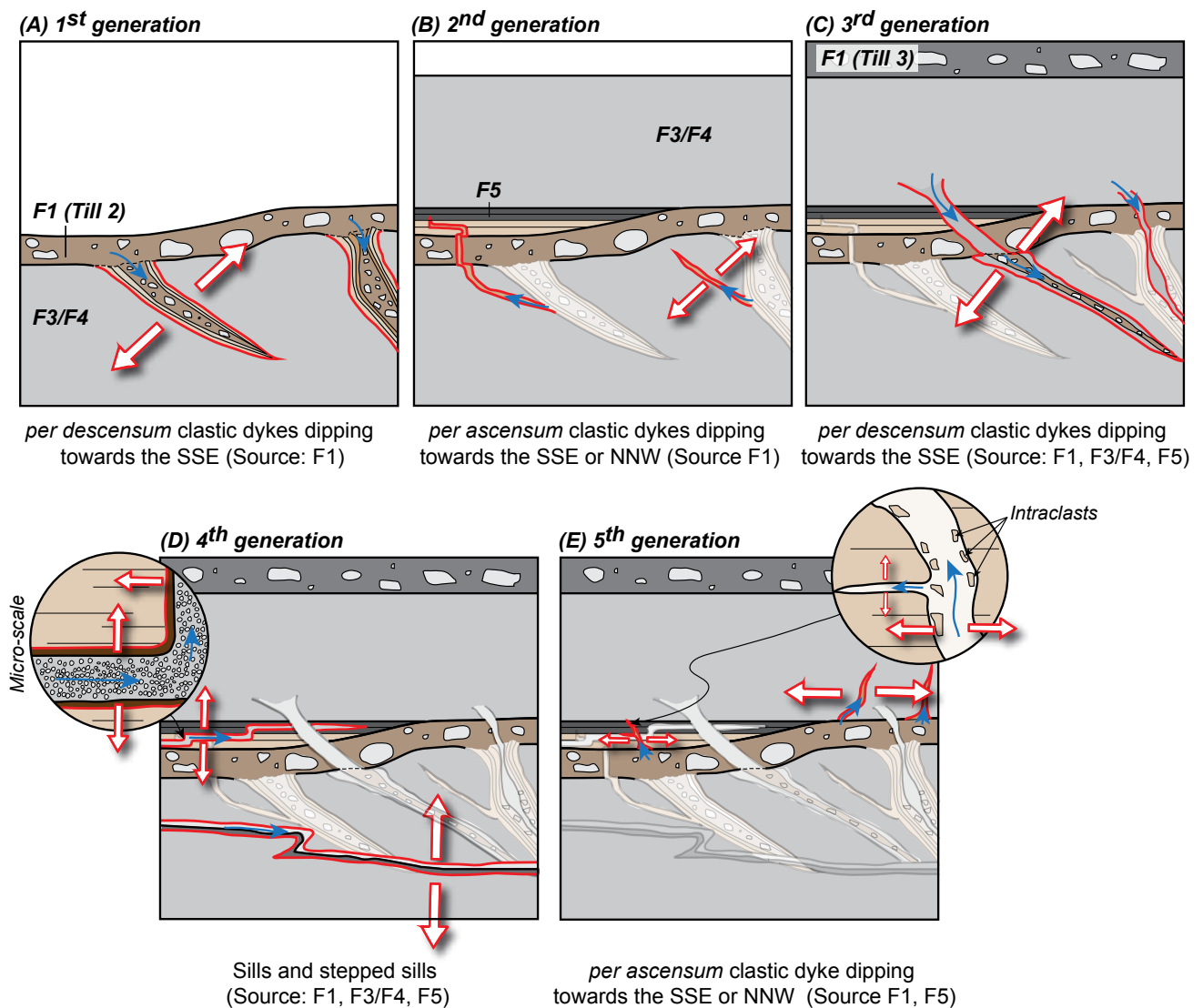


Figure 37. Schematic diagram showing the morphology and sediment-fill of the five main generations of clastic intrusions distinguished in the Sólheimajökull clastic injection network.

fill, from clay to gravel, with locally abundant intraclasts of host sediments (**Fig. 37E**). Sediment fill is generally homogenized and injections often follow preexisting fault planes.

7. Discussion

7.1. Depositional model

The sedimentary sequence was deposited in proglacial to subglacial environments. At the base of the section, glaci-fluvial deposits (F3/F4) record channel incision, infill, and abandonment in a braided network. This depositional setting is evidenced by channelized morphologies, boulder lags, and migration of 2D/3D dunes within channels. The glaci-fluvial deposits are overlain by a 0.5 m thick

and extensive sheet-like subglacial lodgement tills (F1) demonstrating a phase of glacier growth and advance. The top of the till deposits is irregular forming topographic lows where water can accumulate. The localised and thin deposition (up to 1 m) of fine-grained laminated deposits (F5) mainly result from suspension settling, suggesting formation of a pond where quiescent water accumulates. Preservation of tephra layers within the laminated deposits indicate that the pond developed in proglacial settings. The presence of collapsed structures within F5 draped over by laminated sediments suggests melting of buried ice and implies temporary drainage of the pond. This laminated facies, overlain by a 4 m thick sequence of gravely sand (F4), displays trough cross-stratifications and stacked fining-upward sequences, illustrating the development of a proglacial outwash plain. Trough cross-bedding structures are related to sediment deposition by migrating 2D/3D dunes within a channelized system, while repetitive fining-upward sequences suggest sheetflood deposition. This sequence of glacial fluvial sediments is overlain by a 0.8 m thick dark grey fissile and overconsolidated subglacial lodgement tills (F1), suggesting a phase of glacier readvance. The section is topped by a melt-out till deposited by the passive release of subglacial, englacial and supraglacial debris from melting ice during the retreat of the Sólheimajökull outlet glacier.

7.2. Trigger mechanisms and processes involved in the formation of the Sólheimajökull clastic injection network

7.2.1. Hydrofracturing

Assuming that the clastic injection system observed along this section do not represent neptunian dykes (cf. section 7.2.2), the general series of events that leads to the development of a clastic injection network is well known: (1) elevation of porewater pressure into sealed sediments, (2) hydrofracturing, (3) fluidization and injection of clastic material (Jolly and Lonergan, 2002). Most of the clastic injection networks occurring in sedimentary environments including the glacial environments are thought to be initiated by hydrofracturing (Jolly and Lonergan, 2002; van der Meer et al., 2008; Hurst et al., 2010; Phillips et al., 2013). The development of hydrofractures is initiated when porewater pressure exceeds the tensile strength of the host sediments. The generation of high porewater pressure is promoted when permeable and water-saturated aquifers are sealed by low-permeability layers (Janszen et al., 2012; Ravier et al., 2014b). The configuration of the study site, where water-saturated gravely sand

alternates with low-permeability lodgements tills and fine-grained pond deposits, is optimum for the development of high porewater pressures. The high concentration of clastic injections below the localized 1 m thick low-permeability pond deposits (F5) demonstrate the control of the substratum lithology and stacking pattern on the development of hydrofractures (**cf. Fig. 6A**).

Numerous triggering mechanisms are assigned to the formation of hydrofractures and sediment injection, including for the most common case: (1) seismicity, (2) rapid loading by sediments, (3) fluid migrations into porous sediments, and (4) ice load (Obermeier, 1996; Hildebrandt and Egenhoff, 2007; van der Meer et al., 2009). In the area of investigation, these common triggers could all be envisaged.

(1) The outwash plain is located within the eastern volcanic zone of Iceland where active seismic activity is recorded (Jakobsdóttir, 2008). High-magnitude earthquakes (<6) are usually responsible for the formation of clastic injections 15-20 km from seismic epicentres (Rosetti, 1999).

(2) The rapid and massive deposition of sediments during outburst floods (jökhlaupt) will rapidly increase the overburden pressure due to rapid loading and could trigger hydrofracturing (Russell et al., 2005).

(3) The release of subglacial overpressurized meltwater within sealed porous sediments in marginal settings can trigger hydrofracturing (Boulton and Caban, 1995).

(4) The Sólheimajökull outwash plain has been subject to oscillations of the ice front during the Holocene implying that the stresses exerted by the ice load and ice flow on sediments could have triggered hydrofracturing (Sigurdsson, 2010).

The first and third generations of clastic injection are mainly composed of *per descensum* clastic dykes. These generations display a southwesterly dipping direction that is parallel to palaeo-ice flow direction. The formation of *per descensum* injection, characterized by a preferential dip direction oriented parallel to the palaeo ice flow direction, suggests that normal and shear stresses related to ice load and ice flow, were responsible for hydrofracturing (Clerc et al., 2012; Phillips et al., 2013; Ravier et al., 2014b). Glacier-induced hydrofracturing is the trigger mechanism proposed to explain the development of the clastic injections in the Sólheimajökull forefield, as suggested by Le Heron and Etienne (2005).

7.2.2. Processes of sediment injection

Clastic intrusions may result from processes of injection of liquefied/fluidized sand into hydrofractures or may alternatively result from passive infilling of fissures by sediments forming neptunian dykes (Smart et al., 1988; Jolly and Lonergan, 2002). Fluidization is regarded as the main process responsible for the injection of material into hydrofractures. In response to fluidization, sediment-fill is generally structureless, although internal banding or laminations have often been reported in clastic injections, especially within dykes (Diggs, 2007; Hubbard et al., 2007; van der Meer et al., 2009; Phillips et al., 2013).

In the Sólheimajökull injection network, the sediment-fills of clastic injections are characterized by laminae oriented parallel to the margins and are bounded by sharp contacts, defined by differences in grain-size. In addition, the laminae display a symmetrical distribution about the dyke or sill axes. Grain-size and colour analyses show that the material injected within hydrofractures derive from the host sediments including till (F1), glaci-fluvial sediments (F3/F4) and laminated fine-grained sediments (F5). These observations allow to reject a primary depositional origin because of the laminae orientation, distribution, and the identification of the source bed (Le Heron and Etienne, 2005). This implies that the system of intrusions is related to injection of sediments into hydrofractures rather than passive sedimentary infill of fissures. The formation of laminae in dykes and sills have been attributed to multiple episodes of sand injection, irregularities in the rate of fractures opening, or variations in both the velocity and viscosity of the injected material (Peterson, 1968; Taylor, 1982; Diggs, 2007). Le Heron and Etienne (2005) suggested that the symmetry of the laminae about the dyke axes results from repeated cycles of hydrofracturing and injections. This model of injection characterized by repeated opening and sedimentary fill of hydrofracture is similar to the «crack-seal» model (Ramsay, 1980). This model explains the formation of syntectonic veins by multistage crack opening and vein infill, in response to repeated variations in pressures (**Fig. 38**). The successive reopening of injections along the same axis could have been favored by the early clay to silt-rich sediment-fill deposited along the walls of the injection. This first phase of sediment-fill induces sealing of the adjacent hydrofracture walls, thus preferentially concentrating flow and high porewater pressures along the axis of the injection (Phillips et al., 2013).

The state of sediments during injection is difficult to determine. Hydrofractures are commonly followed by injection of fluidized sediments (Duranti and Hurst, 2004). Le Heron and Etienne (2005) suggested

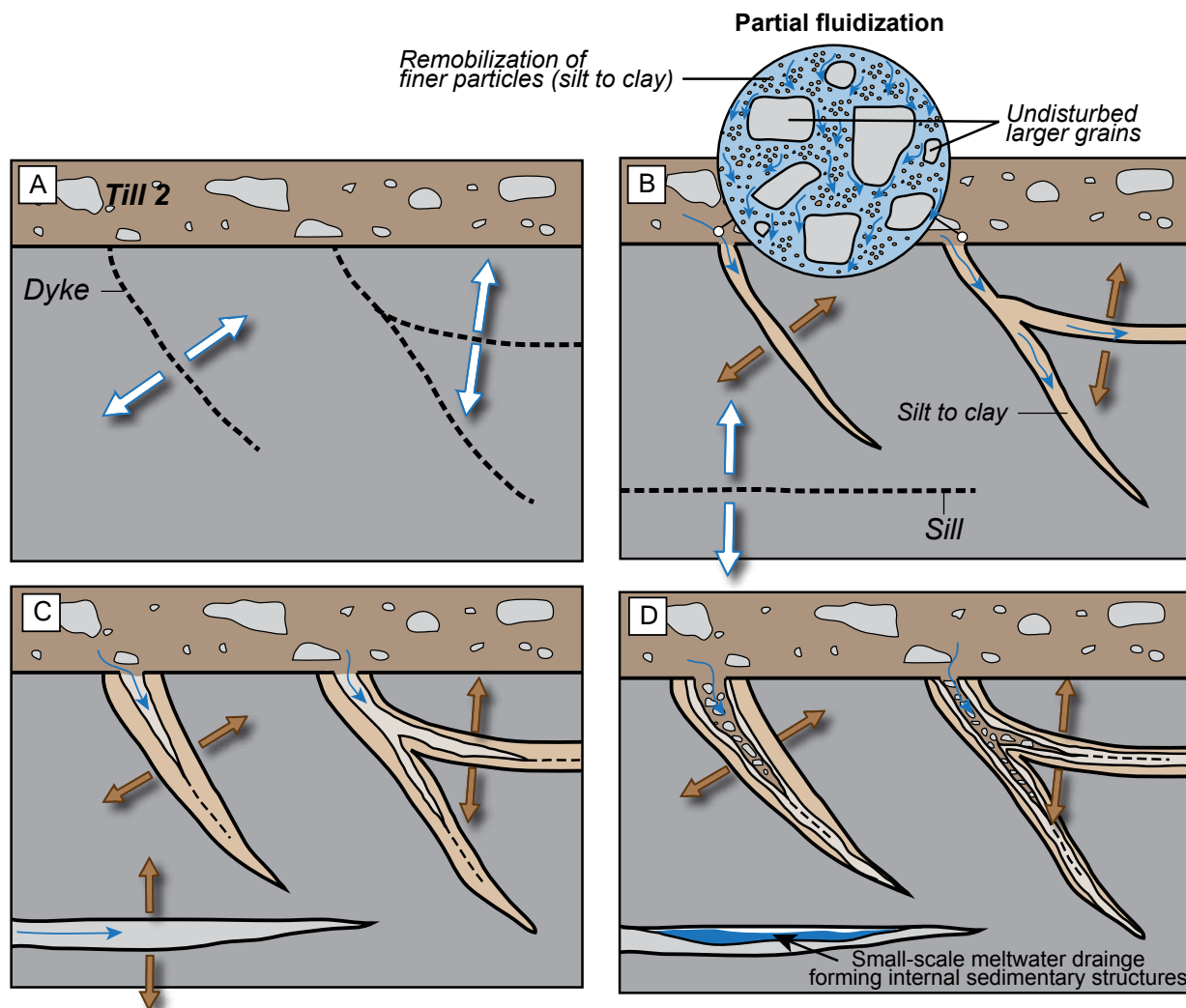


Figure 38. Schematic diagram illustrating the “crack-seal” model responsible for the formation of laminated clastic injections. (A) Hydrofracturing when porewater pressure exceeds the tensile strength of the host sediments. (B) Injection of fluidized sediments into hydrofractures characterized by turbulent flow conditions. Partial fluidization of the till is responsible for the injection of clays into hydrofractures. (C) The increase of porewater pressure leads to a new episode of hydrofracturing reopening the clastic dyke. Reopening is followed by a second phase of sediment-fill. (D) The multistage hydrofracturing and injections are related to the variations in porewater pressure, leading to the formation of laminated dyke-fill. The development of small-scale voids within sill-structures promote the development of traction currents and the deposition of sediments where cross-laminations are sometimes preserved.

that the Sólheimajökull hydrofractures swarm was not filled by injection of fluidized sediments, because of the occurrence of well-defined internal laminae parallel to sidewalls, and the absence of water-escape structures. New micro-scale observations evidence that hydrofracture sediment-fill were sometimes homogenized, indicating that sediments were fluidized during injection. The formation of intraclasts, their impingements along the sidewalls, the staircase erosion, and the overdeepened scours observed along the margins may suggest that turbulent-flow conditions could have operated during injection of sediments. Indeed, the erosion of the margins and the formation of intraclasts record the interaction between high-velocity, turbulent sand to gravel and the fracture surface of the host strata (Scott et al., 2009). In addition, the occurrence of structureless normally graded sequence in some sills indicates that sediment flow may have been turbulent during injection (Talling et al.,

2012) (**Fig. 13A**). Normal grading has been reproduced experimentally during the sedimentation of fluidized grains (Druitt, 1995). Evidence for turbulent flows are good indicators for fluidization as the fluidized flow-regime is thought to be turbulent (Obermeier, 1996; Duranti, 2007; Hubbard et al., 2007; Scott et al., 2009). Grain-size analyses show that injection and deposition of single laminae were not ruled by typical fluvial-like processes as illustrated by the Passega diagram (**Fig. 12**). However, the occasional and localized occurrence of cross-laminations within lenticular pods implies that deposition of sediments by tractive currents may have temporarily occurred during sediment-fill (**Figs. 13B and 36**). The presence of sedimentary structures within subglacial hydrofracture system has been interpreted to be the result of sediment deposition by water flowing through interconnected voids or cavities within clastic injections (Phillips et al., 2013). The sill systems may have behaved as a temporary and small-scale drainage network focusing fluid flows along bedding parallel intrusions, and allowing small-scale sedimentary structures to build up (**Fig. 38D**). The migration of the ripple towards the SSW suggests that water was flowing away from the ice front.

The new micro-scale data collected within the clastic injection system show that several processes of sediment injection may have operated: the injection of fluidized turbulent sediments, and the local deposition by traction currents (**Fig. 38**). Changes of processes involved during injections of sediments into hydrofractures have also been observed in the Meads of St John hydrofracture system where the style of injection was thought to change over time, and to be dependant of the hydrofracture morphologies and orientations (Phillips et al., 2013).

7.2.3. Evolution of the stress field during hydrofracturing: implications for oscillations of the ice margin.

Five main generations of clastic injections with different dips, geometries, and senses of propagation have been evidenced at the different scales. These different generations result from changes of the stress field through time (Clerc et al., 2012; Phillips et al., 2013) and reveal oscillations of the ice margin and variations in porewater pressures.

► The first generation characterized by *per descensum* clastic dykes dipping in a direction parallel to ice flow suggests subglacial hydrofracturing (Le Heron and Etienne, 2005; Clerc et al., 2012). Underneath flowing-ice, when porewater pressure exceeds the tensile strength of the host strata, hydrofractures develop parallel to the direction of principal stress (Cosgrove, 1995; Jolly and

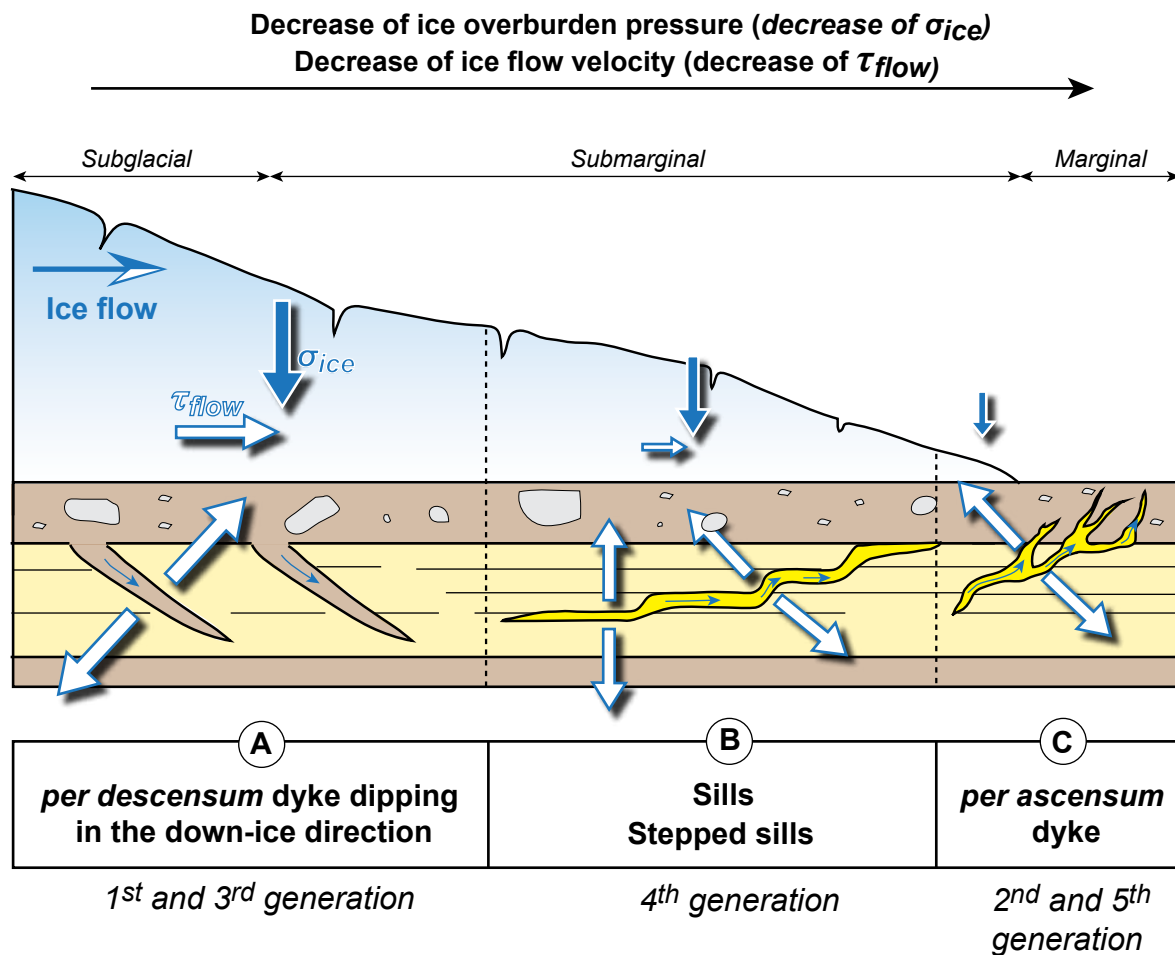


Figure 39. Schematic diagram showing the theoretical distribution of injection morphologies according to their positions underneath the ice. Dip directions, senses of propagation are controlled by stresses exerted on the bed during hydrofracturing. (A) The combination of the vertical stress induced by the ice load (σ_{ice}) and the horizontal stress induced by flowing-ice (τ_{flow}) (1st and 3rd generations) lead to the formation of per descensum dykes dipping down-ice. (B) In submarginal to marginal settings the decrease of the vertical stress related to the decrease of ice thickness favours the development of sills and stepped sills (4th generation). (C) At the ice margin, hydrofractures tend to climb upward in response to the significant decrease in ice overburden pressure (2nd and 5th generations).

Lonergan, 2002). *Per descensum* dykes dipping in the down-ice direction suggest that hydrofractures occurred subglacially due to combined normal and shear stresses, induced by the ice load (σ_{ice}) and the ice flow (τ_{flow}) respectively (**Fig. 39A**).

► The second generation of hydrofractures with prevailing *per ascensum* dyke morphologies suggests a net decrease in the overburden pressure, allowing hydrofractures to climb upwards (Boulton and Caban, 1995; Murdoch, 1995; Phillips et al., 2013). The decrease of overburden pressure is related to a decrease of the ice thickness, indicating that hydrofractures occurred in a marginal position (**Fig. 39C**). This phase of marginal hydrofracturing cross-cut proglacial deposits (ponds and glaciifluvial deposits), illustrating a phase of glacier readvance and southward migration of the ice marginal zone where overpressures and hydrofractures can develop.

► The third generation is composed of *per descensum* clastic dykes dipping parallel to the ice flow

direction, indicating that the ice front was still advancing and migrating towards the south. This third generation developed subglacially during ice-bed coupling and are probably contemporaneous to the deposition of the dark grey fissile subglacial lodgement till (Till 3).

► The fourth and fifth phases of hydrofracturing are formed during progressive retreat of the ice front. The development of sills and stepped sills during the fourth phase suggests a decrease in the vertical overburden stress exerted on the underlying bed (**Fig. 39B**). The last phase of clastic intrusions corresponds the development of *per ascensum* clastic dykes. Clastic dykes climbing upwards indicate that hydrofracturing occurred in marginal settings, and that the overpressure dissipates towards the surface as the result of a net decrease in overburden pressure (**Fig. 39C**). During the development of these two last generations, hydrofractures tend to propagate along planes of weakness as the vertical and horizontal stress considerably decrease in the marginal environment. In this configuration, the bedding anisotropy promotes the formation of sills and stepped sills. When preexisting fractures characterized by little or no tensile strength occur in the host sediments, the porewater pressure only needs to exceed the stress normal to the fracture for hydrofractures to form (Jolly and Lonergan, 2002). This explains the occurrence of numerous dykes using preexisting fault planes to develop.

7.2.4. Porewater pressure variations during sediment-fill

Characteristics of the sediment-fills, with internal variations in grain-size, imply variations in the porewater pressure during the multi-episodic hydrofracturing and sediment injections. The size of particles that can become remobilized during injection is dependant on the fluidization velocity and the porewater pressure (Lowe, 1975). The general trend of grain-size increase towards the centre of the injections could either correspond to variations of porewater pressure during the successive phases of injections, a progressive compositional change in the source bed, or a change in the source bed between the different episodes of injection. In the first generation of hydrofractures, clay and diamicton laminae originating from Till 2 are successively injected into the fractures. These repetitive variations in grain-size suggest that different granulometric classes were remobilized from the same source bed, and injected into hydrofractures. Multimodal sediments are likely to show fluidization of the smaller particles within the pores of undisturbed larger grains explaining the grain-size segregation between the different episodes of injection (Lowe, 1975) (**Fig. 39B**). This type of fluidization is referred to as partial fluidization (Lowe, 1975). The recurring pattern of grain-size increase towards

the centre of the injection suggests a progressive increase of fluidization velocity and porewater pressures during the successive “crack-seal” events. Marginal clay and silt laminae are associated with the elutriation of clay and silt within the pores of the till and are associated with lower porewater pressures, while higher porewater pressures lead to the remobilization of the entire till deposits, including small particles and larger grains (Lowe, 1975).

Although clastic injections have widely been reported as structureless (Hillier and Cosgrove, 2002; Parize et al., 2007), internal laminations are frequently observed in glacially-induced clastic injection networks (Le Heron and Etienne, 2005; van der Meer et al., 2009; Phillips et al., 2013; Phillips et Hughes, 2014). These laminated hydrofracture-fills could be explained by the characteristics of glacial environments. Indeed, these environments represent very dynamic systems where porewater pressures highly fluctuate through time (Boulton et al., 2001), promoting multi-episodic hydrofracturing and injection.

7.3. Possible evidence of small-scale marginal diapirism

Localized and syn-depositional deformation structures affecting the fine-grained laminated deposits (F5) have been evidenced and characterized by the lateral coexistence of intact laminated sediments with deformed laminae. Deformation structures are sealed by underformed laminae, onlapping the topography created by folded structures (**Fig. 5B**). Onlapping geometries suggest that deformation was short-lived and ceased during the deposition of the pond deposits. Deformation structures encompass normal faults, reverse faults, and asymmetrical folds. The combination of NNW or SSE-dipping reverse/thrust faults and stacked NNW or SSE-verging asymmetrical folds indicate frequent switch in the direction of tectonic displacement during the deformation of sediments. Small-scale normal faults are abundant and down-throw either towards the NNW or the SSE. Step normal faults also occur, suggesting collapse of underlying sediments (**Fig. 5A**).

The deformation of these proglacial sediments could result from seismic shaking, or sediment compression during readvance of the Sólheimajökull. Soft-sediment deformation structures induced by earthquakes are laterally extensive, and associated with sediment liquefaction, while deformed zones in the laminated sediments never exceed few meters wide and contain brittle to hydroplastic deformation structures (Obermeier, 1996). In case of glacitectonic deformation during ice readvance, large-scale deformations structures (tens of meters) will affect the whole fine-grained

laminated deposits rather than few laminae (Bennett, 2001). In addition, a single direction of tectonic displacement, related to the compression induced by the advancing glacier, must be recorded within such deformation structures. The localized and stacked asymmetrical folds showing reverse directions of tectonic transport imply that deformation is not triggered by ice-bed interactions.

Groundwater flow models in subglacial to marginal environments demonstrate the existence of a strong upward flow of overpressurized meltwater beyond the glacier margin (Boulton et al., 1993). Overpressures could be enhanced by the low-permeability till deposits and fine-grained sediments deposited upon the permeable glacifluvial sand immediately beyond the glacier margin (**Fig. 40A, B**). Subglacially-driven groundwater wells upwards in proglacial environments where the confining pressure is low, promoting the formation of hydrofracturing, mud diapirs and blow-out structures (Boulton et al., 1993; Boulton and Caban, 1995; van der Meer et al., 1999, Benediktsson et al., 2008). The occurrence of a low permeability deposits sealing the glacifluvial sediments prevents the formation of blow-out structures. The rising of overpressurized flows within permeable and sealed gravely sand triggers small-scale diapirisms (**Fig. 40C**). Active diapirisms will tend to form an uneven and slightly moving till layer during deposition of the overlying laminated sediments. Heterogeneous and localized diapirism will locally form depression evidenced by normal faults and collapsed structures, but could also locally induce compression, illustrated by asymmetrical folds and reverse faults (**Fig. 40C**). Stacked asymmetrical folds showing reverse direction of tectonic displacements suggest radial compression triggered by three-dimensional movements of the underlying till.

Alternatively, the heterogeneous dilatation of the till deposits could also be envisaged as trigger mechanisms for localized deformation of the pond deposits. Dilatancy may occur as a result of porewater pressure increase within the tills that leads to local increase of the till volume.

Syn-sedimentary deformation structures are draped over by onlapping laminated sediments implying that motions of underlying sediments ceased during deposition of fine-grained sediments (**Fig. 40D**). Small-scale diapirism stopped due to the decrease of porewater pressure within the sediments. This decrease of porewater pressure is probably related to the retreat of the ice margin, implying that the study site was no longer situated in the zone where overpressurized groundwater wells upwards.

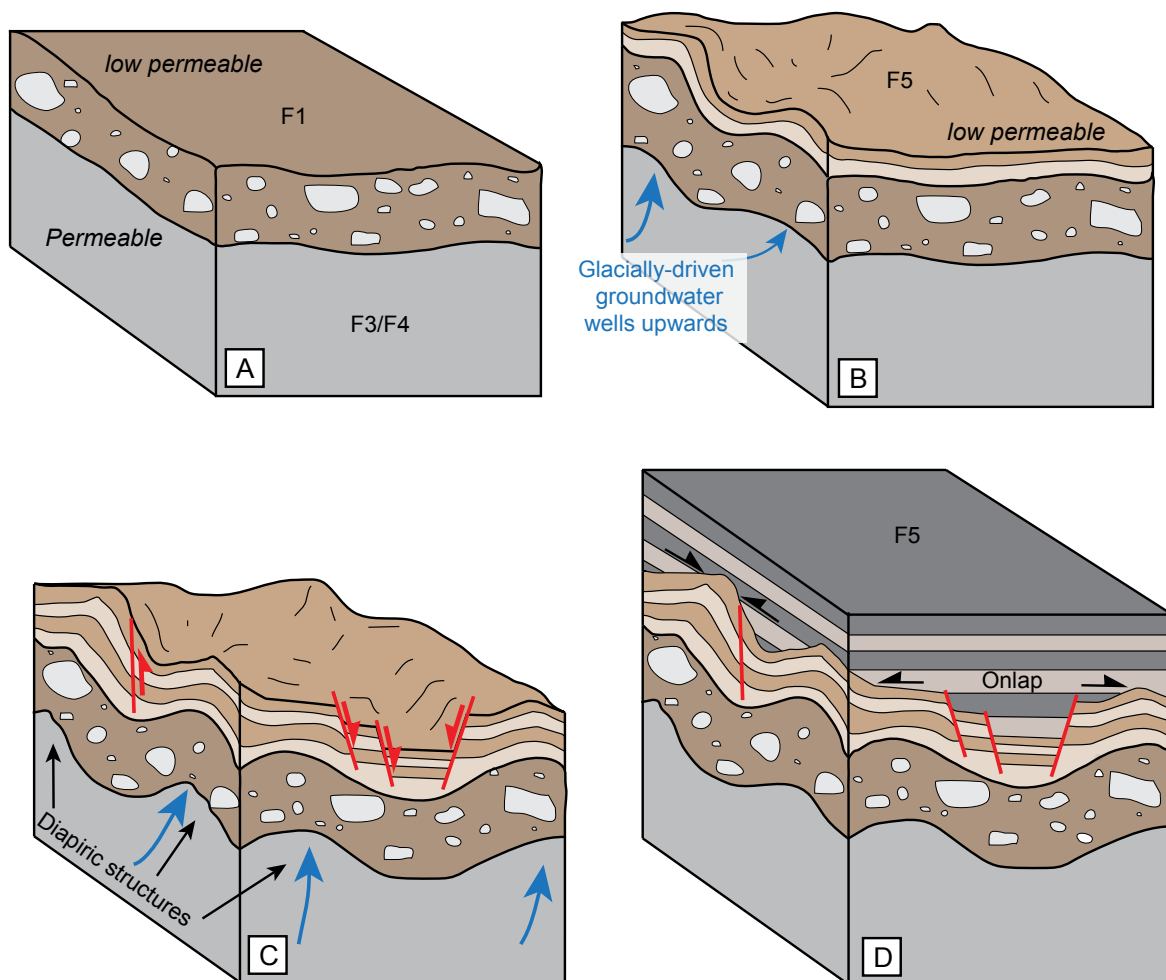


Figure 40. Schematic diagram illustrating the processes involved in the localized and syn-depositional deformation of the laminated pond deposits (F5). (A) Permeable glacialfluvial sand sealed by low-permeability clay-rich till. (B) Glacially-driven meltwater welling upwards is blocked by the low-permeability till and pond deposits. (C) Overpressure in glacialfluvial sediments trigger small-scale diapirism leading to localized and heterogeneous deformation of the laminated fine-grained sediments during their deposition. Diapirism triggers local collapsed structures, but also folds, and reverse faults induced by radial compression. (D) After migration of the marginal overpressurized zone, diapirism ceased while deposition of sediment continues, forming onlap geometries.

8. Synthetic model of the evolution of the clastic injection system through time

Multi-scale sedimentological and deformational observations allow to propose a new and detailed model for the development of the Sólheimajökull clastic injection system (**Fig. 41**).

(A) Deposition of lodgement tills in subglacial settings (F1). The release of subglacial, englacial and supraglacial debris in marginal settings leads to the deposition of melt-out tills (F2). In proglacial settings, the development of an outwash plain is associated with the deposition of a thick sequence of glacialfluvial sediments (F3/F4). Glacialfluvial sediments are composed of gravely sand to sandy gravel, and contained channelized morphologies related to channel erosion, infill, and abandonment in a braided network. The sedimentary sequence observed in the Sólheimajökull forefield is composed

of alternating permeable sand to gravel with low-permeable till deposits, constituting a «layer-cake» configuration (Ravier et al., 2014a) (**Fig. 41A**).

(B) An episode of glacier advance of the Sólheimajökull induces changes of the porewater pressure in the sediments. The increase of porewater pressure within the till beds exceeds the tensile strength of the underlying sediments, thus triggering the formation of hydrofractures filled by injected till. The combination of the vertical stress exerted by the ice load (σ_{ice}) and the horizontal stress exerted by the ice flow (τ_{flow}) generates *per descensum* oblique hydrofractures dipping down-ice. Laminations parallel to clastic dykes suggest repeated hydrofracturing and injection episodes (“crack-seal” model) and imply multi-episodic increase of the porewater pressure. The increase of mean grain-size towards the centre of the dyke suggests progressive increase of porewater pressure during hydrofracture-fill and partial fluidization (**Fig. 41B**).

(C) The retreat of the ice tongue is associated with glacifluvial sediment deposition and formation of small marginal ponds within topographic lows, inside which laminated fine-grained sediments can deposit. The vicinity of the ice margin induces an upward welling of overpressurized glacially-driven groundwater into permeable glacifluvial sediments. The rising overpressurized meltwater triggers small-scale diapirism, and induces heterogenous deformation of the till layer during deposition of sediments into the pond. Diapirism is responsible for the development of faults/folds showing reverse direction of tectonic transport, and collapsed structures evidenced by step normal faults (**Fig. 41C**).

(D) The progressive ice readvance leads to the formation of *per ascensum* clastic dykes in marginal settings. *Per ascensum* clastic dykes form in marginal environments as a response porewater excess release in low confining pressures. At the glacier front, low confining pressures are promoted by the net decrease in ice overburden pressure. This second generation of hydrofractures is filled by silt to clay with occasional granules, originating from the remobilization of sediments that were injected in the first generation of hydrofractures (**Fig. 41D**).

(E) The phase of glacier readvance is further evidenced by the deposition of a fissile and overconsolidated subglacial lodgement till. The deposition of this lodgement till represents the latest glacier maxima recorded in the Sólheimajökull forefield. The till fissility represents syn-depositional deformations triggered by stress exerted by the ice during the plastering of sediments. This phase of ice readvance is associated with the development of the third generation of hydrofractures. Similarly to the first generation, hydrofractures propagating downwards and dipping down-ice demonstrate their subglacial origins. During this second phase of subglacial hydrofracturing, glacifluvial sediments are

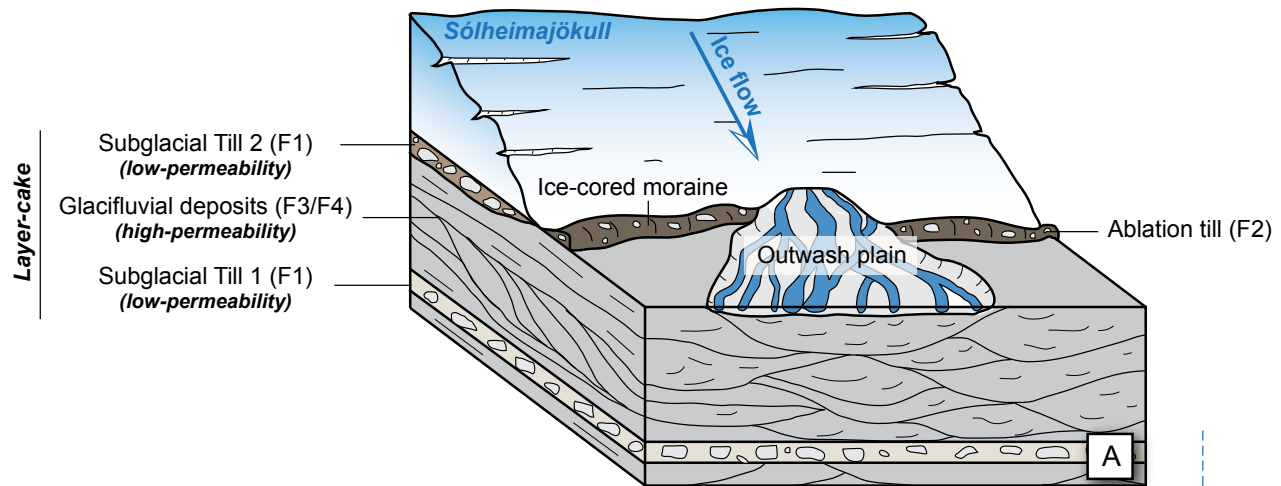
remobilized and injected downwards. The increase of porewater pressure associated with this third episode of hydrofracturing also trigger reopening of older fractures as evidenced by clastic dykes showing a core composed of sandy gravel (**Fig. 41E**).

(F) During the progressive retreat of the ice front, the fourth and fifth generation of clastic injections developed in submarginal to marginal settings.

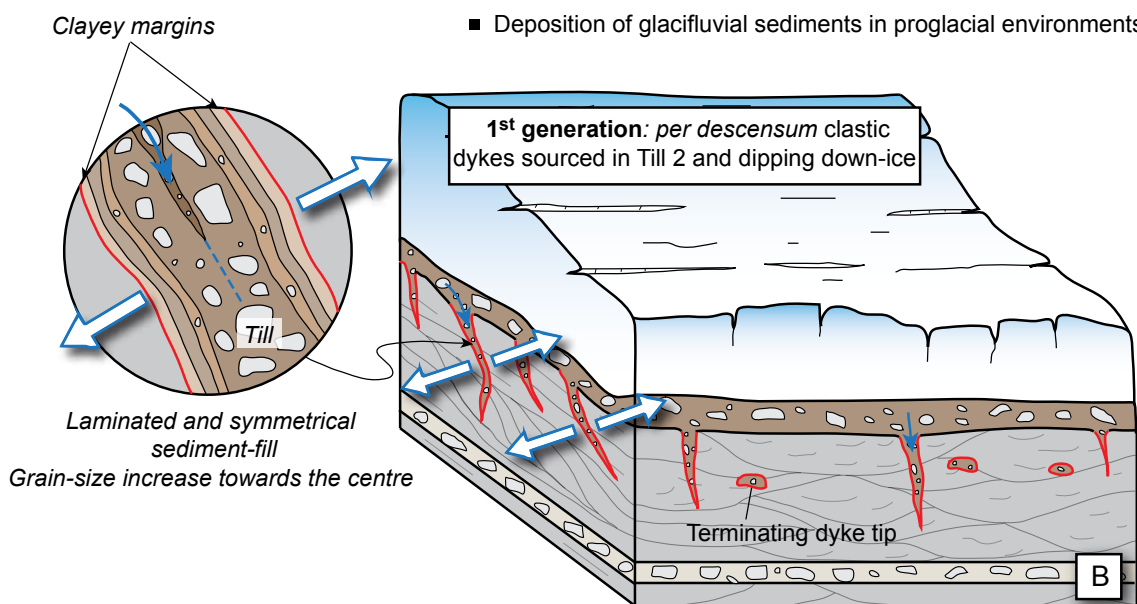
The fourth phase is associated with the formation of sills and stepped sills filled by coarse sand to gravel with clay margins. Sills and stepped sills are typical hydrofractures using bedding anisotropy to propagate when the confining pressure is low. The orientation of clastic dykes connecting the sills is often controlled by the distribution of preexisting faults. A low confining pressure implies low overburden pressure, suggesting that hydrofracturing occurred in submarginal to marginal settings. The fourth generation is generally filled by silt and sand resulting from the remobilization of glaci-fluvial and pond deposits. Lenticular pods containing sedimentary structures occur within the sills, suggesting that deposition by tractive currents locally occurs when groundwater could flow through interconnected small voids or cavities. Alternatively, normal grading observed within some sills suggests that deposition by fluidized turbulent flow may have also occurred.

The fifth generation is mainly composed of *per ascensum* clastic dykes (sometimes connected to small sills) due to marginal hydrofracturing and injection of fluidized sediments. Closely spaced network of hydrofractures lead to the formation of abundant angular and slab-shaped intraclasts detached from the host strata and floating within the injected material (i.e., breccia-like fabric). This last generation of clastic dykes frequently follows preexisting fault planes. During the progressive retreat of the ice tongue, release of englacial, supraglacial and subglacial debris during ice melting lead to deposition of melt-out till (F2) at the top of the section (**Fig. 41F**).

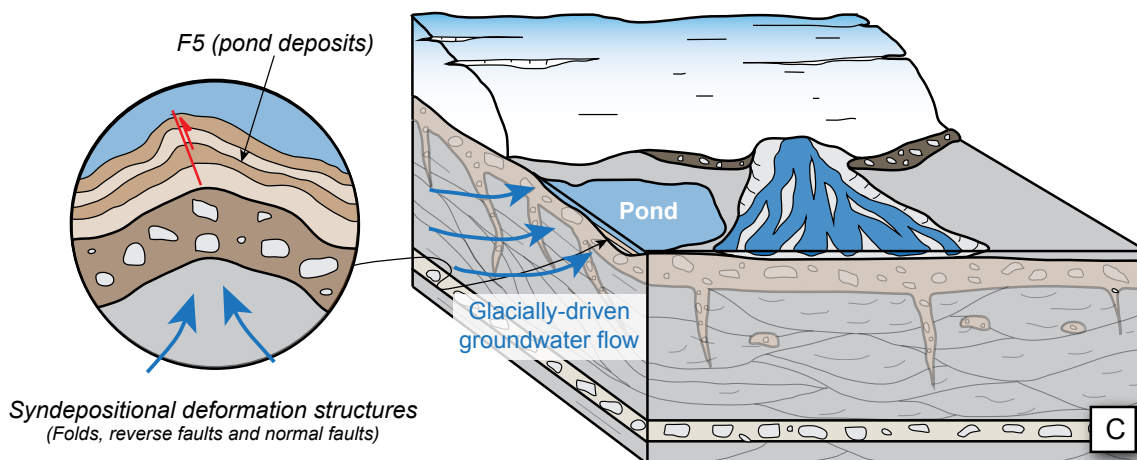
Figure 41. Schematic diagram illustrating the formation and evolution of the Sólheimajökull clastic injections network. (A) Deposition of subglacial lodgement tills in subglacial environments and glaci-fluvial sediments in the proglacial outwash plain forming a layer-cake of permeable and impermeable sediments. (B) An episode of ice advance triggers subglacial hydrofracturing and injection of sediments leading to the formation of *per descensum* clastic dykes dipping down ice (1st generation). (C) Retreat of the ice margin, glacially-driven groundwater flow wells upwards in marginal settings, leading to small-scale marginal diapirism and syn-depositional deformation of the fine-grained laminated sediments. (D) In marginal settings, hydrofractures propagating upwards develop due to low confining pressure and form *per ascensum* clastic dykes (2nd generation). (E) The advance of the ice margin is responsible for the deposition of lodgement tills and for the development of *per descensum* clastic injections dipping down-ice (3rd generation). (F) The retreat of the ice margin is associated with marginal hydrofracturing that promoted the development of sills, stepped sills and *per ascensum* clastic dykes (4th and 5th generation).



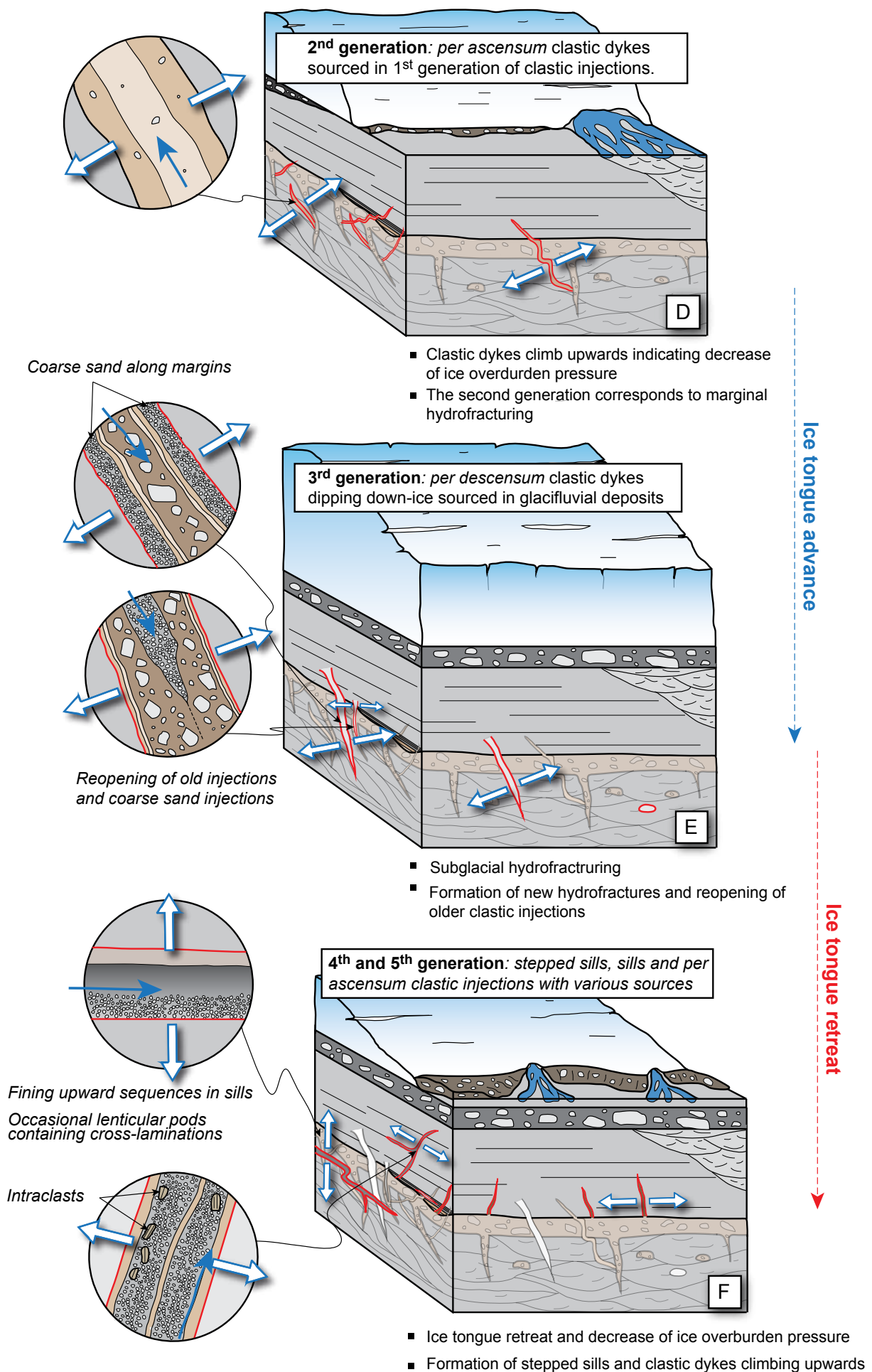
- Deposition of lodgement tills in subglacial environments
- Deposition of glacifluvial sediments in proglacial environments



- Subglacial hydrofracturing / Injection of fluidized sediments
- Multi-phased fracking and injections: «crack-seal» processes
- Porewater pressure fluctuations during successive injection trigger partial fluidization and internal variations in grain-size



- Overpressurized glacially-driven groundwater wells upwards beyond the ice margin
- Upwards stratal disruption (small-scale diapirism) and syn-sedimentary deformation in the vicinity of the ice tongue margin



The extent of Holocene advances of Sólheimajökull as reconstructed from lateral moraines (Dugmore, 1989; Dugmore and Sugden, 1991; Ingólfsson et al., 2010) allow to propose a simplified chronological framework for the development of the Sólheimajökull clastic injection network. The clastic injection network developed in subglacial to submarginal/marginal settings and the deposition of lodgement till deposits suggest that the study site must have been overridden by ice. As suggested by Dugmore and Sugden (1991) the site has been overridden by ice in Pre-Little Ice age times (**Fig. 42**), implying that the emplacement of the clastic injection network also predate the LIA. Subglacial hydrofracturing and injection may be related to the maximum advance of the outlet glacier (i.e., between 7 and 4.5 cal. Ka BP) while marginal hydrofracturing may be penecontemporaneous to the phases of retreat recorded in the 1.3 and 1.0 cal. ka BP end moraines. It is also plausible that episodes of ice readvance dated from the LIA and evidenced by end moraines situated 250 m away from the study area may have reactivated hundreds of years later the clastic injection network. Indeed, the input of overpressurized meltwater in marginal settings could have formed per ascensum dyke morphologies during this period (**Fig. 42**).

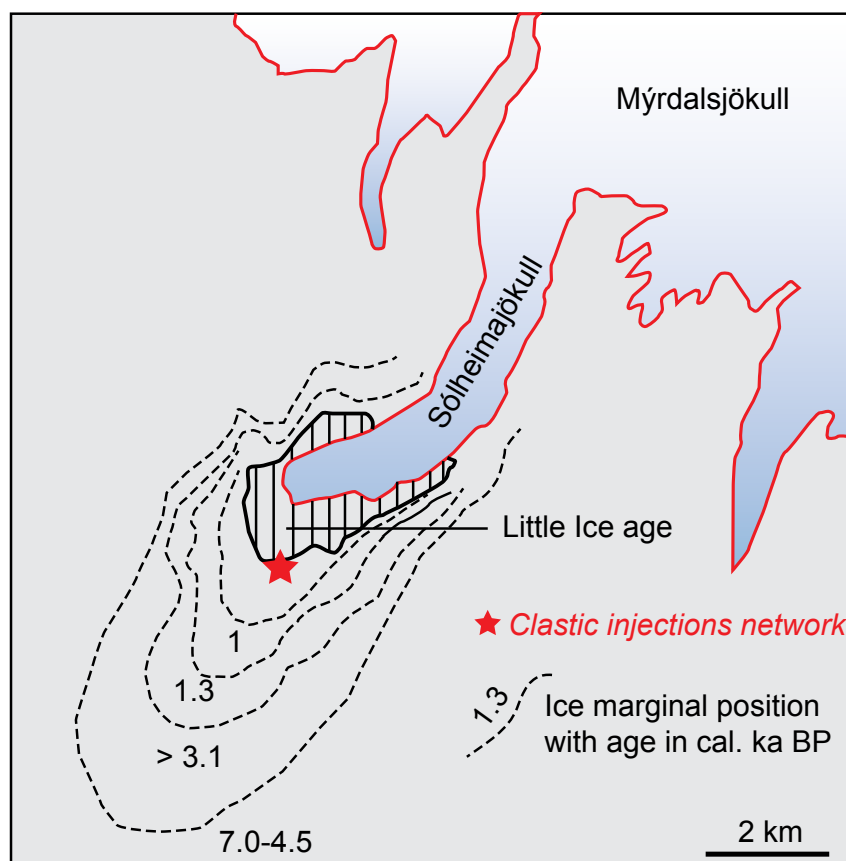


Figure 42. The extent of advances of Sólheimajökull as reconstructed from lateral moraines. Ages are based on tephrochronology and ^{14}C datings. (Modified after Dugmore and Sugden and Ingólfsson et al., 2010).

9. Conclusions

Detailed and multi-scale analyses of the Sólheimajökull clastic injection network permitted to draw a number of conclusions that can be used to better constrain parameters controlling: hydrofracturing, hydrofracture geometries, and injection mechanisms in glacial contexts. The characterization of these different parameters served to reconstruct the oscillations of the ice margin trough time.

- Hydrofractures preferentially develop where the sedimentary sequence is characterized by a layer-cake configuration, with alternating permeable and low-permeable sediments (glacifluvial sediments vs. till and fine-grained pond deposits).
- Hydrofracturing can either occur in subglacial and submarginal/marginal environments. The sense of propagation and dip direction of the hydrofractures are directly linked to the environments in which they form. *Per descensum* clastic dykes dipping down-ice demonstrate subglacial hydrofracturing underneath flowing-ice. In marginal settings, the decrease of overburden pressure promotes the formation of sills, stepped sills and *per ascensum* clastic dykes.
- In marginal settings, hydrofractures preferentially propagate along planes of weakness such as bedding anisotropy and preexisting faults.
- Laminations parallel to injection margins illustrate multiple episodes of hydrofracturing and sediment-fill (crack-seal model). Internal laminations and repetitive variations in grain-size demonstrate frequent variations in porewater pressure, and partial fluidization. Laminated hydrofracture-fills are recurrent in glacial settings and reflect the typical fluctuations of porewater pressures related to such a highly dynamic environment.
- Evidence for turbulent conditions depicted in sediment-fill suggest fluidized flow-regime during injection of sediments. However, lenticular pods containing sedimentary structures within sills suggest localized sediment deposition by traction currents within small internal voids.
- Evidence of small-scale diapirism record upwelling overpressurized groundwater in proglacial environments.
- Sedimentological characteristics, analyses of soft-sediment deformation structures and detailed description of the clastic injection network permit to reconstruct in details the succession of glacial environments induced by repetitive ice front oscillations. Two major cycles of glacier advance and retreat were recorded along the Sólheimajökull outcrop.

References

- Benn, D.I. and Evans, D.J.A., 2010. *Glaciers and Glaciations*, 2nd edn. Edward Arnold, London, 802 pp.
- Benediktsson, I.O., Moller, P., Ingolfsson, O., van der Meer, J.J.M., Kjaer, K.H., Kruger, J., 2008. Instantaneous end moraine and sediment wedge formation during the 1890 glacier surge of Bruarjokull, Iceland. *Quaternary Science Reviews* 27, 209-234.
- Boulton, G.S., Caban, P.E., Vangijssel, K., 1995. Groundwater-flow beneath ice sheets .1. Large-scale patterns. *Quaternary Science Reviews* 14, 545-562.
- Boulton, G.S., Slot, T., Blessing, K., Glasbergen, P., Leijnse, T., Vangijssel, K., 1993. Deep circulation of groundwater in overpressured subglacial aquifers and its geological consequences. *Quaternary Science Reviews* 12, 739-745.
- Boulton, G.S., Dobbie, K.E., Zatsepin, S., 2001. Sediment deformation beneath glaciers and its coupling to the subglacial hydraulic system. *Quaternary International* 86, 3-28.
- Broster, B.E., Dreimanis, A., White, J.C., 1979. A sequence of glacial deformation, erosion and deposition at the ice-rock interface during the Last Glaciation: Cranbook, British Columbian Canada. *Journal of Glaciology* 23, 283-295.
- Clerc, S., Buoncristiani, J.F., Guiraud, M., Desaubliaux, G., Portier, E., 2012. Depositional model in subglacial cavities, Killiney Bay, Ireland. Interactions between sedimentation, deformation and glacial dynamics. *Quaternary Science Reviews* 33, 142-164.
- Collinson, J.D., 1996. Alluvial sediments. In: Reading, H.G. (Ed.), *Sedimentary Environments and Facies*, 3rd edn. Oxford, Blackwell, pp. 37-82.
- Cosgrove, J.W., 2001. Hydraulic fracturing during the formation and deformation of a basin: A factor in the dewatering of low-permeability sediments. *AAPG Bulletin* 85, 737-748.
- Denis, M., Guiraud, M., Konate, M., Buoncristiani, J.F., 2010. Subglacial deformation and waterpressure cycles as a key for understanding ice stream dynamics: evidence from the Late Ordovician succession of the Djado Basin (Niger). *International Journal of Earth Sciences* 99, 1399-1425.
- Diggs, T.N., 2007. An outcrop study of clastic-injection structures in the Carboniferous Tesnus Formation, Marathon basin, Trans-Pecos Texas. In: Hurst, A., Cartwright, J. (Eds.), *Sand Injectites: Implications for Hydrocarbon Exploration and Production: American Association of Petroleum Geologists Memoir*, Tulsa, pp. 209-219.
- Dixon, R.J., Schofield, K., Anderton, R., Reynolds, A.D., Alexander, R.W.S., Williams, M.C., Davies, K.G., 1995. Sandstone diapirism and clastic intrusion in the Tertiary submarine fans of the Bruce Beryl Embayment, Quadrant 9, UKCS. In: Hartley, A.J., Prosser, D.J. (Eds.), *Characterisation of deep-marine clastic systems: Special Publication*, vol. 94. Geological Society, London, pp. 77-94.
- Druitt, T.H., 1995. Settling behavior of concentrated dispersions and some volcanological applications. *Journal of Volcanology and Geothermal Research* 65, 27-39.

- Dugmore, A., 1989. Tephrochronological studies of Holocene glacier fluctuations in south Iceland. In: Oerlemans, J. (Ed), *Glacier fluctuations and climate change*. Dordrecht, Kluwer Academic Publishers, 37–55.
- Dugmore, A.J., Sugden, D.E., 1991. Do the anomalous fluctuations of Sólheimajökull reflect ice-divide migration? *Boreas* 20, 105–113.
- Duranti, D., Hurst, A., 2004. Fluidization and injection in the deep-water sandstones of the Eocene Alba Formation (UK North Sea). *Sedimentology* 51, 503–529.
- Evans, D.J.A., 2003. Ice-Marginal Terrestrial Landsystems: Active Temperate Glacier Margins. In: Evans, D.J.A. (Ed.), *Glacial Landsystems*, Arnold, London, pp. 12–44.
- Evans, D.J.A., Phillips, E.R., Hiemstra, J.F., Auton, C.A., 2006. Subglacial till: Formation, sedimentary characteristics and classification. *Earth-Science Reviews* 78, 115–176.
- Hildebrand, L., Thorssander, P., 1999. Sulphur isotopes in rocks from the Karla volcanic centre, south Iceland. *Geoscience Society of Iceland Spring Meeting Abstract volume*.
- Hildebrandt, C., Egenhoff, S., 2007. Shallow-marine massive sandstone sheets as indicators of palaeoseismic liquefaction - An example from the Ordovician shelf of Central Bolivia. *Sedimentary Geology*, 202, 581–595.
- Hillier, R.D., Cosgrove, J.W., 2002. Core and seismic observations of overpressure-related deformation within Eocene sediments of the Outer Moray Firth, UKCS. *Petroleum Geoscience* 8, 141–149.
- Hubbard, S.M., Romans, B.W., Graham, S.A., 2007. An outcrop example of large-scale conglomeratic intrusions sourced from deep-water channel deposits, Cerro Toro Formation, Magallanes basin, southern Chile. In: Hurst, A., Cartwright, J. (Eds.), *Sand Injectites: Implications for Hydrocarbon Exploration and Production: American Association of Petroleum Geologists Memoir*, Tulsa, pp. 199–207.
- Hurst, A., Scott, A., Vigorito, M., 2011. Physical characteristics of sand injectites. *Earth-Science Reviews* 106, 215–246.
- Ingólfsson, Ó, Norðdahl, H., Schomaker, A., 2010. Deglaciation and Holocene Glacial History of Iceland. In: Schomacker, A., Krüger, J., Kjær, K.H. (Eds.), *The Mýrdalsjökull ice cap, Iceland. Glacial processes, sediments and landforms on an active volcano: Developments in Quaternary Science* 13, pp. 51–68.
- Jakobsdóttir, S.S., 2008. Seismicity in Iceland: 1994–2007. *Jökull* 58, 75–100.
- Janszen, A., Spaak, M., Moscariello, A., 2012. Effects of the substratum on the formation of glacial tunnel valleys: an example from the Middle Pleistocene of the southern North Sea Basin. *Boreas* 41, 629–643.
- Jolly, R.J.H., Lonergan, L., 2002. Mechanisms and controls on the formation of sand intrusions. *Journal of the Geological Society* 159, 605–617.
- Le Heron, D.P., Etienne, J.L., 2005. A complex subglacial clastic dyke swarm, Sólheimajökull, southern Iceland. *Sedimentary Geology* 181, 25–37.

- Lowe, D.R., 1975. Water escape structures in coarse-grained sediments. *Sedimentology* 22, 175–204.
- Mulder, T., Alexander, J., 2001. The physical character of subaqueous sedimentary density flows and their deposits. *Sedimentology* 48, 269–299.
- Norðdahl, H., Ingólfsson, Ó., Pétursson, H.G., Hallsdóttir, M., 2008. Late Weichselian and Holocene environmental history of Iceland. *Jökull* 58, 343–364.
- Obermeier, S.F., 1996. Use of liquefaction-induced features for paleoseismic analysis - An overview of how seismic liquefaction features can be distinguished from other features and how their regional distribution and properties of source sediment can be used to infer the location and strength of Holocene paleo-earthquakes. *Engineering Geology* 44, 1–76.
- Parize, O., Beaudoin, B., Eckert, S., Fries, G., Hadj-hassen, F., Schneider, F., Su, K., Tijani, A., Troullier, A., De Fouquet, C., Vandromme, R., 2007. The Vocontian Aptian and Albian syndepositional clastic sills and dikes: A field-based mechanical approach to predict and model the early fracturing of marly-limy sediments. In: Hurst, A., Cartwright, J. (Eds.), *Sand Injectites: Implications for Hydrocarbon Exploration and Production*: American Association of Petroleum Geologists Memoir, Tulsa, pp. 163–173.
- Passega, R., 1964. Grain size representation by CM patterns as a geological tool. *Journal of Sedimentary Petrology* 34, 830–847.
- Peterson, G.L., 1968. Flow structures in sandstone dykes. *Sedimentary Geology* 2, 177–190.
- Phillips, E., Everest, J., Reeves, H., 2013. Micromorphological evidence for subglacial multiphase sedimentation and deformation during overpressurized fluid flow associated with hydrofracturing. *Boreas* 42, 395–427.
- Phillips, E., Hughes, L., 2014. Hydrofracturing in response to the development of an overpressurized subglacial meltwater system during drumlin formation: an example from Anglesey, NW Wales. *Proceedings of the Geologists' Association*, in press.
- Ramsay, J.G., 1980. Shear zone geometry: a review. *Journal of Structural Geology* 21, 83–99.
- Ravier, E., Buoncristiani, J.-F., Guiraud, M., Menzies, J., Clerc, S., Goupy, B., Portier, E., 2014a. Porewater pressure control on subglacial soft sediment remobilization and tunnel valley formation: A case study from the Alnif tunnel valley (Morocco). *Sedimentary Geology* 304, 71–95.
- Ravier, E., Buoncristiani, J.F., Clerc, S., Guiraud, M., Menzies, J. and Portier, E., 2014b. Sedimentological and deformational criteria for discriminating subglaciofluvial deposits from subaqueous ice-contact fan deposits: A pleistocene example (Ireland). *Sedimentology* 61, 1382–1410.
- Rijsdijk, K.F., Owen, G., Warren, W.P., McCarroll, D., van der Meer, J.J.M., 1999. Clastic dykes in overconsolidated tills: evidence for subglacial hydrofracturing at Killiney Bay, Eastern Ireland. *Sedimentary Geology* 129, 111–126.
- Russell, A.J., Marren, P.M., 1999. Proglacial fluvial sedimentary sequences in Greenland and Iceland: a case study from active proglacial environments subject to jökulhlaups. In: Jones, A.P., Tucker, M.E. and Hart, J.K. (Eds.), *The description and Analysis of Quaternary Stratigraphic Field Sections*. Quaternary Research Association Technical Guide 7, 171–208.
- Russell, A.J., Fay, H., Marren, P.M., Tweed, F.S., Knudsen, Ó., 2005. Icelandic jökulhlaup impacts.

- In: Caseldine, C.J., Russell, A.J., Hardardottir, J. and Knudsen, Ó. (Eds.), *Iceland: Modern Processes and Past Environments. Developments in Quaternary Sciences* 5, Elsevier, Amsterdam, pp. 153-203.
- Russell, A.J., Knudsen, Ó. 2002. The effects of glacier-outburst flood flow dynamics on ice-contact deposits: November 1996 jökulhlaup, Skeiðarársandur, Iceland. In: Martini, I.P., Baker, V.R. and Garzon, G. (Eds.), *Flood and Megaflood Processes and Deposits: Recent and Ancient Examples*. Blackwell, Oxford. International Association of Sedimentologists, Special Publication 32, 67-83.
- Russell, A.J., Duller, R., Mountney, N.P., 2010. Volcanogenic Jökulhlaups (Glacier Outburst Floods) from Mýrdalsjökull: Impacts on Proglacial Environments. In: Schomacker, A., Krüger, J., Kjær, K.H. (Eds.), *The Mýrdalsjökull ice cap, Iceland. Glacial processes, sediments and landforms on an active volcano: Developments in Quaternary Science* 13, pp. 181-207.
- Schomacker, A., Krüger, J., Kjær, K.H., 2010. The Mýrdalsjökull ice cap, Iceland. Glacial processes, sediments and landforms on an active volcano: An Introduction. In: Schomacker, A., Krüger, J., Kjær, K.H. (Eds.), *The Mýrdalsjökull ice cap, Iceland. Glacial processes, sediments and landforms on an active volcano: Developments in Quaternary Science* 13, pp. 1-4.
- Sigurðsson, O., 2010. Variations of Mýrdalsjökull during Postglacial and Historical Times. In: Schomacker, A., Krüger, J., Kjær, K.H. (Eds.), *The Mýrdalsjökull ice cap, Iceland. Glacial processes, sediments and landforms on an active volcano: Developments in Quaternary Science* 13, pp. 69-78.
- Smart, P.L., Palmer, R.J., Whiteaker, F., Wright P.V., 1988. Neptunian Dikes and Fissure Fills: An overview and Account of Some Modern Examples. In: James, N.P., Choquette, P.W. (Eds.), *Paleokarst*, Springer, New York, pp. 149-162.
- Sturkell, E., Einarsson, P., Sigmundsson, F., Hooper, A., Ófeigsson, B.G., Geirsson, H., Ólafsson, H., 2010. Katla and Eyjafjallajökull Volcanoes. In: Schomacker, A., Krüger, J., Kjær, K.H. (Eds.), *The Mýrdalsjökull ice cap, Iceland. Glacial processes, sediments and landforms on an active volcano: Developments in Quaternary Science* 13, pp. 5-22.
- Taylor, B.J., 1982. Sedimentary dykes, pipes and related structures in the Mesozoic sediments of south-eastern Alexander Island. *British Antarctic Survey Bulletin* 51, 1-42.
- Thorarinsson, S., 1943. Vatnajökull. Scientific results of the Swedish-Icelandic investigations 1936-37-38. *Geografiska Annaler* 1-2, 1-54.
- van der Meer, J.J.M., Kjær, K., Krüger, J., 1999. Subglacial water-escape structures, Sléttjökull, Iceland. *Journal of Quaternary Science* 14, 191-205.
- van der Meer, J.J.M., Kjaer, K.H., Kruger, J., Rabassa, J., Kilfeather, A.A., 2009. Under pressure: clastic dykes in glacial settings. *Quaternary Science Reviews* 28, 708-720.
- Vigorito, M., Hurst, A., 2010. Regional sand injectite architecture as a record of pore-pressure evolution and sand redistribution in the shallow crust: insights from the Panoche Giant Injection Complex, California. *Journal of the Geological Society* 167, 889-904.

Chapitre 2

Principaux résultats

Partie 1

- La coexistence de faciès sédimentaires triés sous-glaciaires et proglaciaires au sein d'un même site a permis de différencier les styles de déformation et de sédimentation entre ces deux environnements.
- Les caractéristiques sédimentologiques et structurales facilitant la reconnaissance d'un environnement fluviatile sous-glaciaire sont énumérées dans le **Tableau 1**. Le transport et le dépôt de sédiments par les eaux de fonte, pendant des périodes de découplage de la glace et du substrat, favorisent la mise en place de faciès triés aggradants et granocroissants. Le recouplage de la glace sur le substrat est à l'origine d'une gamme de structures de déformations contrôlées par l'action cisailante de la glace sur les sédiments (i.e., failles inverses, plis asymétriques,...) et par les fortes pressions d'eau interstitielle (dykes *per descensum*, sills, ...). La mise en place de ces déformations est contemporaine de la sédimentation .

Sedimentological & Stratigraphical	Deformational
<ul style="list-style-type: none"> ■ Alternating and interfingering till with sorted sediments ■ Sub and intra-till lenses of sorted sediments ■ Aggrading sorted sediments ■ Overall upward coarsening trend in the ice-bed decoupling sedimentary sequence ■ Amalgamated sorted sediments associated with rapid and rhythmic changes in grain-size ■ Conformable till/sorted sediments contacts ■ Evenly distributed dropstones (debris rain-out) 	<ul style="list-style-type: none"> ■ Coeval and cyclical deposition and deformation ■ Deformation affects discrete beds rather than the entire pile of sediments ■ Preferential horizontal tectonic transport due to simple shear stress exerted by the ice, and limited space for propagation of the deformation ■ Typical subglacial deformation structures induced by ice-bed interactions: <ul style="list-style-type: none"> - Reverse faults - Step normal faulting - Asymmetrical Folds - Clastic dykes propagating downwards - Sills

Table 1. Diagnostic criteria facilitating the recognition of ice-bed decoupling sedimentary sequence. Note that no single features can be used a key diagnostic criterion for identifying a subglaciofluvial environment, instead the interpretation of subglaciofluvial deposits in the sedimentary record must rely on an array of criteria.

- Les sédiments fluviatiles déposés sous la glace présentent des séquences granocroissantes et des séquences de déformation caractéristiques.

- Ces séquences impliquent un contrôle cyclique dans l'augmentation des débits d'eaux de fonte mais également une cyclicité dans les épisodes de couplage et de découplage entre la glace et son substrat.

- L'augmentation des débits pourrait être directement liée à la variation de la production d'eaux de fonte au cours de cycles saisonniers ou pluri-annuels.

- Les séquences de déformation se mettent en place lors du couplage de la glace et du substrat et indiquent une diminution progressive de la pression d'eau interstitielle. La mise en place de ces séquences est liée à des périodes où la production d'eau de fonte est moindre ou nulle.

- La cyclicité dans la production d'eau de fonte contrôle le déclenchement d'épisodes de couplage et de découplage glace/substrat et influence donc la dynamique glaciaire de l'*ice-stream* de la mer d'Irlande.

- Le passage d'un environnement sous-glaciaire/submarginal à un environnement proglaciaire indique une phase de retrait glaciaire. La présence, dans la région d'étude, de dépôts liés à l'écoulement ou le stockage d'eaux de fonte sous l'*ice stream* de la mer d'Irlande (McCabe et O'Cofaigh, 1994; Clerc et al., 2012; cette étude) est probablement causée par l'augmentation de la fonte de surface pendant une phase de déglaciation. Cette présence accrue d'eaux de fonte sous la glace pendant la déglaciation permet d'envisager une augmentation de la vitesse d'écoulement de cet *ice-stream* pendant son retrait.

Partie 2

- L'étude multi-échelle du réseau d'injections clastiques du Sólheimajökull a permis de déterminer les processus et mécanismes impliqués dans la mise en place des injections, mais aussi de reconstruire les oscillations de la marge glaciaire au cours du temps.
- Les dykes et sills composant le réseau se mettent en place par hydrofracturation et injections de sédiments fluidisés.
- Le remplissage des injections est laminé. Cela est dû aux épisodes répétés de fracturation, d'expansion de la roche encaissante et d'injection de sédiments (modèle «crack-seal»). Les variations de granulométrie à l'intérieur des injections témoignent du changement de source au cours du temps et/ou des variations de la pression de fluide, conduisant à des phénomènes de fluidisation partielle.
- La prédominance de remplissages multiphasés dans les injections formées en environnements glaciaires peut s'expliquer par les fluctuations caractéristiques de la pression d'eau interstitielle dans ce type d'environnement.
- L'orientation et le sens de propagation des injections clastiques permettent de déduire l'environnement dans lequel s'est déclenché le processus d'hydrofracturation.
 - Les dykes *per descensum* orientés dans la direction du sens d'écoulement de la glace témoignent d'un environnement sous-glaciaire ou submarginal associé à un couplage entre le substrat et une glace mobile.
 - Les sills sont reliés à des processus d'hydrofracturation en environnements submarginiaux où la diminution de la pression verticale exercée par le poids de la glace favorise le développement d'hydrofractures selon des plans naturels de fragilité (i.e., la stratification et des fractures/failles préexistantes).
 - Les dykes *per descensum* sont associés à des processus d'hydrofracturation à la marge du glacier où l'absence de glace permet aux surpressions de fluide d'être évacuées librement vers le haut, selon le gradient de pression hydrostatique.

- Il existe cinq phases majeurs d'hydrofracturation au sein du réseau d'injection clastique du Sólheimajökull. Ces cinq phases sont caractérisées par des orientations et sens de propagation différents, qui couplés aux caractéristiques sédimentologiques des dépôts encaissants, ont permis de reconstruire en détails la succession des environnements de dépôts et les oscillations de la marge glaciaire.

- Deux cycles majeurs d'avancée et de retrait de la langue glaciaire ont ainsi pu être mis en évidence. Au vue des reconstitutions de la position de la marge glaciaire au cours de l'Holocène, la majeure partie du réseau d'injections clastiques s'est développée avant le Petit Age Glaciaire, bien que la proximité du front glaciaire pendant cette période ait pu réactiver le système.

CHAPITRE III

**Déformations par surpressions de fluide:
Impacts sur les morphologies glaciaires**

Introduction

Le développement de fortes pressions d'eau interstitielle dans les sédiments est capable de contrebalancer temporairement l'augmentation naturelle de leur résistance intrinsèque pendant l'enfouissement. Dans cette configuration, la résistance des sédiments au cisaillement devient tellement faible qu'ils deviennent potentiellement l'objet de remobilisation (Maltman and Bolton, 2003). Le terme de remobilisation sédimentaire est utilisé pour décrire la remise en mouvement du sédiment, déclenchée par une augmentation de la pression de fluide. Les remobilisations sédimentaires sont considérées comme des structures de déformation pré-lithification (Owen et al., 2011) et sont généralement associées à des processus d'hydrofracturation et d'injection de sédiments fluidisés (Lonergan et al., 2000).

Si les remobilisations sédimentaires sont communément associées aux environnements marins profonds (Dixon et al., 1995; Lonergan et al., 2000; Hurst et al., 2011), l'objectif de ce chapitre est de tester si ces processus peuvent se produire dans les environnements sous-glaciaires, puisque des pressions de fluides élevées s'enregistrent dans les sédiments (Boulton et Caban, 1995; van der Meer et al., 2009; Denis et al., 2010; Phillips et al., 2013b). Dans le cas où de tels processus existent, qu'elles pourraient-être leurs implications dans la formation de morphologies glaciaires et plus précisément dans la mise en place des vallées tunnels. Ce chapitre se compose de deux parties, comportant chacune des données interprétées synthétisées dans un articles scientifique, visant à caractériser l'impact de la pression de fluide sur la formation des vallées tunnels.

• **Partie 1:** «Porewater pressure control on subglacial soft sediment remobilization and tunnel valley formation: a case study from the Alnif tunnel valley (Morocco)». (Article 3)

Cette première partie se focalise sur la description des processus de remobilisation sédimentaire induits par des surpressions de fluide et leurs impacts sur les morphologies sous-glaciaires. L'étude se base sur l'analyse du remplissage sédimentaire basal d'une vallée tunnel et des dépôts préglaciaires sous-jacents. Elle combine une analyse faciologique et structurale des sédiments le long d'une vallée tunnel ordovicienne située dans l'Anti-Atlas marocain.

Partie 2: «Porewater pressure-driven (Alnif) vs. Meltwater-driven (Foum Larjamme): two models of tunnel valley formation existing during the Ordovician glaciation, and their relations with Ice-Stream dynamics (Morocco)». (Article 4)

Cette deuxième partie a pour objectif de comparer les processus de formation de deux vallées tunnels ordoviciennes présentant des caractéristiques sédimentologiques, déformationnelles et morphologiques différentes. La comparaison de ces deux vallées permet de mieux comprendre les paramètres contrôlant l'augmentation de la pression de fluide dans le substrat sous-glaciaire, et les processus de remobilisation qui en découlent. De plus, les reconstitutions de la distribution des principaux paléo *ice-stream* de la calotte glaciaire fini-ordovicienne permettront de discuter la relation entre dynamique glaciaire, processus de creusement, et morphologie des vallées tunnels.

Partie 1

«Contrôle de la pression d'eau interstitielle sur les remobilisations sédimentaires sous-glaciaires et sur la formation de vallées tunnels: exemple de la vallée tunnel d'Alnif (Maroc)».

Cette première partie fait l'objet d'une publication dans la revue *Sedimentary Geology*.

Article 3

Ravier, E., Buoncristiani, J.-F., Guiraud, M., Menzies, J., Clerc, S., Goupy, B., Portier, E., 2014. Porewater pressure control on subglacial soft sediment remobilization and tunnel valley formation: A case study from the Alnif tunnel valley (Morocco). *Sedimentary Geology* 304, 71-95.

Objectifs:

- *L'objectif de cette première partie est de décrire les processus de remobilisation sédimentaire ainsi que les différentes étapes de formation conduisant à la mise en place de la vallée tunnel d'Alnif (Maroc) en se basant sur:*

- *une étude sédimentologique des dépôts préglaciaires et du remplissage de la vallée tunnel.*

- *une analyse fine des structures de déformation pré-lithification au sein des dépôts préglaciaires et du remplissage sédimentaire de la vallée.*

- *Le deuxième objectif est de définir les différents paramètres contrôlant l'augmentation de la pression d'eau interstitielle dans les sédiments préglaciaires et donc de déterminer les facteurs qui initient la remobilisation sédimentaire sous une calotte de glace.*

- *Enfin le dernier objectif sera de proposer une liste de critères diagnostiques récoltée sur le terrain permettant de mettre en évidence l'intervention de processus de remobilisation sédimentaire dans le creusement d'une vallée tunnel sur substrat meuble.*

1. Précédents travaux

L'hydrofracturation et la bréchification hydraulique, combinées aux injections de sédiments liquéfiés ou fluidisés, sont considérées comme les principaux mécanismes responsables de la remobilisation sédimentaire (Jolly et Lonergan, 2002; Hurst et al., 2011). Ces processus sont fréquemment décrits dans les environnements marins profonds où l'enfouissement progressif de corps sableux saturés en eau sont remobilisés lors de l'augmentation rapide de la pression d'eau interstitielle. Ces remobilisations sédimentaires peuvent se présenter sous la forme de réseau d'injection clastiques, de volcans de sables, de laccolithes sédimentaires, etc, ... (Hurst et al., 2006; Hurst et Cartwright, 2007; Braccini et al., 2008; Andresen et al., 2009; Hurst et al., 2011; Monnier, 2013) dont l'extension peut atteindre plusieurs kilométriques et les volumes remobilisés plusieurs dizaines de millions de km³ (Parize et al., 2007; Andresen et al., 2009). Si les remobilisations sédimentaires en environnements glaciaires sont communes, comme l'attestent les nombreuses injections clastiques décrites dans le registre sédimentaire (Le Heron et Etienne, 2005; van der Meer et al., 2009; Clerc et al., 2012; Phillips et al., 2013b; 2014), des phénomènes de remobilisation sédimentaire d'échelle kilométrique faisant intervenir de très larges volumes de sédiments n'ont jamais été décrits.

L'augmentation de la pression d'eau interstitielle dans un substrat meuble a déjà été proposée comme un des moteurs de la formation des vallées tunnels d'origine glaciaire. Boulton et Hindmarsh (1987) ont été les premiers à suggérer un tel modèle, où le transfert des eaux de fonte dans les sédiments serait à l'origine du développement de fortes pressions de fluide et de possibles remobilisations sédimentaires. Dans ce modèle, l'augmentation de la pression d'eau interstitielle permet au sédiment de se liquéfier, favorisant ainsi leur remobilisation au sein de chenaux sous-glaciaires. Cette hypothèse de formation repose sur des simulations numériques (Boulton et al., 2007) et a notamment été proposée pour expliquer la formation de certaines vallées tunnels en Allemagne (Piotrowski, 1994). Plus récemment, le rôle majeur de l'augmentation de la pression d'eau interstitielle dans un substrat préglaciaire meuble a été mis en évidence dans les vallées tunnels de la mer du Nord (Janszen et al., 2012). Dans cette récente étude, le rôle majeur du type de substratum dans la génération de fortes pressions de fluide est proposé, de même que l'hypothèse de l'hydrofracturation et de la fluidisation complète de couches sédimentaires. D'autres études ont également démontrées l'importance du substratum dans la génération de surpressions de fluide et donc dans le développement de vallées

tunnels, notamment en démontrant l'existence d'une relation entre la diffusivité du substratum et la morphologie et profondeur des vallées tunnels (Clerc et al., submitted). Cette dernière étude se base sur des données de terrain et insiste sur l'importance du motif stratigraphique et plus particulièrement sur la distribution des aquifères confinés et de l'épaisseur des barrières de perméabilités.

Si les études récentes semblent confirmer l'importance des surpressions de fluide dans la formation des vallées tunnels, il n'existe pas à l'heure actuelle des données de terrain permettant de déterminer la nature et la chronologie des processus intervenant dans la formation de ces dépressions.

2. Contexte de l'étude

Afin d'étudier l'impact des surpressions de fluide sur la formation de vallées tunnel, la vallée tunnel d'Alnif située dans l'anti-Atlas marocain a été sélectionnée. Ce site a été choisi puisque les dépôts préglaciaires étaient meubles au moment du creusement, favorisant ainsi la préservation de structures liées aux fortes pressions de fluide dans le registre sédimentaire (Clerc et al., submitted). De plus, des études précédentes ont caractérisées les faciès et le motif stratigraphique des sédiments préglaciaires (Villas et al., 2006; Alvaro et al., 2007; Clerc et al., 2013), la morphologie de la vallée tunnel, et les caractéristiques de son remplissage sédimentaire (Clerc, 2012; Clerc et al., 2013).

La vallée tunnel d'Alnif se situe dans la partie est de l'anti-Atlas marocain (**Fig. 1A**). Durant la glaciation Hirnantienne (Ordovicien supérieur), le site d'étude était positionné à proximité de l'extrémité nord de la calotte glaciaire gondwanienne, entre deux paléo *ice-streams* (**Fig. 1B, C**) (Ghienne et al., 2007; Le Heron et al., 2007). L'hypothèse «maximale» envisage l'existence d'une seule calotte ayant un diamètre de près de 8000 km centrée sur le Pôle Sud et s'étant développée pendant le maximum d'un épisode froid d'une durée supérieur à 10 Ma (Ghienne et al., 2007; Finnegan et al., 2011). Durant cette épisode glaciaire, une vallée tunnel s'est creusée sur des sédiments alors non lithifiés, déposés dans un environnement marin «offshore» à «shoreface» (Alvaro et al., 2007). La vallée tunnel d'Alnif constitue une dépression de 5 km de large pour 180 m de profondeur comblée par des sédiments clastiques déposés pendant l'épisode glaciaire Hirnantien (Clerc, 2012; Clerc et al., 2013).

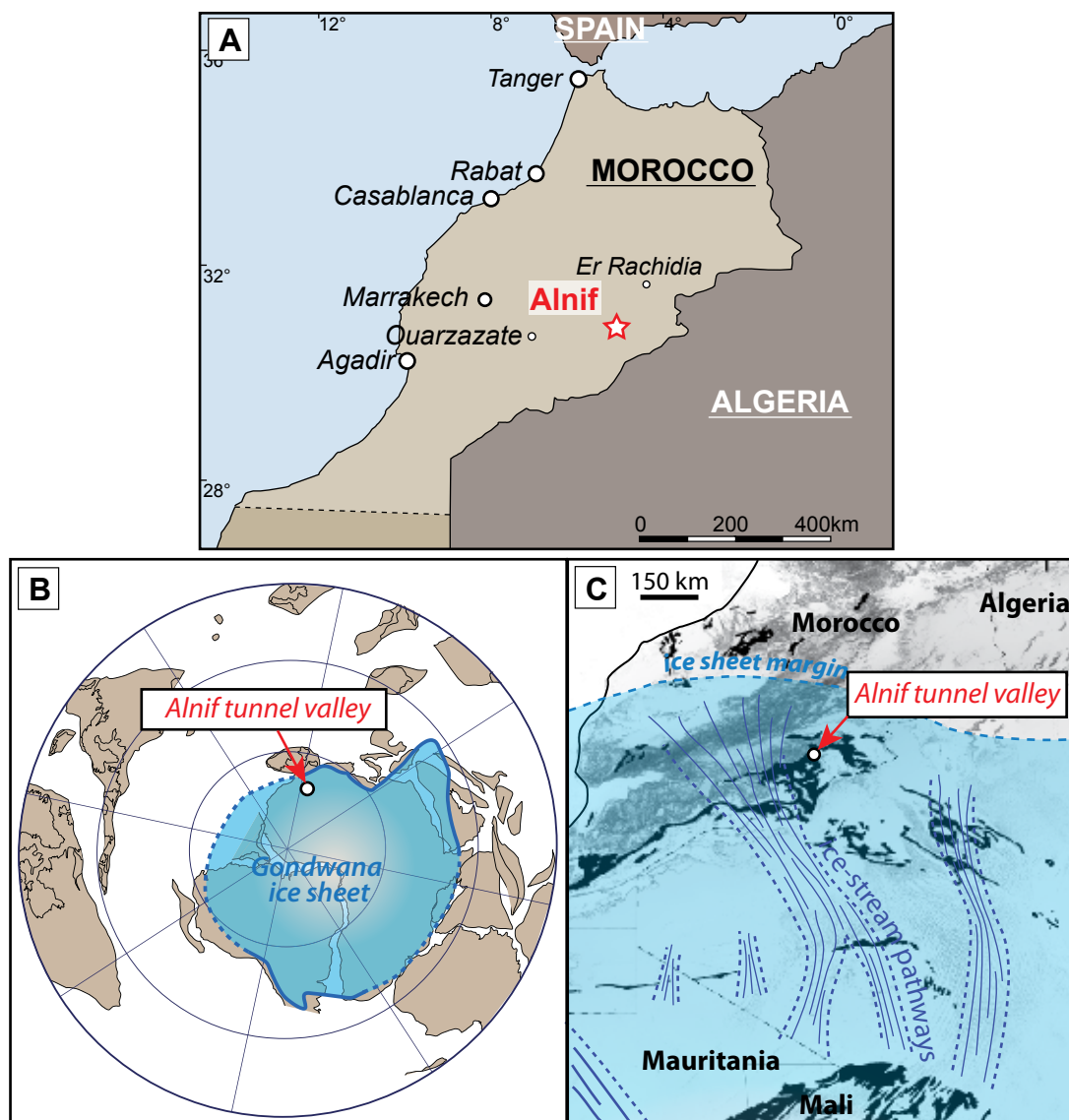


Figure 1. (A) Geographical location of the Alnif tunnel valley. (B) Palaeogeographic reconstructions for the latest Ordovician, adapted from Cocks and Torsvik (2002) and modified after Clerc et al. (2013). The extension of the Hirnantian palaeo-ice sheet, modified from Ghienne et al. (2007) is represented on the Gondwana palaeo continent. (C) Detailed palaeogeographic reconstructions of the ice sheet and associated ice-stream positions in Northwestern Africa are shown (modified after Ghienne et al., 2007 and Le Heron et al., 2007).

3. Méthodes

La méthode utilisée consiste en une analyse sédimentologique et structurale des dépôts préglaciaires et du remplissage sédimentaire basal de la vallée tunnel. Près de 50 échantillons ont été prélevés dans les sédiments préglaciaires et dans le conglomérat déposé à la base de la vallée tunnel afin de réaliser des lames minces. Les structures de déformation pré-lithification observées à l'échelle macroscopique et microscopique ont été décrites, leurs relations chronologiques définies, et leurs cinématiques et mécanismes de déformation déterminés. L'analyse détaillée de ces structures a ensuite permis de reconstruire les différents stades de déformation et l'évolution de la pression d'eau

interstitielle au sein des dépôts préglaciaires et glaciaires au cours du temps.

4. Article publié dans *Sedimentary Geology*

«Porewater pressure control on subglacial soft sediment remobilization and tunnel valley formation: A case study from the Alnif tunnel valley (Morocco)».

L'article est structurée de la façon suivante: (1) Dans une première partie, le cadre stratigraphique, structural, et glaciaire de la région d'Alnif est présenté, ainsi que la morphologie et les grandes caractéristiques du remplissage de la vallée tunnel. (2) Dans une deuxième partie, une description faciologique et stratigraphique détaillée du remplissage basal de la vallée tunnel est réalisée ainsi que l'interprétation des différents faciès définis en termes de processus de dépôt. (3) Dans une troisième partie, les structures de déformations préservées dans les sédiments préglaciaires et dans le remplissage basal de la vallée tunnel sont analysées et interprétés en termes de cinématique, de mécanisme de déformation et de pression de fluide. (4) La quatrième partie discute l'origine et les caractéristiques des phénomènes de remobilisation affectant les dépôts péglaciaires, et comment ils favorisent le creusement de cette vallée tunnel. Dans cette même partie, un modèle de formation de la vallée tunnel d'Alnif en six étapes est proposé. (6) Dans une dernière partie, les critères diagnostiques «terrain» permettant de déterminer si des processus de remobilisations sédimentaires interviennent dans le processus de creusement d'une vallée tunnel sont définis, de même que les paramètres contrôlant l'évolution de la pression d'eau interstitielle dans les dépôts préglaciaires.



Contents lists available at ScienceDirect

Sedimentary Geology

journal homepage: www.elsevier.com/locate/sedgeo

Porewater pressure control on subglacial soft sediment remobilization and tunnel valley formation: A case study from the Alnif tunnel valley (Morocco)

Edouard Ravier^{a,*}, Jean-François Buoncristiani^a, Michel Guiraud^a, John Menzies^b, Sylvain Clerc^c, Bastien Goupy^a, Eric Portier^c

^a Laboratoire Biogéosciences UMR/CNRS 6282 Université de Bourgogne, 6 Bd Gabriel, 21000 Dijon, France

^b Department of Earth Sciences, Brock University, 500 Glenridge Avenue, St. Catharines, Ontario L2S 3A1, Canada

^c GDF Suez, Exploration & Production International, 1 Place Samuel de Champlain, Faubourg de l'Arche, 92930 Paris La Défense Cedex, France

ARTICLE INFO

Article history:

Received 5 December 2013

Received in revised form 17 February 2014

Accepted 19 February 2014

Available online 2 March 2014

Editor: J. Knight

Keywords:

Tunnel valley

Sediment remobilization

Porewater pressure

Hydrofracturing

Subglacial

Ordovician

ABSTRACT

In the eastern part of the Moroccan Anti-Atlas Mountains, the Alnif area exposes a buried Ordovician glacial tunnel valley (5 km wide, 180 m deep) cut into preglacial marine sediments. The preglacial sedimentary sequence, deposited in a marine environment, is characterized by a typical “layer-cake” configuration of permeable (sand) and impermeable (clays and early-cemented sandstones) layers. At the base of the tunnel valley, a discontinuous and fan-shaped glacial conglomeratic unit 10 to 15 m thick occurs, erosively deposited over preglacial marine sediments. The conglomeratic unit is composed of preglacial intraclasts embedded within a sandy matrix. Both preglacial and glacial sediments display soft-sediment deformation structures related to fluctuating porewater pressure and strain rates, including ball structures, clastic dykes, fluted surfaces, turbate structures, folds and radial extensional normal faults. Kinematics and relative chronology of these deformation structures allow the role of porewater pressure in the process of tunnel valley genesis on soft beds to be understood. The tunnel valley formed through multi-phased episodes of intense hydrofracturing of the preglacial bed due to overpressure development promoted by ice sheet growth over the study area, and configuration of the substratum. Transport of the resulting conglomerate composed of preglacial intraclasts and fluidized sand occurred through subglacial pipes. The brecciated material is deposited in subglacial cavities, forming fans of massive sandy conglomerate infilling the base of the tunnel valley. The conglomeratic unit is partially reworked by meltwater and exhibits intense soft-sediment deformations, due to episodes of ice–bed coupling and decoupling.

© 2014 Elsevier B.V. All rights reserved.

1. Introduction

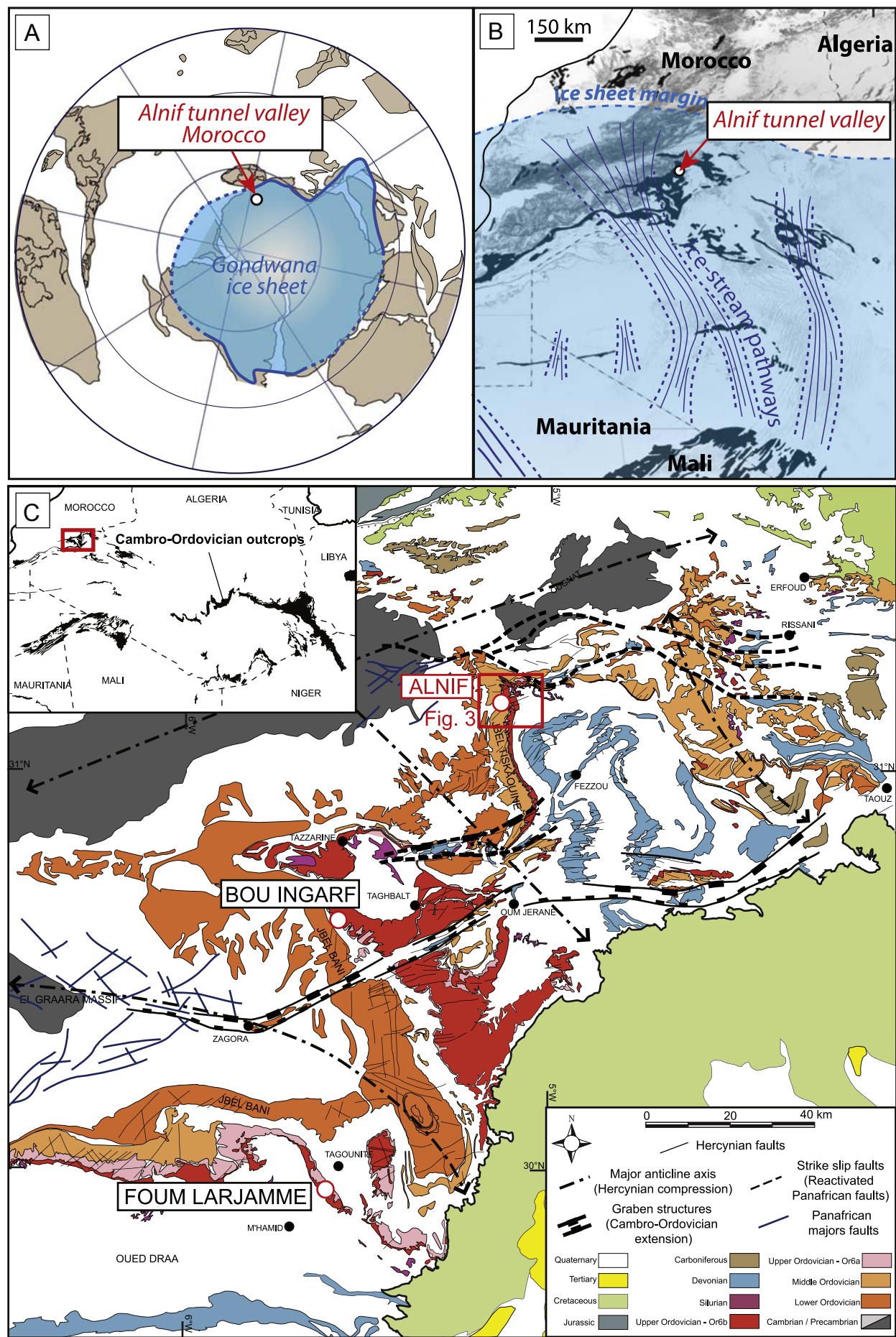
Over the past decades, knowledge about tunnel valley morphologies and their sedimentary infills has greatly improved, but their mechanisms of formation still remain debated (Ó Cofaigh, 1996; Huuse et al., 2012; Kehew et al., 2012). In recent reviews (Kehew et al., 2012; van der Vegt et al., 2012), four major models have been put forward to explain the processes of tunnel valley formation.

Model 1 proposes tunnel valley formation in stable and low pressure subglacial tunnels where subglacial tunnel valleys grow progressively through deformation of basal soft sediments and transport of the

mobilized bed into subglacial conduits (Boulton and Hindmarsh, 1987; Boulton et al., 2007a, 2007b). In Model 2, it is suggested that rapid tunnel valley formation occurs by one or several catastrophic outburst floods. This model requires meltwater accumulation up-ice from a zone of ice–bed coupling, blocking the subglacial drainage (Piotrowski, 1994; Johnson, 1999; Hooke and Jennings, 2006). Stored meltwater is suddenly released when the fluid pressure exceeds the strength of the permafrost or/and the ice pressure exerted on the bed. Model 3 explains the formation of anastomosed or anabranching valleys by bedrock erosion during the collapse of massive sheet floods into channelized flows underneath ice sheets (Shaw, 2002, 2010). Model 4 is a more recent and conceptual model that invokes hydraulic fracturing and fluidization of preglacial material as being responsible for tunnel valley formation (Janszen et al., 2012). According to these models, large quantities of meltwater circulating underneath the ice appear to strongly control tunnel valley formation, even if the processes involved remain unclear.

* Corresponding author. Tel.: +33 380396364.

E-mail addresses: edouard.ravier@u-bourgogne.fr (E. Ravier), jfbuon@u-bourgogne.fr (J.-F. Buoncristiani), michel.guiraud@u-bourgogne.fr (M. Guiraud), jmenzies@brocku.ca (J. Menzies), sylvain.clerc@u-bourgogne.fr (S. Clerc), eric.portier@toutatgaz.com (E. Portier).



The stress exerted by flowing ice over confined and water-saturated aquifers is indirectly responsible for soft-bed deformation including processes of liquefaction/fluidization, hydrofracturing and brecciation (Passchier et al., 1998; van der Meer et al., 2009; Denis et al., 2010; Phillips et al., 2012). Thus, reconsidering the potential of these deformation mechanisms in remobilizing and evacuating sediments beneath an ice mass is essential, in order to evaluate their impact on tunnel valley formation.

This study aims to test the role of fluid overpressure on tunnel valley genesis, through the observations of sediments and their internal deformations within the Ordovician Alnif tunnel valley, located in the eastern Anti-Atlas Mountains (Morocco). This work represents the first Ordovician study case, benefiting from a large-scale and continuous outcrop that provides insights into the process of tunnel valley formation. The morphology of the valley as well as features of glacial and preglacial deposits will be described. The soft-sediment deformation structures (SSDS) affecting both preglacial and glacial sediments at both macro and micro-scale will be analyzed and interpreted. Finally, a new model of subglacial soft bed remobilization and tunnel valley formation will be proposed.

2. Geological setting

2.1. Study area

2.1.1. Stratigraphy

The Alnif tunnel valley is located in the Eastern part of the Moroccan Anti-Atlas Mountains. The valley is situated in the northernmost part of the Gondwana palaeo-ice sheet (Fig. 1A, B). Outcrops in this area expose Upper Ordovician deposits displaying clastic sediments. The stratigraphic succession of Upper Ordovician deposits is composed of the Lower Ktaoua, the Upper Tiouririne and the Upper Ktaoua formations (Villas et al., 2006) (Fig. 2). These formations are characterized by alternating sandstones and shales, with a predominance of shale deposits (2/3 of the preglacial deposits removed during formation of the valley) recording marine deposition within offshore to shoreface environments, frequently affected by storms (Alvaro et al., 2007; Clerc et al., 2013) (Fig. 2B). During the Hirnantian, a thick clastic sedimentary sequence (up to 200 m thick) corresponding to the Upper 2nd Bani Formation (Destombes et al., 1985) was deposited above a major unconformity surface. This surface can be followed through the Anti-Atlas region, along the axis Fom Larjame/Bou Ingarf/Alnif (Figs. 1C, 2A).

2.1.2. Structural situation

The Anti-Atlas Mountains, representing a large antiform structure striking NE–SW were formed by the Late Carboniferous–Permian compression event (Hercynian orogenesis) (Fig. 1C). The Anti-Atlas Mountains basement also records the earlier Panafrican orogenesis and is associated with a predominance of faults oriented NW–SE, following the Panafrican sutures (referred to as the Major Anti-Atlas Suture or Anti-Atlas Major fault) (Burkhard et al., 2006). In North Africa, the Panafrican convergence stops during the Late Proterozoic and is followed by a period of post-orogenic subsidence. During the Paleozoic, the post-orogenic extension results in the formation of tilted blocks and half grabens, controlling the development of E–W to NW–SE basins (Robert-Charreau and Burkhard, 2008) (Fig. 1C). Location and orientation analyses between the position of the Paleozoic depocentres and Panafrican structures highlight a clear correlation between position of Paleozoic basins and formation of basement structures. Orientations of Paleozoic basins seem to have been controlled by Panafrican tectonic events which could have behaved as mobile zones preferentially

affected by post-orogenic subsidence (Destombes et al., 1985; Marante, 2008). Nowadays, these Cambro–Ordovician structures cannot be clearly observed since the Hercynian compression phase at the end of the Early Paleozoic, oriented SSE–NNW, led to folding, faulting, uplift and subsequent partial erosion of the Palaeozoic cover (Figs. 1C, 3A). Most of the deformation responsible for the current structuration of the Anti-Atlas Mountains are dated from the Hercynian and therefore distort the Early Paleozoic subsidence signal.

2.2. Glacial evidence

During the Late Ordovician, an 8000 km diameter ice sheet covered the supercontinent Gondwana from the Arabian Peninsula to South America and from South Africa to Morocco (Beuf et al., 1971; Veevers, 2005; Diaz-Martinez and Graham, 2007) (Fig. 1A). The development of cold conditions during the late Hirnantian (Late Ordovician; Fig. 2A) was evidenced by $\delta^{13}\text{C}$ and $\delta^{18}\text{O}$ positive excursions (Finnegan et al., 2011). The Hirnantian glaciation (1 to 2 Ma in duration) corresponds to the maximum of a cold period that could have lasted over 10 Ma when most of the glacial deposits observed in North Africa and the Arabian Peninsula have been deposited (Brenchley et al., 1994; Hallett, 2002; Ghienne et al., 2007; Denis et al., 2010).

Glacial deposits and tunnel valleys recorded during the Hirnantian episode in Morocco have been the subject of several studies and have been described in the Anti-Atlas and the High-Atlas Mountains (Destombes et al., 1985; Villas et al., 2006; Alvaro et al., 2007; Le Heron et al., 2007; Le Heron, 2007; Loi et al., 2010; Clerc et al., 2013). The glacial origin of these valleys and associated glacial sedimentary deposits have been highlighted by the occurrence of fluted surfaces, striae, grooves, drumlin-like bedforms, hairpin-like structures, notably at Fom Larjame and Bou Ingarf in the Anti-Atlas Mountains or at Isk N'Tazzoult in the High Atlas Mountains.

The temporal and stratigraphical framework of the glacial episode in the Moroccan Anti-Atlas is well constrained (Destombes et al., 1985; Villas et al., 2006). The occurrence of Ashgill fauna (Late Ordovician) in preglacial strata below the synglacial deposits and the widespread occurrence of lowermost Silurian graptolite-bearing shale above the synglacial strata represent a useful lithostratigraphic and biostratigraphic guide permitting large-scale correlation of the glacial deposits in the Anti-Atlas Mountains (Fig. 2A, B).

The Alnif valley is also located in the Anti-Atlas Mountains, respectively 50 km and 150 km away from the Bou Ingarf and Fom Larjame tunnel valleys (Fig. 1C). In Alnif, fauna-rich beds containing Ashgill fauna below the incision combined with the occurrence of Silurian graptolite shales above Hirnantian deposits allow correlation along the major unconformity surface along an axis Fom Larjame/Bou Ingarf/Alnif (Figs. 1C, 2A). The glacial origin of this unconformity surface, resulting in a stratigraphic gap, has been evidenced by striae and subglacial lineations in Fom Larjame and Bou Ingarf (Le Heron, 2007; Loi et al., 2010). Although striae are not observed in Alnif, the base of the glacial incision is characterized by elongated morphologies corresponding to smooth and polished flutes (200 m long/1 m wide/1 m high) oriented towards the palaeo ice flow (e.g., NW) (Clerc et al., 2013). The elongation ratio (Length/Width) varies from 2 to 5. The glacial pavement also displays abundant millimeter-thin lineations which are interpreted as sheet dewatering structures and extensive surfaces displaying radial step normal microfaults probably related to episodes of ice coupling with the bed (Beuf et al., 1971; Biju-Duval et al., 1974; Clerc et al., 2013). The Alnif incision is 5 km wide and 180 m deep with a subhorizontal base and therefore displays a similar morphology to other tunnel valleys described in the Ordovician glacial record (e.g.,

Fig. 1. (A) Palaeogeographic reconstruction for the latest Ordovician, adapted from Cocks and Torsvik (2002) and modified after Clerc et al. (2013). The extension of the Hirnantian palaeo-ice sheet, modified from Ghienne et al. (2007) is represented on the Gondwana palaeo continent. (B) Detailed palaeogeographic reconstructions of the ice sheet and associated ice-stream positions in Northwestern Africa are shown (modified after Ghienne et al., 2007 and Le Heron et al., 2007). (C) Structural situation and geological map of the South Anti-Atlas region, Morocco. Location of the Alnif, Bou Ingarf and Fom Larjame tunnel valleys is reported. Modified from Destombes et al. (1985) and Robert-Charreau and Burkhard (2008).

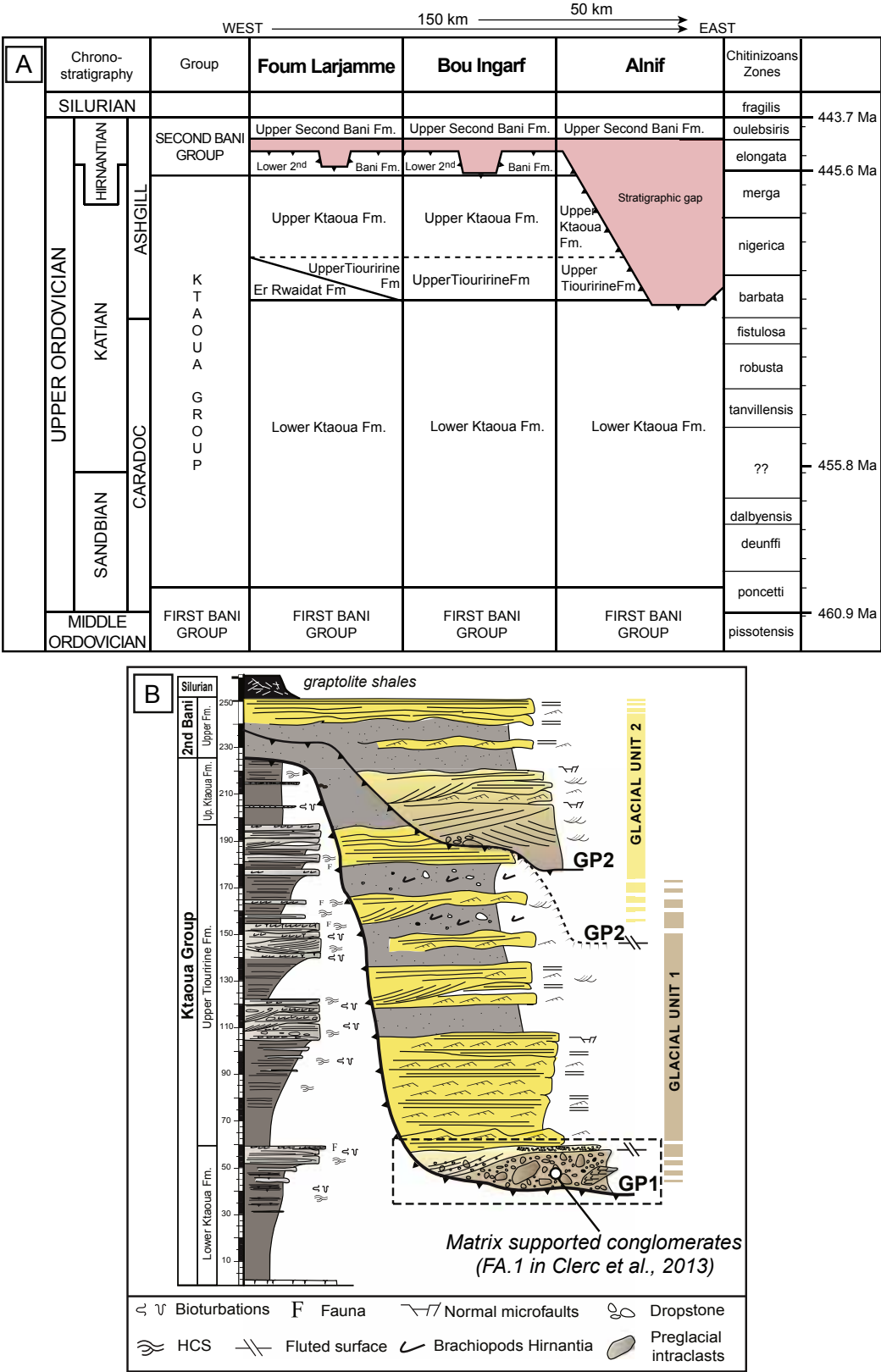


Fig. 2. Chronostratigraphy of Upper Ordovician deposits between Foum Larjamme and Alnif. Synthetic log section showing the polyphased sedimentary infill of the Alnif tunnel valley (Glacial units 1 and 2) and the position of the two glacial pavements (GP1 and 2). Modified after Clerc et al. (2013).

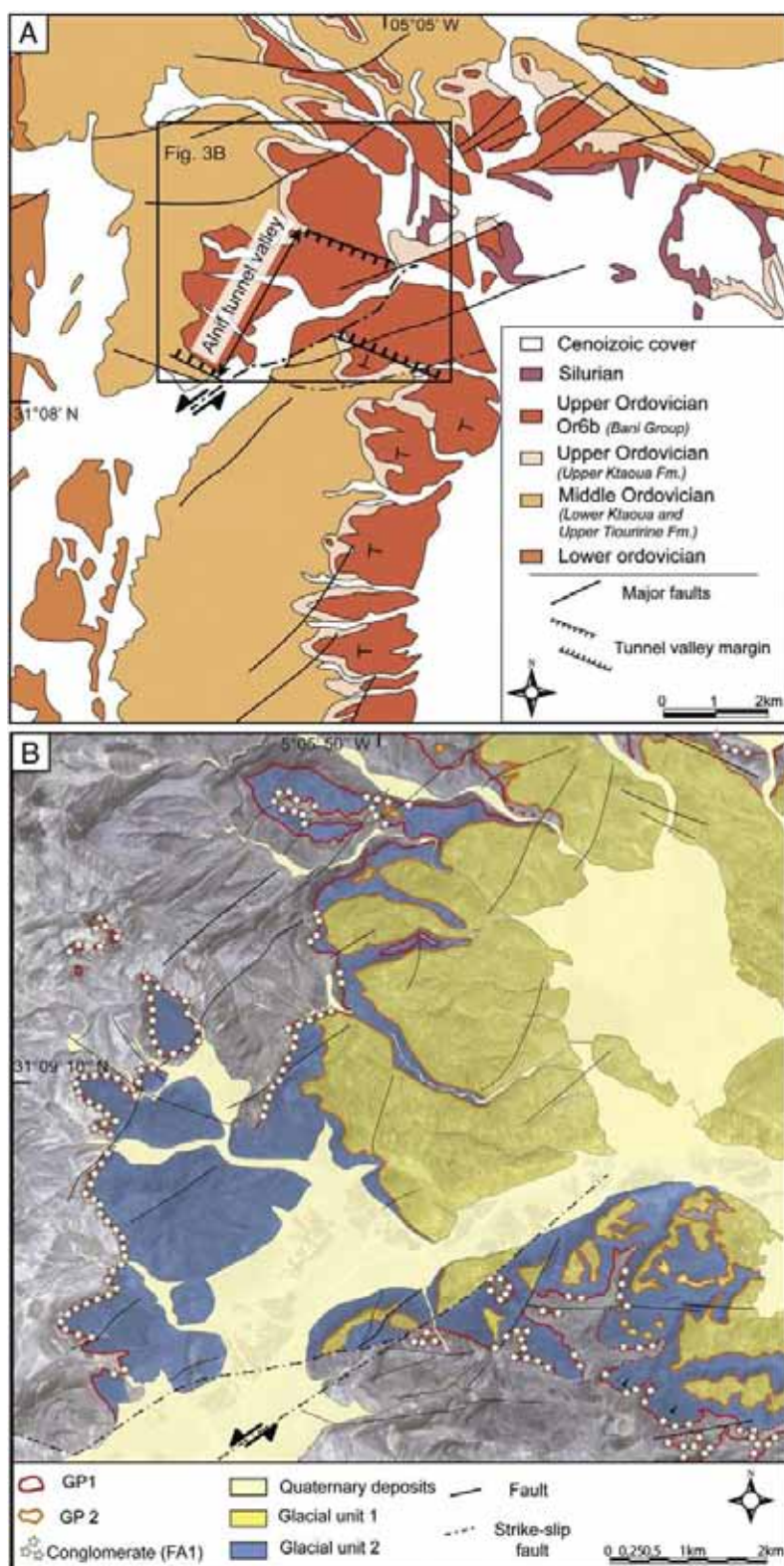


Fig. 3. (A) Detailed geological map in the Alnif area. The position of the Alnif tunnel valley and major faults is reported on this map. (B) Map of glacial pavements 1 and 2 and corresponding glacial units 1 and 2 related to the superimposed system of tunnel valleys described in the Alnif area. The heterogeneous distribution of the conglomerate at the base of the first glacial incision (GP1) is represented by stars.

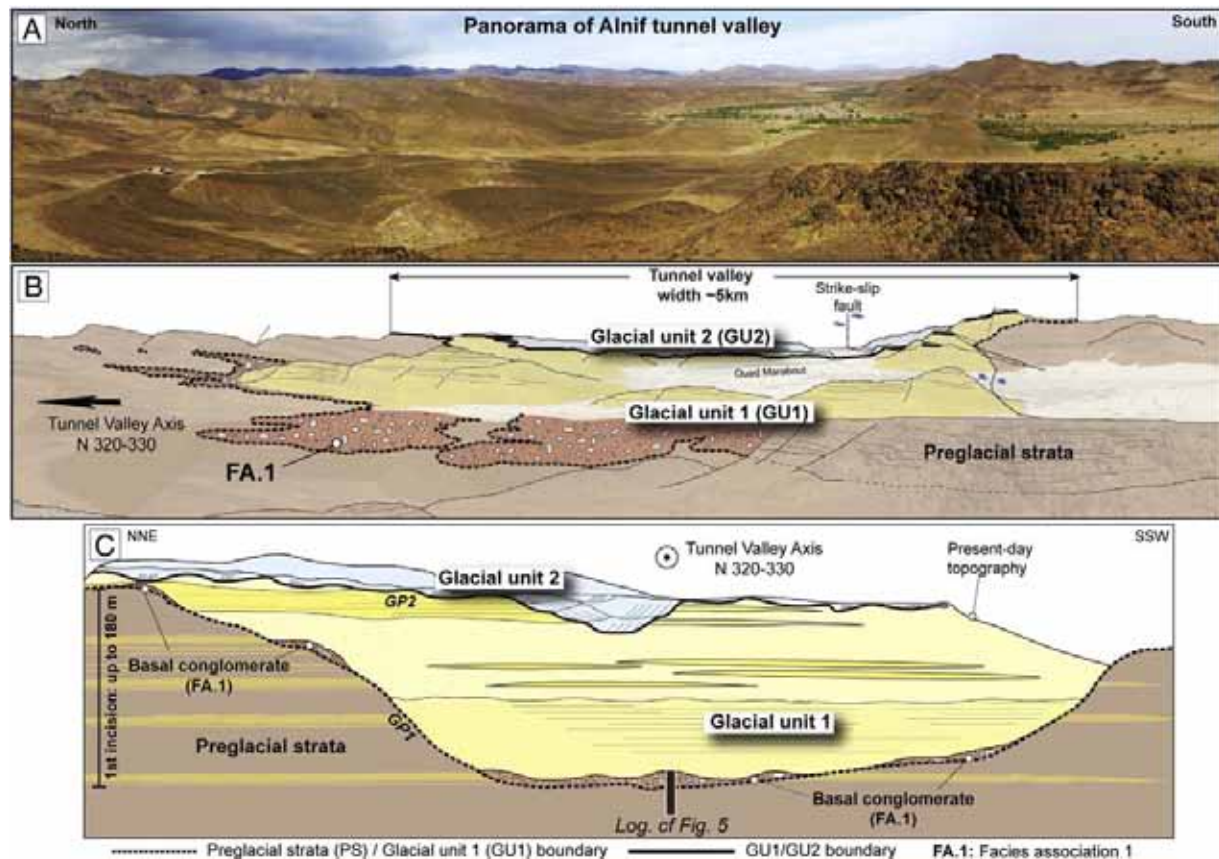


Fig. 4. (A) Panoramic photograph of the Alnif tunnel valley. (B) Interpreted photograph illustrating the geographical extent of the two glacial units (GU1 and GU2). Localisation of FA.1 is reported at the base of GU1 (modified after Clerc et al., 2013). (C) Synthetic model of tunnel valley infill modified after Clerc et al. (2013). Position of the log section described in Fig. 4 is reported on the model.

Algeria, Libya, South Arabia) (Hirst et al., 2002; Ghienne, 2003; Le Heron et al., 2004).

2.3. Tunnel valley sedimentary infill and morphology

Studies of the Hirnantian glacial sediments in the Alnif area revealed two superimposed glacial incisions, representing two major unconformities: Glacial pavement 1 (GP1) related to the base of the glacial record and Glacial pavement 2 (GP2), in the upper part of the glacial sedimentary succession (Clerc et al., 2013) (Figs. 2B, 3B, 4). The upper erosion surface is used to divide the sedimentary sequence infilling this major tunnel valley into a lower and upper unit, successively named Glacial unit 1 (GU1) and Glacial unit 2 (GU2) (Fig. 4). In the Alnif area, preglacial and glacial sediments have been clearly discriminated, based on paleontological, sedimentological and deformational analyses (Destombes et al., 1985; Villas et al., 2006; Alvaro et al., 2007; Clerc et al., 2013). The glacial sedimentary sequence has been interpreted as the result of sediment deposition in subglacial to proglacial/glaciomarine environments (cf., Clerc et al., 2013, for further details).

The buried palaeo tunnel valley related to the first glacial incision is about 5 km wide and 180 m deep, trending SSE–NNW (320° N) (Fig. 4). The base of the tunnel valley is irregular whilst the flanks display slopes averaging 10°. The first glacial unit is characterized by a sharp contact with preglacial facies. This sharp contact is discontinuously overlain by basal conglomeratic deposits (FA.1) along the valley floor, flanks, and beyond the valley margins. Beyond the valley margins, a stratigraphic gap is also observed, corresponding to preglacial material also removed

during the glacial episode. These zones where a thinner pile of preglacial material has been eroded correspond to the interfluvies.

This study will focus on the 10–15 m thick sedimentary succession immediately overlying the first incision, especially on the patchy conglomerate deposited above GP1 (Fig. 3B). This lowermost glacial deposit is defined as the first facies association (FA.1) in the study of Clerc et al. (2013) (Fig. 3). The glacial origin of the conglomeratic unit was illustrated by the internal occurrence of glacial deformation structures, such as smooth and polished fluted structures with long elongation ratios and radial extensional step normal microfaults occurring over extensive areas (Clerc et al., 2013).

3. Results

Sedimentary facies and soft sediment deformation structures affecting both preglacial and glacial sediments will be described. For reasons of clarity, deformation structures are treated separately and not mentioned in the sedimentary facies description. The stratigraphic position of the soft-sediment deformations (SSDS) is reported in the synthetic log section (Fig. 5) and the characteristics of the different sedimentary facies summarized in Table 1.

3.1. Sedimentary facies

3.1.1. Description

The lowermost sediments of the first Glacial unit (GU1) are characterized by matrix-supported conglomeratic deposits forming a

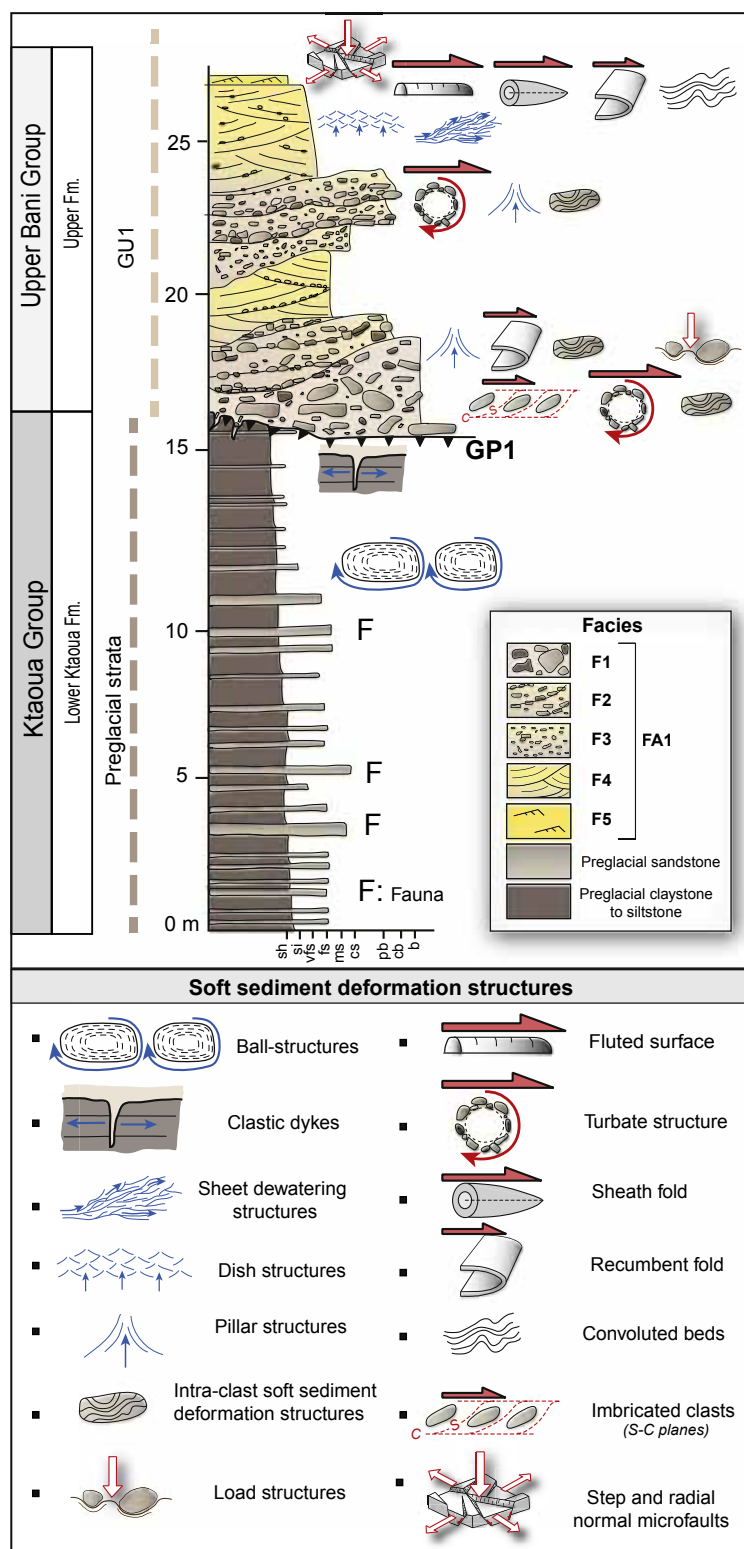


Fig. 5. Synthetic log section illustrating the stacking pattern of the basal unit referred as FA.1 in the study of Clerc et al. (2013), and its stratigraphic relation with underlying preglacial sediments. Position of soft-sediment deformation structures is reported along the log section.

Table 1

Classification of sedimentary facies (F).

	Description	Interpretation
FA.1 Matrix-supported conglomerates (defined by Clerc et al., 2013)	Matrix-supported conglomerate (1 to 15 m thick) containing sandstone and claystone clasts (occasionally containing well-preserved fauna) packed in a coarse to very coarse sandy matrix. Intraclasts are generally angular and mostly display a tabular shape. Locally the conglomerate is incised by large channels with normally graded conglomerates, or medium-grained sandstones.	Debris flows with short-distance transport (local origin)
F1 to F5 Detailed description of FA.1 (this study)		
F1 Matrix-supported conglomerates	Matrix-supported conglomerate, apparently massive, 4 m thick, composed of clasts containing preglacial fauna embedded within a coarse sandy matrix. Intraclasts vary from mm to m-scale with a wide range of shapes including tabular/discoid, ball-shaped and elongated shapes.	Deposition by hyperconcentrated density flows
F2 Channelized conglomerates	Lenses of matrix-supported conglomeratic deposits displaying crude trough cross-bedding structures and occasional normal grading. Lenses are 0.5 to 2 m deep and 3 to 12 m wide. Erosive surfaces are pronounced and often underlined by boulder lags.	Deposition within channels by waning pulses of high density flows
F3 Microconglomerates	Microconglomeratic deposits occur as lenses being 1 m thick and tens of meters wide. Deposits are moderately sorted and contain occasional discrete laminations. Clasts are rounded to well-rounded. Quartz granules are observed.	Deposition within channels by concentrated density flows with localized upper-flow conditions
F4 Channelized fine to medium-grained sandstones	Lenses of medium to fine-grained sandstones displaying cross-bedding structures. Lenses are 1 to 1.5 m thick and generally tens of meters wide. Trains of imbricated granules and mudclasts occur within F4.	Deposition by turbulent flows and downflow migration of 2D/3D dunes
F5 Ripple cross-laminated siltstones to fine-grained sandstones.	0.3 m thick sheets of ripple cross-laminated siltstones to fine-grained sandstones.	Deposition from laminar flow under lower flow regime

discontinuous 10 to 15 m thick unit (cf., Fig. 3B for the heterogeneous distribution of conglomerate (FA.1) at the base of GP1). This unit consists of five sedimentary facies (F1 to F5) characterized by a laterally and upward variable stacking pattern and an upward decrease in mean grain size (Fig. 5). The idealized basal sedimentary sequence is typically 12 m thick and composed, from bottom to top, by matrix-supported conglomerates (F1) deposited upon preglacial strata with

an unconformable contact, erosively overlain by channelized and normally graded conglomerates (F2) (Fig. 6A). Conglomerates pass upwards into microconglomerates (F3), or trough cross-bedded fine to medium sandstones (F4) (Fig. 6B). The basal sedimentary sequence is generally capped by ripple cross-laminated siltstones to fine sandstones (F5). This basal sedimentary sequence is characterized by numerous erosive contacts (Fig. 6).

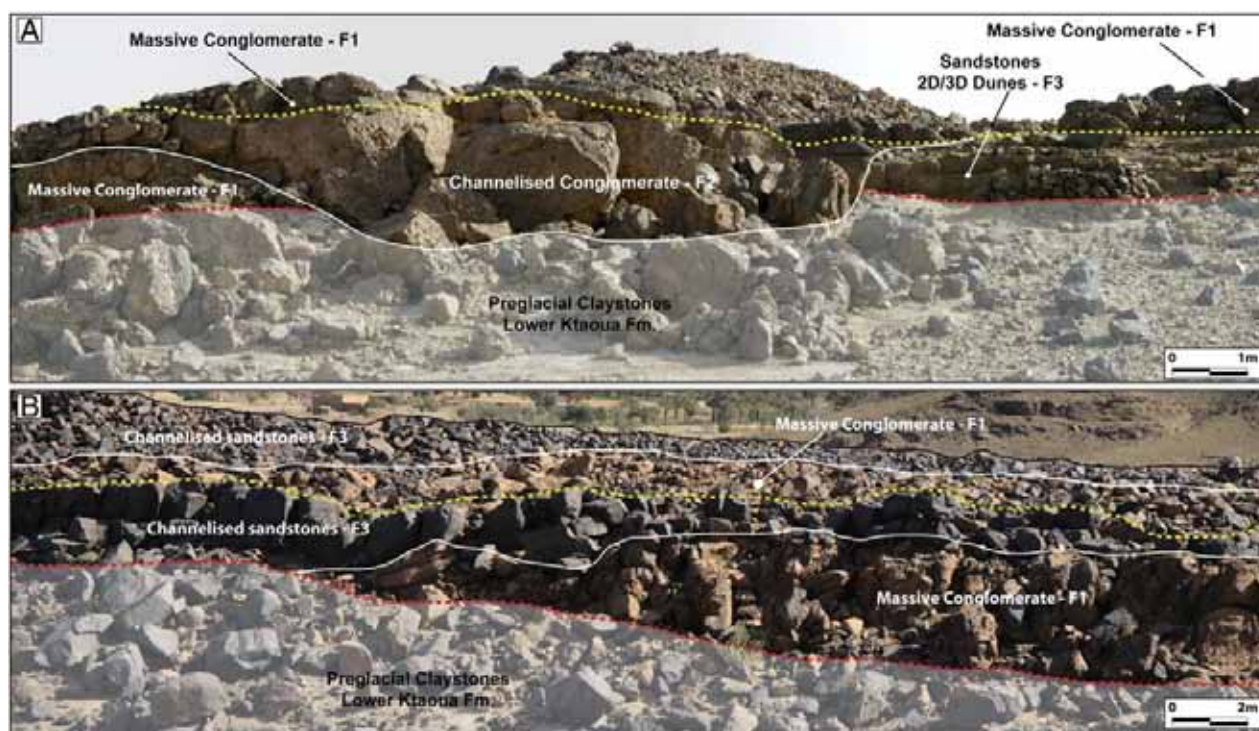


Fig. 6. Interpreted photographs showing the stacking pattern of the basal sedimentary sequence (FA.1). (A) Massive and matrix-supported conglomerates (F1) deposited above preglacial claystones are erosively overlain by sandstone dunes (F4). Channelized conglomerates (F2) erode these deposits down to the preglacial strata. (B) Basal massive conglomerates (F1) deposited on preglacial claystones are erosively overlain by channelized sandstones (F4). A second layer of massive conglomerate (F1) is deposited on top of sandstones.

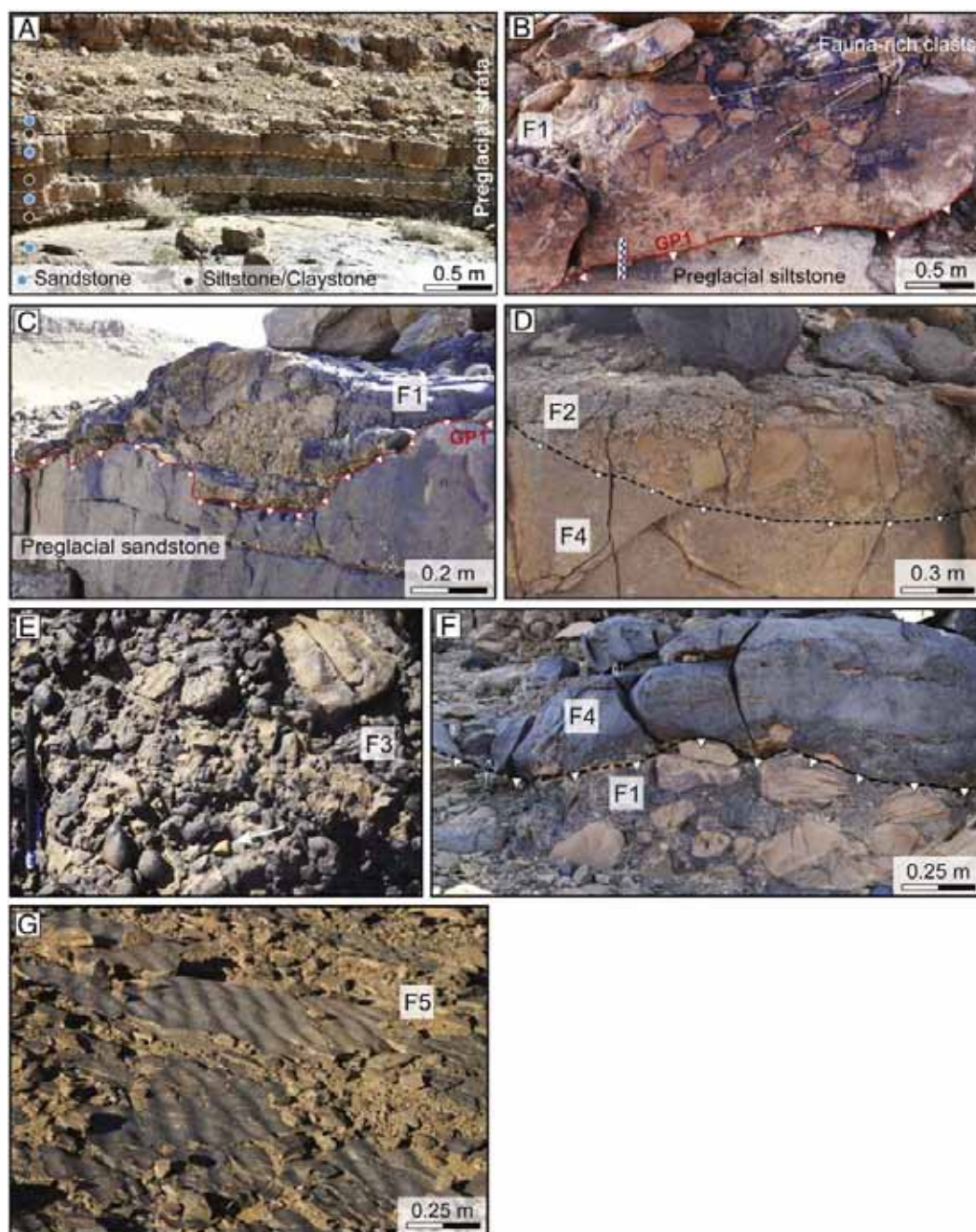


Fig. 7. Facies association 1 exposed at the base of GU1. (A) Typical preglacial alternations of sandstones and claystones/siltstones deposited in a marine environment. (B) Facies 1: Massive matrix-supported conglomerate, containing fauna-rich clasts, lying on preglacial siltstones. (C) Erosive massive conglomerate (F1) deposited upon preglacial sandstones with a sharp and erosive contact. (D) Channelized conglomeratic deposit (F2) eroding glacial sandstone. (E) Microconglomerate (F3) characterized by rounded clasts and frequently polished and smooth quartz granules (white array). (F) Channelized sandstones (F4) erosively deposited upon massive conglomerate (F1). (G) Ripple cross-laminated fine-grained sandstones to siltstones observed at the top of FA.1 (F5).

Discontinuous matrix-supported conglomerates, apparently massive (F1), up to 4 m thick, are generally erosively deposited upon preglacial strata (Figs. 5, 7B, C). This conglomerate corresponds to the base of Glacial unit 1 (GU1) and directly lies on alternating preglacial sandstones and siltstones/claystones containing marine fauna (brachiopods, echinoderms, bivalves) (Figs. 5, 7A).

The conglomerate displays low angle wedge-shape geometry with dimensions up to 600 m long and 500 m wide, associated with a

proximal to distal decrease of conglomerate thickness from approximately 4 to 1 m thick. The matrix of the conglomerate is composed of medium to very coarse sand, with over 90% of quartz grains. Intraclasts display variable grain-size, ranging from clay to medium sand with occasional internal brachiopod shells and calcite cements. Intraclast sizes vary from mm to m-scale in long axis and exhibit a wide range of shapes including tabular/discoid, ball-shaped, elongated, and the coexistence of rounded and angular clasts.

Lenses of matrix-supported conglomeratic deposits (F2) displaying crude trough cross-bedding structures and occasional normal grading frequently occur within the basal unit. The lenticular bodies are 0.5 to 2 m deep and 3 to 12 m wide and display pronounced erosive surfaces occasionally underlined by boulder lags (Figs. 5, 7D).

Lenses of microconglomerates (F3), up to 1 m thick and tens of meters wide, are better sorted compared to F1 and F2 and contain occasional discrete laminations (Fig. 7E). F3 contains rounded to well-rounded preglacial clasts and quartz granules.

Lenses of trough cross-bedded or planar parallel-bedded fine to medium sandstones (F4) are observed within FA.1 and display erosive bases (Figs. 5, 7F). Lenses are 1 to 1.5 m thick and generally tens of meters wide, and display some imbricated granules and mud clasts. The top of the basal unit is often covered by thin (up to 0.3 m thick) and extensive sheets of ripple cross-laminated siltstones to fine sandstones (F5) (Figs. 5, 7G).

3.1.2. Interpretation

At the base of FA.1, the massive and matrix-supported conglomerates with a sandy matrix (F1) are related to sediment deposition by hyperconcentrated density flows (Mulder and Alexander, 2001) and can be referred to as clean-sand debris flows (Talling et al., 2012). Within F1, numerous clasts display a slab-shape and are characterized by sharp edges and angular margins, indicating a very short transport distance or/and a transport within a fluidized matrix preventing clast-to-clast contacts. The occurrence of brachiopods-bearing clasts (Villas et al., 2006; Alvaro et al., 2007) demonstrates the local origin of the material contained in the conglomerate. Calcite cements observed locally within preglacial clasts imply early sandstone diagenesis occurring before fracturing. Shell dissolutions within fauna-rich preglacial layers may occur during burial and compaction, representing the calcite source responsible for early cementation (Tucker and Wright, 1990; Tucker, 2001). The occurrence of angular preglacial clasts implies that preglacial strata have been brecciated.

Lenticular conglomeratic deposits (F2) with normal grading and trough cross-bedding structures are related to reworking and deposition of F1 by high-energy meltwater flows. F2 records sediment deposition within channels by waning and occasional pulses of high density flows and 2D/3D dune migrations under high-energy flows (Mulder and Alexander, 2001). The higher proportion of rounded clasts indicates a longer transport distance, probably related to reworking and transport of massive and matrix-supported conglomerate (F1).

Lenticular bodies of microconglomerates (F3) may indicate reworking and transport/deposition of F1 and F2 by meltwater flow within channels. The better sorting and the decrease in mean grain-size may be related to deposition by concentrated density flows (Mulder and Alexander, 2001).

Occasional faint horizontal laminations indicate localized upper-flow regime conditions within channels. Well-rounded and smoothed quartz granules indicate a long distance transport.

Lenses of trough cross-bedded sandstones (F4) result from the deposition and the downflow migration of 2D/3D sand dunes within channels. Thin sheets of ripple cross-laminated sandstones to siltstones (F5) are related to traction deposition from laminar flow in the lower flow regime (Allen, 1982).

3.2. Deformation structures within preglacial strata

3.2.1. Description

On the interfluvies of the tunnel valley, 5 m below the first glacial incision (GP1), preglacial beds locally display pseudo-ellipsoidal deformation structures with concentric layering, resembling large-scale ball structures. These structures, up to 4 m wide and 1 m high, are constrained to a 600 m zone, 1.5 to 2 m in thickness (Fig. 8A, B). Two superimposed layers of ball structures are observed within this zone, each being delimited by thin clay layers (0.05 m thick). Similar structures are also observed within the glacial sediments below the second glacial incision

(GP2), they are occasionally cross-cut by subvertical clastic dykes that are up to 0.3 m thick (Fig. 8C, D).

At the micro-scale, these cells are characterized by the development of millimeter-sized turbate structures illustrated by circular quartz grain re-arrangements. The turbate structures are overprinted by grain-rearrangements along discrete conjugate bands (Fig. 8E).

Below the glacial incision, preglacial strata are cross-cut by vertical to subvertical clastic dykes propagating downwards, infilled by the overlying massive conglomerate (F1). These structures are up to 1.5 m long and 0.1 to 0.15 m wide.

3.2.2. Interpretation

Ball structures occur in both preglacial and glacial sediments below major glacial erosive surfaces (GP1 and GP2), suggesting that these structures were formed during the glacial episode. Clastic dykes cross-cut ball structures implying that formation of the ball-structures occurred when sediments were still water-saturated and unlithified. Large ball structures indicate liquefaction of the sediment and have been interpreted to be the result of either loading, differential compaction, high sedimentation rate or ground water movement (Maltman, 1994; Pisarska-Jamroz and Weckwerth, 2013). Laboratory studies lead to similar structures when the input of water was conducted within confined and porous sediment layers (Frey et al., 2009). In this configuration, ball structures form when sediments and water are entrained in an upward flow as the confined aquifers need to release the excess of porewater pressure. Beneath GP1, the emplacement of ball structures may be triggered by a combination of meltwater input within preglacial permeable strata or/and the basal shear stress exerted by an overriding ice sheet.

At micro-scale, the turbate structures observed within the ball structures may be formed in response to basal shearing and porewater pressure increase (Hiemstra and Rijdsdijk, 2003). These microstructures are overprinted by conjugate bands, indicating a second phase of deformation induced by a vertical shear stress (Ballas et al., 2013). The shear stress can either be related to the lithostatic weight during sediment burial or ice overloading.

The subvertical injectites indicate hydraulic fracturing related to an applied vertical or subvertical stress, as fractures are opened parallel to the direction of the maximum compressive stress (Cosgrove, 1995, 2001; Rodrigues et al., 2009). In such setting, the ice weight or the lithostatic weight induced by deposition of conglomerates (F1) could represent the inferred vertical stress (Le Heron and Etienne, 2005; Clerc et al., 2012).

3.3. Deformation structures within intraclasts of the conglomerate

3.3.1. Description

Three types of preglacial intraclasts can be defined within conglomeratic deposits, depending on their degree of lithification at time of deposition. (a) Intraclasts with preserved internal sedimentary structures exhibit planar parallel-laminations containing fossil coquinas, trough cross-stratifications and sharp block-to-matrix contacts (Fig. 9A). (b) Intraclasts with disturbed or deformed original sedimentary structures and sharp contact with the matrix. The deformation structures encompass pillar structures, sheet dewatering structures and convolute laminations (Fig. 9B, C). (c) Intraclasts with disturbed original structures and contorted and diffused contact with the surrounding matrix (Fig. 9D, E).

An example of internal SSDS is notably shown in Fig. 9C where pillar structures cross-cutting laminated fine-grained sandstones are constrained to a layer below a coquina bed. Other intra-blocks structures such as disrupted layering, convolute bedding and internal domains that are differentially enriched in clays can be distinguished (Fig. 9D). The outlines of preglacial intraclasts are frequently deformed by the intrusion of the surrounding matrix evidenced by large quartz grains penetrating the margin of clayey clasts. Quartz grains are also sometimes completely embedded within clayey to silty preglacial

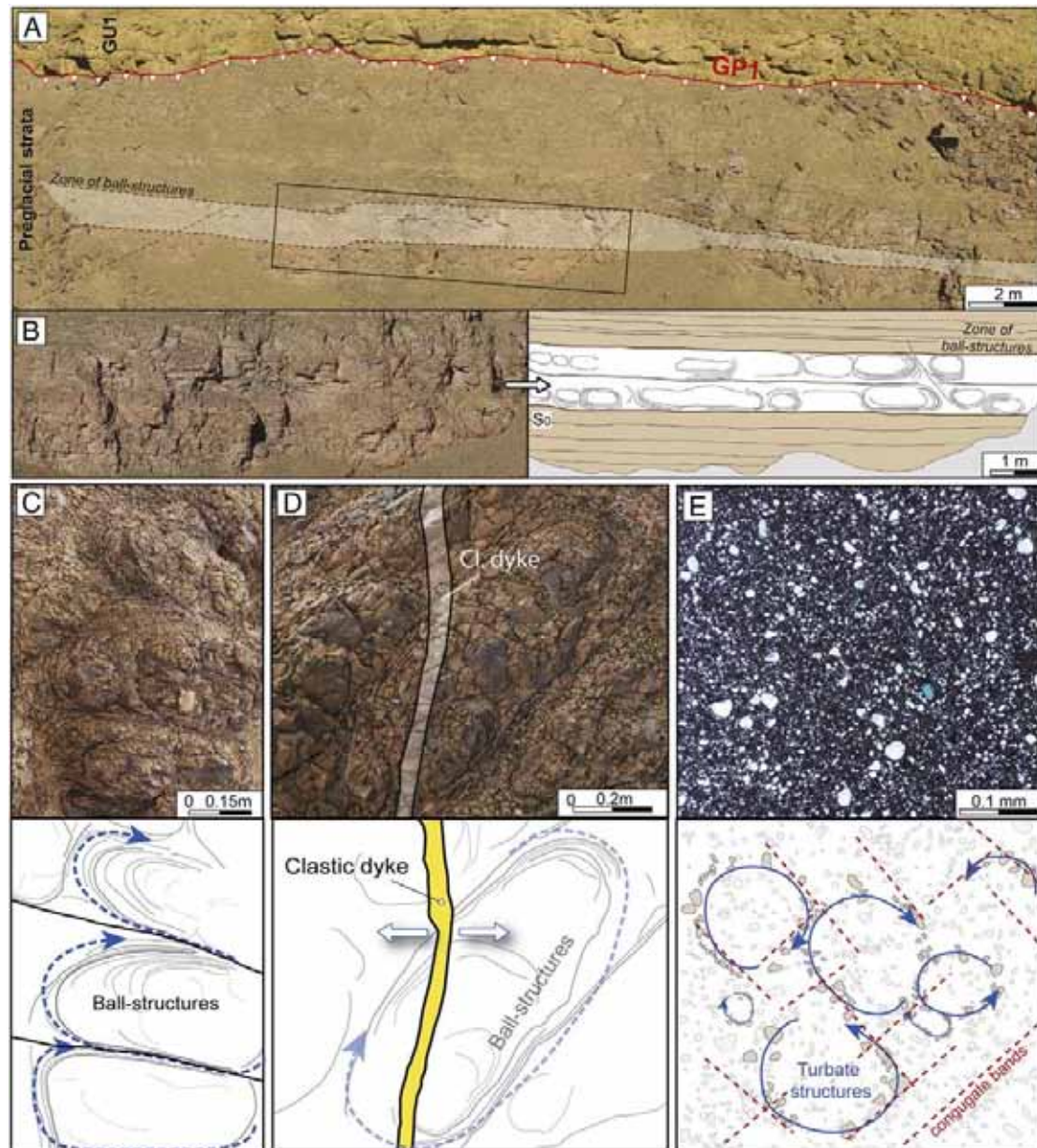


Fig. 8. (A) Zone of large-scale ball structures observed within preglacial silty sediments, located 5 m below the first glacial incision (GP1). (B) Close-up of ball structures, where two layers of deformation structures delimited by thin clay beds occur. (C) Ball structures observed within glacial sediments below GP2. (D) Ball structures cross-cut by a clastic dyke below GP2. (E) Turbate structures associated with conjugate bands observed at microscopic scale within ball structures.

elements (Fig. 9D, E). The abundance of intruded grains frequently leads to the deformation of the margins of preglacial elements or sometimes to in-situ clast fragmentation (Fig. 9E). At the micro-scale, a three-dimensional network of fractures infilled by quartz cement occurs within a soft intraclast (Fig. 9D).

Some hexagonal-shaped intraclasts displaying angular and sharp margins exhibit two sets of obtuse angles ($\approx 90^\circ/110^\circ$) defined as the angles between planes parallel to clast internal laminations (S0) and planes parallel to clast margins (Fig. 10A).

3.3.2. Interpretation

The different types of preglacial blocks reveal that preglacial strata displayed different degrees of lithification prior to the timing

of brecciation. (a) and (b) Preserved sedimentary structures or SSDS and sharp clast-to-matrix contacts indicate that brecciation processes affected lithified or partly lithified preglacial material. (c) Intraclasts with contorted outlines and deformed by matrix intrusion indicate that part of the preglacial material was unlithified during brecciation. In addition, angular clayey intraclasts with embedded quartz grains may derive from clay detachment during hydrofracturing phases affecting preglacial clayey sediments. Similar clasts have been interpreted as a result of fracturing, spalling and corrosion of host clay strata during sand injection (Scott et al., 2009).

Soft-sediment deformations cross-cutting primary sedimentary structures imply post-depositional deformation of the preglacial

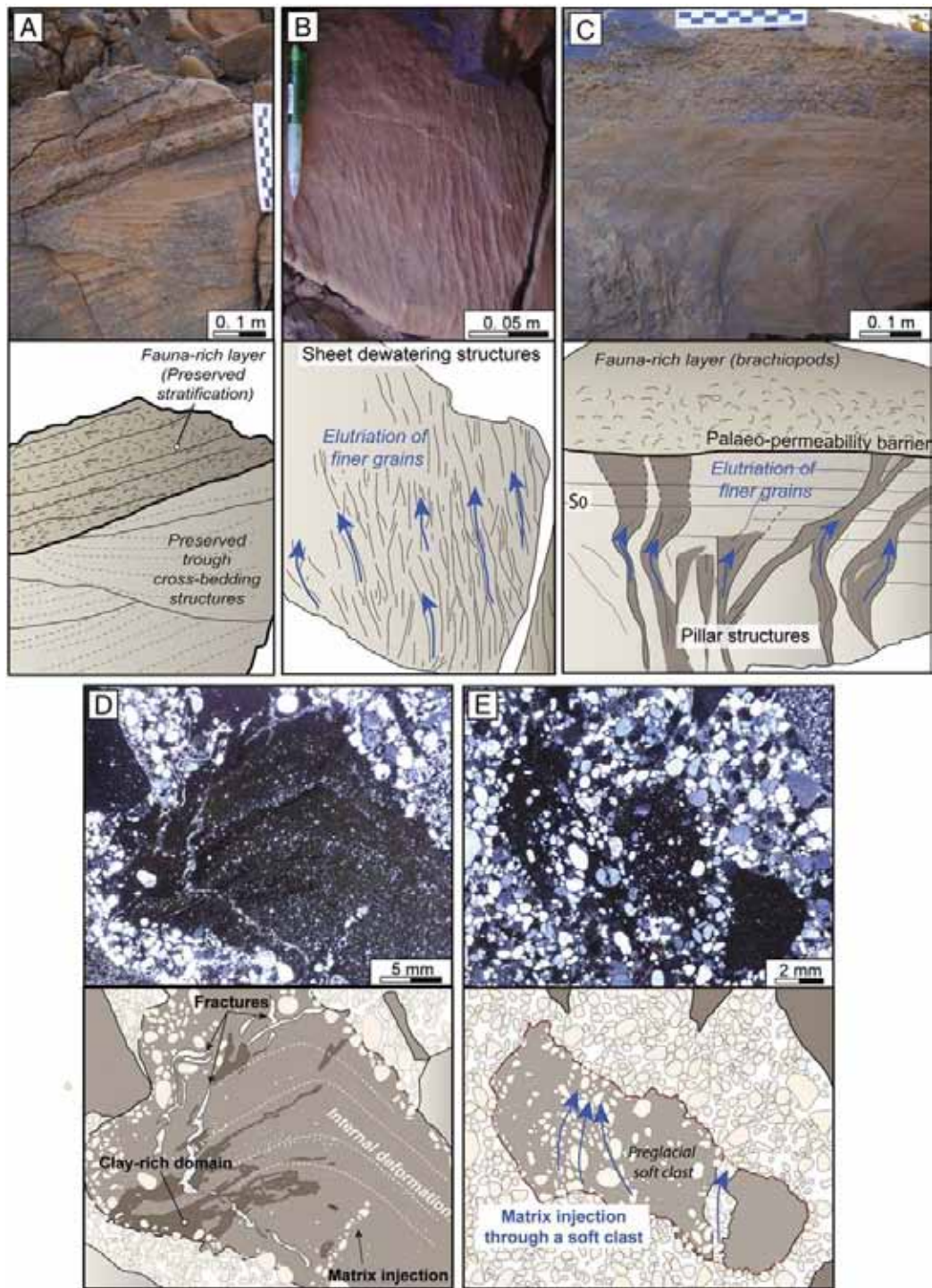


Fig. 9. Intra-clast structures at both macro- and micro-scale. (A) A preglacial clast with preserved trough-cross bedding structures and a fauna-rich laminated bed. (B) Intra-clast sheet dewatering structures related to local clay enrichment along water escape conduits. (C) Pillar structures constrained to a bed located below a fauna-rich layer, related to upward water escape. SSDS do not affect the overlying layer because of the early lithification of the fauna-rich layer. (D) A preglacial intraclast displaying clay-rich domains, injected matrix, and a complex network of fractures constrained to the clast. (E) Preglacial intraclast deformation and brecciation due to matrix intrusion through the clast.

material. Deformation structures including pillar structures, sheet dewatering structures, and convolute laminations are indicative of processes of sediment liquefaction (Lowe, 1975; Owen, 1987; Maltman, 1994). Clay domains indicate that preglacial materials are differentially

enriched in fine particles which may correspond to porewater transmission during dewatering and subsequent clay translocation (Menzies and Ellwanger, 2011). Deformation structures in intraclasts are sometimes constrained to fine-grained sandstone layers (Fig. 9C) and do not extend

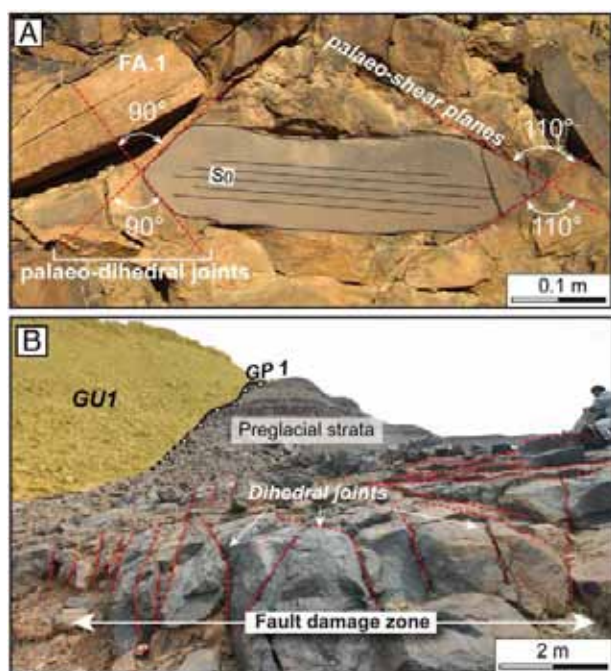


Fig. 10. (A) A preglacial intraclast displaying sharp and well defined margins with two sets of obtuse angles, related to strata fracturing along palaeo-dihedral joints affecting preglacial material. (B) Dihedral joints occurring in preglacial strata below GP1 within a fault damage zone along the border of the tunnel valley.

into overlying fauna-rich layers. These overlying coquina beds act as an impermeable barrier, sealing water-saturated sediments. This permeability barrier is probably linked to early diagenetic processes that led to the lithification of these specific fauna-rich layers. The network of open joints constrained to a soft intraclast demonstrates that a phase of fracturing occurred prior to deposition of the conglomerate while preglacial sediments were still unlithified.

Hexagonal-shaped and angular preglacial clasts displaying sharp margins (Fig. 10A) mimic palaeo-dihedral joints related to brittle shear failures (Price and Cosgrove, 1990). This pattern of joints deduced from intraclast observations is similar to in-situ dihedra joints that have been observed along the margin of the tunnel valley (Fig. 10B). These joints corresponding to brittle deformations are localized along a corridor where preglacial sediments are highly fractured. This fractured zone can be referred to a damaged zone and is generally associated with a nearby fault core. This corridor corresponds to the volume of deformed wall rocks around a fault surface and results from the initiation, interaction and build-up of slip along faults (McGrath and Davison, 1995; Kim et al., 2004). Jointing of preglacial material occurs before the sedimentary infill of the tunnel valley as suggested by the presence of these dihedra joints solely within the preglacial strata. The occurrence of hexagonal-shaped intraclasts and the observation of damage zone may indicate that dihedra joints are used as preferred planes of weakness during processes of preglacial strata brecciation.

3.4. Deformation structures within the conglomerate

3.4.1. Description

Within conglomeratic deposits, numerous evidence of intraclast reorientations and matrix remobilization are observed at both macroscopic (1) and microscopic (2) scales.

(1) Macro-scale turbate structures are distinguished, consisting of a ring of rearranged blocks delimited by a ring of clasts around an axis

that contains matrix or a core stone (Figs. 5, 11A, B). These structures are up to 0.75 m in length and are characterized by zero or limited contacts between the clasts. In Fig. 11B, two adjacent turbate structures with limited clast-to-clast contacts are imbricated, following a S–C fabric with a high θ angle (Fig. 11B). The θ angle is defined as the angle between S and C planes and is an indicator of the strain degree and rate (Choukroune et al., 1987; Passchier and Trouw, 2005). This secondary fabric records the polyphased deformation of the conglomerate.

A NW-verging recumbent fold evidenced by clasts displaying a low θ angle between S and C planes occurs within the conglomerate (Fig. 11C). Clasts are locally reoriented along vertical pipes (Fig. 11D). Occasional matrix deformation structures produced by embedded intraclasts are observed (Fig. 12A). Chaotic flow surfaces within the matrix are locally preserved, these flow surfaces mimic chaotic convolute structures (Fig. 12B).

(2) At micro-scales, necking structures, clay domains and grain-size segregation in the matrix around clasts are observed (Fig. 12C). Large quartz grains are occasionally stacked in the shadow of preglacial clasts. The in-situ fragmentation of a single clast resulting in two tear drop-shaped elements is observed (Fig. 12D). Edge-to-edge grain crushing within the F1 matrix is absent.

3.4.2. Interpretation

(1) Macroscale turbate structures are not diagnostic of a single depositional environment since they can occur either in deforming subglacial beds or in debris flows. In subglacial environments, turbate structures will develop in response to basal shearing, high strain intensity and high porewater pressure induced by an overriding ice flow (Menzies, 2000; Hiemstra and Rijdsdijk, 2003) while turbulent flows within the matrix of a debris flow can produce transitory rotational deformations leading to the same type of structures (Menzies and Zaniewski, 2003; Phillips, 2006). Imbricated turbate structures, displaying a S–C fabric, demonstrate a second phase of deformation, related to simple shear which could be related to stresses exerted by an overriding ice sheet or debris flow. The absence or the limited clast-to-clast contacts in the turbate structures implies that water-saturated sediments were deformed under high porewater pressure as high as limiting or even preventing clast-to-clast contacts (Menzies, 2012). The occurrence of adjacent turbate structures indicates that the structures formed at the same time with mechanical cog rotating in opposite directions or that a first turbate structures developed by shear and then ceased motion to be followed by the formation of a second turbate structure (cf., turbate structures 1 and 2; Fig. 11B).

Recumbent folds, observed within the conglomerates, indicate hydroplastic deformation under a simple shear stress component exerted by ice or debris flow. The decrease of the θ angle illustrates the increase of shear strain intensity (Choukroune et al., 1987; Passchier and Trouw, 2005). Vertical water escape pipes with realigned clasts suggest upwards dewatering of the conglomerate.

Matrix deformations beneath embedded preglacial intraclasts are related to loading, implying that conglomerate deposition was followed by clasts foundering within a water-saturated matrix during compaction of the conglomerate. The occurrence of few flow surfaces within the matrix, together with clasts, suggests that conglomeratic deposits have been fluidized. Similar structures have been observed in fluidized flows (Roussel et al., 2003).

(2) Micro-scale deformations imply post-depositional reworking of the sandy matrix during dewatering of the conglomerate. These structures illustrate that the matrix is reworked by meltwater during release of the porewater excess. Water escape paths are notably controlled by the distribution of large intraclasts within the conglomerate (necking structures, grain-size segregation around clasts and stacked grains). Elongation and fragmentation of preglacial material result in tear drop-shaped intraclasts formed by boudinage of soft intraclasts during early post-depositional dewatering of the conglomerate. The absence of edge-to-edge grain crushing may indicate that conglomerate was

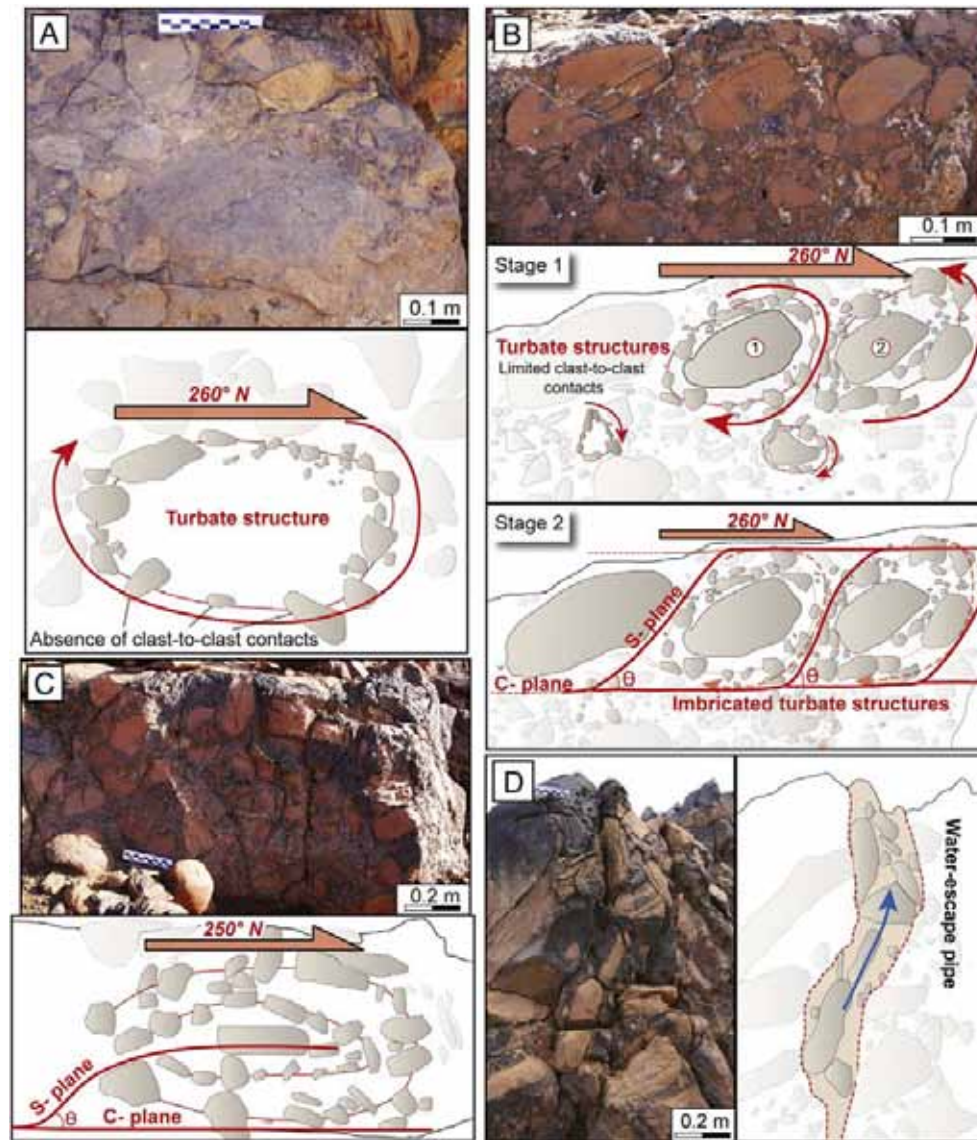


Fig. 11. Macro-scale deformation structures affecting conglomeratic deposits. (A) Macro-scale turbate structures with matrix core and characterized by the absence of clast-to-clast contacts. (B) Aligned macro-scale turbate structures with stone core and limited clast-to-clast contacts, overprinted by a S-C fabric. (C) Clast reorientations following a recumbent fold. (D) Vertically realigned clasts along a water-escape pipe.

characterized by a high porosity, a high porewater pressure and low strain rates, or alternatively high clay matrix component, reducing grain crushing contact events (Reinardy et al., 2011; Menzies et al., 2013).

3.5. SSDS within sandstones

3.5.1. Description

Trough cross-bedded or ripple cross-laminated sandstones (F4 and F5) display a wide range of SSDS that are generally constrained to single beds. These structures include sheath, recumbent and overturned folds; convoluted beds, dish and sheet dewatering structures, step normal faults and fluted surfaces (Figs. 5, 13). Folding is sometimes observed, including sheath and recumbent folds with fold axis oriented W to NW (Fig. 13B). Convoluted beds commonly occur within the sandstone deposits with a prevailing chaotic style (Fig. 13A). Several centimeter-

thick homogenized sandstone beds display flute-like morphologies with polished and smoothed surfaces up to 1 m wide and 2.5 m long, oriented towards 320° N (Fig. 13C). Dish and sheet dewatering structures are locally observed and affect sandstone layers, up to 1 m thick (Fig. 13D, E). At the top of the basal unit, step normal faults with undulating fault planes and centimeter offsets occur over wide areas (over 100 m²) (Fig. 13B).

3.5.2. Interpretation

Sheath and recumbent folds with fold axes dipping in the same directions as the tunnel valley axis indicate hydroplastic deformations under simple shear stress, probably resulting from ice flowing over soft beds during ice/bed coupling events (Lesemann et al., 2010). The different types of folds indicate varying shear strain intensity and/or porewater pressure. Convoluted beds record the internal foundering of liquefied sediment layers upon

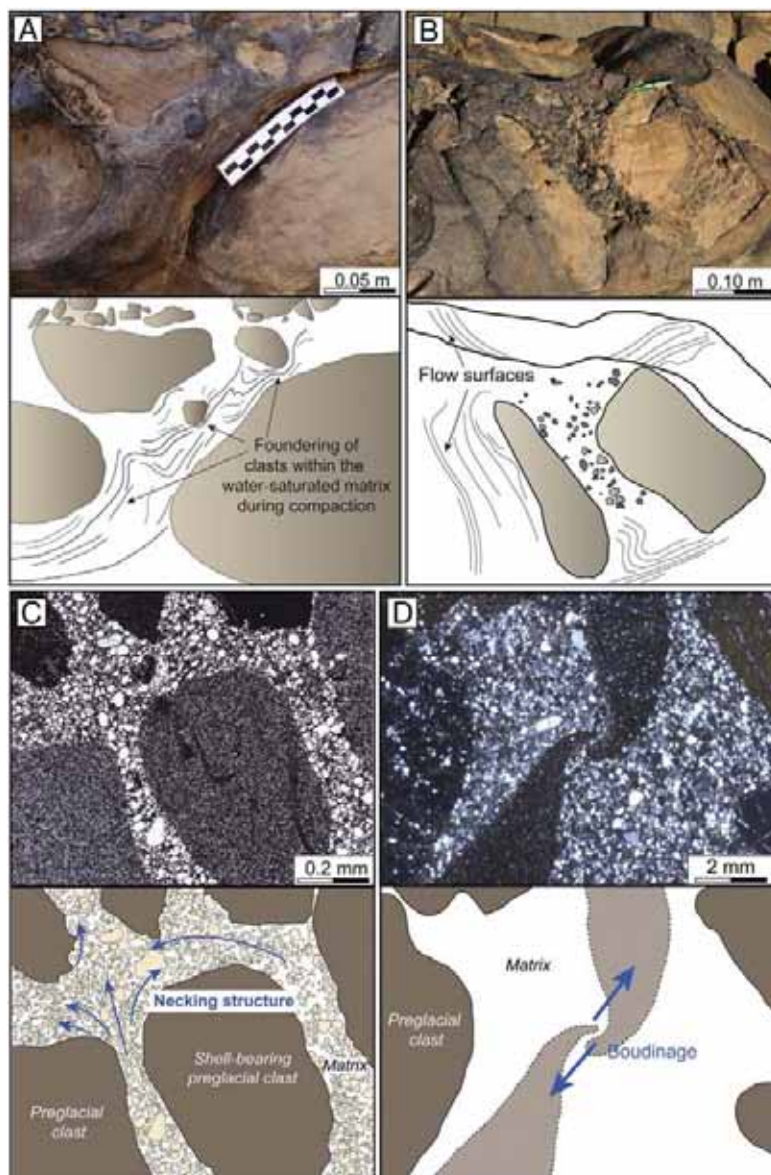


Fig. 12. (A) Matrix deformations by foundering of preglacial intraclasts into water-saturated sediments. (B) Chaotic flow surfaces locally observed within the matrix of the conglomerate, implying matrix fluidization. (C) Micro-scale necking structures related to upward remobilization of the matrix, illustrating porewater movement influenced by the positions of preglacial intraclasts. (D) Micro-scale clast fragmentation by boudinage during upward dewatering of the conglomerate.

themselves, commonly in conjunction with active upward escape of porewater (Maltman, 1994). Such structures are notably triggered by loading which could either be related to compaction due to overlying lithostatic weight or ice being coupled to the water-saturated bed.

Flute-like morphologies indicate soft bed deformations underneath flowing ice (Boulton, 1976). The elongated morphology indicates deformation under simple shear stress and high strain intensity. Sheet dewatering structures and dish structures, related to moderate to intense water escape correspond to a liquefied to fluidized state and can either be related to dewatering of sediments during ice/bed coupling or dewatering during rapid sedimentation. Extensive surfaces affected by step normal faults observed in thin-bedded sandstones correspond to brittle to hydroplastic

(undulating fault planes) deformations induced by radial extensional deformation under low porewater pressure. Radial extension is generally triggered by sediment compaction or overloading (Guiraud and Seguret, 1987). In the Ordovician glacial record, glacial pavements are often associated with extensive surfaces affected by normal microfaults and have been interpreted as being the result of glacial overloading during ice–bed coupling (Beuf et al., 1971; Biju-Duval et al., 1974; Denis et al., 2010; Clerc et al., 2013).

4. Discussion

Kinematics of the deformation structures observed in both preglacial and glacial strata, and their inferred characteristics in

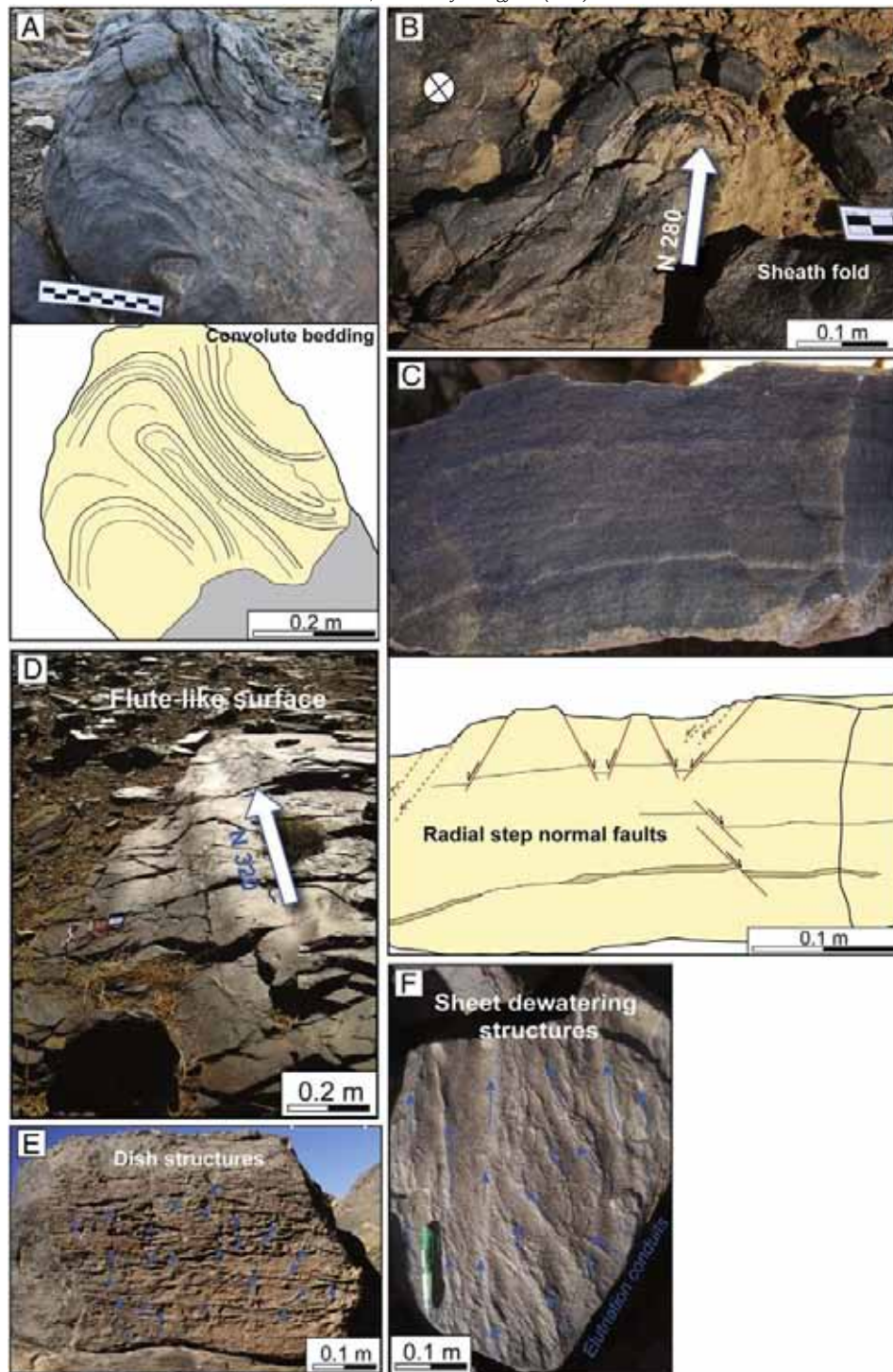


Fig. 13. Macro-scale deformation structures within glacial sandstones (F4 and F5). (A) Convolute beds within channelized sandstones (F4). (B) Sheath fold verging towards the NNW (view from above). (C) Radial step normal faults with millimetric to centimetric offsets within ripple cross-laminated sandstones (F5). (D) A flute-like surface showing a 320° N orientation occurring at the top of FA.1 (F5). (E) Sheet dewatering structures evidenced by clay-rich elutriation conduits (F4). (F) Dish structures related to sand dewatering (F4).

terms of strain intensity and porewater pressure are summarized in Fig. 14. The deformation structures are placed on a theoretical porewater pressure curve showing the high variation of pore pressure within preglacial and glacial sediments during the formation of the tunnel valley and the deformation of the basal glacial deposits.

4.1. Subglacial bed remobilization

4.1.1. Early deformations of preglacial material (prior to glaciation)

Preglacial strata underwent post-depositional modifications in response to extensional tectonic stresses, differential lithification and porewater movement (Fig. 14, stages 1 and 2; 15A).

The occurrence of extensional dihedral joint networks within a fault damage zone along the tunnel valley margin indicates a primary phase of brittle deformation affecting lithified preglacial strata (Fig. 10). This extensional faulting might be related to the Cambro–Ordovician extension (cf., Section 2.2) which led to NE–SW, NW–SE and E–W-oriented graben and half-graben structures in North Africa, notably in the Anti-Atlas region (Robert-Charrue and Burkhard, 2008).

Evidence of a lithification gradient prior to brecciation and formation of the tunnel valley is illustrated by the occurrence of both lithified and unlithified preglacial clasts within the basal conglomerate. Early lithified preglacial strata are illustrated by clasts displaying sharp contact with the surrounding matrix, occasional intra-clast calcite cement related to early diagenesis (i.e., prior to brecciation), and preserved sedimentary structures. The plastic deformation of some preglacial blocks after their deposition indicates the presence of unlithified material. In a sediment burial context, differences in the degree of lithification are related to burial depth, lithology and early cementation (Callot et al., 2008).

Ductile deformation structures, involving porewater movement of water-saturated sediments occur within preglacial blocks. These intra-block structures indicate that porewater pressure was locally significant prior to lithification and brecciation of the preglacial strata (i.e., prior to ice sheet growth). These deformation structures are observed within some preglacial intraclasts that were lithified at time of deposition (sharp clast-to-matrix contact) implying that they probably predate the glacial episode. This first episode of porewater pressure increase within confined and unlithified layers may be related to increasing stress and/or water input within confined layers due to groundwater flow. Intra-clast convoluted laminations, pillar and sheet dewatering structures are the remnants of this first episode of sediment remobilization by fluid pressure.

Several triggers can explain this first deformation episode such as palaeoseismicity, rapid sedimentation, lithostatic stress increase during burial or groundwater circulation within confined, unlithified preglacial strata (Maltman, 1994; Montenat et al., 2007). During the early stages of sediment deformation and remobilization, preglacial aquifers (unlithified silts and sands) were confined by two types of impermeable barriers: (1) preglacial clay beds and (2) early lithified sandstone beds (Fig. 13A). This “layer-cake” configuration of the preglacial deposits with a majority of low-permeability strata (2/3 of the preglacial sedimentary sequence) represents the optimum configuration for the development of overpressure (Janszen et al., 2012; Sandersen and Jørgensen, 2012).

4.1.2. In-situ brecciation of preglacial material

Ice sheet advance over the study area was associated with major changes in the parameters controlling porewater pressure in unlithified and water-saturated preglacial sediments. The resulting increase of basal shear stress combined with meltwater input in aquifers, led to a rapid increase of porewater pressure. Along interfluvies, large ball structures observed 5 m below GP1, with internal turbate structures, may record the first stages of porewater pressure increase and indicate sediment liquefaction within confined aquifers (Fig. 14, stage 3). The discontinuous emplacement of ball structures below both GP1 and GP2 indicates lateral variations in porewater pressure within the subglacial bed, possibly illustrating a mosaic of coexisting deforming and stable areas underneath the ice (Piotrowski and Kraus, 1997; van der Meer et al., 2003; Piotrowski et al., 2004). Areas where preglacial strata display lower potential for meltwater diffusivity or/and areas where groundwater flow brings meltwater within confined aquifers will tend to deform first (deforming zone), as they will develop high porewater pressure earlier when the ice mass is coupled to the bed (Fig. 15B).

The progressive increase of porewater pressure within the confined aquifers continues until pore pressure exceeds the tensile strength of the permeability barriers (lithified sand/clay). When the threshold is passed, hydrofractures develop in order to release the porewater excess (Fig. 14, stage 4; 15C). Sudden ruptures of these barriers allow pore

fluids to escape rapidly, causing injections of sediments, probably in a fluidized state, within open fractures (Onasch and Kahle, 2002). This phase of ‘fracking’ is outlined by the occurrence of angular preglacial blocks within the matrix-supported conglomerate at the base of the tunnel valley. The wide range of preglacial intraclast shapes evidenced by the variety of angles between stratifications and intraclast margins may correspond to randomly orientated hydrofractures, indicating that pore fluid pressure potentially reduced the differential stress state to an effective hydrostatic stress (Mandl and Harkness, 1987; Lorenz et al., 1991; Cosgrove, 1995). In a hydrostatic stress field, the normal stress is the same in every direction, implying that there is no preferential orientation for hydrofractures opening (Cosgrove, 1995). The complex networks of fractures constrained to an unlithified intraclast observed at micro-scale possibly illustrate this process of hydraulic fracturing (Fig. 11D). In addition, the occurrence of clayey intraclasts containing embedded quartz grains within the conglomerate may result from intraclast detachments from the walls of the host clay strata during hydrofracturing and quartz grain impingements related to injection of fluidized sand within the fractures (Scott et al., 2009). The dense network of hydrofractures is probably responsible for the in-situ brecciation of both types of impermeable barriers (Cosgrove, 1995; Chen et al., 2009). The occurrence of hexagonal-shaped angular elements within the conglomerate indicates that some of the preglacial material have been fractured along planes of weakness and may suggest that another process of brecciation locally occurs. Meltwater can rapidly drain within the heavily fractured damage zone (Fig. 8B), leading to local decrease of porewater pressure and ice–bed coupling. Once coupling, the subjacent lithified and heavily fractured bedrock will be quickly and locally loaded, possibly leading to quarrying of preglacial blocks along weakness planes. (Fig. 14, stage 5).

In-situ brecciation processes are described in the literature (Festa et al., 2012), but under-represented in subglacial environments. Passchier et al. (1998) described subglacial in-situ brecciation by hydrofracturing due to ice overload. The concept of “fracking” has also been invoked for the formation of Pleistocene tunnel valleys in the North Sea Basin (Janszen et al., 2012). Processes of hydrofracturing and in-situ brecciation commonly occur underneath mass transport deposits, notably triggered by submarine landslides and debris flows (Callot et al., 2008; Yamamoto et al., 2009; Ogata et al., 2012; Pini et al., 2012). Basal shear, fluid overpressure and the presence of impermeable barriers sealing water-saturated sediments represent the triggers for hydraulic brecciation. Controlling parameters are therefore similar to the parameters producing disruption of the preglacial strata.

The massive upward injections of fluidized material into fractures led to diapiric stratal disruption and mobilization of an admixture of fluidized sand and preglacial clasts (Fig. 15C). Diapiric structures interpreted as the result of fluid overpressure due to rheological gradient between strata, and the abrupt increase of tectonic or lithostatic stress commonly occur in accretionary complexes (Orange, 1990; Kopf, 2002; Yamamoto et al., 2009; Festa, 2011; Codegone et al., 2012). Rare examples of diapiric structures are described in glacial environments, except few examples formed in subglacial environments where diapirs form when the porewater pressure exceeds the ice flotation pressure (Szuman et al., 2013) or in preglacial environments where these structures form in combination with large thrust faults during compression, gravity spreading and loading in front of advancing glaciers (Sadolin et al., 1997). The upward release of the excess of porewater induced by the sudden rupture of the impermeable barriers could drastically decrease the effective pressure. As predicted by Boulton and Hindmarsh (1987) and Boulton et al. (2007b), subglacial pipes develop when the effective pressure is close to zero, promoting subglacial transport of the freshly brecciated preglacial sediments (Fig. 15C). These processes of hydrofracturing, brecciation, and transport of preglacial material through channels contributed to intensify the efficiency of subglacial bed remobilization.

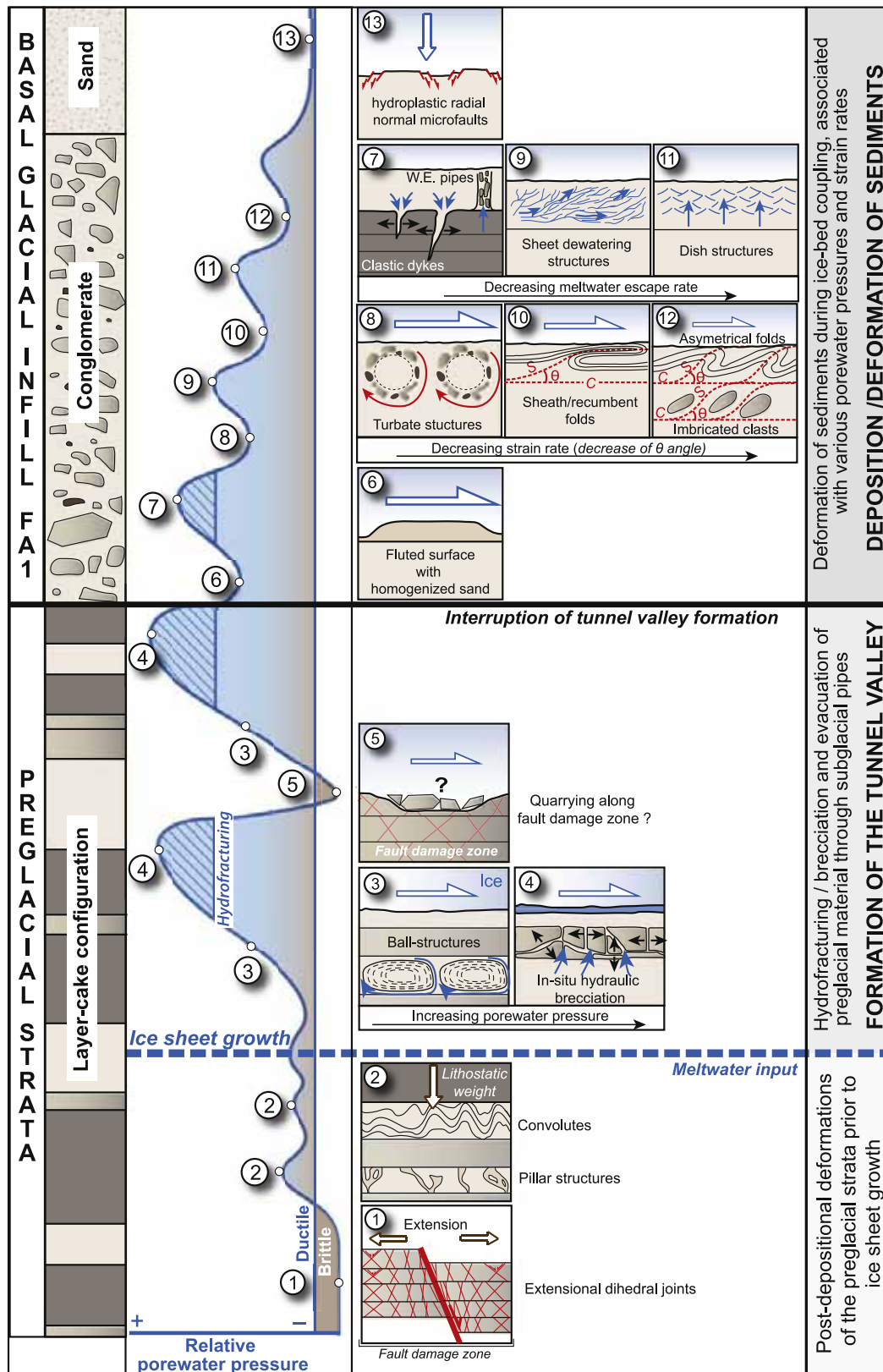


Fig. 14. Kinematics of the deformation structures occurring in both preglacial and glacial sediments before and after the Himantian glaciation. Each structure is replaced on a theoretical porewater pressure curve and corresponds to different strain rates.

4.2. Bed remobilization impact on tunnel valley formation

4.2.1. Diachronic and multi-phased erosion

Once the admixture of preglacial clasts and fluidized material is transported and therefore the excess of porewater pressure within the deforming zone released, the fluid pressure necessary to promote processes of brecciation cannot be reached. Subglacial dynamics is characterized by a high potential for lateral shifting of the deforming zones, cavity and channel positions through time and space (Piotrowski and Kraus, 1997; Piotrowski et al., 2004). Consequently, zones of brecciation, diapirism and piping may continuously form and shift at the base of an ice sheet.

Conglomerates are observed in both the tunnel valley and interfluvies implying that brecciation occurred in both locations in the early stages of subglacial bed remobilization. Along the tunnel valley axis (320° N), subglacial brecciation and remobilization of preglacial strata continued while sediment remobilization stopped along the interfluvies, leading to progressive differential erosion between the valley axis and interfluvies. Along interfluvies, below GP1, ball structures correspond to the immature stage of brecciation, i.e. the stage before porewater pressure is high enough to fracture the overlying impermeable barriers. These structures illustrate that a porewater pressure gradient existed between interfluvies and the emergent tunnel valley (Fig. 15D). This gradient may be explained by an initial palaeotopography, possibly inherited from the Cambro–Ordovician extensional tectonic regime which preferentially drains meltwater along the axis of the tunnel valley. The development of basins during the Paleozoic post-orogenic subsidence was controlled by the location and orientation of Panafrican tectonic accidents, predominantly oriented NW–SE. This orientation is similar to the axis of the Alnif tunnel valley, suggesting that the structural situation of this area may have had an impact on the palaeotopography and subsequently on the position of the tunnel valley.

A tunnel valley formation model with successive and localized episodes of subglacial remobilization of preglacial material during hydraulic brecciation events is here preferred to the steady-state model developed by Boulton and Hindmarsh (1987). Nevertheless, the non-instantaneous model of tunnel valley formation proposed in this study is similar to steady-state models mentioned in several studies (Boulton et al., 2007a, b). The complexity of subglacial dynamics and field observations including the irregular base of the tunnel valley (1), and the fan-morphology of the conglomeratic deposit (2), strengthen this porewater pressure-driven model. Studies conducted on subglacial dynamics in recent decades suggest a coexistence of deforming and stable areas within subglacial bed and that deformation is cumulative through time and space (Piotrowski and Kraus, 1997; Knight, 2002; Piotrowski et al., 2004). (1) The irregular morphology of the tunnel valley base is the result of cumulative and diachronic deformation/remobilization phases beneath the ice sheet. (2) The different fans of matrix-supported conglomerate observed at the base of the tunnel valley suggest several sedimentary influx points related to localized and repetitive piping events underneath the ice. Other models suggest that tunnel valley incision also occurs through successive phases of erosion by one or a range of erosional processes involving meltwater (Piotrowski, 1994; Hooke and Jennings, 2006; Jorgensen and Sandersen, 2006). The Alnif tunnel valley is a single and straight valley which is not part of a valley network and therefore does not fit the Shaw model (2002, 2010) which proposes that the collapse of massive sheet floods into channelized flow is responsible for the genesis of anastomosed tunnel valleys.

4.2.2. Interruption of tunnel valley formation

The combination of subglacial hydraulic brecciation and piping is proposed to explain the formation of the Alnif tunnel valley, implying that a decrease in porewater pressure could interrupt the processes of erosion. Several hypotheses can be raised to explain this decrease of fluid pressure:

- At greater depths, when the ice encountered older preglacial strata, overburden increased sediment shear strength, preventing sediment fluidization and hydrofracturing (Brown, 1994; Collison, 1994; Obermeier, 1996);
- The initial (i.e. prior to or at the time of glaciation) meltwater transfer capacity of preglacial sediments in which the tunnel valley is carved is a key parameter for their formation. Clerc et al. (in prep) demonstrate, using groundwater transfer modeling, that meltwater transfer capacity within the Alnif preglacial sediments is drastically reduced or even null below 170 m of depth (i.e., the depth of the Alnif tunnel valley). These results indicate that processes of tunnel valley formation stop when the effect of overpressure decreases with depth due to reduced capacity for groundwater transfer in deeper strata and subsequent reduction of porewater pressure. Also, a preglacial layer with higher permeability/diffusivity will tend to dissipate the overpressure required to trigger 'fracking' and therefore interrupt the processes responsible for the tunnel valley formation;
- A drastic diminution of meltwater circulation through preglacial aquifers will tend to reduce overpressure within water-saturated sediments. A diminution of meltwater volume within the tunnel valley could either result from changes of meltwater drainage pathways or/and a net decrease in the production of meltwater.

4.3. Deposition and deformation of FA.1

The basal conglomerate (FA.1) has been interpreted as being deposited in a subglacial environment (Clerc et al., 2013). The vertically stacked deposits with pronounced erosional surfaces suggest a constrained accommodation space, concordant with a cavity environment where space available is controlled by an overlying ice roof and a shallow water column. In addition, the conglomerate contains numerous soft-sediment deformation structures triggered by a shear stress and high porewater pressure, interpreted as being the result of ice/bed coupling episodes. The array of subglacial deformation structures is generally constrained to single beds and includes notably flutes, radial extensional normal faults, macro-scale turbate structures, sheath and recumbent folds. The deformation structures have been interpreted as the result of ice–bed interactions since they are associated with fluted surfaces and radial extensional normal faults in FA.1. Such structures have been associated to glacial pavements in the Saharan glacial Ordovician record (Beuf et al., 1971; Bijou-Duval et al., 1974; Deynoux and Ghienne, 2004; Denis et al., 2010; Loi et al., 2010; Clerc et al., 2013).

Fans of massive conglomerate (F1) result from the deposition of an admixture of preglacial blocks packed within a sandy matrix produced by up-ice brecciation and transport of preglacial material (Fig. 15E). The basal conglomerate could be here comparable to a sedimentary mélange since this deposit results from mixing of exotic preglacial clasts within a matrix, leading to a chaotic internal arrangement (Festa et al., 2012). During the piping stage, transport of the massive conglomerate occurred in overpressurized subglacial channels where hydrostatic pressure in meltwater was higher than the porewater pressure within the mélange. In this configuration, overpressure was maintained in the density flow allowing the preglacial material to be transported as a fluidized hyperconcentrated flow (Fig. 15E). The seldom and chaotic flow surfaces observed within the matrix of the conglomerate (F1) may record this stage of matrix fluidization as such structures usually develop when sediments are fluidized (Roussell et al., 2003). Flow surfaces are seldom due to the low preservation potential of such structures. Deposition of the density flow occurred within subglacial cavities, where the drop in meltwater hydrostatic pressure triggered rapid deposition of the fluidized hyperconcentrated flow. Rapid deposition was possibly enhanced by the rapid release of fluid overpressure contained in the flow due to equilibrium re-establishment between the internal porewater pressure and the external hydrostatic pressure in the cavity. Sudden overloading and dewatering related to rapid deposition of this

massive material may be responsible for the formation of vertical to subvertical clastic dykes (Phillips, 2006; Ogata et al., 2012) (Fig. 15E).

After deposition, the basal conglomerate was affected by different episodes of deformation controlled by fluctuating strain rates and porewater pressure changes (Fig. 14 stages 6 to 12; Fig. 15F). These different episodes are evidenced by the different deformation structures, including clastic dykes, folds, radial extensional normal faults, turbate structures, and fluted surfaces. The fluted surfaces indicate sediment deformation under simple shear stress applied by the overriding ice sheet, their elongated morphologies form under high strain rate related to elevate basal shear stress. In the basal sedimentary sequence, other deformation structures triggered by simple shear stress occur in combination with the fluted surfaces (folds, turbate structures, S–C fabrics) suggesting a probable subglacial origin. The different types of folds including sheath to asymmetrical fold types, and the occurrence of turbate structures displaying secondary S–C fabrics illustrate a decrease of the θ angle related to a decrease of the strain intensity (Fig. 14, stages 7, 9, 11). The decrease of strain intensity implies changes in basal shear stress and/or variations in porewater pressure during one or several episodes of ice–bed coupling. Other types of deformation structures, including sheet dewatering structures, dish structures, dewatering pipe or clastic dykes are related to episodes of porewater release (Fig. 14, stages 6, 8, 10). Clastic dykes propagating downwards may suggest hydrofracture development triggered during ice–bed coupling (Clerc et al., 2012; Phillips et al., 2012). Dewatering pipes or dish structures implies a vertical escape of water, related to release of overpressure during overloading of water-saturated sediments. Such structures observed in glacial sediments that are affected by typical subglacial deformation structures (fluted surfaces), suggest that the Hirnantian ice sheet is a plausible cause of overload and might therefore be responsible for sediment dewatering during ice–bed coupling. At the top of FA.1, extensive surfaces affected by step normal faults illustrate a change of sediment behavior during deformation, from liquefaction/fluidization to hydroplastic/brittle, i.e. from high porewater pressure to low porewater pressure. The successive events of porewater escape (dykes, dish structures, etc.) are probably responsible for these changes of sediment behavior during deformation and reveal a decrease of porewater pressure during deformation of the basal sedimentary sequence. The radial extensional normal faults indicate radial extension that is generally triggered by ice overload on the bed (Biju-Duval et al., 1974; Denis et al., 2010; Clerc et al., 2013).

Periods of ice/bed coupling are sometimes interrupted by episodes of decoupling, leading to the development of a subglacial drainage network. The subglacial meltwater flow leads to partial reworking of these basal deposits. Reworking of massive conglomerate resulted in deposition of channelized conglomerates (F2) and microconglomerates (F3) (Fig. 15F). Similarly, sandstones (F4 and F5) may be related to reworking of the conglomeratic matrix or the erosion of preglacial beds by meltwater and subsequent deposition of sand in the subglacial de-coupled space.

5. New model

Unlike previous tunnel valley formation models invoking erosion of the substratum by meltwater flow (Brennand and Shaw, 1994; Hooke and Jenkins, 2006; Boulton et al., 2009), this new model would suggest that single tunnel valleys are formed subglacially under the influence of localized occurrences of high

porewater pressure in the substratum, triggering hydrofracturing. Within zones of high porewater pressure, preglacial sediments were affected by a dense network of hydrofractures, leading to intense brecciation and subsequent glacial evacuation of preglacial material. Brecciation processes led to effective glacial excavation of the valley form that is in turn further exaggerated an inherited topographic relief by coeval glacial processes of evacuation by moving ice and meltwater. The evidence from Alnif substantiates this hypothesis in that the preglacial sediments were brecciated and evacuated. This new model, based upon 3 parameters controlling porewater pressure within the preglacial bed, is derived from field evidence in the Alnif study area.

5.1. Field evidence

The study area reveals the existence of zones of high porewater pressure, where hydrofracturing leads to preglacial stratal brecciation. These evidences rely on sedimentological (1) deformational (2) and geomorphological (3) observations.

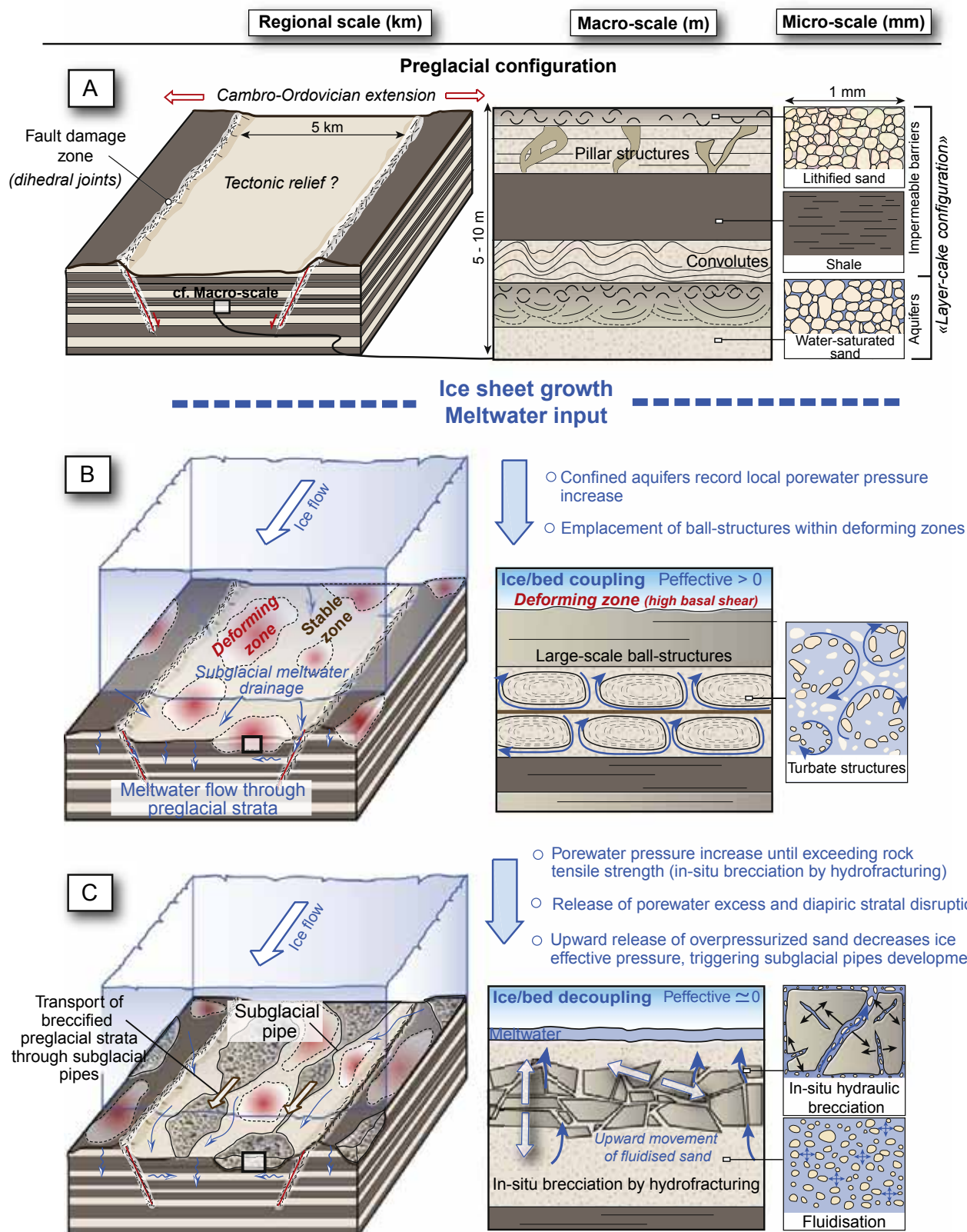
- (1) The occurrence of patchy conglomerate deposits composed of angular preglacial intraclasts at the base of the tunnel valley illustrates the phase of brecciation by hydrofracturing affecting the substratum due to a drastic increase in porewater pressure. Conglomerates are heterogeneous and form different fans with internal flow surfaces related to localized and repetitive brecciation, piping and deposition of the fluidized preglacial material below an active ice flow. The association of soft and lithified preglacial intraclasts within the conglomerate indicates a lithification gradient within the preglacial substratum which formed a 'layer-cake' stratigraphic package.
- (2) The occurrence of deformation structures related to increasing porewater pressure, within both preglacial and glacial sediments, represents major evidence for a porewater pressure-driven model. For example, ball structures and clastic dykes, locally observed below glacial erosional contact surfaces, illustrate the increase of porewater pressure within preglacial strata due to the combination of meltwater input and the stress exerted by the ice on preglacial confined aquifers.
- (3) The occurrence of a preexisting preglacial valley network has not been reported in the Alnif area (nor in any other tunnel valley examples in Morocco) implying that the tunnel valley developed primarily below the ice sheet as a preferential, but system-wise independent meltwater drainage system, where localized high porewater pressures developed.

5.2. Controlling parameters

Principal parameters controlling the evolution of the porewater pressure in the preglacial sediments are: (1) preglacial lithology and stratigraphy, (2) ice thermal regime and dynamics, and (3) inherited preglacial relief.

- (1) This new model of tunnel valley formation hypothesizes that the development of high porewater pressure within the bed, requires that the preglacial strata were likely unlithified. The occurrence of permeable and water-saturated layers (aquifers) is

Fig. 15. Multi-scale model illustrating the characteristics of preglacial bed remobilizations underneath the Hirnantian ice sheet. (A) "Layer-cake" configuration of the preglacial strata. The preglacial material is affected by brittle deformation due to the extensional tectonic stress and ductile deformation due to minor episodes of porewater pressure increase. (B) Meltwater circulation through aquifers associated with the stress exerted by the ice flow lead to a localized increase of porewater pressure within deforming zones. (C) Porewater pressure exceeds the tensile strength of permeability barriers leading to hydrofracturing, in-situ brecciation and diapiric stratal disruption. The upward movement of fluidized material and preglacial clasts leads to ice/bed decoupling and formation of subglacial pipes, capable to evacuate the brecciated material. Multi-scale model of tunnel valley formation by differential erosion and multi-phased remobilizations of preglacial strata. (D) Along interfluvies, porewater pressure does not exceed the threshold required to trigger hydrofracturing while processes of in-situ brecciation continue within the valley, leading to differential erosion. (E) Interruption of tunnel valley digging followed by sedimentary mélange deposition within subglacial cavities, forming fans of massive and matrix-supported conglomerate. (F) Reworking of the conglomerate by meltwater flow and remobilization of the basal deposits (FA.1) during episodes of ice/bed recoupling.



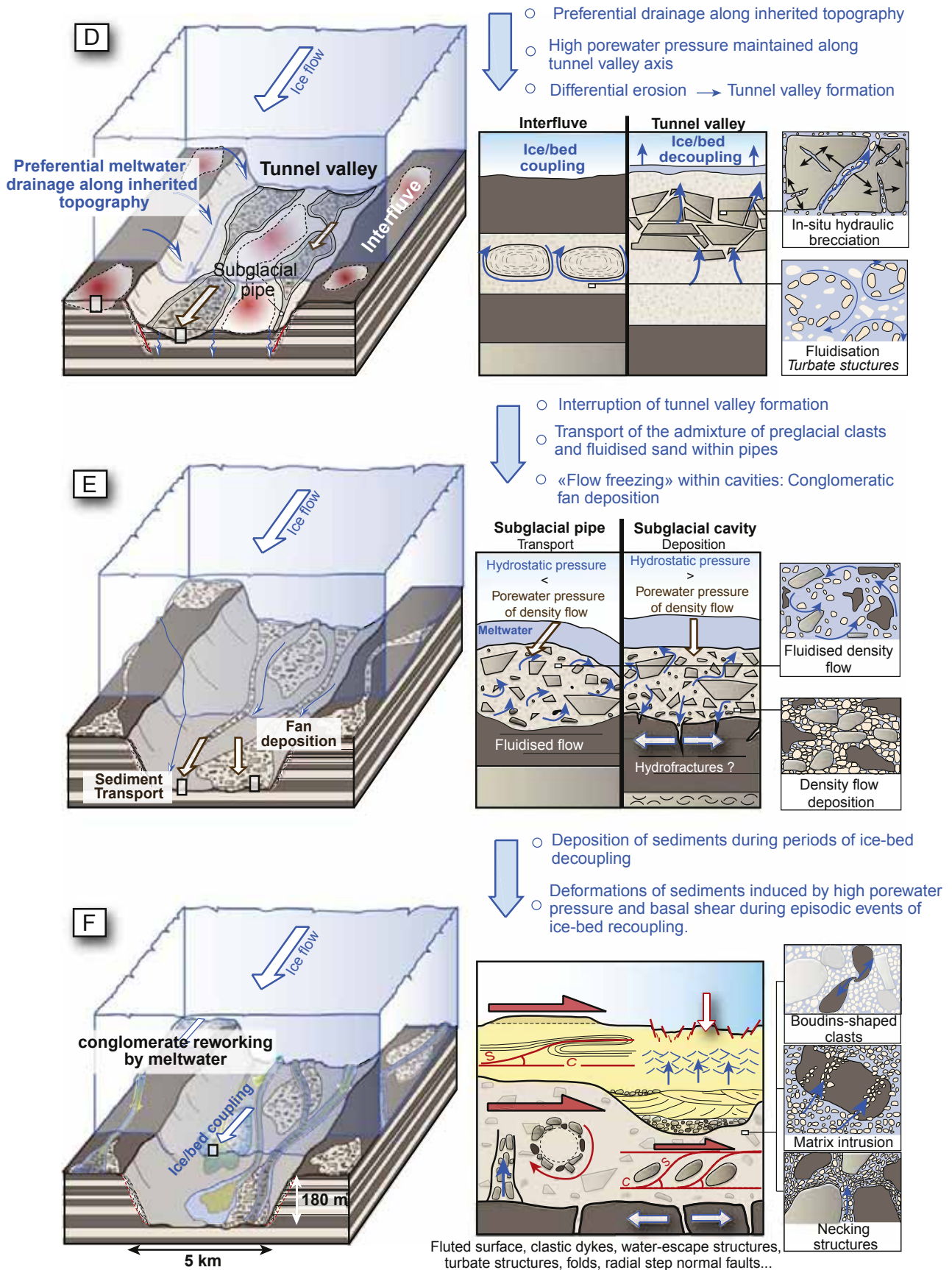


Fig. 15 (continued).

required to the development of high porewater pressure (sand layers in this study). An increase of porewater pressure within aquifers was achieved when water-saturated beds were confined by low permeability barriers (aquitards) (clays and cemented sandstones in this study). The porewater pressure-driven model requires an association of impermeable and permeable layers forming a “layer cake” configuration (Janszen et al., 2012). As suggested by Sandersen and Jørgensen (2012), a preglacial substratum with abundant low-permeable layers will preferentially contribute to the development of tunnel valleys. The Alnif preglacial sequence displays over 2/3 of low permeability strata (see Fig. 2B) triggering high subglacial water pressures caused by the inability of the substratum to entirely drain the meltwater. As a consequence overpressure develops in the bed, potentially leading to hydrofracturing.

- (2) The rapid increase of porewater pressure within confined aquifers was developed and associated with glacial overriding, triggered by a combination of meltwater within the preglacial bed and the basal ice shear exerted on the substratum. Localized and repetitive brecciation events imply the subglacial coexistence of zones of ice-bed coupling and decoupling, occurring in combination with meltwater production. This indicates that the new model of tunnel valley formation is primarily controlled by the development of a mosaic of deforming and stable spots under a warm-based glacier.
- (3) The new model explains the formation of single tunnel valleys, suggesting a localized and linear increase of porewater pressure. The model is dependent on meltwater input within the substratum, implying that the subglacial meltwater drainage path probably influences the position of the tunnel valley. In this study, a palaeorelief was thought to control the position of the Alnif tunnel valley due to preferential meltwater drainage.

This model allows single isolated tunnel valleys to form under active ice masses that in turn may permit subsequent later development of subglacial drainage pathways or/and deposition of sediments underneath the ice mass. At the tunnel valley base, the occurrence of channelized conglomerate or trough cross bedded sandstones, locally deformed, indicates the development of a subglacial drainage system during ice-bed decoupling periods alternating with episodes of ice-bed recoupling.

6. Conclusions

Based on field observations of this Ordovician tunnel valley in Morocco, the study provides new evidence for porewater pressure control on tunnel valley formation. The wider picture of the tunnel valley morphology and sedimentary infill gave new insights into processes of tunnel valley formation. Past studies carried out on this topic suggested that meltwater was the first parameter controlling the formation of tunnel valleys, mainly through catastrophic flows, capable of removing huge volume of sediments. The model proposed here uses meltwater as an indirect trigger for valley formation since fluctuation of porewater pressure at the ice-bed interface is interpreted as being responsible for subglacial sediment remobilization. The high fluid pressure was generated subglacially, by the conjunction of the stress exerted on the bed by flowing ice and the input of meltwater within confined aquifers. Sustained high porewater pressure within unlithified subglacial sediments triggers hydrofracturing, brecciation and diapiric stratal disruption.

Similar to the Boulton and Hindmarsh (1987) model, piping of the freshly brecciated preglacial material occurred through subglacial channels, enhancing erosional efficiency. The genesis of the tunnel valley morphology occurred through successive episodes of localized subglacial bed remobilization followed by evacuation of the resulting fluidized

material, as specified by the observed chronology between the different types of soft-sediment deformations.

The major role of meltwater suggested in this study confirms that tunnel valley may form during periods of ice sheet melting, maybe during short or perennial periods of deglaciation.

Acknowledgments

The work is a contribution from the ‘SEDS’ (Systèmes, Environnements et Dynamique Sédimentaire) research team in the Laboratoire Biogéosciences-UMR/CNRS 6282 at the University of Burgundy and is part of the ANR SeqStrat-Ice (n° 12-B506-0014). The authors thank GDF Suez for the funding of this study. We are also very thankful to Jasper Knight and two anonymous reviewers for their helpful comments that led to improvements to the original manuscript.

References

- Allen, J.R.L., 1982. *Sedimentary structures: their character and physical basis*. Development in Sedimentology, 30. Elsevier, Amsterdam (592 pp.).
- Alvaro, J.J., Vennin, E., Villas, E., Destombes, J., Vizcaino, D., 2007. Pre-Hirnantian (latest Ordovician) benthic community assemblages: controls and replacements in a siliciclastic-dominated platform of the eastern Anti-Atlas, Morocco. *Palaeogeography, Palaeoclimatology, Palaeoecology* 245, 20–36.
- Ballas, G., Soliva, R., Sizun, J.P., Fossen, H., Benedicto, A., Skurtveit, E., 2013. Shear-enhanced compaction bands formed at shallow burial conditions; implications for fluid flow (Provence, France). *Journal of Structural Geology* 47, 3–15.
- Beuf, S., Biju-Duval, B., De Charpal, O., Gariel, O., Bennacef, A., 1971. Les grès du Paléozoïque inférieur au Sahara – Sédimentation et discontinuités, évolution structurale d'un craton. Collection “Science et technique du pétrole”, 18. Publications de l'I.F.P., Paris (464 pp.).
- Biju-Duval, B., Deynoux, M., Rognon, P., 1974. Essai d'interprétation des “fractures en gradins” observées dans les formations glaciaires précambriennes et ordoviciennes du Sahara. *Revue de Géographie Physique et de Géologie Dynamique* 16, 503–512.
- Boulton, G.S., 1976. The origin of glacially-fluted surfaces – observations and theory. *Journal of Glaciology* 17, 287–309.
- Boulton, G.S., Hindmarsh, R.C.A., 1987. Sediment deformation beneath glaciers; rheology and geological consequences. *Journal of Geophysical Research* 92, 9059–9082.
- Boulton, G.S., Lunn, R., Vidstrand, P., Zatsepin, S., 2007a. Subglacial drainage by groundwater-channel coupling, and the origin of esker systems: part I—glaciological observations. *Quaternary Science Reviews* 26, 1067–1090.
- Boulton, G.S., Lunn, R., Vidstrand, P., Zatsepin, S., 2007b. Subglacial drainage by groundwater-channel coupling, and the origin of esker systems: part II—theory and simulation of a modern system. *Quaternary Science Reviews* 26, 1091–1105.
- Boulton, G.S., Hagdorn, M., Maillot, P.B., Zatsepin, S., 2009. Drainage beneath ice sheets: groundwater-channel coupling, and the origin of esker systems from former ice sheets. *Quaternary Science Reviews* 28, 621–638.
- Brentham, P.J., et al., 1994. Bathymetric and isotopic evidence for a short-lived Late Ordovician glaciation in a greenhouse period. *Geology* 22, 295–298.
- Brennand, T.A., Shaw, J., 1994. Tunnel channels and associated landforms, south-central Ontario: their implications for ice-sheet hydrology. *Canadian Journal of Earth Science* 31, 505–522.
- Brown, K.M., 1994. Fluids in deforming sediments. In: Maltman, A.J. (Ed.), *Geological Deformation of Sediments*. Chapman and Hall, London, pp. 205–238.
- Burkhard, M., Carit, S., Helg, U., Robert-Charrier, C., Soulaïmani, S., 2006. Tectonics of the Anti-Atlas of Morocco. *Compte Rendus Geoscience* 338, 11–24.
- Callot, P., Odonne, F., Sempere, T., 2008. Liquefaction and soft-sediment deformation in a limestone megabreccia: the Ayabacas giant collapse, Cretaceous, southern Peru. *Sedimentary Geology* 212, 49–69.
- Chen, J.T., van Loon, A.J., Han, Z.Z., Chough, S.K., 2009. Funnel-shaped, breccia-filled clastic dykes in the Late Cambrian Chaomidian Formation (Shandong Province, China). *Sedimentary Geology* 221, 1–6.
- Choukroune, P., Gapais, D., Merle, O., 1987. Shear criteria and structural symmetry. *Journal of Structural Geology* 9, 525–530.
- Clerc, S., Buoncristiani, J.F., Guiraud, M., Desaubliaux, G., Portier, E., 2012. Depositional model in subglacial cavities, Killiney Bay, Ireland. Interactions between sedimentation, deformation and glacial dynamics. *Quaternary Science Reviews* 33, 142–164.
- Clerc, S., Buoncristiani, J.F., Guiraud, M., Vennin, E., Desaubliaux, G., Portier, E., 2013. Subglacial to proglacial depositional environments in an Ordovician glacial tunnel valley Alnif, Morocco. *Palaeogeography, Palaeoclimatology, Palaeoecology* 370, 127–144.
- Clerc, S., Buoncristiani, J.F., Guiraud, M., Vennin, E., Desaubliaux, G., Portier, E., Evidence for a Combined Influence of Preglacial Lithology, Subglacial Hydrology and Structural Heritage on the Distribution of ORDOVICIAN TUNNEL VALLEYS, (in preparation).
- Cocks, L.R.M., Torsvik, T.H., 2002. Earth geography from 500 to 400 million years ago: a faunal and palaeomagnetic review. *Journal of Geological Society* 159, 631–644.
- Codegone, G., Festa, A., Dilek, Y., Pini, G.A., 2012. Small-scale polygenetic melanges in the Ligurian accretionary complex, Northern Apennines, Italy, and the role of shale diapirism in superposed melange evolution in orogenic belts. *Tectonophysics* 568, 170–184.
- Collison, J., 1994. Sedimentary deformational structures. In: Maltman, A.J. (Ed.), *Geological Deformation of Sediments*. Chapman and Hall, London, pp. 95–125.

- Cosgrove, J.W., 1995. The expression of hydraulic fracturing in rocks and sediments. In: Ameen, M.S. (Ed.), *Fractography: Fracture Topography as a Tool in Fracture Mechanics and Stress Analysis*. Geological Society Special Publication, 92, pp. 187–196.
- Cosgrove, J.W., 2001. Hydraulic fracturing during the formation and deformation of a basin: a factor in the dewatering of low permeability sediments. *AAPG Bulletin* 4, 737–748.
- Denis, M., Guiraud, M., Konate, M., Buoncristiani, J.F., 2010. Subglacial deformation and water-pressure cycles as a key for understanding ice stream dynamics: evidence from the Late Ordovician succession of the Djado Basin (Niger). *International Journal of Earth Sciences* 99, 1399–1425.
- Destombes, J., Hollard, D.H., Willefert, S., 1985. Lower Palaeozoic rocks of Morocco. In: Holland, C.H. (Ed.), *Lower Palaeozoic of North-Western and West Central Africa*. Lower Palaeozoic Rocks of the World. John Wiley and Sons, New York, pp. 91–336.
- Deynoux, M., Ghienne, J.F., 2004. Late Ordovician glacial pavements revisited: a reappraisal of the origin of striated surfaces. *Terra Nova* 16, 95–101.
- Díaz-Martínez, E., Grahn, Y., 2007. Early Silurian glaciation along the western margin of Gondwana (Peru, Bolivia and northern Argentina): palaeogeographic and geodynamic setting. *Palaeogeography, Palaeoclimatology, Palaeoecology* 245, 62–81.
- Festa, A., 2011. Tectonic, sedimentary, and diapiric formation of the Messinian melange: Tertiary Piedmont Basin (northwestern Italy). In: Wakabayashi, J., Dilek, Y. (Eds.), *Melanges: Processes of Formation and Societal Significance*. Geological Society of America Special Paper, 480, pp. 215–232.
- Festa, A., Dilek, Y., Pini, G.A., Codegone, G., Ogata, K., 2012. Mechanisms and processes of stratal disruption and mixing in the development of melanges and broken formations: redefining and classifying melanges. *Tectonophysics* 568, 7–24.
- Finnegan, S., et al., 2011. The magnitude and duration of Late Ordovician–Early Silurian glaciation. *Science* 331, 903–906.
- Frey, S.E., Gingras, M.K., Dashtgard, S.E., 2009. Experimental studies of gas-escape and water-escape structures: mechanisms and morphologies. *Journal of Sedimentary Research* 79, 808–816.
- Ghienne, J.F., 2003. Late Ordovician sedimentary environments, glacial cycles, and post-glacial transgression in the Taoudeni Basin, West Africa. *Palaeogeography, Palaeoclimatology, Palaeoecology* 189, 117–145.
- Ghienne, J.F., Le Heron, D.P., Moreau, J., Denis, M., Deynoux, M., 2007. The Late Ordovician glacial sedimentary system of the North Gondwana platform. In: Hambrey, M.J., Christoffersen, P., Glasser, N.F., Hubbard, B. (Eds.), *Glacial Sedimentary Processes and Products*. International Association of Sedimentologists, Special Publication. Blackwell, Oxford, pp. 295–319.
- Guiraud, M., Seguret, M., 1987. Soft-sediment microfaulting related to compaction within the fluvio-deltaic infill of the Soria strike-slip basin (northern Spain). In: Jones, M.E., Preston, R.M.F. (Eds.), *Deformation of Sediments and Sedimentary Rocks*. Geological Society, London, Special Publication, 29, pp. 123–136.
- Hallett, D., 2002. *Petroleum Geology of Libya*. Elsevier Science (503 pp.).
- Hiemstra, J.F., Rijdsdijk, K.F., 2003. Observing artificially induced strain: implications for subglacial deformation. *Journal of Quaternary Science* 18, 373–383.
- Hirst, J.P.P., Benbakir, A., Payne, D.F., Westlake, I.R., 2002. Tunnel valleys and density flow processes in the upper Ordovician glacial succession, Illizi Basin, Algeria: influence on reservoir quality. *Journal of Petroleum Geology* 25, 297–324.
- Hooke, R.L., Jennings, C.E., 2006. On the formation of the tunnel valleys of the southern Laurentide ice sheet. *Quaternary Science Reviews* 25, 1364–1372.
- Huuse, M., Le Heron, D.P., Dixon, R., Redfern, J., Moscarello, A., Graig, J., 2012. Glaciogenic reservoirs and hydrocarbon systems. In: Huuse, M., Redfern, J., Le Heron, D.P., Dixon, R.J., Moscarello, A., Graig, J. (Eds.), *Glaciogenic Reservoirs and Hydrocarbons systems*. Geological Society of London, Special Publications, 368, pp. 1–28.
- Janszen, A., Spaak, M., Moscarello, A., 2012. Effects of the substratum on the formation of glacial tunnel valleys: an example from the Middle Pleistocene of the southern North Sea Basin. *Boreas* 41, 629–643.
- Johnson, M.D., 1999. Spooner Hill, Northwest Wisconsin: High Relief Hills Carved by Subglacial Meltwater of the Superior Lobe. In: Mickelson, D.M., Attig, J.W. (Eds.), *Glacial Processes Past and Present*. Geological Society of America Special Paper, 337, pp. 83–92.
- Jorgensen, F., Sandersen, P.B.E., 2006. Buried and open tunnel valleys in Denmark – erosion beneath multiple ice sheets. *Quaternary Science Reviews* 25, 1339–1363.
- Kehew, A.E., Piotrowski, J.A., Jorgensen, F., 2012. Tunnel valleys: concepts and controversies – a review. *Earth-Science Reviews* 113, 33–58.
- Kim, Y.S., Peacock, D.C.P., Sanderson, D.J., 2004. Fault damage zones. *Journal of Structural Geology* 26, 503–517.
- Knight, J., 2002. Glacial sedimentary evidence supporting stick-slip basal ice flow. *Quaternary Science Reviews* 21, 975–983.
- Kopf, A.J., 2002. Significance of mud volcanism. *Reviews of Geophysics* 40, 21–52.
- Le Heron, D.P., 2007. Late Ordovician glacial record of the Anti-Atlas, Morocco. *Sedimentary Geology* 201, 93–110.
- Le Heron, D.P., Etienne, J.L., 2005. A complex subglacial clastic dyke swarm, Solheimajökull, southern Iceland. *Sedimentary Geology* 181, 25–37.
- Le Heron, D.P., Sutcliffe, O.E., Bourgeois, K., Craig, J., Visentin, C., Whittington, R.J., 2004. Sedimentary architecture of the Upper Ordovician tunnel valley, Gargaf Arch, Libya: implications for the genesis of a hydrocarbon reservoir. *GeoArabia* 9, 137–160.
- Le Heron, D.P., Ghienne, J.F., El Houichi, M., Khoukhi, Y., Rubino, J.L., 2007. Maximum extent of ice sheets in Morocco during the Late Ordovician glaciation. *Palaeogeography, Palaeoclimatology, Palaeoecology* 245, 200–226.
- Lesemann, J.E., Alsop, G.I., Piotrowski, J.A., 2010. Incremental subglacial meltwater sediment deposition and deformation associated with repeated ice-bed decoupling: a case study from the Island of Funen, Denmark. *Quaternary Science Reviews* 29, 3212–3229.
- Loi, A., Ghienne, J.F., Dabard, M.P., Paris, P., Botquelen, A., Christ, N., Elaouad-Debbaj, Z., Gorini, A., Vidal, M., Videt, B., Destombes, J., 2010. The Late Ordovician glacio-eustatic record from a high-latitude storm-dominated shelf succession: the Bou Ingarf section (Anti-Atlas, Southern Morocco). *Palaeogeography, Palaeoclimatology, Palaeoecology* 296, 332–358.
- Lorenz, J.C., Warpinski, N.R., Teufel, L.W., 1991. Results of the multiwell experiment – in situ stresses, natural fractures, and other geological controls on reservoirs. *Bulletin of the American Association of Petroleum Geologists* 75, 1714–1737.
- Lowe, D.R., 1975. Water escape structures in coarse-grained sediments. *Sedimentology* 22, 175–204.
- Maltman, A.J., 1994. *The Geological Deformation of Sediments*. Chapman and Hall, London (362 pp.).
- Mandl, G., Harkness, R.M., 1987. Hydrocarbon migration by hydraulic fracturing. In: Jones, M.E., Preston, R.M.F. (Eds.), *Deformation of Sediments and Sedimentary Rocks*. Geological Society Special Publication, 29, pp. 39–53 (Bath).
- Marante, A., 2008. Architecture et dynamique des systèmes sédimentaires silico-clastiques sur la "plate-forme géante" nord-gondwanienne – L'Ordovicien moyen de l'Anti-Atlas marocain. PhD Thesis Université Michel Montaigne Bordeaux 3, Bordeaux, France.
- McGrath, A.G., Davison, I., 1995. Damage zone geometry around fault tips. *Journal of Structural Geology* 17, 1011–1024.
- Menzies, J., 2000. Micromorphological analyses of microfabrics and microstructures indicative of deformation processes in glacial sediments. In: Maltman, A.J., Hubbard, B., Hambrey, M.J. (Eds.), *Deformation of Glacial Material*. London, Geological Society, Special Publication, 176, pp. 245–257.
- Menzies, J., 2012. Strain pathways, till internal architecture and microstructures – perspectives on a general kinematic model – a 'blueprint' for till development. *Quaternary Science Reviews* 50, 105–124.
- Menzies, J., Ellwanger, D., 2011. Insights into subglacial processes inferred from the micromorphological analyses of complex diamicton stratigraphy near Illmensee-Lichtenegg, Hochsten, Germany. *Boreas* 40, 271–288.
- Menzies, J., Zaniewski, K., 2003. Microstructures within a modern debris flow deposit derived from Quaternary glacial diamicton – a comparative micromorphological study. *Sedimentary Geology* 157, 31–48.
- Menzies, J., Gao, C., Kodors, C., 2013. Microstructural analyses of a Middle Pliocene till from the James Bay Lowlands, Canada: evidence of "potential" fast ice streaming. *Proceedings of the Geologists' Association* 124, 790–801.
- Montenat, C., Barrier, P., d'Estève, P.O., Hibs, C., 2007. Seismites: an attempt at critical analysis and classification. *Sedimentary Geology* 196, 5–30.
- Mulder, T., Alexander, J., 2001. The physical character of subaqueous sedimentary density flows and their deposits. *Sedimentology* 48, 269–299.
- Ó Cofaigh, C., 1996. Tunnel valley genesis. *Progress in Physical Geography* 20, 1–19.
- Obermeier, S.F., 1996. Use of liquefaction-induced features, as for paleoseismic analysis – an overview of how seismic liquefaction features can be distinguished from other features and how their regional distribution and properties of source sediment can be used to infer the location and strength of Holocene palaeo-earthquakes. *Engineering Geology* 44, 1–76.
- Ogata, K., Mutti, E., Pini, G.A., Tinterri, R., 2012. Mass transport-related stratal disruption within sedimentary melanges: examples from the northern Apennines (Italy) and south-central Pyrenees (Spain). *Tectonophysics* 568, 185–199.
- Onasch, C.M., Kahle, C.F., 2002. Seismically induced soft-sediment deformation in some Silurian carbonates, eastern U.S. Midcontinent. In: Ettensohn, F.R., Rast, N., Brett, C.E. (Eds.), *Ancient Seismites*. Geological Society of America Special Paper, 359, pp. 165–176.
- Orange, D.L., 1990. Criteria helpful in recognizing shear-zone and diapiric melanges: examples from the Hoh accretionary complex, Olympic Peninsula, Washington. *Geological Society of America Bulletin* 102, 935–951.
- Owen, G., 1987. Deformation processes in unconsolidated sands. In: Jones, M.E., Preston, R.M.F. (Eds.), *Deformation of Sediments and Sedimentary Rocks*. Geological Society Special Publication, 29, pp. 11–24.
- Passchier, C.W., Trouw, R.A.J., 2005. *Microtectonics*. Springer, Berlin (366 pp.).
- Passchier, S., Wilson, S., Paulsen, T.S., 1998. Origin of Breccias in the CRP-1 Core. *Terra Antarctica* 5, 401–409.
- Phillips, E., 2006. Micromorphology of a debris flow deposit: evidence of basal shearing, hydrofracturing, liquefaction and rotational deformation during emplacement. *Quaternary Science Reviews* 25, 720–738.
- Phillips, E., Everest, J., Reeves, H., 2012. Micromorphological evidence for subglacial multiphase sedimentation and deformation during overpressurized fluid flow associated with hydrofracturing. *Boreas* 42, 395–427.
- Pini, G.A., Ogata, K., Camerlenghi, A., Festa, A., Lucente, C.C., Codegone, G., 2012. Sedimentary Melanges and Fossil Mass-Transport Complexes: A Key for Better Understanding Submarine Mass Movements. In: Yamada, Y., Kawamura, K., Ikehara, K., Ogawa, Y., Urgeles, R., Mosher, D., Chaytor, J., Strasser, M. (Eds.), *Submarine Mass Movements and Their Consequences*, 31, pp. 585–594.
- Piotrowski, J.A., 1994. Tunnel-valley formation in northwest Germany – geology, mechanisms of formation and subglacial bed conditions for the Bornhöved tunnel valley. *Sedimentary Geology* 89, 107–141.
- Piotrowski, J.A., Kraus, A.M., 1997. Response of sediment to ice-sheet loading in north-western Germany: effective stresses and glacier-bed stability. *Journal of Glaciology* 43, 495–502.
- Piotrowski, J.A., Larsen, N.K., Junge, F.W., 2004. Reflections on soft subglacial beds as a mosaic of deforming and stable spots. *Quaternary Science Reviews* 23, 993–1000.
- Pisarska-Jamroz, M., Weckwerth, P., 2013. Soft-sediment deformation structures in a Pleistocene glaciolacustrine delta and their implications for the recognition of subenvironments in delta deposits. *Sedimentology* 60, 637–665.
- Price, N.J., Cosgrove, J.W., 1990. *Analysis of Geological Structures*. Cambridge University Press, Cambridge (502 pp.).

- Reinardy, B.T.I., Larter, R.D., Hillenbrand, C.D., Murray, R., Hiemstra, J., Booth, A.D., 2011. Streaming flow of an Antarctic Peninsula palaeo-ice stream, both by basal sliding and deformation of substrate. *Journal of Glaciology* 57, 596–608.
- Robert-Charreau, C., Burkhard, M., 2008. Inversion tectonics, interference pattern and extensional fault-related folding in the Eastern Anti-Atlas, Morocco. *Swiss Journal of Geosciences* 10, 397–408.
- Rodrigues, N., Cobbold, P.R., Loseth, H., 2009. Physical modelling of sand injectites. *Tectonophysics* 474, 610–632.
- Rousell, D.H., Fedorowich, J.S., Dressler, B.O., 2003. Sudbury Breccia (Canada): a product of the 1850 Ma Sudbury Event and host to footwall Cu–Ni–PGE deposits. *Earth-Science Reviews* 60, 147–174.
- Sadolin, M., Pedersen, G.K., Pedersen, S.A.S., 1997. Lacustrine sedimentation and tectonics: an example from the Weichselian at Lonstrup Klint, Denmark. *Boreas* 26, 113–126.
- Sandersen, P.B.E., Jørgensen, F., 2012. Substratum control on tunnel-valley formation in Denmark. In: Huuse, M., Redfern, J., Le heron, D.P., Dixon, R.J., Moscariello, A., Graig, J. (Eds.), *Glaciogenic Reservoirs and Hydrocarbon systems*, Geological Society, Special Publications, 368, London, pp. 145–158.
- Scott, A., Vigorito, M., Hurst, A., 2009. The process of sand injection: internal structures and relationships with host strata (Yellowbank Creek Injectite Complex, California, USA). *Journal of Sedimentary Research* 79, 568–583.
- Shaw, J., 2002. The meltwater hypothesis for subglacial bedforms. *Quaternary International* 90, 5–22.
- Shaw, J., 2010. In defence of the meltwater (megaflood) hypothesis for the formation of subglacial bedform fields. *Journal of Quaternary Science* 25, 249–260.
- Szuman, I., Ewertowski, M., Kasprzak, L., 2013. Thermo-mechanical facies representative of fast and slow flowing ice sheets: the Weichselian ice sheet, a central west Poland case study. *Proceedings of the Geologists Association* 124, 818–833.
- Talling, P.J., Masson, D.G., Sumner, E.J., Malgesini, G., 2012. Subaqueous sediment density flows: Depositional processes and deposit types. *Sedimentology* 59, 1937–2003.
- Tucker, M.E., 2001. *Sedimentary Petrology: An introduction to the Origin of Sedimentary Rocks*, 3rd Edition. Blackwell, Oxford (272 pp.).
- Tucker, M.E., Wright, P.V., 1990. *Carbonate Sedimentology*. Blackwell Scientific Publications, Oxford.
- van der Meer, J.J.M., Menzies, J., Rose, J., 2003. Subglacial till: the deforming glacier bed. *Quaternary Science Reviews* 22, 1659–1685.
- van der Meer, J.J.M., Kjaer, K.H., Krüger, J., Rabassa, J., Kilfeather, A.A., 2009. Under pressure: clastic dykes in glacial settings. *Quaternary Science Reviews* 28, 708–720.
- van der Vegt, P., Janszen, A., Moscariello, A., 2012. Tunnel valleys: current knowledge and future perspectives. In: Huuse, M., et al. (Eds.), *Glaciogenic Reservoirs and Hydrocarbons systems*. Geological Society, London, Special Publication, 368, pp. 75–88.
- Veevers, J.J., 2005. Gondwanaland and Gondwana. In: Selley, R.C., Cocks, L.R.M., Plimer, I.R. (Eds.), *Gondwanaland and Gondwana*. Elsevier, Oxford, pp. 128–155.
- Villas, E., Vizcaino, D., Alvaro, J.J., Destombes, J., Vennin, E., 2006. Biostratigraphic control of the latest-Ordovician glaciogenic unconformity in Alnif (Eastern Anti-Atlas, Morocco), based on brachiopods. *Geobios* 39, 727–737.
- Yamamoto, Y., Nidaira, M., Ohta, Y., Ogawa, Y., 2009. Formation of chaotic rock units during primary accretion processes: examples from the Miura-Boso accretionary complex, central Japan. *Island Arc* 18, 496–512.

Partie 2

«Pressions d'eau interstitielle (Alnif) vs. écoulements d'eaux de fonte (Foum Larjamme): deux modèles de formation des vallées tunnels glaciaires ordoviciennes, et leurs relations avec la dynamique des *ice-streams* (Maroc)».

Cette seconde partie fait l'objet d'un article soumis dans la revue *Palaeogeography, Palaeoclimatology, Palaeoecology*

Article 4

Ravier, E., Buoncristiani, J.F., Menzies, J., Guiraud, M., Clerc, S. and Portier E. Porewater pressure-driven (Alnif) vs. Meltwater-driven (Foum Larjamme): two models of tunnel valley formation existing during the Ordovician glaciation, and their relations with Ice-Stream dynamics (Morocco). (Submitted).

Objectifs:

- *L'objectif de cette seconde partie est de comparer deux vallées tunnels ordoviciennes (Alnif vs. Foum Larjamme) se développant sur substrat meuble et présentant des caractéristiques morphologiques, sédimentologiques, et déformationnelles différentes.*
- *Dans la partie 1, la formation de la vallée tunnel d'Alnif par remobilisation sédimentaire a été démontrée. Cependant, l'intérêt et l'objectif de la partie 2 est de tester si il existait un seul modèle de formation des vallées tunnels durant l'Ordovicien (i.e., par remobilisation sédimentaire) alors qu'il existe au moins trois autres principaux modèles expliquant la formation des vallées tunnels au Quaternaire.*
- *Un objectif supplémentaire est d'observer si le remplissage sédimentaire la vallée tunnel varie en fonction du processus de formation, mais également en fonction de l'environnement dans lequel se forme la vallée tunnel.*
- *Enfin, le dernier objectif sera d'analyser si il existe un lien entre la morphologie des vallées tunnels (ainsi que les processus de formation qui leur sont associés) et la dynamique de la calotte glaciaire, plus particulièrement la dynamique et la distribution des «ice-streams».*

1. Précédents travaux

Dans la première partie du chapitre 3, l'impact des remobilisations sédimentaires sur la formation des vallées tunnels ordoviciennes a été démontré. Il existe cependant dans la littérature des autres modèles de formation des vallées tunnels, généralement regroupés sous trois grandes catégories. D'après la synthèse réalisée par Kehew et al. (2012), ces catégories sont les suivantes:

- a. Formation progressive par un écoulement continu.
- b. Formation instantanée par un écoulement catastrophique.
- c. Modèle composite comprenant formation progressive et instantanée.

a. Formation progressive par un écoulement continu

Ce premier modèle, proposé initialement par Boulton et Hindmarsh (1987) et repris plus récemment dans les travaux de Boulton et al. (2007a, b; 2009), envisage qu'une partie des eaux de fonte soit transférée dans le substrat sous-glaciaire meuble et perméable. Le transfert progressif de l'eau de fonte dans l'aquifère se prolonge jusqu'à ce que la capacité de transfert du sédiment soit atteinte. Un fois atteinte, la pression d'eau interstitielle dans le sédiment devient élevée et provoque une chute de la pression effective, qui se traduit alors par la formation d'un chenal sous la glace. L'augmentation de la pression d'eau interstitielle favorise la liquéfaction des sédiments qui sont ensuite entraînés dans le chenal sous-glaciaire.

b. Formation instantanée par écoulement catastrophique

Ce modèle implique l'existence d'un drainage événementiel comme mécanisme principal de la formation des vallées tunnels (Piotrowski, 1994). La formation de la vallée est alors très rapide et considérée comme instantanée comparée au modèle précédent. Ce processus rapide d'érosion lié à l'écoulement chenalisé et catastrophique d'eaux de fonte est proposé par de nombreux auteurs pour expliquer la formation des vallées tunnels au Quaternaire (Shaw, 1983; Ehlers et Linke, 1989; Shaw et al., 1989; Shaw et Gorell, 1991; Brennand et Shaw, 1994; Huuse et Lykke-Andersen, 2000; Hooke et Jennings, 2006).

Les conditions d'existence d'un tel écoulement catastrophique sont liées à la présence d'une couche de permafrost en aval de la marge glaciaire. Ce permafrost favorise le stockage d'une importante réserve d'eau sous la glace, en position submarginale. Cette réserve d'eau se libère de manière catastrophique lorsque la pression de l'eau devient supérieur au poids de la glace. Un modèle alternatif est proposé par Shaw (2002, 2010) qui suggère le développement d'une nappe d'eau pouvant atteindre 100 km de large et près d'une dizaine de m de hauteur sous la calotte glaciaire. Cependant, ce dernier modèle semble très controversé puisqu'il nécessite de gigantesques réserves d'eaux de fonte (Clarke et al., 2005).

c. Modèle composite comprenant formation progressive et instantanée.

Jørgensen et Sandersen (2006) suggèrent que les vallées tunnels peuvent se former par l'alternance au cours du temps d'écoulements catastrophiques et continus. Ce modèle est généralement associé à des processus sous-glaciaires et proglaciaires, liés à des phases de drainage ou de vidanges successives au cours du retrait de la calotte glaciaire (Huuse et Lykke-Andersen, 2000; Kozlowski et al., 2005; Kehew et Kozlowski, 2005). Les vallées tunnels formées par ce type de modèle hybride se composent généralement de multiples incisions et remplissages sédimentaires qui sont associées à des épisodes successifs de vidange catastrophique (Jørgensen et Sandersen, 2006; Sandersen et al., 2009).

Si tous ces modèles découlent d'exemples quaternaires, cette deuxième partie a pour but de démontrer si certains de ces modèles peuvent s'appliquer à des vallées tunnels ordoviciennes, ou alors si toutes ces vallées se sont formées selon le modèle de creusement révélé à Alnif (i.e., par remobilisation sédimentaire).

2. Contexte de l'étude

Les deux vallées tunnels comparées dans cette deuxième partie sont les vallées tunnels d'Alnif et de Foum Larjamme. La vallée tunnel d'Alnif étant constituée de deux incisions superposées, cette deuxième partie se focalise sur les caractéristiques ainsi que sur le modèle de formation intervenant dans le creusement de la deuxième incision (la première incision étant décrite dans la partie 1).

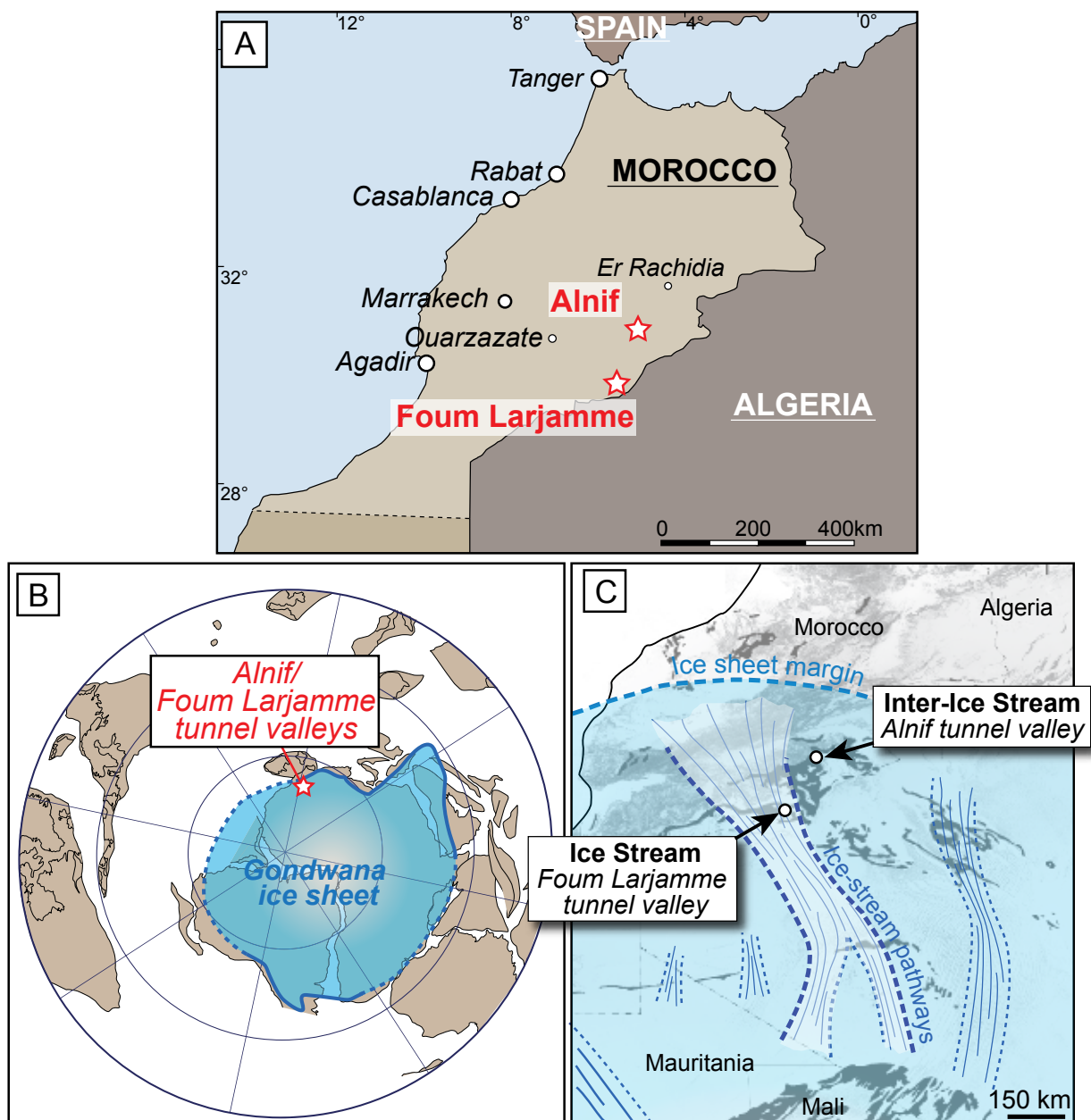


Figure 1. (A) Geographical location of the Alnif tunnel and Foug Larjamme tunnel valleys. (B) Palaeogeographic reconstructions for the latest Ordovician, adapted from Cocks and Torsvik (2002) and modified after Clerc et al. (2013). The extension of the Hirnantian palaeo-ice sheet, modified from Ghienne et al. (2007) is represented on the Gondwana palaeo continent. (C) Detailed palaeogeographic reconstructions of the ice sheet and associated ice-stream positions in Northwestern Africa are shown (modified after Ghienne et al., 2007 and Le Heron et al., 2007). Note that the Foug Larjamme area was situated along a palaeo ice stream pathway, while the Alnif tunnel valley was situated in an inter-ice stream zone (i.e., between two major ice streams).

Les caractéristiques morphologiques, sédimentologiques, et déformationnelles de cette deuxième incision sont donc comparées aux caractéristiques de la vallée tunnel de Foug Larjamme, située à 150 km au sud-est d'Alnif, dans l'anti-Atlas marocain (**Fig. 1A**). La vallée tunnel de Foug Larjamme mesure approximativement 1 km de large pour 100 m de profondeur, et repose sur des sédiments préglaciaires marins déposés durant l'Ordovicien. La vallée tunnel de Foug Larjamme a fait l'objet d'une publication par Le Heron (2007) qui se focalise principalement sur la nature de son remplissage sédimentaire.

Ces deux sites d'études étaient situés à proximité du front nord de la calotte glaciaire gondwanienne lors de son maximum d'avancée (**Fig. 1B,C**). La distribution géographique des paléo *ice-streams* de l'Afrique du nord, proposée par Ghienne et al. (2007) et Le Heron et al. (2007), a permis de situer les deux vallées tunnels par rapport à la paléo dynamique glaciaire. En admettant que la formation de ces vallées tunnels soient contemporaine du fonctionnement des *ice-streams*, la vallée tunnel d'Alnif était alors située dans une zone comprise entre deux *ice-streams*, tandis que la vallée tunnel de Foug Larjamme était alors située dans l'axe d'un *ice-stream* (**Fig. 1C**).

3. Méthodes

La méthode utilisée consiste en une analyse morphologique et sédimentologique couplée à une étude détaillée des structures de déformation pré-lithification contenues dans les dépôts préglaciaires, et dans le remplissage sédimentaire des vallées tunnels. Une vingtaine d'échantillons a été prélevée dans les sédiments préglaciaires et dans le remplissage basal des deux vallées tunnels afin de réaliser des lames minces. Les structures de déformation pré-lithification observées à l'échelle macroscopique et microscopique ont été décrites, de même que leurs relations chronologiques et leurs cinématiques. Les données morphologiques, sédimentologiques et structurales récoltées sur les deux sites d'études ont ensuite été analysées et comparées afin de déterminer le modèle de formation associé à chacune des deux vallées tunnels.

4. Articles soumis à *Palaeogeography, Palaeoclimatology, Palaeoecology*

«Porewater pressure-driven (Alnif) vs. Meltwater-driven (Foug Larjamme): two models of tunnel valley formation existing during the Ordovician glaciation, and their relations with Ice-Stream dynamics (Morocco).»

L'article est structuré de la façon suivante: (1) Dans une première partie, le cadre stratigraphique ainsi que la morphologie des vallées tunnels d'Alnif et de Foug Larjamme sont présentés. (2) Dans une deuxième partie, une description faciologique et stratigraphique détaillée des dépôts préglaciaires et du remplissage basal des deux vallées tunnels est réalisée. Dans cette même partie, les structures de déformation pré-lithification préservées dans les sédiments préglaciaires ainsi que dans le remplissage

basal de la vallée tunnel sont analysées. Chaque structure de déformation est interprétée en termes de cinématique, de mécanismes de déformation, et de pressions de fluide. (3) La troisième partie présente les modèles de creusement associés à chacune des vallées en se basant sur les données morphologiques, sédimentologiques, et déformationnelles précédemment récoltées. (4) Dans une quatrième partie, la reconstruction des environnements de dépôt relatifs au remplissage sédimentaire basal de chaque vallée tunnel est proposée. (5) Dans une dernière partie, le contrôle de la dynamique glaciaire sur les processus de creusement des vallées tunnels, et donc sur leurs morphologies, sera discuté en s'appuyant sur les cartes de distribution des paléo *ice-streams*.

**Porewater pressure-driven (Alnif) vs. Meltwater-driven (Foum Larjamme):
two models of tunnel valley formation existing during the Ordovician glaciation,
and their relations with Ice-Stream dynamics (Morocco).**

Edouard Ravier^a, Jean-François Buoncristiani^a, John Menzies^b, Michel Guiraud^a, Sylvain Clerc^c, Eric Portier^c.

^aLaboratoire Biogeosciences UMR/CNRS 6282 Université de Bourgogne, 6 Bd Gabriel, 21000 DIJON, France.

^bDepartment of Earth Sciences, Brock University, 500 Glenridge Avenue, St. Catharines, Ontario L2S 3A1, Canada

^cGDF Suez, Exploration Production International, 1 place Samuel de Champlain – Faubourg de l'Arche 92930 Paris La Défense Cedex – France.

1. Introduction

Tunnel valleys are described as up to hundreds of kilometers long, several kilometers wide, and hundreds of meters deep. Research on tunnel valleys used to be focused on their morphologies and sedimentary infills due to their economical and societal interest (groundwater, gas, and oil resources), while recent studies also focused on their mechanisms of formation (Jørgensen and Sandersen, 2006; Huuse et al., 2012; Janszen et al., 2012, van der Vegt et al., 2012; Ravier et al., 2014a).

There are four major models of tunnel valley formation proposed in the literature, principally based on numerical modelling and field investigations. The mechanisms involved in the formation of tunnel valleys depend on the nature of the substratum, the characteristics of the subglacial meltwater drainage, the amount of meltwater available, glaciodynamics, and the erosion rate. Some models suggest tunnel valley formation by steady-state processes and progressive erosion and evacuation of material through subglacial pipes (e.g., N- or C-channels), while others mention rapid tunnel valley formation by outburst flooding and subsequent bed erosion by considerable amounts of meltwater (Boulton & Hindmarsh, 1987; Piotrowski, 1994; Hooke and Jennings, 2006; Shaw, 2010). Recently, models invoking tunnel valley formation by hydraulic fracturing due to the localized development of fluid overpressure have been proposed (Janszen et al., 2012; Ravier et al., 2014a).

In this study, we compare different processes involved in the formation and infill of Ordovician tunnel valleys growing into soft beds in the eastern Anti-Atlas Mountains (Morocco), via analyses conducted along the Alnif and Foug Larjamme tunnel valleys. The Alnif and Foug Larjamme troughs were situated close to the northern margin of the Ordovician ice sheet, respectively in and between palaeo-ice stream pathways. Sedimentological and deformational analyses of these tunnel valleys, displaying exceptional outcrop qualities, lead to two different models of tunnel valley formation being proposed. A first model controlled by the subglacial development of high porewater pressures (Alnif) promoting bed remobilization (Alnif) and a second model resulting from bed erosion by meltwater flows (Foug Larjamme).

2. Geological setting and tunnel valley morphologies

Based on stratigraphical, sedimentological, and deformational analyses, tunnel valleys in Alnif and Foug Larjamme were formed during the Hirnantian glacial episode, although the relative timing for

the emplacement of both Tunnel valleys cannot be established. (Destombes, 1985; Villas et al., 2006; Le Heron, 2007; Clerc et al., 2013a).

2.1. Alnif

The Alnif tunnel valley is situated in the eastern part of the Moroccan Anti-Atlas Mountains. This region corresponded to the northernmost part of the Gondwana palaeo-ice sheet (Figs. 1A and 1B).

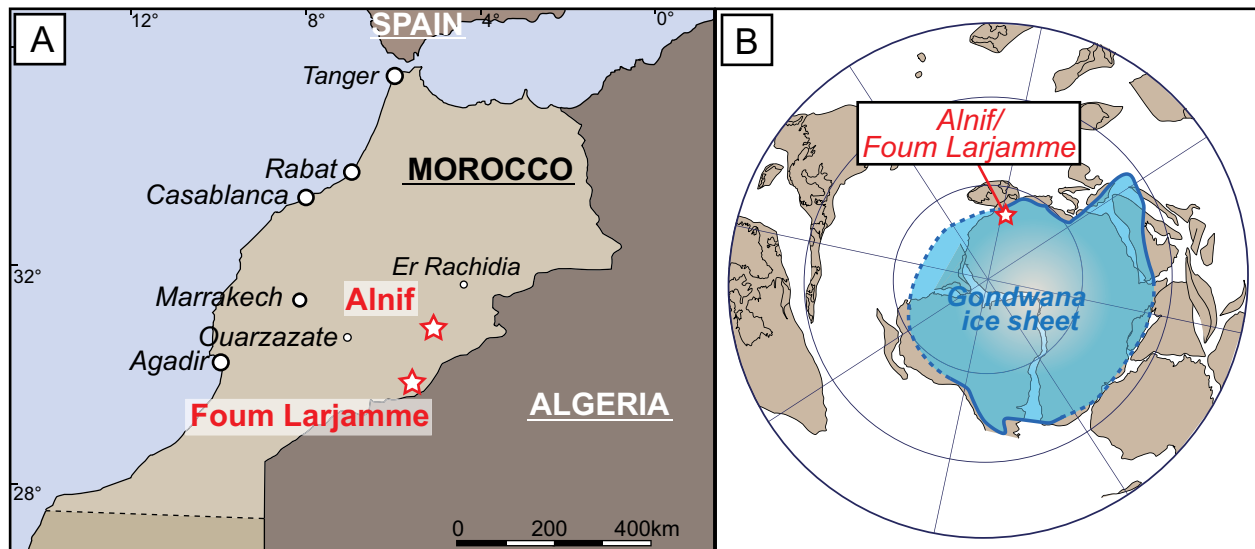


Figure 1. (A) Locations of the Alnif and Foug Larjamme tunnel valleys. (B) Palaeogeographic reconstruction for the latest Ordovician, adapted from Cocks and Torsvik (2002) and modified after Clerc et al. (2013a). The extension of the Hirnantian palaeo- ice sheet, modified from Ghienne et al. (2007) is represented on the Gondwana palaeo continent.

Outcrops in this area expose Upper Ordovician deposits displaying both preglacial and glacial sedimentary successions. The stratigraphic succession of Upper Ordovician preglacial deposits is composed of the lower Ktaoua, the upper Tiouririne and the upper Ktaoua Formations (Villas et al., 2006) (**Fig. 2**). During the Hirnantian, the glacial erosion cut through preglacial sediments down to the lower Ktaoua Formation (Destombes, 1985) (**Fig. 2**). Above this major unconformity surface, a 200 meters thick sedimentary sequence infilling the tunnel valley, corresponding to the upper formation of the upper Bani Group, was deposited in subglacial to glaciomarine environments (Clerc et al., 2013a). The Alnif tunnel valley is composed of two superimposed and imbricated tunnel valleys, underlain by two unconformity surfaces: glacial pavement 1 (GP1), related to the first phase of glacial erosion into preglacial marine sediments, and glacial pavement 2 (GP2) related to a second episode of glacial erosion affecting glacial sediments. The two glacial incisions are successively filled by Glacial sedimentary Unit 1 (GU1) and Glacial sedimentary Unit 2 (GU2) (cf. Clerc et al., 2013a; Ravier et al., 2014a). The buried palaeo tunnel valley related to the first glacial incision (GP1) is about 5 km

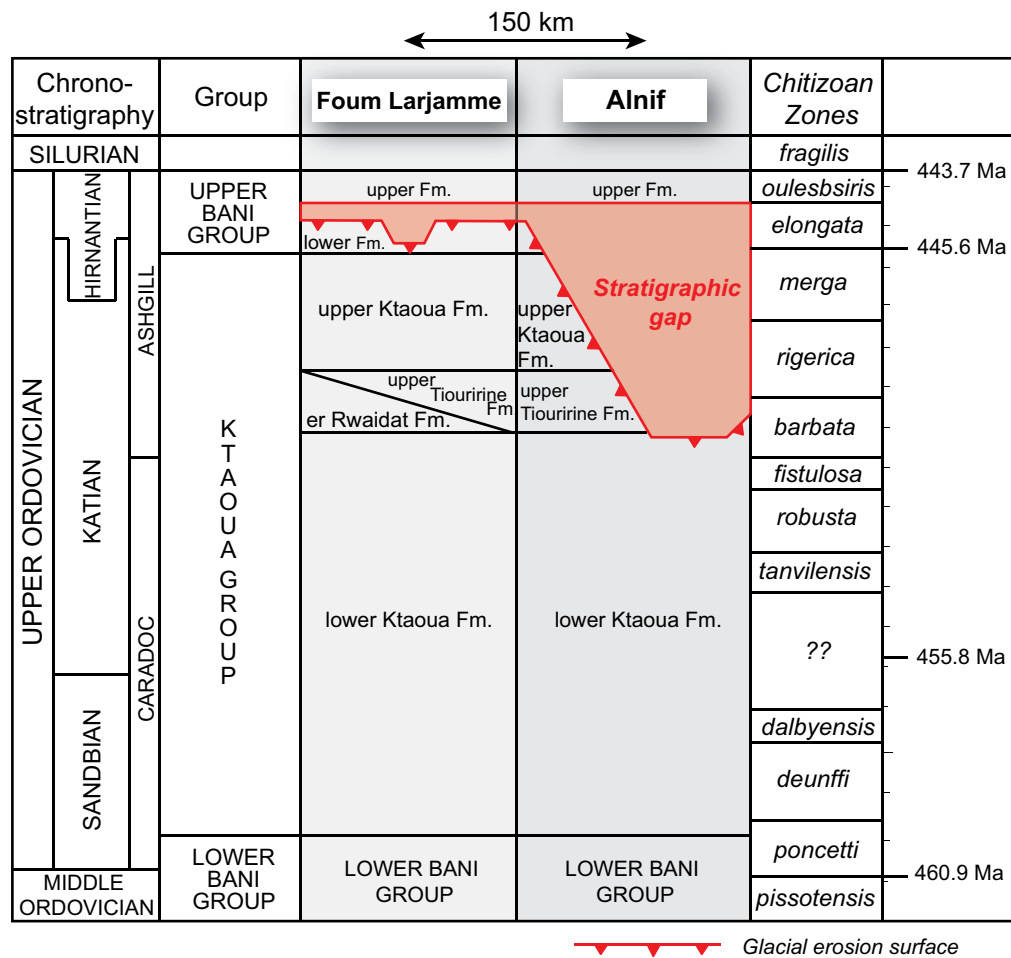


Figure 2. Upper Ordovician stratigraphic correlations between the Foug Larjamme and Alnif areas (modified after Villas et al., 2006 and Clerc et al., 2013a).

wide and 180 m deep, trending SSE-NNW (320° N), while the second tunnel valley (GP2) cut GU1 down to 70 m (up to 100 m in the central part of the valley) and displays a similar width (Fig. 3A). The bases of both tunnel valleys are slightly irregular but generally smooth (Fig. 3A, C). This study will integrate observations realized below both incisions (e.g., GP1 and GP2) and within both valley sedimentary infills (GU1 and GU2). The mechanisms involved in the formation of the first glacial incision (GU1) have been subject to an earlier study where the impact of high porewater pressure on tunnel valley formation has been demonstrated (Ravier et al., 2014a).

2.2. Foug Larjamme

Foug Larjamme is located 150 km SE of the Alnif tunnel valley (Fig. 1A). This site was located in the northern outer part of the Hirnantian ice sheet. In the Foug Larjamme area, Upper Ordovician deposits are also characterized by both preglacial and glacial sedimentary sequences separated by

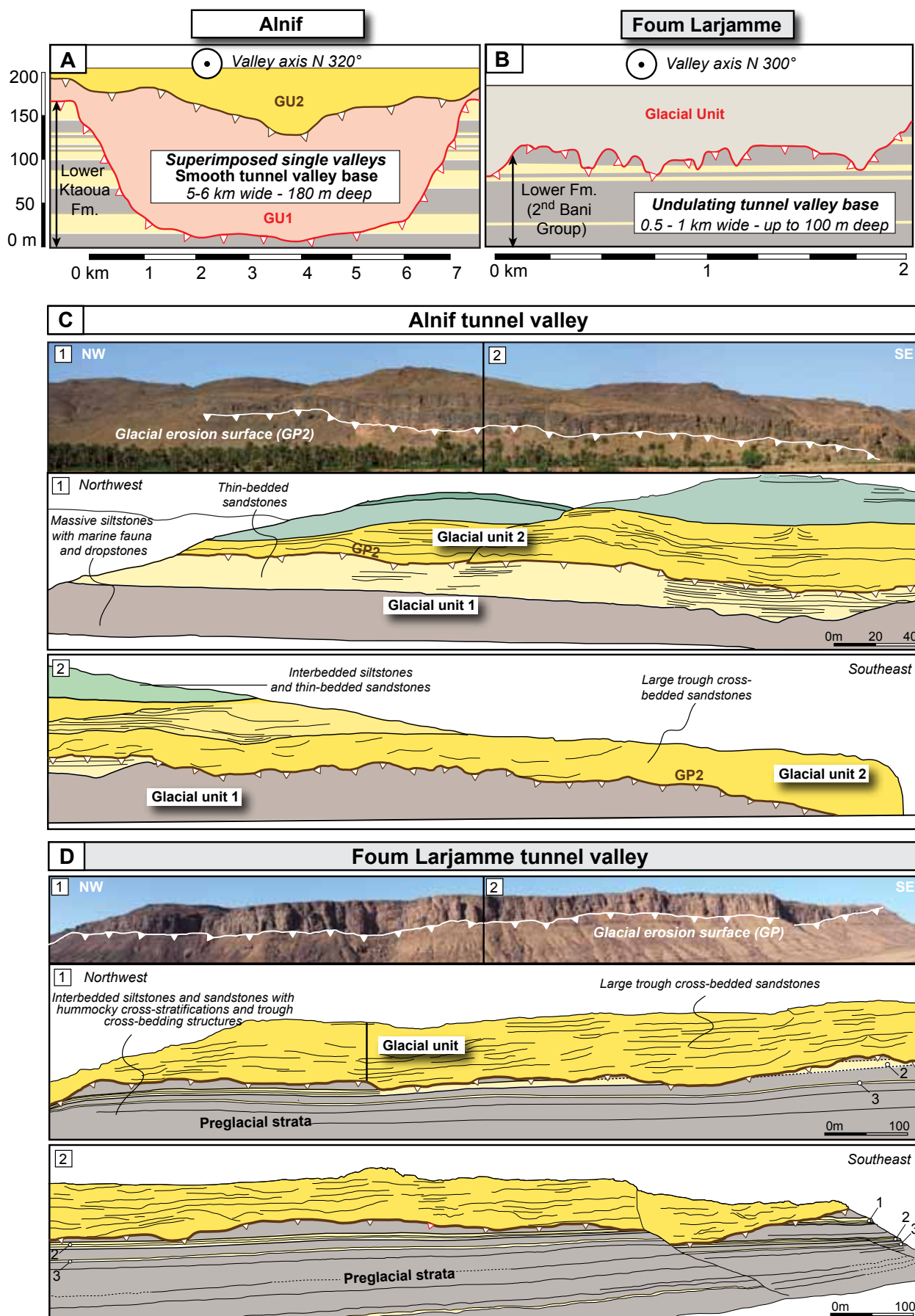


Figure 3. Diagrams showing morphologies of the Alnif (A) and Foug Larjamme (B) tunnel valleys. Panoramic photograph and interpretative scheme of the Alnif (C) and Foug Larjamme (D) tunnel valleys highlighting the morphology of the glacial incisions. In Foug Larjamme, numbers 1, 2, and 3 correspond to laterally extensive sandstone beds that can be used as marker beds to track the glacial truncation surface.

a major erosive and unconformable contact (**Fig. 2**). The Late Ordovician glaciogenic rocks are referred to as the upper formation of the upper Bani Group and overly preglacial rocks deposited in a marine environment (Destombes, 1985). The Foug Larjamme tunnel valley is shallow and cuts into preglacial strata down to the lower formation of the upper Bani Group. The tunnel valley is approximately 1 km wide and up to 100 m in depth (**Fig. 3B, D**).

The tunnel valley, trending SSE-NNW (N 300°), is characterized by an irregular and undulating base (**Fig. 3B, D**). Laterally, the Foug Larjamme tunnel valley truncates another tunnel valley in Tizi N'Tazzounghart indicating that the emplacement of this tunnel valley is related to a second episode of tunnel valley genesis in this area (Le Heron, 2007). Le Heron (2007) proposed that the Foug Larjamme tunnel valley may have formed under a combination of ice sheet loading and elevated subglacial hydrostatic pressures.

3. Sedimentological and deformational analyses

Sedimentological and deformational characteristics of sediments deposited below and above glacial pavements in Alnif and Foug Larjamme are presented below. In the Alnif area, two glacial incisions described as a system of superimposed tunnel valleys are distinguished, while in Foug Larjamme a single tunnel valley truncating preglacial sediments is observed. Sediments deposited below glacial unconformity surfaces (i.e., below the base of tunnel valleys), are considered as “pre-incision” deposits in this study.

3.1. Sedimentological characteristics of pre-incision deposits

3.1.1. Alnif

The superimposed tunnel valleys (GP1 and GP2) are associated with two glacial incisions, the first one truncates preglacial sediments while the second one is related to erosion of GU1.

Below GP1, the preglacial Upper Ordovician stratigraphic succession in the Alnif area has been defined, described and interpreted by Villas et al. (2006), Alvaro et al. (2007), and Clerc et al. (2013a). Preglacial sediments described in the Alnif area include the lower Ktaoua Formation, the upper Tiouririne Formation and upper Ktaoua Formation (**Fig. 2**). The preglacial sedimentary succession

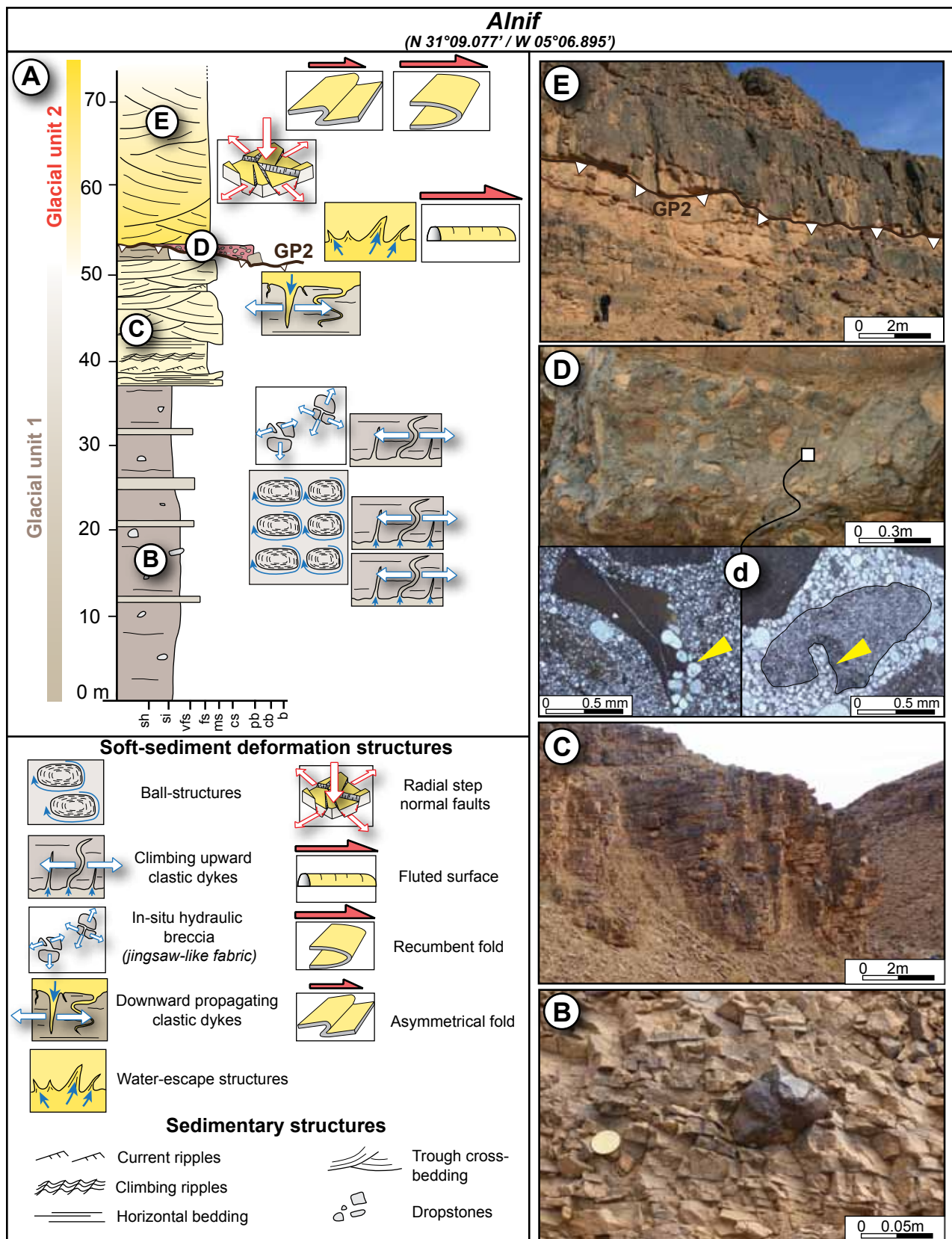


Figure 4. Sedimentological characteristics of the Alnif tunnel valley. (A) Synthetic log section illustrating the transition between deposits from glacial unit 1 (GU1) occurring below the second glacial incision (GP2) and the base of glacial unit 2 (GU2) corresponding to sediments deposited at the base of the second tunnel valley. Positions of soft-sediment deformation structures are reported along the log section. (B) A floating clast embedded in siltstones interpreted as a dropstone. (C) A 15 m thick sequence of stacked thin-bedded fine-grained sandstones. (D) Matrix-supported massive conglomerate containing clayey intraclasts characterized by embedded quartz grains and internal sand-filled microfractures (d). (E) Thick sequence of trough cross-bedded sandstones above GP2 composed of medium to coarse-grained sandstones.

displays an alternation of sandstones beds and shales with a predominance of shale deposits. These preglacial formations record sediment deposition within offshore to shoreface environments frequently affected by storms, illustrated by hummocky cross-stratifications structures (Alvaro et al., 2007; Clerc et al., 2013a). During the Hirnantian glacial episode, the preglacial sediments remained predominantly unlithified although some fauna-rich sand layers have certainly experienced early carbonate cementation and subsequent early lithification (Ravier et al., 2014a). Alternations of unlithified sand with shales and early lithified sandstone beds define a typical “layer-cake” configuration involving aquifers and impermeable barriers (Ravier et al., 2014a).

Below GP2, glacial sediments infilling the underlying tunnel valleys has been described and referred to as GU1 (Clerc et al., 2013a). Within GU1, Clerc et al. (2013a) described three sedimentary units corresponding to three different facies associations. At the base of the valley, matrix-supported conglomerates containing preglacial clasts and displaying a laterally variable thickness (from 1 to 15 m thick) represent the first facies association. This first unit has been interpreted as the result of subglacial deposition by fluidized hyperconcentrated density flows (Clerc et al., 2013a, Ravier et al. 2014a). Conglomeratic deposits are overlain by 80 m of sheet-like bedded, rippled medium-grained sandstones to siltstones. These deposits were characterized by alternating ripple cross-laminations and planar parallel-laminations, sometimes truncated by shallow and low-angle channels infilled by coarser material. This second unit has been interpreted as formed under waning density flows within a subglacial fan system (Clerc et al., 2013a). Upwards, the last unit is composed of faintly laminated siltstones interbedded with very fine to fine-grained sandstones (**Figs. 4A, B, C**). The sandstones beds are locally stacked in 10 to 15 m thick packages with the complete unit reaching over 110 m of thickness. These siltstones are dropstone-rich and contain preserved shells of Hirnantia fauna (**Fig.4B**). This uppermost unit likely records the deposition of a proglacial fan associated with a calving ice margin in a glaciomarine environment (Clerc et al., 2013a).

3.1.2. Fout Lamjamme

Below the glacial unconformity in Fout Lamjamme, preglacial strata corresponding to the lower formation of the upper Bani Group were deposited in a marine environment, and are characterized by alternating weathering-resistant fine sandstone beds and claystone to siltstone beds (**Figs. 2, 5A**). Sandstone beds display hummocky cross-stratifications (HCS), trough cross-stratifications and

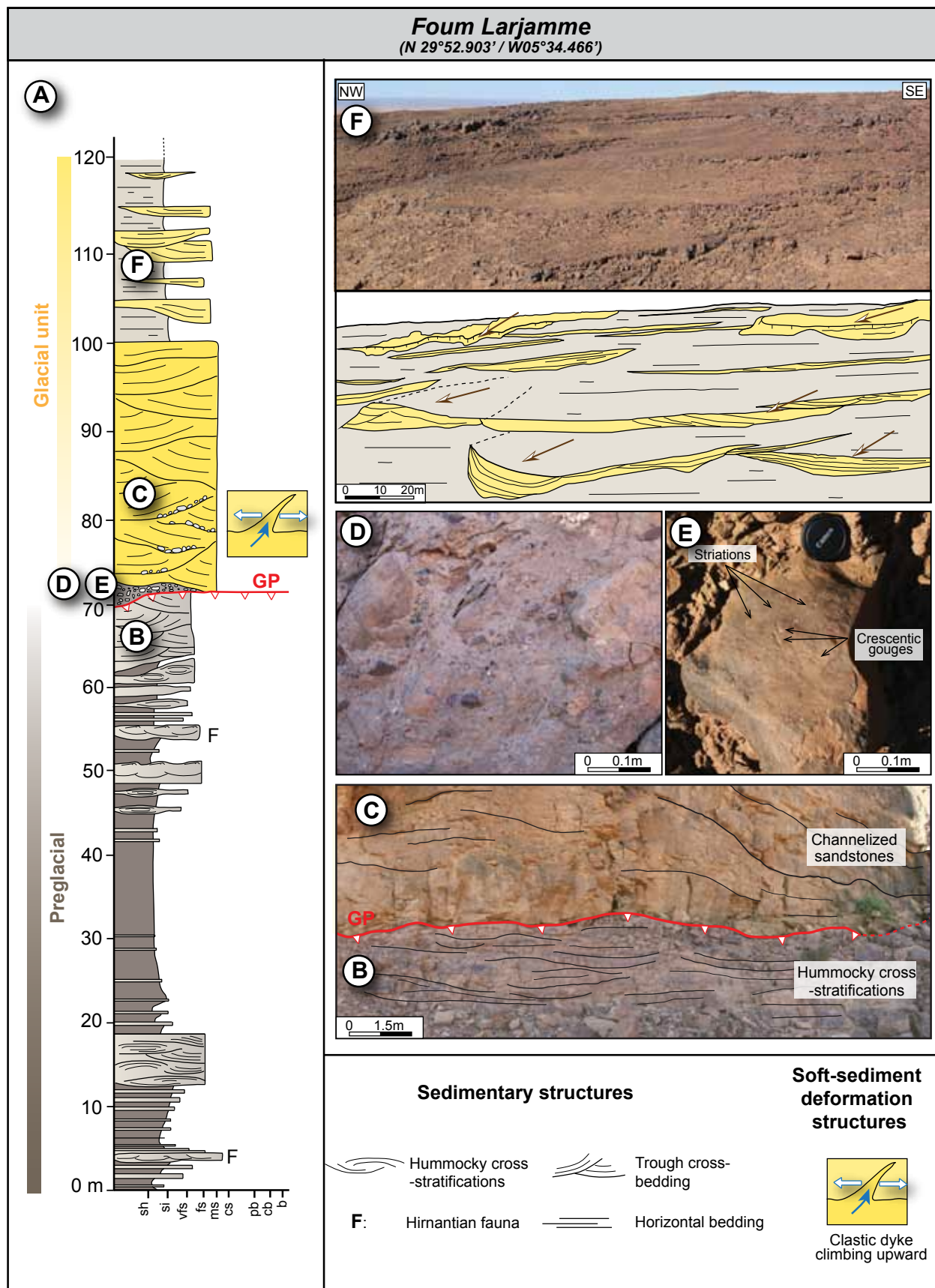


Figure 5. Sedimentological characteristics of the Foum Larjamme tunnel valley. (A) Synthetic log section illustrating the transition between preglacial strata and sediments deposited above the glacial incision (GP) corresponding to the glacial sedimentary unit. (B) Preglacial marine strata with preserved hummocky cross-stratifications (HCS) below the glacial erosion surface (GP). (C) Trough cross bedded-sandstones deposited above the glacial incision. (D) Patchy conglomeratic deposits with rounded and polygenic clasts deposited above the glacial incision (GP). (E) Angular clasts displaying striations and crescentic gouges observed within basal conglomerate. (F) Lenticular sandstone bodies embedded within siltstones. Arrows correspond to palaeo flow indicators.

planar parallel-laminations (**Fig. 5A, B**). Shell debris, including fragments of *Hirnantia* brachiopods are frequently observed within the sandstones beds. Claystones to siltstones beds occasionally contain thin-walled bivalves. The occurrences of trough cross-bedding structures, hummocky cross-stratifications, and planar parallel-laminations, in combination with marine fauna, indicate a storm-dominated shoreface environment. The high proportion of claystones to siltstones at the base of the logged section measured in Fouta Larjamme corresponds to a deep-marine environment, illustrative of sediment deposition in an offshore environment (Le Heron., 2007). Below the glacial incision, an upward increase of sandstone is observed within pre-incision sediments (**Fig. 5A**).

3.2. *Soft-sediment deformation structures in pre-incision deposits*

3.2.1 *Alnif*

Description

Below GP1 and GP2, deposits containing ball-structures occur in the close vicinity of glacial erosion surfaces. A 2 m wide zone situated 5 m below GP1 where such deformation structures occur, has been observed in the Alnif area (Ravier et al., 2014a). Similarly, a 15 m thick sedimentary sequence affected by ball-structures occurs approximately 20 m below GP2 (**Fig. 4A**). Below GP2, superimposed layers containing ball-structures are 0.3 to 0.5 m thick each (**Fig. 6A**). At the microscopic scale, ball-structures display turbate structures illustrated by circular quartz grain re-arrangements. The distribution of ball-structures is heterogeneous below both glacial incisions (Ravier et al., 2014a). Clastic dykes infilled by fine-grained sand are numerous below GP2 and notably cross-cut ball-structures (**Fig. 6B, C**). Clastic dykes are up to 0.4 m thick and are generally subvertical with an upward decrease of their thickness. In combination with dykes and ball-structures, in-situ brecciated clasts are observed, resulting in a “jigsaw-like” fabric (**Fig. 6D, E, F**). Brecciated clasts are associated with chaotic and faint convoluted sandstones beds (**Fig. 6D**).

Interpretation

Ball-structures below GP1 and GP2 indicate liquefaction of the sediments as the result of porewater pressure increase within water-saturated sediments (Maltman, 1994). The increase of porewater pressure might be triggered by loading, differential compaction, high sedimentation rate, or

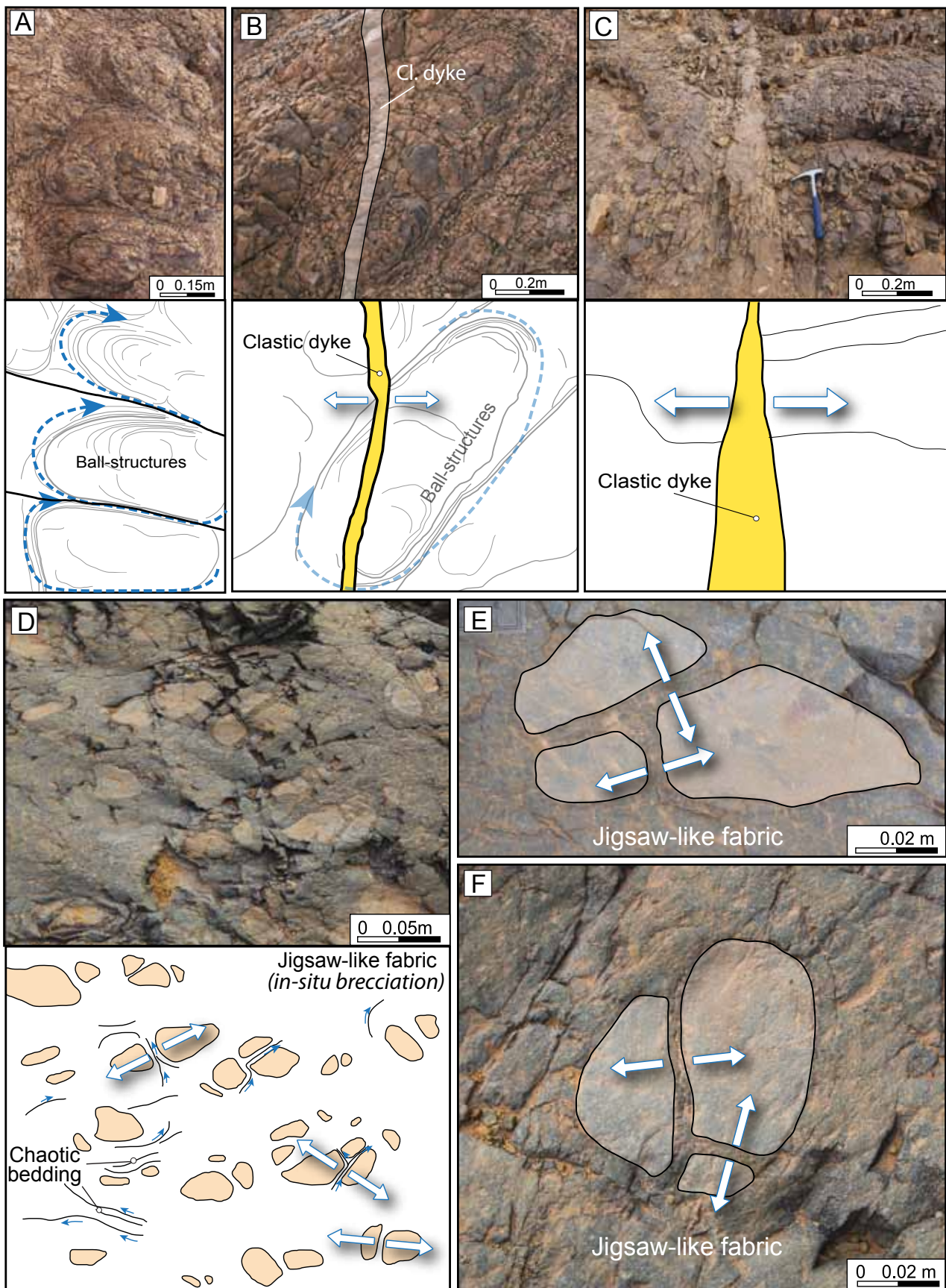


Figure 6. Soft-sediment deformation structures within pre-incision deposits (below GP2) in the Alnif area. (A) Ball-structures occurring up to 35 m below GP2. (B) A clastic dyke cross-cutting ball-structures. (C) Fine-grained sandstone dyke cross-cutting siltstones. (D) In-situ brecciated fine-grained sandstone layer resulting in a «jigsaw-like» fabric associated with chaotic bedding. (E) Close-up on brecciated clasts forming the «jigsaw-like» fabric.

groundwater movement (Pisarska-Jamrozy and Weckwerth, 2013). Below GP1, the discontinuous distribution of ball-structures has been interpreted to be the result of localized porewater increase within the subglacial bed, possibly illustrating a mosaic of coexisting deforming and stable areas underneath the ice (van der Meer et al., 2003; Piotrowski et al., 2004; Ravier et al., 2014a). Similarly, the occurrence of ball-structures below GP2 may record a localized increase of porewater pressure in a deforming zone. This increase of porewater pressure forms in response to the meltwater input within the bed and the local increase of basal shear stress exerted by the overriding ice sheet. At the micro-scale, the turbate structures observed within the ball-structures may be formed in response to basal shearing and porewater pressure increase (Hiemstra and Risdjik, 2003; Menzies et al., 2013). Clastic dykes cross-cutting ball-structures are related to the release of overpressurized water through hydrofractures when porewater pressure within the bed continued to increase until it overcame tensile strength of the host strata. Beds displaying in-situ brecciation combined with chaotic convoluted beds also indicate high porewater pressure, triggering a network of hydrofractures with the circulation of liquefied to fluidized fine-grained sediments within fractures.

3.2.2. Foug Larjamme

Description

Below the Foug Larjamme tunnel valley, pre-incision deposits are not affected by soft-sediment deformation structures, instead undisturbed hummocky cross-stratifications and trough cross-bedding structures can be observed at both scales (**Fig. 7A, 7B**).

Interpretation

In Foug Larjamme, Preglacial sediments display undisturbed sedimentary structures. The absence of perceptible deformation indicates that prevailing stress did not exceed sediment strength for a period of time long enough to achieve deformation. This characteristic implies that predominant parameters controlling deformation of sediments, including porewater pressure and basal shear stress, were in a different configuration between the Alnif and Foug Larjamme areas.

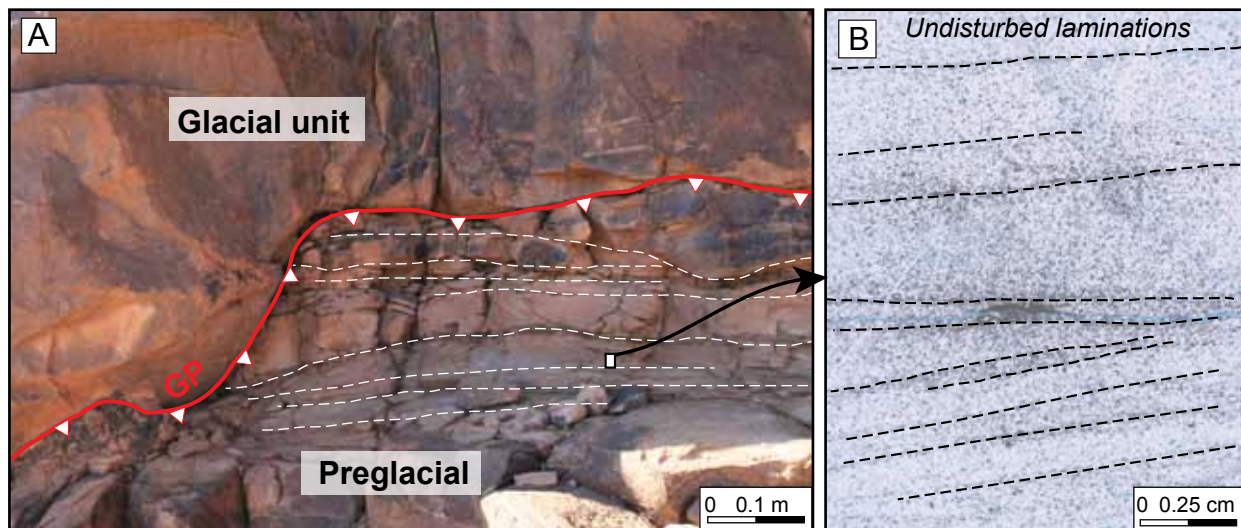


Figure 7. Preserved sedimentary structures below the glacial incision (GP) in the Fouta Larjamme area, at macroscopic (A) and microscopic scale (B).

3.3. Sedimentological characteristics of tunnel valley infills

3.3.1. Alnif

Description

In the Alnif area, the glacial sedimentary infill is divided into two units, GU1 and GU2, successively infilling the two superimposed tunnel valleys GP1 and GP2.

The base of both tunnel valleys is infilled by a patchy conglomeratic unit. Above GP1, a 10 to 12 m thick and discontinuous unit composed of matrix-supported conglomerates is observed. At the microscale, some intraclasts display sharp contacts with the matrix while others display contorted and diffused outlines with the matrix. This basal deposit is characterized by vertically stacked deposits with a predominance of erosive contacts between single beds (cf. Ravier et al., 2014a for further details). Similarly, the base of GU2 is characterized by the presence of a 0.5 to 1.5 m thick and patchy conglomeratic unit composed of subrounded to rounded clasts (**Fig. 4D**). At the micro-scale, some clasts display sharp contacts with the matrix while others display contorted and diffused outlines with the matrix. Some angular clay intraclasts contain embedded quartz grains and internal sand-filled microfractures (**Fig. 4d**).

Within the first incision (GP1), conglomerates are overlain by 80 m of sheet-like bedded, rippled medium-grained sandstones to siltstones and a 110 m thick unit composed of siltstones interbedded with fine-grained sandstones (cf. section 3.1.1. and **Fig. 4A**). The second conglomeratic unit infilling

the base of GP2 is overlain by a 20-25 m thick medium to coarse-grained sandstone unit composed of vertically stacked and amalgamated lenticular bodies containing trough cross-stratifications (**Fig. 3C, 4E**). The base of trough cross-bedding structures is often characterized by mudclasts alignments. Upwards, massive siltstones interbedded with thin-bedded sandstones are observed.

Interpretation

Patchy conglomeratic units occurring at the base of both valleys record sediment deposition by hyperconcentrated density flows (e.g., clean sand debris flow) (Mulder and Alexander, 2001; Talling et al., 2012; Ravier et al., 2014a). The different types of clast-to-matrix contacts indicate that soft and lithified clasts coexist within the conglomerate, related to different degrees of lithification of pre-incision deposits (Ravier et al., 2014a). The occurrence of clay intraclasts with embedded quartz grains, sometimes containing sand-filled microfractures, is interpreted to be the result of fracturing, spalling, and corrosion of encasing strata during sand injection into hydrofractures (Scott et al., 2009). The occurrence of such intraclasts has been described in injectites networks in deep-marine environments and may illustrate the remobilization of preglacial strata fragments that have undergone an early phase of hydrofracturing (Kawakami and Kawamura, 2002).

Above both conglomeratic units, the overlying channelized systems composed of coarse-grained sandstones indicates sediment deposition by turbulent flows under upper flow regime conditions (Clerc et al., 2013a). The numerous erosive surfaces between the lenticular deposits demonstrate a high degree of cannibalization which in turns indicates a tendency for frequent lateral shifting of the meltwater flow (Clerc et al., 2013a). Together with the vertical stacking pattern, the amalgamation of sandstones lenses suggest a limited space available for sediment deposition and rapid changes of flow directions (Catania and Paola, 2001). This sandstone unit has been interpreted as deposited subglacially within a subglacial braided canal network (Clerc et al., 2013a). Above the channelized subglacial deposits, massive siltstones containing marine fauna with thin-bedded sandstones indicate a proglacial environment dominated by suspension fall-out. Suspension settling alternates with sand bed deposition by concentrated flows in a subaqueous fan system (cf. Clerc et al., 2013a for further details).

3.3.2. Fout Larjamme

Description

The sedimentary infill of the Fout Larjamme tunnel valley is composed of three main sedimentary facies. At the base of the tunnel valley, a 0.2 to 1.5 m thick discontinuous conglomeratic unit composed of clasts up to boulder size embedded within a coarse sandy matrix occurs (**Fig. 5D**). Clasts, occasionally containing shell fragments, are principally subrounded to rounded and clast-to-matrix contacts are sharp. Striations and crescentic gouges are occasionally observed on the surface of polished clasts that are predominantly subangular to angular (**Fig. 5E**). Conglomeratic deposits are erosively overlain by a 50 m thick unit composed of vertically stacked lenses (1 to 7 m thick and tens of m wide) of medium to coarse grained sandstones. Sandstones occasionally display cross-bedding structures underlined by pebble and/or cobble deposits (**Figs. 3D, 5C**). Clayey rip-up clasts are frequently observed within these sandstones deposits. The uppermost unit displays individual lenticular bodies of medium to coarse-grained sandstones surrounded by thinly bedded siltstones (**Fig. 5F**). Lenticular bodies are up to tens of meter wide and 4 m thick and contain thinly-bedded to more massive sandstones, with ripple cross-laminated beds. Within these lenses, beds contain frequent mudclasts alignments and load structures. The sandstones lenses have been mapped out on the field by Le Heron (2007) and reveal their meandriform geometries.

Interpretation

The basal massive conglomerate, containing clasts up to boulder size embedded in a sandy matrix, suggests deposition by non-cohesive debris flows reworking preglacial clasts. The roundness index of intraclasts implies long distance transport. Striations on blocks were initially formed by subglacial abrasion of preglacial lithified sediments. The occurrence of angular blocks among rounded clasts possibly indicates that they derive from another source. The conglomerate represents proximal facies, recording efflux adjacent to an ice front, in a subaqueous fan system, or within a subaerial environment (Le Heron, 2007). The overlying thick sequence of lenticular bodies of sandstones is related to deposition by turbulent flows with upper flow conditions within channels. The lenses of thin-bedded sandstones, with ripple cross-laminations are associated with turbulent flow processes, from lower to upper flow regime. Load structures related to sediment foundering have often been described in sediment density flows (Talling et al., 2012). The absence of gravel lag and well-

expressed grading is not consistent with deposition within a proglacial fluvial channel (Posamentier and Walker, 2006). The surrounding massive to faintly laminated siltstones demonstrates predominant suspension settling processes. These channelized deposits may correspond to sediment deposition within a subaqueous medium to distal fan where suspension settling is predominant (silt), and where occasional density flows form superficial scours and small channels infilled by thin sand beds. The whole glacial sequence is here interpreted to have been deposited in a subaqueous environment.

3.4. Soft-sediment deformation structures within tunnel valley infill

3.4.1. Alnif

Description

The basal sedimentary infill of both glacial valleys in Alnif contains a wide range of deformation structures including fluted surfaces, folds, radial step normal faults, clastic dykes and dewatering structures.

At the base of GP1 and GP2, fluted sandstone with polished surfaces up to 1 m wide and tens of meters long are observed (**Fig. 8A**). Recumbent, overturned and sheath fold types, with fold axis oriented towards the SSE occur, generally within single beds (**Figs. 8C, D**). Surfaces displaying radial step normal faults with centimetric offsets and undulating fault planes occur within sandstones (**Fig. 8G**). Clastic dykes up to 0.5 m wide, infilled by conglomerate or sand propagate downwards into siltstones (**Fig. 8B**). In the basal conglomerates, bedding is locally verticalized within the sandy matrix (**Fig. 8E**). Other structures related to dewatering are observed and consist in upward disruption of the layering (0.8 m wide; 1 m thick) (**Fig. 8H**). Sheet dewatering structures or water-escape pipes have also been described at the base of GU1 (Ravier et al., 2014a). At microscopic scale, dewatering structures are characterized by preferential zones of vertical grain re-alignments and necking structures (**Fig. 8F**).

Interpretation

The coexistence of clastic dykes, various fold types and radial step normal faults within the tunnel valley sedimentary infill implies that sediments were deformed under fluctuating strain rates and porewater pressures.

Flute-like structures with elongated morphologies indicate soft-bed deformations underneath flowing-

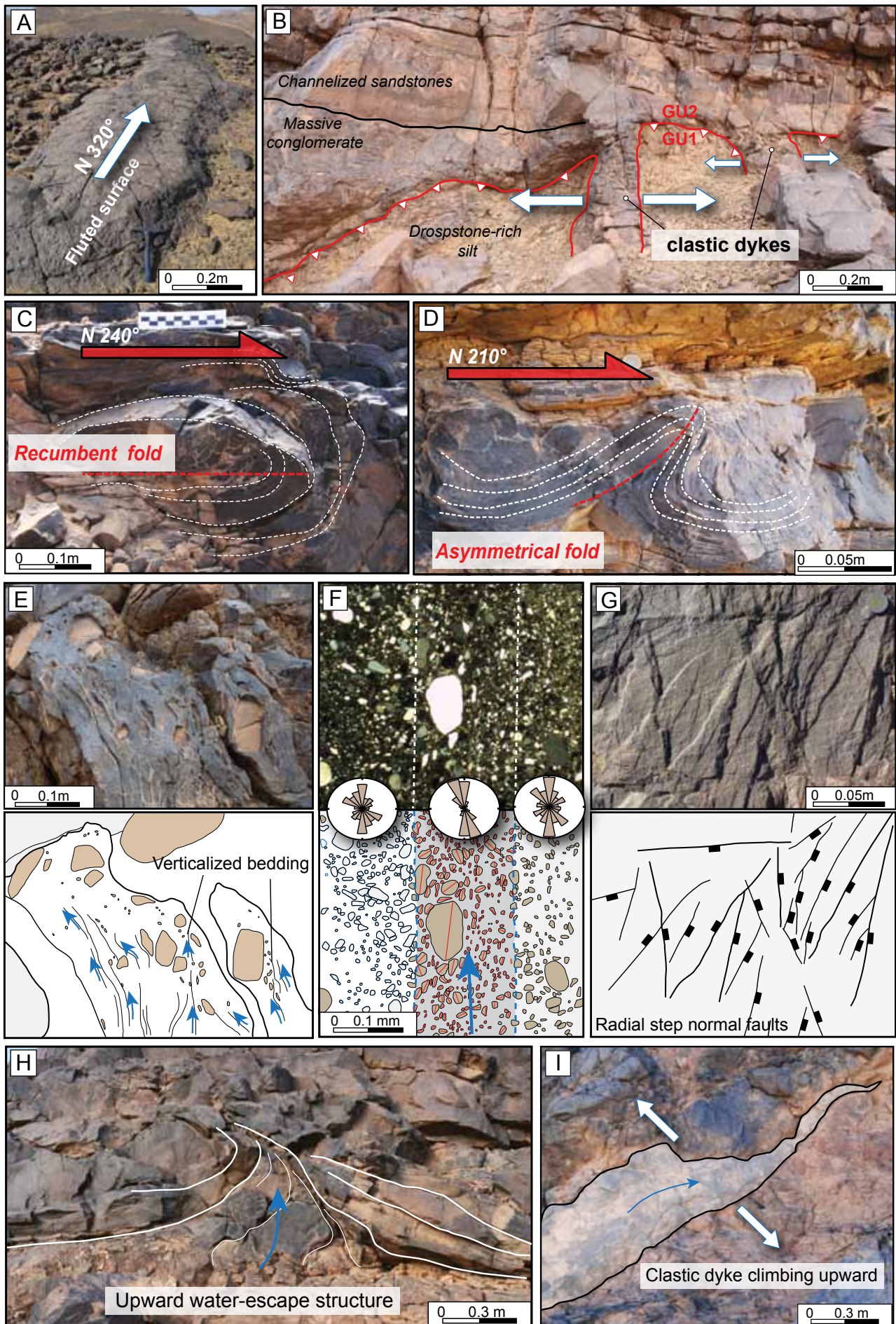


Figure 8. Soft-sediment deformation structures observed within the tunnel valley sedimentary infill. (A) Fluted surface oriented parallel to the tunnel valley axis in the Alnif area (cf. Fig. 4 for stratigraphical position) (B) Clastic dykes propagating downwards occurring along glacial pavement 2 with material from GU2 being injected into GU1 (Alnif). Recumbent (C) and asymmetrical (D) folds affecting single beds and oriented towards the SSE, i.e., parallel to the ice flow direction (Alnif). (E) Verticalized bedding occurring in the basal conglomerate indicating fluidization of the sandy matrix (Alnif). (F) Vertical water-escape observed at the microscopic scale illustrated by the localized vertical realignment of quartz grain long axis in the central part of the thin section (grey zone). (G) Radial step normal microfaults with undulating fault planes triggered by a vertical stress applied on sediments (Alnif). (H) Upward water-escape structures resembling a large-scale dish structure. (I) A clastic dyke climbing upward observed at the base of the sedimentary infill in the Foug Larjamme tunnel valley.

ice associated with high basal shear stress and high strain intensity (Boulton, 1976). Recumbent, asymmetrical or sheath folds observed within glacial sediments indicate that hydroplastic deformations occur in conjunction with a simple shear component parallel to the axis of the tunnel valley which either result from the overlying flow of sediments or ice. Folds are generally restricted to single beds and may suggest sediment deformation during episodes of ice recoupling with the bed (Lesemann et al., 2010; Ravier et al., 2014b). The different fold types correspond to sediment deformation under various strain rates and/or porewater pressures. Extensive surfaces affected by radial step normal faults with undulating fault planes observed in thin-bedded sandstones correspond to hydroplastic/brittle deformations induced by radial extensional deformation (Guiraud and Seguret, 1987). Radial extension is triggered by a dominant vertical stress leading to pure-shear deformations. In a glacial context, such stress configuration may be due to overloading implied by ice promptly recoupling the bed (Boeuf et al., 1971; Denis et al., 2010; Clerc et al., 2013a). The presence of oblique clastic dykes propagating downwards indicates that hydrofracturing triggered by high porewater pressure occurred in conjunction with a shear stress. Such stress could result from the basal shear transmitted to the subglacial bed during periods of ice-bed coupling (Phillips et al., 2012; Ravier et al., 2014b). Other dewatering structures, including dish structures, grain realignments or verticalized bedding related to sediment liquefaction/fluidization may either indicate episodes of porewater excess release during periods of ice-bed coupling or release of water excess due to high sedimentation rate (Maltman, 1994).

3.4.2. Foug Larjamme

Description

Similarly to the preglacial sequence, the glacial sedimentary sequence in Foug Larjamme is characterized by the relative absence of soft-sediment deformation structures. In some places, upward

dewatering structures are observed at the base of the tunnel valley infill, including a few upward clastic injections that are up to 0.7 wide and 2 to 4 m long (**Fig. 8I**).

Interpretation

The scarcity of deformation structures may be related to low basal shear stress and minor and localized increases in porewater pressures. In glacial settings, clastic dykes climbing upwards have generally been interpreted as the result of hydrofracturing in marginal settings when the ice overburden pressure decreases, allowing hydrofractures to climb upward (Phillips et al., 2013; Ravier et al., 2014b).

4. Models of tunnel valley formation

4.1. Porewater pressure-driven model (Alnif)

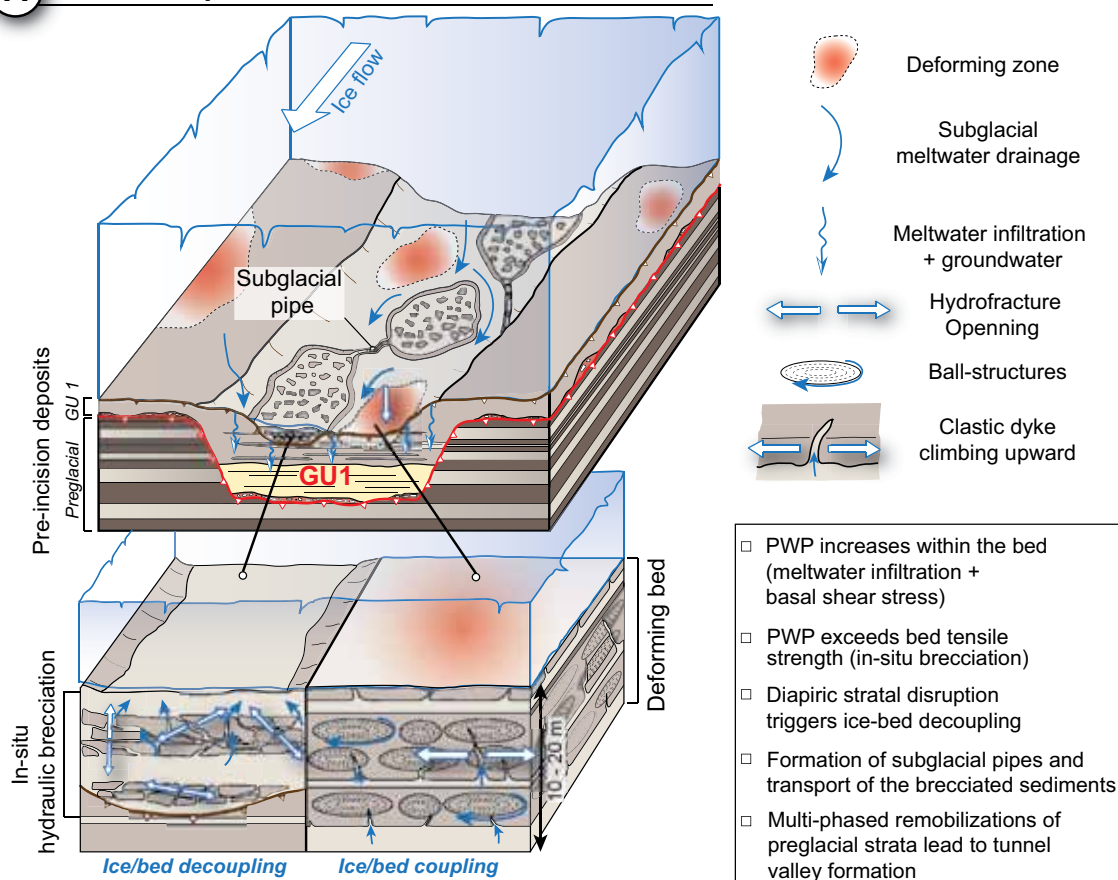
Sedimentary deposits below GP1 and GP2 are characterized by a “layer-cake configuration” with alternating claystones and sandstones, resulting in an association of water-saturated aquifers (sand, silt beds) confined by impermeable layers (clay beds, lithified beds) (Ravier et al., 2014a). Each valleys constituting this system of superimposed tunnel valleys in the Alnif area result from ice sheet advance/readvance over an unlithified substratum (Clerc et al., 2013a; Ravier et al., 2014a). These episodes of ice advance/retreat were probably associated with meltwater input in the subglacial bed and an increase of the basal shear stress beneath areas of ice-bed coupling, thus triggering a localized increase of porewater pressure. The increase of porewater pressure was locally illustrated by the formation of ball-structures with internal turbate structures triggered by sediment liquefaction (Maltman, 1994; Pisarska-Jamroz and Weckwerth, 2013; Ravier et al., 2014a) (**Fig. 9A**). These structures are often cross-cut by fine-grained clastic dykes climbing upwards. The occurrence of clastic dykes cross-cutting liquefied structures indicates an increase of porewater pressure that is sufficient to trigger hydrofracturing (Cosgrove, 1995). Locally, jigsaw-like fabrics related to in-situ brecciated layers induced by hydrofractures network occur below the glacial incision. Areas containing deformation structures below glacial incisions are discontinuous indicating that the increase of porewater pressure is confined to restricted zones, thus defining a mosaic of deforming (e.g., high porewater pressure) and stable (e.g., low porewater pressure) zones. This localized increase of basal shear stress was proposed by Piotrowski and Kraus (1997), Piotrowski et al. (2004), and van der Meer

et al. (2003) where the occurrence of a mosaic of coexisting deforming and stable areas underneath the ice has been demonstrated in Pleistocene sediments. Computed basal shear stress distributions underneath the Antarctic ice sheet also revealed the presence of riblike patterns of very high basal shear stress embedded within areas of low to zero basal shear stress (Sergienko and Hindmarsh, 2013). The progressive increase of porewater pressure within the subglacial bed leads to preglacial strata brecciation within deforming zones, due to the development of dense hydrofractures networks (**Fig. 9A**). The occurrence of patchy conglomerate composed of preglacial intraclasts along GP1 and GP2 illustrates these episodes of subglacial ‘fracking’ affecting the subglacial bed. Angular clayey intraclasts with embedded individual quartz grains and internal sand-filled microfractures also reveal this hydrofracturing phase (**Fig. 4d**). These particular clasts may be the result of clast detachments from the host low-permeable clay strata during hydrofracturing and quartz grains impingements along the walls during the injection of fluidized sand (Kawakami and Kawamura, 2002; Scott et al., 2009). Similarly to the processes proposed for the formation of the first tunnel valley (GP1), in-situ brecciation triggered by upward injections of fluidized sand into hydrofractures led to diapiric disruption of preglacial strata, contributing to bed remobilization and tunnel valley formation (Ravier et al., 2014a). The upwards release of overpressure contained in the subglacial bed is capable to significantly decrease the ice effective pressure, causing ice-bed decoupling and development of subglacial pipes (Boulton and Hindmarsh, 1987; Boulton et al., 2007) (**Fig. 9A**). The establishment of subglacial pipes triggers the evacuation of freshly brecciated sediments, thus promoting subglacial bed remobilization in the down-ice direction. Deforming zones where high basal shear stress and elevated porewater pressure occur are likely to shift through time, implying that zones of in-situ hydraulic brecciation, upwards stratal disruption and piping, continuously form and shift underneath the ice sheet.

The first generation of tunnel valley (GP1) formed due to the optimum bed configuration (e.g., “layer-cake”) and a palaeotopography preferentially draining meltwater along the axis of the tunnel valley, thus favoring the infiltration of meltwater and the subsequent development of localized high porewater pressures (Ravier et al., 2014a). The second generation of tunnel valley in the Alnif area developed along an axis parallel to GP1 as demonstrated by the thick and unlithified Glacial Unit 2 erosively deposited upon Glacial Unit 1 (**Fig. 9A**). Once formed and filled, tunnel valleys cause a change of the substratum hydraulic properties and if subglacial water pressures are sufficiently high after a phase of ice readvance, old tunnel valleys will be prone to reactivation (Jørgensen and Sandersen, 2006).

Alnif tunnel valley: formation and sedimentary infill

A Porewater pressure-driven model of formation



B Subglacial sedimentary infill and deformation

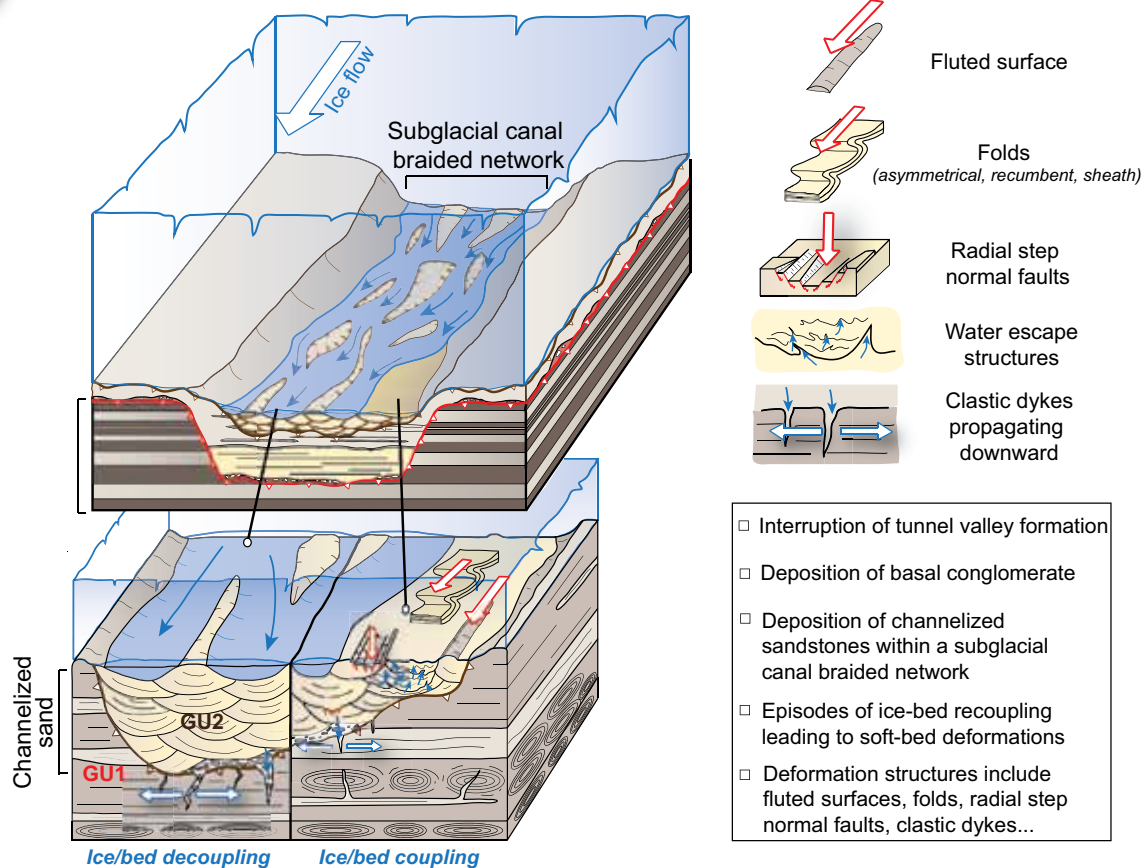


Figure 9. Model of the Alnif tunnel valley formation and sedimentary infill. (A) The development of high porewater pressure (PWP) beneath zones of ice-bed coupling contributes to sediment remobilization through processes of hydraulic brecciation. In the first stages of porewater increase, ball-structures and clastic dykes form until porewater pressure becomes high enough to trigger in-situ hydraulic brecciation (subglacial “fracking”). Subglacial brecciation induced by the development of a dense network of hydrofractures led to diapiric stratal disruption and upward release of the porewater excess. The release of considerable amount of pore fluids decreased the ice effective pressure, triggering ice bed-decoupling, leading to the emplacement of subglacial pipes where the brecciated material can be evacuated. (B) The characteristics of the basal sedimentary infill is typical of a confined environment and the sediments are affected by subglacial deformation structures (e.g. downward clastic dykes, fluted surface, folds, radial step normal faults) indicating a subglacial depositional environment.

GU1, characterized by a layer-cake configuration, probably acted as a preferential drainage pathway for meltwater during ice readvance, therefore representing a preferential zone for the development of high porewater pressures. These high porewater pressures promoted the remobilization of the subglacial bed and the formation of GP2.

4.2. Meltwater-driven model (Foum Larjamme)

Le Heron (2007) suggested that the Foum Larjamme tunnel valley may have formed under a combination of ice sheet loading and elevated subglacial hydrostatic pressures. Preglacial sediments observed below the glacial incision display preserved sedimentary structures at both macroscopic and microscopic scales, with no evidence for deformation structures related to high porewater pressures (**Figs. 7, 10A**). The porewater pressure-driven model suggested for the formation of tunnel valleys in Alnif cannot be applied in the present case because the field evidence listed in the study of Ravier et al. (2014a) have not been observed along the Foum Larjamme tunnel valley. In addition, the absence of soft-sediment deformation structures along the glacial incision permits to refute the Boulton and Hindmarsh hypothesis (1987) in which tunnel valleys grow by deformation of basal sediment into conduits.

An alternative model must be envisaged to explain the formation of this tunnel valley. The morphology of the glacial incision allows to discuss plausible alternative models of tunnel valley formation. The undulating base of the tunnel valley is characteristics of erosion by meltwater channels (**Fig. 10A**) (Nitsche et al., 2013), implying that models invoking meltwater as the main erosional agent must be preferentially considered. The formation of tunnel valleys by meltwater erosion are divided into two major processes: (1) a steady-state formation where streams erode gradually into the substratum over a long period via N- or C-channels, (2) and a catastrophic formation where erosion of the bed occurs through one or several outburst events (**Fig. 10A**).

(1) Subglacial meltwater pathways can be relatively stable over hundreds of years (Boulton et al., 2007; Le Brocq et al., 2013; Nitsche et al., 2013). Channels incised down into sediments must be considered here, i.e., N-channels or C-channels, representing a combination of N-channels and R-channels (Clarke et al., 1984). Such channels can occur as single isolated features or in braided networks covering large areas (Sharp et al., 1989; Walder and Fowler, 1994). The undulating base suggests soft-bed erosion by several channels either contemporaneous or not. The Foug Larjamme tunnel valley morphology composed of interconnected overdeepenings indicates tunnel-valley segments that were once an integrated anastomosed/anabranched drainage network. Relatively constant meltwater input required to maintain subglacial meltwater channels over long period may either be driven by basal meltwater production or by increasing supraglacial meltwater production descending to the bed (Mooers, 1989).

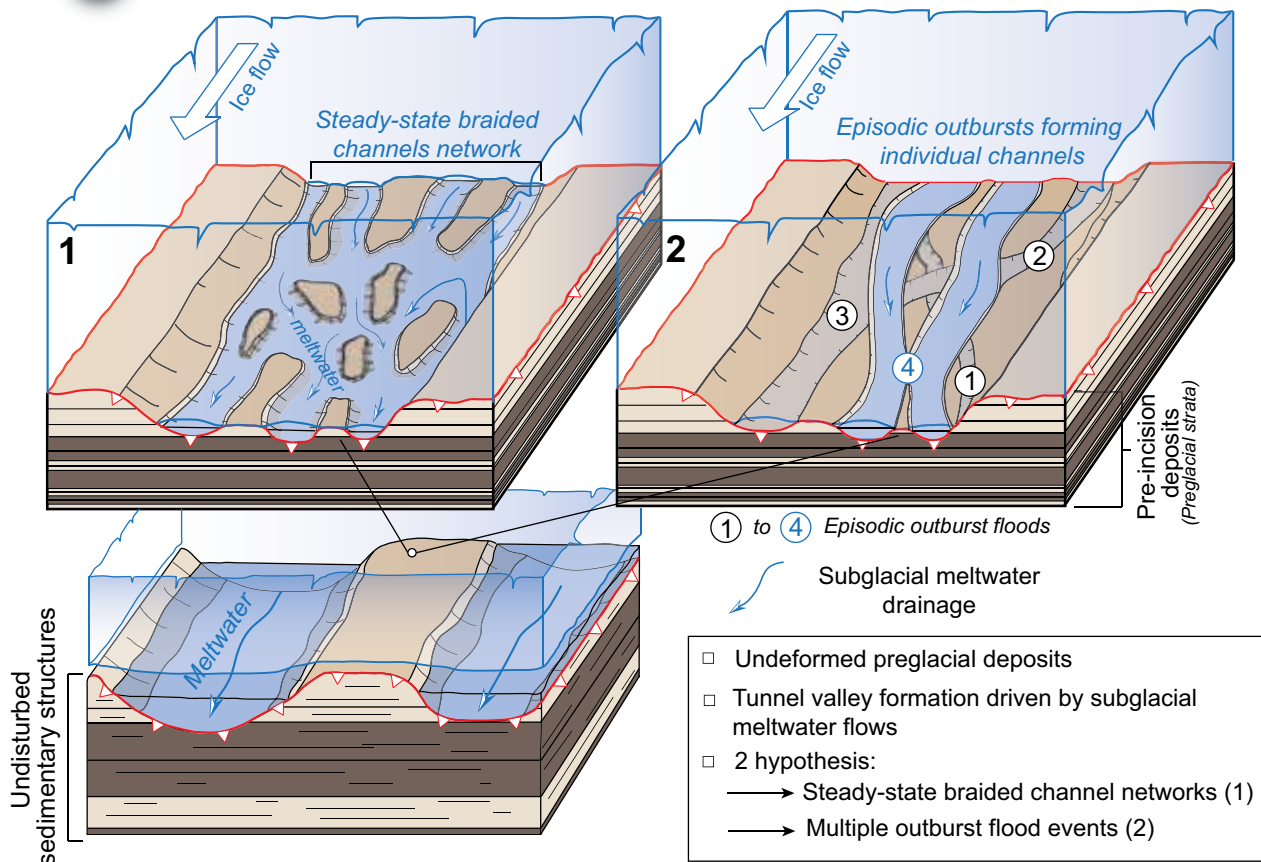
(2) Alternatively, the Foug Larjamme tunnel valley could result from substratum erosion during outburst events releasing huge amount of meltwater, as it is frequently proposed for tunnel valley genesis (Brennand and Shaw, 1994; Piotrowski, 1994; Jørgensen and Sandersen, 2006; Kehew et al., 2013). The undulating glacial pavement observed at the base of the valley may alternatively represent composite valleys that either result from simultaneous or diachronous developments of meltwater channels during episodic outbursts (**Fig. 10A**).

Anastomosing or anabranched tunnel valley networks underneath the Laurentide Ice Sheet have been interpreted as the result of substratum erosion by massive sheetfloods collapsing into channelized flows (Shaw, 2002, 2010; Fisher et al., 2005). This model is proposed for forming simultaneous network of tunnel valleys that could result in the formation of an irregular and undulating tunnel valley base. This catastrophic model has been strongly criticized notably because of the size and location of subglacial lakes that must be involved to validate the model (Clark et al., 2005). Although recent studies led on Ordovician deposits have underlined the occurrence of large subglacial lakes (10's km²) connected to tunnel valley networks (Illizi Basin, Algeria) (Hirst et al., 2002; Clerc et al., 2013b), volumes of meltwater required to form such megafloods have been debated and seem unrealistic (Ó Cofaigh, 1996; Clarke et al., 2005; Eyles, 2006).

An alternative model controlled by huge and rapid release of meltwater relies on the occurrence of repetitive outbursts events. Glacial outbursts have been documented in the Ordovician sedimentary record in Algeria and Lybia (Ghienne et al., 2010; Girard et al., 2012) implying that sudden release of

Foum Larjamme tunnel valley formation and sedimentary infill

A Meltwater-driven model of formation



B Proglacial sedimentary infill

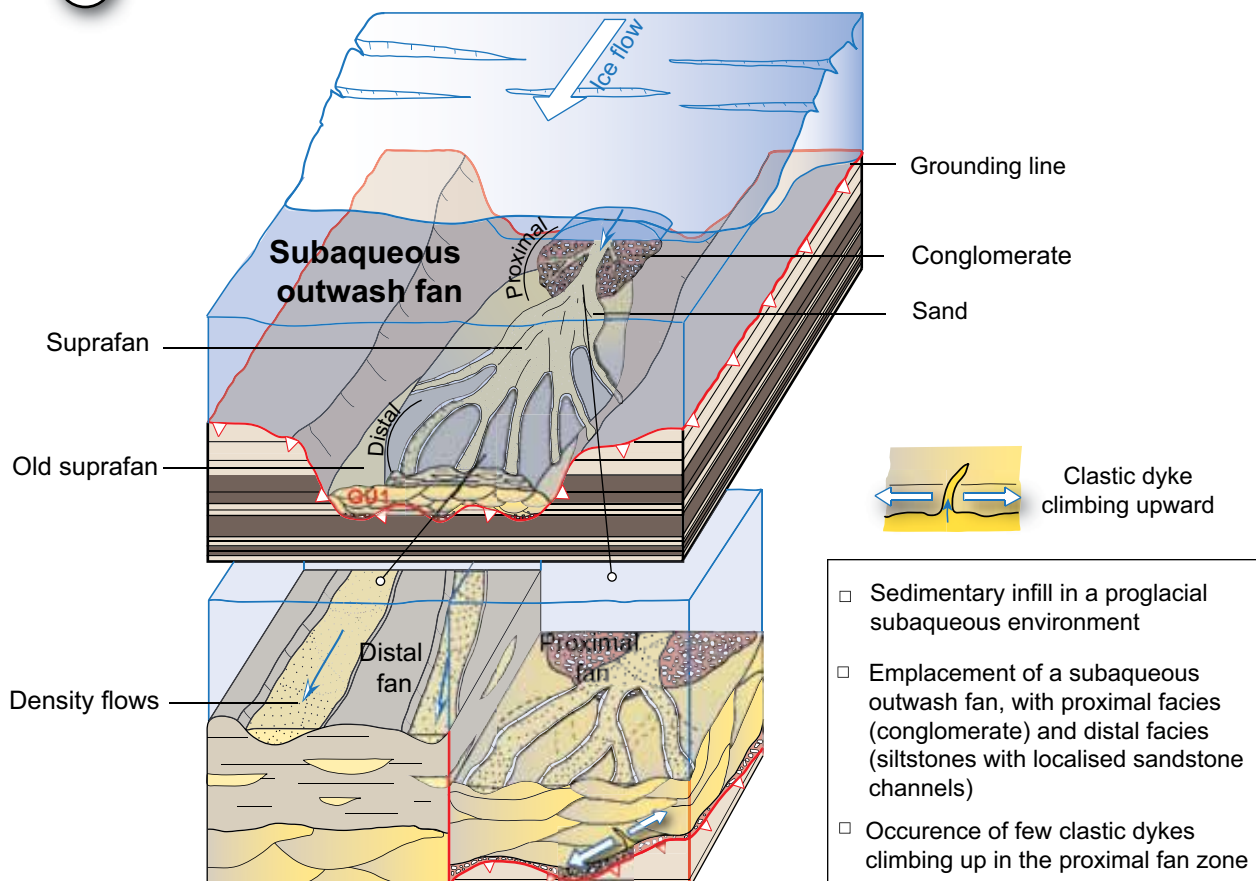


Figure 10. Model of the Foug Larjamme tunnel valley formation and sedimentary infill. (A) The absence of deformation structures within preglacial sediments associated with the undulating morphology of the tunnel valley base indicate that formation of this tunnel valley results from bed erosion by meltwater. The undulating base can either be the result of a contemporaneous anastomosing subglacial channel networks (1) or the lateral migration of channels through time during episodic outburst events (2). (B) The tunnel valley is infilled by an ice-marginal subaqueous outwash fan in the proximity of the grounding line. Deformation structures are sparse and concentrated at the tunnel valley base where few clastic dykes climbing upwards form. Sedimentological and deformational characteristics indicate that sedimentation occur in a proglacial subaqueous environment.

meltwater (stored beneath the ice), occurred during the Hirnantian glaciation. A model of tunnel valley formation by outburst flooding evokes catastrophic meltwater release at the margin of continental glaciers when permafrost wedges block meltwater drainage (Piotrowski, 1994; Hooke and Jennings, 2006). In this configuration, meltwater can accumulate and form marginal subglacial lakes until fluid pressure exceeds the strength of the permafrost causing catastrophic release of meltwater, and formation of tunnel valleys. Evidence for permafrost zones have been documented in Morocco, where structures related to cryogenic processes demonstrate the localized occurrence of discontinuous permafrost zones during the Ordovician (Nutz et al, 2013). The occurrence of permafrost zones during the Late Ordovician allows to envisage the Piotrowski model (1994) in this study case, although formation of a single valley during one major outburst cannot fully explained the undulating pattern of this tunnel valley. The base of the Foug Larjamme tunnel valley is irregular and consists of overdeepenings related to a plausible anastomosing/anabranching channel patterns. Jørgensen and Sandersen (2006) proposed that such patterns are controlled by successive formation of channels during episodic and diachronous minor outbursts events. The hypothesis of lateral shifting of meltwater conduit positions through time, resulting in undulating tunnel valley bases, is illustrated by several tunnel valleys from Denmark and the North Sea (Jørgensen and Sandersen, 2006; Huuse and Lykke-Andersen, 2000; Lonergan et al., 2006). Similarly to the steady-state model, this meltwater-driven model controlled by episodic outbursts suggests formation of tunnel valleys over a long period relative to a single outburst. Although soft-bed erosion is surely controlled by meltwater flow, data collected along the Foug Larjamme tunnel valley do not permit to preferentially designate a model of tunnel valley formation and both steady-state and outburst models must be considered.

5. Models of tunnel valley sedimentary infill

5.1. Subglacial infill (Alnif)

The basal sedimentary infill of both tunnel valleys, including patchy conglomerates, sheet-like bedded rippled sandstones and trough cross-bedded sandstones have been interpreted as a result of deposition in a confined accommodation space under ungrounded ice, in a marginal environment (Clerc et al., 2013a). The subglacial origin of the basal sedimentary infill was notably illustrated by the vertical stacking pattern with pronounced erosional surfaces, suggesting a limited space for sediment deposition that is expected in a subglacial environment (**Fig. 9B**). In addition, numerous deformation structures typical of subglacial deformation during ice-bed coupling occur within this basal sedimentary infill, strengthening the hypothesis of a subglacial depositional environment. The deformation structures include fluted surfaces, step radial normal faults, recumbent/asymmetrical/sheath folds, clastic dykes, dish structures or sheet dewatering structures (**Fig. 9B**). The emplacement of these different types of deformation structures suggests fluctuating strain and water-escape rates. Elongated fluted surfaces indicate subglacial sediment deformation under simple shear and high strain rates. Asymmetrical to sheath folds demonstrate different strain intensities induced by changes in basal shear stress and/or variations in porewater pressures during one or several episodes of ice-bed coupling (Lesemann et al., 2010). Clastic dykes, large-scale dish structures, and vertical grain realignments are related to episodes of porewater release. Clastic dykes propagating downwards suggest hydrofracturing triggered during ice-bed coupling and high porewater pressure conditions (Phillips et al., 2013, Ravier et al., 2014b). Dish structures and vertical grain realignments indicate liquefaction/fluidization of sediments and vertical release of porewater excess that may be triggered by rapid sedimentation or ice-bed coupling episodes (Maltman, 1994; Ravier et al., 2014a). Surfaces displaying radial step normal faults indicate brittle to hydroplastic deformation induced by radial extensional deformation under low porewater pressure (Guiraud and Seguret, 1987; Denis et al., 2010). Radial step normal faults are often closely associated with fluted surfaces in Alnif and have been interpreted as being the result of glacial overloading during ice-bed coupling (Beuf et al., 1971; Denis et al., 2010; Clerc et al., 2013a). In Alnif, the formation of the two tunnel valleys occurred subglacially as well as the basal sedimentary infill that has been locally deformed during episodic ice-bed recoupling.

5.2. Proglacial infill (Foum Larjamme)

The sedimentary infill of the Foum Larjamme tunnel valley displays a general fining upward pattern, starting with thin and patchy conglomeratic deposits at the base, overlain by massive channelized sandstones, ending with lenticular sandstone bodies embedded within siltstones (**Fig. 10B**). Le Heron (2007) interpreted this sedimentary sequence as an ice-contact fan sequence evolving into either an underflow-dominated fan or a system of laterally migrating fluvial channels. At the top of the sequence, the occurrence of mudclasts alignments and load structures in embedded sandstone lenses, characterized by the absence of gravel lags and well-expressed grading, are diagnostic of subaqueous sediment deposition (Posamentier and Walker, 2006; Talling et al., 2012) (**Fig. 10B**). Conglomerates record high-energy sediment deposition (e.g., debris flow) at the ice margin, near the subglacial conduit exit while channelized sandstones record deposition by density flows with down-current migration of channels. Conglomeratic clasts are generally rounded to well-rounded indicating a significant distance of transport while few other clasts are angular and sometimes display striae and crescentic gouges on their surfaces. The presence of these small-scale forms, although of limited potential of preservation while transported in water, may rather suggest that they derive from rain-out processes during ice shelf or iceberg melting, in a marginal environment. The thick sandstones succession represents proximal facies of the subaqueous outwash fan associated with high sediment supply. Lenticular sandstones embedded within fine-grained sediments represent the distal part of the subaqueous outwash fan where isolated and density flow channels form, eroding the fine sediments deposited by suspension settling. This overall fining upward sequence may indicate a phase of glacier retreat and subsequent migration of the subglacial conduit exit or/and a decrease in meltwater discharge.

The sedimentary infill in Foum Larjamme is generally undisturbed and display very few deformation structures. In the basal part of the sedimentary infill, few clastic dykes migrating upwards occur, indicating occasional upwards hydrofracturing (**Fig. 10B**). Clastic dykes climbing upwards are common in marginal settings when the reduced vertical ice stress allow hydrofractures to climb upwards (Boulton and Caban, 1995; Phillips et al., 2013; Ravier et al., 2014b).

The tunnel valley sedimentary infill in Foum Larjamme occurs at the vicinity of the grounding line, in a marine proglacial environment.

6. Control of ice stream distributions on tunnel valley morphologies

Using the distribution of glacial troughs and ice-flow orientation indicators, Ghienne et al. (2007) and Le Heron et al. (2007) proposed a palaeogeographic reconstruction for major ice stream pathways in North Africa (**Fig. 11**).

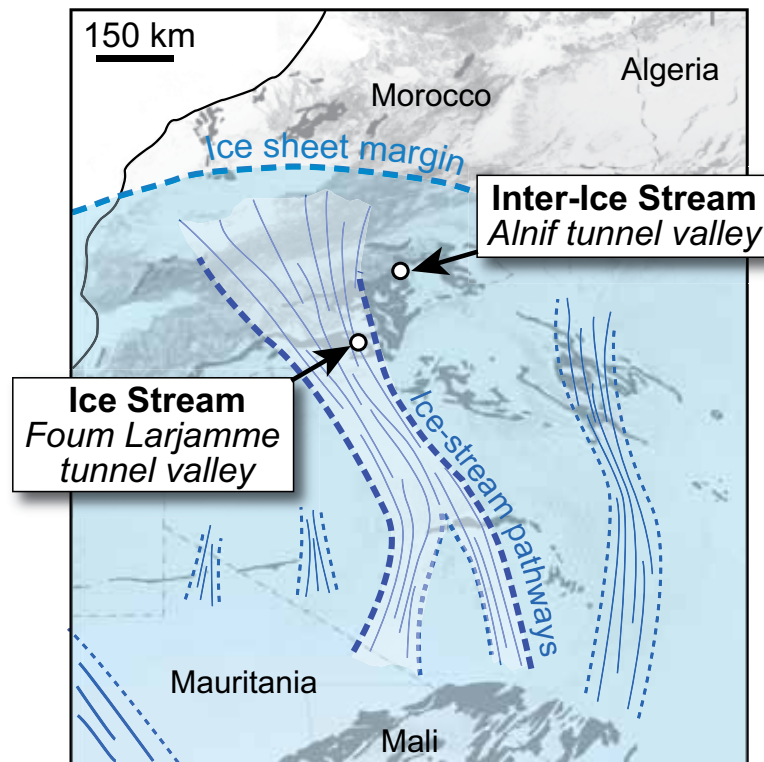


Figure 11. Locations of the Alnif and Fom Larjamme tunnel valleys relative to the distributions of reconstructed palaeo-ice streams in the west part of North Africa (Ghienne et al., 2007; Le Heron et al., 2007).

A major ice-stream taking its source in southern Algeria and terminating in marginal position in the Moroccan Atlas Mountains has been delimited. Although the temporal and spatial frameworks of these ice streams are not clearly established, these reconstructions highlight that the Alnif tunnel valley is located in an inter-ice stream position while the Fom Larjamme tunnel valley is situated within the ice stream pathway (**Fig. 11**). Assuming that the formation of both valleys are contemporaneous to this ice stream, the variations in tunnel valley morphologies between Alnif and Fom Larjamme permit the opportunity to envisage a predictable distribution of tunnel valley type morphologies related to ice stream locations and geographies.

The ice flow movement and the development of ice streams on soft beds are highly controlled by the passage of subglacial water at the ice-bed interface or by basal deformation of water-saturated sediments (Kamb, 2001; Shepherd et al., 2009; Bartholomew et al., 2011, Sole et al., 2011; Richter et al., 2013). Subglacial water flow originates from basal melting, surface melting associated with

meltwater transfer to the base of the ice sheet, and periodical drainage of subglacial lakes (Bell, 2008). The deformation of sediments capable of maintaining fast flowing-ice occur within thin shear zones at the top of subglacial soft beds (Tulaczyk et al., 2000; Kamb, 2001; Reinardy et al., 2011; Menzies et al., 2013). The meltwater control on ice flow velocities indicates that tunnel valleys formed by meltwater-driven processes must preferentially develop along ice-stream corridors. The Foug Larjamme tunnel valley is located along a palaeo-ice stream pathway and the associated morphology characterized by an undulating base indicates that meltwater flow was abundant during its formation (**Fig. 12**). Very similar tunnel valley morphologies corresponding to subglacial channel networks have been depicted in West Antarctica underneath the palaeo-Pine Island and Thwaites ice streams and interpreted as structures resulting from considerable subglacial meltwater flows (Lowe and Anderson, 2003; Nitsche et al., 2013). Recent studies highlighted a clear link between subglacial lakes and ice streaming (Bell et al., 2007; Fricker et al., 2009). The storage of subglacial meltwater within subglacial lakes encourages fast ice flow through the supply of subglacial meltwater and/or through the erosion of bed channels during lake drainage events (Winsborrow et al., 2010). Subglacial lake drainage events induce rapid release of water promoting circulation of water at the ice-bed interface rather than diffusion within the subglacial soft bed because infiltration capacity of subglacial meltwater into the bed is exceeded (Passchier et al., 2010) (**Fig. 12**). The development of a water layer at the ice-bed interface enhances basal sliding, thus favoring fast ice flow.

In inter-ice stream positions (i.e., between ice streams), the Alnif tunnel valley displays a different morphology with a deeper trough and a smoother tunnel valley base resulting from porewater-pressure driven processes (**Fig. 12**). The amount of meltwater available is probably lower, therefore promoting meltwater infiltration and groundwater circulation within the subglacial soft bed (Boulton et al., 1995). The resulting increase of meltwater content within deeper strata of the subglacial bed is responsible for the development of elevated porewater pressures, promoting remobilization of sediments by porewater pressure-driven processes (i.e., hydraulic brecciation) (**Fig. 12**).

The distributions of ice streams are influenced by subglacial meltwater lubricating the base of the ice sheet and the present observations indicate that meltwater-driven processes leading to the formation of the Foug Larjamme tunnel valley type will preferentially occur beneath ice stream pathways. Between ice stream pathways, where ice flow velocity is moderate, meltwater is transferred within the subjacent bed rather than being integrated within a subglacial channel network, resulting in the Alnif tunnel valley type where basal porewater pressure-driven processes predominate. Subglacial

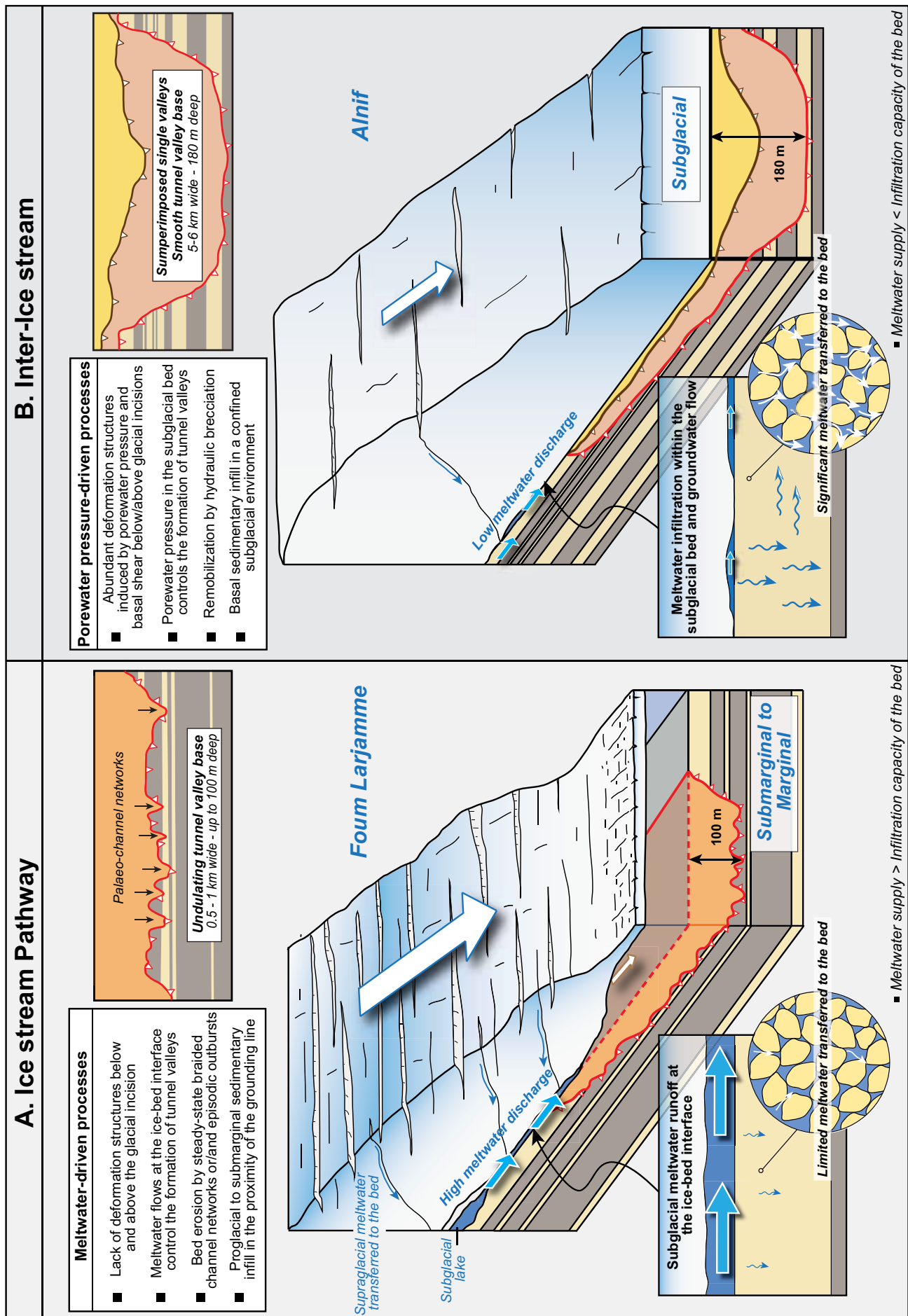


Figure 12. Synthetic diagram showing the main characteristics of the Alnif and Foug Larjamme tunnel valleys including the processes involved in their formations, their resulting geometries and incision depths, their respective depositional environments and their relations with ice stream geographical distributions. The two models of tunnel valley formations and tunnel valley geometries depend on their geographical distributions, i.e., in or between ice stream pathways.

characteristics inferred from the distribution of tunnel valley types indicate that during the Ordovician, water circulating within channels at the ice-bed interface (Foug Larjamme / ice stream zone) could have had a greater impact on the increase of ice flow velocities than basal deformation of soft and water-saturated sediments underneath ice-bed coupling zones (Alnif / inter-ice stream zone).

The characteristics of the tunnel valleys permit the identification of zones where meltwater is available at the ice-bed interface in contrast with zones where meltwater is preferentially diffused within the bed (**Fig. 12**). These different zones indicate that underneath the Gondwana ice sheet, different sets of basal processes were ongoing, therefore controlling subglacial erosional processes and tunnel valley morphologies. Assuming that palaeo-ice streams were contemporaneous to the formation of these tunnel valleys, the lateral variations in meltwater flow dynamics may in turn help to understand the location and functioning of ice streams and the parameters that control their distributions during the Ordovician glaciation. These parameters include (1) the local rate of basal and supraglacial melting, (2) the bed topography influencing subglacial meltwater drainage and storage, and (3) bed characteristics, involving capacity for meltwater diffusion and the impermeable to permeable strata ratio.

7. Conclusions

Analyses of the Alnif and Foug Larjamme tunnel valley infills served to identify major sedimentological and deformational differences at a regional scale (**Fig. 12**). The Alnif tunnel valley displays deformation structures related to high porewater below glacial pavements (e.g. ball-structures, clastic dykes) while the Foug Larjamme tunnel valley is characterized by relatively undisturbed sediments below the glacial incision. The sedimentary infill of both valleys was also characterized by major differences in the types of deformation structures. The Alnif site displays deformation structures related to high shear stresses and elevated porewater pressures related to episodes of ice-bed coupling (e.g., fluted surface, folds, clastic dykes) while the Foug Larjamme valley presents minor deformations except for a few upward dewatering structures (e.g., clastic dykes). The analyses of these two tunnel valleys were used to develop two different models of tunnel valley formation and highlighted the regional-

scale variability of processes involved in their formation.

The Alnif tunnel valley was formed subglacially under a combination of elevated basal shear stresses and high porewater pressures triggering hydraulic brecciation and remobilization of sediments. The base of the glacial sedimentary infills in the Alnif area was characterized by sediments deposited in a confined environment and affected by typical subglacial deformation structures recording a subglacial sediment deposition. The Foug Larjamme tunnel valley was formed in a marginal position by substratum erosion by meltwater, either controlled by the sudden release of meltwater (outbursts) or by the continuous meltwater flow in a steady-state configuration. The Foug Larjamme tunnel valley was infilled by a proglacial subaqueous outwash fan in the proximity of the grounding-line.

The Foug Larjamme and Alnif tunnel valleys are respectively situated within and between palaeo-ice stream pathways suggesting a control of ice stream distributions on tunnel valley morphologies. Beneath ice streams, developments of channel networks lubricate the ice-bed interface, thus promoting high ice flow velocity and the development of tunnel valleys driven by meltwater processes (Foug Larjamme). In inter-ice stream zones, the lower meltwater availability favors meltwater infiltration into the subglacial soft bed, thus promoting tunnel valley formation by porewater pressure-driven processes.

Acknowledgments

This work is a contribution from the ‘SEDS’ (Systèmes, Environments et Dynamique Sédimentaire) research team in the Laboratoire Biogésociences-UMR/CNRS 6282 at the University of Burgundy and is part of the ANR SeqStrat-Ice (n° 12-B506-0014). The authors thank GDF Suez for the funding of this study which is part of the “Impact des pressions de fluides sur les qualités réservoirs” project.

References

- Alvaro, J.J., Vennin, E., Villas, E., Destombes, J., Vizcaino, D., 2007. Pre-Hirnantian (latest Ordovician) benthic community assemblages: Controls and replacements in a siliciclastic-dominated platform of the eastern Anti-Atlas, Morocco. *Palaeogeography Palaeoclimatology Palaeoecology* 245, 20-36.
- Bartholomew, I.D., Nienow, P., Sole, A., Mair, D., Cowton, T., King, M.A., Palmer, S., 2011. Seasonal variations in Greenland Ice Sheet motion: Inland extent and behaviour at higher elevations. *Earth and Planetary Science Letters* 307, 271-278.
- Bell, R.E., Studinger, M., Shuman, C.A., Fahnestock, M.A., Joughin, I., 2007. Large subglacial lakes in East Antarctica at the onset of fast-flowing ice streams. *Nature* 445, 904-907.
- Bell, R.E., 2008. The role of subglacial water in ice-sheet mass balance. *Nature Geoscience* 1, 297-304.
- Beuf, S., Biju-Duval, B., De Charpal, O., Gariel, O., Bennacef, A., 1971. Les grès du Paléozoïque inférieur au Sahara – Sédimentation et discontinuités, évolution structurale d'un craton. Collection « Science et technique du pétrole », Volume 18, Publications de l'I.F.P., Paris, 464 pp.
- Boulton, G.S., 1976. The origin of glacially-fluted surfaces – observations and theory. *Journal of glaciology* 17, 287-309.
- Boulton, G.S., Hindmarsh, R.C.A., 1987. Sediment deformation beneath glaciers; rheology and geological consequences. *Journal of Geophysical Research* 92, 9059-9082.
- Boulton, G.S., Caban, P.E., Vangijssel, K., 1995. Groundwater-flow beneath ice sheets: Part I - Large-scale patterns. *Quaternary Science Reviews* 14, 545-562.
- Boulton G.S., Caban, P.E., 1995. Groundwater-flow beneath ice sheets: Part II – Its impact on glacier tectonic structures and moraine formation. *Quaternary Science Reviews* 14, 563-587.
- Boulton, G.S., Lunn, R., Vidstrand, P., Zatsepin, S., 2007a. Subglacial drainage by groundwater-channel coupling and the origin of esker systems: Part I - glaciological observations. *Quaternary Science Reviews* 26, 1067-1090.
- Boulton, G.S., Lunn, R., Vidstrand, P., Zatsepin, S., 2007b. Subglacial drainage by groundwater-channel coupling, and the origin of esker systems: Part II - theory and simulation of a modern system. *Quaternary Science Reviews* 26, 1091-1105.
- Boulton, G.S., Hagdorn, M., Maillot, P.B., Zatsepin, S., 2009. Drainage beneath ice sheets: groundwater-channel coupling, and the origin of esker systems from former ice sheets. *Quaternary Science Reviews* 28, 621-638.
- Brennand, T.A., Shaw, J., 1994. Tunnel channels and associated landforms, south-central Ontario: their implications for ice-sheet hydrology. *Canadian Journal of Earth Sciences* 31, 505-522.
- Catania, G., Paola, C., 2001. Braiding under glass. *Geology* 29, 259-262.
- Clarke, G.K.C., Collins, S.G., Thompson, D.E., 1984. Flow, thermal structure, and subglacial conditions of a surge-type glacier. *Canadian Journal of Earth Sciences* 21, 232-240.

- Clarke, G.K.C., Leverington, D.W., Teller, J.T., Dyke, A.S., Marshall, S.J., 2005. Fresh arguments against the Shaw megaflood hypothesis. A reply to comments by David Sharpe on «Paleohydraulics of the last outburst flood from glacial Lake Agassiz and the 8200 BP cold event». *Quaternary Science Reviews* 24, 1533-1541.
- Clerc, S., Buoncristiani, J. F., Guiraud, M., Vennin, E., Desaubliaux, G., Portier, E., 2013a. Subglacial to proglacial depositional environments in an Ordovician glacial tunnel valley, Alnif, Morocco. *Palaeogeography, Palaeoclimatology, Palaeoecology* 370, 127-144.
- Clerc, S., Castellano, P., Mattioni, L., Portier E., 2013b. Contrôle structural du réseau de vallées tunnel de l'Ordovicien supérieur du bassin d'Ilizi, Algérie. Vers l'existence de dépressions/lacs sous-glaciaires. 14ème Congrès Français de Sédimentologie, oral communication.
- Cocks, L.R.M., Torsvik, T.H., 2002. Earth geography from 500 to 400 million years ago: a faunal and palaeomagnetic review. *Journal of Geological Society* 159, 631–644.
- Cofaigh, C.O., 1996. Tunnel valley genesis. *Progress in Physical Geography* 20, 1-19.
- Cosgrove, J.W., 1995. The expression of hydraulic fracturing in rocks and sediments. In: Ameen, M.S. (Ed.), *Fractography: Fracture Topography as a Tool in Fracture Mechanics and Stress Analysis*. Geological Society Special Publication, 92, pp. 187–196.
- Denis, M., Guiraud, M., Konate, M., Buoncristiani, J.F., 2010. Subglacial deformation and water-pressure cycles as a key for understanding ice stream dynamics: evidence from the Late Ordovician succession of the Djado Basin (Niger). *International Journal of Earth Sciences* 99, 1399-1425.
- Destombes, J., Hollard, D.H., and Willefert, S., 1985. Lower Palaeozoic Rocks of Morocco. In: C.H. Holland (Ed.), *Lower Palaeozoic of north-western and west central Africa. Lower Palaeozoic rocks of the World*. John Wiley and Sons, New York, pp. 91–336.
- Ehlers, J., Linke, G., 1989. The origin of deep buried channels of Elsterian age in north-west Germany. *Journal of Quaternary Science* 4, 255-265.
- Eyles, N., 2006. The role of meltwater in glacial processes. *Sedimentary Geology* 190, 257-268.
- Fisher, T.G., Jol, H.M., Boudreau, A.M., 2005. Saginaw Lobe tunnel channels (Laurentide Ice Sheet) and their significance in south-central Michigan, USA. *Quaternary Science Reviews* 24, 2375-2391.
- Fricker, H.A., Scambos, T., 2009. Connected subglacial lake activity on lower Mercer and Whillans Ice Streams, West Antarctica, 2003-2008. *Journal of Glaciology* 55, 303-315.
- Ghienne, J.F., Le Heron, D.P., Moreau, J., Denis, M., Deynoux, M., 2007. The Late Ordovician glacial sedimentary system of the North Gondwana platform. In: Hambrey, M.J., Christoffersen, P., Glasser, N.F., Hubbard, B. (Eds.), *Glacial Sedimentary Processes and Products*. International Association of Sedimentologists, Special Publication. Blackwell, Oxford, pp. 295–319.
- Ghienne, J.F., Girard, F., Moreau, J., Rubino, J.L., 2010. Late Ordovician climbing-dune cross-stratification: a signature of outburst floods in proglacial outwash environments? *Sedimentology* 57, 1175-1198.
- Girard, F., Ghienne, J.F., Rubino, J.L., 2012. Occurrence of hyperpycnal flows and hybrid event beds related to glacial outburst events in a late ordovician proglacial delta (Murzuq basin, SW Libya).

Journal of Sedimentary Research 82, 688-708.

Guiraud, M., Seguret, M., 1987. Soft-sediment microfaulting related to compaction within the fluvio-deltaic infill of the Soria strike-slip basin (northern Spain) In: Jones, M.E., Preston, R.M.F. (Eds.), Deformation of sediments and sedimentary rocks. Geological Society, London, Special Publication 29, pp. 123-136.

Hiemstra, J.F., Rijdsdijk, K.F., 2003. Observing artificially induced strain: implications for subglacial deformation. Journal of Quaternary Science 18, 373-383.

Hirst, J.P.P., Benbakir, A., Payne, D.F., Westlake, I.R., 2002. Tunnel valleys and density flow processes in the upper Ordovician glacial succession, Illizi Basin, Algeria: Influence on reservoir quality. Journal of Petroleum Geology 25, 297-324.

Hooke, R.L., Jennings, C.E., 2006. On the formation of the tunnel valleys of the southern Laurentide ice sheet. Quaternary Science Reviews 25, 1364-1372.

Huuse, M., Lykke-Andersen, H., 2000. Overdeepened Quaternary valleys in the eastern Danish North Sea: morphology and origin. Quaternary Science Reviews 19, 1233-1253.

Huuse, M., Le Heron, D.P., Dixon, R., Redfern, J., Moscariello, A., Graig, J., 2012. Glaciogenic reservoirs and hydrocarbon systems. Geological Society of London, Special Publications 368, 1-28.

Janszen, A., Spaak, M., Moscariello, A., 2012. Effects of the substratum on the formation of glacial tunnel valleys: an example from the Middle Pleistocene of the southern North Sea Basin. Boreas, 41, 629-643.

Jørgensen, F., Sandersen, P.B.E., 2006. Buried and open tunnel valleys in Denmark - erosion beneath multiple ice sheets. Quaternary Science Reviews 25, 1339-1363.

Kamb, B., 2001. Basal zone of the West Antarctic Ice Streams and its role in lubrication of their rapid motion. In Alley, R.B. and Bindshchaller, R.A. (Eds.), The West Antarctic Ice sheet: Behavior and Environment. American Geophysical Union, Antarctic Research 77, 157-199.

Kawakami, G., Kawamura, M., 2002. Sediment flow and deformation (SFD) layers: evidence for intrastratal flow in laminated muddy sediments of the Triassic Osawa Formation, northeast Japan. Journal of Sedimentary Research 72, 171-181.

Kehew, A.E., Kozlowski, A.L., 2007. Tunnel channels of the Saginaw Lobe, Michigan, USA. In: Johansson, P., Sarala, P. (Eds.), Applied Quaternary Research in the Central Part of Glaciated Terrain. Geological Survey of Finland, Special Paper 46, 69-78.

Kehew, A.E., Piotrowski, J.A., Jørgensen, F., 2012. Tunnel valleys: Concepts and controversies – A review. Earth-Science Reviews 113, 33-58.

Kehew, A.E., Ewald, S.K., Esch, J.M., Kozlowski, A.L., 2013. On the origin of tunnel valleys of the Saginaw Lobe of the Laurentide Ice Sheet; Michigan, USA. Boreas 42, 442-462.

Kozlowski, A.L., Kehew, A.E., Bird, B.C., 2005. Outburst flood origin of the Central Kalamazoo River Valley, Michigan, U.S.A. Quaternary Science Reviews 24, 2354-2374.

Le Brocq, A.M., Ross, N., Griggs, J.A., Bingham, R.G., Corr, H.F.J., Ferraccioli, F., Jenkins, A., 332

- Jordan, T.A., Payne, A.J., Rippin, D.M., Siegert, M.J., 2013. Evidence from ice shelves for channelized meltwater flow beneath the Antarctic Ice Sheet. *Nature Geoscience* 6, 945-948.
- Le Heron, D.P., 2007. Late Ordovician glacial record of the Anti-Atlas, Morocco. *Sedimentary Geology* 201, 93–110.
- Le Heron, D.P., Ghienne, J.F., El Houicha, M., Khoukhi, Y., Rubino, J.L., 2007. Maximum extent of ice sheets in Morocco during the Late Ordovician glaciation. *Palaeogeography Palaeoclimatology Palaeoecology* 245, 200-226.
- Lesemann, J.E., Alsop, G.I., Piotrowski, J.A., 2010. Incremental subglacial meltwater sediment deposition and deformation associated with repeated ice-bed decoupling a case study from the Island of Funen, Denmark. *Quaternary Science Reviews* 29, 3212-3229.
- Lonergan, L., Maidment, S.C.R. and Collier, J.S., 2006. Pleistocene subglacial tunnel valleys in the central North Sea basin: 3-D morphology and evolution. *Journal of Quaternary Science* 21, 891-903.
- Lowe, A.L., Anderson, J.B., 2003. Evidence for abundant subglacial meltwater beneath the paleo-ice sheet in Pine Island Bay, Antarctica. *Journal of Glaciology* 49, 125-138.
- Menzies, J., Gao, C., Kodors, C., 2013. Microstructural analyses of a Middle Pliocene till from the James Bay Lowlands, Canada-evidence of «potential» fast ice streaming. *Proceedings of the Geologists Association* 124, 790-801.
- Mooers, H.D., 1989. On the formation of the tunnel valleys of the Superior Lobe, Central Minnesota. *Quaternary Research* 32, 24-35.
- Mulder, T., Alexander, J., 2001. The physical character of subaqueous sedimentary density flows and their deposits. *Sedimentology* 48, 269-299.
- Nitsche, F.O., Gohl, K., Larter, R.D., Hillenbrand, C.D., Kuhn, G., Smith, J.A., Jacobs, S., Anderson, J.B., Jakobsson, M., 2013. Paleo ice flow and subglacial meltwater dynamics in Pine Island Bay, West Antarctica. *Cryosphere* 7, 249-262.
- Nutz, A., Ghienne, J.F., Storch, P., 2013. Circular, cryogenic structures from the Hirnantian deglaciation sequence (Anti-Atlas, Morocco). *Journal of Sedimentary Research* 83, 87-103.
- Passchier, S., Laban, C., Mesdag, C.S., Rijdsdijk, K.F., 2010. Subglacial bed conditions during Late Pleistocene glaciations and their impact on ice dynamics in the southern North Sea. *Boreas* 39, 633-647.
- Phillips, E., Everest, J., Reeves, H., 2013. Micromorphological evidence for subglacial multiphase sedimentation and deformation during overpressurized fluid flow associated with hydrofracturing. *Boreas* 42, 395-427.
- Piotrowski, J.A., 1994. Tunnel-valley formation in northwest Germany - geology, mechanisms of formation and subglacial bed conditions for the Bornhöved tunnel valley. *Sedimentary Geology* 89, 107-141.
- Piotrowski J.A., Kraus, A.M., 1997. Response of sediment to ice-sheet loading in northwestern Germany: effective stresses and glacier-bed stability. *Journal of Glaciology* 145, 498-502.

- Piotrowski, J.A., Larsen, N.K., Junge, F.W., 2004. Reflections on soft subglacial beds as a mosaic of deforming and stable spots. *Quaternary Science Reviews* 23, 993-1000.
- Pisarska-Jamrozy, M., Weckwerth, P., 2013. Soft-sediment deformation structures in a Pleistocene glaciolacustrine delta and their implications for the recognition of subenvironments in delta deposits. *Sedimentology* 60, 637-665.
- Posamentier, H.W., Walker, R.G., 2006. Facies model revisited. *SEPM Special Publication* 84, 1-17.
- Ravier, E., Buoncristiani, J.F., Guiraud, M., Menzies, J., Clerc, S., Goupy, B., Portier E., 2014a. Porewater pressure control on subglacial soft sediment remobilization and tunnel valley formation: A case study from the Alnif tunnel valley (Morocco). *Sedimentary Geology* 304, 71-95.
- Ravier, E., Buoncristiani, J.F., Clerc, S., Guiraud, M., Menzies J., Portier, E., 2014b. Sedimentological and deformational criteria for discriminating subglaciofluvial deposits from subaqueous ice-contact fan deposits: a Pleistocene example (Ireland). *Sedimentology* 61, 1382-1410.
- Reinardy, T.I., Larter, R.D., Hillenbrand, C.D., Murray, T., Hiemstra, J.F., Booth, A.D., 2011. Streaming flow of an Antarctic Peninsula palaeo-ice stream, both by basal sliding and deformation of substrate. *Journal of Glaciology* 57, 596-608.
- Richter, A., Fedorov, D.V., Fritsche, M., Popov, S.V., Lipenkov, V.Y., Ekaykin, A.A., Lukin, V.V., Matveev, A.Y., Grebnev, V.P., Rosenau, R. and Dietrich, R., 2013. Ice flow velocities over Vostok Subglacial Lake, East Antarctica, determined by 10 years of GNSS observations. *Journal of Glaciology* 59, 315-326.
- Sandersen, P.B.E., Jørgensen, F., Larsen, N.K., Westergaard, J.H.W., Auken, E., 2009. Rapid tunnel-valley formation beneath the receding Late Weichselian ice sheet in Vendsyssel, Denmark. *Boreas* 38, 834-851.
- Scott, A., Vigorito, M., Hurst, A., 2009. The process of sand injection: internal structures and relationships with host strata (Yellowbank Creek Injectite Complex, California, USA). *Journal of Sedimentary Research* 79, 568-583.
- Sergienko, O.V., Hindmarsh, R.C.A., 2013. Regular Patterns in Frictional Resistance of Ice-Stream Beds Seen by Surface Data Inversion. *Science* 342, 1086-1089.
- Sharp, M. J., Gemmemm, J.C., Tison, J.L., 1989. Structure and stability of the former subglacial drainage system of the Glacier de Tsanfleuron, Switzerland. *Earth Surface Processes and Landforms* 14, 119-134.
- Shaw, J., 1983. Drumlin formation related to inverted meltwater erosional marks. *Journal of Glaciology* 29, 461-479.
- Shaw, J., 2002. The meltwater hypothesis for subglacial bedforms. *Quaternary International* 90, 5-22.
- Shaw, J., 2010. In defence of the meltwater (megaflood) hypothesis for the formation of subglacial bedform fields. *Journal of Quaternary Science* 25, 249-260.
- Shaw, J., Kvill, D., Rains, R.B., 1989. Drumlins and catastrophic subglacial floods. *Sedimentary Geology* 62, 177-202.

- Shaw, J., Gorell, G., 1991. Subglacially formed dunes with bimodal and graded gravel in the Trenton drumlin field, Ontario. *Géographie Physique et Quaternaire* 45, 21-34.
- Shepherd, A., Hubbard, A., Nienow, P., King, M., McMillan, M., Joughin, I., 2009. Greenland ice sheet motion coupled with daily melting in late summer. *Geophysical Research Letters* 36, L01501.
- Sole, A.J., Mair, D.W.F., Nienow, P.W., Bartholomew, I.D., King, M.A., Burke, M.J. and Joughin, I., 2011. Seasonal speedup of a Greenland marine-terminating outlet glacier forced by surface melt-induced changes in subglacial hydrology. *Journal of Geophysical Research-Earth Surface* 116, F03014.
- Talling, P.J., Masson, D.G., Sumner, E.J., Malgesini, G., 2012. Subaqueous sediment density flows: Depositional processes and deposit types. *Sedimentology* 59, 1937-2003.
- Tulaczyk, S., Kamb, W.B. and Engelhardt, H.F., 2000. Basal mechanics of Ice Stream B, West Antarctica 1. Till mechanics. *Journal of Geophysical Research-Solid Earth* 105, 463-481.
- van der Vegt, P., Janszen, A., Moscariello, A., 2012. Tunnel valleys: current knowledge and future perspectives. Geological Society, London, Special Publication 368.
- Villas, E., Vizcaino, D., Alvaro, J.J., Destombes, J., Vennin, E., 2006. Biostratigraphic control of the latest-Ordovician glaciogenic unconformity in Alnif (Eastern Anti-Atlas, Morocco), based on brachiopods. *Geobios* 39, 727-737.
- Winsborrow, M.C.M., Clark, C.D., Stokes, C.R., 2010. What controls the location of ice streams? *Earth-Science Reviews* 103, 45-59.
- Walder, J.S., Fowler, A., 1994. Channelized subglacial drainage over a deformable bed. *Journal of Glaciology* 40, 3-15.

Chapitre 3

Principaux résultats

Partie 1

- L'étude des dépôts sédimentaires de la région d'Alnif a permis de mettre en évidence l'impact de l'augmentation de la pression d'eau interstitielle dans le matériel préglaciaire sur les processus de creusement de la vallée tunnel d'Alnif.

- Cette étude a donc permis de mettre en évidence:

- **(1) Les processus intervenant dans le creusement de la vallée tunnel, et leurs chronologies.**
- **(2) Les paramètres contrôlant l'augmentation de la pression d'eau interstitielle.**
- **(3) Les observations terrain démontrant un creusement contrôlé par des processus de remobilisation sédimentaire.**

□ (1) Sous la glace, l'augmentation de la pression d'eau interstitielle dans les dépôts préglaciaires a pour conséquence de déclencher des processus d'hydrofracturation. Le développement d'un dense réseau d'hydrofracture donne lieu à des phénomènes de bréchification hydraulique. Cette bréchification hydraulique est associée à l'injection de sédiments fluidisés, permettant ainsi au matériel fracturé d'être remobilisé. L'augmentation notable de la pression d'eau interstitielle dans les sédiments préglaciaires est responsable de la diminution de la pression effective. L'instabilité qui en résulte favorise la création de chenaux sous-glaciaires à l'intérieur desquels le «mélange» de matériel préglaciaire fracturé et de sédiments fluidisés peut être évacué. La répétition de ces remobilisations sédimentaires favorise l'évacuation du matériel préglaciaire et contribue donc au creusement de la vallée tunnel d'Alnif.

□ (2) Le modèle de creusement induit par surpressions de fluide proposé pour la vallée tunnel d'Alnif est contrôlé par: (a) les caractéristiques lithologiques du matériel préglaciaire, (b) le régime thermique et la dynamique de la calotte de glaciaire, (c) l'héritage topographique.

(a) L'augmentation de la pression d'eau interstitielle dans les dépôts préglaciaires repose sur la présence de sédiments non lithifiés et d'aquifères confinés. La configuration du matériel préglaciaire de type «layer-cake» dans la région d'Alnif où couches sableuses perméables alternent avec des couches imperméables (couches argileuses ou niveaux sableux cimentés) est idéale pour le développement de surpressions de fluides.

(b) L'augmentation de la pression de fluide dans les dépôts préglaciaires est contrôlée d'une part par le transfert d'eaux de fonte dans le substrat mais aussi par le couplage local de la glace sur le substrat. Ces deux facteurs de contrôle suggèrent la coexistence de zones de couplage et de découplages entre la glace et le substrat, ainsi que la production d'eaux de fonte. En d'autres termes, les creusements par remobilisations sédimentaires peuvent se produire uniquement sous une glace tempérée où une mosaïque de zones de couplage (déformation du substrat) et de découplage (transfert d'eau de fonte dans le substrat) peut se mettre en place.

(c) La vallée tunnel d'Alnif constitue une dépression linéaire, ce qui implique une concentration particulière des phénomènes de remobilisations sédimentaires. Puisque le modèle s'appuie sur l'augmentation de la pression d'eau interstitielle dans le substrat sous-glaciaire, l'écoulement préférentiel d'eau de fonte au sein d'une dépression préexistante (d'origine tectonique dans le cas d'étude) favoriserait un transfert localisé d'eau dans le substrat. Ce transfert d'eau de fonte est alors responsable de l'augmentation locale de la pression de fluide et de la remobilisation préférentielle des sédiments préglaciaires le long de l'axe de la future vallée tunnel.

□ (3) Le modèle de creusement contrôlé par l'augmentation de la pression d'eau interstitielle repose sur des observations qui sont d'ordre (a) sédimentologique, (b) structurale, et (c) stratigraphique.

(a) La présence d'un conglomérat composé d'éléments préglaciaires anguleux, incorporés dans une matrice fluidisée, et formant des cônes de déjection épars, témoigne des processus d'hydrofracturation, d'injection et de remobilisation sédimentaire du matériel préglaciaire.

(b) La présence abondante de structures de déformation pré-lithification liées à l'augmentation de la pression d'eau interstitielle (structures en boules, dykes clastiques, «jigsaw-like» fabrique, micro- and macro-scale turbate structures, etc...), au sein du matériel préglaciaire et dans le remplissage glaciaire, est un argument majeur en faveur d'un modèle contrôlé par des fortes pressions de fluide.

(c) La stratigraphie et les caractéristiques lithologiques du matériel préglaciaire constitué d'aquifères confinés («layer-cake») représente également un argument en faveur d'un modèle de creusement

induit par des pressions de fluides élevées.

Partie 2

- La comparaison de deux vallées tunnels aux caractéristiques morphologiques, sédimentaires, et déformationnelles différentes a permis de mettre en évidence la coexistence de deux modèles de formation des vallées tunnels à l'Ordovicien:

- (1) un modèle contrôlé par les remobilisations sédimentaires induites par pressions de fluides élevées (vallée tunnel d'Alnif).
- (2) un modèle où les processus d'érosion et de formation d'une vallée tunnel sont contrôlés par les écoulements d'eaux de fonte à l'interface glace-substrat (vallée tunnel de Fourn Larjamme).

(1) Les caractéristiques du modèle de formation de la vallée tunnel d'Alnif sont décrites dans la partie 1 de ce chapitre.

(2) La vallée tunnel de Fourn Larjamme se forme par écoulement d'eaux de fonte à l'interface glace/substrat, probablement à proximité de la marge glaciaire.

L'absence de déformations induites par des pressions d'eau interstitielle élevées, et l'absence d'un conglomérat basal épais contenant des blocs anguleux et une matrice fluidisée permettent de réfuter un modèle de creusement contrôlé par des processus de remobilisations sédimentaires. La morphologie ondulante de la base de la vallée glaciaire est caractéristique d'un modèle de creusement dominé par l'écoulement d'eaux de fonte. Il est cependant difficile de caractériser la nature de ces écoulements puisque la formation de la vallée tunnel pourrait être le résultat d'une érosion progressive par un écoulement d'eau stable, ou alors d'un ou plusieurs écoulements catastrophiques.

- L'analyse sédimentologique et déformationnelle a permis de reconstruire les environnements de dépôt du remplissage sédimentaire de chaque vallée tunnel:

- Le remplissage sédimentaire basal de la vallée tunnel d'Alnif est d'origine sous-glaciaire comme l'atteste les dépôts sédimentaires amalgamés (i.e., faible espace d'accommodation) et les nombreuses structures de déformation liées au cisaillement de la glace et à l'augmentation de la pression d'eau

interstitielle.

- Le remplissage sédimentaire de la vallée tunnel de Foug Larjamme se compose de dépôts hyperpicnaux au sein d'un cône de déjection et est caractérisé par l'absence de déformations pré-lithifications (exceptés quelques dykes *per ascensum*). Ces caractéristiques indiquent un environnement de dépôt subaquatique juxtaglacière.

- D'après la distribution des *ice-streams* sur le secteur d'étude, la vallée d'Alnif et son modèle de creusement contrôlé par les pressions d'eau interstitielle était situé entre deux *ice-streams*. En revanche, la vallée tunnel de Foug Larjamme et son modèle de formation contrôlé par les écoulements d'eaux de fonte se situait dans l'axe d'un *ice-stream*. Cette distribution particulière met en évidence l'influence de la dynamique glaciaire et de la dynamique des eaux de fonte sur les processus d'érosion sous-glaciaires et donc sur le modèle de formation et la morphologie des vallées tunnels.

CHAPITRE IV

**Déformations par surpressions de fluide:
Impacts sur les propriétés réservoirs**

Introduction

Les dépôts glaciaires et marins profonds comportent généralement des dépôts sableux triés, poreux, et perméables, représentant de potentiels réservoirs géologiques. Les hydrocarbures contenus dans les sédiments glaciaires ordoviciens d’Afrique ou du Moyen-Orient (Davidson et al., 2000; Hirst et al., 2002; Le Heron et al., 2009) et dans les sédiments marins profonds de la Mer du Nord ou des marges ouest-africaine et brésilienne (Pettingil et Weimer, 2002) illustrent le fort potentiel réservoir de ce type de dépôt. Dans ces environnements, l’augmentation de la pression d’eau interstitielle dans les aquifères confinés provoque des phénomènes de remobilisation sédimentaire par l’intermédiaire d’hydrofracturation et d’injection de sables fluidisés (Jolly et Lonergan, 2002; van der Meer et al., 2009). Les impacts de ces remobilisations sur l’architecture des réservoirs sont bien documentés, notamment sur la géométrie des réservoirs et sur leurs connectivités (Lonergan et al., 2000). Les processus de fluidisations associés aux remobilisations sédimentaires tendent à homogénéiser les dépôts sableux, modifier la structuration du réseau granulaire, et éluier les particules les plus fines (Lowe et al., 1975; Owen et al., 1987; Maltman et Bolton, 2003). Les modifications de la structure granulaire engendrent des modifications des propriétés pétrophysiques du sédiment (porosité, perméabilité) comme il l’a notamment été démontré dans certains systèmes d’injections clastiques (Duranti et al., 2002; Duranti et Hurst, 2004; Briedis et al., 2007; Lonergan et al., 2007; Scott et al., 2013). Cependant, il subsiste de nombreuses interrogations sur la distribution des propriétés pétrophysiques à l’échelle d’un affleurement affecté par ces remobilisations sédimentaires, ou encore des questions concernant l’impact des processus d’éluier sur les valeurs de porosité/perméabilité.

Les objectifs principaux de ce chapitre sont: (1) de caractériser la distribution des propriétés pétrophysiques à grande échelle dans le cas d’un système d’injections clastiques et (2) de déterminer l’impact de la pression de fluide et des processus d’éluier sur les propriétés pétrophysiques des réservoirs sableux. Le chapitre 4 se compose donc de deux parties à l’intérieur desquels l’impact des pressions de fluides sur les propriétés pétrophysiques sera respectivement discuté dans les environnements marins profonds et glaciaires.

• **Partie 1:** «Micro- to Macroscale internal Structures, Diagenesis and Petrophysical evolution of Injectite networks in the Vocontian Basin (France): implications for Fluid Flows». (Article 5)

Cette première partie se focalise sur la description et la caractérisation de deux réseaux d'injections clastiques formés en domaine marin profond, à échelles microscopique et macroscopique. Les deux principaux objectifs de cette première partie sont de (1) caractériser l'évolution de la porosité au sein de systèmes d'intrusions sableuses, de leurs mises en place jusqu'à nos jours, et (2) d'analyser la distribution de ces valeurs de porosité au sein de ces systèmes. Ces deux objectifs permettront de mieux contraindre les facteurs contrôlant la distribution et l'évolution de la porosité, et de discuter leurs impacts sur les écoulements de fluides au cours du temps. Pour remplir ces objectifs, une analyse des structures microscopiques et macroscopiques du réseau d'injection, une étude diagénétique et une estimation des valeurs de porosité primaire à l'échelle de l'affleurement ont été réalisées.

• **Partie 2:** Les coatings argileux» dans les grès glaciaires ordoviciens du bassin de Sbaa (Algérie): processus de mise en place et implications pétrophysiques.

Dans cette deuxième partie, l'impact de l'augmentation de la pression d'eau interstitielle sur les remobilisations sédimentaires dans les environnements glaciaires sera étudié, et plus particulièrement son effet sur les processus d'élutriation. L'élutriation des particules les plus fines a pour conséquence de former des coatings argileux qui modifient les propriétés pétrophysiques des sédiments. Les objectifs principaux de cette deuxième partie seront de discuter l'origine des coatings argileux, leurs impacts sur les propriété réservoirs, et leurs processus de mise en place.

Partie 1

«Structures microscopiques et macroscopiques, évolution pétrophysique et diagénétique de deux réseaux d'injectites dans le bassin Vocontien (France): impacts sur les écoulement de fluides».

Cette seconde partie fait l'objet d'un article soumis à la revue *Marine and Petroleum Geology*

Article 5

Ravier, E., Guiraud, M., Guillien A., Vennin, E., Buoncristiani, J.F. et Portier, E. Micro- to Macroscale internal Structures, Diagenesis and Petrophysical evolution of Injectite networks in the Vocontian Basin (France): implications for Fluid Flows (Submitted).

Objectifs:

- *L'objectif principal de cette première partie est d'étudier deux réseaux d'injectites situés dans le bassin Vocontien, de l'échelle microscopique à macroscopique.*
- *Dans cette partie, le but est d'établir une synthèse et une chronologie de la mise en place des différentes structures observées à l'intérieur des injectites, ainsi que des différentes phases diagénétiques.*
- *Afin d'estimer l'impact des pressions de fluide sur les propriétés réservoirs des réseaux d'injectites, les valeurs et la distribution de la porosité primaire (i.e., porosité moins-ciment) seront quantifiées. L'échantillonnage sera effectué à l'échelle de l'affleurement dans l'objectif de visualiser les variations de la porosité à échelle pluricentimétrique.*
- *Les observations multi-échelles structurales et diagénétiques, couplée aux estimations de la porosité primaire et actuelle, permettront de: (1) contraindre l'évolution de la porosité au sein du système d'injectite, de sa mise en place à aujourd'hui, et de (2) caractériser l'évolution des écoulements de fluides au sein des réseaux d'injectites au cours du temps.*

1. Précédents travaux

De nombreux travaux portent sur l'étude des systèmes d'injections clastiques en domaines marins profonds, et s'appuient sur l'analyse de données sismiques (Huuse et al., 2007), de carottes sédimentaires (Duranti et Hurst, 2004) ou encore de données terrain (Parize et al., 2007; Vigorito et al., 2010). Dans cette première partie, le travail réalisé sur les injectites du bassin Vocontien se focalise sur trois principaux aspects:

- (1) Les structures internes à micro- et macro-échelles.
- (2) La séquence diagénétique.
- (3) L'estimation des valeurs de porosité.

(1) Le remplissage des injections clastiques est communément décrit comme homogène et sans structures (Truswell, 1972; Hillier et Cosgrove, 2002; Parize et al., 2007). Cependant, des lamines disposées parallèlement aux marges des injections, et caractérisées par des granulométries différentes ont parfois été observées (Hubbard et al., 2007; Macdonald et Flecker, 2007). Des granoclassements sont occasionnellement distingués dans le remplissage, perpendiculairement à la marge (Hubbard et al., 2007) et le long des injections (Obermeier, 1996; Ross et White, 2005). Ces granoclassements sont généralement dûs à la distribution préférentielle des galets mous au sein du remplissage des injectites (Taylor, 1982; Diggs, 2007). Des bandes de déformation ont fréquemment été observées à l'intérieur des dykes clastiques. Elles sont interprétées comme résultant de la compaction mécanique induite par le poids lithostatique (Duranti et Hurst, 2004; Jonk et al., 2005).

(2) Jonk et al. (2003, 2005a, b) ont effectué plusieurs études sur les séquences diagénétiques types caractérisant les injectites et leurs influences sur les écoulements de fluides au cours du temps. Des phases de cimentation siliceuses authigéniques précoces, en relation avec la mise en place des bandes de déformation, ont été mises en évidence. Cependant la phase diagénétique majeure des réseaux d'injectites est le développement d'un ciment carbonaté. Cette phase de cimentation est généralement plus développée dans les injectites que dans les unités parentes, et se développe sous la forme d'une calcite de blocage, limitant ou inhibant les écoulements de fluides dans les injectites.

(3) La majorité des valeurs pétrophysiques obtenue au sein des injectites provient de sondages. Les valeurs obtenues montrent que la porosité et la perméabilité sont légèrement plus faibles dans les intrusions, comparées aux unités parentes. Récemment, une première étude visant à caractériser les valeurs de porosité et de perméabilité d'un système d'injectites affleurant dans les «Panoche Hills» (Californie) a été conduite (Scott et al., 2013). Des données de porosité visuelle, de porosité moins-ciment ou encore de perméabilité ont été récoltées sur le terrain, ou après analyses de lames minces. Si les données de porosité primaire (porosité moins-ciment) n'ont pas été analysées, ou leur distribution à l'échelle de l'affleurement non présentée, les données de perméabilité ont permis de mettre en évidence l'influence de l'angle de pendage des dykes ou encore de la morphologie des sills sur les propriétés réservoirs (Scott et al., 2013).

Dans l'optique de mieux caractériser la distribution et l'évolution des propriétés pétrophysiques au sein d'un système d'injections clastiques ainsi que les paramètres qui contrôlent ses propriétés, une étude a été menée dans le Bassin Vocontien (SE France).

2. Contexte de l'étude

Deux sites d'études localisés dans le Bassin Vocontien ont été sélectionnés. Le bassin vocontien est une paléo marge passive qui s'est développé durant le Crétacé Inferieur entre la partie Nord-Ouest de L'océan Alpin téthysien et le Rift Atlantique (Ziegler, 1990; Dercourt et al., 1993) (**Fig. 1**). Les deux sites d'études sont respectivement localisés à proximité des localités de Bevens et de Rosans dans le Sud-Est de la France et se situent à plus de 40 kilomètres de la plateforme de la paléo fosse vocontienne (**Fig. 1**). Les deux sites présentent des réseaux d'injectites qui recoupent des sédiments Aptien-Albien (Crétacé Inférieur). Les systèmes d'injectites sableuses sont dominés par la présence de dykes sur le site de Bevens et dominés par la présence de sills sur le site de Rosans.

De nombreuses études se sont focalisées sur ces sites de renommée internationale (Beaudoin et Friès, 1982; Huang, 1988; Parize, 1988; Friès et Parize, 2003; Parize et Friès, 2003; Parize et al., 2007a, 2007b; Monnier, 2013). Les différentes travaux ont principalement décrit l'architecture à grande échelle de ces systèmes d'injections afin de déterminer les mécanismes contrôlant l'hydrofracturation et le sens de propagation des injections sableuses. L'observation à plus fines échelles des réseaux d'injections sableuses du bassin vocontien, ou encore leurs caractéristiques pétrophysiques, n'ont à

l'heure actuelle pas fait l'objet de travaux publiés.

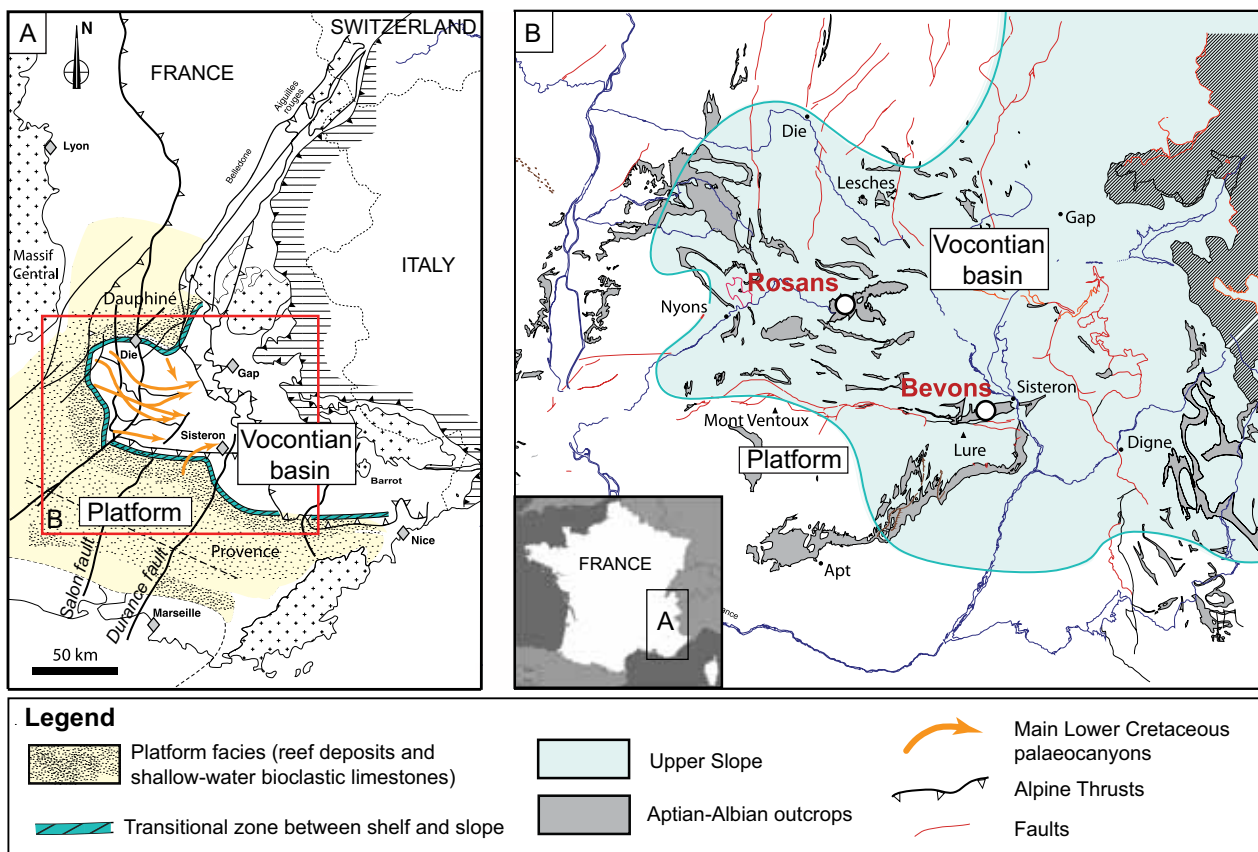


Figure 1. (A) Regional map showing contours separating the Shelf from the Vocontian Basin, and positions of the submarine valleys during the Lower Cretaceous. (B) Close up on the Vocontian Basin where the distribution of Aptian-Albian deposits is highlighted. Rosans and Bevens correspond to the areas where injectite networks are described in this study. Modified after Parize et al. (2007a).

3. Méthodes

Une description des deux systèmes d'injections sableuses a été réalisée à échelle macroscopique et microscopique. Sur les sites de Bevens et Rosans, 115 échantillons ont été collectés au sein de dykes, sills, et turbidites (i.e., unité parente). Pour chaque échantillon, la position, le type d'échantillon (i.e., dykes, sills ou turbidites), l'épaisseur de l'élément échantillonné, l'angle de pendage des dykes et la distance à l'unité parente ont été mesurés. A partir de ces échantillons, des lames minces ont pu être réalisées et imprégnées avec de l'araldite bleue (mise en évidence de la porosité) puis colorées à l'aide d'une solution de ferricyanure de potassium (mise en évidence de la proportion de ciment carbonaté). Chaque lame mince a été analysée afin de déterminer la minéralogie, la granulométrie, la porosité visuelle, et la porosité moins-ciment des différents échantillons. Les valeurs de porosité ont été déterminées par comptage de points sur les différentes lames minces (800 points par lames

minces) à l'aide du logiciel JMicrovision©. Afin de déterminer la séquence diagénétique caractérisant les systèmes d'injectites, certains échantillons ont été observés en cathodoluminescence.

L'objectif principal de cette étude étant d'analyser l'évolution et les paramètres qui contrôlent la distribution des valeurs de porosité primaire, des tests statistiques ont été effectués entre les valeurs de porosité et les différentes caractéristiques des injectites (épaisseur, angle de pendage, distance à la source, etc.). En parallèle, des cartes d'interpolation ont été réalisées à l'aide du logiciel ArcGIS© afin d'analyser la distribution des valeurs de porosité à l'échelle de l'affleurement.

4. Article soumis dans la revue *Marine and Petroleum Geology*

«Micro- to Macroscale internal Structures, Diagenesis and Petrophysical evolution of Injectite networks in the Vocontian Basin (France): implications for Fluid Flows.»

L'article est structuré de la façon suivante: (1) Dans une première partie, les cadres paléogéographiques, structuraux et sédimentologiques des deux secteurs sont présentés. (2) Les différentes méthodes utilisées dans cette étude sont ensuite présentées. (3) Suit la description des deux systèmes d'injectites à l'échelle de l'affleurement et des différents types d'injectites qui les composent. (4) Dans une quatrième partie, les différentes structures observées au sein des injectites sont décrites successivement à l'échelle macroscopique et microscopique, puis interprétées en terme de mécanisme de formation. (5) Les différentes phases diagénétiques affectant le système d'injection sont ensuite exposées par ordre chronologique. (6) Dans une sixième partie, les estimations des valeurs de porosité primaire sont présentées et analysées en fonction de plusieurs paramètres incluant: le type d'élément échantillonné (i.e., dykes, sills, ou turbidites), l'épaisseur de l'injection ou encore la distance à la source. (7) Dans une dernière partie, les différents résultats seront discutés et plus particulièrement l'évolution des valeurs de porosité, de la mise en place du système d'injection à aujourd'hui. L'implication des variations de la porosité sur les écoulements de fluides au cours du temps sera également abordée dans cette partie.

**Micro- to Macroscale internal Structures, Diagenesis and Petrophysical
evolution of Injectite networks in the Vocontian Basin (France):
Implications for Fluid Flows. (*submitted*)**

Edouard Ravier^a, Michel Guiraud^a, Arthur Guillien^a, Emmanuelle Vennin^a, Jean-François Buoncristiani^a, Eric Portier^b.

^aLaboratoire Biogeosciences UMR/CNRS 6282 Université de Bourgogne, 6 Bd Gabriel, 21000 DIJON, France.

^bGDF Suez, Exploration Production International, 1 place Samuel de Champlain – Faubourg de l’Arche 92930 Paris La Défense Cedex – France.

1. Introduction

Injectites are lithified intrusions of clastic sediments that are either discordant (dykes) or concordant (sills) to the bedding of their host strata. Injectites are related to injections of remobilized liquefied to fluidized clastic material within hydrofractures propagating within an encasing seal lithology (Cosgrove, 2001; Jolly and Lonergan, 2002). Hydrofractures and clastic injections form as a response of water excess release from an overpressurized parent unit. Clastic injections occur in many depositional environments including fluvial, glacial, deltaic and for the most part in marine deep-water environments (Plint, 1985; Hardie, 1999; van der Meer et al., 2009; Hurst et al., 2011). In deep-water environments, turbiditic sandy channels mainly represent the parent units being injected within fine-grained and low permeable strata (e.g., mudstones, shales). In such configuration, sills and dykes behave as porous and permeable conduits focusing fluid flows within hundred-meter thick low-permeability lithologies (Huuse et al., 2005). Although injectites have first been described in 1827 (Murchison), active research have started over 150 years later when their roles in hydrocarbon systems have undeniably been recognized (Dixon et al., 1995). Injectites notably form vertical communications between reservoirs separated by low-permeability sedimentary intervals (Hurst et al., 2003). Large injectite networks also represent intrusive traps for fluids and excellent reservoirs containing substantial volume of porous and permeable sand, forming excellent pay zones (Hurst and Catwright, 2007; Braccini et al., 2008). Numerous studies based on seismic data have been conducted on hydrocarbon reservoirs, principally in the North Sea where architectures and geometries of large-scale sand intrusions have been explored (Briedis et al., 2007; Huuse et al., 2007; Jackson, 2007). Field investigations have increased during the past decade as they serve to improve geometrical models, but also to characterize petrophysical and diagenetic characteristics of injectite networks. Both diagenetic and petrophysical characteristics are essential parameters to comprehend fluid flow characteristics through time within an intruded sand network (Mazzini et al., 2003; Jonk et al., 2005b, 2010, Scott et al., 2013). Well-known outcrops benefiting from optimum exposure conditions are notably located in California (Panoche hills, Yellowbank Creek), East Greenland (Kangerlussuaq Basin) or Southeast France (Vocontian Basin) (Surlyk and Noe-Nygaard, 2001; Jonk et al., 2005a; Whitman et al., 2004; Parize and Friès, 2003; Parize et al., 2007a,b; Vigorito et al., 2008, 2010; Scott et al., 2009, 2013).

This present study deals with field investigations and sampling conducted in the ‘classic’ Vocontian

injectite exposures (SE France), more particularly in the Bevons and Rosans areas. This study aims to describe and interpret structures observed within injectites at both macro- and microscales and their impacts on the granular framework. In parallel, timing of the diagenetic phases affecting the injectite networks have been established in order to estimate the porosity evolution through time. Precementation porosity values have been estimated and their geographical distributions analyzed. Integrations of structural and diagenetic observations combined with distributions of precementation porosity values were used to construct a model of porosity evolution from time of injection to modern time. This evolution serves to approach the impact of injectite networks on fluid flows through time.

2. Geological setting

2.1. General setting

The Bevons and Rosans areas are located near Sisteron in the upper slope domain of the Vocontian Basin (SE France). These areas display high-quality outcrops where two injectite networks cross-cut Aptian-Albian deposits (**Fig. 1**).

The Vocontian Basin corresponds to a palaeo passive margin, which developed in the Early Cretaceous between the NW part of the Alpine Tethys Ocean and the Atlantic Rift (Ziegler, 1990; Dercourt et al., 1993). This palaeomargin formed part of the northern margin of the Pyrenean-Valais oceanic area, linking the Gulf of Biscay and the East Tethys Ocean during the Aptian (Stampfli et al., 2002).

This basin was segmented into three distinct areas: the platform, the slope and the basin floor (Friès and Parize, 2003). These areas defined two main depositional environments: a platform characterized by reef deposits and shallow-water bioclastic limestones, notably preserved in Provence, Ardèche, Chartreuse and Vercors (Rubino, 1989; Arnaud-Vanneau and Arnaud, 1991; Quesne, 1998) and an upper slope domain where pelagic sediments displaying marl/limestone alternations are disrupted by gravity deposits (e.g., slumps, debris flows, sandy turbidites) (**Fig. 1**).

In the Vocontian Basin, the Bevons area is located 40 km away from the platform while the Rosans area is situated in the central part of the upper slope Vocontian domain (**Fig. 1B**). Both sites provide excellent outcrop qualities where pelagic sediments and gravity deposits dated from the Aptian-Albian are exposed (**Fig. 1B**). In this study, the “Puy Hill” and “Saint-André-de-Rosans” sections have been respectively selected in the Bevons and Rosans areas, for reasons of exposure conditions.

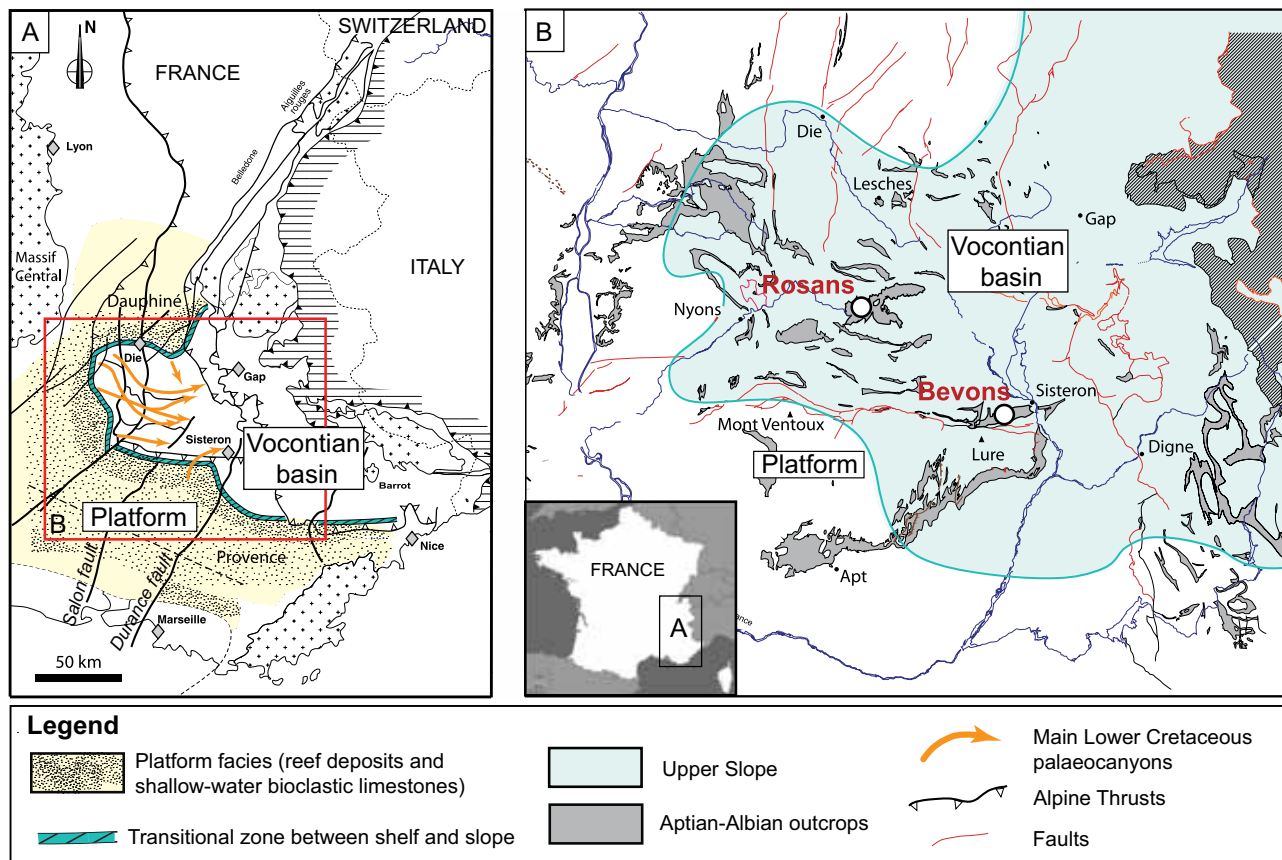


Figure 1. (A) Regional map showing contours separating the Shelf from the Vocontian Basin, and positions of the submarine valleys during the Lower Cretaceous. (B) Close up on the Vocontian Basin where the distribution of Aptian-Albian deposits is highlighted. Rosans and Bevens correspond to the areas where injectite networks are described in this study. Modified after Parize et al. (2007a).

2.2. Structural setting

The Vocontian Basin is structured by two sets of faults respectively oriented N-S (N100°) and E-W (N020°), corresponding to two major tectonic phases (**Fig. 1**). The first phase corresponds to the E-W extensional tectonic regime occurring during Trias to Jurassic times, attributed to the evolution of the western Thetys rift while the Central Atlantic opens (Manatschal and Bernouilli, 1998). In the Vocontian Basin, this first tectonic phase is responsible for the development of N-S (N100°) trending faults inherited from the Hercynian structuration. During the Late Jurassic to Early Cretaceous, the diachronous subduction of the NeoTethys mid-oceanic ridge probably triggered changes in Late Jurassic to Early Cretaceous plate tectonics (Bonin et al., 2012). From the late Jurassic to Early Cretaceous, the second active tectonic phase results from the evolution of the main Alpine northern Tethyan rift in a westward propagating oblique rift, and coincides with the opening of the Bay of Biscay along the intracontinental Pyrenean fault (Bonin et al., 2012). The angle between the rift trend and the extensional direction of less than 20° implies transform-to-oblique rifting in the Bay

of Biscay and the Vocontian Basin. The transform-to-oblique rifting in the study area triggered the formation of faults oriented E-W that is nowadays structuring the Vocontian Basin. Numerous faults sealed by Cenomanian deposits, with offsets reaching several tens of meters, demonstrate the active synsedimentary tectonics during the Early Cretaceous (Beaudoin et al., 1986; Joseph et al., 1987; Maillart et al., 1987). In agreement with the low subsidence rate of the Early Cretaceous, the Vocontian Basin evolved in an aborted rift away from the active stretching center. After this last phase of tectonic extension, the platform of the Vocontian Basin was affected by compression leading to formation of E-W antiform axis during the Albo-Cenomanian (e.g., Durancian Uplift), either attributed to the Africa-Eurasia collision or induced by a thermal uplift during a NW-SE extensive regime (Chorowicz and Mekarnia, 1992; Hibschi et al., 1992). Nowadays, the study area is limited to the south by a major southward-dipping E-W thrust, and to the west and the east by the Salon and Durance faults (**Fig. 1A**).

2.3. Sedimentary setting

2.3.1 Hemipelagic deposits

From the Aptian to the Albian, a 700-800 m thick pile of pelagic sediments was deposited in the Vocontian Basin (Friès, 1987). Bevons and Rosans areas display marls alternating with limestones, referred to as the “blue marls Formation” (**Figs. 2, 3A**). The “blue marls Formation” is characterized by a maximum total thickness of 300 m and appears abruptly above a marly calcareous succession of Lower Cretaceous age (**Fig. 2**). Marls typically contain 50% of carbonate, 30 % of clays, 15 % of quartz and the remainder consists of accessory mineral such as pyrite and feldspar (Parize and Friès, 2003). Micropalaeontological data, facies, and geometric considerations permitted to estimate the palaeobathymetry of the Vocontian Basin during deposition of the marls. When deposition of the hemipelagic sediments commenced during the Aptian, maximum depth of the slope domain was around 1000 m, while at the Aptian-Albian boundary the depth was reduced to only a few hundred of meters (Friès, 1987; Bréhéret, 1997). This Formation contains several cm to dm thick “key” beds allowing basin-scale correlations of the Aptian-Albian sedimentary sequence. These key beds include individual limestone beds, limy and black shale bundles, and bentonites (i.e., ash layers) (**Fig. 2**).

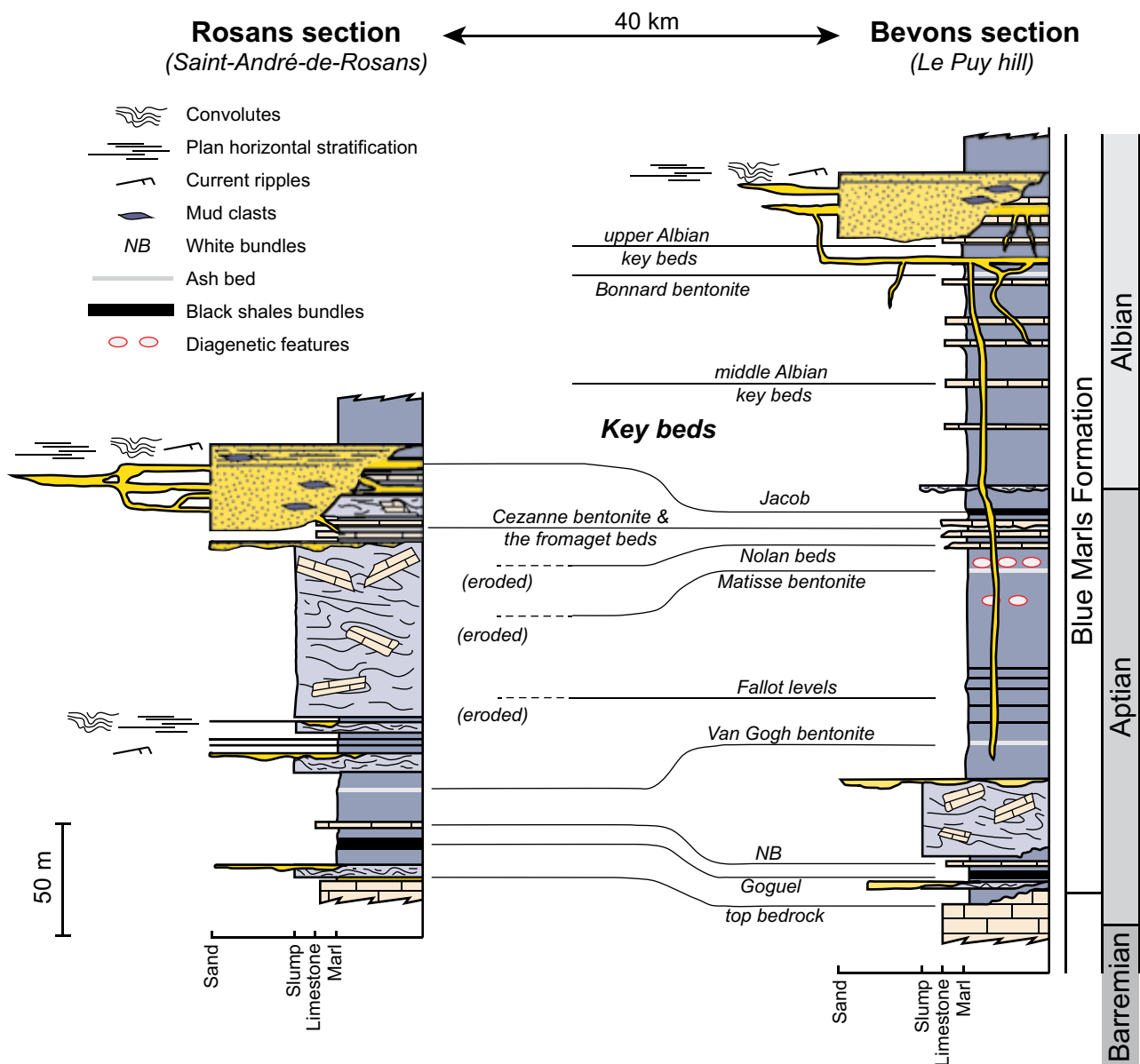


Figure 2. Lithostratigraphic succession of the Aptian-Albian “blue marls” Formation in the Bevens and Rosans areas. Stratigraphic correlations between these two sites rely on key beds traced throughout the Basin. Modified after Parize et al. (2007a).

2.3.2. Gravity-driven deposits

Numerous gravity-driven deposits, including thin-bedded turbidites, thick massive turbidites, debris flows, and slumps are intercalated within the hemipelagic deposits. Over 20 Aptian-Albian slumps have been mapped in the area with a maximum extent of 50 km away from the shelf break (Friès and Parize, 2003). Slumps are characterized by contorted blocks up to several hundreds of m, often disaggregated in a marly matrix. A wide range of folds is associated with these slumped deposits (**Fig. 3B**).

Turbidites occur as up to 80 km away from the shelf break and were triggered by the relative sea level fall during the Aptian (Friès and Parize, 2003). Sorted sands forming tens of m-thick dunes in

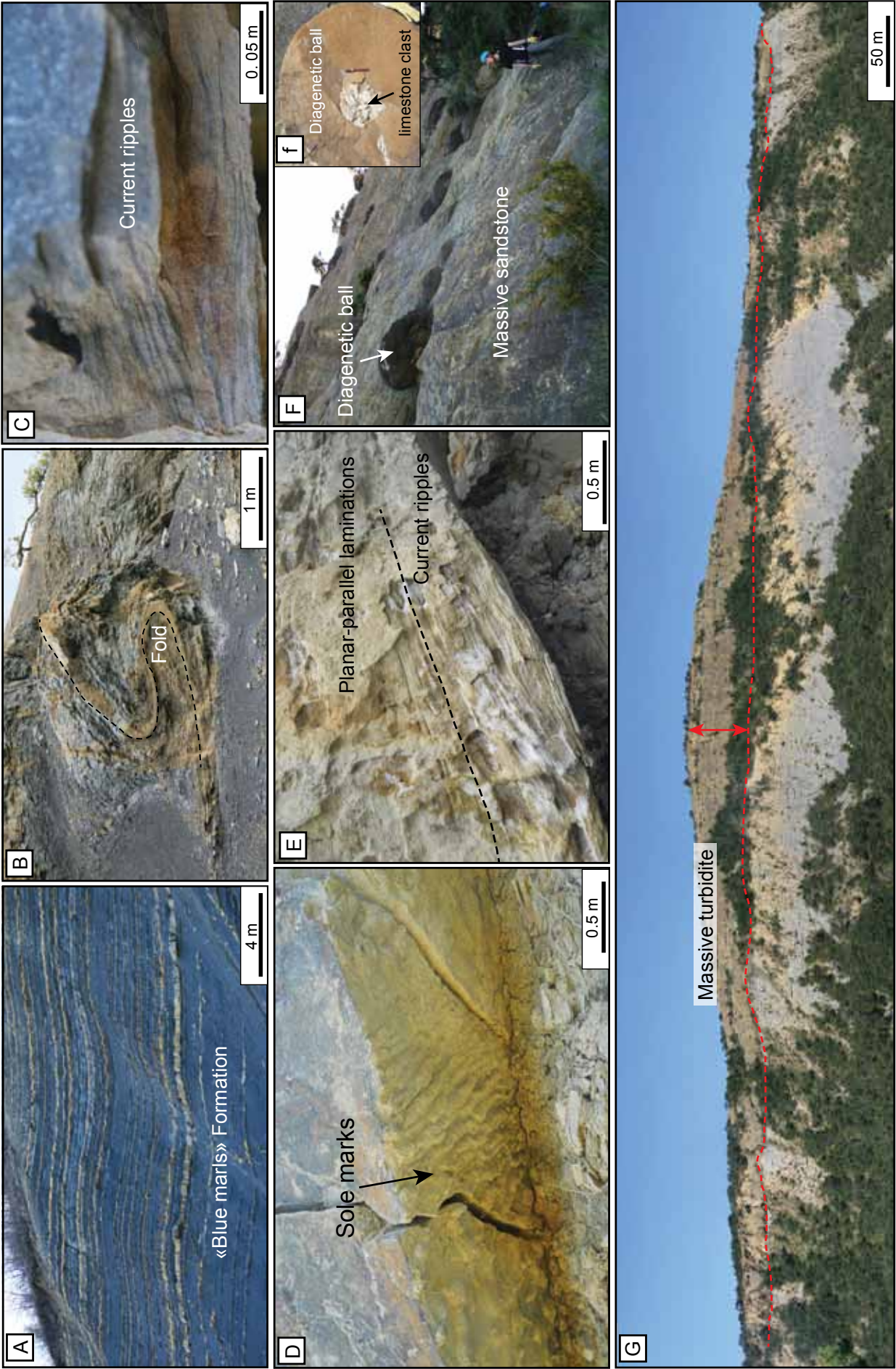


Figure 3. (A) The Aptian-Albian “blue marls” Formation with typical marls/limestone alternations. (B) A fold observed in a slump that frequently disturbs the “blue marls” Formation. (C) Climbing current ripples observed at the base of a thin-bedded turbidite. (D) Soles marks observed at the base of a thin-bedded turbidite. (E) Current ripples overlain by planar stratifications in a sandstone turbidite. (F) Massive sandstones containing aligned diagenetic balls. (f) Detailed section within a diagenetic ball showing a central limestone clast. (G) A 40 m-thick turbiditic channel infilled by massive sandstones along the “Saint-André-de-Rosans” outcrop (Rosans area). This channel lies on slumped hemipelagic deposits corresponding to the “blue marls” Formation.

the shelf-break area represented the source for the development of these turbidity currents (Friès, 1987; Parize, 1988; Friès and Parize 2003). A series of palaeocanyons (10-15km wide and 60-80km long) channelized sandy flows in the basin, leading to deposition of massive turbidites in the distal part of the Vocontian Basin (Parize and Friès, 2003). Two types of turbidites are distinguished in the Vocontian Basin: classical turbidites (up to several m thick) characterized by the presence of Bouma sequences (1962), and massive turbidites (up to 40 m thick). In the first type, fining-upward sequences containing sole marks at the base, convolutes, current ripples and planar parallel laminations occur (**Fig. 3C, D, E**), while the second type, much thicker, contains scarce sedimentary structures except at the channel top where ripples and planar-convoluted laminations are observed (**Fig. 2**). Turbidites evidenced by Bouma sequences demonstrate sediment deposition by low-density turbidity flows while massive turbidites result from the deposition of high-density turbidity flows (Lowe, 1982; Mulder and Alexander, 2001; Friès and Parize, 2003). The occurrence of rip-up limestone clasts within massive turbidites leads to the formation of scattered m-sized diagenetic nodules (**Fig. 3F, f**). The Bevens and Rosans outcrops are characterized by the presence of massive turbidites. Using lithostratigraphic and biostratigraphic markers, the massive turbiditic channels observed in Bevens are inferred to be Albian while the Rosans thick and massive turbiditic channel is dated from the Aptian-Albian boundary (Friès, 1987; Friès and Parize, 2003) (**Fig. 2**).

In the Bevens area, the “Puy Hill” outcrop displays the largest section (200 m high; 720 m long) with best exposure conditions. At the top of this section, the Albian sandstones consist of two turbiditic channels (a and b) composed of massive sandstones, lying on a 200 m thick pile of undisturbed hemipelagic deposits (**Fig. 4**). The first channel is 150 m wide and 30 m thick while the second channel is 90 m wide and 30 m thick. In the central part of the Vocontian Basin, the Rosans area has been studied principally through the “Saint-André-de-Rosans” section. This section displays a 5 km long outcrop where a 40 m thick and 500 m wide sandstone turbiditic channel occurs (**Figs. 2, 5**). The turbiditic channel lies on the well-stratified “Fromaget beds” intercalated between two slumped deposits (**Fig. 2**). On both sites, massive turbidites are composed of well-sorted fine-grained

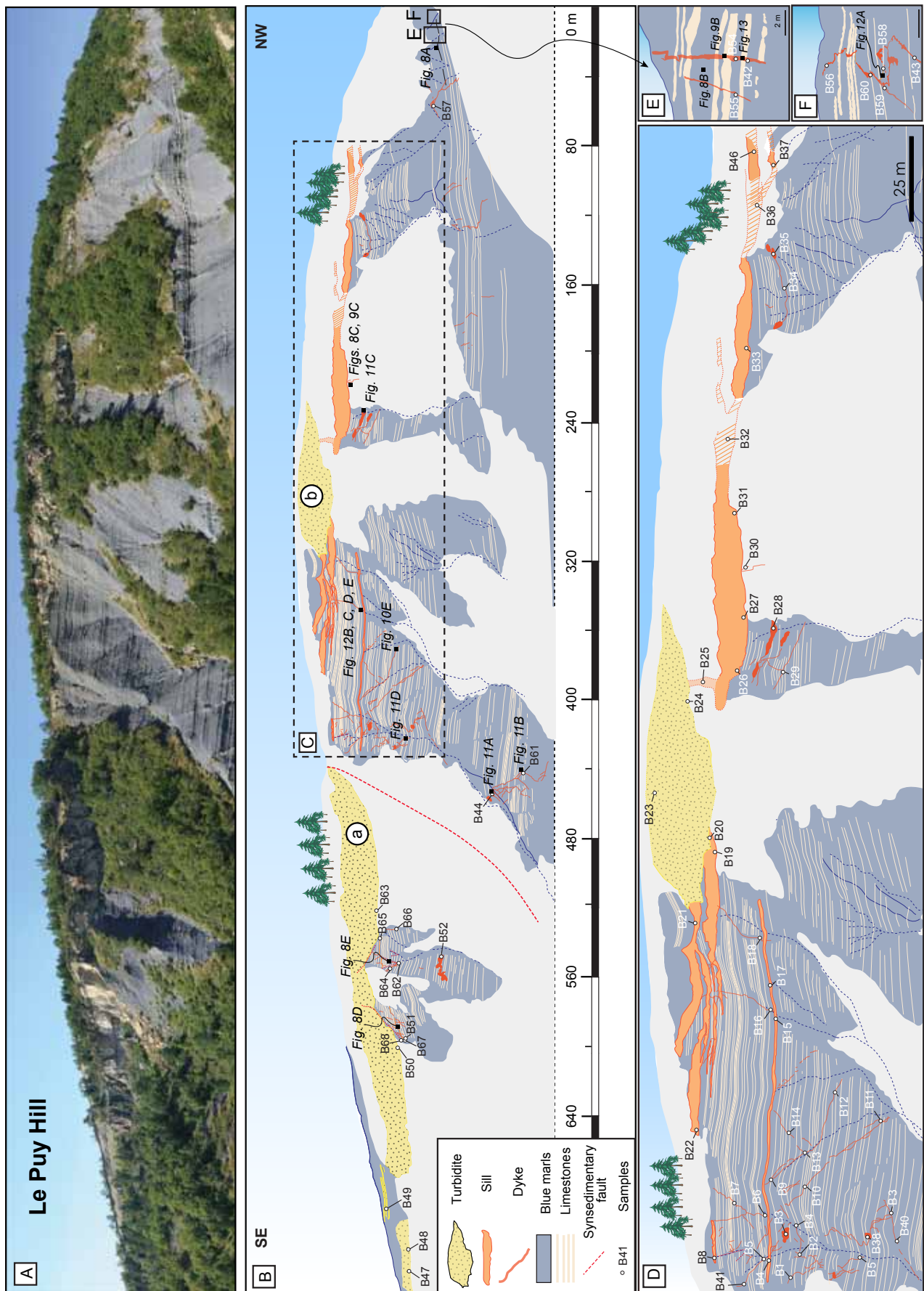


Figure 4. (A) Panoramic photograph of the “Puy hill” outcrop in the Bevens area. (B) Interpreted sketch highlighting the distribution of parent beds (turbiditic channels a and b) and the associated injectite system. Positions of the collected samples are represented. (C) Close-up on the central part of the injectites network with positions of the samples. (E), (F) Close-up on injectites situated at the base of the outcrop where few samples have been collected.

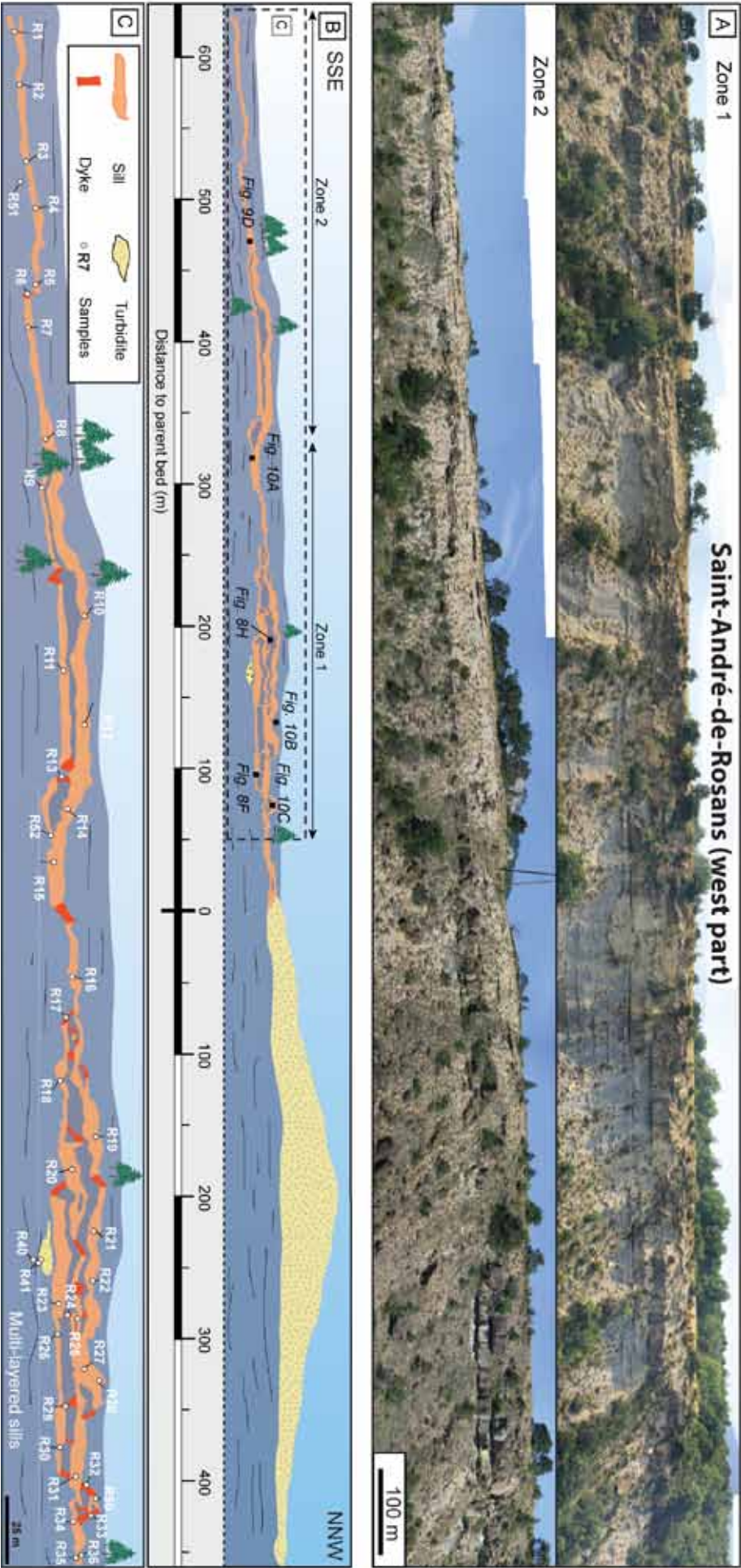


Figure 5. Panoramic photograph of the western part of the “Saint-André-de-Rosans” outcrop in the Rosans area. (B) Interpreted sketch highlighting the distribution of the parent bed (turbiditic channel) and the associated injectite system. Positions of the collected samples are represented. (C) Close-up on the injectites system with the distribution of samples.

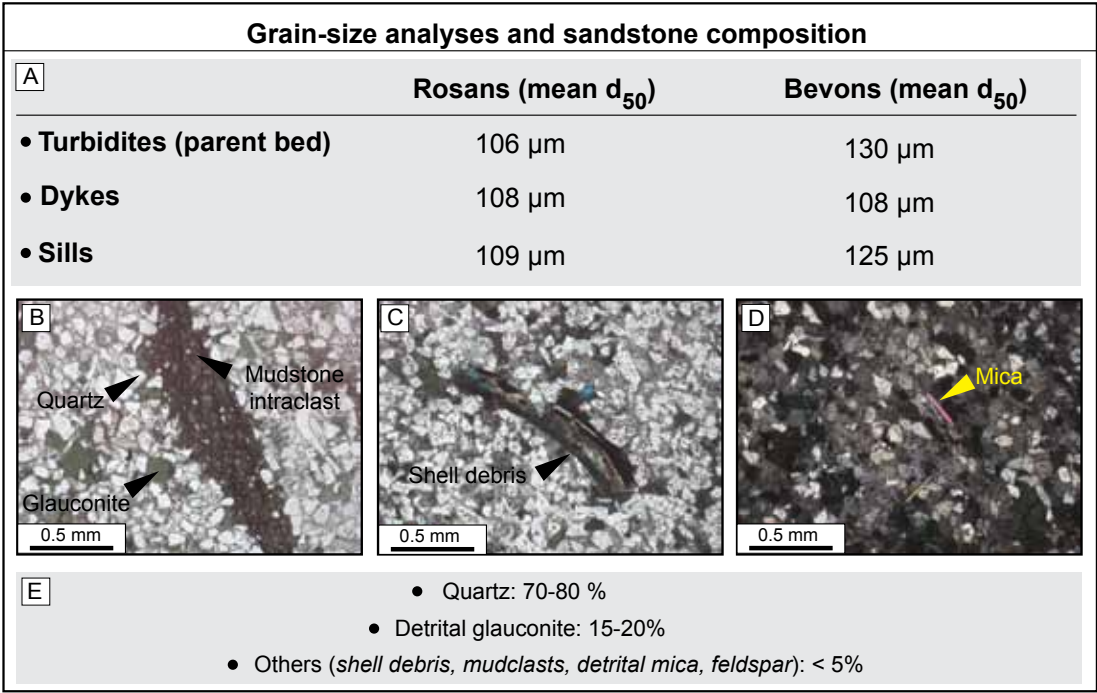


Figure 6. Grain-size distribution and sandstone composition (A) Mean d_{50} of parent beds, dykes and sills in the Bevons and Rosans areas. (B) A Mudstone intraclast observed within injected sandstone. (C) Shell debris observed within injected sand. (D) Micaceous within intruded sand. (E) Averaged values of sandstone composition in the Bevons and Rosans areas.

glauconitic sandstones. The mean d_{50} of the turbidites is 130 μm for Bevons and 106 μm for Rosans (Fig. 6). Sandstones are predominantly composed of quartz grains (70-80%) and detrital glauconite (15-20%) associated with siliceous and carbonate shell debris, feldspars, micas and mudclasts (Fig. 6B, C, D, E).

3. Methods

Along the two selected outcrops (e.g., “Le Puy hill” and “Saint-André-de-Rosans”) corresponding to the two areas of interest (Bevons and Rosans), a detailed study of the injectite networks has been carried out. Both macro- and micro-scale descriptions of the injectite networks were performed. In the Bevons area, 65 samples were collected in 38 dykes, 20 sills and 7 turbidites while 50 samples were collected in the Rosans area, in 13 dykes, 31 sills and 6 turbidites. For each samples, positions, orientations, typologies (dykes, sills, or turbidites), injectite thickness, dyke dip angles and the distance to parent bed (when possible) were recorded. Thin sections, impregnated with blue araldite dye have been produced (i.e., 115 thin sections) and then mounted on glass slides measuring 30 ×

45 mm, without glass cover slips. The mineralogy, grain-size distribution, visual and minus-cement porosity were determined by point counting (800 counts per thin section) using the JMicrovision © software. The grain-size has been characterized using the d_{50} index known as the median diameter or the medium value of the particle size distribution. Visual porosity (\emptyset_v) consists in measuring void spaces highlighted by blue dye in thin sections (1). Minus-cement porosity (\emptyset_c) is the percent of void spaces (blue dye), volume of cements and volume of clays to the total volume (2) (**Fig. 7**).

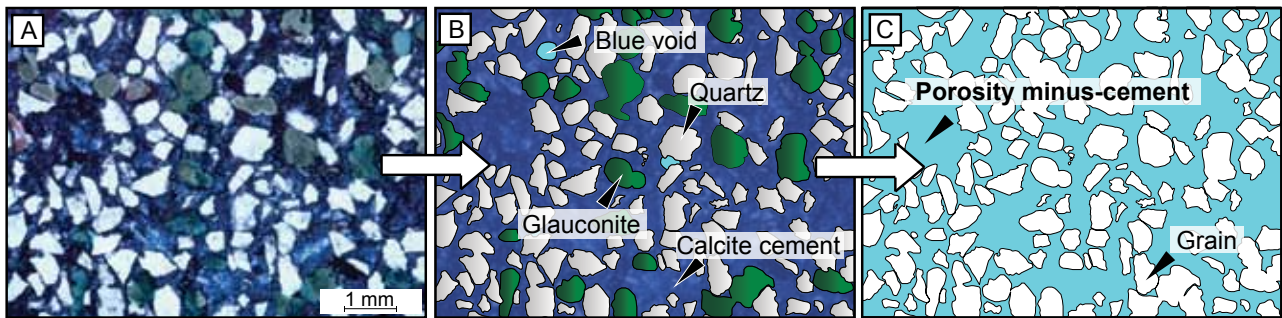


Figure 7. Diagram illustrating the method to estimate minus-cement porosities. (A), (B) Thin section photograph with quartz grains, glauconites, calcite cement evidenced by blue stain, and voids illustrated by blue dye. (C) Interpreted sketch illustrating in blue the area corresponding to the porosity-minus cement volume estimated for each samples in this study.

1. Visual porosity (\emptyset_v) = (point - counted volume of blue dye)/(point - counted total volume)
2. Minus-cement porosity (\emptyset_c) = (point-counted volume of blue dye+cement+ clays)/(point-counted total volume)

Each sample has been stained using an alizarin-potassium ferricyanide solution to highlight calcite cement and facilitate minus-cement porosity measurements (Dickson, 1966). Mercury intrusion porosimetry measurements have also been estimated on some samples to validate results obtained on visual porosity by point counting (\emptyset_v). Cathodoluminescence petrography was also performed with a cold cathode luminescence Technosyn 8200 Mk2 to determine cement composition and establish a chronological diagenetic succession.

This study particularly focuses on minus-cement porosities to assess characteristics of early porosity values. Covariance and regression analyses between minus-cement porosities and injectite sites (Bevons vs. Rosans), injectite types, injectite thickness, dyke dip angles, and distance to parent bed have been conducted. The distribution and interpolation of minus-cement porosity values at outcrop scale were constructed using “inverse distance weight” interpolation model in the ArcGIS software

4. Macro-scale characteristics and architecture of the injectite networks

4.1. Bevens: a dyke-dominated injectite system

Although a majority of sills are directly connected to the two turbiditic channels (e.g., parent bed), dykes are predominant and define a dyke-dominated injectite system. Along this outcrop, injectites are mainly connected to channel b while a few are connected to channel a (**Fig. 4**). Injectites are intruded within the “blue marls” Formation laterally and below the parent bed, indicating that hydrofractures and injections did not reach the palaeo-sea-floor at the moment of turbidite deposition (Friès and Parize, 2003). Two major models of injection are debated for the Bevens area, a model implying per descensus sand injection (Parize et al., 1987, 2007a; Parize and Friès, 2003) and another implying per ascensus sand injection (Monnier, 2013). Nevertheless, the model of sand injection is beyond the scope of the present study and will not be further discussed.

4.1.1. Dykes

Dykes are up to 2.5 m wide with a majority below 0.5 m and can be traced down to 275 m within the “blue marls” Formation (**Fig. 4**). The dyke network is well-defined, and single elements are predominantly high angle ($>45^\circ$) with straight and planar margins (**Fig. 4**). Dykes can also be bifurcating, branching, anastomosing, “en echelon” or displaying a “zig-zag” trajectory (**Fig. 8A, B**). The variety of morphology is directly controlled by lithological contrasts at bedding surfaces, bed thickness, bedding dips, and palaeo-fractures. Ptygmatic folds due to post-sand-injection compaction of the host strata are occasionally observed along dykes. Dykes are often connected to sills and thicker near their source with a progressive decrease of their thickness downward (**Fig. 8C**). Dykes display two preferential strike directions (Huang, 1988; Parize and Friès 2003; Parize et al., 2007b). Preferential strike directions are the N-S and E-W directions corresponding to the two families of faults structuring the Vocontian Basin (cf. 2.2) (Parize et al., 2007b). A higher dyke concentration has been recognized close to synsedimentary faults (Parize and Friès, 2003) (**Fig. 4**). In addition, dykes occasionally follow synsedimentary faults as illustrated by a dyke developing along a conjugate set of normal faults (**Fig. 8E**). Sand injected within the dykes are slightly finer-grained ($d_{50} = 108\mu\text{m}$) and displays a similar mineralogical composition compared to the turbidite (**Fig. 6**).

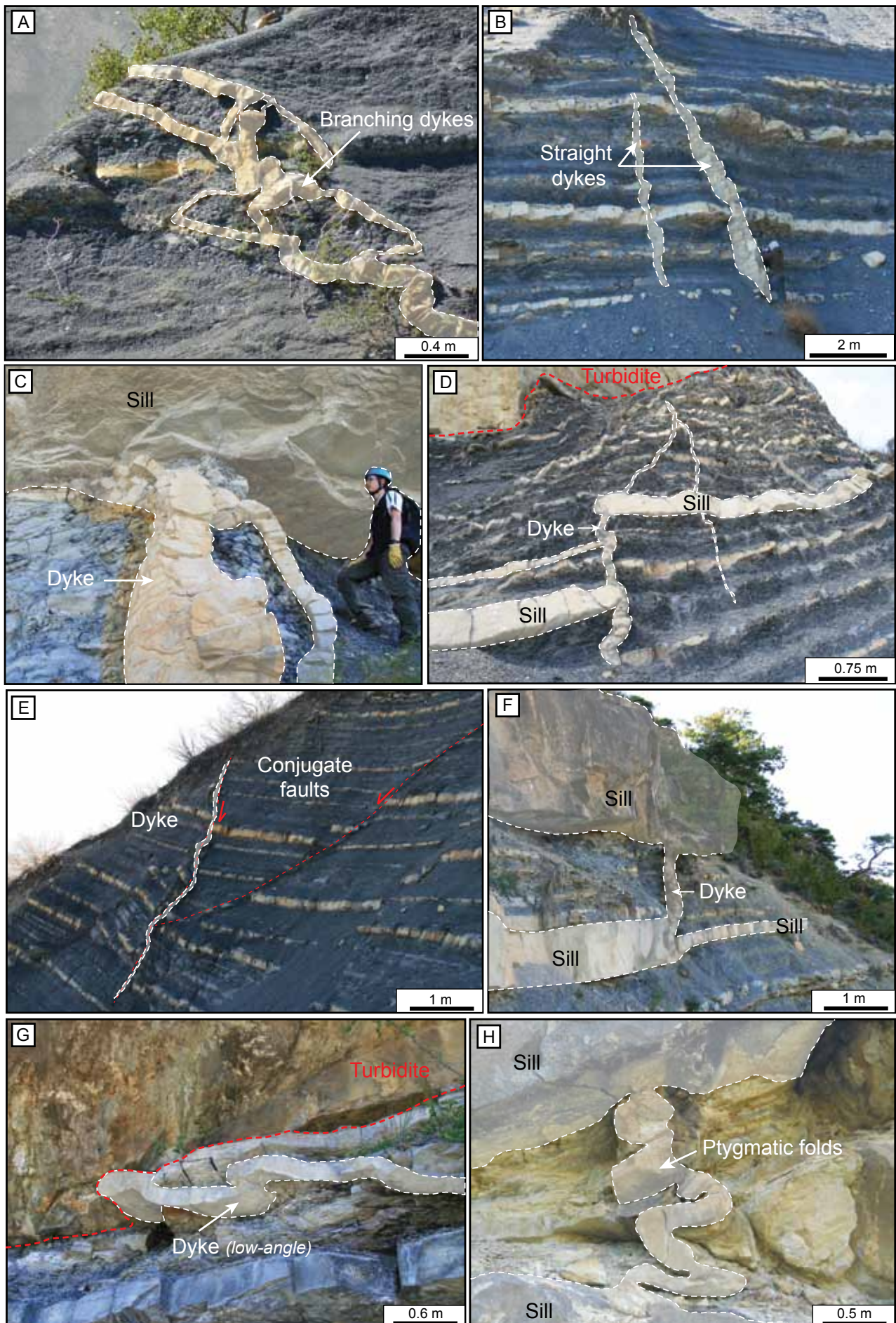


Figure 8. (A) Branching dykes in the Bevens area. (B) Straight dykes in the Bevens area. (C) A set of conjugate dykes connected to a sill in the Bevens area. (C) A dyke-sill complex connected to the overlying turbidite in the Bevens area. (E) A set of syn-sedimentary conjugate faults affecting the “blue marls” Formation in the Bevens area. Note that a clastic dyke is injected within one of these faults. (D) A dyke-sill system observed in the Rosans area. Note the lateral increase of the sill thickness when a dyke becomes connected. (G) A low-angle sand dyke directly connected to the parent bed in the Rosans area. (H) Ptygmatic folding of a high-angle sandstone dyke within the Rosans injectites network. Cf. location of photographs on the outcrop on Figures 4 and 5.

4.1.2. Sills

Sills are predominantly situated near the sand source, i.e. the turbiditic channel (**Fig. 4**). Their dimensions vary from 0.1 m to 10 m thick and can laterally extend over hundreds of m (**Fig. 4**). Some sills are connected to channel (b) and display steps refer to as “stepped sills” or “wing sills” (**Fig. 4**). Few examples of stepped sills occur when sills transgress from one horizon to another to form a dyke-sill system, notably below channel 1 (**Fig. 8D**). Other sills are straight, following strata composing the host marls. Grains injected within the sills are slightly finer ($d_{50} = 106 \mu\text{m}$) and display a similar composition with the turbidite (i.e., the parent bed) and dykes.

4.2. Rosans: a sill-dominated injectite system

An injectite network, dominated by sills, develops laterally into channel banks on both sides of the turbiditic channel, defining a sill-dominated injectite system in “Saint-André-de-Rosans” (**Fig. 5**). The sand volume injected in the area reaches 20 % of the total volume of the massive turbiditic channel (Parize, 1988; Parize and Friès, 2003). Parize and Friès (2003) suggested that the development of the injectite network in Rosans is contemporaneous to the deposition of the massive turbidite because the channel banks are fractured, thus indicating that injection took place during channel infilling.

4.2.1. Sills

Sills are up to 6 m thick and extend laterally over 2.5 km (Parize and Friès, 2003). Sill thickness decreases away from the source (**Fig. 5**). Laterally, sill thickness can vary when dykes become connected, resulting in additional sand supply (**Fig. 8F**). A multi-layered sill network rapidly develops away from the source (**Fig. 5**). The sill network frequently presents dykes connecting sills between each other, thus forming a dyke-sill system referred to as “stepped sills” (Hurst et al., 2011). The sill network is very chaotic and sometimes difficult to laterally track. The chaotic pattern of the injectite

network may result from the slumped deposits being cross-cut by the network, leading to a tortuous fractured system that will influence hydrofracture geometries (Parize et al., 2007a). Sand injected within the sills displays similar grain-size ($d_{50} = 106\mu\text{m}$) and a similar mineralogical composition compared to the turbidite.

4.2.2. Dykes

Dykes mainly occur as connections between sills (**Figs. 5, 8F**). Single dykes propagating downwards are occasionally observed below the turbidites, and are low- to high-angle and generally straight (**Fig. 8G**). Dykes affected by ptygmatic folding frequently occur (**Fig. 8H**).

Dykes that are part of the sill system can reach 4 to 5 m in width and up to 4 m long while single and isolated dykes are generally up to 0.5 m wide and 3 m long (**Fig. 5**). Sand injected within the dykes displays similar grain-size ($d_{50} = 109\mu\text{m}$) and composition than the associated parent bed and sills.

5. Macro-to microscale internal structures

Injectites are characterized by homogenized sand, however internal structures formed during hydrofracturing and injection are observed. Other structures observed in the injectites postdate injection and are related to porewater movement and compaction. These structures can be deciphered at both macro- and microscopic scales.

5.1 Structures formed during hydrofracturing/injection

5.1.1. At the injectite margin

Marls in contact with the injectites are occasionally deformed. Zones affected by the deformation never exceed one m wide. In the vicinity of dyke margins, marls are slightly deformed downwards or upwards or even verticalized (**Fig. 9A, B**). Along injection, ball-structures locally developed within the marls (**Fig. 9C**). Below few sills, low-angle S-C planes paralleling the sense of hydrofractures propagation occasionally occur (**Fig. 9D**). These structures are constrained to a 0.1 m thick zone below sills. The base of sandstone sills sometimes displays crenulations, resembling flute casts, and

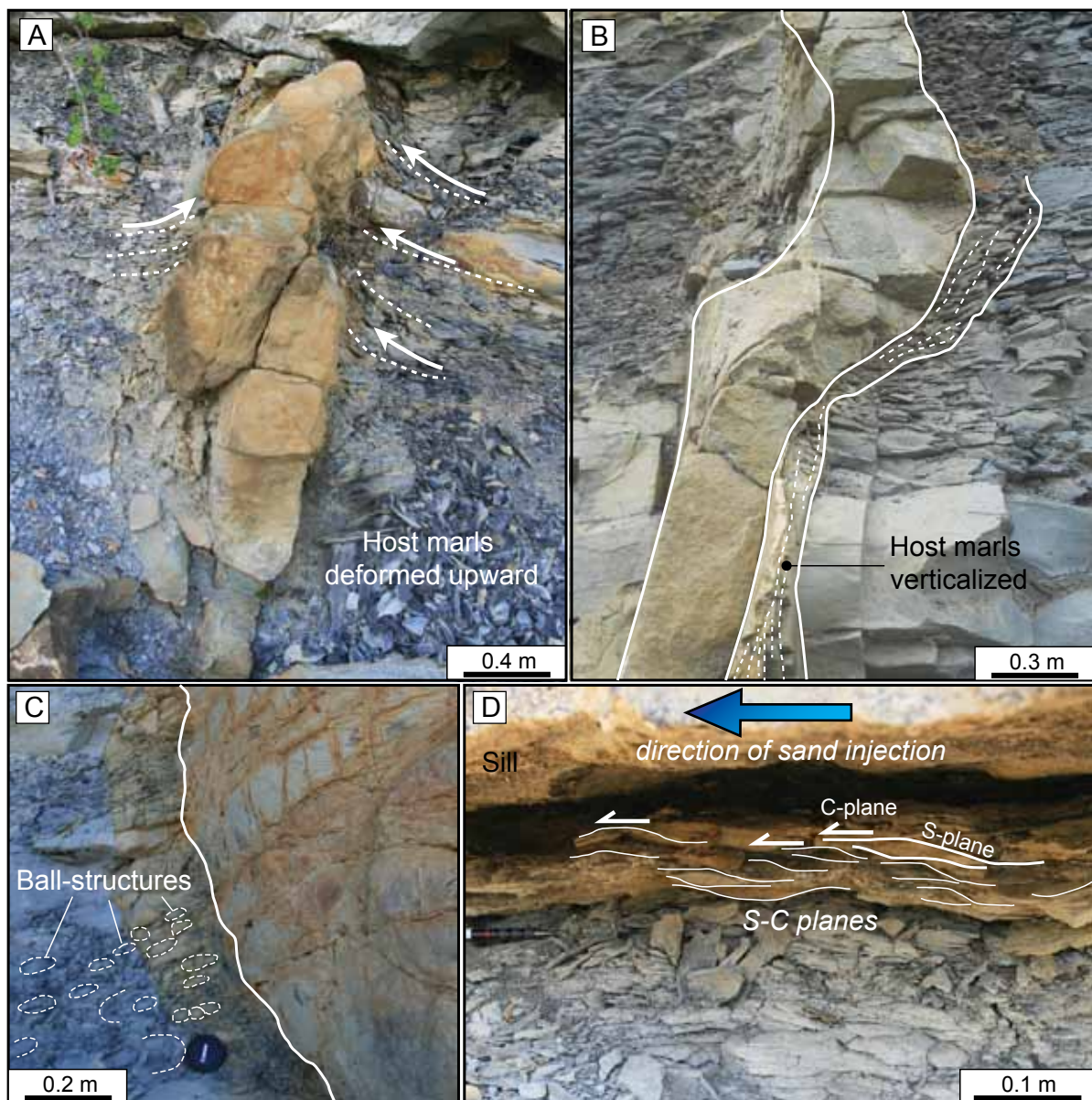


Figure 9. Deformation of the encasing “blue marls” Formation along injectite margins. (A) Upward deformation of marls in the vicinity of a high-angle sand dyke. (B) A narrow fringe of verticalized marls occurring at the dyke margin. (C) Ball structures affecting marls along the margin of a sand dyke. (D) Marls display S-C-like structures paralleling direction of sand injection in the overlying sill. Cf. location of photographs on the outcrop on Figures 4 and 5.

paralleling the direction of sill propagation (**Fig. 10A**).

Deformations along dyke margins are common in injectite networks and have been interpreted to be the result of the stress exerted on the encasing sediments during the injection phase (Rowe et al., 2002; Kane, 2010). Marls in contact with dykes are either deformed upward or downward, suggesting that sand injection can occur in either upward or downward directions. Hydrofracturing geometries and directions of propagation are governed by stress states and overpressure conditions during seal failure (Jolly and Lonergan, 2002). The combination of *per ascensum* and *per descensum* sand injections illustrates the complexity of these injectite networks and probably implies that the entire network developed during several hydrofracturing and sand injection phases. The deformation of marls in the

vicinity of dykes has alternatively been attributed to the pillar effect played by sandstone dykes during marls compaction (Hiscott, 1979; Parize, 1988). At the dyke margins, the occasional occurrence of ball-structures suggests that they are related to the adjacent injectite. Similar ball-structures have been interpreted as the result of fluid pressure increase in sediments or could alternatively represent localized diagenetic features due to the nearby sand injection (Ravier et al., 2014). S-C structures observed below few sills indicate deformation of the marls by simple shear (Passchier and Trouw, 2005, Denis et al., 2010). In addition, the low angle displayed between the S and C planes suggests that simple shear deformation operated in conjunction with a relatively high strain rate (Choukroune et al., 1987). The sense of shear (deduced from S-C structures) parallel direction of injection of the overlying sill, indicating that shear stress is likely triggered by sand being laterally injected within horizontal hydrofractures. Crenulations with crests paralleling the direction of sill propagation represent flow-induced structures recording processes of sand injection into hydrofractures (Kane, 2010).

5.1.2. Inside injectites

Sand injected into hydrofractures is homogenized due to the fluidization processes commonly associated with clastic injections, implying a general lack of internal structures (Jolly and Lonergan, 2002). However, few structures remaining from the hydrofracturing/injection phase can be observed. Marly and limy clasts are frequently observed within dykes and sills. Clasts vary from mm to m in size and are generally very angular and elongated (**Fig. 10B, C, D, E**). Clasts are sometimes isolated but can also be locally clustered forming a breccia-like fabric (**Fig. 10C**). Clasts generally display preferential imbrications, with their long axis paralleling the dyke margins. At the microscale, clasts contain frequent embedded quartz grains (**Fig. 10E**). Mudstone clasts are sometimes cut by sandstone-filled mm-wide microfractures (**Fig. 10D**).

Clasts detached from the encasing hemipelagic deposits are evidence of host strata erosion during sand injection. The occurrences of mudstone clasts within injectites are very common (Kawakami and Kawamura, 2002; Scott et al., 2009). The formation of such clasts results from the corrasion, scouring, and fracturing of the margin during injection of the fluidized sand (**Fig. 10F**).

Clast imbrications suggest sustained periods of traction occurring during sand injection within the hydrofractures (Kawakami and Kawamura, 2002). Embedded quartz grains observed in clasts

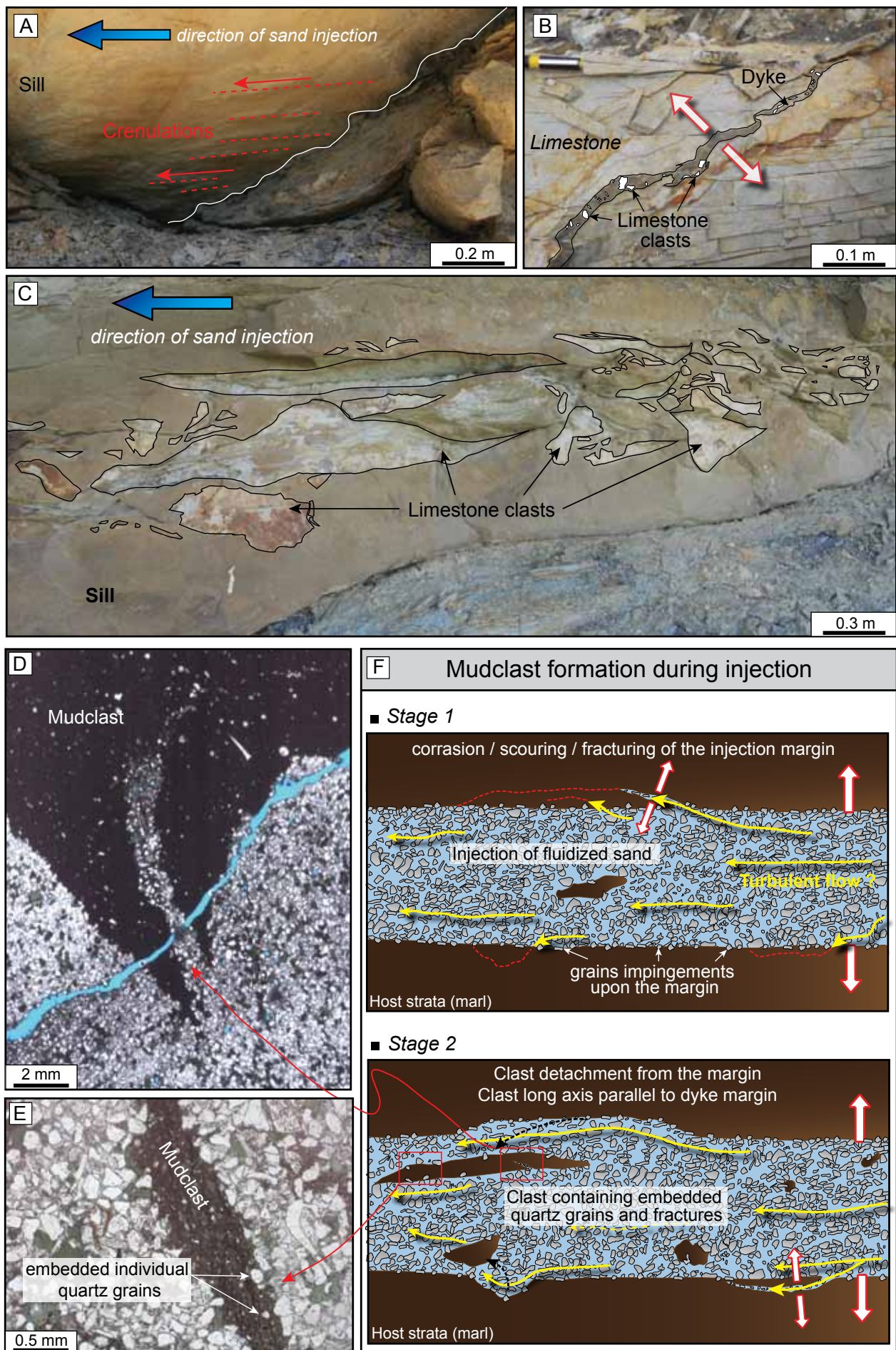


Figure 10. (A) Crenulations, resembling flute-like structures, observed at base of a sill in Rosans. (B) Angular limestone clasts (in white) observed within a dyke and ripped off from the encasing limestone strata. (C) Large and angular limestone intraclasts in a sill displaying a preferential imbrication parallel to the margin of the injectite. (D) An intraclast observed in thin section, displaying a microfracture infilled by fine-grained sand. (E) An intraclast containing embedded quartz grains floating in an injectite. (F) Formation of mudstone intraclasts during injection of fluidized sand into hydrofractures. Stage 1: during injection, a turbulent flow triggers corrasion, scouring, and fracturing of the injection margins. As a result of margins erosion, fragments of host strata are ripped off. In addition, during injection, the turbulent flow leads to grain impingements along the margins as evidenced by embedded quartz grains within intraclasts. Stage 2: when sand is injected into hydrofractures, detached clasts tend to become imbricated parallel to the direction of injection. Cf. location of photographs on the outcrop on Figures 4 and 5.

illustrate processes of grains impingements upon the injection margins at high velocity and at non zero angles (Scott et al., 2009). Intraclast microfractures infilled by sand record the fracturing phase affecting the dyke margins before the detachment of larger clasts from the host marls (**Fig. 10D, F**). Corrasion along the dyke margins and quartz grains impingements during injection of the fluidized sand may indicate that the fluid motion throughout hydrofractures is associated with sand grains suspended in a turbulent flow (Allen, 1982; Scott et al., 2009).

5.2. Internal structures induced by early variations in porewater pressure

Elutriation bands are occasionally observed in injectites, principally within dykes. These structures, up to 5 cm wide and up to 1 m long, are characterized by vertical conduits enriched in clay-size particles. Elutriation conduits display a wide range of geometries including straight, anastomosed, or branched conduits (**Fig. 11A, B**). Locally, complex networks of clay conduits locally mimic dish structures that generally display a high clay content (**Fig. 11C**).

At the microscopic scale, these elutriation bands display relatively straight or slightly diffused margins and contain quartz grains that have their long axis preferentially reoriented parallel to the orientation of the elutriation conduits (**Fig. 11D**).

Elutriation processes postdate the injection of sand as fluidized material will tend to homogenize the material without preservation of preferential water escape conduits (Scott et al., 2009). The localized post injection increase of porewater pressure illustrated by elutriation structures implies that clastic injections are still unlithified. These structures may be triggered by stresses exerted on water-saturated sand by overburden pressure or/and by sand compression during margins retractions once injection ceased. This increase of porewater pressure is naturally associated with minor water escapes segregating clay-size particles that are preferentially remobilized along vertical conduits (Lowe and LoPiccolo, 1974). Elutriation bands are generally parallel to the dyke margins and are combined with

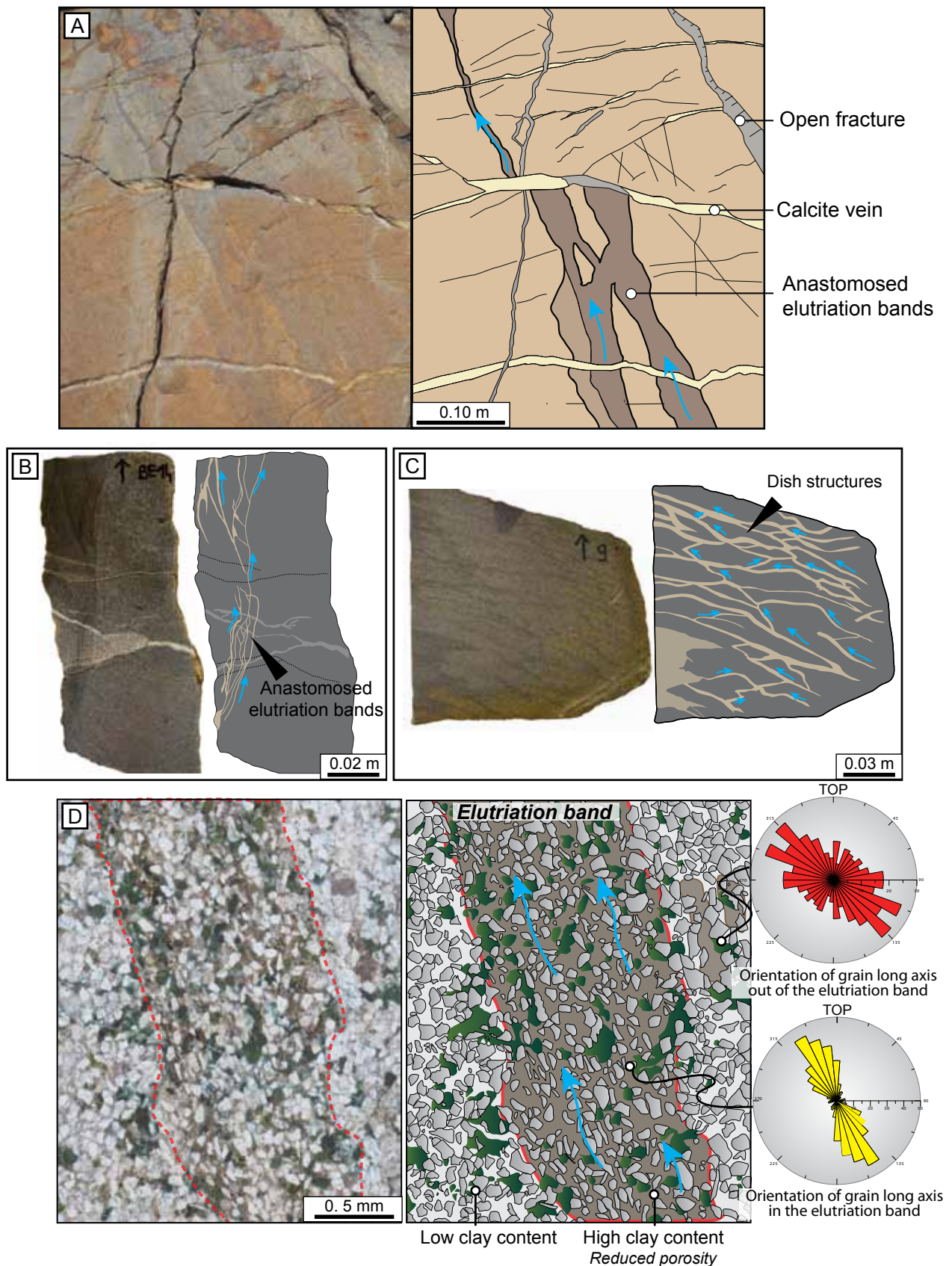


Figure 11. Internal structures related to porewater movement within injectites. (A) Vertical and anastomosed elutriation bands observed at the macroscale in a sandstone dyke. Blue arrows indicate directions of water-escape paths. (B) Polished section of a sample collected within a sandstone dyke showing an anastomosed network of elutriation bands. (C) Complex network of elutriation structures mimicking dish structures observed in a sand dyke. (D) An elutriation band observed at the microscale where grains embedded within the band are characterized by a preferential subvertical orientation paralleling the margins. The red and yellow rose diagram corresponds to orientation of grain long axis out and within the elutriation band respectively. Cf. location of photographs on the outcrop on Figure 4.

grain reorientations due to porewater movement during localized dewatering.

5.3. Structures induced by compaction

Deformation structures related to the compaction of sand are observed within sandstone injections, predominantly within dykes. Dykes are occasionally deformed inducing cm to dm ptigmatic folds (**Fig. 8H**). At the margin of low-angle sandstone dykes and few sills, step normal faults with mm to cm-scale offsets and undulating fault planes occasionally occur (**Fig. 12A**). High-angle dykes are sometimes affected by 2 mm-wide bands occurring parallel to each other, or displaying a dihedral pattern with sets of conjugate bands showing an angle between 30° and 45° with the dyke axis (**Fig. 12B, C**). At the microscopic scale, these bands are characterized by a significant grain-size reduction, cataclased grains and authigenic micro-quartz cements (**Fig. 12D, E**). Except few grains exceeding 100 µm, grains are smaller than 50 µm along the band axis (**Fig. 12E**).

Ptygmatic folds occur because of the mechanical response of dykes to compaction (Parize et al., 2007b). Assuming that the mechanical compaction of sand is negligible, ptygmatic folds formed as a response to marls compaction during burial, implying that clastic injections had to deform preferentially to counterbalance the reduction of marls thickness (Parize et al., 2007b).

Step normal faults with undulating fault planes occurring at the margin of low-angle dykes are related to hydroplastic deformations triggered by a vertical stress. Such fault patterns have been associated to pure shear due to overloading (Guiraud et al., 1987; Denis et al., 2010). In this context, the lithostatic stress exerted by the overlying “blue marls” Formation represents the trigger for early faulting of the unlithified sand intrusions.

Bands characterized by grain-size reduction, grain cataclasis, and microquartz cementation correspond to deformation bands (sensu Aydin, 1978). The significant grain cataclasis occurring along the deformation bands indicates that they correspond to cataclastic deformation bands (Fossen et al., 2007). Grain cataclasis is triggered by the localized abrasion, crushing, and fracturing of quartz grains along discrete shear bands (Borja and Aydin, 2004). Such processes promoting grain cataclasis are reflected by the intense grain-size reduction along the bands. Conjugate sets of deformation bands may indicate pure-shear enhanced bands induced by compaction, indicating that they formed in conjunction with a vertical stress related to the overburden pressure (Eichhubl et al., 2010). The relative drop of fluid pressure once injection of the fluidized sand ceased triggered collapse of the grain framework

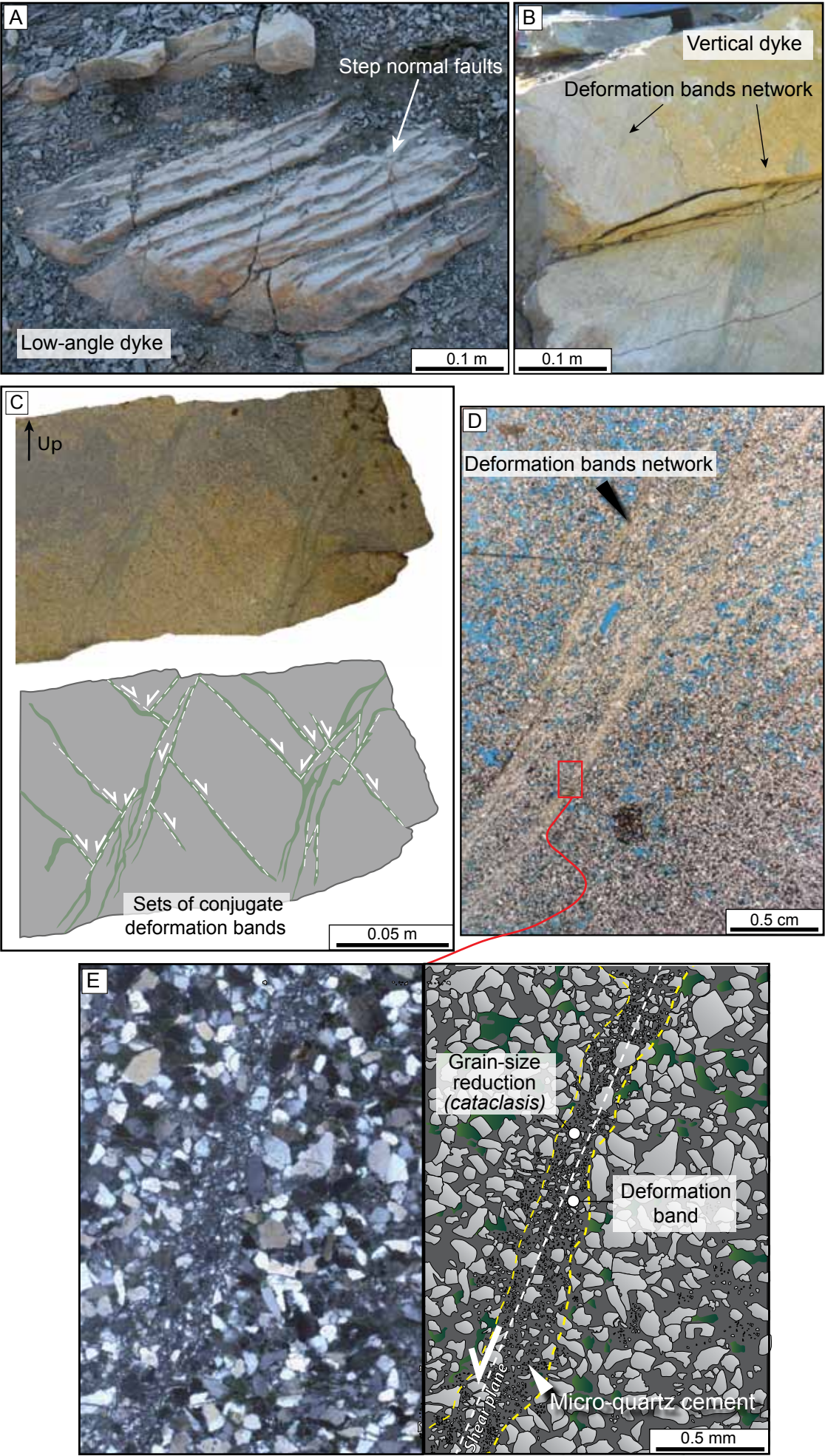


Figure. 12. Internal structures related to sand compaction induced by overburden pressure. (A) Step normal faults with undulating fault planes observed at the top of a low-angle sandstone dyke. (B) A pattern of parallel deformation bands observed within a high-angle sandstone dyke. (C) Polished section displaying conjugate sets of deformation bands. (D) Close-up on deformation bands. Bands are characterized by narrow zones where a significant grain-size reduction related to cataclastic processes is observed. (E) Detailed deformation bands where grain-size reduction and microquartz cement is observed. Cf. location of photographs on the outcrop on Figure 4.

(Jonk et al., 2005b; Parize et al., 2007a). Once grain framework collapsed, grains were subject to the lithostatic weight resulting in the onset of numerous compaction-induced shear planes (Ballas et al., 2013). These structures related to early compaction are only observed within some high-angle dykes, indicating that the drop of fluid pressure invoked as a trigger for the formation of shear planes did not affect the entire clastic injection network. This reveals that fluid pressures within sand, once injection ceased, were characterized by a heterogeneous distribution at outcrop scale, resulting in heterogeneous sand compaction rates and subsequent heterogeneous distributions of compaction-induced structures. Authigenic microquartz cements formed in the axis of the bands are related to pressure-solution processes enhanced by deformation. The cementation occurs preferentially along deformation bands, during or more commonly after deformation ceased, and is promoted by fresh and highly reactive surfaces formed during abrasion and crushing of quartz along shear planes (Fossen et al., 2007). Parallel bands (cf. **Fig. 12B**) could illustrate the successive formation of new cataclastic bands when the nearby band experienced cementation and local lithification while stresses exerted on the dykes remained active (Lucas and Moore, 1986).

5.4. Secondary injections

A 0.2 mm wide clayey injection containing several floating quartz grains has been observed within a vertical dyke (**Fig. 13A, B**). This mm-sized clayey dyke is high-angle, straight and displays sharp margins with the host sandstones. Grain cataclasis and microquartz cements are observed on both sides of this micro-dyke (**Fig. 13A, B**), indicating that the clayey injection propagates inside a cemented cataclastic deformation band (cf. section 5.3 for descriptions of processes involved in the development of cataclastic deformation bands). This clay injection implies that the deformation band has been reopened by hydrofracturing. After hydrofracturing, clay particles were flushed out and injected within the fracture (**Fig. 13C**). This episode indicates that porewater pressure remained high after sand injection and early sand compaction. The propagation of this late hydrofracturing phase was promoted by the occurrence of deformation bands, representing internal planes of weakness. The

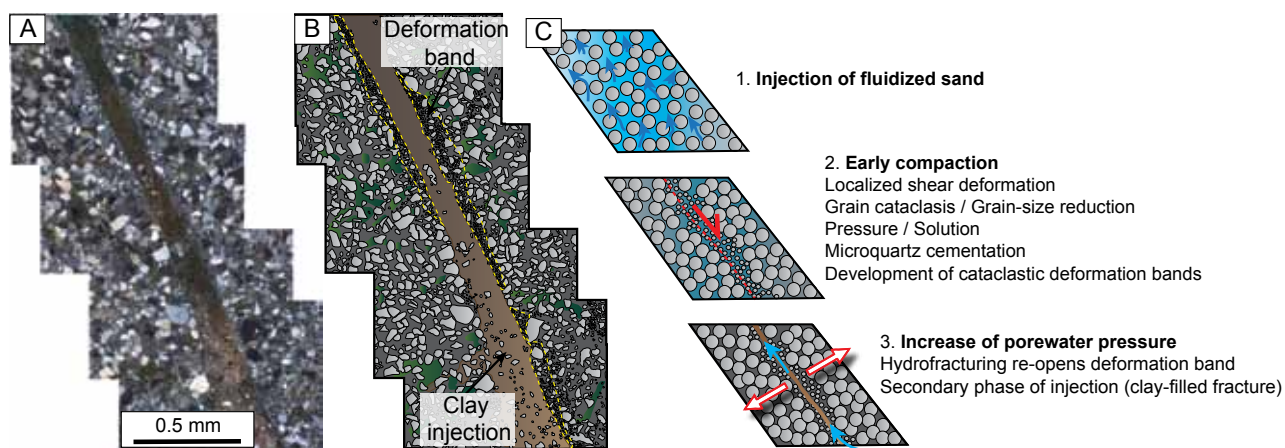


Figure 13. (A) (B) Photograph and associated interpreted sketch of a subvertical clay injection along a deformation cataclastic band within a clastic dyke. The deformation band is used as a preferential plane of weakness for the development of this second phase of injection. (C) Model for the development of a secondary injection forming clay veins within sand injectites. Cf. location of photographs on the outcrop on Figure 4.

late porewater pressure increase could be related to the lithostatic pressure increase during burial or/ and water input with the intrusive sand resulting from host marls dehydration or water transmitted to the sand injection through syn-sedimentary faults (Monnier, 2013).

5.5. Chronology of early deformations in sand injections

All the structures previously described correspond to deformational processes affecting the early evolution of the granular media. Cross-cutting relationships between these different structures allow to reconstruct the relative chronology of the early phases of sand deformation modifying injectite internal structures (**Fig. 14**).

The first stage corresponds to hydrofracturing (Porewater Pressure (PWP) $> \sigma_h$) of the “blue marls” Formation, followed by the injection of fluidized sand (**Fig. 14A**). This episode is generally associated with deformation of the encasing marls (i.e., upward/downward marls deformations at dyke margins, S-C planes along sill margins) and occasional crenulations at the base of sills. During injection, the fluidized sand behaves as a turbulent flow which is capable to trigger corrosion, scouring, and fracturing of the injection margins, resulting in the formation of intraclasts imbricated parallel to injection margins. During the injection, grains impingements upon the margins are also common as illustrated by the numerous quartz grains embedded within intraclasts. Once injection ceased, local porewater increase promoted by the combined action of lithostatic weight and margin retractions, triggers upward flushing of clay particles forming elutriation bands and dish structures (PWP $>$

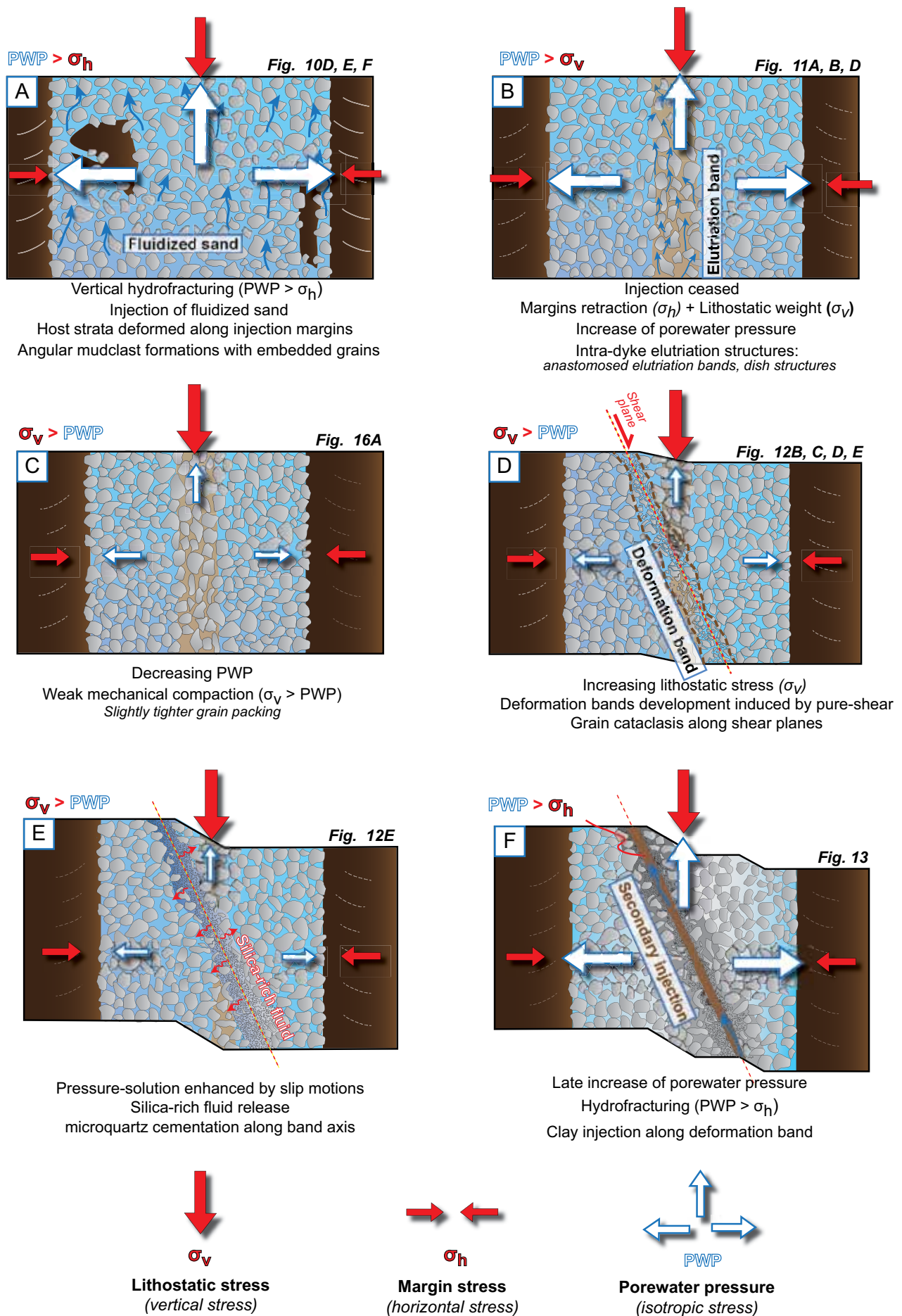


Figure 14. Chronology and processes involved in the formation of early structures affecting the intruded sand.

σ_v) (**Fig. 14B**). After these early elutriation processes, the increase of lithostatic stress induced by progressive burial leads to minor sand compaction and slight decrease of the pore volume ($\sigma_v > \text{PWP}$) (**Fig. 14C**). Within dykes, the increase of vertical stress due to the overburden pressure will enhance development of parallel to dihedral compaction-induced shear planes ($\sigma_v > \text{PWP}$). This will tend to develop bands where grain-size is reduced due to grain cataclasis along shear planes (**Fig. 14D**). Along these deformation bands, pressure-solution processes enhanced by freshly crushed quartz grains lead to localized authigenic microquartz cementation (**Fig. 14E**). In the early stages of clastic injection deformation and remobilization, injections remain unlithified. In this configuration, episodes of porewater pressure increase can potentially trigger a secondary phase of hydrofracturing affecting the internal structure of sand injections ($\text{PWP} > \sigma_h$). This episode is evidenced by the occurrence of a clayey vein being injected within a deformation band (**Fig. 14F**). The early deformations and diagenetic imprints observed in sand injections have an impact on the evolution of porosity that will be later discussed.

6. Diagenetic sequence

Given the broadly similar diagenetic successions in Rosans and Bevens areas, we will describe thereafter a single diagenetic sequence. Cross-cutting relationships between the different diagenetic structures allow to reconstruct the relative chronology of the diagenetic phases. The diagenetic sequence, subdivided in 7 phases and described in their order of appearance, is as follows (**Fig. 15**):

(1) The first phase corresponds to compaction (mechanical and chemical) of the glauconite-rich sand composing the clastic injections (**Fig. 15.1**). Mechanical compaction is evidenced by deformation of glauconites and mud intraclasts. These ductile clasts tend to rapidly deform during compaction and occur in association with quartz grains, leading to ductile lithic grains deformation and grains diffusion into free pore spaces (Pittman and Larese, 1991; Ali et al., 2010). The chemical compaction highlighted by interpenetrating quartz grains also occurs (**Fig. 16A**), and results from pressure/solution processes induced by intergranular pressures during compaction (Bjorkum, 1996; Yang, 2000).

(2) The second phase corresponds to localized microquartz cementation (**Fig. 15.2**). Intergranular microquartz cements are observed within approximately 10 % of the collected samples (**Fig. 16B**). Most of the samples containing microquartz cements are associated with deformation bands (**Fig. 12E**). Near deformation bands, microquartz cements result from pressure/solution processes and are

promoted by fresh and highly reactive surfaces formed during abrasion and crushing of quartz along shear planes (Fossen et al., 2007). Silica-rich fluids released during chemical compaction of quartz grains also lead to localized development of microquartz cements.

(3) The third phase corresponds to quartz overgrowths (**Fig. 15.3**). Quartz overgrowths affect approximately 5 % of the collected samples and are generally limited to few grains. Syntaxial overgrowths are generally inferior to 10 μm thick and do not cover the entire grain perimeters (**Fig. 16C**). It is assumed that temperatures of solution required to form quartz overgrowths must be superior to 70°C to 80°C (Ajdukiewicz and Lander, 2010), however diagenesis analyses of clay mineral in bentonites have demonstrated that the “blue marls” Formation burial temperature did not exceed 80°C (Dauphin, 2002). High porewater pressures maintained within sediments may lower the minimum temperature required to form quartz cement overgrowths (Wilson and Staton, 1994). Processes of hydrofracturing and injection are associated with very high porewater pressures and the encasing impermeable marls maintain high fluid pressure conditions, possibly promoting shallow formation of quartz overgrowths.

(4) The fourth phase represents the pervasive phase of cementation affecting both depositional sandstones and associated injectites mapped in the Vocontian Basin. The blue stain produced by alizarin-potassium ferricyanide solution enhanced the visualization of a Fe-rich blocky calcite (**Figs. 15.4, 16D**). Similarly, the non-luminescent brown to dull red character of intergranular cements in cathodoluminescence microscopy illustrates the occurrence of a single phase of calcite cementation infilling all the pores (**Fig. 16E**). The carbonate source responsible for the emplacement of the blocky calcite results from the release of Ca-rich fluids during compaction of the encasing host strata (e.g., marl/limestone alternations). Injectites are generally thinner than parent beds (e.g., turbidite sandstones) implying that they probably become more quickly cemented by calcite (Jonk et al., 2005b).

(5) The rim of quartz grains occasionally displays optical birefringences related to quartz corrosion (**Fig. 15.5**). The outer corroded margins are generally irregular and totally or partially surround the grain (**Fig. 16F**). Quartz grains are corroded and replaced by calcite cements during the pervasive phase of carbonate cementation (Ali et al., 2010). This is notably due to the opposite pH condition of precipitation/solution of carbonate and silica. This phase of corrosion is certainly contemporaneous to the formation of the blocky calcite (phase 4).

(6) Abundant veins infilled by fibrous carbonate cements cross-cut all diagenetic phases previously

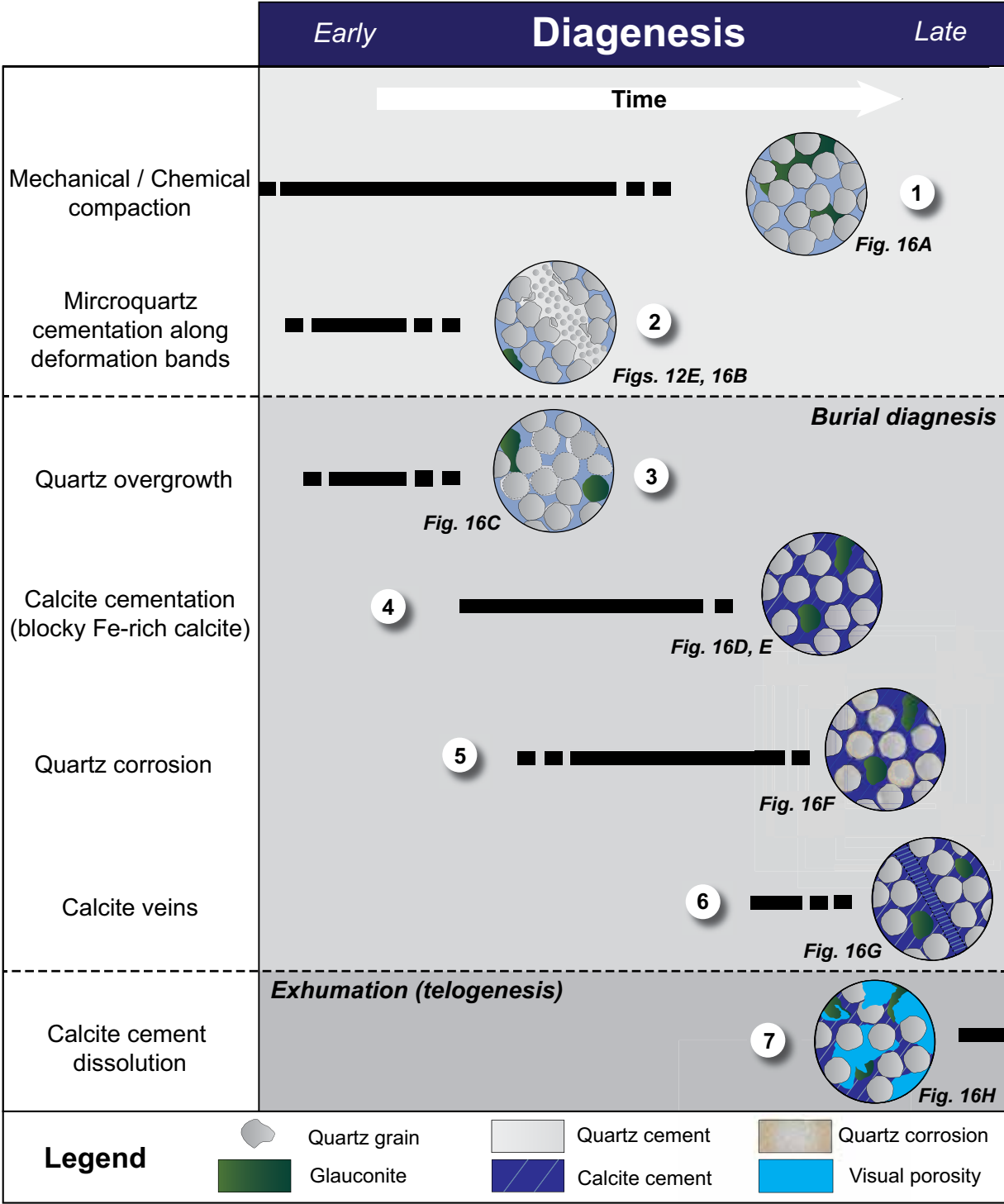


Figure 15. Generalized diagenetic sequence for the Aptian-Albian sandstones, including parent beds and injectites.

described (Fig. 15.6). The blue stain evidence by alizarin-potassium ferricyanide solution highlights a Fe-rich calcite (Fig. 16G). Calcite veins are straight to slightly undulating and their thickness vary from mm to cm. These veins related to brittle fracturing indicate that lithified injectites can be reactivated as fluid conduits (Ca-rich fluid circulation) during tectonic deformation.

(7) The last phase affecting the injectite network corresponds to telogenesis during exhumation of the “blue marls” Formation (Fig. 15.7). Numerous samples are affected by dissolution evidenced by voids

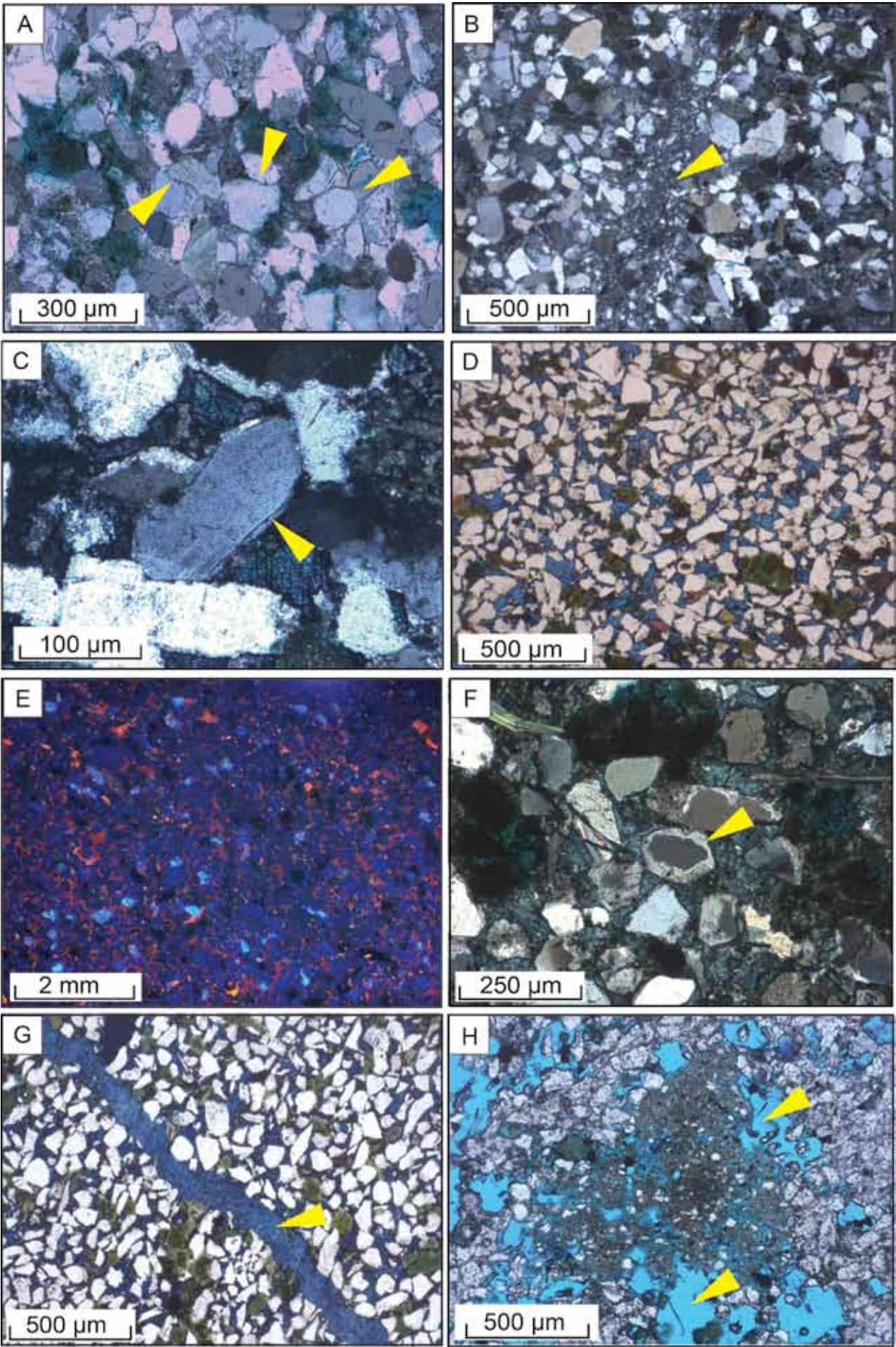


Figure 16. Photographs illustrating the different phases involved in the diagenetic sequence. (A) Chemical compaction evidenced by interpenetrating quartz grains. (B) Localized emplacement of microquartz cements along cataclastic deformation bands. (C) Quartz overgrowth illustrated by quartz cements growing in optical continuity with the involved quartz grain. (D) Fe-rich blocky calcite evidenced by blue stain. (E) Non-luminescent brown to dull red character of intergranular calcite cement in cathodoluminescence microscopy. (F) Quartz grains affected by corrosion during emplacement of the calcite cement. (G) Veins infilled by Fe-rich calcite. (H) Dissolution of glauconites and carbonate cements evidenced by numerous blue voids (blue dye).

infilled by blue dye (**Fig. 16H**). The calcite cements and glauconites are preferentially affected by dissolution. The recent dissolution by meteoric water is the major porosity-forming process affecting sandstones in this study. Although dissolution processes affect the entire sand network, turbidites are preferentially affected by the dissolution of cements. This dissolution gradient could be explained by the larger size of turbidites that tend to be not entirely cemented, thus favoring meteoric fluid circulation and subsequent dissolution. Large turbidites may probably be preferentially cemented by carbonate in proximity to their contacts with the host blue marls. The contact between the sandy turbidites and the blues marls may enhance fluid flux along the bedding compared to across bedding, thus creating a carbonate cemented rim (Scott et al., 2013). As a consequence the inner part of the turbidites that is less pervasively cemented is subject to abundant meteoric fluid circulations.

7. Petrophysical characteristics of the injectite networks.

7.1. Mercury porosity vs. minus-cement porosity.

Mercury intrusion porosimetry measurements have first been conducted on 10 injectites samples. The resulting values display a wide range of porosity varying from 1.5 % to 23%. Thin sections and rock samples corresponding to these mercury porosity measurements were analyzed and showed very different degrees of dissolution as evidenced by significant variations in blue void percents (2 to 30%). Collected samples have been differentially subject to telogenesis as shown by samples 1 to 3 (**Fig. 17**), where a range of mercury porosity values induced by various cement dissolutions is illustrated. As a consequence, direct estimations of porosities give petrophysical information on the modern granular structuration, which is principally controlled by recent telogenetic processes. However, knowing the characteristics of the diagenetic sequence, minus-cement porosity values can be estimated and have a greater significance in the present study where the evolution of porosity wants to be characterized. The carbonate cementation phase affecting turbidites and injectites represents the

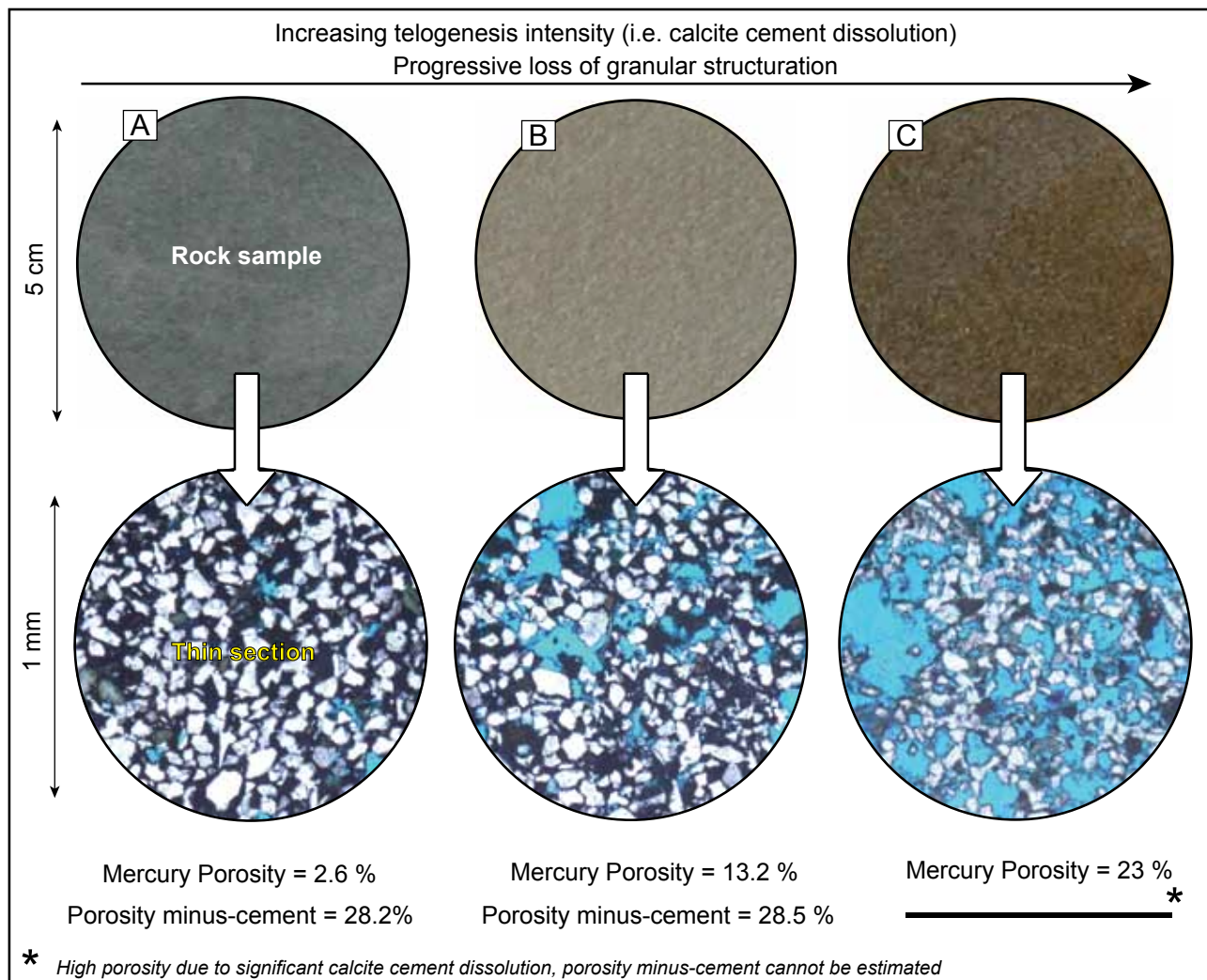


Figure 17. Three samples illustrating the range of mercury-porosity values and blue voids contents and the associated minus-cement porosity values (A) A sample characterised by low modern porosity (2.6%) illustrated by the low blue voids percent and the grey color of the associated rock sample. (B) A sample characterised by moderate modern porosity (13.2%). The increase of porosity is illustrated by higher blue voids content and the yellow brownish rock sample indicating alteration during exhumation of the injectite. (C) A sample characterised by elevated modern porosity (23%). This increase is evidenced by the associated rust-colored rock sample (i.e., high alteration) and the very high blue voids volume. Modern porosity is greatly influenced by post-exhumation dissolution processes and therefore disrupt the original signal represented by minus-cement porosities.

single and pervasive phase infilling free pores after weak compaction and at relatively low burial depth, implying that true minus-cement porosities can be investigated (Jonk et al., 2005a). Minus-cement porosities (i.e. precementation porosities) correspond to the porosity before sand lithification, allowing to estimate original porosity values (i.e., once sand was injected into hydrofractures) (Jonk et al., 2005a; Scott et al., 2013).

7.2. Minus-cement porosity values

7.2.1 Injectites

The 58-collected injectite samples in the Bevens area display an average of 26.5 % minus-cement porosity with a 5.7% standard deviation (sd). The 44 injectites sampled in the Rosans area display slightly higher porosities with an average of 31.6% and higher dispersions from the average (sd = 11%) (**Fig. 18A, B**). Mean precementation porosities between Rosans and Bevens are not statistically different ($p = 0.99$) (**Fig. 18 C, D**).

7.2.2. Dykes and sills

In Bevens, dykes ($n = 38$) show a 26.7 % minus-cement porosity average and 5.7% standard deviation while dykes measured in Rosans display a higher porosity average with 33.9% and a standard deviation of 10.3%. Dyke porosities in Bevens are not statistically different to dyke porosities in Rosans due to elevated standard deviation for the Rosans site (**Fig. 18C, D**).

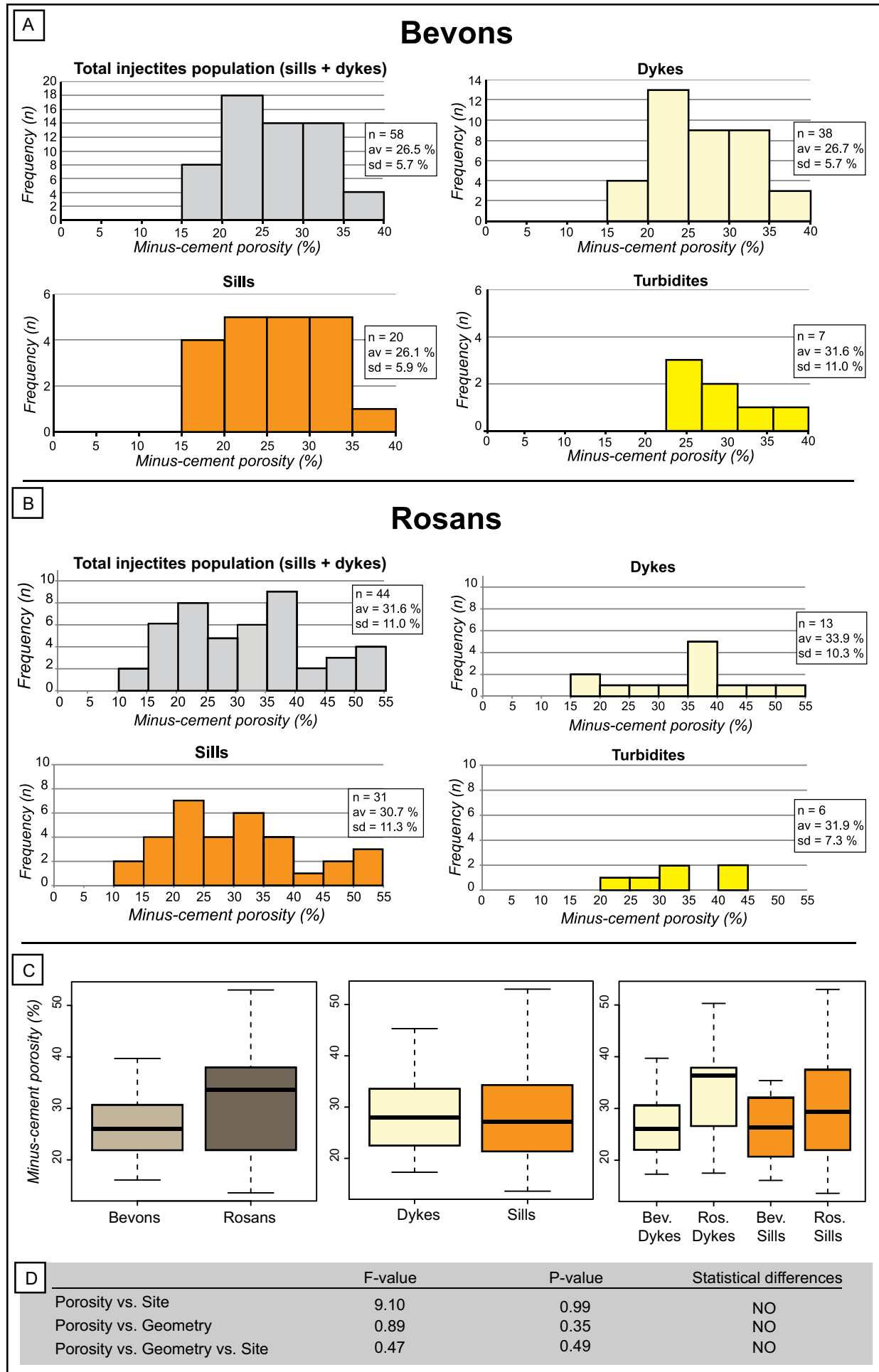
In Bevens, the 20 sills collected are characterized by a 26.1 % porosity average with a 5.9 % standard deviation, while the 31 sills sampled in Rosans display a 30.7% porosity average and a high dispersion of values (sd = 11.3%). Similarly to dykes, there is no site effect (Bevens vs. Rosans) on sill precementation porosities ($p = 0.49$) (**Fig. 18C, D**).

According to our results, averaged porosity values of dykes and sills collected in both sites are not statistically different ($p = 0.35$) and display very similar porosity averages (27-28%) (**Fig. 18D**).

7.2.3. Parent beds

Although the amount of collected samples in turbidites are reduced ($n = 13$) due to the significant cement dissolution of parent beds, minus-cement porosities are similar for both sites with an average of 31.6 % and 31.9% for Bevens and Rosans, respectively (**Fig. 18A, B**).

Figure 18. Distribution of minus-cement porosity values of injectites (sills + dykes), dykes, sills, and turbidites successively for Bevens (A) and Rosans (B). (C) Box plots with minus-cement porosity plotted against site, injectite geometries, and combined injectite geometry and site. (D) Analyses of variance (ANOVA) realized between sites, injectite geometries, and combined injectite geometries and sites. No statistical differences are observed within the tested groups.



7.3. Parameters controlling the distribution of minus-cement porosity values

Several parameters potentially controlling the geographical distribution of early petrophysical properties have been statistically tested. The effect of these parameters on petrophysical characteristics has been highlighted in past studies and includes injectite thickness, distance to parent bed, dyke dip angles, and the relative vertical distance to parent bed vs. minus-cement porosity values (Scott et al., 2013). Relations between injectite thickness and distance to parent bed vs. minus-cement porosity will be presented thereafter as they represent the only parameters displaying satisfactory statistical relations.

7.3.1. Injectite thickness

In the Bevens area, injectites are predominantly inferior to 0.5 m thick ($n = 41$). Consequently, for testing the potential influence of dyke thickness on minus-cement porosity, we discriminated injectites < 0.5 m from those that are > 0.5 m (**Fig. 19A**).

Injectites (sills and dykes together) thickness < 0.5 m plotted against minus-cement porosity do not display any statistical trends as demonstrated by the slope of the curve that is not significantly different from 0 ($p = 0.17$), whereas injectites > 0.5 m display a significant statistic trend ($P = 0.027$). Injectites > 0.5 m display a positive correlation with minus-cement porosities ($R^2 = 0.29$) (**Fig. 19B, C**).

When plotting dykes < 0.5 m, a modest but statistically significant trend is observed ($P = 0.005$) and is characterized by a negative correlation with respect to minus-cement porosity ($R^2 = 0.21$). The lack of dykes being > 0.5 m does not permit to draw any conclusions concerning a possible correlation between dyke thickness and porosity. Sills are predominately superior to 0.5 m and display a statistically significant and positive correlation between precementation porosity and thickness ($P = 0.01$; $R^2 = 0.43$) (**Fig. 19E**).

In the Rosans area, injectite thickness plotted vs. minus-cement porosity is characterized by the absence of significant relation ($P = 0.17$). Similarly, when discriminating dykes from sills, the relation thickness vs. minus-cement porosity displays slopes that are not significantly different from 0 and are therefore not statistically correlated (**Fig. 20A, B**).

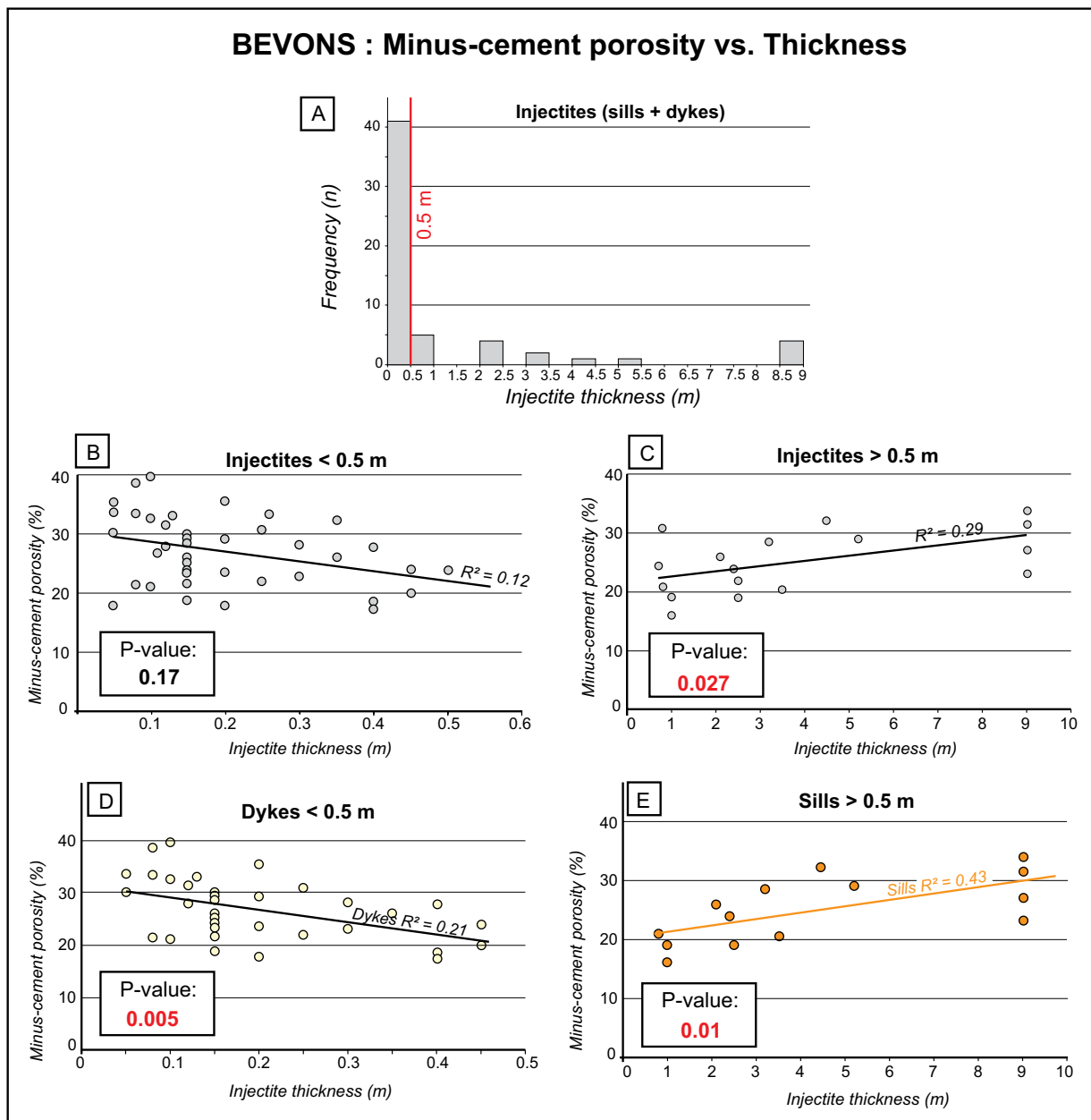


Figure 19. Minus-cement porosity vs. injectite thickness in the Bevens area. (A) Injectite thickness distribution and frequency. Minus-cement porosity is plotted against (B) injectite thickness < 0.5m; (C) injectite thickness > 0.5 m; (D) dykes thickness < 0.5 m; (E) sills thickness > 0.5 m.

7.3.2. Injectite distance to parent bed

In the Rosans area, the clear connection between the turbidite and the injectite network combined with the significant lateral extent (~ 700 m) of this intruded sand system permits to measure the distance separating the collected samples and the source (e.g., parent bed). No statistical relations are found between the distance to the source and the collected samples when mixing dykes and sill precementation porosity values ($P = 0.18$) (**Fig. 20C**). Nevertheless, when segregating dykes and sills, a significant correlation occurs between sill minus-cement porosities and distance to parent bed (P

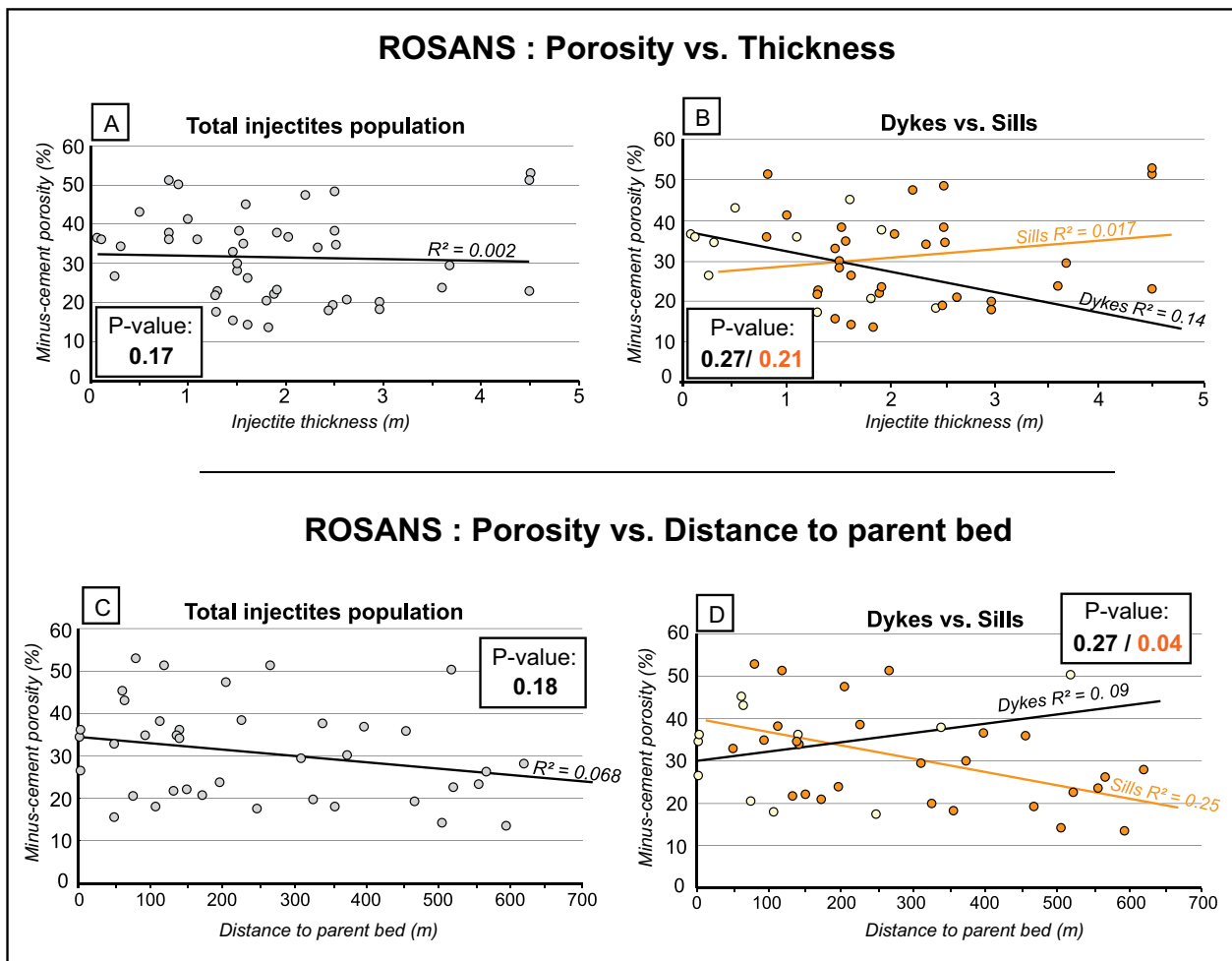


Figure 20. Minus-cement porosity vs. injectite thickness in the Rosans area. (A) Minus-cement porosity (%) plotted against injectite thickness. (B) Minus-cement porosity (%) plotted against sill vs. dyke thickness. (C) Minus-cement porosity (%) plotted against distance to parent bed (i.e., turbiditic channel). (D) Minus-cement porosity (%) plotted against sill and dyke distance to parent bed, respectively.

= 0.04). The negative correlation is characterized by a modest correlation coefficient ($R^2 = 0.25$) but remains the only parameter that has a statistical significance in the Rosans area.

Twelve sill samples collected in the Bevens area are visually connected to the parent bed; distance has been estimated and then plotted vs minus-cement porosity. A modest negative correlation is evidenced ($R^2 = 0.23$) although the P-value is superior to the confidence level fixed in this study ($P = 0.11$).

7.4. Distribution of minus-cement porosity values at outcrop scale

Geographical distributions of precementation porosities have been constructed and interpolation realized using the “inverse distance weighted” method. These interpolations serve to visualize the partitioning of the porosity characteristics at outcrop scale. The “Inverse distance weighted” interpolation method has been selected as it gives greater weights to values closest to the prediction

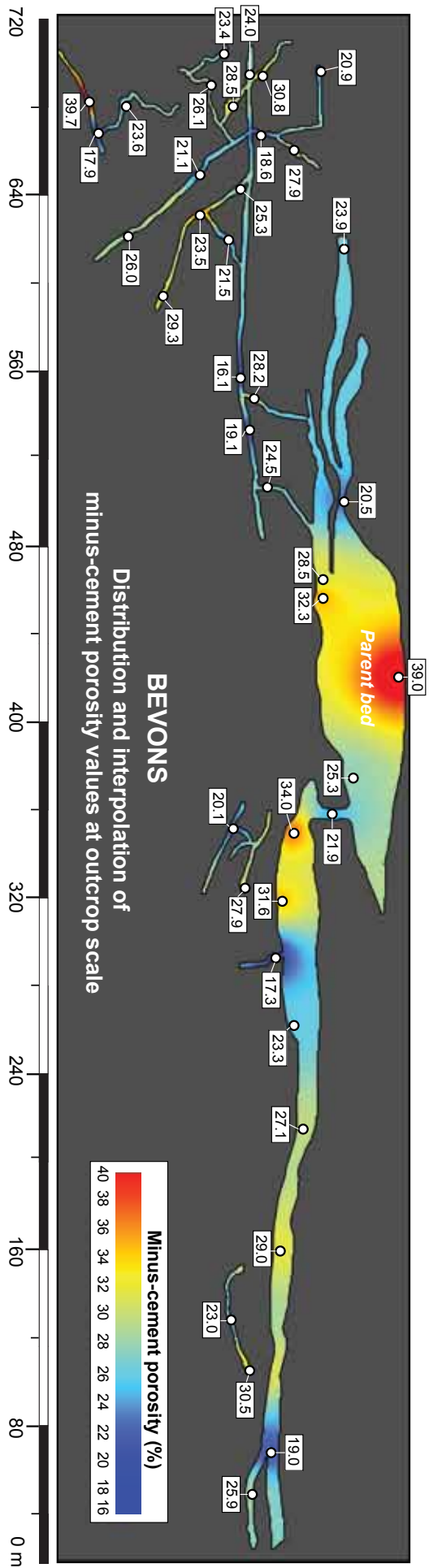


Figure 21. Distribution and interpolation of minus-cement porosity values at outcrop scale along the “Puy Hill” outcrop (Bevons). Interpolation has been established using an “inverse distance weight” interpolation model. The 2D visualization highlights the heterogeneous distribution of the precementation porosities. Cf. dashed line box in figure 4 for position of the present map on the “Puy hill” outcrop.

location, and the weights diminish as a function of distance. These interpolations highlight possible large-scale relations with respect to the distance to parent beds although the complexity of the 3D injectite network underlines a major limitation to the validity of full-field interpolated models. Outcrop scale analyses in Bevons evidence a very heterogeneous distribution of the minus-cement porosity as suggested by parameters previously tested (**Fig. 21**). The heterogeneous minus-cement porosity distributions could be explained by multi-phased sand injections. This model is proposed by Monnier (2013) where fluid excess, triggering overpressure and hydrofracturing, is episodically carried to the parent bed through faults (fault-valve behavior). Each injection phase certainly displays their own characteristics with different porewater pressures, burial depths, geometries, and thickness. These variations of sand injection characteristics can impact initial porosities and mechanical compaction once injection ceased, therefore leading to the heterogeneous distribution of minus-cement porosities observed at outcrop-scale. In addition, the heterogeneous distribution could also reflect the wide range of grain textures and grain packing caused by fluidization (Scott et al., 2009; Hurst et al., 2011). In the Rosans area, the distribution of dykes and sills minus-cement porosity values appears to be heterogeneous without any clear trends (**Fig. 22A**). However, when dykes are removed, minus-cement porosity values display an overall trend of porosity decrease away from the parent bed (**Fig. 22B, C**). Apart from few samples, the first zone displays values that are significantly above the sill porosity average value with several values exceeding 45%. The second zone corresponding to samples collected in the distal part of the injectite network display porosity that are generally inferior to the average porosity with a mean value of 25% (**Fig. 22C**). These results imply that processes ongoing for the development of dykes connecting multi-layered sills promote porosity heterogeneities within the injectite network. Although the sills network displays a lateral trend of porosity decrease, the network appears locally segmented into zones where minus-cementation porosity values vary locally. The occurrence of such zones may suggest that a second generation of sills or dykes developed, locally establishing connections in three-dimensions with the preexisting sill network, thus locally modifying precementation porosities along the outcrop.

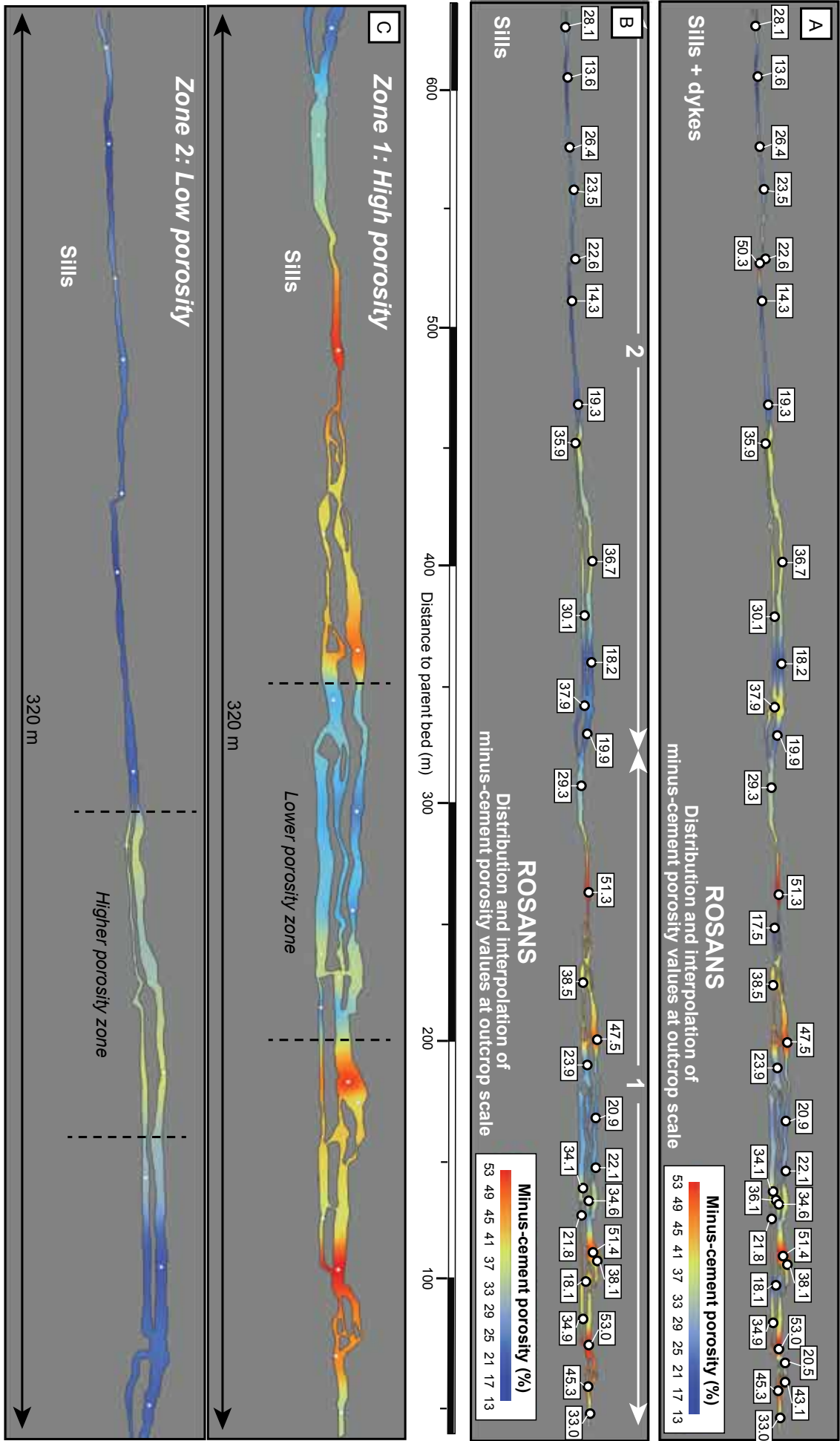


Figure 22. Distribution and interpolation of minus-cement porosity values at outcrop scale along the “Saint-André-de-Rosans” outcrop (Rosans). (A) Minus-cement porosity values collected from both dykes and sills. (B) Minus-cement porosity values collected from sills only. (C) Close up on minus-cement porosity distribution where only values collected from sills are represented. A general trend of precementation porosity decrease is observed away from the parent bed with a proximal zone (zone 1) with averaged high porosities and a distal zone (zone 2) with lower porosity values. Interpolation has been established using an “inverse distance weight” interpolation model. Cf. dashed line box in figure 4 for position of the map on the “Saint-André-de-Rosans” outcrop.

8. Discussion

This section integrates internal structures, diagenetic phases, and values of precementation porosity collected in injectites in order to determine the porosity evolution of the sand injection networks. Minus-cement porosities correspond to porosity values just after sand injection ceased. The chronological emplacement of the different deformation and remobilization structures and the timing of the successive diagenetic phases have been established and permit to approach the evolution of porosity from time of injection to present-day. This evolution permits the opportunity to discuss the potential impact of injectites networks on fluid flows through time.

8.1. Evolution of porosities from time of injection to present-day

8.1.1. High primary porosity inferred from injection processes

These two injectite networks initially result from processes of hydrofracturing and injection of fluidized sand into open fractures when porewater pressure within turbidites became higher than the tensile strength of the host low-permeable marls.

Maximum precementation porosity values calculated for both sites suggest that seal failure and hydrofracturing occurred at different burial depths. When replaced on a typical sandstone compaction curve (depth vs. porosity), the maximum minus-cement porosity value recorded in Bevens indicates that cementation occurred within the first km (~ 0.7 km) (**Fig. 23**). This maximum porosity value recorded in the Bevens area (up to 39.7 %) indicates that sand injections became quickly cemented prior to significant compaction. Bevens is a dyke-dominated system implying that the porewater pressure must exceed the horizontal stress (σ_h) for dykes to form (Jolly and Lonergan, 2002), this configuration requires a significant vertical stress inferred from the lithostatic pressure increase during burial of the parent bed (**Fig. 23A**). The maximum precementation value obtained at the Rosans site

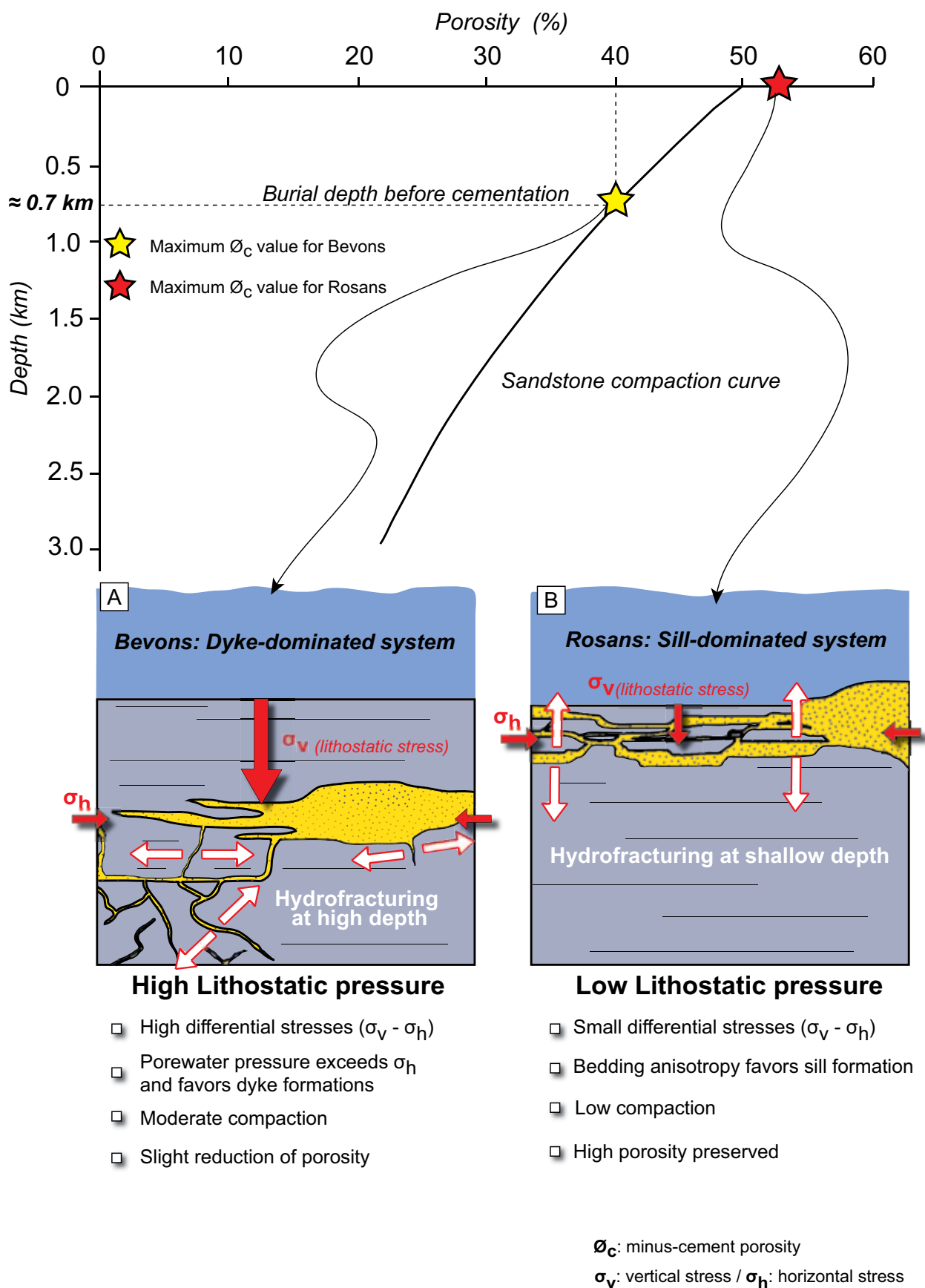
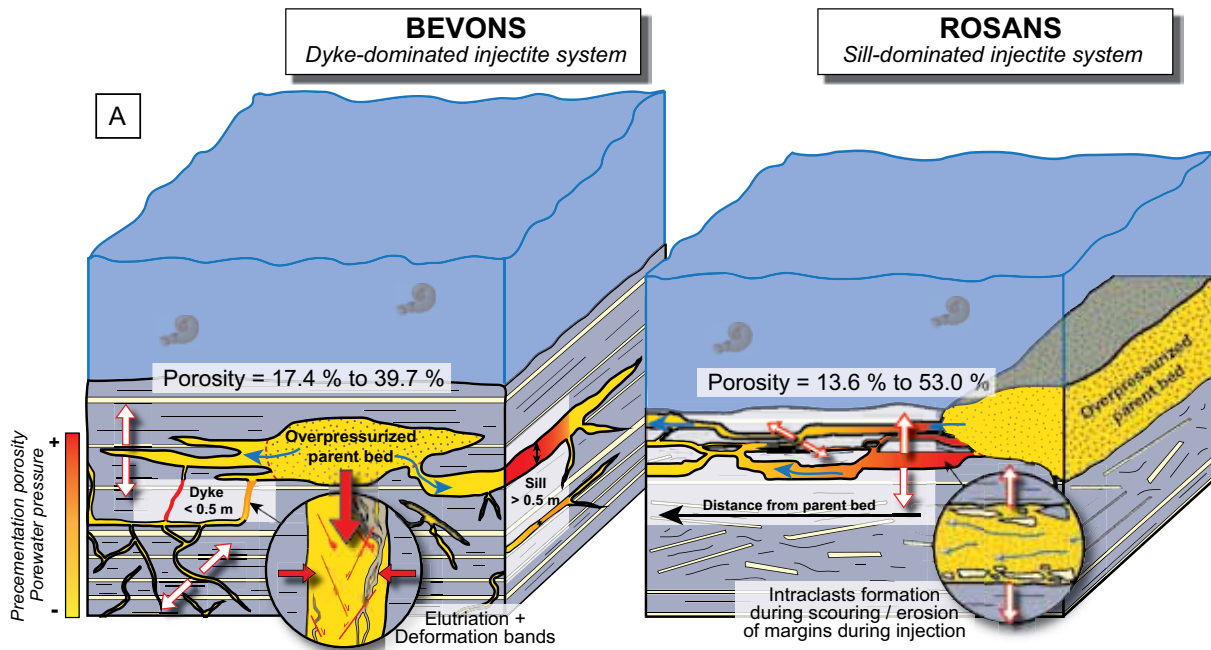


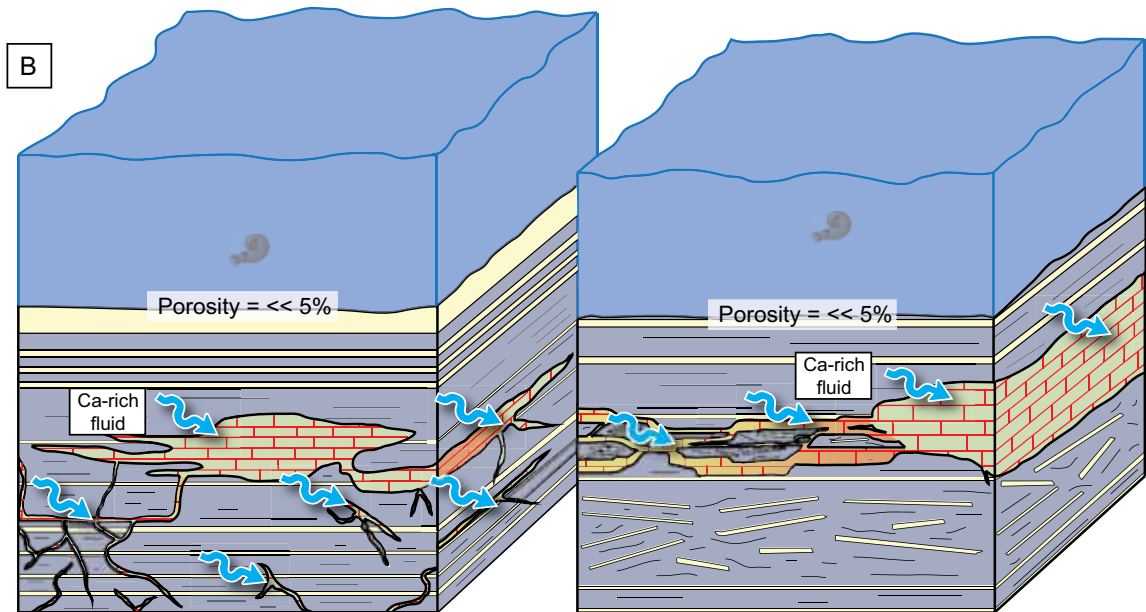
Figure 23. Typical compaction curve of sandstones (depth vs. porosity) (based on data presented in Allen and Allen, 1990) with the indicative burial range over which carbonate cementation occurred within injected sand, based on maximum precementation porosity values estimated for both sites. (A) In Bevens, cementation occurred around 0.7 km in depth, the increase of lithostatic pressure preferentially triggers the formation of dykes leading to the development of a dyke-dominated system. (B) In Rosans, cementation occurred in subsurface. The reduced lithostatic stress and the bedding anisotropy favors the formation of sills.

indicates that the sill-dominated injectite network became cemented in subsurface (**Fig. 23B**). Sill-dominated systems typically form at very shallow depths when the vertical stress (σ_v) exerted by the lithostatic weight is reduced. In this configuration, differential stresses are small ($\sigma_v - \sigma_h$) and the bedding anisotropy favors the formation of sills (Jolly and Lonergan, 2002; Vigorito et al., 2010). Once injection ceased, injected sediments preserved high porewater pressures as they remained sealed by the encasing “blue marls” Formation, considered as a material of very-low permeability. In this configuration, high porewater pressures resist mechanical compaction by the overburden, thus maintaining a metastable grain fabric characterized by high porosity values (Taylor et al., 2010; Nguyen et al., 2013). The weak compaction and the high porewater pressures are respectively illustrated by limited pressure/solution processes affecting quartz grains and high minus-cement porosity values (up to 40 and 53% for the Rosans and Bevens areas respectively). The precementation porosities display heterogeneous distributions with values ranging from 17.4% to 39.7% for the Bevens area and 13.6 % to 53 % for the Rosans area (**Figs. 21, 22, 24A**), implying that porewater pressures and/or compaction rates were variable just after injection ceased. Several factors can explain the heterogeneous distribution of early porosities: the variability of grain packing resulting from sediment fluidization, thickness of the injection, distance to the parent bed, and the multi-phased three-dimensional development of the sand injection networks (Scott et al., 2009; Hurst et al., 2011). Maximum precementation porosities are observed in Rosans where the injectite network is characterized by a sill-dominated network (up to 53%). Sills generally form close to the surface, as supra-lithostatic pressure needs to be reached (Jolly and Lonergan, 2002; Vigorito et al., 2010). As a consequence, the highest precementation porosity values occurring in Rosans may be related to high porewater pressures and weak compaction due to low overburden pressure. Although the precementation porosity distribution seems heterogeneous, few parameters play a role in early porosity distributions including injectite thickness and distance to parent bed. The Bevens area shows a thickness control on early porosity (**Figs. 19, 24A**). Dykes < 0.5 m display a modest negative correlation implying that thinner dykes tend to present high porosities. This could be due to the effect of post-injection margin retractions on thin sand dykes that tends to maintain higher fluid pressures and subsequent high porosities due to lateral compression. Alternatively, this relation could illustrate that thin dykes become quicker carbonate-cemented, thus preserving the granular framework to further compaction and porosity reduction

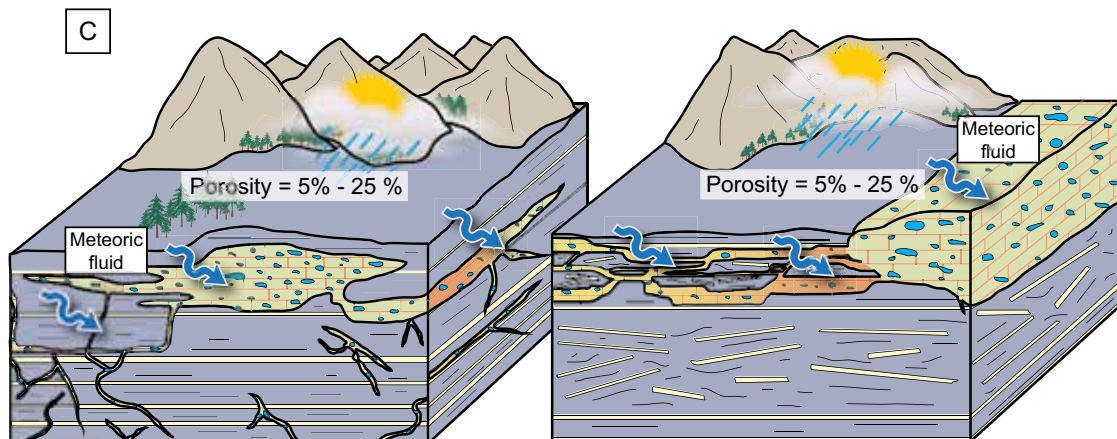
Figure 24. Schematic diagram illustrating the three major phases (A to C) affecting the evolution of porosity values in the injectites networks of Bevens and Rosans areas.



Stage 1. Hydrofracturing / injection of fluidized sand
Distance to parent bed and injection thickness control precementation porosities
Deformation bands / elutriation / intraclasts accumulations → Localized porosity reduction



Stage 2. Burial, Ca-rich fluid released during marls compaction
Pervasive carbonate cementation → Drastic porosity reduction



Stage 3. Exhumation. Circulation of meteoric water
Carbonate cement dissolution → Modern porosity increase

(Jonk, 2003; Jonk et al., 2005a, b). Sill thickness > 0.5 m shows a positive correlation with minus-cement porosity implying that porosities increase together with the widths of injections. Sills are a record of supra-lithostatic pressures and the increase of sill thickness could plausibly involve higher porewater pressures inducing the preservation of higher precementation porosities. In the Rosans area, the distance to the parent bed has an influence on the distribution of early porosity values (**Fig. 24A**). The general trend of precementation porosity decrease may derive from the progressive decrease of the fluid pressure away from the source during sand injection. Processes of hydrofracturing stop when the overpressure laterally dissipates away from the source and when the porewater pressure threshold required to fracture the encasing marls cannot be reached anymore. Similarly, during sand injection into hydrofractures, progressive dissipation of the porewater pressure away from the source could result in a lateral gradient of grain packing (from loose to more tightly packed) and subsequent decrease in porosity. Alternatively, sill thickness decreases away from the parent bed, implying that the effect of compaction will be potentially strengthened away from the source, thus creating a lateral precementation porosity gradient. Indeed, thinner beds tend to be quicker affected by mechanical compaction when the overburden pressure exerts a stress on the sediments.

The emplacement of intraclasts within injectites produced by erosion, scouring, and fracturing of margins during sand injection may also locally affect the original porosity. When mudclasts of various sizes are locally abundant, they could potentially have an impact on precementation porosities and permeabilities. Scott et al. (2009, 2013) demonstrated that lower porosities and permeabilities were correlated with an increase of the mudstone clasts abundance.

8.1.2. Early porosity reduction

After the development of the sand injection networks but prior to sandstones lithification, processes related to compaction and porewater pressure fluctuations altered the early porosity of sand injections. Elutriation processes evidenced by anastomosed elutriation bands or dish structures are occasionally observed within the injectite networks and consist of zones enriched in clays that tend to locally affect original porosities (**Fig. 24A**). Although the quantities of clay particles observed in dykes are rather low (mm to cm wide elutriation bands), it has been demonstrated that it has a detectable influence on both porosity and permeability of sandstones (Hurst and Buller, 1984; Scott et al., 2009). Elutriation

processes can trigger a double and opposite effect on porosity. Elutriation dynamics tend to locally increase porosity in zones where vertical elutriation bands are observed as a result of clay flushing through narrow elutriation conduits. Alternatively, such processes tend to decrease porosity within dish structure zones where the clay content is the highest (Hurst and Buller, 1984).

Although the effect of compaction is weak, some evidence of interpenetrating quartz grains suggest that the porosity slightly decreased due to compaction induced by the lithostatic stress exerted on sand injections. Increasing lithostatic stress also led to fracturing of unlithified sediments illustrated by the occasional presence of step normal faults and deformation bands. Deformation bands have a significant impact on both porosities and permeabilities of sandstones (Fossen, 2010; Schultz et al., 2010; Ballas et al., 2013). Previous studies have demonstrated that the porosity of cataclastic deformation bands is reduced by up to an order of magnitude because of intense grain crushing leading to changes in grain-size distribution (Rotevatn et al., 2008; Balsamo and Storti, 2010; Fossen, 2010). In addition these deformation cataclastic bands are associated with microquartz cements along the bands but also in the immediate vicinity of these structures. This cementation phase, enhanced by the chemical reactivity of fresh broken grains, seriously lower the porosity of the injected sand (Ogilvie and Glover, 2001).

Injections with sharp margins following deformation bands have been observed within sand injections. This secondary phase of injection infilled by clay-sized material indicates a minor increase of porewater pressure capable to remobilize fine-grained particles. Similarly to elutriation bands, the impact of such bands on the porosity is variable. Clay injections will locally reduce the porosity as clays represent impermeable material, whereas such structures also imply porosity enhancement in the source zone where the fine particles have been flushed out.

In the early stages of sand injections evolution, porosity is highly controlled by the compaction and the variations in porewater pressure. The control of compaction and porewater pressures on porosities is respectively illustrated by the development of deformation bands and the formation of elutriation structures (**Fig. 24A**).

8.1.3. Pervasive porosity reduction

Early phases of porosity reduction were followed by a major phase of calcite cementation leading to a drastic porosity destruction. This phase occurred during burial and is characterized by a single

carbonate cement phase. Maximum minus-cement porosity values plotted on a classic sand compaction curve indicate that cementation occurs in subsurface in the Rosans injectite network while around 0.7 km in depth for the Bevens injectite network (**Fig. 23**).

The source responsible for calcite cementation is the carbonate-enriched water deriving from the encasing “blue marls” Formation that is composed of limestone and marls alternations. Typical marls contain 50 % of carbonate, 30% of clays (< 15 % of chlorite, 30-40% of illite, 15-25% of mixed-layer clays, 15% of smectite and 20-25% of Kaolinite) and 15% of quartz (Deconinck, 1984). The circulation of these carbonate-rich fluids certainly led to the development of a pervasive blocky calcite in the porous injected sand (**Fig. 24B**). This major diagenetic phase led to a drastic and general diminution of the porosity that was close to null as evidenced by porosity measurements on samples that were not affected by cement dissolution (between 1 and 5 %). After carbonate cementation, clastic injections are no longer unlithified and can be considered as injectites. The late porosity evolution of the sand injectites is driven by diagenetic processes.

8.1.4. Late porosity increase

The occurrence of numerous carbonate veins, in both injectites and host strata, cross-cutting all structures and diagenetic phases illustrates a late fracturing phase related to the tectonic reactivation of the entire pile of sediments. Deformations focused in competent and lithified sand injectites resulting in the formation of open joints. Joints influence permeability of the injectites as they represent drains for fluid flows. Open joints promoted the circulation of carbonate-rich fluid leading to their cementation by fibrous calcite, thus blocking these permeable pathways.

At last, the Alpine compression led to the uplift and exhumation of the Vocontian passive margin and the associated Aptian-Albian deposits. Telogenetic processes enhanced by meteoric fluids affected and still affect the injected sandstones as demonstrated by the dissolution of calcite cements and glauconites. The dissolution affecting the injectites corresponds to a major porosity-forming process that configures the modern porosity. Modern porosity is locally as high as 25 % because of dissolution processes (**Fig. 17C**). The intensity of dissolution is variable and heterogeneous, illustrated by the wide range of modern porosity values (from 1.5 to 25 %).

8.2. Implications for fluid flows in sand injectite networks

Sand injections play a major role in fluid flows as they potentially form vertical communications between reservoirs separated by low-permeability sedimentary intervals, e.g., between different turbiditic channels in the present study. Large injectite networks also represent intrusive traps for fluids and excellent reservoirs containing substantial volume of porous and permeable sand (Hurst and Catwright, 2007). As a consequence, networks of sand intrusions have a considerable impact on fluid flow patterns in sedimentary basins and a primordial importance for understanding the behavior of petroleum reservoirs and aquifers affected by injectites. By reconstructing the evolution of porosity of injection networks through time, we can estimate when sand injections behaved as potential fluid flow pathways (**Fig. 25**).

In the Vocontian Basin, fluid flow characteristics associated with the development of injectite networks can be divided in two major phases: (1) an early phase where porosity evolution was controlled by deformations induced by compaction and porewater pressure variations, and (2) a late phase where porosity evolution was dominated by diagenetic processes (**Fig. 25**).

8.2.1. Early impacts on fluid flows

The early phase represents the best configuration for fluid migrations because sand injections were unlithified, with averaged porosity values exceeding 25 %. This early phase corresponds to the injection stage where highly porous and permeable sand intrusions were formed and prematurely modified by deformational processes.

Overpressures developed in depositional sand bodies until it exceeded tensile strength of the encasing impermeable formation, triggering hydrofracturing. Hydrofracturing induced significant increase of permeability within marls sealing the depositional sand bodies (Jonk, 2010). Hydrofractures were infilled by fluidized and porous sand resulting in a highly connected and porous network formed in low-permeability marls. The sand injections formed conduits at shallow to very shallow burial depth (< 0.7 km) in which water contained within the host marls could have laterally drained (Hurst and Catwright, 2007).

Although the sand injection networks were characterized by high early porosities, the geographical distribution of the porosity values was rather heterogeneous. Once injection ceased, very high

porosities (up to 53%) were maintained in the injected sand network due to high porewater pressures, leading to the development of efficient drains. Although no evidence for petroleum migration has been evidenced in the study area, the petrophysical properties differences between the injected sand and the low-permeable host strata could have greatly influenced rates of fluid drainage and therefore enhanced rates of hydrocarbon migration (Duranti et al., 2002; Briedis et al., 2007).

Post-injection developments of elutriations bands, dish structures and deformation cataclastic bands led to a significant but localized reduction of porosity (**Fig. 25**). These structures create porosity and permeability heterogeneities at sub 0.01 m scale that could have notably affected fluid circulation through the intrusive sand network (Hurst and Buller, 1984; Scott et al., 2009). The early diagenetic imprints represented by quartz cemented deformation bands have been found in other sites, including the North Sea (Viking Graben, Eocene-Paleocene) and North East Scotland (Kimmeridgian). Fluid inclusions analyses of the early quartz cement in Scotland demonstrated the migration of deep-seated basinal fluids, therefore illustrating that injections were used as pathways for deeper fluids. Similarly, the Viking graben displays petroleum inclusions in this early cement, possibly indicating hydrocarbon migration from deeper buried sandstones (Jolly and Lonergan, 2002; Jonk et al., 2005a).

Sand injectites represent an emerging play in deep-water environments and were thought to be characterized by typically good and homogeneous reservoir qualities (Hurst et al., 2005). The present study highlights that sand injection networks display high porosity and therefore constitute efficient drains for fluid flows and good reservoirs. However, the heterogeneous distribution of precementation porosities and the localized porosity reductions caused by elutriation and deformation bands indicate that the reservoir quality is rather heterogeneous.

8.2.1. Late impacts on fluid flows

The late evolution of the injectite network is controlled by diagenetic processes and tectonic deformations occurring during burial and exhumation of the “blue marls” Formation. A single phase of carbonate cement blocking the high porosity maintained by high porewater pressures before significant compaction occurred within both depositional sandstones and injectites. In many samples, calcite cements are well preserved with volumes up to 40-50%, indicating that cements considerably reduced porosity and blocked fluid flows (Fig. 25). Precementation porosities indicate that carbonate

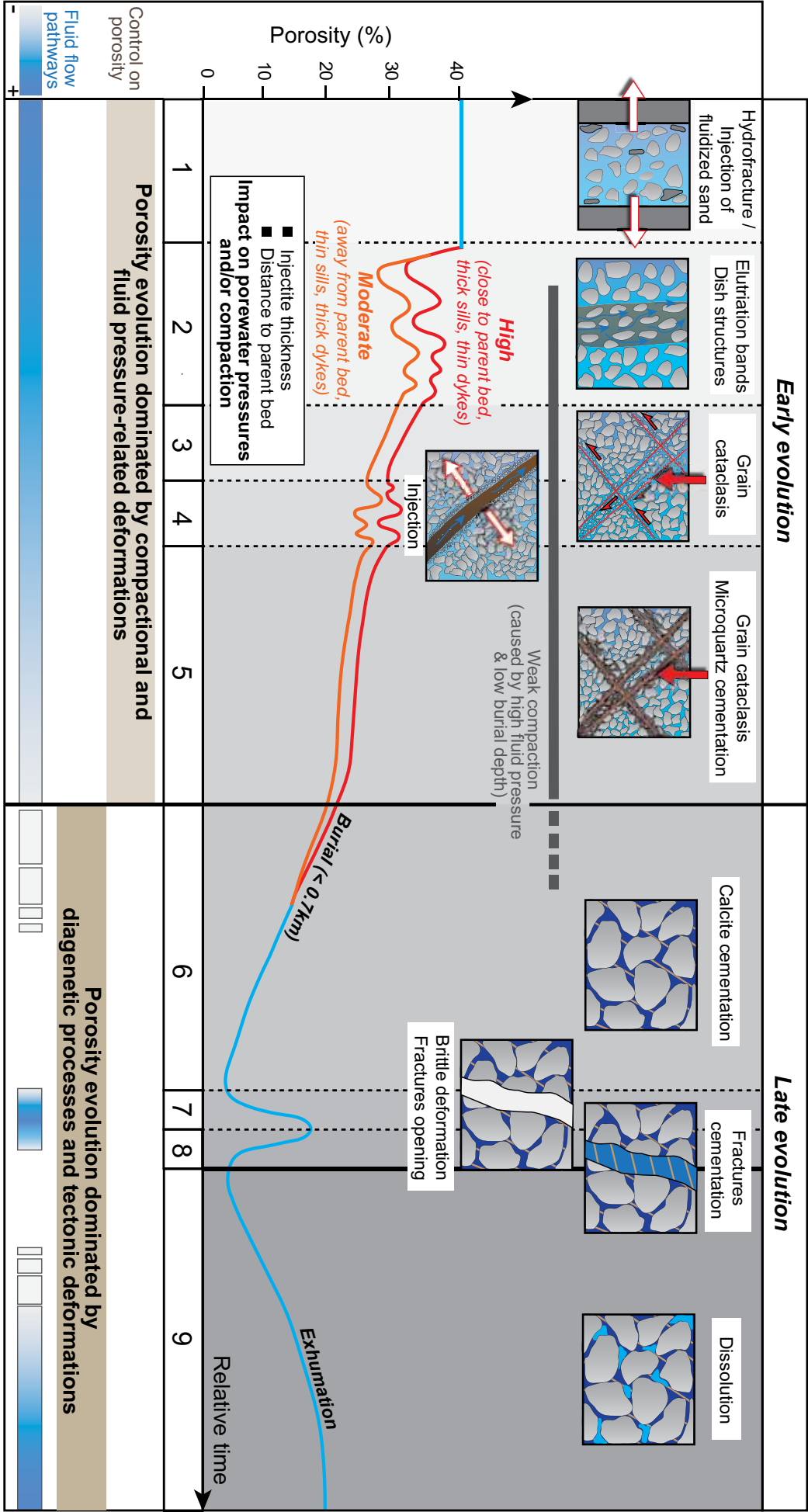


Figure 25. *Relative evolution of the porosity through time associated with the chronological development of the different structures and diagenetic phases that played a role in porosity variations. In the early evolution stages, porosity is predominantly influenced by variations in porewater pressure while the late evolution of injectite porosity is mainly controlled by diagenetic phases. The evolution of porosity directly controls fluid flows within the intrusive sand networks.*

cementation occurred within the first kilometer (~ 0.7 km) or even in subsurface indicating that clastic injections behaved as fluid conduits in the first km or less before entire lithification of the intruded sand. A pervasive phase of carbonate cementation affecting injectites networks is very common as sand injections are usually surrounded by carbonate-rich fine-grained sediments (Jonk et al., 2005a,b, 2010; Scott et al., 2013). During cementation of the injected sand, water and petroleum could keep migrating through injections as evidenced by numerous petroleum inclusions observed within blocky calcite in the North Sea (Paleocene-Eocene) (Mazzini et al., 2003; Jonk et al., 2005a; Jonk, 2010).

Although injectites behaved as flow barriers after lithification, late tectonic deformation led to reactivation of injectites through fracturing and jointing of the competent cemented sandstones. During reactivation, fluids can migrate through open joints as illustrated by petroleum inclusions within reactivated zones in Central Scotland (Lower Carboniferous) that have been used as pathways for oil migration from surrounding shales (Jonk, 2010). Fibrous calcite infilling these joints indicate that they have been later sealed, preventing further fluid flows within injectites. The very last phase affecting porosity and fluid flows within injectites networks postdates the exhumation of the Aptian-Albian series in the Vocontian Basin. Significant cement dissolutions affecting numerous samples indicate that meteoric water circulates within both depositional sandstones and injectites implying that the complex sandy network behaves as modern conduits for meteoric fluids (**Fig. 25**).

9. Conclusions

Injectite networks have been considered as geological oddities for a long time until geologists discovered that such anomalies represent attractive exploration targets and must be considered of a huge significance when planning hydrocarbon and water recovery. Recent studies have integrated structural, diagenetic and petrophysical analyses of sand intrusions network to better constrain their impacts on fluid flow dynamics (Jonk et al., 2010; Scott et al., 2013). This study used an integrated method combining structural, diagenetic, and petrophysical analyses to characterize these injectite networks, with a special focus on the geographical distributions of precementation porosities at outcrop scale. Data collected were used to determine how injection processes, early structurations

and diagenetic imprints, pervasive cementation, and modern exhumation affected the porosity of the injectite networks. The key conclusions on chronological porosity evolution resulting from this study are as follows:

- (1) Injection of fluidized sand into hydrofractures led to the emplacement of porous (up to 53%) and permeable conduits within thick impermeable strata.
- (2) Early porosity (i.e. once the injection ceased), evidenced by minus-cement porosity values, appears to be primary controlled by injectite thickness and distance to parent bed, although heterogeneous values prevailed.
- (3) Injectites are affected by early structures, including elutriation structures (elutriation bands and dish structures) and deformation bands, locally reducing the porosity.
- (4) During burial, at relatively low depth (< 0.7 km), the circulation of carbonate-rich fluids within the porous and permeable sand injection networks led to the development of a pervasive blocky calcite reducing porosity ($<< 5\%$).
- (5) Late tectonic deformations led to fracturing of the competent and cemented injectites, re-opening porous and permeable conduits.
- (6) After exhumation, injectites were subject to intense cement and glauconite dissolution by meteoric water which significantly increased porosity (up to 25%).

This study highlighted that injectite networks are characterised by high but heterogeneous precementation porosities and alternate periods of fluid pathways and fluid barriers through time. These results have a great significance in the comprehension of petroleum and aqueous fluids flows within injectite networks, and therefore contribute to understand how to explore and develop these types of reservoirs.

Acknowledgments

This work is a contribution from the ‘SEDS’ (Systèmes, Environnements et Dynamique Sédimentaire) research team in the Laboratoire Biogésosciences-UMR/CNRS 6282 at the University of Burgundy. The authors thank GDF Suez for the funding of this study. The authors also would like to thank Cédric Talloire, Julien Boule and Agathe Germain for their contributions on the field.

References

- Ajdukiewicz, J.M., Lander, R.H., 2010. Sandstone reservoir quality prediction: The state of the art. *AAPG Bulletin* 94, 1083-1091.
- Ali, S.A., Clark, W.J., Moore, W.R., Dribus, J.R., 2010. Diagenesis and Reservoir Quality. *Oilfield Review* 22, 1-14.
- Allen, J.R., 1982. *Sedimentary Structures: Their Character and Physical Basis*. Amsterdam, Elsevier edition, *Developments in Sedimentology* 30, 2 volumes, 663 pp.
- Allen, P.A., Allen, J.R., 1990. *Basin Analyses, Principles and Applications*. Blackwell Scientific Publications, Oxford, 451 pp.
- Arnaud-Vanneau, A., Arnaud, H., 1991. Sédimentation et variations relatives du niveau de la mer sur les plates-formes carbonatées du Berriasien-Valanginien et du Barrémien dans les massifs subalpins septentrionaux et le Jura (SE de la France). *Bulletin de la Société Géologique de France*, 162, 535–545.
- Aydin, A., 1978. Small faults formed as deformation bands in sandstone. *Pure and Applied Geophysics* 116, 913–930.
- Ballas, G., Soliva, R., Sizun, J.P., Fossen H., Benedicto, E., Skurtveit, E., 2013. Shear enhanced compaction bands formed at shallow burial conditions; implications for fluid flow (Provence, France). *Journal of Structural Geology* 47, 3-15.
- Balsamo, F., Storti F., 2010. Grain size and permeability evolution of soft-sediment extensional sub-seismic and seismic fault zones in high-porosity sediments from the Croton basin, southern Apennines, Italy. *Marine and Petroleum Geology* 27, 822-837.
- Beaudoin, B., Friès, G., Joseph, P., Bouchet, R., Cabrol, C., 1986. Tectonique sédimentaire crétacée à l'Ouest de la Durance (S.E. de la France). *Comptes Rendus à l'Académie des Sciences, Paris*, 303, 857-862.
- Bjorkum, P.A., 1996. How important is pressure in causing dissolution of quartz in sandstones? *Journal of Sedimentary Research* 66, 147-154.
- Bonin, A., Vennin, E., Puceat, E., Guiraud, M., Arnaud-Vanneau, A., Adatte, T., Pittet, B., Mattioli, E., 2012. Community replacement of neritic carbonate organisms during the late Valanginian platform demise: A new record from the Provence Platform. *Palaeogeography Palaeoclimatology Palaeoecology* 365, 57-80.
- Bouma, A.H., 1962. *Sedimentology of some flysch deposits. A graphic approach of facies interpretation*. Thesis. University Utrecht. Elsevier Publishers, Amsterdam, 168 pp.
- Borja, R.I., Aydin, A., 2004. Computational modeling of deformation bands in granular media. I. Geological and mathematical framework. *Computer Methods in Applied Mechanics and Engineering* 193, 2667-2698.
- Braccini, E., de Boer, W., Hurst, A., Huuse, M., Vigorito, M., Templeton, G., 2008. Sand injectites. *Oilfield review*, summer 2008.

- Bréhéret, J.G., 1997. L'Aptien et l'Albien de la fosse vocontienne (des bordures au bassin). Evolution de la sédimentation et enseignements sur les événements anoxiques. Thèse Doctorat Sciences. University Tours, 1995. Publications de la Société Géologique du Nord 25, 614 pp.
- Briedis, N.A., Bergslien, D., Hjellbakk, A., Hill, R.E., Moir, G.J., 2007. Recognition Criteria, Significance to Field Performance, and Reservoir Modeling of Sand Injections in the Balder Field, North Sea. In: Hurst, A., Cartwright, J. (Eds.), Sand injectites: Implications for Hydrocarbon Exploration and Production: American Association of Petroleum Geologists Memoir, Tulsa, pp. 91–102.
- Chorowicz, J., Mekarnia, A., 1992. Mise en évidence d'une extension albo-aptienne orientée NW-SE en Provence (SE de la France). Comptes Rendus de l'Académie des Sciences, Paris, 315, 861-866.
- Choukroune, P., Gapais, D., Merle, O., 1987. Shear criteria and structural symmetry. Journal of Structural Geology 9, 525-530.
- Cosgrove, J.W., 2001. Hydraulic fracturing during the formation and deformation of a basin: A factor in the dewatering of low-permeability sediments. AAPG Bulletin 85, 737-748.
- Denis, M., Guiraud, M., Konate, M., Buoncristiani, J.F., 2010. Subglacial deformation and water-pressure cycles as a key for understanding ice stream dynamics: evidence from the Late Ordovician succession of the Djado Basin (Niger). International Journal of Earth Sciences 99, 1399-1425.
- Dickson, J.A.D., 1966. Carbonate identification and genesis as revealed by staining. Journal of Sedimentary Petrology 27, 107-118.
- Dixon, R.J., Schofield, K., Anderton, R., Reynolds, A.D., Alexander, R.W.S., Williams, M.C., Davies, K.G., 1995. Sandstone diapirism and clastic intrusion in the Tertiary submarine fans of the Bruce-Beryl Embayment, Quadrant 9, UKCS. In: Hartley, A.J., Prosser, D.J. (Eds.), Characterisation of deep-marine clastic systems: Special Publication, vol. 94. Geological Society, London, pp. 77–94.
- Dauphin, L., 2002. Litho-, bio-, chrono-stratigraphie comparées dans le bassin Vocontien à l'Aptien. Thèse Doctorat Géologie, ENS Mines Paris. Mémoires des Sciences de la Terre, École des Mines de Paris, 516 pp.
- Deconinck, J.F., 1984. Sédimentation et diagénèse des minéraux argileux du Jurassique supérieur-Crétacé dans le Jura méridional et le domaine subalpin (France Sud-Est); comparaison avec le domaine Atlantique Nord. Unpubl. Thèse Doctorat III cycle. University Lille, 150 pp.
- Dercourt, J., Ricou, L.E. and Vrielynck, B., 1993. Atlas Tethys Palaeoenvironmental Maps. Gauthier-Villars Publishers, Paris, 307 pp.
- Eichhubl, P., Hooker, J.N., Laubach, S.E., 2010. Pure and shear-enhanced compaction bands in Aztec Sandstone. Journal of structural Geology 32, 1873-1886.
- Fossen, H., 2010. Deformation bands formed during soft-sediment deformation: Observations from SE Utah. Marine and Petroleum Geology 27, 215-222.
- Fossen, H., Schultz, R.A., Shipton, Z.K., Mair, K., 2007. Deformation bands in sandstone: a review. Journal of the Geological Society 164, 755-769.
- Friès G., 1987. Dynamique du bassin subalpin méridional de l'Aptien au Cénomanién: Thèse Doctorat

- ès Sciences Université Paris VI, 1986: Mémoire des Sciences de la Terre, Ecole des Mines de Paris, 370 p.
- Fries, G., Parize, O., 2003. Anatomy of ancient passive margin slope systems: Aptian gravity-driven deposition on the Vocontian palaeomargin, western Alps, south-east France. *Sedimentology* 50, 1231-1270.
- Guiraud, M., Seguret, M., 1987. Soft-sediment microfaulting related to compaction within the fluvio-deltaic infill of the Soria strike-slip basin (northern Spain) In: Jones, M.E., Preston, R.M.F. (Eds.), *Deformation of sediments and sedimentary rocks*. Geological Society, London, Special Publication 29, pp. 123-136.
- Hardie, J.K., 1999. Clastic dikes Intruding Cretaceous Coals of Western Colorado. *Bulletin of the Colorado Geological Survey* 53, 1-48.
- Hibsch, C., Kandel, D., Montenat, C., Ott d'Estevou, P., 1992. Evénements tectoniques crétacés dans la partie méridionale du bassin subalpine (massif Ventoux-Lure et partie orientale de l'arc de Castellane, SE France). Implications géodynamiques. *Bulletin de la Société de Géologie de France* 163, 147-158.
- Hiscott, R.N., 1979. Clastic sills and dikes associated with deep-water sandstone, Tourelle Formation, Ordovician, Québec. *Journal of Sedimentology and petroleum* 49, 1-10.
- Huang, Q., 1988. Geometry and tectonic significance of Albian sedimentary dikes in the Sisteron area, SE France: *Journal of Structural Geology* 10, 453-462.
- Hurst, A., Buller, A.T., 1984. Dish structures in some Palaeocene deep-sea sandstones (Norwegian sector, North Sea); origin of the dish-forming clays and their effect on reservoir quality. *Journal of Sedimentary Petrology* 54, 1206-1211.
- Hurst, A., Cartwright, J.A., Huuse, M., Jonk, R., Schwab, D., Duranti, D., Cronin, B., 2003. Significance of large-scale sand injectites as long-term fluid conduits: evidence from seismic data. *Geofluids* 3, 263-274.
- Hurst, A., Cartwright, J.A., Duranti, D., Huuse, M., Nelson, M., 2005. Sand injectites: an emerging global play in deep-water clastic environments. In: Doré, A., Vining, B. (Eds.), *Petroleum Geology: North-west Europe and Global Perspectives*. Proceedings of the 6th Petroleum Geology conference. Geological Society, London, pp. 133-144.
- Hurst, A., Cartwright, J., 2007. Relevance of sand injectites to hydrocarbon exploration and production, in Hurst, A., Cartwright J. (Eds.), *Sand injectites: Implications for hydrocarbon exploration and production*. AAPG Memoir 87, 1-19.
- Hurst, A., Scott, A., Vigorito, M., 2011. Physical characteristics of sand injectites. *Earth-Science Reviews* 106, 215-246.
- Huuse, M.J., Cartwright, J.A., Hurst, A., Steinsland, N., 2007. Seismic characterization of large-scale sandstone intrusions. In: Hurst, A., Cartwright, J. (Eds.), *Sand Injectites: Implications for Hydrocarbon Exploration and Production*: American Association of Petroleum Geologists Memoir, Tulsa, pp. 21-35.
- Huuse, M., Cartwright, J.A., Gras, R., Hurst, A., 2005. Kilometre-scale sandstone intrusions. In:

- Doré, A.G., Vining, B.A. (Eds.), *Petroleum Geology: North-West Europe and Global Perspectives—Proceedings of the 6th Petroleum Geology Conference*. Geological Society of London, pp. 1577–1594.
- Jackson, C.A.L., 2007. The Geometry, Distribution, and Development of Clastic Injections in Slope Systems: Seismic Examples from the Upper Cretaceous Kyrre Formation, Måløy Slope, Norwegian Margin. In: Hurst, A., Cartwright, J. (Eds.), *Sand Injectites: Implications for Hydrocarbon Exploration and Production: American Association of Petroleum Geologists Memoir*, Tulsa, pp. 21–35.
- Jolly, R.J.H., Lonergan, L., 2002. Mechanisms and controls on the formation of sand intrusions. *Journal of the Geological Society* 159, 605–617.
- Jonk, R., 2010. Sand-rich injectites in the context of short-lived and long-lived fluid flow. *Basin Research* 22, 603–621.
- Jonk, R., Hurst, A., Duranti, D., Parnell, J., Mazzini, A., Fallick, A.E., 2005a. Origin and timing of sand injection, petroleum migration, and diagenesis in Tertiary reservoirs, South Viking Graben, North Sea. *AAPG Bulletin* 89, 329–357.
- Jonk, R., Parnell, J., Hurst, A., 2005b. Aqueous and petroleum fluid flow associated with sand injectites. *Basin Research* 17, 241–257.
- Joseph, Ph., Cabrol, C., Friès, G., 1987. Blocs bascules et passes sous-marines dans le Champ de Banon (France S.E.) à l'Apto-Albien : une paléotopographie directement contrôlée par la tectonique synsédimentaire décrochante. *Comptes Rendus de l'Académie des Sciences* 9, 447–452.
- Kane, I.A., 2010. Development and flow structures of sand injectites: The Hind Sandstone Member injectite complex, Carboniferous, UK. *Marine and Petroleum Geology* 27, 1200–1215.
- Kawakami, G., Kawamura, M., 2002. Sediment flow and deformation (SFD) layers: evidence for intrastratal flow in laminated muddy sediments of the Triassic Osawa Formation, northeast Japan. *Journal of Sedimentary Research* 72, 171–181.
- Lowe, D.L., 1982. Sediment gravity flows. II. Depositional models with special reference to the deposits of high-density turbidity currents. *Journal of Sedimentary Petrology* 52, 280–297.
- Lowe, D.R., Lopiccolo, R.D., 1974. The characteristics and origins of dish and pillar structures. *Journal of Sedimentary Petrology* 44, 484–501.
- Lucas, S.E., Moore, J.C., 1986. Cataclastic deformation in accretionary wedges: Deep Sea Drilling Project Leg 66, southern Mexico, and on-land examples from Barbados and Kodiak Islands. In: Moore, C.D. (ed.) *Structural fabrics in Deep Sea Drilling Project cores from forearc region*. Geological Society of America, *Memoirs* 166, 89–103.
- Maillart, J., Beaudoin, B., Cojan, I., Joseph, P., Pinoteau, B., 1987. Déformation synsédimentaire ou compaction différentielle: exemples dans le Sud-Est de la France. *Notes et Mémoires – Compagnie Française des Pétroles* 21, 249–257.
- Manatschal, G., Bernoulli, D., 1998. Rifting and early evolution of ancient ocean basins; the record of the Mesozoic Tethys and the Galicia-Newfoundland margins. In: Erzinger, J., Sibuet Jean, C., Talwani, M. (Eds.), *Volcanic Margins. : Marine Geophysical Researches*. Kluwer Academic Publishers, Dordrecht, Netherlands, pp. 371–381.

Mazzini, A., Jonk, R., Duranti, D., Parnell, J., Cronin, B., Hurst, A., 2003. Fluid escape from reservoirs: implications from cold seeps, fractures and injected sands - Part I. The fluid flow system. *Journal of Geochemical Exploration* 78, 293-296.

Monnier, D., 2013. Dynamique de mise en place des réseaux d'intrusions sableuses dans les bassins sédimentaires : Impact sur l'évolution post-dépôt des réservoirs et le réseau de migration associé. Ph.D thesis, University of Montpellier 2, France, 294 pp.

Murchison, R.I., 1827. On the coal field of Bora in Sutherlandshire and some other stratified deposits in the North of Scotland. *Geological Society of London* 2, 293–326.

Ogilvie, S.R., Glover, P.W.J., 2001. The petrophysical properties of deformation bands in relation to their microstructure. *Earth and Planetary Science Letters* 193, 129-142.

Parize, O., 1988. Sills et dykes gréseux sédimentaires: paléomorphologie, fracturation précoce, injection et compaction: Thèse Doctorat Géologie, Ecole Nationale Supérieure des Mines de Paris–Université Lille I: Mémoire des Sciences de la Terre, Ecole des Mines de Paris, 7, 333 pp.

Parize, O., Friès, G., 2003. The Vocontian clastic dykes and sills: a geometric model. In: Van Rensbergen, P., Maltman, A.J., Morely, C.J. (Eds.), *Sub-surface sediment mobilization: Geological Society of London Special Publication* 216, 51–72.

Parize, O., Beaudoin, B., Eckert, S., Fries, G., Hadj-hassen, F., Schneider, F., Su, K., Tijani, A., Troullier, A., De Fouquet, C., Vandromme, R., 2007a. The Vocontian Aptian and Albian syndepositional clastic sills and dikes: A field-based mechanical approach to predict and model the early fracturing of marly-limy sediments. In: Hurst, A., Cartwright, J. (Eds.), *Sand Injectites: Implications for Hydrocarbon Exploration and Production: American Association of Petroleum Geologists Memoir*, Tulsa, pp. 163–173.

Parize, O., Beaudoin, B., Champanhet, J.M., Friès, G., Imbert, P., Labourdette, R., Paternoster, B., Rubino, J.L., Schneider, F., 2007b. A Methodical Approach to Clastic Injectites: From Field Analysis to Seismic Modeling—Examples of the Vocontian Aptian and Albian Injectites (Southeast France). In: Hurst, A., Cartwright, J. (Eds.), *Sand Injectites: Implications for Hydrocarbon Exploration and Production: American Association of Petroleum Geologists Memoir*, Tulsa, pp. 173–183.

Passchier, C.W., Trouw R.A.J., 2005. *Microtectonics*. Springer, Berlin, 366 p.

Pittman, E. D., R. E. Larese, 1991. Compaction of lithic sands: Experimental results and applications. *AAPG Bulletin* 75, 1279–1299.

Plint, A.G., 1985. Possible earthquake-induced soft-sediment faulting and remobilization in Pennsylvanian alluvial strata, southern New Brunswick, Canada. *Canadian Journal of Earth Sciences* 22, 907-912.

Quesne, D., 1998. Propositions pour une nouvelle interprétation séquentielle du Vercors méridional, à l'échelle de la paraséquence. *Bulletin Société Géologique de France* 169, 537–546.

Ravier, E., Buoncristiani, J.F., Guiraud, M., Menzies, J., Clerc S., Goupy B., Portier E., 2014. Porewater pressure control on subglacial soft-sediment remobilization and tunnel valley formation: a case study from the Alnif Tunnel Valley (Morocco). *Sedimentary Geology* 304, 71-95.

- Rotevatn, A., Torabi, A., Fossen, H., Braathen, A., 2008. Slipped deformation bands: A new type of cataclastic deformation bands in Western Sinai, Suez rift, Egypt. *Journal of Structural Geology* 30, 1317-1331.
- Rowe, C.A., Mustard, P.S., Mahoney, J.B., Katnick, D.C., 2002. Oriented clastic dike swarms as indicators of paleoslope? - An example from the Upper Cretaceous Nanaimo Group, Canada. *Journal of Sedimentary Research* 72, 192-200.
- Rubino, J.-L., 1989. Introductory remarks on Upper Aptian to Albian siliciclastic/carbonate depositional sequences. In: Ferry, S., Rubino, J.-L. (Eds.), *Mesozoic Eustasy on Western Tethyan Margins; Post-Meeting Field Trip in the "Vocontian Trough"*. Publication de l'Association des Sédimentologues Français 12, 28-45.
- Schultz, R.A., Okubo, C.H., Fossen, H., 2010. Porosity and grain size controls on compaction band formation in Jurassic Navajo Sandstone. *Geophysical Research Letters* 37, L22306.
- Scott, A., Vigorito, M., Hurst, A., 2009. The process of sand injection: internal structures and relationships with host strata (Yellowbank Creek Injectite Complex, California, USA). *Journal of Sedimentary Research* 79, 568-583.
- Scott, A., Hurst, A., Vigorito, M., 2013. Outcrop-based reservoir characterization of a kilometer-scale sand-injectite complex. *AAPG Bulletin* 97, 309-343.
- Stampfli, G.M., Borel, G.D., Marchant, R., Mosar, J., 2002. Western Alps geological constraints on western Tethyan reconstructions. In: Rosenbaum, G., Lister, G. (Eds.), *Reconstruction of the Evolution of the Alpine Himalayan Orogen*. *Journal of the Virtual Explorer* 7, 75-104.
- Surlyk, F., Noe-Nygaard, N., 2001. Sand remobilization and intrusion in the Upper Jurassic Hareelv Formation of East Greenland. *Bulletin of the Geological society of Denmark* 48, 169-188.
- Vigorito, M., Hurst, A., 2010. Regional sand injectite architecture as a record of pore-pressure evolution and sand redistribution in the shallow crust: insights from the Panoche Giant Injection Complex, California. *Journal of the Geological Society* 167, 889-904.
- Vigorito, M., Hurst, A., Cartwright, J., Scott, A., 2008. Regional-scale subsurface sand remobilization: geometry and architecture. *Journal of the Geological Society* 165, 609-612.
- Whitman, A.G., Morton, A.C., Fanning, G., 2004. Insights into Cretaceous-Palaeocene sediment transport paths and basin evolution in the North Atlantic from a heavy mineral study of sandstones from southern East Greenland. *Petroleum Geosciences* 10, 61-72.
- Wilson, M.D., Stanton, P.T., 1994. Diagenetic mechanisms of porosity and permeability reduction and enhancement. In: *Reservoir Quality Assessment and Predictions in Clastic Rocks*. SEPM Short Course Notes 30, 59-117.
- Yang, X.S., 2000. Pressure solution in sedimentary basins: effect of temperature gradient. *Earth and Planetary Science Letters* 176, 233-243.
- Ziegler, P.A., 1990. *Geological Atlas of Western and Central Europe*. Shell International Petrol. Mij., Den Haag, 239 pp.

Partie 2

Les coatings argileux dans les grès glaciaires ordoviciens du bassin de Sbaa (Algérie): processus de mise en place et implications pétrophysiques

Processes of clay coating emplacement in Ordovician glacial sandstones and their impact on petrophysical properties (Sbaa Basin, Algeria).

Objectifs:

La présence de coatings argileux (i.e., tapissages argileux) et leurs impacts sur les propriétés pétrophysiques des sédiments glaciaires ordoviciens du bassin de Sbaa ont été démontrés (Tournier, 2010; Tournier et al., 2010.)

- *L'objectif principal de cette seconde partie est de tester le potentiel impact des surpressions de fluides et des remobilisations sédimentaires sur la mise en place de ces coatings argileux dans les sédiments glaciaires ordoviciens.*

- *Afin de pouvoir discuter cette éventuelle relation, il sera nécessaire d'effectuer dans un premier temps une analyse des structures de déformation pré-lithification et de leur distribution le long des carottes sédimentaires, ainsi qu'une caractérisation des différents environnements de dépôts.*

- *Dans un deuxième temps, la nature et l'origine des coatings argileux présents dans les sables glaciaires devront être déterminées, de même que la distribution de l'abondance de ces coatings le long des carottes sédimentaires.*

- *Les relations entre structures de déformation pré-lithification, environnements de dépôts et distribution de l'abondance des coatings argileux permettront de discuter les facteurs contrôlant la mise en place de ces tapissages argileux.*

1. Précédents travaux

Cette deuxième partie aborde deux grands aspects: (1) L'influence des surpressions de fluide et des processus de remobilisation sédimentaire sur la mise en place des coatings argileux en domaine glaciaire, et (2) l'impact des coatings argileux sur les propriétés pétrophysiques des sédiments glaciaires.

(1) L'impact de l'augmentation de la pression d'eau interstitielle sur les processus d'élutriation, et sur la mise en place de coatings argileux dans les sédiments glaciaires a déjà été discuté dans certains travaux (Menzies, 2000; van der Meer et al., 2003; Menzies et Ellwanger, 2011; Phillips et al., 2013). La mise en place de ces coatings argileux a notamment été interprétée comme le résultat de processus d'illuvations guidés par des pressions d'eau interstitielle élevées (Menzies et Ellwanger, 2011), favorisant ainsi la dispersion des particules argileuses et la formation de tapissages argileux (Menzies, 2000; van der Meer et al., 2003). La mise en place des coatings argileux a également été associée à des processus de liquéfaction sédimentaire (Phillips et al., 2007, 2013).

(2) La majeure partie des études caractérisant les déformations pré-lithifications et les processus de remobilisation sédimentaire au sein des dépôts glaciaires s'appuie sur des exemples quaternaires. Les sédiments quaternaires glaciaires sont meubles, expliquant ainsi l'absence de données pétrophysiques et les connaissances limitées de l'impact des pressions de fluide sur la porosité ou la perméabilité des sédiments. Cependant, des études menées dans d'autres environnements sédimentaires ont déjà démontré l'impact des pressions de fluides sur les processus d'élutriation et leurs impacts sur les propriétés réservoirs (Lowe et LoPiccolo, 1974; Hurst et Buller, 1984). Ces études ont démontrées une réduction précoce (i.e., avant diagénèse et lithification du sédiment) de la perméabilité dans les zones où les coatings argileux sont abondants.

Les études menées par Tournier (2010) et Tournier et al. (2010) représentent les seules données pétrophysiques disponibles dans des sédiments glaciaires. Dans ces études, une caractérisation pétrophysique et diagénétique de dépôts clastiques glaciaires ordoviciens est proposée. Tournier (2010) décrit la présence de coatings argileux dans des sables glaciaires et détermine l'impact de ces coatings argileux sur la séquence diagénétique, et à terme sur les propriétés pétrophysiques et réservoirs

des sédiments. En effet, plusieurs études montrent que la dissolution de quartz intergranulaire est favorisée par la présence de fins tapissages argileux et plus particulièrement de coatings illitiques (Weyl, 1959; Heald et Larese, 1974; Sibley et Blatt, 1976; Dewers et Ortoleva, 1991; Renard et al., 1997; Fisher et al., 2000), réduisant ainsi considérablement les valeurs de porosité et de perméabilité des réservoirs clastiques (Weyl, 1959 ; Dewers et Ortoleva, 1991 ; Oelkers et al., 1992 ; Bjorkum, 1996 ; Renard et Ortoleva, 1997).

Tournier (2010) suggère que les coatings argileux composés d'illites sont d'origine détritique et proviennent de la circulation, sous la glace, d'eaux de fonte en surpression chargées en particules argileuses.

2. Contexte de l'étude

Il est proposé de réétudier les données sédimentologiques et pétrophysiques des sédiments glaciaires ordoviciens du bassin de Sbaa à la lumière de nouvelles données (i.e., analyses des structures de déformation pré-lithification et quantification/distribution de l'abondance des coatings argileux). Cette étude repose sur l'analyse de carottes sédimentaires (> 60 m d'épaisseur) issues d'un puits foré au sein du Bassin de Sbaa, et plus particulièrement au sein du remplissage d'un système de paléo vallée tunnels ordoviciennes. Le bassin sédimentaire de Sbaa, d'une superficie de 32000 km², est localisé dans le Sud-Ouest de l'Algérie et correspond à une dépression synclinale (**Fig. 1A**). Durant l'Hirnantien (Ordovicien supérieur) et d'après les reconstitutions de la paléogéographie glaciaire, le site d'étude se trouvait alors à proximité de la marge nord de la calotte glaciaire gondwannienne (Ghienne et al., 2007; Le Heron et al., 2007) (**Fig. 1B**).

3. Méthodes

Une méthode classique de description des carottes sédimentaires à échelle macroscopique a tout d'abord été réalisée. Elle consiste en une description des différents faciès sédimentaires et des structures de déformation pré-lithification afin d'élaborer un modèle de dépôt. Les différentes structures de déformation ont été interprétées en terme de cinématique et de pression d'eau interstitielle. A partir des carottes sédimentaires, des «plugs» ont été réalisés à intervalles réguliers afin de déterminer: (1) la nature et la morphologies des coatings argileux, (2) leurs impacts sur les propriétés pétrophysiques,

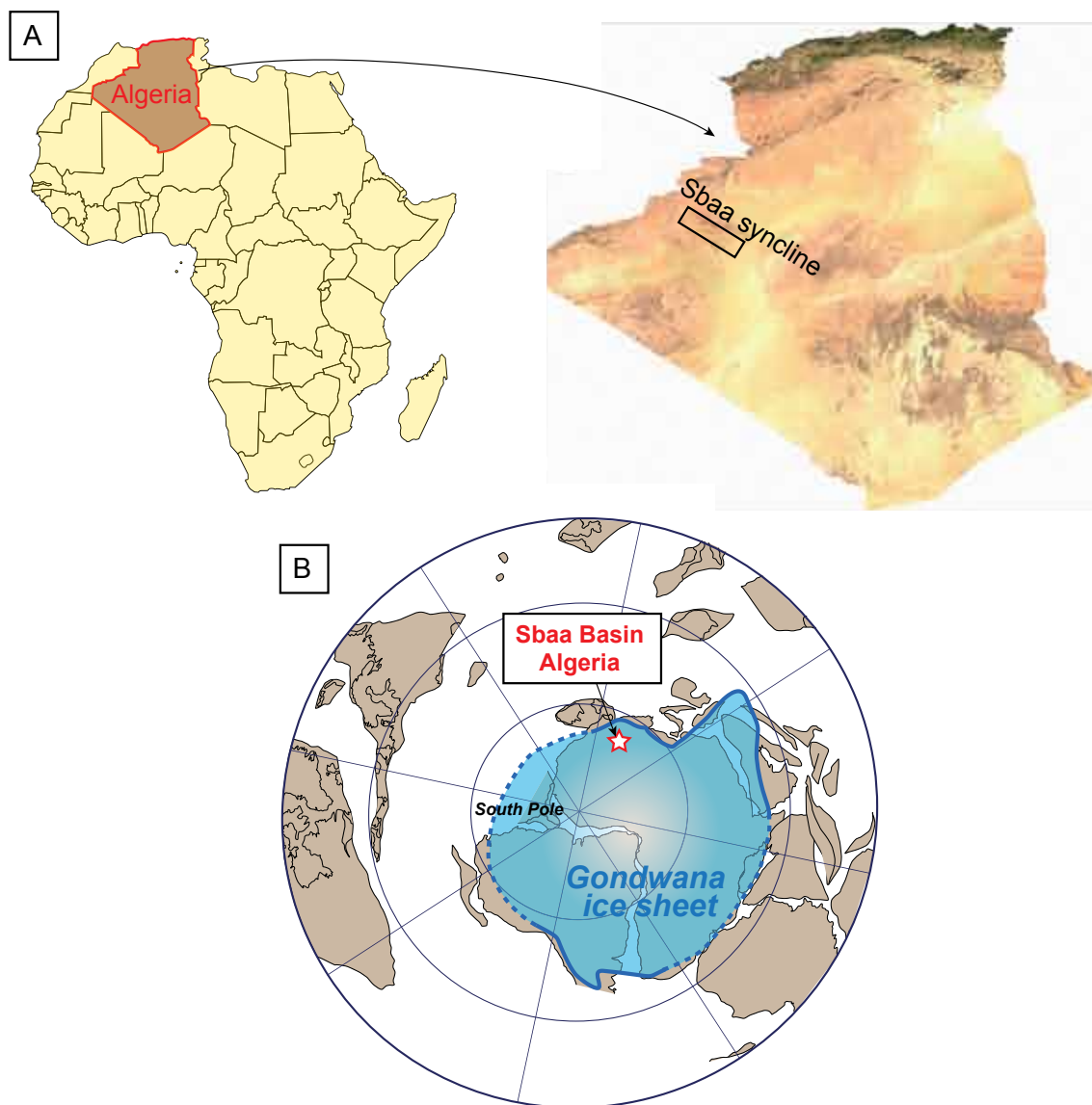


Figure 1. (A) Location of the Sbaa basin. (B) The extension of the Hirnantian palaeo-ice sheet represented on the Gondwana palaeo continent (reconstructions adapted from Cocks and Torsvik, 2002 and Ghienne et al., 2007). Note the location of the Sbaa Basin in the Northern margin of the ice sheet.

et (3) la distribution de l'abondance des coatings argileux. A partir des plugs, 70 lames minces ont été réalisées et étudiées, notamment afin de quantifier les variations d'abondance des coatings argileux le long des carottes. L'abondance des coatings argileux a été estimée par comptage de points à l'aide du logiciel JMicrovision©, avec un minimum de 200 points pour chaque échantillon. Certains échantillons ont été observés au microscope électronique à balayage et analysés au diffractomètre à Rayon X afin de discuter la nature et l'origine des coatings argileux présents dans les différents échantillons. Afin de caractériser l'évolution des caractéristiques pétrophysiques le long des carottes sédimentaires, les valeurs de porosité et de perméabilité ont été mesurées sur les plugs prélevés.

4. Rédaction de la partie 2

Cette deuxième partie est construite de la façon suivante: (1) Dans une première partie, une introduction étendue sur les coatings argileux est proposée au sein de laquelle, leurs caractéristiques et leurs processus de mise en place sous la glace sont présentées ainsi que leurs impacts sur les propriétés pétrophysiques. (2) Dans une deuxième partie, le contextes géographique, structural, glaciaire et sédimentaire du secteur d'étude sont introduits. (3) Après la présentation des méthodes utilisées durant cette étude, (4) les principaux résultats seront présentés. (i) Les différents faciès et les environnements de dépôts seront d'abord définis, (ii) puis les structures de déformation pré-lithification décrites et interprétées, et enfin (c) les données pétrophysiques et les pourcentages d'abondance de coatings représentées le long d'un log sédimentaire. Dans cette même partie, (iii) la nature, la morphologie, l'origine et la distribution des coatings argileux seront présentées, ainsi que la (iv) relation entre les valeurs d'abondance de coatings et les propriétés pétrophysiques. (5) Dans une cinquième partie, l'origine des coatings argileux ainsi que les facteurs contrôlant la distribution de l'abondance des coatings argileux seront discutés (i.e., distance au plancher glaciaire, distance au niveau argileux, dynamique sédimentaire). Enfin dans une dernière partie (6), un modèle de mise en place des coatings argileux dans les grès glaciaires du bassin de Sbaa sera proposé.

Les coatings argileux» dans les grès glaciaires ordoviciens du bassin de Sbaa (Algérie): processus de mise en place et implications pétrophysiques

Processes of clay coating emplacement in Ordovician glacial sandstones and their impact on petrophysical properties (Sbaa, Algeria).

1. Les coatings en environnements glaciaires

1.1 Définition

Dans les roches sédimentaires gréseuses, les grains sont parfois revêtis d'une fine pellicule d'origine sédimentaire, organique, ou diagénétique, qui tapissent les grains de façon plus ou moins continue, celle-ci est appelée «coating» ou tapissage (**Fig. 1**). Ces fines pellicules sont constituées par différents types de minéraux et de structures, incluant voiles microbiens, oxydes de fer, carbonates, zéolithes, microquartz asyntaxiaux ou encore des argiles (Pittman et al., 1992). Les coatings argileux sont les plus communs et les mieux documentés dans la littérature, notamment en raison de leurs impacts sur la préservation de la porosité et de la perméabilité dans les réservoirs gréseux très profondément enfouis (Pittman et al., 1992).

Il existe deux principaux types de coatings argileux: les coatings argileux allogéniques correspondant à la mise en place précoce d'argiles dans des sables, et les coatings argileux authigéniques qui se développent par des processus diagénétiques pendant l'enfouissement progressif des sables. Durant la mésogénèse, la chimie des eaux interstitielles ainsi que la composition minéralogique du sable influencent grandement la croissance d'argiles authigènes et la néoformation d'argiles (Pittman et al., 1982). Les environnements de dépôts ont également un rôle majeur sur les processus éodiagénétiques puisque les conditions environnementales contrôlent: la composition chimique et la quantité d'eau présente dans le sédiments, la différence entre l'apport d'eau et l'évaporation, la température, l'exposition ou non des sédiments à l'oxygène atmosphérique, ou encore la quantité de matière organique (Worden and Morad, 2003).

1.2 Les coatings argileux détritiques

Tous les types d'argiles peuvent présenter des origines détritiques (Chamley, 1989). Ces argiles détritiques peuvent se déposer de manière précoce avant enfouissement et transformation diagénétique, mais ils peuvent également se mettre en place plus tardivement lors de l'exhumation de grès longuement enfouis (i.e., pendant la télogénèse). Les coatings argileux peuvent être continus, discontinus, isopaques ou anisopaques et s'observent à l'échelle microscopique (**Fig. 1**).

Les coatings argileux détritiques précoces peuvent se mettre en place dans une multitude

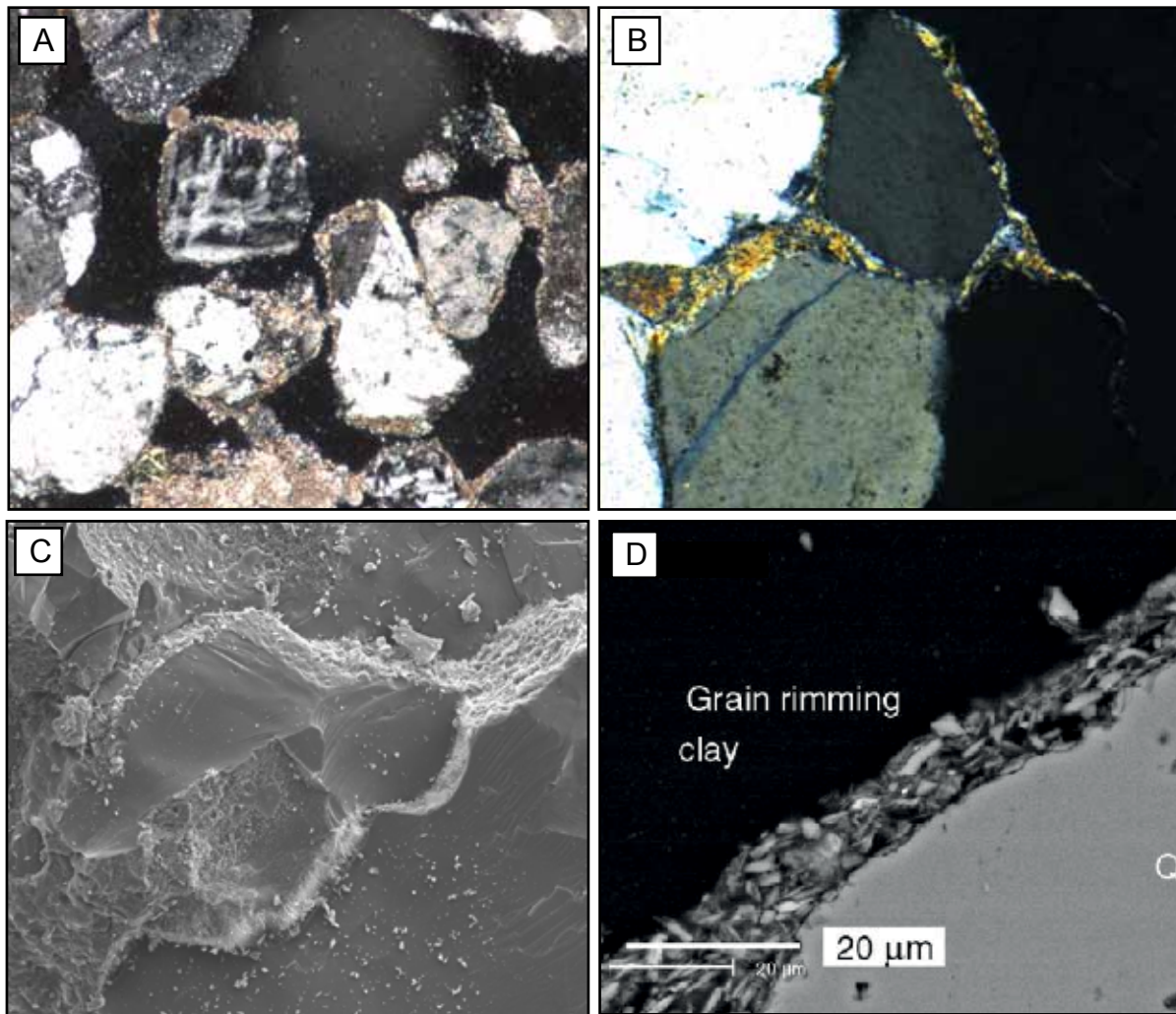


Figure 1. (A) Discontinuous and anisopachous clay coatings emplaced in glacial sand (Pleistocene, Switzerland). (B) Discontinuous and anisopachous clay coatings observed in glacial sandstones (Ordovician, Algeria). (C) Observations of continuous clay coatings around quartz grains using a Digital Electron Microscope (DEM) (Ordovician, Algeria). (D) Close up on platy clay coatings deposited along the margin of a quartz grain (DEM observation) (Worden et al., 2006).

d'environnements sédimentaires comprenant les environnements turbiditiques (i.e., marins profonds), estuariens, deltaïque, fluviaux, éoliens, ou encore glaciaires (Matchlack et al., 1989; Houseknecht et Ross Jr., 1992; Storvoll et al., 2002; Tournier et al., 2010).

Dans les environnements marins, les bioturbations, les écoulements de masse (mass flows), et les déformations pré-lithifications liées aux fortes pressions de fluides sont notamment responsables de la remobilisation et de l'introduction d'argiles détritiques dans les sables (Hurst et Buller, 1984; Houseknecht et Ross Jr., 1992; Ali et al., 2010). La mise en place de coatings argileux d'origine détritique dans les environnements continentaux résulte de l'infiltration mécanique d'eau météorique et de la percolation de cette eau riche en argile en milieu vadose (Buurman et al., 1998). Dans les sables glaciaires, les infiltrations d'eaux de fonte chargées en argiles ou encore les déformations sédimentaires induites par des fortes pressions de fluide peuvent être responsables de l'introduction

de particules argileuses et du tapissage des grains (Menzies, 2000; ven der Meer et al., 2003; Tournier et al., 2010; Menzies et Ellwanger, 2011; Phillips et al., 2013).

Le type et l'orientation des coatings argileux par rapport aux grains sont directement induits par les processus découlant de leur mise en place (e.g., décantation, illuviation, infiltration, translocation, remobilisation, etc...).

1.3. Les coatings détritiques en environnements glaciaires: modèles de mise en place.

Les coatings argileux dans des environnements sous-glaciaires sont largement sous-étudiés, cependant certains processus de mise en place ont été suggérés dans la littérature (Tournier, 2010; Menzies, 2000; van der Meer et al., 2003; Menzies and Ellwanger, 2011; Phillips et al., 2007; 2013). Trois principaux modèles peuvent être proposés: (1) un modèle où les coatings se mettraient en place durant le dépôt des sédiments, (2) un second modèle où l'infiltration d'eaux de fonte en surpression et riches en particules argileuses favorise la mise en place de coatings et enfin, (3) un dernier modèle impliquant les remobilisations argileuses engendrées par des fortes pressions de fluide (**Fig. 2**).

(1) Les différents environnements sédimentaires et leurs dynamiques singulières ont une influence notable sur la distribution des coatings. Les lois d'hydrodynamique suggèrent que le dépôt des argiles n'est pas contemporain du sable. Cependant le dépôt rapide de sédiments induits par une diminution très rapide des vitesses d'écoulement peut favoriser l'incorporation de fines particules dans le sable, notamment dans les turbidites ou dans les débris flows (Worden et Morad, 2003). Dans les environnements sous-glaciaires, la chute rapide de la pression hydrostatique dans les cavités sous-glaciaires pourrait provoquer le dépôt quasi- instantané des sédiments, et donc le dépôt simultané des sables et des argiles (Ravier et al., 2014) (**Fig. 2**). Dans les environnements proglaciaires, de telles variations de pression ne sont pas attendues, la diminution de l'énergie avec l'éloignement de la marge glaciaire peut cependant favoriser le dépôt des particules les plus fines (i.e., argiles) et donc former des tapissages argileux (Wilson, 1992) (**Fig. 2**). Malgré des processus de mise en place différents, des coatings argileux détritiques peuvent potentiellement se mettre en place en environnements sous-glaciaires et proglaciaires.

L'étude de la répartition et de l'abondance des coatings en fonction des environnements de dépôts peut permettre d'estimer si la dynamique sédimentaire contrôle la mise en place des coatings argileux.

(2) Lors de périodes de découplage entre la glace et le substrat, des eaux de fonte en surpression

et riches en particules argileuses peuvent circuler à l'interface glace/substrat (Boulton et al., 2009; Piotrowski et al., 2009). Lorsque le substrat est sableux, non lithifié, poreux et perméable, une quantité notable d'eaux de fonte peut s'y infiltrer et circuler. Ces eaux de fonte, riches en argiles, peuvent circuler profondément dans les sables poreux et sont ainsi responsables de la mise en place des tapissages argileux (Tournier, 2010) (**Fig. 2**). L'étude de la distribution et de l'abondance verticale des coatings par rapport au plancher pourrait permettre de mettre en évidence ce processus de mise en place. Dans cette configuration, une décroissance de l'abondance des coatings depuis le plancher glaciaire pourrait être attendue (Tournier, 2010).

(3) Le troisième modèle suggère une remobilisation post dépôt des particules argileuses lors de l'augmentation de la pression de fluide. Cette augmentation peut déclencher des processus de liquéfaction et de fluidisation des sédiments. Houseknecht et Ross Jr (1992) ont décrit une mise en place de tapissages illitiques au sein de turbidites marines entièrement fluidisées. De la même manière, les remaniements sédimentaires et les phénomènes de fluidisation sont également fréquents dans le registre sédimentaire glaciaire (van der Meer et al., 2009; Denis et al., 2010; Phillips et al., 2013).

La liquéfaction et la fluidisation des sédiments sont associées à des phénomènes d'élutriation qui consistent en une remobilisation accrue des particules les plus fines (i.e, des argiles) (Lowe, 1975). Des réseaux de petits conduits se forment, à l'intérieur desquels les particules argileuses sont transportées (e.g., conduits d'élutriations) (**Fig. 2**). Lorsque la pression de pore n'est plus suffisante pour prolonger le transport des argiles, ces fines particules se déposent et peuvent ainsi tapisser les grains de sable. L'impact de l'augmentation de la pression de fluide sur la mise en place des coatings argileux a notamment été mise en évidence au sein des structures en «dish». En effet, les processus d'élutriation associés à ces structures de déformations pré-lithification provoquent un enrichissement très localisé du sable en particules argileuses (Hurst et Buller, 1984).

Lorsque des contraintes verticales et/ou horizontales sont associées aux processus de fluidisation/liquéfaction des sédiments, les chemins d'élutriations peuvent se développer selon une orientation préférentielle. Lors du couplage entre la glace et le substrat, les conduits d'élutriation devraient principalement se propager vers le bas en raison de la contrainte verticale imposée par le poids de la glace (Phillips et al., 2013) (**Fig. 2**). A proximité de la marge glaciaire, la nette diminution de la contrainte verticale facilite la progression des conduits d'élutriation vers le haut (**Fig. 2**).

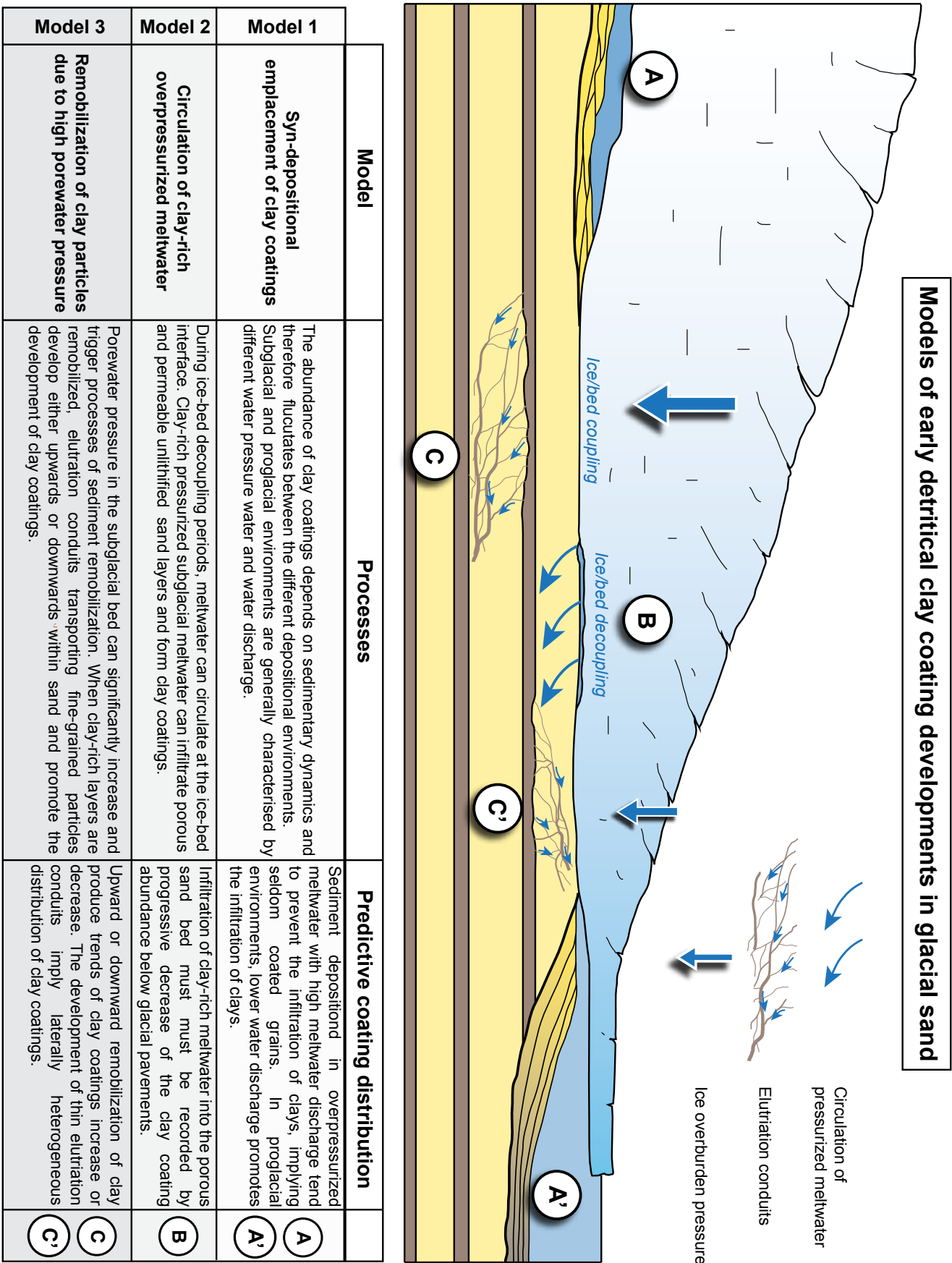


Figure 2. Schematic diagram illustrating the three models of detrital clay coating establishment in glacial environments.

1.4 Impact des coatings argileux sur les propriétés pétrophysiques

La présence de coatings argileux peut avoir différentes conséquences sur la séquence diagénétique et donc a posteriori sur les propriétés pétrophysiques des grès. En effet, ces tapissages argileux ont deux effets opposés sur la porosité/perméabilité (Byrnes et Wilson, 1994).

La mise en place de coatings argileux est largement décrite comme un facteur majeur dans la préservation de la porosité et de la perméabilité dans les grès enfouis à de grandes profondeurs (Amhed, 2008; Ajdukiewicz et Larese, 2012). Les coatings parviennent à maintenir une porosité élevée à de fortes profondeurs en inhibant la formation de ciment siliceux tardif. Les tapissages argileux ralentissent voire empêchent la nucléation des auréoles de silicification sur les grains détritiques de quartz, et donc préservent la porosité (Ajdukiewicz et Larese, 2012). Dans cette première configuration, la présence de coatings argileux a pour conséquence de former de bons réservoirs, dits «conventionnels».

En revanche, les coatings argileux tapissant les grains de quartz dans les réservoirs sableux ont également pour conséquence de catalyser les phénomènes de pression-dissolution durant l'enfouissement progressif du sable. Cette catalyse favorise la compaction chimique et donc la libération de fluides riches en silice (Bjorkum, 1996; Bloch et al., 2002). La cristallisation de ces fluides riches en silice est à l'origine de la mise en place d'un ciment siliceux précoce. La poronécrose majeure associée à la mise en place de ce ciment siliceux précoce est à l'origine des mauvais réservoirs (i.e., réservoirs «tights»).

2. Exemple des grès glaciaires de Sbaa (Algérie)

Afin de mieux contraindre les processus de mise en place des coatings argileux, une étude a été menée sur les grès glaciaires ordoviciens du bassin de Sbaa (Algérie). Des études précédentes ont démontré la présence de coatings argileux dans ces grès, ainsi que leurs impacts significatifs sur la séquence diagénétique et sur les propriétés réservoirs (Tournier et al., 2010; Tournier, 2010). Une hypothèse de mise en place précoce des argiles, liée à la dynamique des eaux de fonte, a été proposée (Tournier, 2010). Dans ce modèle, une infiltration d'eaux de fonte sous hautes pressions et riches en argiles serait à l'origine des coatings argileux dans les grès.

Afin de mieux contraindre les processus intervenant dans la mise en place des coatings, une quantification de l'abondance de ces tapissages argileux a été réalisée. Dans un deuxième temps,

les différents paramètres contrôlant la distribution de l'abondance des coatings ont été analysés (distribution verticale par rapport au plancher, distribution en fonction des environnements sédimentaires, distribution par rapport aux niveaux argileux). Les résultats obtenus permettront de discuter le ou les modèles responsables de la mise en place des coatings argileux dans les grès glaciaires ordoviciens du bassin de Sbaa (Algérie).

2.1. Contexte géologique.

2.1.1. Localisation géographique

La présente étude utilise les données issues d'un puits foré au sein du bassin de Sbaa (puits ODZ-6). Le bassin sédimentaire de Sbaa est localisé dans le Sud-Ouest de l'Algérie (**Fig. 3A et B**). Ce bassin intracratonique correspond à une dépression synclinale située à l'intersection de la chaîne de l'Ougarta, la voûte d'Azzène ainsi que le Bled El Mas et s'étend sur une surface d'environ 32000km². Il présente une orientation principalement NW-SE dans le prolongement de la chaîne des Monts de l'Ougarta (**Fig. 3C**). Il est situé entre deux bassins sédimentaires, le bassin de Timimoun au Nord et le bassin de Reggane au Sud (**Fig. 3C**).

2.1.2. Contexte structural

L'initiation du bassin de Sbaa a lieu lors de l'orogénèse panafricaine, en raison de la collision entre le craton Ouest Africain et Est Africain à la fin du Protérozoïque (Bumby et Guiraud, 2005). La phase panafricaine provoque la surrection du massif du Hoggar et la mise en place de grands linéaments de socle orientés N-S (Bumby et Guiraud, 2005). Ces grands linéaments sont interprétés comme des décrochements (NW-SE et conjugués) résultant d'une compression horizontale orientée E-W (**Fig. 3C**). Ces différents accidents tectoniques formés durant l'orogénèse panafricaine sont à l'origine de la structuration du socle précambrien sur l'ensemble de la plate-forme saharienne. Ils forment ainsi l'édifice sur lequel vont s'installer les différents bassins paléozoïques, dont le bassin de Sbaa. Suite à l'orogénèse panafricaine, une phase majeure de distension orientée NW-SE, provoquant une subsidence générale, correspond à l'extension Cambro-Ordovicienne. Durant cet épisode extensif, la formation de structures en demi-graben conduit à l'individualisation des bassins de la plate-forme

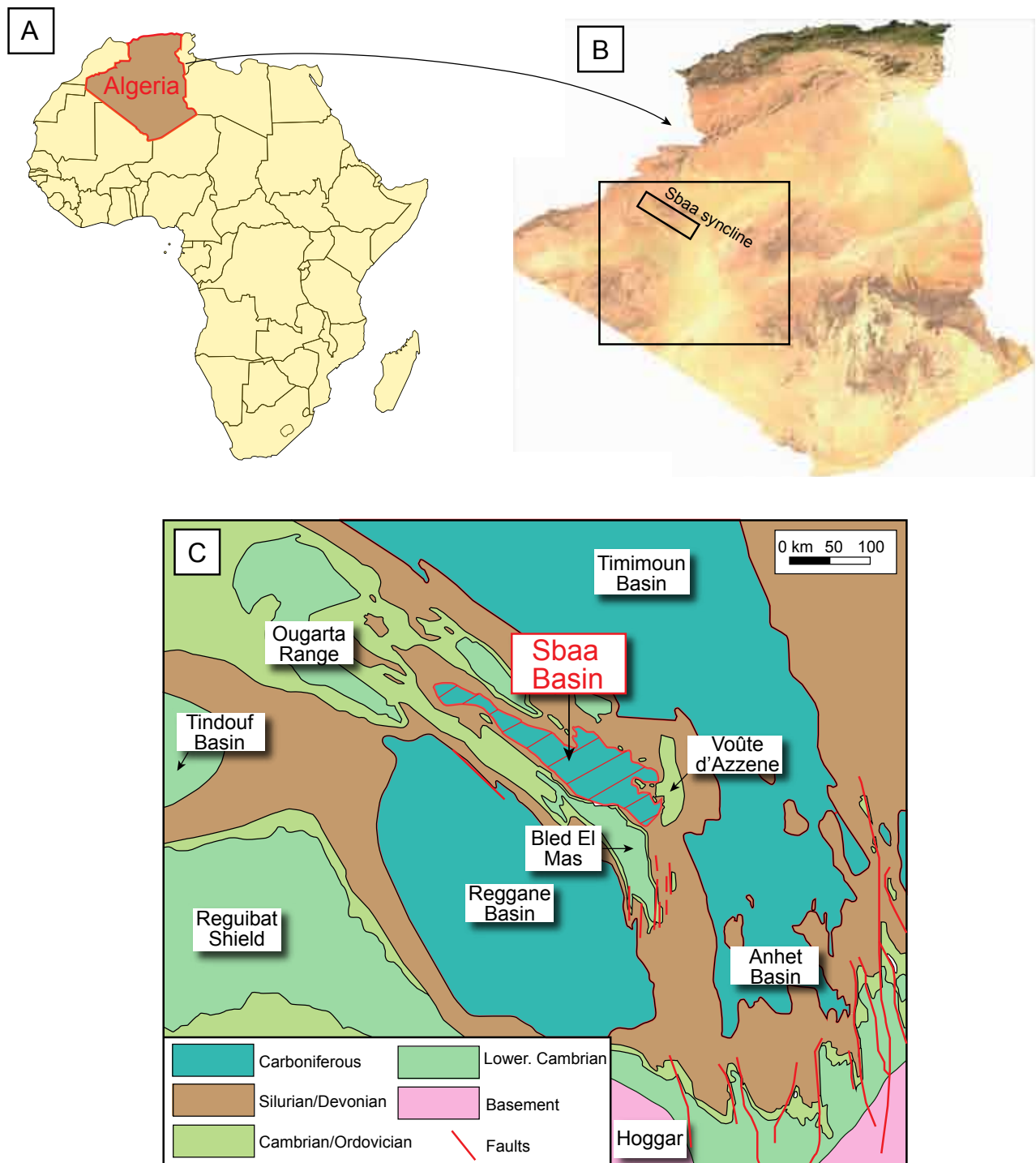


Figure 3. (A) (B) Location of the Sbaa basin in Algeria. (C) Geological map of Palaeozoic units in Algeria and locations of the main sedimentary basins.

saharienne (Beuf et al., 1971). A l'Ordovicien supérieur, un nouvel épisode compressif associé au cycle Calédonien réactive des accidents panafricains et génère des plis d'axe N-S (Lüning et al., 2005). La phase Hercynienne provoque une intense structuration, la création, et la réactivation de nombreux systèmes de failles. Au paroxysme de l'orogénèse hercynienne, la chaîne de l'Ougarta se forme véritablement par d'importants plissements et chevauchements. Ce maximum de déformation se traduit par une surrection du socle, formant une ride d'orientation NS-SE entre le bassin de Reggane

et le bassin de Sbaa (**Fig. 3C**). Le bassin de Sbaa s'individualise véritablement lors de cette orogénée hercynienne, par l'inversion et le soulèvement de la Voute d'Azzène et la réactivation du chaînon Sud de l'Ougarta et du Bled El Mas, formant les bordures actuelles Nord et Sud du bassin (**Fig. 3C**). La bassin de Sbaa constitue alors un synclinal d'axe NW-SE, situé en position haute par rapport aux bassins voisins de Reggane au sud, et Timimoun au Nord.

2.1.3. Contexte sédimentaire durant l'Ordovicien

L'ensemble des unités sédimentaires présentes et observées dans le bassin de Sbâa reposent sur un substratum pré-cambrien (**Fig. 4**). Les sédiments cambriens se sont mis en place dans un système fluvial en tresse et sont ensuite remaniés dans un environnement de type tidal (Tournier, 2010). Les sédiments ordoviciens déposés au sein du bassin de Sbâa peuvent être divisés en deux unités sédimentaires :

- l'unité III, caractérisée par des alternances argilo-gréseuses (**Fig. 4**).
- l'unité IV, caractérisée par des dépôts glaciaires gréseux contenant quelques passages silto-argileux (**Fig. 4**) (Tournier, 2010). Cet ensemble sédimentaire est composé de quatre sous unités (IV.1, IV.2, IV.3 et IV.4). Les sédiments glaciaires ordoviciens se sont déposés dans un système de vallées tunnels creusées pendant plusieurs phases d'avancées glaciaires.

Les quatre carottes sédimentaires issues du puits ODZ-6 analysées au cours de cette étude contiennent des sédiments issus de l'unité IV.3 et IV.4, pour une épaisseur total de 54 m (**Figs. 4, 7**).

2.1.4. Paléogéographie et glaciation fini-ordovicienne

Durant la fin du Protérozoïque, l'initiation de la phase panafricaine engendre un assemblage de masses continentales et la mise en place d'un super continent appelé Gondwana (Cocks et Torsvik, 2002; Ghienne, 2003; Bumby et Guiraud, 2005). À la fin du Protérozoïque et début du Paléozoïque, la migration de Gondwana vers le Pôle Sud, associée à des facteurs climatiques et géologiques, engendre une modification des conditions climatiques sur Terre et l'initiation d'une période de type «ice house». Cette période coïncide avec la mise en place d'une importante calotte de glace sur ce super continent (Scotese et al., 1999; Finlay et al., 2010; Torsvik et Cocks, 2011) (**Fig. 5**).

La durée de la glaciation varie entre 0,5 et 2 Ma (Brenchley et al., 1994; El-ghali et al., 2006; Ghienne

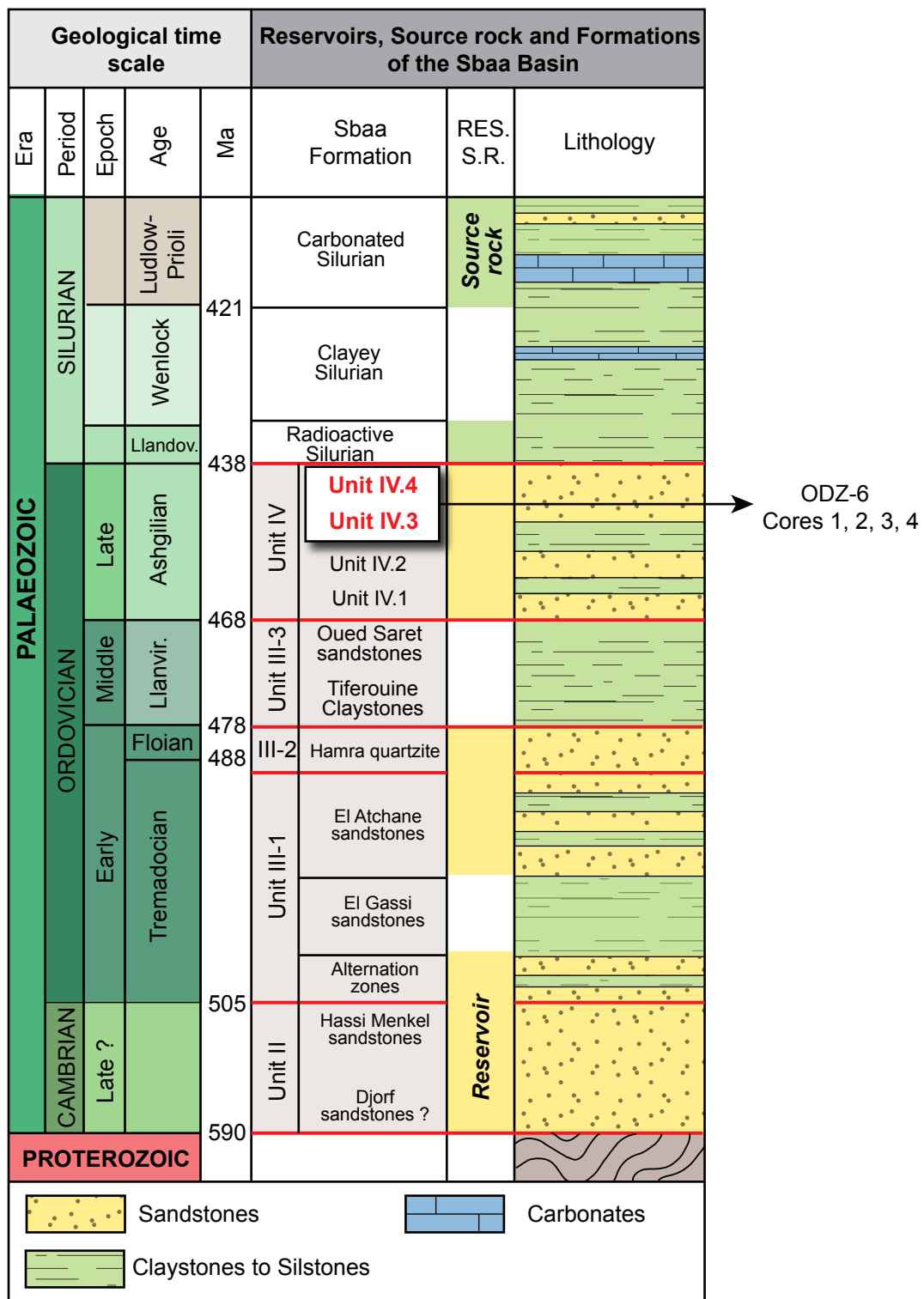


Figure 4. Stratigraphic scheme of the sediments contained in the Sbaa basin (modified after Fernandez, 2004 and Tournier, 2010). Sediment cores analyzed in this study correspond to the Unit IV.4 and IV.3. These sedimentary units were deposited during the Late Ordovician and correspond to sediments deposited during the Hirnantian glaciation.

et al., 2007; Le Heron et al., 2009). L'épisode glaciaire hirnantien marque le maximum d'une période froide qui aurait duré environ 10 Ma (Brenchley et al., 1994; Ghienne et al., 2007).

La période glaciaire Hirnantienne est marquée par des cycles de retrait et d'avancée de la calotte de glace, exprimée par des phases d'érosion suivies d'accumulation de sédiments, ainsi que des variations eustatiques (Sutcliffe et al., 2000; Ghienne et al., 2003; Huuse et al., 2012; Clerc et al., 2013). Deux

phases de glaciation sont enregistrées et séparées par une période de transgression correspondant à la fonte de la calotte (Sutcliffe et al., 2000; Ghienne et al., 2007). Le bassin de Sbaa était situé à proximité de la marge nord de la calotte glaciaire gondwanienne (**Fig. 5**).

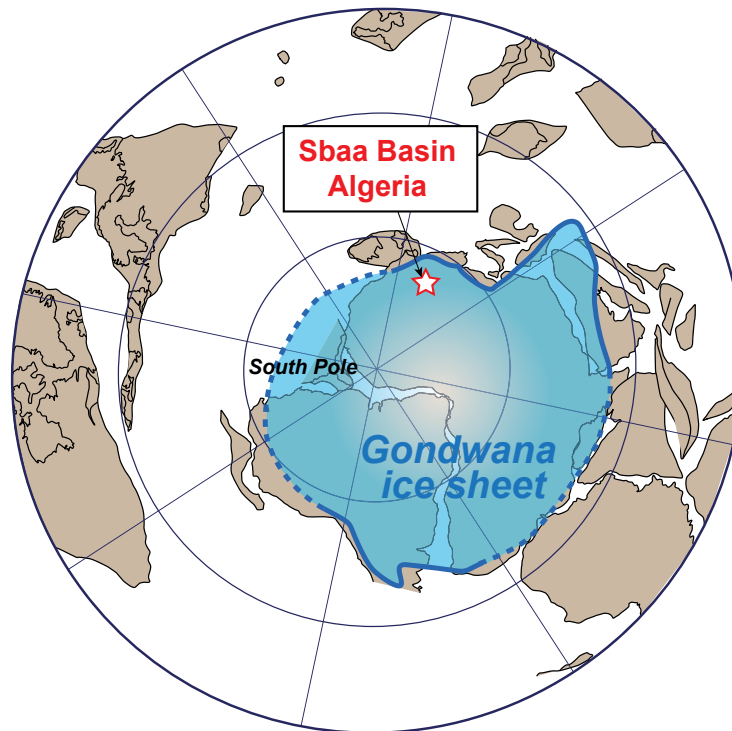


Figure 5. The extension of the Hirnantian palaeo-ice sheet represented on the Gondwana palaeo continent (reconstructions adapted from Cocks and Torsvik, 2002 and Ghienne et al., 2007). Note the location of the Sbaa basin, in the Northern margin of the ice sheet.

2.2. Méthodologie

Une analyse faciologique et une étude détaillée des structures de déformations pré-lithification ont tout d'abord été réalisées le long des carottes sédimentaires.

A partir de ces carottes, des plugs ont été réalisés à intervalles réguliers afin de déterminer: (1) la nature et la morphologie des coatings argileux, (2) leurs impacts sur les propriétés pétrophysiques, (3) l'abondance des coatings argileux et leur distribution (**Fig. 6**).

(1) Les nature et morphologie des coatings argileux ont été déterminées grâce à une étude microscopique détaillée. 70 lames minces ont été analysés, quelques cassures fraîches de fragments ont été observées au microscope électronique à balayage et les poudres ($< 2 \mu\text{m}$) de 18 échantillons analysés au diffractomètre à Rayon X.

(2) Des mesures pétrophysiques (porosité, perméabilité) ont été réalisées sur les plugs prélevés le long des carottes.

(3) La quantification de l'abondance des coatings argileux a été effectuée à l'aide du logiciel

JMicroVision©. Sur chaque lame mince, le pourcentage de grains coatés (i.e., tapissé par des argiles) a été mesuré par comptage de points, avec un minimum de 200 points.

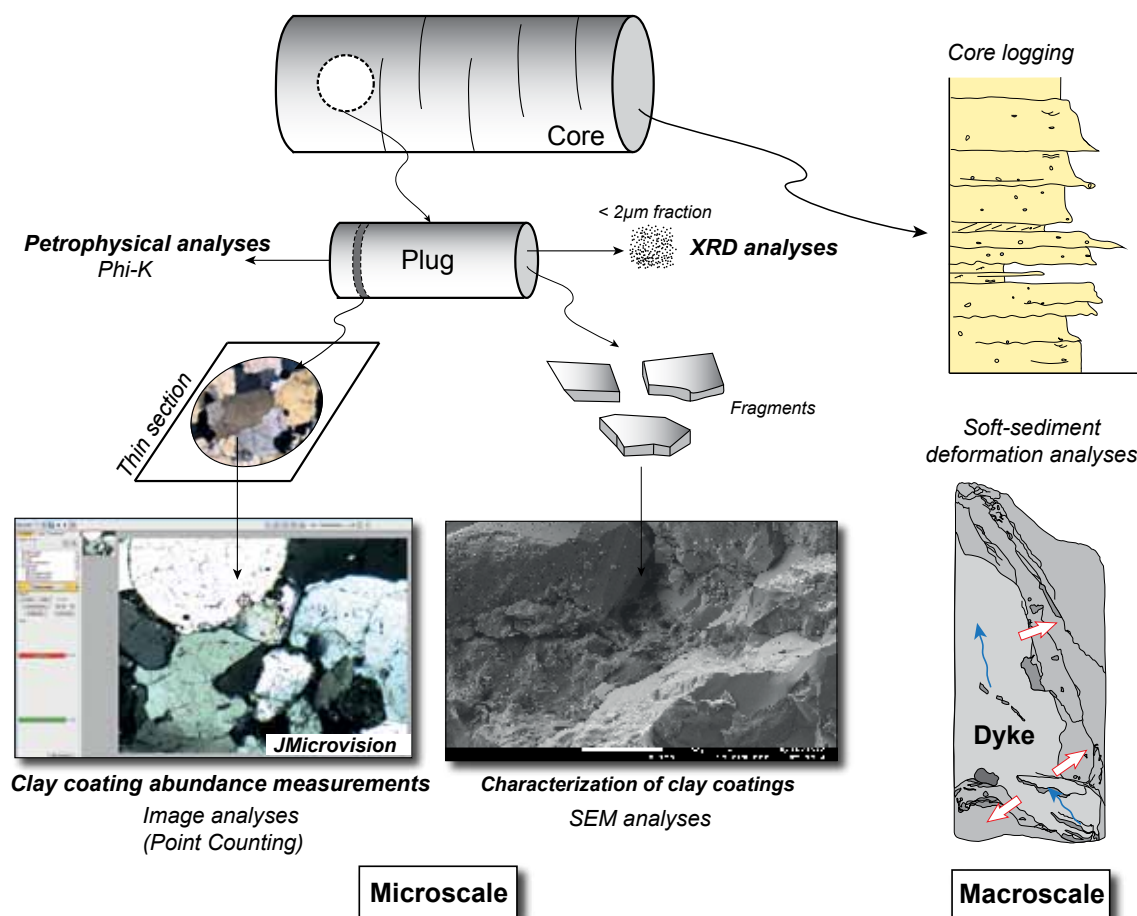


Figure 6. Schematic diagram illustrating the different methods used to determine the type of clay coatings, their abundance, and their impact on petrophysical properties.

2.3. Résultats

Le log sédimentaire, les données pétrophysiques (porosité et perméabilité), ainsi que la distribution de l'abondance des coatings argileux sont synthétisés dans la figure 7.

Les carottes récoltées le long du puits ODZ-6 ont permis d'observer la présence de deux planchers glaciaires. Un premier plancher situé à la cote 2521m et un second à 2440m. Ces deux planchers ont été mis en évidence par une augmentation notable de la granulométrie et par la présence de nombreuses structures de déformation pré-lithification. Ces structures se mettent en place sous les planchers et sont induites par un cisaillement simple (boudins asymétriques, plans de schistosité «S-C», plis en fourreaux), mais aussi par l'augmentation de la pression d'eau interstitielle (dykes clastiques, structures d'échappements d'eau). Ces types de déformation suggèrent des épisodes de couplage entre la glace et le substrat.

2.3.1. Faciès sédimentaires et environnements de dépôts

Les carottes sédimentaires C1 à C4 contiennent des dépôts appartenant aux unités IV.3 Inf. et IV. 4 (**Fig. 4**). La granulométrie entre ces deux unités varie entre des sables fins bien triés et des sables grossiers assez mal triés, avec quelques fois l'apparition de niveau silto-argileux de faible épaisseur (< 25 cm), notamment dans l'unité IV.3.Inf où trois passages argileux sont observés (**Fig. 7**).

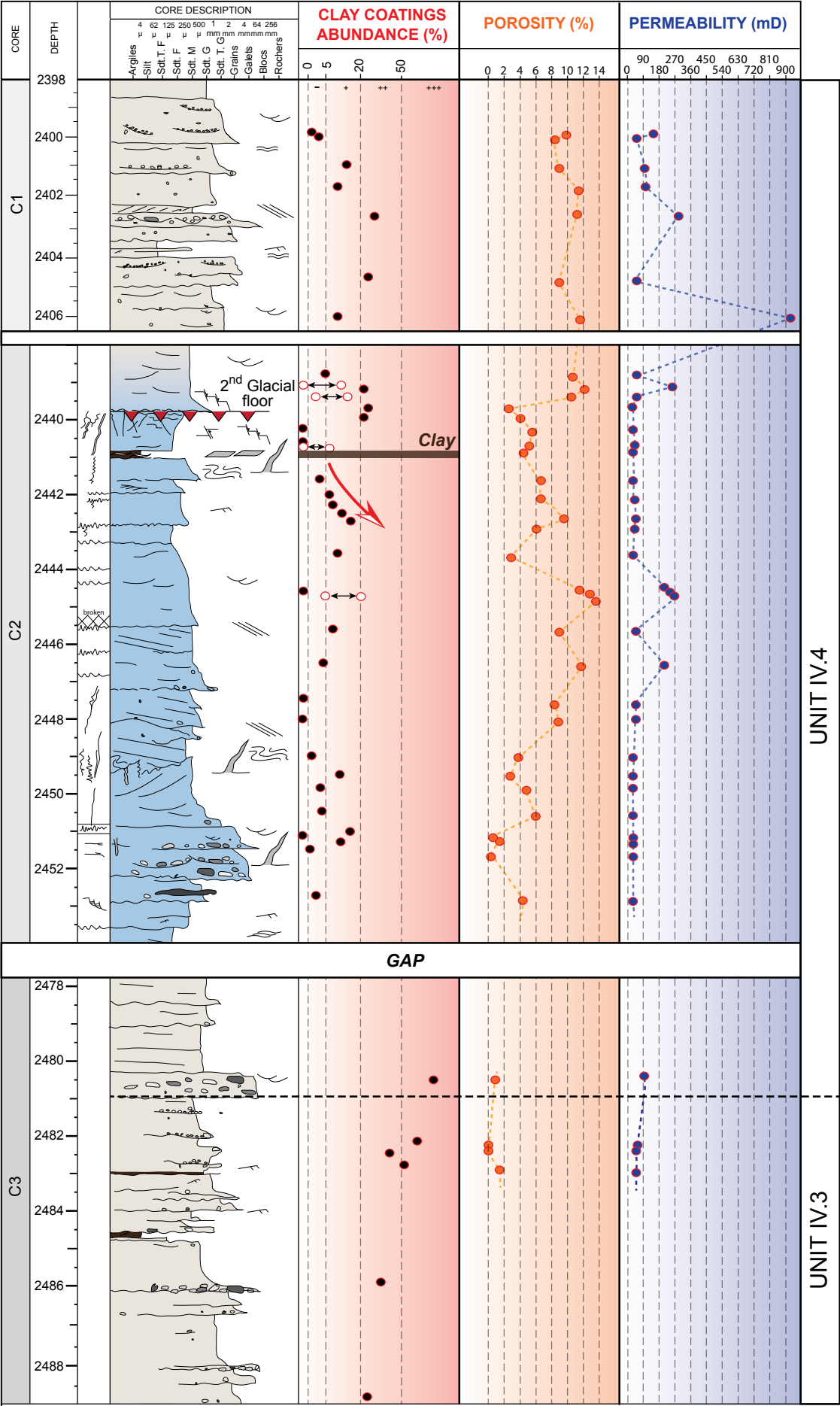
L'unité IV.3.Inf. (carottes 3 et 4) est caractérisée par la présence de litages en auges, stratifications entrecroisées, litages obliques à plans avec bases érosives, localement marquées par des reprises granulométriques (graviers). L'unité IV.3 Inf. présente peu de structures de déformation pré-lithification. Néanmoins, à la base de la carotte 4, la présence d'un plancher glaciaire est mise en évidence par une augmentation de la granulométrie et par la présence de nombreuses structures de déformation pré-lithification (**Fig. 7**).

L'unité IV.4 (carottes 1 et 2) est caractérisée par différentes structures sédimentaires associées à des dépôts de chenaux et de levées. Des rides de courants, des litages obliques, mais également des stratifications entrecroisées ont été observées. Des reprises granulométriques sont également fréquemment enregistrées (**Fig. 7**). La carotte C2 présente de nombreuses structures de déformation pré-lithification ainsi que la présence d'un plancher glaciaire positionné à la cote 2440 m. En revanche, la carotte C1 est complètement dépourvue de structures de déformation.

Deux grands environnements sédimentaires sont proposés pour le dépôt des sédiments dans les unités IV.3 Inf. et IV.4 (GDF internal report). Un environnement de dépôt sous-glaciaire, enregistré dans la carotte C2 et à la base de la carotte C4, se caractérise par la récurrence de déformations induites par des fortes pressions de fluide et par le cisaillement de la glace (cf. section 2.3.2) (**Fig. 7**). Les carottes C4 et C1 contiennent des sédiments déposés en environnement proglaciaire et enregistrent des dépôts tractifs marqués par l'absence de structures de déformation (**Fig. 7**). La transition entre ces deux environnements se produit pendant des phases de déglaciation, elle est par conséquent progressive et difficile à délimiter.

2.3.2. Structures de déformation pré-lithification

De nombreuses structures de déformation pré-lithification ont pu être observées à l'échelle macroscopique. Ces déformations se concentrent souvent sous les planchers glaciaires, et sont liées à



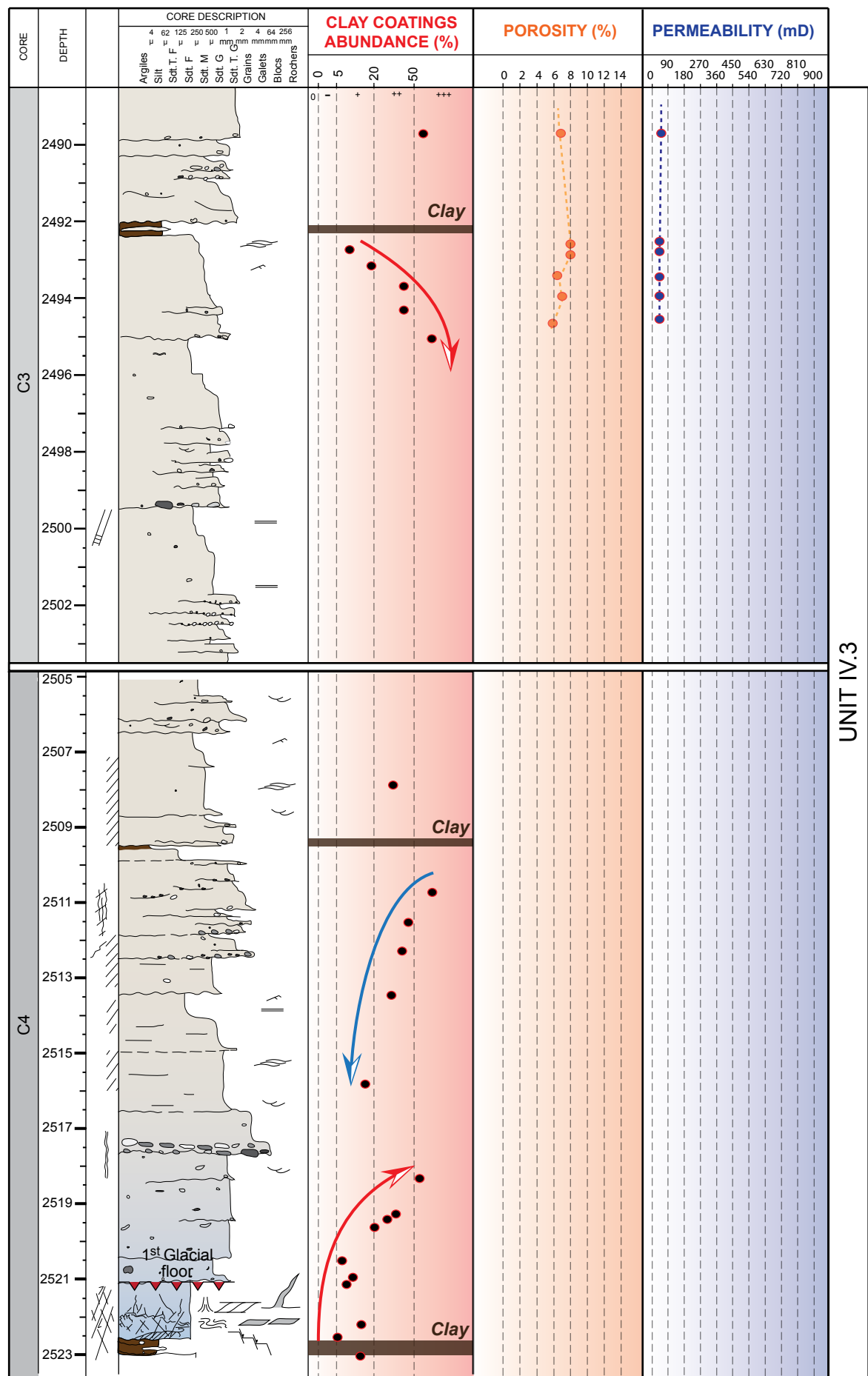


Figure 7. Sedimentary log of ODZ-6 with corresponding petrophysical data and clay coating abundance values. The location of the soft-sediment deformation structures and the sedimentary structures is replaced along the log as well as the interpreted depositional environments (Cf. legend in Fig. 8).

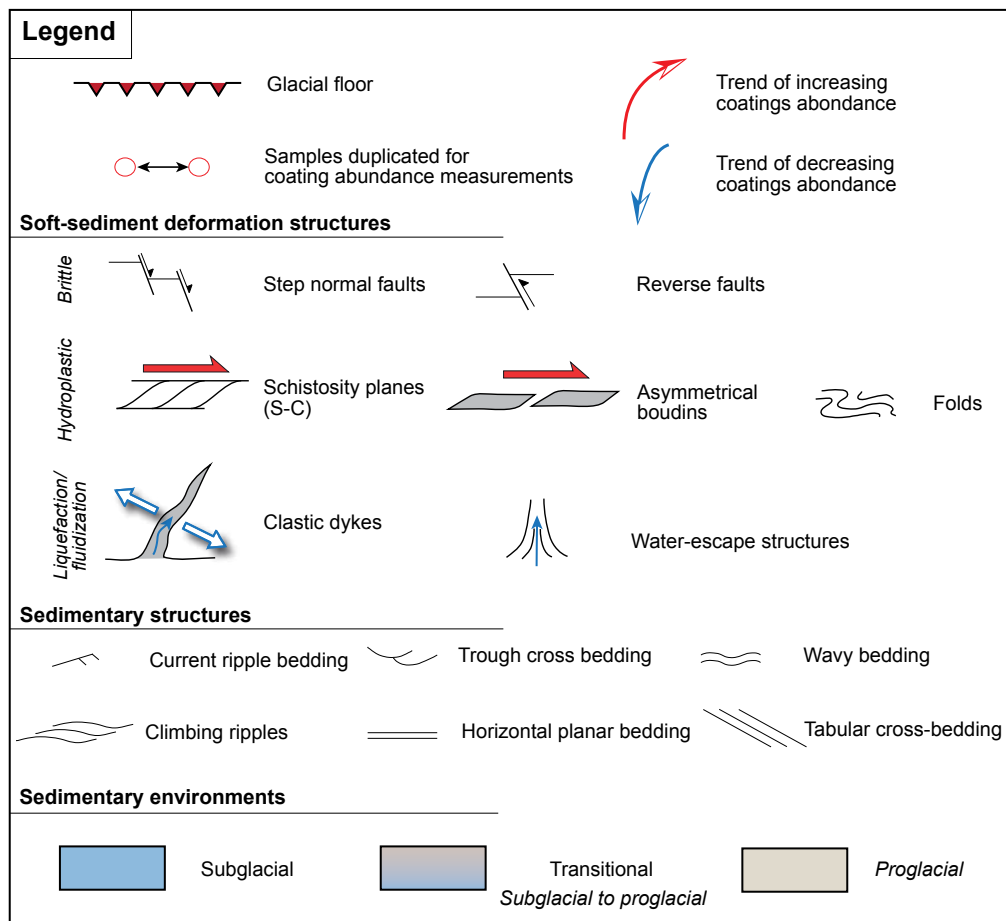


Figure 8. Legend used for the description of the ODZ-6 sedimentary log.

des processus de déformation fragile, hydroplastique ou de fluidisation/liquéfaction (Figs. 7, 8).

Les déformations fragiles sont caractérisées par des failles normales en gradins qui témoignent d'une déformation liée à une contrainte verticale affectant des sables peu saturés en eau. Les failles normales en gradins sont fréquentes dans les environnements sous-glaciaires, où la contrainte verticale exercée par le poids de la glace sur les sédiments déclenche la mise en place de ces structures (Biju-Duval et al., 1974; Denis et al., 2010; Ravier et al., 2014). Quelques failles inverses ont été également

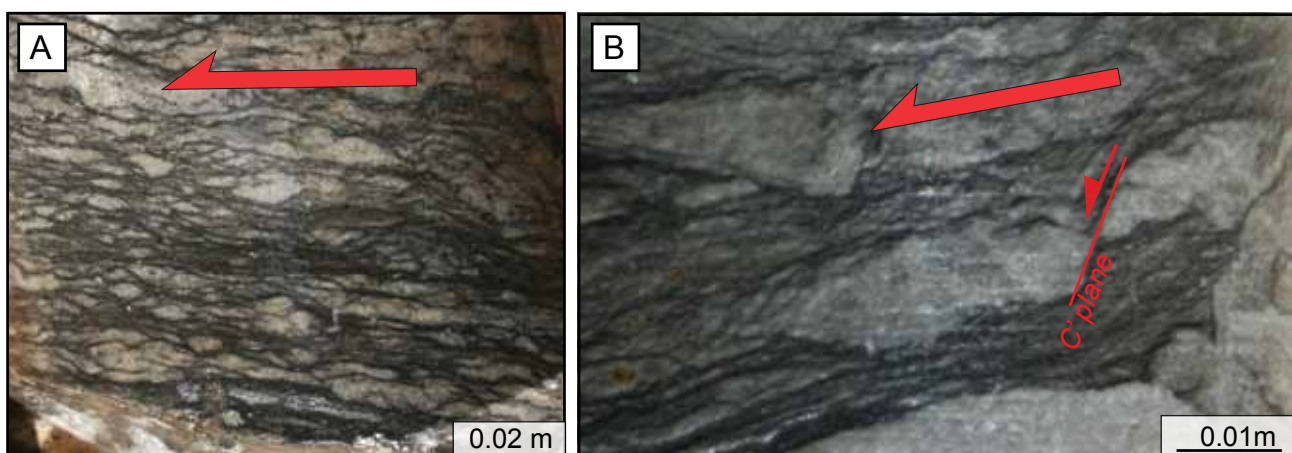


Figure 9. (A) Boundins formed by general shear below the glacial floor. (B) Close up on asymmetrical boudins (also referred as shearband boudins) where typical C' plane form due to intense shear. Red arrows indicate sense of shear.

observées sous les planchers glaciaires, et sont probablement liées à l'action cisailante de la glace sur les sédiments.

Un certain nombre de déformations hydroplastiques ont été également observées à proximité des planchers glaciaires. Elles incluent des boudins asymétriques, des plans de schistosité caractérisés par des structures de type «S-C» et quelques structures plissées (**Fig. 9A, B**). La déformation hydroplastique indique une légère augmentation de la saturation en eau et/ou à l'augmentation de l'argilosité. Les différentes structures observées sont le produit d'une déformation par cisaillement général (i.e., pure + simple shear). Lorsqu'elles se forment à proximité d'un plancher glaciaire, il est probable que ces structures soient produites par l'action cisailante de la glace sur les sédiments lors

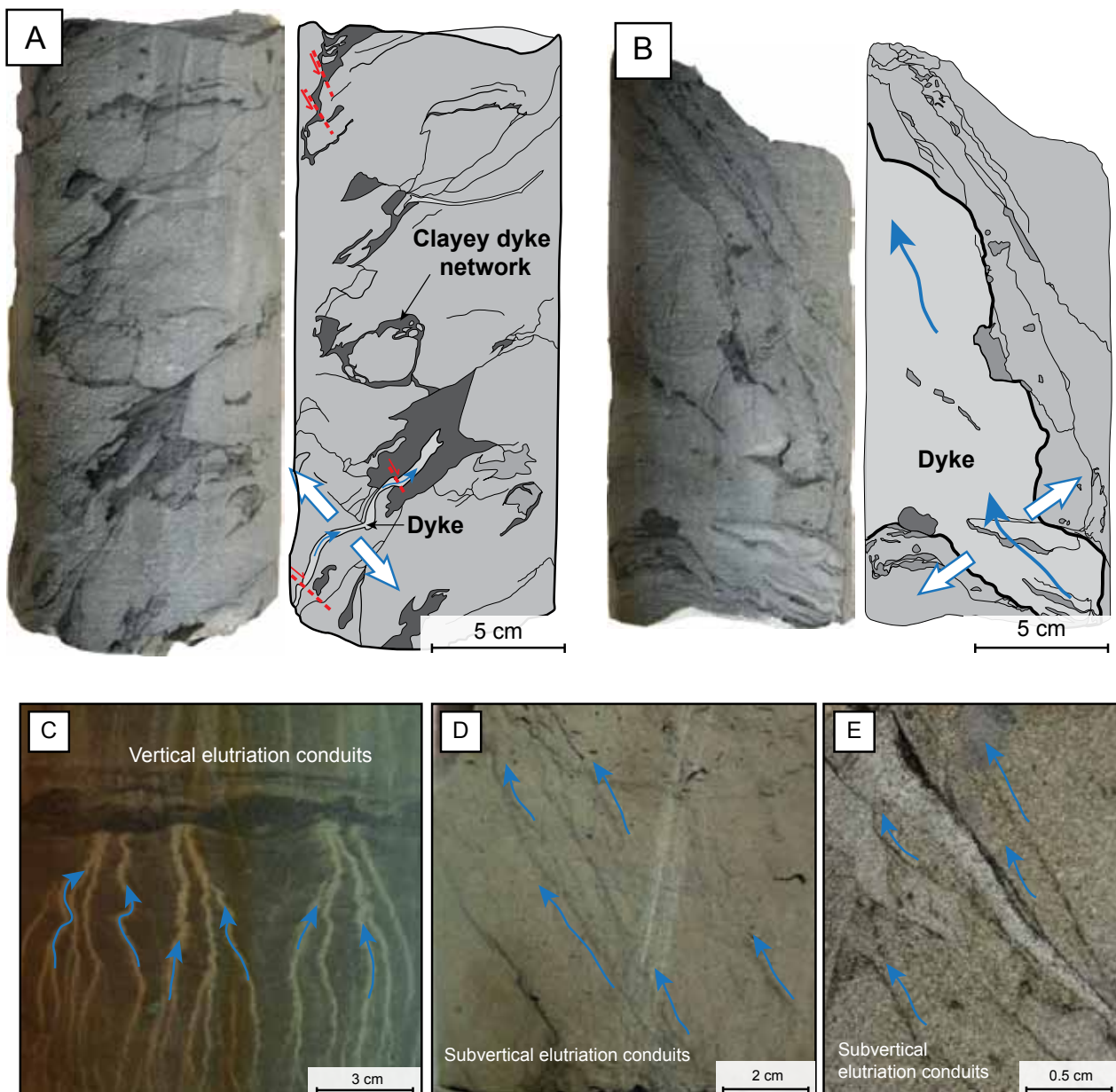


Figure 10. (A) A network composed of clayey dyke that is later fractured by a set of normal faults. (B) A dyke filled by homogenized sand. (C) Network of elutriation conduits transporting material. (D) Anastomosed elutriation conduits remobilizing clay particles under the effect of high porewater pressures. (E) Subvertical elutriation conduits in ODZ-6.

de périodes de couplage entre la glace et le substrat (Denis et al., 2010, Lesemann et al., 2010, Ravier et al., 2014).

Enfin, la dernière catégorie de déformation pré-lithification est constituée de structures liées à des processus de liquéfaction/fluidisation, telles que des dykes clastiques et des structures d'échappement d'eau. Le remplissage des dykes clastiques varie des argiles au sable (**Fig. 10A, B**). Au sein d'ODZ6, mais aussi dans un autre puits foré à proximité, de nombreuses structures d'élutriation ont été également observées (**Fig. 10C, D, E**). Ces structures se composent de réseaux de conduits à l'intérieur desquels les particules fines (argiles et silts) sont remobilisées sous l'effet de l'augmentation de la pression d'eau interstitielle. Ces réseaux d'élutriation peuvent parfois remanier et remobiliser complètement des niveaux argilo-silteux. Les types de structures liées aux processus de liquéfaction, fluidisation ont un rôle important dans la remobilisation des particules les plus fines, et notamment des argiles puisque ces deux processus sont fréquemment associés à des phénomènes d'élutriations (Lowe, 1975).

L'augmentation de la pression de fluide à proximité des planchers glaciaire est due à l'action de la glace qui comprime des sédiments saturés en eau. Les apports d'eaux de fonte peuvent également jouer un rôle dans l'augmentation de la pression d'eau interstitielle (van der Meer et al., 2009; Denis et al., 2010; Phillips et al., 2013; Ravier et al., 2014).

2.3.3. Morphologie et nature des coatings

Dans les 70 lames minces étudiées, les variations d'abondance de coatings argileux sont très importantes, avec des valeurs s'échelonnant de 0 à 77%. Les coatings argileux du puits ODZ-6 sont caractérisés par différentes morphologies. Ces coatings sont constitués par des argiles biréfringentes qui tapissent des grains de quartz détritiques de manières continues ou discontinues (**Fig. 11C, D**). En revanche, certains échantillons montrent une absence totale de tapissages argileux autour des grains de quartz (**Fig. 11A, B**). Les tapissages argileux sont parfois isopaques mais présentent parfois des variations d'épaisseur donnant lieu à des coatings anisopaques. L'analyse au diffractomètre à rayon X de la fraction argileuse de 18 échantillons prélevés dans les différentes carottes ont révélé la présence de 100 % d'illite (**annexe 1; cf. p. 453**). L'observation des coatings argileux au MEB a

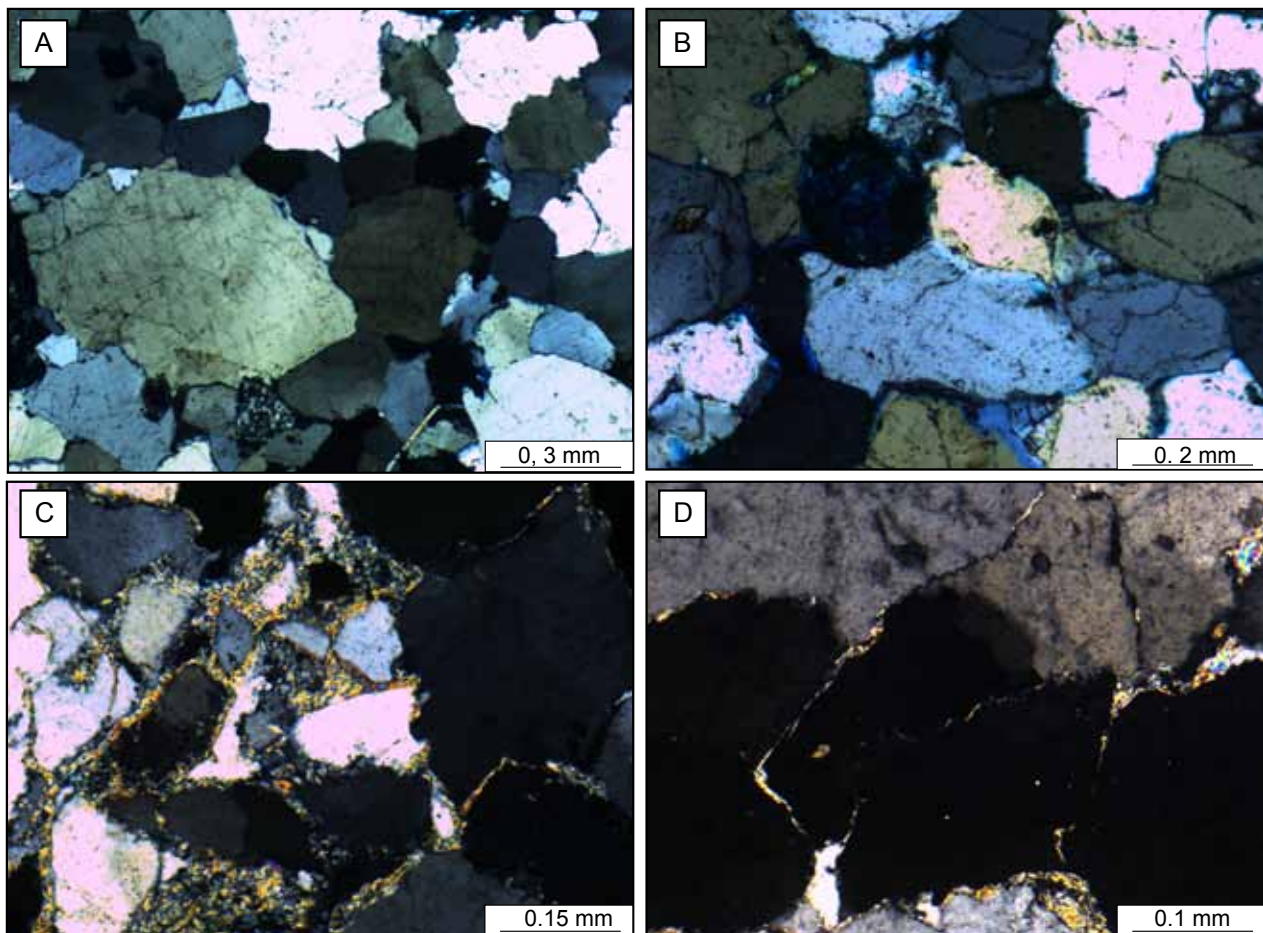


Figure 11. (A) (B) Two thin sections showing quartz grains without clay coatings. (C) Quartz grains with birefringent clay films partially or totally surrounding the quartz grains. (D) Quartz grains with discontinuous thin clay coatings.

permis de mettre en évidence des morphologies fibreuses typiques des tapissages argileux illitiques d'origine diagénétique (**Fig. 12A, B**) (Desbois et al., 2011; Wilson et al., 2014). Des morphologies lamellaires, formant des plaquettes disposées parallèlement par rapport à la surface du grain et qui sont généralement associées à des illites d'origine détritique, ont également pu être distinguées (**Fig. 12 C**) (Matlack et al., 1989). Les tapissages illitiques englobent totalement ou partiellement les grains de quartz mais peuvent également former de grandes plages lorsqu'elles proviennent du remplacement de feldspaths potassiques durant la diagenèse (**Fig. 12D**).

2.3.4. Abondance des coatings vs. Perméabilité/Porosité

Le graphique présentant la relation entre abondance des coatings et porosité met en évidence la présence de deux groupes distincts:

(1) Pour de faibles pourcentages de grains coatés (0 à 20%), les valeurs de porosités (2 à 16%) et de perméabilité (0.01 à 1000 mD) sont très variables (**Fig. 13A**).

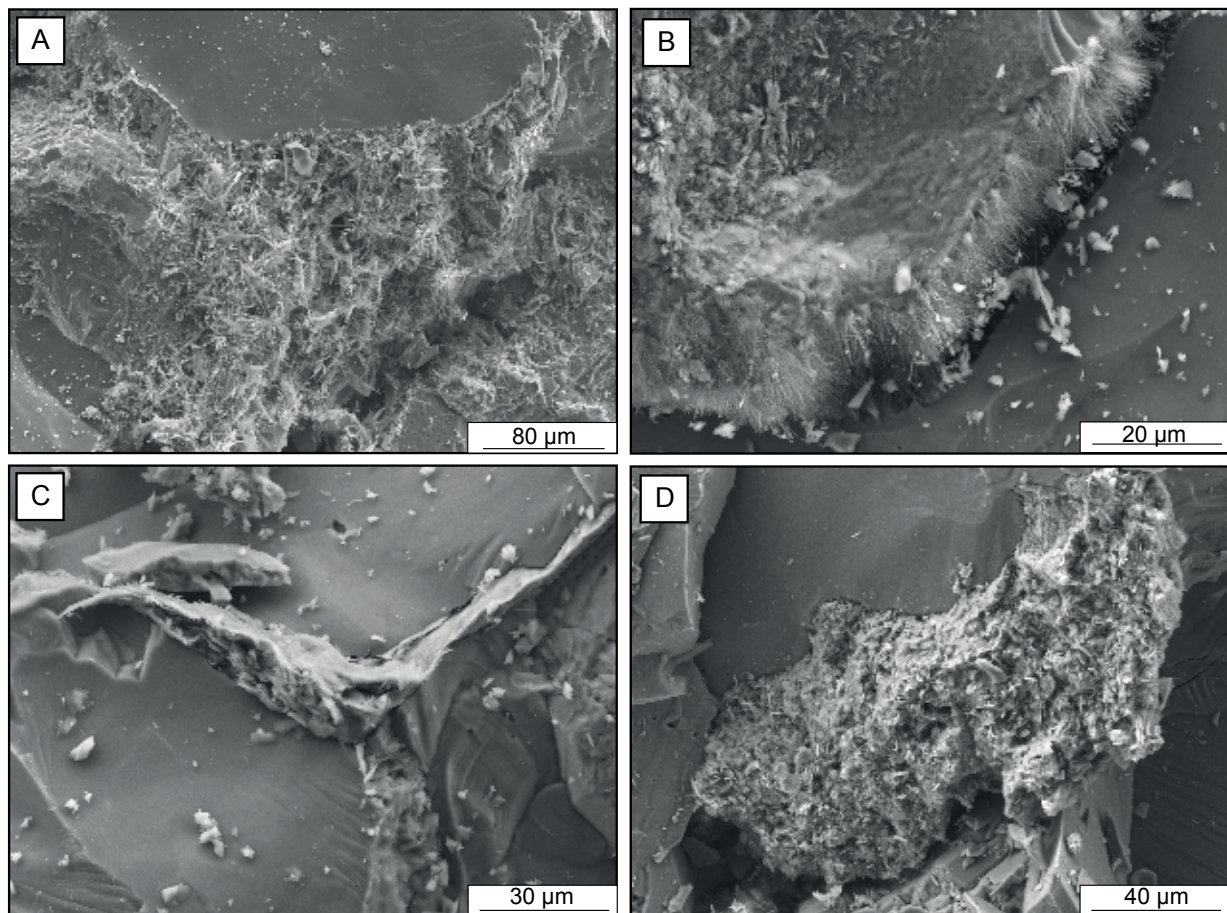


Figure 12. Scanning electron microscope photograph of clay coatings observed in ODZ-6. (A) (B) Illite coating with fibrous morphologies. (C) Illite coating with platy morphologies. (D) Illite formed by feldspar substitution.

(2) Pour des pourcentages de grains coatés élevés ($> 40\%$), les grès sont caractérisés par des faibles valeurs de porosité (entre 2 et 6%) et de perméabilité (0.01 à 0.1 mD) (**Fig. 13A**).

Après contrôle des échantillons, les trois points où des valeurs d'abondance de coatings élevées sont associées à des fortes perméabilités (10 à 100 mD) correspondent à des échantillons microfracturés (**Fig. 13B**).

Plusieurs études montrent que la dissolution de quartz intergranulaire est favorisée par la présence de fins tapissages d'illite autour des grains détritiques de quartz (Weyl, 1959; Heald et Larese, 1974; Sibley et Blatt, 1976; Dewers et Ortoleva, 1991; Renard et al., 1997; Fisher et al., 2000). Au contact entre deux grains de quartz, l'illite catalyse la dissolution du quartz par l'amélioration de la diffusion des solutés sur la surface des argiles. La dissolution et la recristallisation du quartz est responsable de la réduction des valeurs de porosité et de perméabilité (Weyl, 1959 ; Dewers et Ortoleva, 1991 ; Oelkers et al., 1992 ; Bjorkum, 1996 ; Renard et Ortoleva, 1997).

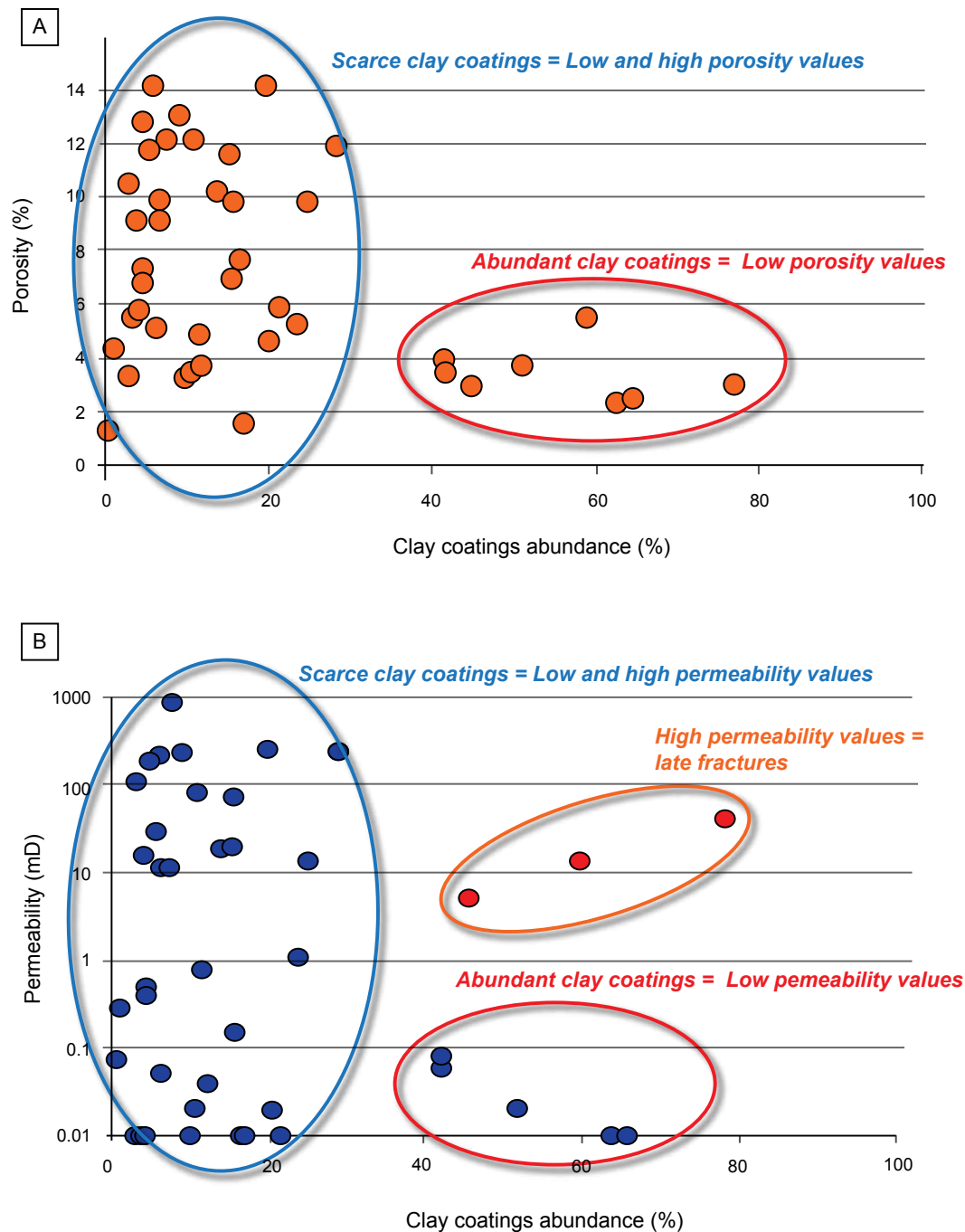


Figure 13. (A) Porosity vs. clay coatings abundance in ODZ-6. (B) Permeability vs. clay coatings abundance in ODZ-6.

2.3.5. Analyse de la distribution des coatings argileux

► Distribution depuis les planchers glaciaires

Sous le plancher glaciaire numéro 2, les 14 m continus de carottes sédimentaires contiennent 26 mesures d'abondance en coatings à intervalles réguliers (**Figs. 7 et 14**). Aucune tendance ou relation n'est observée dans la distribution verticale des coatings sous le plancher. Il n'existe donc pas de

relation entre la mise en place des coatings argileux et la distance au plancher glaciaire (**Fig. 14**).

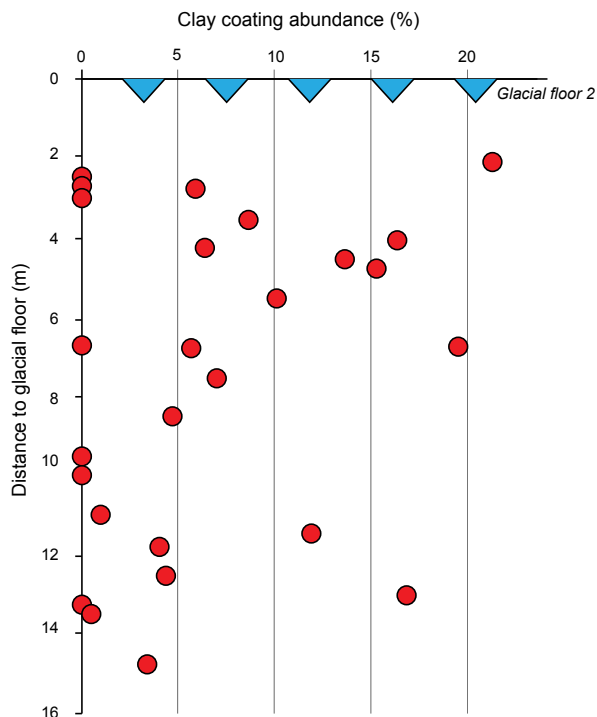


Figure 14. Distribution of the abundance of clay coatings from the glacial floor 2. Note the absence of relation between clay coatings abundance and distance to the glacial floor.

► Distribution depuis les niveaux argilo-silteux

Les sables représentent la granulométrie dominante des carottes sédimentaires du puits ODZ-6. Cependant, cinq niveaux argilo-silteux mesurant de 10 à 25 cm d'épaisseur ont été observés. Il est possible de distinguer des tendances d'augmentation ou de diminution de l'abondance en coatings argileux à proximité de ces fins bancs argilo-silteux (**Fig. 7**). En dessous du premier plancher glaciaire, une tendance à l'augmentation de l'abondance en coatings vers le haut est observée depuis un niveau argileux situé à la cote 2523 m, avec un passage progressif de 5 à 53 % de grains coatés. Au dessus de ce premier plancher glaciaire, une décroissance du pourcentage de grains tapissés par des argiles est observée dans une zone située à proximité d'un niveau argileux épais de quelques centimètres (2509, 50 m) (**Fig. 7**). Cette décroissance s'observe sur environ 5 m et est associée à une chute de l'abondance en coatings de 65 % à 18 %. Une augmentation progressive du pourcentage de grain coatés vers le bas est observée à proximité d'une fine couche argilo-silteuse située à la cote 2492 m (**Fig. 7**). En dessous de cette fine couche de 25 cm d'épaisseur, l'abondance en coatings argileux passe de 11% à 64 % sur environ 3 m d'épaisseur. Enfin, sous le plancher glaciaire 2, une augmentation vers le bas de l'abondance en coatings est observée depuis une couche argilo-silteuse de 20 cm d'épaisseur située à

la cote 2441m (**Fig. 7**). Les valeurs de pourcentage de grains coatés augmentent très progressivement de 4.5 % à 16%.

► *Variations latérales à très fines échelles.*

Quelques échantillons ont été dupliqués afin d'estimer les variations locales d'abondance en coatings argileux. Au sein d'un même plug, des variations importantes de pourcentage de grains coatés sont observées, illustrant le caractère hétérogène de la répartition des coatings à échelle centimétrique. L'abondance des coatings peut parfois tripler entre deux doublons (**Fig. 15**). De la même manière, ces variations en abondance de coatings peuvent être très importantes à l'échelle métrique. Autour de la cote 2240 m, des fortes variations sont observées sur 1 m d'épaisseur démontrant également le caractère très hétérogène de la répartition des coatings argileux (**Fig. 15**).

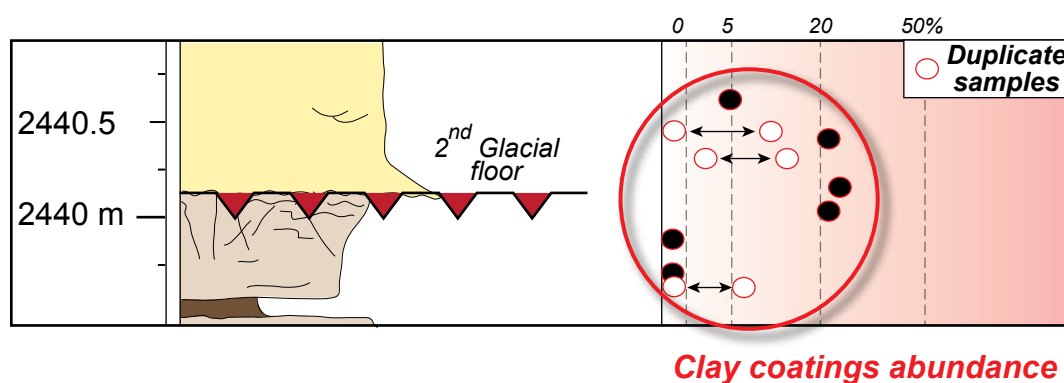


Figure 15. Variations of clay coating abundance at centimetric scale and between duplicates, illustrating the heterogeneous distribution of clay coatings.

► *Influence des environnements sédimentaires*

L'enregistrement sédimentaire suggère la présence de deux grands environnements de dépôt: un environnement sous-glaciaire et un environnement proglaciaire (**Fig. 7**).

L'abondance des coatings entre ces deux environnements sédimentaires est sensiblement différente. La moyenne des pourcentages de grains coatés est de 8, 2 % dans les échantillons issus de sables sous-glaciaires alors que les échantillons issus de sables proglaciaires présentent des valeurs quatre fois supérieures (34.6%) (**Tableau 1**). Un test U de Mann-Whitney a permis de démontrer que ses deux moyennes sont significativement différentes ($p < 0.05$), démontrant ainsi une influence de l'environnement de dépôt sur l'abondance des coatings argileux (**Tableau 1**).

	Samples	Mean (μ)	Std. deviation
Subglacial coating abundance	n = 32	8.2 %	7.09
Proglacial coating abundance	n = 27	34.6 %	19.2
<hr/>			
	U index	P-value	
Mann-Whitney U-test ($\sigma = 0.05$)	93	$2.51 \cdot 10^{-7}$	

Table 1. Comparison of clay coatings abundance between subglacial and proglacial sand. Mann-Whitney U-test results confirms that coatings abundance are different between subglacial and proglacial environments.

2.4. Discussion

2.4.1. Origine des coatings argileux.

Les coatings argileux au sein du puits ODZ-6 sont constitués d'illites. Ces tapissages illitiques peuvent être d'origine détritique et mis en place de manière précoce, ou alors ils peuvent être authigéniques et donc se mettre en place plus tardivement, pendant la diagenèse (Houseknecht et Ross, 1992; Jahren et Aagaard, 1992; Buurman et al., 1998). Une majorité des coatings illitiques est caractérisée par des morphologies fibreuses, ce qui induit donc une formation tardive durant la diagenèse (Desbois et al., 2011; Wilson et al., 2014). Néanmoins, certaines illites montrent des morphologies en plaquettes disposées parallèlement au grains de quartz qui témoignent d'une possible origine détritique (Matlack et al., 1989). La mise en place d'illites détritiques est bien connue dans les environnements fluviatiles où elles s'installent lors de l'infiltration précoce d'eaux chargées en argiles (Matlack, 1989; Moraes et De Ros, 1990; Buurman et al., 1998). Des tapissages illitiques ont également été enregistrés dans des sables turbiditiques liquéfiés et mise en place par des phénomènes d'élutriations lors de l'augmentation de la pression d'eau interstitielle (Houseknecht et Ross Jr., 1992).

De plus, la distribution spécifique de l'abondance des coatings argileux à proximité des couches argilo-silteuses ou alors en fonction de l'environnement de dépôt suggèrent une mise en place précoce de ces tapissages illitiques. Enfin, un dernier argument pour l'origine détritique des coatings concerne la minéralogie des argiles tapissant les grains de quartz. En effet, les illites sont des argiles se formant

fréquemment par altération mécanique sous climat froid et sec. Des études ont démontrées que l'illite est l'argile dominante transportée à la mer par les glaciers de hautes latitudes (Chamley, 1989).

Les coatings illitiques observés au sein du puits ODZ-6 présentent des arguments en faveur d'une mise en place précoce et d'origine détritique. Cette origine détritique était déjà suggérée dans l'étude diagénétique et minéralogique détaillée des grès du bassin de Sbaa réalisée par Tournier (2010).

2.4.2. Paramètres contrôlant la distribution des coatings argileux

L'analyse de la distribution de l'abondance des coatings argileux au sein du puits ODZ-6 a permis de mettre en évidence deux facteurs contrôlant leur distribution: (1) les environnements de dépôt, et (2) les remobilisations sédimentaires associées à l'augmentation de la pression de fluide.

► (1) Environnements sédimentaires

L'analyse de l'abondance des coatings entre les sédiments sous- et proglaciaires a permis de mettre en évidence un facteur de contrôle syn-dépositionnel sur la distribution des coatings argileux, propre à la dynamique sédimentaire. En effet, les sédiments sous-glaciaires présentent un coating argileux moins abondant comparés aux sédiments déposés au devant la calotte glaciaire. Cette distribution préférentielle des coatings argileux peut s'expliquer par une variation de la dynamique sédimentaire entre les environnements sous-glaciaires et proglaciaires (**Fig. 16A**). Le dépôt de sédiment sous la glace est généralement associé à des écoulements de hautes énergies et des forts débits en raison du drainage de grandes quantités d'eau de fonte en direction de la marge glaciaire (Clerc et al., 2013). Les forts débits associés à ces dépôts chenalisés sous-glaciaires ont tendance à évacuer et transporter les particules les plus fines, provoquant un appauvrissement en particules argileuses. Cet appauvrissement peut notamment expliquer la faible abondance de coatings argileux dans les grès sous-glaciaires (**Fig. 16A**).

En revanche, en environnement proglaciaire, l'éloignement progressive de la marge glaciaire entraîne une diminution des débits et favorise donc le dépôt de particules plus fines, notamment par décantation et/ou par percolation. Cette diminution de l'hydrodynamisme favorise le développement de tapissages argileux et pourrait expliquer la forte abondance de coatings dans les grès proglaciaires (**Fig. 16A**).

► (2) *Remobilisations liées à l'augmentation de la pression de fluide*

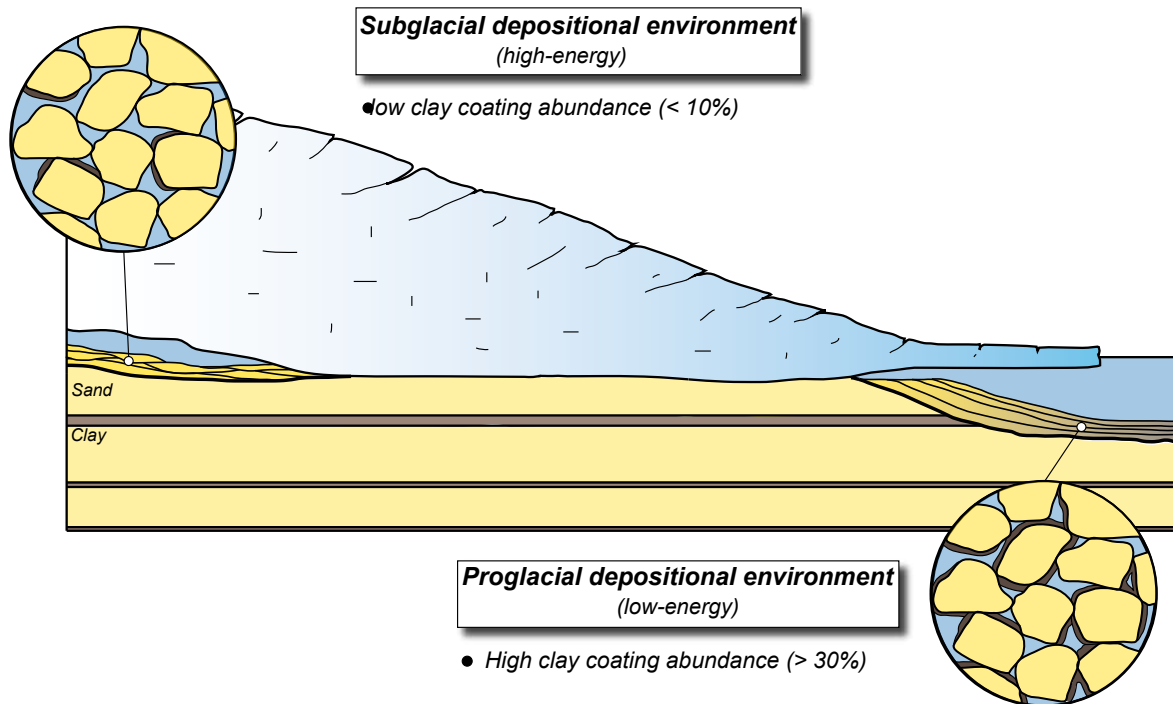
Une hypothèse alternative, expliquant les variations d'abondance de coatings entre environnements proglaciaires et sous-glaciaires, réside dans la remobilisation des particules argileuses lors de l'augmentation de la pression d'eau interstitielle. Lors d'une phase d'avancée glaciaire, les sédiments déposés en environnements proglaciaires se retrouvent sous la calotte de glace et peuvent donc être sujets à d'importantes déformations. La contrainte exercée par le poids de la glace sur ces sédiments saturés en eau provoque une augmentation significative de la pression d'eau interstitielle, entraînant des phénomènes de remobilisations sédimentaires (Lowe, 1975; Ravier et al., 2014). Ces remobilisations sont généralement associées à des processus de liquéfaction/fluidisation des sédiments, comme l'illustre les nombreux dykes observés dans la carotte C2 (**Fig. 7**). Dans cette configuration, la remobilisation des particules les plus fines, connue sous le terme d'élutriation, est commune et peut provoquer un appauvrissement des sédiments en argile. Si les coatings argileux sont naturellement plus abondants en domaine proglaciaire, l'appauvrissement en argile provoqué par les processus d'élutriation pourrait être à l'origine des plus faibles valeurs observées dans les sédiments déformés sous la glace.

De la même manière, l'enrichissement et l'appauvrissement en coatings argileux à proximité des bancs argilo-silteux, témoignent de processus de remobilisations sédimentaires post-dépôt. Ces tendances, associées aux nombreuses structures de déformation induites par des surpressions de fluide, témoignent de la remobilisation des fines couches argilo-silteuses. Ces processus de remobilisations sédimentaires s'enregistrent notamment dans les dykes argileux ou encore dans les réseaux de conduits d'élutriation (**Figs. 7, 10**). L'élutriation des particules fines permet le transport et le dépôt d'illites au sein des sables poreux à travers un réseau de conduits infracentimétriques (**Fig. 16B**). Les illites tapissent très localement les grains de quartz comme l'illustrent notamment les variations d'abondance de coatings au sein d'un même échantillon (**Fig. 15**). Les coatings argileux mis en place par des surpressions de fluides ont été fréquemment décrits dans les environnements glaciaires (van der Meer et al., 2003; Menzies et Elwanger, 2011; Phillips et al., 2013). L'augmentation de la pression de pore est souvent liée aux poids de la glace et/ou en raison de l'apport important d'eaux de fonte dans des aquifères confinés.

La répartition des coatings argileux à proximité des niveaux argilo-silteux au sein du puits ODZ-6 démontre que les processus de remobilisations sédimentaires peuvent se produire vers le bas (cote 2492 m, 2442 m) mais aussi vers le haut (cote 2523 m) (**Figs. 7, 16B**). Dans la littérature, les

Processes of clay coating emplacement in the Ordovician glacial sandstones (Sbaa basin, Algeria)

A) Sedimentary environment control



B) Porewater pressure control

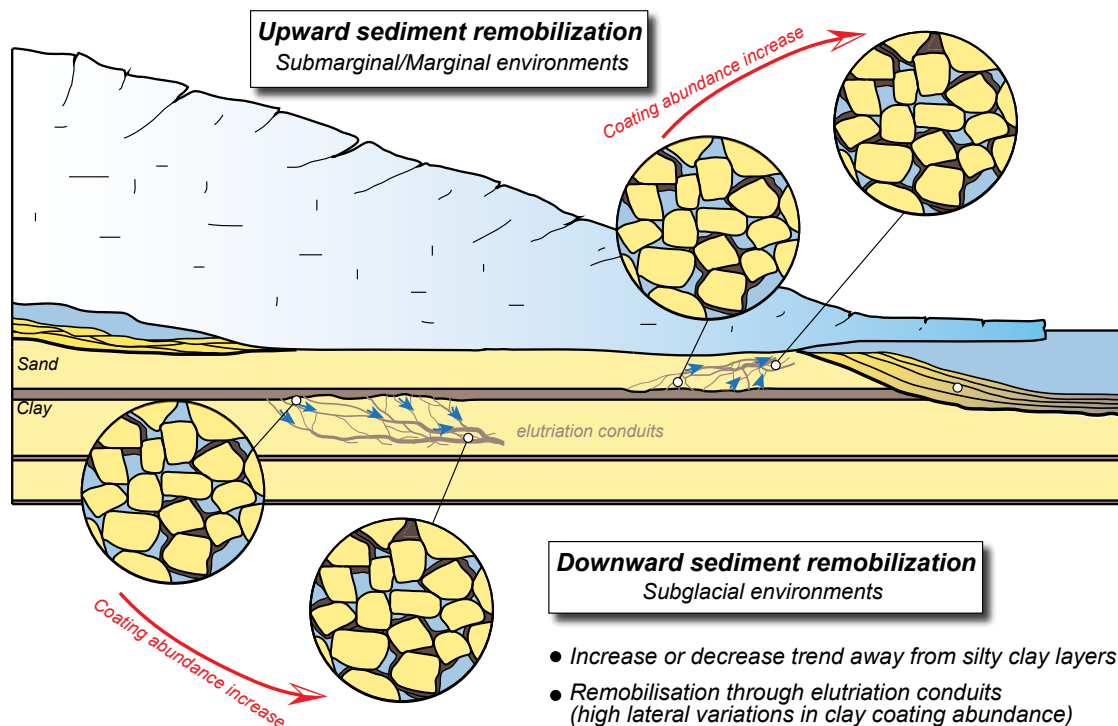


Figure 16. Schematic diagram illustrating the different processes responsible for the distribution of clay coatings within the Ordovician glacial sandstones (Sbaa Basin, Algeria). (A) Clay coatings distribution controlled by the depositional environment. (B) Clay coatings distribution controlled by sediment remobilisation during periods of porewater pressure increase.

remobilisations sédimentaires liées à l'hydrofracturation et l'injection de sédiments peuvent se faire à la fois vers le haut (i.e., *per ascensum*) ou vers le bas (i.e., *per descensum*) (Boulton and Caban, 1995; van der Meer et al., 1999; Phillips et al., 2013). Dans les environnements sous-glaciaires, le poids exercé par la colonne de glace a pour conséquence de diriger la majeure partie des remobilisations sédimentaires vers le bas. En revanche, à proximité du front glaciaire, la diminution considérable de la contrainte exercée par le poids de la glace (e.g., amincissement de la calotte glaciaire) favorise les remobilisations sédimentaires ascendantes.

2.5. Modèles de mise en place des coatings argileux du bassin de Sbaa.

Deux modèles peuvent donc être proposés pour la mise en place des coatings argileux détritiques au sein des grès glaciaires du bassin de Sbaa. Un premier modèle syn-dépôt, où les caractéristiques de la dynamique sédimentaire des environnements sous-glaciaires et proglaciaires contrôlent la distribution des coatings argileux (**Fig. 16A**). Un deuxième modèle, où les remobilisations sédimentaires liées à l'augmentation de la pression d'eau interstitielle influence la distribution des tapissages argileux (**Fig. 16B**). La remobilisation des particules argileuses peut se faire vers le haut ou vers le bas, probablement en fonction des contraintes exercées par la glace sur les sédiments.

3. Conclusions

De nombreuses études ont démontré l'influence des coatings argileux sur la diagenèse des grès et donc leurs impacts sur les propriétés pétrophysiques des réservoirs sableux. Dans cette étude, la quantification de l'abondance des coatings argileux a permis de mettre en évidence l'influence significative de ces tapissages argileux sur les propriétés pétrophysiques des grès glaciaires du bassin de Sbaa. En effet, l'augmentation de l'abondance des tapissages illitiques a pour conséquence de diminuer la porosité et la perméabilité des grès pendant la diagenèse et donc de former des réservoirs dits «tights». Afin de mieux contraindre les hétérogénéités de ces réservoirs, une analyse de la distribution des coatings argileux dans les carottes sédimentaires du bassin de Sbaa a permis de déterminer leurs modèles de mise en place:

(1) La différence significative d'abondance en coatings entre les sables déposés sous et devant la glace met en évidence un contrôle de l'environnement de dépôt et donc de la dynamique sédimentaire

sur la distribution des coatings. La baisse de l'hydrodynamisme associée à l'éloignement de la marge glaciaire favorise le développement de tapissages argileux.

(2) La distribution des coatings argileux a proximité des niveaux argilo-silteux démontre l'importance des remobilisations sédimentaires dans la répartition des coatings argileux. Les fortes pressions d'eau interstitielle, induites par le poids de la glace et/ou des apports important d'eaux de fonte dans des aquifères confinés, provoquent une remobilisation des particules les plus fines correspondant à des phénomènes d'élutriations. Les fins conduits d'élutriations transportent et déposent localement les argiles autour des grains de quartz et forment des gradients d'abondance en coatings argileux depuis les niveaux argilo-silteux.

Dans le cas où ces deux modèles seraient validés à plus grandes échelles, une analyse des faciès sédimentaires, des structures de déformation pré-lithification, et de la distribution des niveaux argilo-silteux, permettrait de déterminer les zones potentiellement enrichies ou appauvries en tapissages argileux au sein d'un réservoir sableux.

Bibliographie

- Ahmed, W., 2008. Contrast in clay mineralogy and their effect on reservoir properties in sandstones formations. *Bulletin of Chemical Society of Ethiopia* 22, 41-65.
- Ajdukiewicz, J.M., Larese, R.E., 2012. How clay grain coats inhibit quartz cement and preserve porosity in deeply buried sandstones: Observations and experiments. *AAPG Bulletin* 96, 2091–2119.
- Ali, S.A., Clark, W.J., Ray Moore, W., Dribus, J.R., 2010. Diagenesis and Reservoir quality. *Oilfield review* 22, 1-14.
- BEICIP, 1996. Etude de la cuvette de Sbâa: GDF SUEZ Internal Report.
- Beuf, S., Biju-Duval, B., De Charpal, O., Rogonon, P., Gariel, O., Bennacef, A., 1971. Les grès du Paléozoïque inférieur au Sahara. Sédimentation et discontinuité: évolution structurale d'un craton: Institut Français du Pétrole: Paris, Collection Sciences et Techniques du Pétrole, eds Technip, 464 pp.
- Biju-Duval, B., Deynoux, M., Rogonon, P., 1974. Essai d'interprétation des "fractures en gradins" observées dans les formations glaciaires précambriennes et ordoviciennes du Sahara. *Revue de Géographie Physique et de Géologie Dynamique* 16, 503–512.
- Bjorkum, P.A., 1996. How important is pressure in causing dissolution of quartz in sandstones: *Journal of Sedimentary Research* 6, 147-154.
- Bloch, S., Lander, R.H., Bonnell, L., 2002. Anomalously high porosity and permeability in deeply buried sandstone reservoirs: Origin and predictability: *AAPG Bulletin* 86, 301-328.
- Brenchley, P.J., Marshall, J.D., Carden, G. a. F., Robertson, D.B.R., Long, D.G.F., Meidla, T., Hints, L., Anderson, T.F., 1994. Bathymetric and isotopic evidence for a short-lived Late Ordovician glaciation in a greenhouse period. *Geology* 22, 295–298.
- Bumby, A.J., Guiraud, R., 2005. The geodynamic setting of the Phanerozoic basins of Africa. *Journal of African Earth Sciences* 43, 1–12.
- Boulton, G.S., Caban, P.E., Vangijssel, K., 1995. Groundwater-flow beneath ice sheets .1. Large-scale patterns. *Quaternary Science Reviews* 14, 545-562.
- Boulton, G.S., Hagdorn, M., Maillot, P.B., Zatsepin, S., 2009. Drainage beneath ice sheets: groundwater-channel coupling, and the origin of esker systems from former ice sheets. *Quaternary Science Reviews* 28, 621-638.
- Byrnes, A.P., Wilson, M.D., 1994. Case history - St. Peter and Mt. Simon sandstones, Illinois basin, in: Wilson, M.D. (ed), *Reservoir quality assessment and prediction in clastic rocks: SEPM Short Course* 30, 385-394.
- Chamley, H., 1989. *Clay sedimentology*. Springer-Verlag, 623 pp.
- Clerc, S., Buoncristiani, J.-F., Guiraud, M., Vennin, E., Desaubliaux, G., Portier, E., 2013. Subglacial to proglacial depositional environments in an Ordovician glacial tunnel valley, Alnif, Morocco.

Palaeogeography, Palaeoclimatology, Palaeoecology 370, 127–144.

Cocks, L.R.M., Torsvik, T.H., 2002. Earth geography from 500 to 400 million years ago: a faunal and palaeomagnetic review. *Journal of the Geological Society* 159, 631–644.

Denis, M., Guiraud, M., Konaté, M., Buoncristiani, J.-F., 2010. Subglacial deformation and water-pressure cycles as a key for understanding ice stream dynamics: evidence from the Late Ordovician succession of the Djado Basin (Niger). *International Journal of Earth Sciences* 99, 1399–1425.

Desbois, G., Urai, J.L., Kukla, P.A., Konstanty, J., Baerle, C., 2011. High-resolution 3D fabric and porosity model in a tight gas sandstone reservoir: A new approach to investigate microstructures from mm- to nm-scale combining argon beam cross-sectioning and SEM imaging. *Journal of Petroleum Science and Engineering* 78, 243–257.

Dewers, T., Ortoleva, P., 1991. Influences of clay minerals on sandstone cementation and pressure solution. *Geology* 19, 1045–1048.

El-ghali, M.A.K., Mansurbeg, H., Morad, S., Al-Aasm, I., Ramseier, K., 2006. Distribution of diagenetic alterations in glaciogenic sandstones within a depositional facies and sequence stratigraphic framework: Evidence from the Upper Ordovician of the Murzuq Basin, SW Libya. *Sedimentary Geology* 190, 323–351.

Fernandez, N., 2004. Touat Project - Sbaa field, geological model: GDF SUEZ internal report.

Fisher, Q.J., Knipe, R.J., Worden, R.H., 2000. Microstructures of deformed and non-deformed sandstones from the North Sea: implications for the origins of quartz cement in sandstones, in: Worden, R.H., and Morad, S. (Eds.), *Quartz Cementation in Sandstones: International Association of Sedimentologists, Special Publication 29*, 129–146.

Ghienne, J.-F., 2003. Late Ordovician sedimentary environments, glacial cycles, and post-glacial transgression in the Taoudeni Basin, West Africa. *Palaeogeography Palaeoclimatology, Palaeoecology* 189, 117–145.

Ghienne, J.-F., Le Heron, D.P., Moreau, J., Denis, M., Deynoux, M., 2007. The Late Ordovician glacial sedimentary system of the North Gondwana platform, in: *Glacial Sedimentary Processes and Products*. Hambrey, M.J., Christoffersen, P., Glasser, N.F., Hubbard, B., Blackwell, Oxford, pp. 295–319.

Heald, M.T., Larese, R.E., 1974. Influence of coatings on quartz cementation. *Journal of Sedimentary Research* 44, 1269–1274.

Housknecht, D.W., Ross Jr., L.M., 1992. Clay minerals in Atokan deep-water sandstone facies, Arkoma basin: origins and influence on diagenesis and reservoir quality, in: Housknecht, D.W., and Pittman, E.D. (eds), *Origin, diagenesis, and petrophysics of clay minerals in sandstones: SEPM Special Publication 47*, 227–240.

Hurst, A., Buller, A.T., 1984. Dish structures in some Paleocene deep-sea sandstones (Norwegian sector, North Sea): Origin of the dish-forming clays and their effect on reservoir quality. *Journal of Sedimentary Petrology* 54, 1206–1211.

- Huuse, M., Heron, D.P.L., Dixon, R., Redfern, J., Moscariello, A., Craig, J., 2012. Glaciogenic reservoirs and hydrocarbon systems: an introduction. Geological Society of London, Special Publications 368, 1-28.
- Jahren, J.S., Aagaard, P., 1992. Diagenetic Illite-Chlorite assemblages in Arenites. I. Chemical evolution. *Clays and Clay Minerals* 40, 540-546.
- Le Heron, D.P., Craig, J., Etienne, J.L., 2009. Ancient glaciations and hydrocarbon accumulations in North Africa and the Middle East. *Earth-Science Reviews* 93, 47–76.
- Le Heron, D.P., Ghienne, J.-F., El Houicha, M., Khoukhi, Y., Rubino, J.-L., 2007. Maximum extent of ice sheets in Morocco during the Late Ordovician glaciation. *Palaeogeography, Palaeoclimatology, Palaeoecology* 245, 200–226.
- Lesemann, J.E., Alsop, G.I., Piotrowski, J.A., 2010. Incremental subglacial meltwater sediment deposition and deformation associated with repeated ice-bed decoupling a case study from the Island of Funen, Denmark. *Quaternary Science Reviews* 29, 3212-3229.
- Lowe, D.R., 1975. Water escape structures in coarse-grained sediments. *Sedimentology* 22, 157–204.
- Lüning, S., Shahin, Y.M., Loydell, D., Al-Rabi, H.T., Masri, A., Tarawneh, B., Kolonic, S., 2005. Anatomy of a world-class source rock: Distribution and depositional model of Silurian organic-rich shales in Jordan and implications for hydrocarbon potential. *AAPG Bulletin* 89, 1397–1427.
- Matclack, K.S., Houseknecht, D.W., Appling, K.R., 1989. Emplacement of clay into sand by infiltration. *Journal of Sedimentary Petrology* 59, 77-87.
- Menzies, J., 2000. Micromorphological analyses of microfabrics and microstructures indicative of deformation processes in glacial sediments. In: Maltman, A.J., Hubbard, B., Hambrey, M.J. (Eds.), *Deformation of Glacial Materials*. Geological Society Special Publication No. 176, London, pp. 245-257.
- Morad, S., Al-Ramadan, K., Ketzer, J.M., De Ros, L.F., 2010. The impact of diagenesis on the heterogeneity of sandstone reservoirs: A review of the role of depositional facies and sequence stratigraphy. *AAPG Bulletin* 94, 1267-1309.
- Moraes, M.A.S., De Ros, L.F., 1990. Infiltrated clays in fluvial Jurassic sandstones of Reconcavo Basin, Northeastern Brazil: *Journal of Sedimentary Petrology* 60, 809-819.
- Oelkers, E.H., Bjorkum, P.A., Murphy, W.M., 1992. The mechanism of porosity reduction, stylolite development and quartz cementation in North Sea sandstones, in: Kharaka, Y.K., and Maest, A.S. (Eds.), *Water-Rock Interaction*, Rotterdam, US Geological Survey, pp. 1183-1186.
- Phillips, E., Everest, J., Reeves, H., 2013. Micromorphological evidence for subglacial multiphase sedimentation and deformation during overpressurized fluid flow associated with hydrofracturing. *Boreas* 42, 395–427.
- Pittman, E.D., Larese, R.E., Heald, M.T., 1992. Clay coats: Occurrence and relevance to preservation of porosity in sandstones, in: Houseknecht, D.W., and Pittman, E.D. (Eds.), *Origin, diagenesis, and petrophysics of clay minerals in sandstones: SEPM Special Publications* 47, 241-264.

- Ravier, E., Buoncristiani, J.-F., Guiraud, M., Menzies, J., Clerc, S., Goupy, B., Portier, E., 2014. Porewater pressure control on subglacial soft sediment remobilization and tunnel valley formation: A case study from the Alnif tunnel valley (Morocco). *Sedimentary Geology* 304, 71–95.
- Renard, F., Ortoleva, P., 1997. Water film at grain–grain contacts: Debye–Hückel, osmotic model of stress, salinity and mineralogy dependence: *Geochimica and Cosmochimica Acta* 61, 1963–1970.
- Renard, F., Ortoleva, P., Gratier, J.P., 1997. Pressure solution in sandstones: influence of clays and dependence on temperature and stress. *Tectonophysics* 280, 257–266.
- Scotese, C.R., Boucot, A.J., McKerrow, W.S., 1999. Gondwanan palaeogeography and palaeoclimatology. *Journal of African Earth Sciences* 28, 99–114.
- Sibley, D.F., Blatt, H., 1976. Intergranular pressure solution and cementation of the Tuscarora orthoquartzite: *Journal of Sedimentary Petrology* 46, 881–896.
- Storvoll, V., Bjørlykke, K., Karlsen, D., Saigal, G., 2002. Porosity preservation in reservoir sandstones due to grain-coating illite: a study of the Jurassic Garn Formation from the Kristin and Lavrans fields, offshore Mid-Norway. *Marine and Petroleum Geology* 19, 767–781.
- Sutcliffe, O.E., Dowdeswell, J.A., Whittington, R.J., Theron, J.N., Craig, J., 2000. Calibrating the Late Ordovician glaciation and mass extinction by the eccentricity cycles of Earth's orbit. *Geology* 28, 967–970.
- Torsvik, T.H., Cocks, L.R.M., 2011. The Palaeozoic palaeogeography of central Gondwana. *Geological Society of London, Special Publications* 357, 137–166.
- Tournier, F., 2010. Mécanismes et contrôle des phénomènes diagénétiques en milieu acide dans les grès de l'Ordovicien glaciaire du bassin de Sbâa, Algérie. *Campus d'Orsay, Paris 6, Paris*, 403 pp.
- Tournier, F., Pagel, M., Portier, E., Wazir, I., Fiet, N., 2010. Relationship between deep diagenetic quartz cementation and sedimentary facies in a late ordovician glacial environment (Sbaa basin, Algeria). *Journal of Sedimentary Research* 80, 1068–1084.
- van der Meer, J.J.M., Menzies, J., Rose, J., 2003. Subglacial till: the deforming glacier bed. *Quaternary Science Reviews* 22, 1659–1685.
- van der Meer, J.J.M., Kjaer, K.H., Kruger, J., Rabassa, J., Kilfeather, A.A., 2009. Under pressure: clastic dykes in glacial settings. *Quaternary Science Reviews* 28, 708–720.
- Weyl, P.K., 1959. Pressure solution and the force of crystallisation - a phenomenological theory: *Journal of Geophysical Research* 64, 2001–2025.
- Worden, R.H., Morad, S., 2003. Clay minerals in sandstones: controls on formation, distribution and evolution, in: Worden, R.H., and Morad, S. (Eds.), *Clay Mineral Cements in Sandstones*: International Association of Sedimentologists, Special Publication 34, 3–41.
- Worden, R.H., Needham, S.J., Cuadros, J., 2006. The worm gut; a natural clay mineral factory and a possible cause of diagenetic grain coats in sandstones. *Journal of Geochemical Exploration* 89, 428–431.

Wilson M.D., 1992. Inherited grain-rimming clays in sandstones from eolian and shelf environments: Their origin and control on reservoir properties: in Houseknecht, D.W., and Pittman, E.D., (Eds.), Diagenesis and petrophysics of clay minerals in sandstones, SEPM Special Publication 47, 209-225.

Wilson, L., Wilson, M.J., Green, J., Patey, I., 2014. The influence of clay mineralogy on formation damage in North Sea reservoir sandstones: A review with illustrative examples. *Earth-Science Reviews* 134, 70–80.

Annexe

Depth (m)	Kaolin (%)	Illite (%)
2439.15	0	100
2439.60	0	100
2439.85	0	100
2442.05	0	100
2442.80	0	100
2445.60	0	100
2452.75	0	100
2480.75	0	100
2488.75	0	100
2489.50	0	100
2492.50	0	100
2493.10	0	100
2494.10	0	100
2494.75	0	100
2507.95	0	100
2511.30	0	100
2511.80	0	100

Supplementary data 1. Results of XRD analyses.

Chapitre 4

Principaux résultats

Partie I

- La première partie s'est focalisée sur l'étude à plusieurs échelles de deux réseaux d'injectites dans un ancien domaine marin profond (bassin Vocontien). Une méthode intégrée a été mise en oeuvre, combinant des analyses structurales, diagénétiques, et pétrophysiques afin de caractériser les valeurs, la distribution, et l'évolution de la porosité le long des systèmes d'injectites.

- La porosité primaire (i.e., porosité moins-ciment) peut être estimée au sein des système d'injectites en raison d'une séquence diagénétique caractérisée par la mise en place précoce d'une calcite de blocage.

- Cette étude a permis de déterminer l'évolution de la porosité de l'injection à nos jours et les différents paramètres contrôlant cette évolution:

- (1) Après hydrofracturation, l'injection de sable fluidisé est à l'origine de l'emplacement d'un vaste réseau d'intrusions clastiques poreux (porosité moyenne $> 25\%$), atteignant localement 53% , au sein d'une épaisse formation très faiblement perméable.

- (2) La distribution des valeurs de porosité primaire à l'échelle de l'affleurement permet de mettre en évidence la répartition hétérogène des valeurs de porosité, même si l'épaisseur des injectites et la distance à la source (i.e., distance séparant l'injection de l'unité parente) semblent influencer ces valeurs.

- (3) Avant un enfouissement significatif, le réseau d'injections est localement affecté par la présence de structures d'élutriations et de bandes de déformation. Ces structures ont pour conséquence de réduire localement la porosité au sein des injectites.

- (4) Durant l'enfouissement, la circulation de fluides riches en carbonate au sein du système d'injection poreux conduit à la mise en place d'une calcite de blocage qui a pour conséquence de réduire fortement la porosité ($< 5\%$).

(5) Des déformations tardives d'origine tectonique provoquent la fracturation et la ré-ouverture du système d'injection alors lithifié et imperméable. Ces fractures sont rapidement cimentées par de la calcite.

(6) Le dernier événement est induit par l'exhumation des réseaux d'injectites. Les phénomènes de dissolution des ciments carbonatés et des glauconies provoqués par les eaux météoriques ont pour conséquence d'augmenter significativement la porosité (jusqu'à 25 % localement).

- Les variations de la porosité au cours du temps au sein de ces deux systèmes d'injectites ont un impact direct sur les écoulements des fluides au cours du temps. Le système d'intrusions peut se comporter à la fois comme un drain préférentiel pour les écoulements de fluide (i.e., eau, hydrocarbure) pendant les périodes où la porosité est élevée, mais aussi comme des barrières imperméables lorsque la porosité est fortement réduite.

Partie 2

- Dans la deuxième partie, l'impact des surpressions de fluides sur les propriétés physiques des sédiments glaciaires a été testé. L'influence des coatings argileux sur la diagénèse et, a posteriori, sur les propriétés physiques des sédiments a été démontrée auparavant (Tournier et al., 2010). L'étude s'est donc naturellement portée sur la caractérisation des processus de mise en place de ces coatings argileux.

- La morphologie des coatings argileux illitiques, leur distribution spécifique à proximité des couches argilo-silteuses, ainsi que la présence récurrente d'illites détritiques dans les sédiments glaciaires ont permis de déduire une mise en place précoce et d'origine détritique des coatings argileux.

- La quantification de l'abondance des coatings argileux a permis de mettre en évidence la relation entre valeurs d'abondances et propriétés pétrophysiques. L'augmentation de l'abondance des coatings argileux dans les grès glaciaires a pour conséquence de diminuer la porosité et la perméabilité des grès, formant ainsi des réservoirs dits «tights».

- L'analyse de la distribution de l'abondance des coatings argileux a permis de mettre en évidence

deux facteurs de contrôle prédominants:

(1) L'environnement de dépôt influence la quantité de coatings argileux présents dans les grès glaciaires. En effet, les sédiments sous-glaciaires présentent des faibles abondances de coatings argileux, contrairement aux grès proglaciaires qui possèdent des coatings argileux quatre fois plus abondants. L'augmentation des coatings argileux dans les environnements proglaciaires peut être expliquée par la baisse de l'hydrodynamisme et la décantation de particules plus fines.

(2) Les remobilisations sédimentaires, et plus précisément les processus d'élutriation associés à l'augmentation de la pression d'eau interstitielle, semblent influencer la distribution des coatings argileux. Des dykes argileux et des réseaux composés de fins conduits d'élutriation transportant les argiles enregistrent ces processus de remobilisation sédimentaire. L'élutriation des particules fines permet le transport et le dépôt d'illites au sein de conduits infracentimétriques. Ces processus de remobilisation sédimentaire sont notamment mis en évidence par l'enrichissement ou l'appauvrissement des grès en coatings argileux à proximité des bancs argilo-silteux et par la présence de bandes (e.g., conduits) d'élutriations.

- Dans le cas où ces deux modèles contrôleraient la distribution des coatings argileux au sein des grès glaciaires ordoviciens, certains paramètres devront être définis afin de déterminer les zones potentiellement enrichies ou appauvries en tapissages argileux. Les paramètres à définir sont: les environnements sédimentaires, la répartition des structures de déformation induites par surpression de fluide, et la distribution des niveaux argilo-silteux.

CONCLUSIONS & PERSPECTIVES

Conclusions & Perspectives

1. Synthèse des principaux résultats

L'analyse et l'interprétation des structures de déformation pré-lithification ont représenté le sujet principal de ce travail. Les études se sont particulièrement focalisées sur l'analyse des structures induites par des surpressions de fluide en environnements sous-glaciaires et marins profonds. Les différents travaux menés durant cette thèse se sont principalement appuyés sur l'acquisition et l'analyse de données de terrains à échelles microscopique et macroscopique.

Les principaux résultats des différents chantiers peuvent être synthétisés selon les trois grandes problématiques définies en introduction de ce travail:

A) Structures de déformation pré-lithification et reconstruction paléoenvironnementale.

B) Structures de déformation pré-lithification et impacts sur les morphologies glaciaires.

C) Structures de déformation pré-lithification et impacts réservoirs.

Afin de répondre aux questions soulevées au sein de ces trois grandes problématiques de recherche (cf., introduction générale), six chantiers ont été menés durant lesquels des analyses de la déformation pré-lithification, des études sédimentologiques, et des mesures pétrophysiques ont été réalisées.

A. Reconstruction paléoenvironnementale

Quels sont les critères sédimentologiques et déformationnels qui permettent d'identifier les faciès sédimentaires triés déposés sous la glace ?

Le chantier Irlande a permis de répondre à cette question en raison de la coexistence de faciès sédimentaires triés sous-glaciaires et proglaciaires au sein du même site d'étude, permettant ainsi leur comparaison et leur discrimination.

Des dépôts triés mis en place dans un système fluvatile sous-glaciaire (probablement situé à proximité de la marge) ont été mis en évidence par des observations (a) stratigraphiques, (b) sédimentologiques,

et (c) déformationnelles:

► (a) La présence de larges lentilles de sables triés au sein de couches de tills sous-glaciaires témoignent du découplage localisé et épisodique entre la glace et le substrat.

► (b) Les séquences sédimentaires sous-glaciaires sont aggradantes et présentent des forts taux d'amalgamation en raison d'un espace d'accommodation contraint par la base du glacier. Les séquences sédimentaires sous-glaciaires sont caractérisées par des variations rapides et cycliques de la granulométrie.

► (c) Les dépôts proglaciaires ne présentent que des structures de déformation d'origine gravitaire sur le site d'étude, alors que les faciès triés sous-glaciaires sont caractérisés par une large gamme de structures, principalement liées à l'action de la glace sur les sédiments. Les failles inverses et les plis asymétriques sont liés à l'action cisailante du glacier lors d'épisodes de couplage de la glace et du substrat. Les injections clastiques sont les indicateurs de l'augmentation de la pression d'eau interstitielle lors de l'interaction entre la glace et les sédiments saturés en eau. La mise en place de ces structures de déformation au sein des faciès sous-glaciaires est contemporaine de la sédimentation et affecte généralement quelques niveaux sédimentaires.

L'ensemble des critères terrain permettant de discriminer des faciès triés déposés sous la glace d'autres faciès similaires déposés au devant la marge glaciaire sont de nature stratigraphique, sédimentologique et déformationnel. Ces critères permettront ainsi de mieux contraindre les reconstructions paléoenvironnementales dans le registre sédimentaire fossile.

**L'identification de dépôts fluviaux sous-glaciaires
permet-elle de caractériser la dynamique sédimentaire sous-glaciaire ?**

L'identification de faciès triés d'origine sous-glaciaire a permis d'obtenir de nouvelles informations sur la dynamique sédimentaire caractéristique d'un système fluvial sous-glaciaire. Quatre séquences sédimentaires déposées durant des épisodes de découplage de la glace et du substrat ont été mises en évidence dans la carrière de Ballyhorsey (Irlande). Elles présentent toutes le même motif stratigraphique granocroissant. La récurrence de ce motif granulométrique au sein de ce type de dépôt sous-glaciaire indique une variation cyclique (saisonnière ou pluri-annuelle ?) de la production des eaux de fonte et des débits associés, contrôlant ainsi la granulométrie des sédiments transportés et déposés au sein du système fluvial sous-glaciaire.

Le facteur climatique semble influencer l'augmentation de la production et des débits d'eaux de fonte et contrôle ainsi la dynamique sédimentaire d'un système de drainage sous-glaciaire selon des cycles annuels et/ou pluri-annuels.

Peut-on reconstruire la dynamique glaciaire et estimer les variations de la pression de fluide en se basant sur une analyse détaillée des structures de déformation ?

Les séquences sédimentaires caractéristiques de l'environnement fluvial sous-glaciaire ont été mises en évidence précédemment. Lorsque la production d'eau de fonte est moindre, la pression effective diminue provoquant le recouplage de la glace avec le substrat. Le cisaillement et le poids exercés par la glace sur les sédiments sont responsables du développement de structures de déformation pré-lithification. La séquence typique de déformation est caractérisée par un passage progressif d'injections clastiques obliques *per descensum* à des failles normales en gradins en passant par des plis asymétriques. Les mécanismes de déformation et les contraintes associées à ces différentes structures illustrent la diminution progressive de la pression d'eau interstitielle (fluidisation, hydroplastique, fragile) et de la vitesse d'écoulement de la glace (cisaillement général à cisaillement pur) au cours du temps. L'augmentation de la vitesse d'écoulement de la glace est au contraire favorisée durant les épisodes de découplage de la glace et du substrat (dépôt des faciès triés sous-glaciaires). En revanche, elle diminue progressivement durant les épisodes de couplage en raison de l'évacuation progressive de la surpression de fluide initiée par les processus d'hydrofracturation.

Le chantier Islande et l'analyse du système d'injection clastique a également permis de mettre en évidence les variations récurrentes de la pression d'eau interstitielle dans le substrat, sous et à la marge du glacier. Ces variations se manifestent par les remplissages d'injections multi-phasés caractérisés par des lamines de granulométries différentes, mais aussi par les nombreux épisodes d'injection au cours du temps. Les fréquentes variations de la pression d'eau interstitielle au sein du substrat peuvent s'expliquer par des épisodes de couplage et découplage de la glace et de son substrat et/ou par les variations de la production et du transfert d'eaux de fonte dans les sédiments.

L'analyse de l'enregistrement sédimentaire et des structures de déformation pré-lithification permet de reconstruire localement et sur des courtes échelles de temps (saisons ?) les variations de la paléo-dynamique glaciaire (plus particulièrement les vitesses d'écoulement de la glace) ainsi que les variations de la pression d'eau interstitielle.

Peut-on mettre en évidence des séquences de déformation liées à des oscillations de la marge glaciaire ? Quels impacts pour les reconstitutions paléogéographiques ?

Différentes phases d'injection clastiques caractérisées par des orientations et des sens de propagation différents ont été observés en Islande. Le sens de propagation et l'orientation des injections clastiques sont directement liés aux contraintes exercées sur le sédiment durant le processus d'hydrofracturation. En contexte glaciaire, la contrainte varie en fonction de l'épaisseur de la calotte (contrainte verticale) et de la vitesse d'écoulement de la glace (contrainte horizontale). Trois types d'injection ont pu être définis: (1) les dykes *per descensum* liés à une hydrofracturation sous-glaciaire, (2) les sills et sills en «marches d'escaliers» («stepped sills») liés à des processus d'hydrofracturation submarginale et enfin (3) les dykes *per ascensum* liés à une hydrofracturation en domaine margino-glaciaire. Les recoupements entre ces différentes phases d'injections permettent de reconstruire les oscillations de la marge glaciaire en déterminant dans quel environnement s'est produit chaque épisode d'hydrofracturation.

L'analyse de la cinématique associée aux différentes structures de déformation permet donc de déterminer précisément dans quel environnement s'est produit la déformation. L'établissement d'une chronologie entre les différentes phases de déformation permet de caractériser la succession des environnements et donc de reconstituer localement l'évolution de la paléogéographie d'une calotte glaciaire.

L'étude détaillée des structures de déformation pré-lithification dans les environnements glaciaires a permis de reconstruire avec précision les environnements de dépôts et de discriminer les domaines sous-glaciaire, submarginal ou encore margino-glaciaire.

L'analyse de la cinématique et des mécanismes de déformation associée à chaque structure a permis de reconstruire la dynamique glaciaire locale (i.e., estimation de la vitesse d'écoulement), les variations de la production d'eaux de fonte et l'évolution de la pression d'eau interstitielle dans le substrat. Ces structures de déformation ont également permis de reconstituer les oscillations d'une marge glaciaire et donc de discuter l'évolution paléogéographique d'une calotte glaciaire.

B. Impacts sur les morphologies glaciaires

Quels sont les processus intervenant dans l'évacuation du matériel préglaciaire et dans la formation des vallées tunnels contrôlées par l'augmentation de la pression d'eau interstitielle ?

Dans le chapitre trois, un nouveau modèle de creusement des vallées tunnels induit par des remobilisations sédimentaires est proposé. Ce modèle repose sur l'augmentation de la pression d'eau interstitielle dans les dépôts préglaciaires de la région d'Alnif. Lorsque l'augmentation de la pression d'eau dans les aquifères devient supérieure à la résistance intrinsèque des dépôts encaissants, des processus de bréchification hydraulique et d'injection de matériel fluidisé peuvent affecter les dépôts préglaciaires. Le «mélange» qui résulte de ces processus d'hydrofracturation et d'injection est composé de fragments de matériels préglaciaires flottant dans une matrice de sable fluidisé. Les fortes pressions d'eau interstitielle présentent alors dans le substrat préglaciaire diminuent considérablement la pression effective et provoquent le découplage de la glace et du substrat, ainsi que la mise en place de chenaux sous-glaciaires. Ces chenaux sous-glaciaires vont permettre au «mélange» fluidisé d'être évacué et donc de contribuer à la création d'une vallée sous la glace. La répétition de ces processus de bréchification et de transport de matériel préglaciaire en direction de la marge contrôle le développement de la vallée tunnel d'Alnif.

Le modèle de creusement par remobilisation sédimentaire est conditionné par l'augmentation de la pression de fluide dans le substrat, et se caractérise par la bréchification hydraulique des dépôts préglaciaires, puis l'évacuation de cette brèche fluidisée par l'intermédiaire de chenaux sous-glaciaires.

Quels sont les paramètres contrôlant l'augmentation de la pression d'eau interstitielle dans les sédiments meubles préglaciaires ?

L'augmentation de la pression d'eau interstitielle est contrôlée par: (1) les caractéristiques lithologiques du matériel préglaciaire, (2) le régime thermique et la dynamique de la calotte glaciaire, et (3) l'héritage topographique.

(1) L'augmentation de la pression de fluide est liée à la configuration stratigraphique et lithologique des dépôts préglaciaires. Une configuration de type «layer-cake», où les couches sableuses perméables (aquifères) alternent avec les couches argileuses ou cimentées imperméables, favorise le

développement de surpressions de fluide dans les aquifères préglaciaires confinés.

(2) L'augmentation de la pression de fluide est également contrôlée par le transfert d'eaux de fonte dans le substrat mais aussi par la contrainte exercée par la glace sur les aquifères confinés. Les remobilisations sédimentaires sont donc favorisées par une calotte glaciaire tempérée sous laquelle zones de découplage et de couplage peuvent coexister.

(3) L'augmentation de la pression d'eau interstitielle doit être locale dans un tel modèle de creusement et implique donc l'existence d'une paléotopographie où les eaux de fonte peuvent préférentiellement s'infiltrer dans le substrat, formant ainsi un gradient de pression de fluide entre l'axe de la vallée et les interfluvés.

Le processus de creusement contrôlé par les remobilisations sédimentaires implique une forte augmentation de la pression d'eau interstitielle dans les dépôts préglaciaires. Cette augmentation de la pression de fluide est contrôlée par des paramètres lithologiques, stratigraphiques, glaciodynamiques et topographiques.

Quels sont les critères terrains permettant de démontrer l'impact des surpressions de fluide et des processus de remobilisation sédimentaire dans le creusement des vallées tunnels ?

A partir de l'étude terrain, des critères (1) déformationnels, (2) sédimentologiques et (3) stratigraphiques ont été établis:

(1) Des structures de déformation pré-lithification enregistrant des surpressions de fluide ont été observées dans les dépôts préglaciaires, à proximité de la base de la vallée tunnel. Certaines de ces structures démontrent l'initiation de processus de remobilisation du matériel préglaciaire, notamment par l'intermédiaire d'hydrofracturation, de bréchification hydraulique, et d'injection.

(2) La présence localisée de cônes de déjection composés de brèches à la base de la vallée tunnel enregistre le dépôt du matériel préglaciaire remobilisé et transporté par les chenaux sous-glaciaires. En effet, cette brèche est composée de fragments de matériels préglaciaires anguleux (issus de l'hydrofracturation des strates préglaciaires) flottant dans une matrice sableuse fluidisée.

(3) La configuration stratigraphique et lithologique du matériel préglaciaire affectée les processus de remobilisation représente également un critère terrain essentiel. Une configuration de type «layer-cake» du matériel préglaciaire est essentielle dans un modèle de creusement induit par des surpressions de fluide.

L'identification sur le terrain d'un modèle de creusement contrôlé par les remobilisations sédimentaires est principalement basé sur: (1) l'observation de déformation pré-lithification induites par des surpressions de fluide sous la vallée, (2) la présence d'une brèche à la base de la vallée où des fragments de matériel préglaciaire flottent dans une matrice fluidisée, et (3) une configuration stratigraphique des dépôts préglaciaires de type «layer-cake».

Les vallées tunnels mises en place sur substrats meubles sont-elles toutes initiées par l'augmentation de la pression d'eau interstitielle ?

Le modèle de creusement de la vallée tunnel d'Alnif, contrôlé par l'augmentation de la pression d'eau interstitielle dans le matériel préglaciaire, n'est pas applicable à toutes les vallées tunnels creusées sur substrat meuble. Les observations sédimentologiques (conglomérats peu épais, clasts émoussés, matrice non fluidisée) et déformationnelles (absence de déformation sous et à la base de la vallée) dans les dépôts préglaciaires et dans le remplissage sédimentaire de la vallée tunnel de Foug Larjamme n'ont pas permis de valider un modèle de creusement par surpressions de fluide. La morphologie ondulante de la base de la vallée tunnel de Foug Larjamme indique un creusement où l'érosion du substrat est contrôlé par l'écoulement d'eaux de fonte. Il est cependant difficile de déterminer si l'érosion est progressive, liée à un écoulement continu, ou quasi-instantanée lors d'écoulements catastrophiques d'eaux de fonte.

La comparaison des vallées tunnels d'Alnif et de Foug Larjamme a permis de mettre en évidence la coexistence de plusieurs modèles de creusement des vallées tunnels ordoviciennes. Des modèles contrôlés par l'augmentation de la pression de fluide dans les dépôts préglaciaires (Alnif) et d'autres où l'érosion est contrôlée par des écoulements d'eaux de fonte (Foug Larjamme).

Existe-t-il un lien entre les processus de creusement des vallées tunnels et la dynamique glaciaire grande échelle (*ice-stream* vs. *inter ice-stream*) ?

La localisation des vallées tunnels d'Alnif et de Foug Larjamme sur les cartes de reconstitution des paléo *ice-streams* ordoviciens permet de discuter les relations entre leurs processus de creusement et la paléo dynamique glaciaire. La vallée tunnel d'Alnif est située entre deux *ice-streams* et présente une morphologie différente de la vallée tunnel de Foug Larjamme alors située sous la trajectoire d'un paléo *ice-stream* majeur. Le modèle de creusement proposé pour Foug Larjamme est conditionné par

des écoulements d'eaux de fonte sous la glace. La vallée se positionnait alors sous un paléo *ice-stream* dont le fonctionnement était probablement induit par des circulations d'eaux de fonte favorisant la lubrification de la base de la calotte glaciaire, et l'augmentation de sa vitesse d'écoulement. La vallée tunnel d'Alnif est en revanche positionnée entre deux paléo *ice-streams* et son modèle de formation est principalement contrôlé par le transfert de l'eau de fonte dans le matériel préglaciaire. La diffusion de l'eau de fonte dans les sédiments sous la glace semble influencer les processus d'écoulement de la glace et engendre des vitesses d'écoulement plus modérées.

La distribution des ice-streams à L'Ordovicien pourrait être contrôlée par la dynamique des eaux de fonte (i.e., transfert dans le substrat vs. écoulement à l'interface glace/substrat) et donc avoir une influence sur les processus de creusement et les morphologies des vallées tunnels.

Dans ce travail, deux modèles de formation des vallées tunnels ordoviciennes ont été proposés. Un nouveau modèle de creusement contrôlé par des pressions d'eau interstitielle élevées et des processus de remobilisation sédimentaire (bréchification hydraulique, injection de matériel fluidisé), mettant ainsi en évidence l'impact des surpressions de fluide sur les morphologies glaciaires. Un deuxième modèle où la formation des vallées tunnels est contrôlée par des écoulements d'eaux de fonte à l'interface glace/substrat.

Les reconstitutions paléoenvironnementales semblent démontrer l'existence d'un lien entre le modèle de creusement, la morphologie de la vallée tunnel, et la dynamique d'écoulement de la glace (*ice-stream* vs. *inter ice-stream*). A terme, si cette spatialisation des modèles se confirme, il serait alors possible de déterminer le modèle de creusement et la morphologie de la vallée tunnel en fonction de la distribution des *ice-streams*.

C. Impacts réservoirs

Quelles sont les valeurs de porosité primaire (i.e., porosité pré-lithification) associées aux injections sableuses ?

La séquence diagénétique déterminée dans les réseaux d'injectites sableuses du bassin Vocontien indique la mise en place précoce d'une calcite de blocage permettant d'estimer la porosité primaire (i.e., porosité pré-lithification). Cette porosité primaire correspond à la porosité initiale après l'injection, permettant ainsi de quantifier l'impact des surpressions de fluides sur les propriétés pétrophysiques des réservoirs sableux. La porosité moyenne du réseau d'injection avoisine les 30 % avec des valeurs maximum atteignant les 53 %. De la même manière, les turbidites remobilisées pendant l'injection présentent des valeurs de porosité primaire autour des 30 %. Ces porosités élevées sont liées à l'augmentation de la pression d'eau interstitielle et les processus de fluidisation qui en découlent. En effet, lorsque la pression d'eau interstitielle devient supérieur au poids des grains, les grains se désolidarisent et flottent dans un fluide en surpression, induisant ainsi les fortes porosités primaires enregistrées dans ces réseaux d'injectites. Ces fortes porosités sont préservées après injection puisque les pressions d'eau interstitielle au sein du système sableux confiné restent élevées. Ces pressions élevées sont donc capable de contrebalancer la compaction mécanique induite par la charge lithostatique.

Les fortes valeurs de porosité primaire (~ 30 %) associées aux réseaux d'injectites témoignent de l'impact des surpressions de fluide sur les propriétés pétrophysiques. En effet, l'augmentation de la pression d'eau interstitielle engendre une diminution des contacts entre les grains et donc une augmentation sensible de la porosité.

Quels paramètres contrôlent la distribution de la porosité primaire au sein d'un réseau d'injectites (à l'échelle de l'affleurement) ?

Les campagnes d'échantillonnage menées le long de deux réseaux d'injectites ont permis d'estimer les variations de la porosité primaire à l'échelle de l'affleurement et de déterminer les principaux facteurs de contrôle de la distribution des propriétés pétrophysiques au sein de ces réseaux. Le type d'injection (dykes, sills), l'épaisseur de l'injection, l'angle de pendage des dykes ou encore la distance à la source sont autant de facteurs dont l'influence sur la porosité primaire a

été testée. La distribution de la porosité primaire est relativement hétérogène au sein des réseaux d'injectites, principalement en raison des processus de fluidisation qui sont capables de générer une grande variabilité dans la structuration granulaire du sédiment. L'occurrence de plusieurs épisodes d'injections qui se recoupent et se connectent dans un espace tri-dimensionnel pourrait également expliquer cette distribution hétérogène. Les résultats et tests statistiques démontrent cependant que l'épaisseur des injections et la distance à la source exercent un contrôle sur la distribution de la porosité.

La distribution des valeurs de porosité primaire à l'échelle de l'affleurement semble majoritairement hétérogène au sein des réseaux d'injectites. En revanche, l'épaisseur des injectites et la distance à la source semblent exercer un contrôle sur la porosité des intrusions sableuses.

Quelle est l'évolution de la porosité primaire au sein d'un système d'injectites au cours du temps et les différents paramètres contrôlant cette évolution ?

Le calcul des valeurs de porosité primaire et de porosité actuelle, la détermination de la séquence diagénétique, et l'identification des structures de déformation au sein des réseaux d'injectites ont permis d'estimer l'évolution de la porosité, depuis l'injection jusqu'à aujourd'hui. Après injection, les valeurs de porosité sont élevées (~ 30 %) en raison des fortes pressions d'eau interstitielle. Dans l'histoire précoce de ces injections, les valeurs de porosité peuvent être localement réduites en raison de la concentration de galets mous provenant de l'encaissant argileux, de la mise en place de bandes d'élutriations argileuses, ou encore du développement de bandes de déformation. La phase majeure de réduction de la porosité est associée à la mise en place d'une calcite de blocage qui divise les valeurs de porosité par six (< 5%), même si auparavant quelques ciments siliceux associé saux bandes de déformation ont très localement réduit la porosité des injectites. Dans l'histoire tardive de ces injectites, des déformations tectoniques ont provoqué la réouverture locale du système permettant la circulation tardive de fluides comme l'atteste la présence de veines de calcite. Enfin lors de l'exhumation des réseaux d'injectites, l'impact des eaux météoriques sur les ciments calcitiques a pour conséquence d'augmenter localement la porosité (> 25%).

L'évolution de la porosité au sein des réseaux d'injectites est influencée par les processus d'injection, par les structures de déformation pré-lithification, par la diagénèse et par les phases de déformation tectonique. Ces différents facteurs de contrôle ont pour conséquence d'influencer

les écoulements de fluides (eau, hydrocarbures). En effet, le réseau d'injectites peut se comporter comme un drain (porosité élevée) ou comme une barrière imperméable (faible porosité) au cours du temps.

Quelle est l'origine des coatings argileux dans les grès glaciaires ordoviciens et quels impacts ont-ils sur les propriétés réservoirs?

Les observations morphologiques, la distribution préférentielle selon les environnements de dépôts, et la nature illitique des coatings argileux indiquent leur origine détritique, probablement liée à une mise place précoce. Si l'impact de la présence de coatings argileux sur la diagenèse des sables et donc a fortiori sur leurs propriétés pétrophysiques a déjà été démontré (Byrnes et Wilson, 1994; Tournier et al., 2010), cette étude a mis en évidence l'influence de l'abondance des coatings sur les propriétés pétrophysiques. L'augmentation de l'abondance des coatings argileux est en effet responsable de la réduction de la porosité/perméabilité des grès glaciaires ordoviciens d'Algérie.

Les coatings argileux se mettent en place de manière précoce dans les grès glaciaires ordoviciens d'Algérie et sont d'origine détritique. L'abondance des coatings argileux varie au sein des carottes sédimentaires étudiées et influence directement les propriétés pétrophysiques des grès (porosité et perméabilité).

Quels sont les processus de mise en place des coatings argileux détritiques dans les grès glaciaires ordoviciens ? Leur distribution est-elle contrôlée par les processus d'élutriation induits par des surpressions de fluide ?

Cette étude a permis de proposer deux modèles de mise en place des coatings grâce à l'analyse conjuguée de l'abondance des coatings argileux, des faciès sédimentaires, et des déformations pré-lithifications.

(1) Le premier modèle de mise en place fait intervenir la dynamique sédimentaire et l'environnement de dépôt comme facteur de contrôle de la distribution des coatings argileux. Ce modèle s'appuie sur la distribution de l'abondance des coatings argileux en fonction des environnements de dépôts (sous-glaciaires vs. proglaciaires). Il apparaît alors que les coatings sont quatre fois plus abondants dans les environnements proglaciaires, probablement en raison d'une dynamique sédimentaire plus propice à la décantation de particules fines au sein des sables.

(2) Dans le deuxième modèle, la distribution de l'abondance des coatings argileux est contrôlée par des processus de remobilisations sédimentaires induits par des pressions de fluides élevées. L'augmentation de la pression d'eau interstitielle est souvent associée à des processus d'élutriations (e.g., remobilisation des particules les plus fines). L'occurrence de tels processus est mise en évidence par la présence de dykes argileux et de réseaux d'élutriations composés de fins conduits argileux au sein des grès. Ces processus d'élutriation ont un impact sur la distribution des coatings argileux comme l'attestent notamment les gradients d'abondance à proximité des bancs argilo-silteux.

L'analyse de la distribution de l'abondance des coatings argileux au sein des grès glaciaires ordoviciens d'Algérie a permis de proposer deux nouveaux paramètres pouvant contrôler la répartition des coatings. Dans un premier modèle, l'environnement sédimentaire influence la distribution des coatings alors que dans le deuxième modèle, les surpressions de fluide contrôlent la mise en place des coatings.

L'étude des propriétés pétrophysiques dans deux environnements comportant de nombreuses structures de déformation pré-lithifications (marin profond et glaciaire) a permis de mettre en évidence l'impact des surpressions de fluide sur les propriétés réservoirs. Si les processus de remobilisation sédimentaire induits par pressions de fluide élevées sont capable de former des réservoirs très poreux, les processus d'élutriations qui sont associés peuvent avoir un effet inverse et ainsi réduire la porosité. Les processus de fluidisation sédimentaire sont responsable de l'hétérogénéité des propriétés pétrophysiques au sein des réservoirs clastiques marins profonds ou glaciaires. Cependant, certains paramètres exercent un contrôle sur la distribution des propriétés pétrophysiques au sein des systèmes clastiques (épaisseur des injectites, distance à la source, distance au niveau argileux, et environnement de dépôt). Ces paramètres permettent ainsi de mieux prédire les variations internes de la qualité d'un réservoir.

2. Perspectives

Les résultats de ce mémoire de thèse permettent de dresser les perspectives ouvertes par ce travail de recherche. Différentes perspectives peuvent être envisagées:

► Les informations paléoenvironnementales et paléogéographiques transmises par l'étude des structures de déformation pré-lithification pourront être utilisées dans l'étude des dépôts liés aux glaciations très anciennes (ex: glaciation Néoprotérozoïque). Les sédiments glaciaires Néoprotérozoïque sont fréquemment affectés par du métamorphisme et/ou ne présentent pas toujours des conditions d'affleurements optimales. La préservation de structures de déformation pré-lithification au sein de sédiments glaciaires Néoprotérozoïque a déjà été démontrée (Menzies, 2000 ; Benn et Prave, 2006; Le Heron et al., 2012; Busfield et Le Heron, 2013). Leur analyse détaillée (mécanisme de déformation, cinématique, reconstruction des champs de contrainte, recoupement, etc...) pourrait permettre d'estimer la paléo dynamique glaciaire, l'environnement dans lequel s'est produit la déformation (sous-glaciaire, submarginale et marginal), et de mieux contraindre la paléogéographie des calottes glaciaires très anciennes. Cette approche terrain combinant des analyses de la déformation et des études sédimentologiques permettraient peut-être d'apporter de nouveaux éléments dans les très controversées épisodes de «snowball earth».

► Les environnements sédimentaires glaciaires enregistrent une succession de zones de dépôts spécifiques (sous-glaciaire, marginal, subaquatique proximal et distal, etc...) permettant de définir les cycles d'avancée et de retrait des glaciers. Les différents critères sédimentologiques et déformationnels, permettant de contraindre les environnements de dépôts de manière plus fine, sont essentiels dans le développement de la stratigraphie séquentielle adaptée aux environnements glaciaires. Les cortèges sédimentaires déposés durant l'avancée et le retrait d'un glacier sont séparés par des surfaces d'érosion ou des planchers glaciaires (Brookfield et Martini, 1999). Or, ils peuvent également se manifester par des niveaux sédimentaires présentant des structures de déformation induites par l'action de la glace sur un substrat meuble.

► La majorité des sables et graviers ont été interprétée comme des faciès sédimentaires proglaciaires (fluvatile, glaciolacustre ou glaciomarin), cependant ce type de dépôt peut également

se mettre en place dans des systèmes fluviaux, ou encore des cavités et lacs sous-glaciaires (McCabe et O'Cofaigh, 1994; Munro-Stasick, 2000; Lesemann et al., 2010; Livingstone et al., 2012; Ravier et al., 2014a). L'utilisation des critères sédimentologiques, stratigraphiques, et déformationnels définis dans cette étude permet de mettre en évidence l'origine sous-glaciaire de certains de ces faciès sédimentaires. Il serait donc possible d'évaluer leur proportion dans le registre sédimentaire, mais aussi leur potentiel de préservation au cours des cycles d'avancée et de retrait d'une calotte glaciaire.

► L'analyse de la cinématique ou encore des mécanismes de déformations associés aux différentes structures de déformations permet d'estimer de manière approximative les gammes de vitesses d'écoulement, d'épaisseur de glace, ou encore de pressions d'eau interstitielle. La modélisation numérique et/ou analogique pourrait permettre de quantifier ces différents paramètres qui sont essentielles dans la reconstitution de la paléo dynamique glaciaire. Les différents paramètres à simuler seraient tout d'abord la pression verticale (σ), la contrainte cisailante (τ), et la vitesse de déformation (ϵ). Ces paramètres permettent de modéliser l'impact de la variation de l'épaisseur de glace et de la vitesse d'écoulement sur la déformation. Deux autres paramètres essentiels dans la modélisation de la déformation d'un substrat meuble sont la pression d'eau interstitielle et la lithologie (i.e., tris granulométrique et taille des grains). Les caractéristiques des structures de déformation simulées (type de déformation, amplitude, taille, ...) permettrait d'établir un catalogue où chaque structure serait associée à une configuration particulière de ces cinq paramètres.

► Afin de valider le modèle de creusement des vallées tunnels par remobilisation sédimentaire, l'apport de la modélisation numérique et/ou analogique est également essentiel. Seul quelques travaux de modélisation analogique simulant l'impact des écoulements d'eaux sous-hautes pressions sur la morphologie des chenaux ont été jusqu'à réalisés (Catania et Paola, 2000; Lelandais, 2014). Les différents paramètres contrôlant la pression d'eau interstitielle et les processus de remobilisation ont été déterminés dans cette étude, et pourrait ainsi être modélisés analogiquement. La stratigraphie préglaciaire pourrait être modélisée en alternant couches sableuses perméables et imperméables argileuses. La glace serait modélisée par un couvercle rigide et imperméable sur lequel des fortes pressions seraient exercées (verticalement et horizontalement), tandis qu'un écoulement d'eau à l'interface sédiment/couvercle rigide permettrait de simuler l'apport d'eau de fonte dans le système. Une simulation avec ou sans paléotopographie permettrait également de déterminer l'impact de

l'héritage topographique sur la distribution des vallées tunnels. De même, les variations du ratio niveaux perméables/niveaux imperméables dans la simulation lithologique et stratigraphique du substrat préglaciaire permettrait de mieux définir l'impact du substratum sur les processus de remobilisation sédimentaire. La simulation de ces différents paramètres permettrait de pouvoir prédire l'emplacement des vallées tunnels en fonction de l'héritage structural et de la stratigraphie des sédiments préglaciaires.

► La comparaison des vallées tunnels de Foum Larjamme et d'Alnif a permis de mettre en évidence les différences de morphologie et de modèle de creusement sous et entre les *ice-streams*. Afin de valider ce modèle, il serait important d'observer la relation entre la morphologie des vallées tunnels et la distribution des *ice-streams* sur des exemples quaternaires. La distribution des paléo *ice-streams* de la mer du Nord et de la mer de Norvège durant le Quaternaire est géographiquement bien définie (Ottesen, 2005a, b). Les données de subsurface sont nombreuses dans ces régions (Huuse et Lykke-Andersen, 2000; Jørgensen et Sandersen, 2006; Sandersen et al., 2009; Janszen et al., 2012) en raison de l'intérêt économique (hydrocarbures) que ces vallées représentent. L'étude de ces vallées permettrait ainsi de comparer leurs morphologies en fonction de leur localisation par rapport aux «*ice-streams*». A terme, comparer les morphologies et les processus de creusement sous et entre les «*ice-streams*» permettraient de mieux contraindre les processus responsable des fortes vitesses d'écoulement le long de ces «*ice-streams*». Une des questions étant de déterminer le processus prédominant dans l'initiation d'un *ice-stream*: la circulation d'eau de fonte à l'interface glace/substrat ou bien le développement de fortes pressions de fluide dans le substrat.

► L'impact des pressions de fluide sur les propriétés pétrophysiques dans les domaines glaciaires et marins profonds a été démontré dans ce manuscrit. Si la distribution des propriétés pétrophysiques semblent hétérogène, elle pourrait être due à un pas d'échantillonnage trop large. Les cartes d'interpolation de la distribution de la porosité primaire pourraient être améliorées en augmentant le nombre d'échantillons. Concernant la distribution des coatings argileux dans les grès glaciaires du bassin de Sbaa, il faudrait répliquer la méthode à d'autres puits et d'autres carottes sédimentaires afin de valider les différents modèles de mise en place de ces tapissages argileux.

► L'évolution de la porosité au sein du système d'injectites a permis de mettre en évidence l'alternance de phase où le réseau se comporte comme un drain et des phases où le réseau d'injectites se comporte comme une barrière de perméabilité. Dans le but de mieux contraindre ces écoulements au cours du temps, ainsi que l'origine et le type de fluide circulant pendant les phases où le système d'injection est poreux et perméable, une analyse des inclusions fluides pourrait être réalisée. Les inclusions fluides présentes dans les ciments siliceux précoces permettraient de déterminer l'impact des fortes porosités associées aux pressions d'eau interstitielle élevées sur la migration des fluides profonds et des hydrocarbures. Après avoir validé l'impact des pressions de fluide sur les propriétés réservoirs, ces analyses permettraient d'illustrer si elles ont un rôle dans la migration des hydrocarbures.

BIBLIOGRAPHIE

Bibliographie

- Allen, J.R., 1982. *Sedimentary Structures: Their Character and Physical Basis*. Amsterdam, Elsevier edition, *Developments in Sedimentology* 30, 663 pp.
- Alvaro, J.J., Vennin, E., Villas, E., Destombes, J., Vizcaino, D., 2007. Pre-Hirnantian (latest Ordovician) benthic community assemblages: Controls and replacements in a siliciclastic-dominated platform of the eastern Anti-Atlas, Morocco. *Palaeogeography Palaeoclimatology Palaeoecology* 245, 20-36.
- Andresen, K.J., Clausen, O.R., Huuse, M., 2009. A giant (3.3×10^7 m³) middle Miocene (c. 15 Ma) sediment mound (M1) above the Siri Canyon, Norwegian-Danish Basin: Origin and Significance. *Marine and Petroleum Geology* 26, 1640-1655.
- Arnaud, E., 2012. The paleoclimatic significance of deformation structures in Neoproterozoic successions. *Sedimentary Geology* 243, 33-56.
- Asbjørn, S., Pedersen, S.A.S., 1996. Progressive glaciotectonic deformation in Weichselian and Palaeogene deposits at Feggeklit, northern Denmark. *Bulletin of the Geological Society of Denmark* 42, 153-174.
- Alsop, G.I., Marco, S., 2012. Tsunami and seiche-triggered deformation within offshore sediments. *Sedimentary Geology* 261, 90-107.
- Alsop, G.I., Marco, S., 2013. Seismogenic slump folds formed by gravity-driven tectonics down a negligible subaqueous slope. *Tectonophysics* 605, 48-69.
- Ballas, G., Soliva, R., Sizun, J.P., Fossen, H., Benedicto, A., Skurtveit, E., 2013. Shear-enhanced compaction bands formed at shallow burial conditions; implications for fluid flow (Provence, France). *Journal of Structural Geology* 47, 3-15.
- Banham, P.H., 1975. Glacitectonic structures: a general discussion with particular reference to the contorted drift of Norfolk. In: Wright A.E. and Moseley F. (Eds.), *Ice Ages: Ancient and Modern*. Geological Journal Special Issue 6. Seel House Press, Liverpool, pp. 69-94.
- Banham, P.H., 1977. Glacitectonites in till stratigraphy. *Boreas* 6, 101-105.
- Bartholomew, I.D., Nienow, P., Sole, A., Mair, D., Cowton, T., King, M.A., Palmer, S., 2011. Seasonal variations in Greenland Ice Sheet motion: Inland extent and behaviour at higher elevations. *Earth and Planetary Science Letters* 307, 271-278.
- Bartholomew, I., Nienow, P., Sole, A., Mair, D., Cowton, T., King, M.A., 2012. Short-term variability in Greenland Ice Sheet motion forced by time-varying meltwater drainage: Implications for the relationship between subglacial drainage system behavior and ice velocity. *Journal of Geophysical Research-Earth Surface* 117, F03002.
- Benediktsson, I.O., Moller, P., Ingolfsson, O., van der Meer, J.J.M., Kjaer, K.H., Kruger, J., 2008. Instantaneous end moraine and sediment wedge formation during the 1890 glacier surge of Brúarjökull, Iceland. *Quaternary Science Reviews* 27, 209-234.

- Benn, D.I., Evans, D.J.A., 1996. The interpretation and classification of subglacially deformed materials. *Quaternary Science Reviews* 15, 23-52.
- Benn, D.I., Evans, D.J.A., 2010. *Glaciers and Glaciations*, 2nd edn. Edward Arnold, London.
- Benn, D.I., Prave, A.R., 2006. Subglacial and proglacial glaciectonic deformation in the neoproterozoic Port Askaig Formation, Scotland. *Geomorphology* 75, 266-280.
- Bennett, M.P., 2001. The morphology, structural evolution and significance of push moraines. *Earth-Science Reviews* 53, 197-236.
- Bennett, M.R., 2003. Ice streams as the arteries of an ice sheet: their mechanics, stability and significance. *Earth-Science Reviews* 61, 309-339.
- Bjorkum, P.A., 1996. How important is pressure in causing dissolution of quartz in sandstones: *Journal of Sedimentary Research* 6, 147-154.
- Brennand, T.A., 2000. Deglacial meltwater drainage and glaciodynamics: inferences from Laurentide eskers, Canada. *Geomorphology* 32, 263-293.
- Boehm, A. and Moore, J.C., 2002. Fluidized sandstone intrusions as an indicator of Paleostress orientation, Santa Cruz, California. *Geofluids* 2, 147-161.
- Bolton, A.J., Maltman, A.J., Clennell, M.B., 1998. The importance of overpressure timing and permeability evolution in fine-grained sediments undergoing shear. *Journal of Structural Geology* 20, 1013-1022.
- Boon, S., Sharpe, M.J., 2003. The role of hydrologically-driven ice fracture in drainage system evolution of an Arctic glacier. *Geophysical Research Letters* 30, 1916.
- Boulton, G.S., 1974. Processes and patterns of subglacial erosion. In: Coates, D.R. (Ed.), *Glacial Geomorphology*. University of New York, Binghamton, pp. 41-87.
- Boulton, G.S., 1976. The origin of glacially-fluted surfaces — observations and theory. *Journal of Glaciology* 17, 287-309.
- Boulton, G.S., Hindmarsh, R.C.A., 1987. Sediment deformation beneath glaciers; rheology and geological consequences. *Journal of Geophysical Research* 92, 9059–9082.
- Boulton, G.S. and Jones, A.S., 1987. Stability of temperate ice caps and ice sheets resting on beds of deformable sediment. *Journal of Glaciology* 90, 29-43.
- Boulton, G.S., Caban, P.E., Vangijssel, K., 1995. Groundwater-flow beneath ice sheets .1. Large-scale patterns. *Quaternary Science Reviews* 14, 545-562.
- Boulton, G.S., Dobbie, K.E., Zatsepin, S., 2001. Sediment deformation beneath glaciers and its coupling to the subglacial hydraulic system. *Quaternary International* 86, 3-28.
- Boulton, G.S., Lunn, R., Vidstrand, P., Zatsepin, S., 2007. Subglacial drainage by groundwater-channel coupling and the origin of esker systems: Part I - glaciological observations. *Quaternary Science Reviews* 26, 1067-1090.

- Boulton, G.S., Hagdorn, M., Maillot, P.B., Zatsepin, S., 2009. Drainage beneath ice sheets: groundwater-channel coupling, and the origin of esker systems from former ice sheets. *Quaternary Science Reviews* 28, 621-638.
- Bouma, A.H., 1962. Sedimentology of some flysch deposits. A graphic approach of facies interpretation. Thesis. University Utrecht. Elsevier Publishers, Amsterdam, 168 pp.
- Boyce, J.I., Eyles, N., 1991. Drumlins carved by deforming till streams below the Laurentide ice sheet. *Geology* 19, 787-790.
- Braccini, E., de Boer, W., Hurst, A., Huuse, M., Vigorito, M., Templeton, G., 2008. Sand injectites. *Oilfield Review*, summer 2008, 34-49.
- Brandes, C., Le Heron, D.P., 2010. The glaciotectonic deformation of Quaternary sediments by fault-propagation folding. *Proceedings of the Geologists' Association* 121, 270-280.
- Brandes, C., Winsemann, J., 2013. Soft-sediment deformation structures in NW Germany caused by Late Pleistocene seismicity. *International Journal of Earth Sciences* 102, 2255-2274.
- Brennand, T.A., Shaw, J., 1994. Tunnel channels and associated landforms, south-central Ontario: their implications for ice-sheet hydrology. *Canadian Journal of Earth Sciences* 31, 505-522.
- Briedis, N.A., Bergslien, D., Hjellbakk, A., Hill, R.E., Moir, G.J., 2007. Recognition Criteria, Significance to Field Performance, and Reservoir Modeling of Sand Injections in the Balder Field, North Sea. In: Hurst, A., Cartwright, J. (Eds.), *Sand injectites: Implications for Hydrocarbon Exploration and Production: American Association of Petroleum Geologists Memoir*, Tulsa, pp. 91-102.
- Brodzikowski, K., Van Loon, A.J., 1980. Sedimentary deformations in Saalian glaciolimnic deposits near Włostów (Zary area, western Poland). *Geologie en Mijnbouw* 59, 251-272.
- Brodzikowski, K., Van Loon, A.J., 1983. Sedimentology and deformational history of unconsolidated Quaternary sediments of the Jarosław Zone (Sudetic Foreland). *Geologia Sudetica* 18, 121-196.
- Brodzikowski, K., Van Loon, A.J., 1985. Inventory of deformational structures as a tool for unravelling the Quaternary geology of glaciated areas. *Boreas* 14, 175-188.
- Brodzikowski, K., van Loon, A.J., 1991. Glacigenic Sediments, In: *Collection Development in Sedimentology* 19, Elsevier, Amsterdam.
- Brooke, C.M., Trimble, T.J., Mackay, T.A., 1995. Mounded shallow gas sands from the Quaternary of the North Sea: analogues for the formation of sand mounds in deep water Tertiary sediments? In: Hartley, A.J., Prosser, D.J. (Eds.), *Characterisation of Deep Marine Clastic Systems: Special Publication*, vol. 94. Geological Society, London, pp. 95-101.
- Brookfield, B.E., Martini, I.P., 1999. Facies architecture and sequence stratigraphy in glacially influenced basins: basic problems and water-level/glacier input-point controls (with an example from the Quaternary of Ontario, Canada). *Sedimentary Geology* 123, 183-197.
- Brown, R.J., Kokelaar, B.P., Branney, M.J., 2007. Widespread transport of pyroclastic density currents from a large silicic tuff ring: the Glaramara tuff, Scafell caldera, English Lake District, UK.

Sedimentology 54, 1163-1189.

Busfield, M.E., Le Heron, D.P., 2013. Glacitectonic deformation in the Chuos Formation of northern Namibia: implications for Neoproterozoic ice dynamics. *Proceedings of the Geologists Association* 124, 778-789.

Carr, S., 2001. Micromorphological criteria for discriminating subglacial and glacial marine sediments: evidence from a contemporary tidewater glacier, Spitsbergen. *Quaternary International* 86, 71-79.

Carr, S.J., 2004. Micro-scale features and structures. In: Evans, D.J.A. and Benn, D.I. (Eds.), *A practical Guide to the Study of Glacial Sediments*. Arnold, London, 115-144.

Cartwright, J., James, D., Huuse, M., Vetel, W. and Hurst, A., 2008. The geometry and emplacement of conical sandstone intrusions. *Journal of Structural Geology* 30, 854-867.

Catania, G., Paola, C., 2001. Braiding under glass. *Geology* 29, 259-262.

Cheel, R.J., Rust, B.R., 1986. A sequence of soft-sediment deformation (dewatering) structures in Late Quaternary subaqueous outwash near Ottawa, Canada. *Sedimentary Geology* 47, 77-93.

Chen, J., Chough, S.K., Chun, S.S., Han, Z., 2009. Limestone pseudoconglomerates in the Late Cambrian Gushan and Chaomidian Formations (Shandong Province, China): soft-sediment deformation induced by storm-wave loading. *Sedimentology* 56, 1174-1195.

Choukroune, P., Gapais, D., Merle, O., 1987. Shear criteria and structural symmetry. *Journal of Structural Geology* 9, 525-530.

Christoffersen, P., Tulaczyk, S., Wattrus, N.J., Peterson, J., Quintana-Krupinski, N., Clark, C.D. and Sjunneskog, C., 2008. Large subglacial lake beneath the Laurentide Ice Sheet inferred from sedimentary sequences. *Geology* 36, 563-566.

Clark, C.D., 1994. Large-scale ice-moulding: a discussion of genesis and glaciological significance. *Sedimentary Geology* 91, 253-268.

Clarke, G.K.C., Leverington, D.W., Teller, J.T., Dyke, A.S., Marshall, S.J., 2005. Fresh arguments against the Shaw megaflood hypothesis. A reply to comments by David Sharpe on «Paleohydraulics of the last outburst flood from glacial Lake Agassiz and the 8200 BP cold event». *Quaternary Science Reviews* 24, 1533-1541.

Clerc, S., 2012. Modèles de dépôt sous-glaciaires et dynamique de remplissages des vallées tunnel. Exemple au Quaternaire (Bray, Irlande) et application à l'Ordovicien supérieur de l'Anti-Atlas (Alnif, Maroc). Ph.D thesis, University of Burgundy, Dijon, France, 312 pp.

Clerc, S., Buoncristiani, J.F., Guiraud, M., Desaubliaux, G., Portier, E., 2012. Depositional model in subglacial cavities, Killiney Bay, Ireland. Interactions between sedimentation, deformation and glacial dynamics. *Quaternary Science Reviews* 33, 142-164.

Clerc, S., Buoncristiani, J.F., Guiraud, M., Vennin, E., Desaubliaux, G., Portier, E., 2013. Subglacial to proglacial depositional environments in an Ordovician glacial tunnel valley Alnif, Morocco. *Palaeogeography, Palaeoclimatology, Palaeoecology* 370, 127-144.

Clerc S., Buoncristiani J.F., Guiraud M., Vennin E., Desaubliaux G., Ravier, E., Portier E., 2014.

- Evidence for a Combined Influence of Preglacial Lithology, Subglacial Hydrology and Structural Heritage on the Distribution of Ordovician Tunnel Valleys, (submitted).
- Cocks, L.R.M., Torsvik, T.H., 2002. Earth geography from 500 to 400 million years ago: a faunal and palaeomagnetic review. *Journal of the Geological Society* 159, 631–644.
- Collinson, J.D., 2003. Deformation of sediments. In: Middleton, G.V. (Ed.), *Encyclopedia of sediments and sedimentary rocks*. Kluwer Academic Publishers, Dordrecht, pp. 190–193.
- Coulomb, C. A., 1776. Essai sur une application des règles des maximis et minimis à quelques problèmes de statique relatifs, à la architecture. *Mem. Acad. Roy. Div. Sav.* 7, 343–387.
- Cosgrove, J.W., 1995. The expression of hydraulic fracturing in rocks and sediments. In: Ameen, M.S. (Ed.), *Fractography: Fracture Topography as a Tool in Fracture Mechanics and Stress Analysis*. Geological Society Special Publication 92, 187–196.
- Dana, J.D., 1849. *Geology. United States exploring expedition during the years 1838, 1839, 1840, 1841, 1842, under the command of Charles Wilkes, U.S.N., Vol. 10*. Philadelphia, 756 pp.
- Dardis, G.F., Hanvey, P.M., 1994. Sedimentation in a drumlin lee-side subglacial wave cavity, Northwest Ireland. *Sedimentary Geology* 91, 97–114.
- Darwin, Ch., 1851. *Geological observations on coral reefs, volcanic islands and on South America, part III*. Smith, Elder and Co., London.
- Davis, G. H., Reynolds, S. J., 1996. *Structural Geology of Rocks and Regions*. New York, John Wiley and Sons, 776 pp.
- Davies, R.J., Huuse, M., Hirst, P., Cartwright, J., Yang, Y., 2006. Giant clastic intrusions primed by silica diagenesis. *Geology* 34, 917–920.
- Davidson, L., Beswetherick, S., Craig, J., Eales, M., Fisher, A., Himmali, A., Jho, J., Mejrab, B., Smart, J., 2000. The structure, stratigraphy and petroleum geology of the Murzuq Basin, southwest Libya. In: Sola, M.A., Worsley, D. (Eds.), *Geological Exploration of the Murzuq Basin*. Elsevier, Amsterdam, pp. 295–320.
- Dehandschutter, B., Vandycke, S., Sintubin, M., Vandenberghe, N., Wouters, L., 2005. Brittle fractures and ductile shear bands in argillaceous sediments: inferences from Oligocene Boom Clay (Belgium). *Journal of Structural Geology* 27, 1095–1112.
- Deichmann, N.J., Ansorge, F., Scherbaum, A., Aschwanden, Bernardi, F., Gudmundsson, G.H., 2000. Evidence for deep icequakes in an Alpinr Glacier. *Annals of Glaciology* 31, 85–90.
- Delaney, P.T., Pollard, D.D., Ziony, J.I., McKee, E.H., 1986. Field relations between dikes and joints: emplacement processes and paleostress analysis. *Journal of Geophysical Research* 91, 4920–4938.
- Denis, M., Buoncristiani, J.F., Guiraud, M., 2009. Fluid-pressure controlled soft-bed deformation sequence beneath the surging Breiðamerkurjökull (Iceland, Little Ice Age). *Sedimentary Geology* 221, 71–86.
- Denis, M., Guiraud, M., Konate, M., Buoncristiani, J.F., 2010. Subglacial deformation and water-pressure cycles as a key for understanding ice stream dynamics: evidence from the Late Ordovician

succession of the Djado Basin (Niger). *International Journal of Earth Sciences* 99, 1399-1425.

Dewers, T., Ortoleva, P., 1991. Influences of clay minerals on sandstone cementation and pressure solution. *Geology* 19, 1045–1048.

Diggs, T.N., 2007. An outcrop study of clastic-injection structures in the Carboniferous Tesnus Formation, Marathon basin, Trans-Pecos Texas. In: Hurst, A., Cartwright, J. (Eds.), *Sand Injectites: Implications for Hydrocarbon Exploration and Production*: American Association of Petroleum Geologists Memoir, Tulsa, pp. 209–219.

Dixon, R.J., Schofield, K., Anderton, R., Reynolds, A.D., Alexander, R.W.S., Williams, M.C., Davies, K.G., 1995. Sandstone diapirism and clastic intrusion in the Tertiary submarine fans of the Bruce-Beryl Embayment, Quadrant 9, UKCS. In: Hartley, A.J., Prosser, D.J. (Eds.), *Characterisation of deep-marine clastic systems*: Special Publication, vol. 94. Geological Society, London, pp. 77–94.

Dugan, B., Flemings, P.B., 2002. Fluid flow and stability of the US continental slope offshore New Jersey from the Pleistocene to the present. *Geofluids* 2, 137-146.

Duranti, D., Hurst, A., Bell, C., Groves, S., Hanson, R., 2002. Injected and remobilised Eocene sandstones from the Alba Field, UKCS: core and wireline characteristics. *Petroleum Geoscience* 8, 99–107.

Duranti, D., Hurst, A., 2004. Fluidization and injection in the deep-water sandstones of the Eocene Alba Formation (UK North Sea). *Sedimentology* 51, 503-529.

Duranti, D., 2007. Large-scale sand injection in the Paleogene of the North Sea: Modeling of energy and flow velocities. In: Hurst, A., Cartwright, J. (Eds.), *Sand Injectites: Implications for Hydrocarbon Exploration and Production*: American Association of Petroleum Geologists Memoir, Tulsa, pp. 129-139.

Dyke, A.S., 1993. Landscapes of cold-centred Late Wisconsinian ice caps, Arctic Canada. *Progress in Physical Geography* 17, 223-247.

Dzuffyński, S., Walton, E.K., 1965. *Sedimentary features of flysch and greywackes*. Elsevier, Amsterdam, 274 pp.

Ehlers, J., Linke, G., 1989. The origin of deep buried channels of Elsterian age in north-west Germany. *Journal of Quaternary Science* 4, 255-265.

Ehlers, J., Gibbard, P. L., 2004. *Quaternary Glaciations - Extent and Chronology Part I: Europe*. Elsevier, Amsterdam. 457 pp.

Engelhardt, H., 2004. Thermal regime and dynamics of the West Antarctic ice sheet. *Annals of Glaciology* 39, 85-92.

Evans, D.J.A., Phillips, E.R., Hiemstra, J.F., Auton, C.A., 2006. Subglacial till: Formation, sedimentary characteristics and classification. *Earth-Science Reviews* 78, 115-176.

Eyles, N., Miall, A.D., 1984. Glacial facies. In: R.G. Walker (Ed.) *Facies Models*. Geoscience Canada Reprint Series 1, Second Edition, pp. 15-38.

Eyles, N., McCabe, A.M., 1989. Glaciomarine facies within subglacial tunnel valleys: the sedimentary

- record of glacioisostatic downwarping in the Irish Sea basin. *Sedimentology* 36, 431-448.
- Ferguson, J., 1994. *Introduction to Linear Algebra in Geology*, New York, Chapman & Hall, 203 pp.
- Finnegan, S., et al., 2011. The magnitude and duration of Late Ordovician–Early Silurian glaciation. *Science* 331, 903–906.
- Fisher, Q.J., Knipe, R.J., Worden, R.H., 2000. Microstructures of deformed and non-deformed sandstones from the North Sea: implications for the origins of quartz cement in sandstones, in: Worden, R.H., and Morad, S. (Eds.), *Quartz Cementation in Sandstones: International Association of Sedimentologists, Special Publication 29*, 129-146.
- Fisher, T.G., Taylor, L.D., 2002. Sedimentary and stratigraphic evidence for subglacial flooding, south-central Michigan, USA. *Quaternary International* 90, 87-115.
- Fleming, E.J., Stevenson, C.T.E., Petronis, M.S., 2013. New insights into the deformation of a Middle Pleistocene glaciotectionised sequence in Norfolk, England through magnetic and structural analysis. *Proceedings of the Geologists Association* 124, 834-854.
- Fossen, H., Tikoff, B., 1993. The deformation matrix for simultaneous simple shearing, pure shearing, and volume change, and its application to transpression/transtension tectonics. *Journal of Structural Geology* 15, 413-422.
- Fossen, H., Schultz, R.A., Shipton, Z.K., Mair, K., 2007. Deformation bands in sandstone: a review. *Journal of the Geological Society* 164, 755-769.
- Fossen, H., 2010. *Structural Geology*. Cambridge University Press, 272 pp.
- Fries, G., Parize, O., 2003. Anatomy of ancient passive margin slope systems: Aptian gravity-driven deposition on the Vocontian palaeomargin, western Alps, south-east France. *Sedimentology* 50, 1231-1270.
- Gallo, F., Woods, W., 2004. On steady homogeneous sand–water flows in a vertical conduit. *Sedimentology* 51, 195–210.
- Ghienne, J.F., Le Heron, D.P., Moreau, J., Denis, M., Deynoux, M., 2007. The Late Ordovician glacial sedimentary system of the North Gondwana platform. *Glacial Sedimentary Processes and Products* 39, 295-319.
- Gibbard, P., 1980. The origin of stratified Catfish Creek till by basal melting. *Boreas* 9, 71-85.
- Gibbard, P., Cohen K.M., 2008. Global chronostratigraphical correlation table for the last 2.7 million years. *Episodes* 31, 243-247.
- Girard, F., Ghienne, J.F., Rubino, J.L., 2012. Occurrence of hyperpycnal flows and hybrid event beds related to glacial outburst events in a late ordovician proglacial delta (Murzuq Basin, SW Libya). *Journal of Sedimentary Research* 82, 688-708.
- Glennie, K., Hurst, A., 2007. Fluidization and Associated Soft-sediment Deformation in Eolian Sandstones: Hopeman Sandstone (Permian), Scotland, and Rotliegend, North Sea. In: Hurst, A., Cartwright, J. (Eds.), *Sand Injectites: Implications for Hydrocarbon Exploration and Production: American Association of Petroleum Geologists Memoir*, Tulsa, pp. 245–252.

- Gordon, J.E., Whalley, W.B., Gellatly, A.F., Vere, D.M., 1992. The formation of glacial flutes: assessment of models with evidence from Lyngsdalen, north Norwat. *Quaternary Science Reviews* 11, 709-731.
- Goscombe, B.D., Passchier, C.W., Hand, M., 2004. Boudinage classification: end-member boudin types and modified boudin structures. *Journal of Structural Geology* 26, 739-763.
- Hart, J.K., 2007. An investigation of subglacial shear zone processes from Weybourne, Norfolk, UK. *Quaternary Science Reviews* 26, 2354-2374.
- Greb, S.F., Archer, A.W., 2007. Soft-sediment deformation produced by tides in a meizoseismic area, Turnagain Arm, Alaska. *Geology* 35, 435-438.
- Gruszka, B., van Loon, A.J., 2007. Pleistocene glaciolacustrine breccias of seismic origin in an active graben (central Poland). *Sedimentary Geology* 193, 93-104.
- Guiraud, M., Plaziat, J.C., 1993. Seismites in the fluvial Bima sandstones: identification of paleoseisms and discussion of their magnitudes in a Cretaceous synsedimentary strike-slip basin (Upper Benue, Nigeria). *Tectonophysics* 225, 493-522.
- Habermann, M., Truffer, M., Maxwell, D., 2013. Changing basal conditions during the speed-up of Jakobshavn Isbrae, Greenland. *Cryosphere* 7, 1679-1692.
- Hart, J.K., Smith, B., 1997. Subglacial deformation associated with fast ice flow, from the Columbia Glacier, Alaska. *Sedimentary Geology* 111, 177-197.
- Hart, J.K., 1998. The deforming bed debris-rich basal ice continuum and its implications for the formation of glacial landforms (flutes) and sediments (melt-out till). *Quaternary Science Reviews* 17, 737-754.
- Hart, J.K., Boulton, G.S., 1991. The interrelation of glaciotectonic and glaciodepositional processes within the glacial environment. *Quaternary Science Reviews* 10, 335-350.
- Haughton, P., Davis, C., McCaffrey, W., 2006. «Facies Prediction in turbidite Fan Systems – Nature and Significance of ‘Linked Debrites’ in Sand-Rich Versus Mixed Sand-Mud Systems» Recent Advances in Siliciclastic Facies Models: Implications for Reservoir Characterization II (SEPM), AAPG Annual Convention, April 9-12, 2006 Technical Program.
- Heald, M.T., Larese, R.E., 1974. Influence of coatings on quartz cementation. *Journal of Sedimentary Research* 44, 1269-1274.
- Hickson, T.A., Lowe, D.R., 2002. Facies architecture of a submarine fan channel-levee complex: The Juniper Ridge Conglomerate, Coalinga, California. *Sedimentology* 49, 335-362.
- Hicock, S.R., 1990. Genetic Till Prism. *Geology* 18, 517-519.
- Hiemstra, J.F., van der Meer, J.J.M., 1997. Pore-water controlled grain fracturing as an indicator for subglacial shearing in tills. *Journal of Glaciology* 43, 446-454.
- Hildebrandt, C., Egenhoff, S., 2007. Shallow-marine massive sandstone sheets as indicators of palaeoseismic liquefaction - An example from the Ordovician shelf of Central Bolivia. *Sedimentary*

Geology 202, 581-595.

Hillier, R.D., Cosgrove, J.W., 2002. Core and seismic observations of overpressure-related deformation within Eocene sediments of the Outer Moray Firth, UKCS. *Petroleum Geoscience* 8, 141-149.

Hirst, J.P.P., Benbakir, A., Payne, D.F., Westlake, I.R., 2002. Tunnel valleys and density flow processes in the Upper Ordovician glacial succession, Illizi Basin, Algeria: influence on reservoir quality. *Journal of Petroleum Geology* 25, 297-324.

Hiscott, R.N., 1979. Clastic sills and dikes associated with deep-water sandstones, Tourelle formation, Ordovician, Quebec. *Journal of Sedimentary Petrology* 49, 1-10.

Hoek, J.D., 1991. A classification of dyke-fracture geometry with examples from Precambrian dyke swarms in the Vestfold Hills, Antarctica. *Gologische Rundschau* 80, 233-248.

Hooke, R.L., Jennings, C.E., 2006. On the formation of the tunnel valleys of the southern Laurentide ice sheet. *Quaternary Science Reviews* 25, 1364-1372.

Huang, Q., 1988. Geometry and tectonic significance of Albian sedimentary dikes in the Sisteron area, SE France: *Journal of Structural Geology* 10, 453-462.

Hubbard, S.M., Romans, B.W., Graham, S.A., 2007. An outcrop example of large-scale conglomeratic intrusions sourced from deep-water channel deposits, Cerro Toro Formation, Magallanes basin, southern Chile. In: Hurst, A., Cartwright, J. (Eds.), *Sand Injectites: Implications for Hydrocarbon Exploration and Production: American Association of Petroleum Geologists Memoir*, Tulsa, pp. 199-207.

Huguen, C., Guiraud, M., Benkhelil, J., Mascle, J., 2001. Synlithification deformation processes of the Cretaceous sediments of the Ivory Coast-Ghana transform margin: A way to detail the margin history. *Tectonics* 20, 959-975.

Hughes, T., Sargent, A., Fastook, J., 2011. Ice-bed coupling beneath and beyond ice streams: Byrd Glacier, Antarctica. *Journal of Geophysical Research-Earth Surface* 116, F03005.

Hulbe, C.L., Joughin, I.R., Morse, D.L., Bindschadler, R.A., 2000. Tributaries to West Antarctic ice streams: characteristics deduced from numerical modelling of ice flow. *Annals of Glaciology* 31, 184-190.

Hurst, A., 2004. Sedimentology of seafloor sand extrusions: an example from the Miocene of central California. *British Sedimentological Research Group Annual General Meeting*. BSRG, Manchester, England, pp. 1.

Hurst, A., Buller, A.T., 1984. Dish structures in some Palaeocene deep-sea sandstones (Norwegian sector, North Sea); origin of the dish-forming clays and their effect on reservoir quality. *Journal of Sedimentary Petrology* 54, 1206-1211.

Hurst, A., Cronin, B.T., 2001. The origin of consolidation laminae and dish structures in some deep-water sandstones. *Journal of Sedimentary Research* 71, 136-143

Hurst, A., Cartwright, J.A., Duranti, D., 2003. Fluidization structures produced by upward injection of sand through a sealing lithology. In: Van Rensbergen, P., Hillis, R.R., Maltman, A.J., Morley, C.K. (Eds.), *Subsurface Sediment Mobilization: Special Publication*, vol. 216. Geological Society,

London, pp. 123–137.

Hurst, A., Cartwright, J.A. (Eds.), 2007. Implications for Hydrocarbon Exploration and Production: American Association of Petroleum Geologists Memoir, Tulsa. 274 pp.

Hurst, A., Cartwright, J.A., Huuse, M., Duranti, D., 2006. Extrusive sandstones (extrudites): a new class of stratigraphic trap? In: Allen, M.R., Goffey, G.P., Morgan, R.K., Walker, I.M. (Eds.), *The Deliberate Search for the Stratigraphic Trap. : Special Publication*, vol. 254. Geological Society, London, pp. 289–300.

Hurst, A., Scott, A., Vigorito, M., 2011. Physical characteristics of sand injectites. *Earth-Science Reviews* 106, 215–246.

Huuse, M., Lykke-Andersen, H., 2000. Overdeepened Quaternary valleys in the eastern Danish North Sea: morphology and origin. *Quaternary Science Reviews* 19, 1233–1253.

Huuse, M., Mickelson, M., 2004. Eocene sandstone intrusions in the Tampen Spur area (Norwegian North Sea Quad 34) imaged by 3D seismic data. *Marine and Petroleum Geology* 21, 141–155.

Huuse, M., Duranti, D., Steinsland, N., Guaranga, C.G., Prat, P., Holm, K., Cartwright, J.A., Hurst, A., 2004. Seismic characteristics of large-scale sandstones intrusions in the Paleogene of the South Viking Graben, UK and Norwegian North Sea. In: Davies, R.J., Cartwright, J.A., Stewart, S.A., Lappin, M., Underhill, J.R. (Eds.), *Seismic technology: Application to the Exploration of Sedimentary basins*: Geological Society, London Memoir, 29, pp. 263–277.

Huuse, M.J., Cartwright, J.A., Hurst, A., Steinsland, N., 2007. Seismic characterization of large-scale sandstone intrusions. In: Hurst, A., Cartwright, J. (Eds.), *Sand Injectites: Implications for Hydrocarbon Exploration and Production*: American Association of Petroleum Geologists Memoir, Tulsa, pp. 21–35.

Ingólfsson, Ó., Norðdahl, H., Schomaker, A., 2010. Deglaciation and Holocene Glacial History of Iceland. In: Schomacker, A., Krüger, J., Kjær, K.H. (Eds.), *The Mýrdalsjökull ice cap, Iceland. Glacial processes, sediments and landforms on an active volcano*: *Developments in Quaternary Science* 13, 51–68.

Iverson, N.R., Hoojer, T.S., Hooke, R. L.B., 1996. A laboratory study of sediment deformation: stress heterogeneity and grain-size evolution. *Annals of Glaciology* 22, 167–175.

Janszen, A., Spaak, M., Moscariello, A., 2012. Effects of the substratum on the formation of glacial tunnel valleys: an example from the Middle Pleistocene of the southern North Sea Basin. *Boreas* 41, 629–643.

Jackson, C.A.L., 2007. The geometry, distribution, and development of clastic injections in slope systems: seismic examples from the Upper Cretaceous Kyrre Formation, Maloy Slope, Norwegian margin, In: Hurst, A., and Cartwright, J., (Eds.), *Sand injectites: Implications for hydrocarbon exploration and production*: AAPG Memoir, 87, pp. 37–48.

Jackson, C.A.L., Huuse, M., Barber, G.P., 2011. Geometry of winglike clastic intrusions adjacent to a deep-water channel complex: Implications for hydrocarbon exploration and production. *AAPG Bulletin* 95, 559–584.

Johnson, M.D., 1999. Spooner Hill, Northwest Wisconsin: High Relief Hills Carved by Subglacial

- Meltwater of the Superior Lobe. In: Mickelson, D.M., Attig, J.W. (Eds.), *Glacial Processes Past and Present: Geological Society of America Special Paper*, 337, pp. 83–92.
- Jolly, R., Sanderson, D., 1997. A Mohr circle construction for the opening of a preexisting fracture. *Journal of Structural Geology* 19, 887–892.
- Jolly, R.J.H., Lonergan, L., 2002. Mechanisms and controls on the formation of sand intrusions. *Journal of the Geological Society* 159, 605–617.
- Jonk, R., Duranti, D., Parnell, J., Hurst, A., Fallick, A.E., 2003. The structural and diagenetic evolution of injected sandstones: examples from the Kimmeridgian of NE Scotland. *Journal of the Geological Society* 160, 881–894.
- Jonk, R., Hurst, A., Duranti, D., Parnell, J., Mazzini, A., Fallick, A.E., 2005a. Origin and timing of sand injection, petroleum migration, and diagenesis in Tertiary reservoirs, South Viking Graben, North Sea. *AAPG Bulletin* 89, 329–357.
- Jonk, R., Parnell, J., Hurst, A., 2005b. Aqueous and petroleum fluid flow associated with sand injectites. *Basin Research* 17, 241–257.
- Jonk, R., Cronin, B.T., Hurst, A., 2007. Variations in Sediment Extrusion in Basin-floor, Slope, and Delta-front Settings: Sand Volcanoes and Extruded Sand Sheets from the Namurian of County Clare, Ireland. In: Hurst, A., Cartwright, J. (Eds.), *Sand Injectites: Implications for Hydrocarbon Exploration and Production: American Association of Petroleum Geologists Memoir*, Tulsa, pp. 221–226.
- Jorgensen, F., Sandersen, P.B.E., 2006. Buried and open tunnel valleys in Denmark — erosion beneath multiple ice sheets. *Quaternary Science Reviews* 25, 1339–1363.
- Joughin, I., MacAyeal, D.R., Tulaczyk, S., 2004. Basal shear stress of the Ross ice streams from control method inversions. *Journal of Geophysical Research* 109, B09405.
- Joughin, I., Das, S.B., King, M.A., Smith, B.E., Howat, I.M., Moon, T., 2008. Seasonal speedup along the western flank of the Greenland Ice Sheet. *Science* 320, 781–783.
- Kamb, B., 1987. Glacier surge mechanism based on linked cavity configuration of the basal water conduit system. *Journal of Geophysical Research* 92, 9083–9100.
- Kane, I.A., 2010. Development and flow structures of sand injectites: The Hind Sandstone Member injectite complex, Carboniferous, UK. *Marine and Petroleum Geology* 27, 1200–1215.
- Kawakami, G., Kawamura, M., 2002. Sediment flow and deformation (SFD) layers: evidence for intrastratal flow in laminated muddy sediments of the Triassic Osawa Formation, northeast Japan. *Journal of Sedimentary Research* 72, 171–181.
- Kehew, A.E., Piotrowski, J.A., Jørgensen, F., 2012. Tunnel valleys: Concepts and controversies – A review. *Earth-Science Reviews* 113, 33–58.
- Keighley, D.G., Pickerill, R.K., 1994. Flute-like marks and associated structures from the Carboniferous Port Hood formation of eastern Canada: Evidence of secondary origin in association with sediment intrusion. *Journal of Sedimentary Research* 64, 253–263.
- Kjaer, K.H., Larsen, E., van der Meer, J., Ingolfsson, O., Kruger, J., Benediktsson, I.O., Knudsen, C.G.,

- Schomacker, A., 2006. Subglacial decoupling at the sediment/bedrock interface: a new mechanism for rapid flowing ice. *Quaternary Science Reviews* 25, 2704-2712.
- Kleman, J., Borgström, I., 1996. Reconstruction of palaeo-ice-sheets: the use of geomorphological data. *Earth Surface Processes and Landforms* 21, 893-909.
- Kleman, J., Glasser, N.F., 2007. The subglacial thermal organisation (STO) of ice sheets. *Quaternary Science Reviews* 26, 585-597.
- Kleman, J., Hättestrand, C., 1999. Frozen-bed Fennoscandian and Laurentide ice sheets during the Last Glacial Maximum. *Nature* 402, 63-66.
- Knipe, R.J., 1986. Deformation mechanism path diagrams for sediments undergoing lithification. *Geological Society of America Memoir* 166, 151-160.
- Kozlowski, A.L., Kehew, A.E., Bird, B.C., 2005. Outburst flood origin of the Central Kalamazoo River Valley, Michigan, U.S.A. *Quaternary Science Reviews* 24, 2354-2374.
- Le Heron, D.P., 2007. Late ordovician glacial record of the Anti-Atlas, Morocco. *Sedimentary Geology* 201, 93-110.
- Le Heron, D.P., Sutcliffe, O.E., Whittington, R.J., Craig, J., 2005a. The origins of glacially related soft-sediment deformation structures in Upper Ordovician glaciogenic rocks: implication for ice-sheet dynamics. *Palaeogeography Palaeoclimatology Palaeoecology* 218, 75-103.
- Le Heron, D.P., Etienne, J.L., 2005b. A complex subglacial clastic dyke swarm, Sólheimajökull, southern Iceland. *Sedimentary Geology* 181, 25-37.
- Le Heron, D.P., Ghienne, J.F., El Houicha, M., Khoukhi, Y., Rubino, J.L., 2007. Maximum extent of ice sheets in Morocco during the Late Ordovician glaciation. *Palaeogeography Palaeoclimatology Palaeoecology* 245, 200-226.
- Le Heron, D.P., Craig, J., Etienne, J.L., 2009. Ancient glaciations and hydrocarbon accumulations in North Africa and the Middle East. *Earth-Science Reviews* 93, 47-76.
- Le Heron, D.P., Busfield, M.E., Kamona, F., 2013. An interglacial on snowball Earth? Dynamic ice behaviour revealed in the Chuos Formation, Namibia. *Sedimentology* 60, 411-427.
- Lelandais, T., 2014. Modélisation analogique des écoulement d'eaux sous-glaicaires. TER, Université du Maine, 32 pp.
- Lee, J.R., Phillips, E.R., 2008. Progressive soft sediment deformation within a subglacial shear zone - a hybrid mosaic-pervasive deformation model for Middle Pleistocene glaciotectionised sediments from eastern England. *Quaternary Science Reviews* 27, 1350-1362.
- Le Roux, J.P., Nielsen, S.N., Kemnitz, H. & Henriquez, Á., 2008. A Pliocene mega-tsunami deposit and associated features in the Ranquil Formation, southern Chile. *Sedimentary Geology* 203, 164-180.
- Lesemann, J.E., Alsop, G.I., Piotrowski, J.A., 2010. Incremental subglacial meltwater sediment deposition and deformation associated with repeated ice-bed decoupling a case study from the Island of Funen, Denmark. *Quaternary Science Reviews* 29, 3212-3229.

- Levi, T., Weinberger, R., Eyal, Y., 2011. A coupled fluid-fracture approach to propagation of elastic dikes during earthquakes. *Tectonophysics* 498, 35-44.
- Libboutry, L., 1979. Local friction laws for glaciers: a critical review and new openings. *Journal of Glaciology* 39, 67-95.
- Lien T., Walker, R. G., Martinsen, O. J., 2003. Turbidites in the Upper Carboniferous Ross Formation, Western Ireland - reconstruction of a sinuous channel and sandy spillover system. *Sedimentology* 50, 113-148.
- Livingstone, S.J., Clark, C.D., Piotrowski, J.A., Tranter, M., Bentley, M.J., Hodson, A., Swift, D.A., Woodward, J., 2012. Theoretical framework and diagnostic criteria for the identification of palaeo-subglacial lakes. *Quaternary Science Reviews* 53, 88-110.
- Lonergan, L., Lee, N., Johnson, H.D., Cartwright, J.A., Jolly, R.J.H., 2000. Remobilization and injection in deep-water depositional systems: Implications for reservoir architecture and prediction, in P. Weimer, R. M. Slatt, J. Coleman, N. C. Rosen, H. Nelson, A. H. Bouma, M. J. Styzen, and D. T. Lawrence (Eds.), *Deep-water reservoirs of the world: Gulf Coast Section SEPM Foundation, 20th Annual Conference*, Houston, pp. 515–532.
- Lonergan, J., Borlandelli, C., Taylor, A., Quine, M., Flanagan, K., 2007. The Three-dimensional Geometry of Sandstone Injection Complexes in the Gryphon Field, United Kingdom, North Sea. In: Hurst, A., Cartwright, J. (Eds.), *Sand Injectites: Implications for Hydrocarbon Exploration and Production: American Association of Petroleum Geologists Memoir*, Tulsa, pp. 103–112.
- Lowe, D.R., 1975. Water escape structures in coarse-grained sediments. *Sedimentology* 22, 157–204.
- Lowe, D.R., 1982. Sediment gravity flows: II. Depositional models with special reference to the deposits of high-density turbidity currents. *Journal of Sedimentary Petrology* 52, 279-297.
- Lowe, D.R., Lopiccolo, R.D., 1974. The characteristics and origins of dish and pillar structures. *Journal of Sedimentary Petrology* 44, 484–501.
- Lyell, Ch., 1841. *Elements of geology* (2nd ed.). London.
- MacAyeal, D. R., 1992. The basal stress distribution of Ice Stream E, Antarctica, inferred by control methods, *Journal of Geophysical Research* 97, 595–603.
- MacLeod, M.K., Hanson, R.A., Bell, C.R., McHugo, S., 1999. The Alba Field ocean bottom cable seismic survey: Impact on development. *The Leading Edge* 18, 136-1312.
- Mair, D., Willis, I., Fischer, U.H., Hubbard, B., Nienow, P., Hubbard, A., 2003. Hydrological controls on patterns of surface, internal and basal motion during three «spring events»: Haut Glacier d’Arolla, Switzerland. *Journal of Glaciology* 49, 555-567.
- Maltman, A.J., 1984. On the term «soft-sediment deformation». *Journal of Structural Geology* 6, 589-592.
- Maltman, A.J., 1994. *The Geological Deformation of Sediments*. Chapman and Hall, London 362 pp.

- Maltman, A.J., Bolton, A., 2003. How sediments become mobilized. In Van Rensbergen, P., Hillis, R.R., Maltman, A.J. and Morley, C.K. (Eds.), *Subsurface Sediment Mobilization*. Geological Society, London, Special Publications 216, 9-20.
- Martill, D.M., Hudson, J.D., 1989. Injection clastic dykes in the Lower Oxford Clay (Jurassic) of central England: relationship to compaction and concretion formation. *Sedimentology* 36, 1127–1133.
- McCabe, A. M., Clark, P. U., Clark, J., 2005. AMS 14C dating of deglacial events in the Irish Sea Basin and other sectors of the British-Irish ice sheet. *Quaternary Science Reviews* 24, 1673-1690.
- McCabe, A. M., Clark, P. U., Clark, J., Dunlop, P., 2007. Radiocarbon constraints on readvances of the British-Irish Ice Sheet in the northern Irish Sea Basin during the last deglaciation. *Quaternary Science Reviews* 26, 1204-1211.
- McCarroll, D., Rijdsdijk, K.F., 2003. Deformation styles as a key for interpreting glacial depositional environments. *Journal of Quaternary Science* 18, 473-489.
- Marshall, J.D., 2000. Sedimentology of a Devonian fault-bounded braidplain and lacustrine fill in the lower part of the Skrinkle Sandstones, Dyfed, Wales. *Sedimentology* 47, 325-342.
- Menzies, J., 2000a. Micromorphological analyses of microfabrics and microstructures, indicative of deformation processes, in glacial sediments. In: Maltman, A.J., Hubbard, B., Hambrey, M.J. (Eds.), *Deformation of Glacial Materials*. Geological Society, London, pp. 245-258.
- Menzies, J., 2000b. Microstructures in diamictites of the Lower Gowaganda Formation (Huronian), near Elliott lake, Ontario: evidence for deforming-bed conditions at the grounding line? *Journal of Sedimentary Research* 7, 21 -216.
- Menzies, J., 1989. Subglacial hydraulic conditions and their possible impact upon subglacial bed deformation. *Sedimentary Geology* 62, 125-150.
- Menzies, J., 2012. Strain pathways, till internal architecture and microstructures - perspectives on a general kinematic model - a 'blueprint' for till development. *Quaternary Science Reviews* 50, 105-124.
- Menzies, J., van der Meer, J.J.M., Rose, J., 2006. Till-as a glacial «tectomict», its internal architecture, and the development of a «typing» method for till differentiation. *Geomorphology* 75, 172-200.
- Menzies, J., Ellwanger, D., 2011. Insights into subglacial processes inferred from the micromorphological analyses of complex diamicton stratigraphy near Illmensee-Lichtenegg, Hochsten, Germany. *Boreas* 40, 271-288.
- Meshram, D.C., Sangode, S.J., Gujar, A.R., Ambre, N.V., Dhongle, D., Porate, S., 2011. Occurrence of soft sediment deformation at Dive Agar beach, west coast of India: possible record of the Indian Ocean tsunami (2004). *Natural Hazards* 57, 385-393.
- Middleton, G. V., Hampton, M. A., 1973. Sediment gravity flows: mechanics of flow and deposition. In *Turbidites and Deep Water Sedimentation* G. V. Middleton and A. H. Bouma (Eds.). Anaheim, California, SEPM. Short Course Notes, 38 pp.
- Mills, P.C., 1983. Genesis and diagnostic value of soft-sediment deformation structures - review. *Sedimentary Geology* 35, 83-104.

- Minoura, K., Nakata, T., 1994. Discovery of an ancient tsunami deposit in coastal sequence of southwest Japan, verification of a large historic tsunami. *Island Arc* 3, 66-72.
- Molina, J.M., Alfaro, P., Moretti, M., Soria, J.M., 1998. Soft-sediment deformation structures induced by cyclic stress of storm waves in tempestites (Miocene, Guadalquivir Basin, Spain). *Terra Nova* 10, 145-150.
- Molyneux, S., Cartwright, J.A., Lonergan, L., 2002. Conical sandstone injection structures imaged by 3D seismic in the central North Sea, UK. *First break* 20, 383-393.
- Monnier, D., 2013. Dynamique de mise en place des réseaux d'intrusions sableuses dans les bassins sédimentaires : Impact sur l'évolution post-dépôt des réservoirs et le réseau de migration associé. Ph.D thesis, University of Montpellier 2, France, 294 pp.
- Monnier, D., Imbert, P., Gay, A., Mourgues, R., Lopez, M., 2014. Pliocene sand injectites from a submarine lobe fringe during hydrocarbon migration and salt diapirism: a seismic example from the Lower Congo Basin. *Geofluids* 14, 1-19.
- Moreau, J., Ghienne, J.F., Hurst, A., 2012. Kilometre-scale sand injectites in the intracratonic Murzuq Basin (South-west Libya): an igneous trigger? *Sedimentology* 59, 1321-1344.
- Mugnier, J.L., Huyghe, P., Gajurel, A.P., Upreti, B.N., Jouanne, F., 2011. Seismites in the Kathmandu basin and seismic hazard in central Himalaya. *Tectonophysics* 509, 33-49.
- Muir Wood, D., 1998. Life Cycles of Granular Materials. In: *Philosophical Transactions of the Royal Society London* 356, 2453-2470.
- Mulder, T., Alexander, J., 2001. The physical character of subaqueous sedimentary density flows and their deposits. *Sedimentology* 48, 269-299.
- Mulder T., 2011. Gravity Processes and Deposits on Continental Slope, Rise and Abyssal Plains. In: Hüeneke, H. and Mulder, T. (Eds.), *Deep-sea Sediments. Developments in Sedimentology* 63, pp. 25-148.
- Mulder T., Hüeneke, H., Van Loon A.J., 2011b. Progress in Deep-Sea Sedimentology In: Hüeneke, H. and Mulder, T. (Eds.), *Deep-sea Sediments. Developments in Sedimentology* 63, pp. 1-24.
- Muller, E., 1983. Dewatering during lodgement of till. In: *Tills and related deposits* (Eds E.B. Evenson, C. Schluchter, and J. Rabassa). Balkema, Rotterdam, pp. 3-12.
- Munro-Stasiuk, M.J., 2000. Rhythmic till sedimentation: Evidence for repeated hydraulic lifting of a stagnant ice mass. *Journal of Sedimentary Research* 70, 94-106.
- Mutti, E., 1985. Turbidite systems and their relations to depositional sequences. In: Zuffa, G. (Ed.), *Provenance of Arenites*, D. Reidel Publishing Co, Dordrecht, Holland, pp. 65-93.
- Mutti, E., 1992. *Turbidite Sandstones*. Agip, Istituto di Geologia, Università di Parma, San Donato Milanese 275 pp.
- Mutti, E., Tinterri, R., Remacha, E., Mavilla, N., Angella, S., Fava, L., 1999. An introduction to the Analysis of ancient Turbidite Basins from an Outcrop Perspective. *American Association Petroleum Geologists Continuing Education Course Note Series* 39, 61pp.

- Nagtegaal, P.J.C., 1965. An approximation to the genetic classification of non-organic sedimentary structures. *Geologie en Mijnbouw* 44, 347–352.
- Ng, F., 2000. Canals under sediment-based ice sheets. *Annals of glaciology* 30, 146–152.
- Nichols, R.J., 1995. The liquefaction and remobilization of sandy sediments. In: Hartley, A.J., Prosser, D.J. (Eds.), *Characterization of Deep Marine Clastic Systems: Geological Society of London Special Publication* 94, 63–76.
- Norðdahl, H., Ingólfsson, Ó., Pétursson, H.G., & Hallsdóttir, M., 2008. Late Weichselian and Holocene environmental history of Iceland. *Jökull* 58, 343–364.
- Nye, J.F., 1976. Water flow in glaciers; jökulhlaups, tunnels and veins. *Journal of Glaciology* 17, 181–207.
- Obermeier, S.F., 1996. Use of liquefaction-induced features for paleoseismic analysis - An overview of how seismic liquefaction features can be distinguished from other features and how their regional distribution and properties of source sediment can be used to infer the location and strength of Holocene paleo-earthquakes. *Engineering Geology* 44, 1–76.
- Ó Cofaigh, C., Evans, D.J.A., 2007. Radiocarbon constraints on the age of the maximum advance of the British-Irish Ice Sheet in the Celtic Sea. *Quaternary Science Reviews* 26, 1197–1203.
- Oelkers, E.H., Bjorkum, P.A., Murphy, W.M., 1992. The mechanism of porosity reduction, stylolite development and quartz cementation in North Sea sandstones, in: Kharaka, Y.K., and Maest, A.S. (Eds.), *Water-Rock Interaction*, Rotterdam, US Geological Survey, pp. 1183–1186.
- Oliveira, C.M.M., Hodgson, D.M., Flint, S.S., 2009. Aseismic controls on in situ soft-sediment deformation processes and products in submarine slope deposits of the Karoo Basin, South Africa. *Sedimentology* 56, 1201–1225.
- Oliveira, C.M.M., Hodgson, D.M., Flint, S.S., 2011. Distribution of soft-sediment deformation structures in clinoform successions of the Permian Ecca Group, Karoo Basin, South Africa. *Sedimentary Geology* 235, 314–330.
- Ottesen, D., Dowdeswell, J.A., Rise, L., 2005. Submarine landforms and the reconstruction of fast-flowing ice streams within a large Quaternary ice sheet: The 25 -km-long Norwegian–Svalbard margin (57°–8 °N). *Geological Society of America Bulletin*, 117, 1033–1050.
- Ottesen, D., Rise, L., Knies, J., Olsen, L. and Henriksen, S., 2005b. The Vestfjorden – Trænadjupet palaeo-ice stream drainage system, mid-Norwegian continental shelf. *Marine Geology* 218, 175–189.
- Owen, G., 1987. Deformation processes in unconsolidated sands. In: Jones, M.E., Preston, R.M.F. (Eds.), *Deformation of Sediments and Sedimentary Rocks: Geological Society, London, Special Publication* 29, 11–24.
- Owen, G., Moretti, M., Alfaro, P., 2011. Recognising triggers for soft-sediment deformation: Current understanding and future directions. *Sedimentary Geology* 235, 133–140.
- Parize, O., 1988. Sills et dykes gréseux sédimentaires: paléomorphologie, fracturation précoce, injection et compaction: Thèse Doctorat Géologie, Ecole Nationale Supérieure des Mines de Paris–

Université Lille I: Mémoire des Sciences de la Terre, Ecole des Mines de Paris, 7, 333 pp.

Parize, O., Beaudoin, B., Eckert, S., Fries, G., Hadj-hassen, F., Schneider, F., Su, K., Tijani, A., Troullier, A., De Fouquet, C., Vandromme, R., 2007. The Vocontian Aptian and Albian syndepositional clastic sills and dikes: A field-based mechanical approach to predict and model the early fracturing of marly-limy sediments. In: Hurst, A., Cartwright, J. (Eds.), *Sand Injectites: Implications for Hydrocarbon Exploration and Production: American Association of Petroleum Geologists Memoir*, Tulsa, pp. 163–173.

Passchier, S., Wilson, S., Paulsen, T.S., 1998. Origin of Breccias in the CRP-1 Core. *Terra Antarctica* 5, 401–409.

Passchier, C.W., Trouw, R.A.J., 2005. *Microtectonics*. Springer, Berlin, 366 pp.

Pedersen, S.A.S., 1993. The glaciodynamic event and glaciodynamic sequence. In: Aber, J.S. (Ed.) *Glaciotectonics and Mapping Glacial Deposits*. Canadian Plains Research Center, University of Regina, Saskatchewan, 67–85.

Pedersen, S.A.S., 1996. Progressive glaciotectonic deformation in Weichselian and Palaeogene deposits at Feggeklit, northern Denmark. *Bulletin of the Geological Society of Denmark* 42, 153–174.

Pedersen, S.A.S., 2005. Structural analysis of the Rubjerg Knude Glaciotectonic Complex, Vendsyssel, northern Denmark. *Geological Survey of Denmark and Greenland Bulletin* 8, 1–192.

Peterson, G.L., 1968. Flow structures in sandstone dykes. *Sedimentary Geology* 2, 177–190.

Pettijohn, F.J., Potter, P.E., 1964. *Atlas and glossary of primary sedimentary structures*. Springer, New York, 370 pp.

Pettingill, H.S., Weimer, P., 2002. "Worldwide deepwater exploration and production: Past, present, and future." *Worldwide deepwater exploration and production: Past, present, and future* 21, 371–376.

Phillips, E., Merritt, J., Auton, C., Golledge, N., 2007. Microstructures in subglacial and proglacial sediments: understanding faults, folds and fabrics, and the influence of water on the style of deformation. *Quaternary Science Reviews* 26, 1499–1528.

Phillips, E., Lee, J.R., Burke, H., 2008. Progressive proglacial to subglacial deformation and syntectonic sedimentation at the margins of the Mid-Pleistocene British Ice Sheet: evidence from north Norfolk, UK. *Quaternary Science Reviews* 27, 1848–1871.

Phillips, E., van der Meer, J.J.M., Ferguson, A., 2011. A new 'microstructural mapping' methodology for the identification, analysis and interpretation of polyphase deformation within subglacial sediments. *Quaternary Science Reviews* 30, 2570–2596.

Phillips, E., Lee, J.R., Riding, J.B., Kendall, R., Hughes, L., 2013a. Periglacial disruption and subsequent glaciectonic deformation of bedrock: an example from Anglesey, North Wales, UK. *Proceedings of the Geologists Association* 124, 802–817.

Phillips, E., Everest, J., Reeves, H., 2013b. Micromorphological evidence for subglacial multiphase sedimentation and deformation during overpressurized fluid flow associated with hydrofracturing. *Boreas* 42, 395–427.

- Phillips, E., Hughes, L., 2014. Hydrofracturing in response to the development of an overpressurized subglacial meltwater system during drumlin formation: an example from Anglesey, NW Wales. *Proceedings of the Geologists' Association*, (in press).
- Pickering, K.T., 1987. Wet-sediment deformation in the Upper Ordovician Point Leamington Formation: an active thrust-imbricate system during sedimentation, Notre Dame Bay, north-central Newfoundland. In: Jones, M.E., Preston, R. M.F. (Eds.), *Deformation of Sediments and Sedimentary Rocks*. Geological Society of London Special Publication 29, 213-239.
- Piotrowski, J.A., 1994. Tunnel-valley formation in northwest Germany - geology, mechanisms of formation and subglacial bed conditions for the Bornhöved tunnel valley. *Sedimentary Geology* 89, 107-141.
- Piotrowski, J.A., Kraus, A.M., 1997. Response of sediment to ice-sheet loading in northwestern Germany: effective stresses and glacier-bed stability. *Journal of Glaciology* 43, 495–502.
- Piotrowski, J.A., Larsen, N.K., Junge, F.W., 2004. Reflections on soft subglacial beds as a mosaic of deforming and stable spots. *Quaternary Science Reviews* 23, 993-1000.
- Piotrowski, J.A., Larsen, N.K., Menzies, J., Wysota, W., 2006. Formation of subglacial till under transient bed conditions: deposition, deformation, and basal decoupling under a Weichselian ice sheet lobe, central Poland. *Sedimentology* 53, 83-106.
- Pisarska-Jamrozy, M., Weckwerth, P., 2013. Soft-sediment deformation structures in a Pleistocene glaciolacustrine delta and their implications for the recognition of subenvironments in delta deposits. *Sedimentology* 60, 637-665.
- Potter, P.E., Pettijohn, F.J., 1963. *Paleocurrents and basin analysis*. Springer, Berlin, 296 pp.
- Price, N.J., Cosgrove, J.W., 1990. *Analysis of geological structures*. Cambridge University Press, Cambridge, 502 pp.
- Pringle, J.K., Westerman, D.A., Stanbrook, D.A., Tatum, D.I., Gardiner, A.R., 2007. Sand Volcanoes of the Carboniferous Ross Formation, County Clare, Western Ireland: 3-D Internal Sedimentary Structure and Formation. In: Hurst, A., Cartwright, J. (Eds.), *Sand Injectites: Implications for Hydrocarbon Exploration and Production*: American Association of Petroleum Geologists Memoir, Tulsa, pp. 227–231.
- Ravier, E., Buoncristiani, J.F., Clerc, S., Guiraud, M., Menzies, J., Portier, E., 2014a. Sedimentological and deformational criteria for discriminating subglaciofluvial deposits from subaqueous ice-contact fan deposits: A Pleistocene example (Ireland). *Sedimentology* 61, 1382-1410.
- Ravier, E., Buoncristiani, J.-F., Guiraud, M., Menzies, J., Clerc, S., Goupy, B., Portier, E., 2014b. Porewater pressure control on subglacial soft sediment remobilization and tunnel valley formation: A case study from the Alnif tunnel valley (Morocco). *Sedimentary Geology* 304, 71-95.
- Reinardy, B.T.I., Larter, R.D., Hillenbrand, C.D., Murray, T., Hiemstra, J.F., Booth, A.D., 2011. Streaming flow of an Antarctic Peninsula palaeo-ice stream, both by basal sliding and deformation of substrate. *Journal of Glaciology* 57, 596-608.
- Renard, F., and Ortoleva, P., 1997. Water film at grain–grain contacts: Debye–Hückel, osmotic model

- of stress, salinity and mineralogy dependence: *Geochimica and Cosmochimica Acta* 61, 1963-1970.
- Renard, F., Ortoleva, P., Gratier, J.P., 1997. Pressure solution in sandstones: influence of clays and dependence on temperature and stress. *Tectonophysics* 280, 257-266.
- Roberts, D., 1995. The development of criteria to distinguish glaciotectonic and glaciomarine sedimentary environments. Unpublished Ph.D. Thesis, University of Southampton.
- Roberts, D.H., Hart, J.K., 2005. The deforming bed characteristics of a stratified till assemblage in north East Anglia, UK: investigating controls on sediment rheology and strain signatures. *Quaternary Science Reviews* 24, 123-140.
- Roberts, D.H., Yde, J.C., Knudsen, N.T., Long, A.J., Lloyd, J.M., 2009. Ice marginal dynamics during surge activity, Kuannersuit Glacier, Disko Island, West Greenland. *Quaternary Science Reviews* 28, 209-222.
- Rose, J., 1987. Drumlins as part of a glacier bedform continuum. In Menzies, J. and Rose, J. (Eds.), *Drumlin Symposium*. Balkema, Rotterdam, pp. 103-116.
- Rose, K.E., 1979. Characteristics of flow in Marie Byrd Land, Antarctica. *Journal of Glaciology* 11, 177-203.
- Rossetti, D.D.F., 1999. Soft-sediment deformation structures in late Albian to Cenomanian deposits, São Luís Basin, northern Brazil: evidence for palaeoseismicity. *Sedimentology* 46, 1065-1081.
- Rotnicki, K., 1976. The theoretical basis for and a model of the origin of glaciotectonic deformations. *Questiones Geographicae* 3, 103-139.
- Rousell, D.H., Fedorowich, J.S., Dressler, B.O., 2003. Sudbury Breccia (Canada): a product of the 1850 Ma Sudbury Event and host to footwall Cu-Ni-PGE deposits. *Earth-Science Reviews* 60, 147-174.
- Rowe, C.A., Mustard, P.S., Mahoney, J.B., Katnick, D.C., 2002. Oriented clastic dike swarms as indicators of paleoslope? - An example from the Upper Cretaceous Nanaimo Group, Canada. *Journal of Sedimentary Research* 72, 192-200.
- Rye-Larsen, M., 1994. The Balder Field: Refined reservoir interpretation with the aid of high resolution seismic data and seismic attribute mapping, in: J.O. Aasen, E. Berg, A.T. Buller, O. Hjelmeland, R.M. Holt, J. Kleppe and O. Torsaeter, (Eds.), *North Sea Oil and Gas Reservoirs III*: Kluwer, p. 115-124.
- Sanders, J.E., 1965. Primary sedimentary structures formed by turbidity currents and related resedimentation mechanisms. In: Middleton, G.V. (Ed.), *Primary Sedimentary Structures and their Hydrodynamic Interpretation*, SEPM Special Publication 12, 192-219.
- Sandersen, P.B.E., Jørgensen, F., Larsen, N.K., Westergaard, J.H.W., Auken, E., 2009. Rapid tunnel-valley formation beneath the receding Late Weichslian ice sheet in Vendsyssel, Denmark. *Boreas* 38, 834-851.
- Schmid, S.M., Handy, M.R., 1991. Towards a genetic classification of fault rocks: geological usage and tectonophysical implications. In Müller, D.W., McKenzie, J.A., Weissert, H. (Eds.) *Controversies in modern geology, evolution of geological theories in sedimentology, earth history and tectonics*. Academic Press, London, pp 369-361.

- Scholz, H., Frieling, D., Aehnelt, M., 2010. Synsedimentary deformational structures caused by tectonics and seismic events – Example from the Cambrian of Sweden, Permian and Cenozoic of Germany. *New Frontiers In: Tectonic Research - General Problems, Sedimentary Basins and Island Arcs*, Evgenii V. Sharkov (Ed.).
- Scott, A., Vigorito, M., Hurst, A., 2009. The process of sand injection: internal structures and relationships with host strata (Yellowbank Creek Injectite Complex, California, USA). *Journal of Sedimentary Research* 79, 568-583.
- Scott, A., Hurst, A., Vigorito, M., 2013. Outcrop-based reservoir characterization of a kilometer-scale sand-injectite complex. *AAPG Bulletin* 97, 309-343.
- Selby, M.J., 1993. *Hillslope Materials and Processes*. Oxford University Press, 264 pp.
- Sergienko, O.V., Hindmarsh, R.C.A., 2013. Regular Patterns in Frictional Resistance of Ice-Stream Beds Seen by Surface Data Inversion. *Science* 342, 1086-1089.
- Shanmugan, G., 2000. 50 years of the turbidite paradigms (1950s-1990s): deep-water processes and facies models - a critical perspective. *Marine and Petroleum Geology* 17, 285-342.
- Shanmugam, G., Moiola, R.J., 1988. Submarine fans: characteristics, models, classification, and reservoir potential. *Earth Science Reviews* 24, 383-428.
- Shaw, J., 1983. Forms associated with boulders in melt-out till. In: *Tills and related deposits* (Eds E.B. Evenson, C. Schluchter, and J. Rabassa). Balkema, Rotterdam, pp. 3-12.
- Shaw, J., 1987. Glacial sedimentary processes and environmental reconstructions based on Lithofacies. *Sedimentology* 34, 103-16.
- Shaw, J., 2002. The meltwater hypothesis for subglacial bedforms. *Quaternary International* 90, 5-22.
- Shaw, J., 2010. In defence of the meltwater (megaflood) hypothesis for the formation of subglacial bedform fields. *Journal of Quaternary Science* 25, 249-260.
- Shaw, J., Kvill, D., Rains, R.B., 1989. Drumlins and catastrophic subglacial floods. *Sedimentary Geology* 62, 177-202.
- Shaw, J., Gorell, G., 1991. Subglacially formed dunes with bimodal and graded gravel in the Trenton drumlin field, Ontario. *Géographie Physique et Quaternaire* 45, 21-34.
- Shoemaker, E. M., 2003. Effects of bed depressions upon floods from subglacial lakes. *Global and Planetary Change* 35, 175-184.
- Sibley, D.F., Blatt, H., 1976. Intergranular pressure solution and cementation of the Tuscarora orthoquartzite: *Journal of Sedimentary Petrology* 46, 881-896.
- Sigurðsson, O., 2010. Variations of Mýrdalsjökull during Postglacial and Historical Times. In: Schomacker, A., Krüger, J., Kjær, K.H. (Eds.), *The Mýrdalsjökull ice cap, Iceland. Glacial processes, sediments and landforms on an active volcano: Developments in Quaternary Science* 13, pp. 69-78.
- Sims, J.D., 1978. Annotated bibliography of penecontemporaneous deformational structures in

sediments. United States Geological Survey Open File Report 78–510, 79 pp.

Slater, G., 1926. Glacial tectonics as reflected in disturbed drift deposits. *Proceedings of the Geologists Association* 37, 392–400.

Smellie, J., Nelson, A., Williams, M., 2006. Fire and ice: unravelling the climatic and volcanic history of James Ross Island, Antarctic Peninsula. *Geology Today* 22, 220–226.

Smyers, N.B., Peterson, G.L., 1971. Sandstone dikes and sills in the Moreno shale, Panoche hills, California. *Geological Society of America Bulletin* 82, 3201–3207.

Storti, F., Vannucchi, P., 2007. Deformation of Soft Sediment in Nature and Laboratory: *Sedimentary Geology* 196, 278 pp.

Strachan, L.J., 2002. Slump-initiated and controlled syndepositional sandstone remobilization: an example from the Namurian of County Clare, Ireland. *Sedimentology* 49, 25–41.

Stromberg, S.G., Bluck, B., 1997. Turbidite facies, fluidescape structures and mechanisms of emplacement of the Oligo-Miocene Aljibe Flysch, Gibraltar Arc, Betics, southern Spain. *Sedimentary Geology* 115, 267–288.

Sugden, D.E., Glasser, N.F., Clapperton, C.M., 1992. Evolution of large roches moutonnées. *Geografiska Annaler: Physical Geography* 74, 253–264.

Surlyk, F., Noe-Nygaard, N., 2001. Sand remobilisation and intrusion in the Upper Jurassic Hareelv Formation of East Greenland. *Geological Society of Denmark Bulletin* 48, 169–188.

Takahama, N., Otsuka, T., Brahmantyo, B., 2000. A new phenomenon in ancient liquefaction - the draw-in process, its final stage. *Sedimentary Geology* 135, 157–165.

Talling, P.J., Masson, D.G., Sumner, E.J., Malgesini, G., 2012. Subaqueous sediment density flows: Depositional processes and deposit types. *Sedimentology* 59, 1937–2003.

Tarplee, M.F., van der Meer, J.J.M., Davis, G.R., 2011. The 3D microscopic ‘signature’ of strain within glacial sediments revealed using X-ray computed microtomography. *Quaternary Science Reviews* 30, 3501–3532.

Taylor, B.J., 1982. Sedimentary dykes, pipes and related structures in the Mesozoic sediments of south-eastern Alexander Island. *British Antarctic Survey Bulletin* 51, 1–42.

Terzaghi, C., 1925. Principles of Soil Mechanics. *Engineering News-Record* 95, 19–27.

Thomas, G.S.P., Chiverrell, R.C., 2007. Structural and depositional evidence for repeated ice-marginal oscillation along the eastern margin of the Late Devensian Irish Sea Ice Stream. *Quaternary Science Reviews* 26, 2375–2405

Thomason, J.F., Iverson, N.R., 2006. Microfabric and microshear evolution in deformed till. *Quaternary Science Reviews* 25, 1027–1038.

Thorarinsson, S., 1943. Vatnajökull. Scientific results of the Swedish-Icelandic investigations 1936 37–38. *Geografiska Annaler* 1–2, 1–54.

- Tournier, F., 2010. Mécanismes et contrôle des phénomènes diagénétiques en milieu acide dans les grès de l'Ordovicien glaciaire du bassin de Sbâa, Algérie. Campus d'Orsay, Paris 6, Paris, 403 pp.
- Tournier, F., Pagel, M., Portier, E., Wazir, I., Fiet, N., 2010. Relationship between deep diagenetic quartz cementation and sedimentary facies in a late ordovician glacial environment (Sbaa basin, Algeria). *Journal of Sedimentary Research* 80, 1068-1084.
- Truswell, J.F., 1972. Sandstone sheets and related intrusions from Coffee bay, Transkei, South Africa. *Journal of Sedimentary Petrology* 42, 578-583.
- Tulaczyk, S., 1999. Ice sliding over weak, fine-grained tills: dependence of ice-till interactions on till granulometry. *Geological Society of America Special Papers* 337, 159-177.
- Twiss, R.J., Moores, E.M., 1992. *Structural Geology*. Freeman, New York, 532 pp.
- Vetel, W., Cartwright, J., 2010. Emplacement mechanics of sandstone intrusions: insights from the Panoche Giant Injection Complex, California. *Basin Research* 22, 783-807.
- Van den Driessche, J. and Brun, J.P., 1987. Rolling structures at large shear strain. *Journal of Structural Geology* 9, 691-704.
- van der Meer, J.J.M., 1993. Microscopic evidence of subglacial deformation. *Quaternary Science Reviews* 12, 553-587.
- van der Meer, J.J.M., Kjær, K., Krüger, J., 1999. Subglacial water-escape structures, Sléttjökull, Iceland. *Journal of Quaternary Science* 14, 191-205.
- van der Meer, J.J.M., Menzies, J., Rose, J., 2003. Subglacial till: the deforming glacier bed. *Quaternary Science Reviews* 22, 1659-1685.
- van der Meer, J.J.M., Kjaer, K.H., Kruger, J., Rabassa, J., Kilfeather, A.A., 2009. Under pressure: clastic dykes in glacial settings. *Quaternary Science Reviews* 28, 708-720.
- van der Meer, J.J.M., and Menzies, J., 2011. The micromorphology of unconsolidated sediments. *Sedimentary Geology* 238, 213-232.
- Van der Wateren, F.M., 1999. Structural geology and sedimentology of the Heiligenhafen till section, Northern Germany. *Quaternary Science Reviews* 18, 1625-1639.
- van der Wateren, F.M., Kluiving, S.J., Bartek, L.R., 1995. Kinematics indicators of subglacial shearing. In : Maltman, A.J., Hubbard, B. and Hambrey, M.J. (Eds.): *Deformation of Glacial Materials*. Geological Society, London, Special Publications 176, 259-278.
- van der Wateren, F.M., Kluiving, S.J., Bartek, L.R., 2000. Kinematic indicators of subglacial shearing. In: A.J. Maltman, B. Hubbard, M.J. Hambrey (Eds.) *Deformation of glacial materials*. Geological Society of London, Special Publications 176, 259-278.
- van Loon, A.J., 2009. Soft-sediment deformation structures in siliciclastic sediments: an overview. *Geologos* 15, 3-55.
- Vanuxem, L., 1842. *Geology of New York, Pt. III, Survey of the 3rd District*, 306 pp.

- Vetel, W., Cartwright, J., 2010. Emplacement mechanics of sandstone intrusions: insights from the Panoche Giant Injection Complex, California. *Basin Research* 22, 783-807.
- Vigorito, M., Hurst, A., Cartwright, J., Scott, A., 2008. Regional-scale subsurface sand remobilization: geometry and architecture. *Journal of the Geological Society* 165, 609-612.
- Vigorito, M., Hurst, A., 2010. Regional sand injectite architecture as a record of pore-pressure evolution and sand redistribution in the shallow crust: insights from the Panoche Giant Injection Complex, California. *Journal of the Geological Society* 167, 889-904.
- Villas, E., Vizcaino, D., Alvaro, J.J., Destombes, J., Vennin, E., 2006. Biostratigraphic control of the latest-Ordovician glaciogenic unconformity in Alnif (Eastern Anti-Atlas, Morocco), based on brachiopods. *Geobios* 39, 727-737.
- Vogel, S.W., Tulaczyk, S., Joughin, I.R., 2003. Distribution of basal melting and freezing beneath tributaries of Ice Stream C: implication for the Holocene decay of the West Antarctic ice sheet. *Annals of Glaciology* 36, 273-282.
- Waldron, J.W.F., 2004. Anatomy and evolution of a pull-apart basin, Stellarton, Nova Scotia. *Geological Society of America Bulletin* 116, 109-127.
- Waldron, J.W.F., Gagnon, J.F., 2011. Recognizing soft-sediment structures in deformed rocks of orogens. *Journal of Structural Geology* 33, 271-279.
- Waller, R., Phillips, E., Murton, J., Lee, J., Whiteman, C., 2011. Sand intraclasts as evidence of subglacial deformation of Middle Pleistocene permafrost, North Norfolk, UK. *Quaternary Science Reviews* 30, 3481-3500.
- Waterson, C.D., 1950. Note on the sandstone injections of Eathie Haven, Cromarty. *Geological Magazine* 87, 133-139.
- Walter, F., Deichmann, N., Funk, M., 2008. Basal icequakes during changing subglacial water pressures beneath Gornergletscher, Switzerland. *Journal of Glaciology* 54, 511-521.
- Went, D.J., 2005. Pre-vegetation alluvial fan facies and processes: an example from the Cambro-Ordovician Rozel Conglomerate Formation, Jersey, Channel Islands. *Sedimentology* 52, 693-713.
- Werther, J., Reppenhagen, J., 2003. Attrition. In: Yang, W.C. (Ed.), *Handbook of fluidization and fluid-particles systems*. Marcel Dekker, New York, pp. 201-237.
- Weyl, P.K., 1959. Pressure solution and the force of crystallisation - a phenomenological theory: *Journal of Geophysical Research* 64, 2001-2025.
- Wiebe, R.A., Collins, W.J., 1998. Depositional features and stratigraphical sections in granitic plutons: implications for the emplacement and crystallization of granitic magmas. *Journal of Structural Geology* 20, 1273-1289.
- Wignall, P.B., Best, J.L., 2000. The Western Irish Namurian Basin reassessed. *Basin Research* 12, 59-78.
- Williams, G., 1996. Soft-sediment deformation structures from the Marinoan glacial succession, Adelaide foldbelt: implications for the palaeolatitude of late Neoproterozoic glaciation. *Sedimentary*

Geology 106, 165-175.

Williams, G.D., Brabham, P.J., Eaton, G.P., Harris, C., 2001. Late Devensian glaciotectionic deformation at St Bees, Cumbria: a critical wedge model. *Journal of the Geological Society of London* 158, 125-135.

Winsborrow, M.C.N, Clark, C.D., Stokes, C.R., 2010. What controls the location of ice streams? *Earth Science Reviews* 103, 45-59.

Winsemann, J., Asprion, U., Meyer, T., Schultz, H., Victor, P., 2003. Evidence of iceberg-ploughing in a subaqueous ice-contact fan, glacial Lake Rinteln, NW Germany. *Boreas* 32, 386-398.

Zwally, H.J., Abdalati, W., Herring, T., Larson, K., Saba, J., Steffen, K., 2002. Surface melt-induced acceleration of Greenland ice-sheet flow. *Science* 297, 218-222.

